



GE Energy

David H. Hinds  
Manager, ESBWR

PO Box 780 M/C L60  
Wilmington, NC 28402-0780  
USA

T 910 675 6363  
F 910 362 6363  
david.hinds@ge.com

MFN 05-127

Project 717

November 17, 2005

U.S. Nuclear Regulatory Commission  
Document Control Desk  
Washington, D.C. 20555-0001

Subject: **NEDO-33083-A, "TRACG Application for ESBWR," October 2005  
(TAC # MC8168)**

This letter submits the "A" (accepted) version of the subject Licensing Topical Report (LTR) which incorporates the Reference 1 NRC letter and the non-proprietary safety evaluation. The LTR is contained in Enclosure 1. This report is the non-proprietary version of NEDC-33083P-A, *TRACG Application for ESBWR*, March 2005, which was submitted in the Reference 2 letter.

If you have any questions about the information provided here, please let me know.

Sincerely,

David H. Hinds  
Manager, ESBWR

DBL 8

References:

1. MFN 04-119, Letter from William D. Beckner to Louis M. Quintana, *Reissuance of Safety Evaluation Report Regarding the Application of General Electric Nuclear Energy's TRACG Code to ESBWR Loss-of-Coolant Accident (LOCA) Analyses (TAC Nos. MB6279, MB6280, MB6281, MB6282, MB6283, MB6801 and MB7255)*, October 28, 2004
2. MFN 05-017, Robert E. Gamble to U.S. Nuclear Regulatory Commission, *Accepted Version of GE Licensing Topical Report NEDC-33083P-A, "TRACG Application for ESBWR," March 2005, April 8, 2005*

Enclosure:

1. MFN 05-127 – NEDO-33083-A, "TRACG Application for ESBWR," October 2005

cc: WD Beckner USNRC (w/o enclosure)  
LA Dudes USNRC (w/o enclosure)  
AE Cabbage USNRC (with enclosure)  
GB Stramback GE (with enclosure)  
eDRF 0000-0046-6821

NEDO-33083-A  
Class I  
DRF 0000-0009-4180  
October 2005

# **TRACG Application for ESBWR**

B. S. Shiralkar  
Y. K. Cheung

## **NON PROPRIETARY NOTICE**

This is a non proprietary version of the document NEDC-33083P-A, which has the proprietary information removed. Portions of the document that have been removed are indicated either by an open and closed bracket as shown here [[ ]] or by sidebars in the right margin.

## **IMPORTANT NOTICE REGARDING CONTENTS OF THIS REPORT PLEASE READ CAREFULLY**

Neither the General Electric Company nor any of the contributors to this document:

a. Makes any warranty or representation, express or implied, with respect to the accuracy, completeness, or usefulness of the information contained in this document, or that the use of any information, apparatus, method, or process disclosed in this document may not infringe privately owned rights;

or

b. Assumes any liabilities, including but not limited to nuclear liability, with respect to the use of, or for damages resulting from the use of any information, apparatus, method, or process disclosed in this document.

This work was performed partially as part of a contract between various utilities and GE for "ESBWR Development".

**CHANGES FROM REV. 0**

Some of the GENE responses to NRC requests for additional information (RAIs) committed to revise certain report sections. Plus, the NRC acceptance letter “requests that GENE publish an accepted version of the revised NEDC-33083P”...and add an “-A”(designating accepted) following the report identification number,” and that a copy of the NRC acceptance letter and safety evaluation be incorporated into the report. This document is the non proprietary version of NEDC-33083P-A. The NRC-requested and RAI-related changes are incorporated herein, and are denoted by “bars” in the left-hand margins of the affected paragraphs and figure (as shown to the left of this paragraph). An attachment is added to provide copies of all of the RAIs and their associated responses.



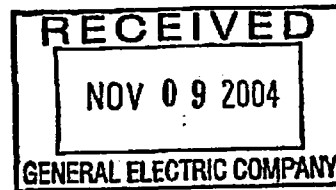
UNITED STATES  
NUCLEAR REGULATORY COMMISSION

WASHINGTON, D.C. 20555-0001

October 28, 2004

MFN:04-119

Mr. Louis M. Quintana  
Manager, GENE Licensing  
General Electric Company  
175 Curtner Avenue, M/C 365  
San Jose, CA 95125-1014



**SUBJECT: REISSUANCE OF SAFETY EVALUATION REPORT REGARDING THE APPLICATION OF GENERAL ELECTRIC NUCLEAR ENERGY'S TRACG CODE TO ESBWR LOSS-OF-COOLANT ACCIDENT (LOCA) ANALYSES (TAC NOS. MB6279, MB6280, MB6281, MB6282, MB6283, MB6801 AND MB7255)**

Dear Mr. Quintana:

By letter dated April 18, 2002, General Electric Nuclear Energy (GENE) requested a preapplication review of the economic simplified boiling water reactor (ESBWR) advanced passive reactor design. At GENE's request, the preapplication review is focused on the TRACG thermal-hydraulic analysis computer code and the testing and scaling programs relevant to assessment of the computer code. By letters dated August 30 and November 19, 2002, and January 9, 2003, General Electric Company (GE) submitted the following eight topical reports (TR) in support of the ESBWR preapplication review:

- NEDC-32606P, SBWR Testing Summary Report;
- NEDC-32725P, TRACG Qualification for SBWR, Rev.1, Vol. 1 and 2;
- NEDC-33079P, ESBWR Test and Analysis Program Description;
- NEDC-33080P, TRACG Qualification for ESBWR;
- NEDC-33081P, ESBWR Test Report;
- NEDC-33082P, ESBWR Scaling Report;
- NEDC-33083P, TRACG Application for ESBWR; and
- NEDC-33084P, ESBWR Design Description, Rev.1.

By letter dated August 19, 2004, the Nuclear Regulatory Commission (NRC) staff issued a safety evaluation (SE) regarding the application of TRACG to ESBWR loss-of-coolant accident (LOCA) analyses. The letter requested that you review the SE for proprietary information. By letter dated September 10, 2004, as revised by letter dated September 23, 2004, from Robert E. Gamble, you identified this information line by line pursuant to the criteria of Title 10 of the *Code of Federal Regulations* (10 CFR) Section 2.390. The proprietary information contained in the SE (Enclosure 1) is indicated by marginal lines. We have prepared a non-proprietary version of the SE (Enclosure 2 - ADAMS Accession No. ML04300303) that does not contain proprietary information.

The enclosed SE is limited to the application of TRACG to the ESBWR LOCA analyses and the relevant testing programs and scaling analyses. The staff concludes that TRACG, including the application methodology, is an acceptable evaluation model for ESBWR LOCA analyses. Therefore, the staff finds that NEDC-33083P, *TRACG Application for ESBWR*, is acceptable for

referencing during the ESBWR design certification to the extent specified and under the limitations delineated in the TR and in the associated NRC SE. The SE, which is enclosed, defines the basis for acceptance of the TR.

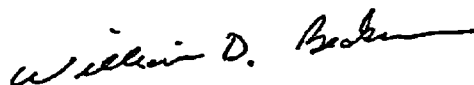
The NRC requests that GENE publish revised versions of the topical reports listed above within 3 months of receipt of this letter. The accepted version of NEDC-33083P shall incorporate this letter and the enclosed SE between the title page and the abstract, and add an "-A" (designating accepted) following the report identification number (i.e., NEDC-33083P-A).

If the NRC's criteria or regulations change so that its conclusion that the TR is acceptable is invalidated, GENE and/or the applicant referencing the TR will be expected to revise and resubmit its respective documentation, or submit justification for the continued applicability of the TR without revision of the respective documentation.

The subject TR and supporting documentation have been reviewed by the Advisory Committee on Reactor Safeguards (ACRS) which has agreed with the staff recommendation for approval by their letter of February 12, 2004.

If you have any further questions regarding this review, please contact Amy E. Cabbage (301-415-2875).

Sincerely,



William D. Beckner, Program Director  
New, Research and Test Reactors Program  
Division of Regulatory Improvement Programs  
Office of Nuclear Reactor Regulation

Project No. 717

Enclosures: 1. Safety Evaluation (Proprietary)  
2. Safety Evaluation ( Non-Proprietary)

cc: See next page (w/o enclosure 1)

ESBWR

cc:

Dr. Robert E. Gamble  
Manager, ESBWR  
GE Nuclear Energy  
175 Curtner Avenue, MC 365  
San Jose, CA 95125

Mr. George B. Stramback  
Manager, Regulatory Services  
GE Nuclear Energy  
175 Curtner Avenue, MC 747  
San Jose, CA 95125

Mr. J. Alan Beard  
GE Nuclear Energy  
13113 Chestnut Oak Drive  
Darnestown, MD 20878-3554

Mr. David Lochbaum, Nuclear Safety Engineer  
Union of Concerned Scientists  
1707 H Street, NW., Suite 600  
Washington, DC 20006-3919

Mr. Paul Gunter  
Nuclear Information & Resource Service  
1424 16th Street, NW, Suite 404  
Washington, DC 20036

Mr. James Riccio  
Greenpeace  
702 H Street, Suite 300  
Washington, DC 20001

Mr. Adrian Heymer  
Nuclear Energy Institute  
Suite 400  
1776 I Street, NW  
Washington, DC 20006-3708

Mr. Thomas P. Miller  
U.S. Dept. of Energy, NE-20, Rm. A286  
Headquarters - Germantown  
19901 Germantown Road  
Germantown, MD 20874-1290

Mr. Paul Leventhal  
Nuclear Control Institute  
1000 Connecticut Avenue, NW  
Suite 410  
Washington, DC 20036

Mr. Jack W. Roe  
SCIENTECH, INC.  
910 Clopper Road  
Gaithersburg, MD 20878

Mr. Brendan Hoffman  
Research Associate on Nuclear Energy  
and Environmental Program  
215 Pennsylvania Avenue, SE  
Washington, DC 20003

Mr. Tom Clements  
6703 Gude Avenue  
Takoma Park, MD 20912

Ms. Patricia Campbell  
Winston & Strawn  
1400 L Street, NW  
Washington, DC 20005

Mr. Glenn H. Archinoff  
5275 Westview Drive  
ACR Suite  
Frederick, MD. 21703-8306

Mr. Gary Wright, Director  
Division of Nuclear Facility Safety  
Illinois Emergency Management Agency  
1035 Outer Park Drive  
Springfield, IL 62704

Mr. Charles Brinkman  
Westinghouse Electric Co.  
Washington Operations  
12300 Twinbrook Pkwy., Suite 330  
Rockville, MD 20852

Mr. Ronald P. Vijuk  
Manager of Passive Plant Engineering  
AP1000 Project  
Westinghouse Electric Company  
P. O. Box 355  
Pittsburgh, PA 15230-0355

Mr. Ed Wallace, General Manager  
Projects  
PBMR Pty LTD  
PO Box 9396  
Centurion 0046  
Republic of South Africa

Mr. Russell Bell  
Nuclear Energy Institute  
Suite 400  
1776 I Street, NW  
Washington, DC 20006-3708

Mr. Ron Simard  
6170 Masters Club Drive  
Suwanne, GA 30024

E-Mail:  
[jim.mallay@framatome-anp.com](mailto:jim.mallay@framatome-anp.com)

## SAFETY EVALUATION BY THE OFFICE OF NUCLEAR REACTOR REGULATION

### NEDC-33083P, "TRACG APPLICATION FOR ESBWR"

#### GE NUCLEAR ENERGY

### PROJECT 717 - ESBWR PREAPPLICATION REVIEW

#### 1.0 INTRODUCTION

By letter dated April 18, 2002, General Electric Nuclear Energy (GENE) requested a preapplication review of the economic simplified boiling water reactor (ESBWR) advanced passive reactor design. The ESBWR is a 4000 MWth (1390 MWe), natural circulation, boiling water reactor design, which utilizes passive safety systems. The staff has held several public meetings, including meetings with the Advisory Committee on Reactor Safeguards, to discuss the preapplication review scope and schedule, and the ESBWR design and technology basis. The staff documented the scope, schedule, and cost for the preapplication review in a letter to GENE dated December 19, 2002.

The preapplication review is focused on the TRACG thermal-hydraulic analysis computer code and the testing and scaling programs relevant to assessment of the computer code. The scope of the preapplication review does not address the design of the ESBWR. The scope of this safety evaluation report (SER) is limited to the application of TRACG to ESBWR loss-of-coolant accident (LOCA) analyses and the relevant testing programs and scaling analyses. The NRC's Offices of Nuclear Reactor Regulation and Nuclear Regulatory Research, and their contractors, performed this review.

#### 2.0 REGULATORY BASIS

##### 2.1 Regulatory Basis for Loss-of-Coolant Accidents

The requirements of 10 CFR 50.46 specify that each boiling or pressurized light-water cooled nuclear power reactor fueled with uranium oxide pellets within cylindrical zircaloy or ZIRLO cladding must be provided with an emergency core cooling system (ECCS) that must be designed so that its calculated cooling performance following a postulated LOCA conforms to the criteria contained in that section.

Section 50.46 states further that this requirement can be met through an evaluation model for which an uncertainty analysis has been performed, specifically, section 50.46(a) states that:

*the evaluation model must include sufficient supporting justification to show that the analytical technique realistically describes the behavior of the reactor system during a loss-of-coolant accident. Comparisons to*

*applicable experimental data must be made and uncertainties in the analysis method and inputs must be identified and assessed so that the uncertainty in the calculated results can be estimated. This uncertainty must be accounted for, so that, when the calculated ECCS cooling performance is compared to the criteria set forth in paragraph (b) of this section, there is a high level of probability that the criteria would not be exceeded.*

Section 50.46(b) specifies that the calculated peak cladding temperature (PCT) must not exceed 2200 °F, the maximum cladding oxidation must not exceed 0.17 times the total cladding thickness before oxidation, the maximum hydrogen generation must not exceed 0.01 times the hypothetical amount that would be generated if all of the metal in the cladding surrounding the fuel pellets were to react, the core must remain in a coolable geometry, and, after calculated successful ECCS initiation, the core temperature shall be maintained at an acceptably low level and decay heat shall be removed for the extended period of time required by the long-lived radioactivity remaining in the core.

## 2.2 Containment Regulatory Basis

The staff reviews the containment design to ensure compliance with the relevant requirements of General Design Criteria (GDC) 4, "Environmental and Dynamic Effects Design Bases," GDC 16, "Containment Design," GDC 38, "Containment Heat Removal," GDC 50, "Containment Design Basis," and GDC 53, "Provisions for Containment Testing and Inspection." The relevant requirements for this review are as follows.

GDC 16, insofar as it requires that reactor containment be provided to establish an essentially leak-tight barrier against the uncontrolled release of radioactivity to the environment;

GDC 38, insofar as it requires that a system to remove heat from the containment be provided, and that the system's safety function be to reduce rapidly, consistent with the functioning of other associated systems, the containment pressure and temperature following any LOCA and maintain them at acceptably low levels; and

GDC 50, insofar as it requires that the containment structure be designed so that it and its internal compartments can accommodate, without exceeding the design leakage rate and with sufficient margin, the calculated pressure and temperature conditions resulting from any LOCA.

Unlike the transient response for other containment designs where the containment pressure peaks rapidly, the ESBWR pressure transient does not rapidly increase to a peak value from which it must be rapidly reduced. The pressure increases slowly over several hours and is expected to remain well below the design limits for the duration of the transient (72 hours). The passive containment cooling system (PCCS) removes the decay heat from the containment and the containment pressure is determined by the transport of noncondensibles into the wetwell and the heat input to the containment. GENE concluded that the intent of GDC 38 can be satisfied by the use of a decay heat removal system that maintains the containment pressure

below the design pressure at all times. ESBWR calculations for radiological releases from the containment will be based on the assumption that the containment remains at the design pressure throughout the 72 hours, and no credit for pressure reduction will be used for design basis analyses during design certification.

The Standard Review Plan (SRP) for the Review of Safety Analysis Reports for Nuclear Power Plants, draft NUREG-0800, June 1996, describes the responsibilities and guidelines for the staff's review. The section of the SRP that is relevant to the TRACG analysis for the ESBWR is Section 6.2.1, "Containment Functional Design." Two statements from the introduction of SRP Section 6.2.1 relate directly to the staff's review of the use of the TRACG code for the analysis of the ESBWR Containment/LOCA response:

- *The containment structure must be capable of withstanding, without loss of function, the pressure and temperature conditions resulting from postulated loss-of-coolant, steam line, or feedwater line break accidents.*
- *GDC 50, among other things, requires that consideration be given to the potential consequences of degraded engineered safety features, such as the containment heat removal system and the emergency core cooling system, the limitations in defining accident phenomena, and the conservatism of calculational models and input parameters, in assessing containment design margins.*

Guidelines specific to boiling water reactor (BWR) pressure suppression containments are contained in SRP Section 6.2.1.1.C, "Pressure-Suppression Type BWR Containments." This SRP addresses GENE Mark I, II, and III pressure-suppression containments, and was also used by the staff as the basis for the review of the Advanced Boiling Water Reactor (ABWR) containment design. The ESBWR containment design has developed from the Mark III and ABWR containments. Therefore, these guidelines are considered by the staff to be an applicable basis for the review of the ESBWR containment analysis.

The SRP, developed prior to the promulgation of 10 CFR Part 52, provides a two-step approach to acceptance of calculated containment pressure and drywell/containment [wetwell] pressure differential. At the construction permit stage, the containment design pressure should provide at least a 15 percent margin above the peak calculated containment pressure, and the design differential pressure between drywell and containment [wetwell] should provide at least a 30 percent margin above the peak calculated differential pressure. At the operating license stage, the peak calculated containment pressure and the differential pressure between the drywell and the containment [wetwell] should be less than their respective design values.

The other containment acceptance criteria are related to missile and pipe whip protection (GDC 4), periodic inspections (GDC 53), containment dynamic loads, allowable bypass leakage rates, design leakage rate, containment negative pressures, external pressures, safety relief valve (SRV) in-plant tests, local suppression pool (SP) temperature limits during SRV discharges, and instrumentation for post-accident monitoring. These criteria are not relevant to

this TRACG application method review and they will be addressed by other analytical methods or procedures in the design certification application.

### 2.3 Standard Design Regulatory Basis

The Commission promulgated specific regulatory requirements for the acceptance, review, and approval of standardized nuclear power plant designs. Those requirements are found in 10 CFR Part 52. Specifically applicable to the review of the TRACG analysis methodology, 10 CFR 52.47(b), "Contents of Applications," requires the following:

(2)(i) Certification of a standard design which differs significantly from the light water reactor designs described in paragraph (b)(1) of this section or utilizes simplified, inherent, passive, or other innovative means to accomplish its safety functions will be granted only if

(A)(1) The performance of each safety feature of the design has been demonstrated through either analysis, appropriate test programs, experience, or a combination thereof;

(2) Interdependent effects among the safety features of the design have been found acceptable by analysis, appropriate test programs, experience, or a combination thereof; [and]

(3) Sufficient data exist on the safety features of the design to assess the analytical tools used for safety analyses over a sufficient range of normal operating conditions, transient conditions, and specified accident sequences, including equilibrium core conditions[.]

For the qualification of TRACG, GENE used a broad range of tests that span and bound the important ESBWR parameters and passive safety features. In particular, a full-scale prototype of the isolation condenser (IC) and a near-full scale PCCS were tested at PANTHERS. The various test programs are discussed in Section 3.7.1 of this report. Reduced scale PCCS units were tested at GIRAFFE (3 tubes) and PANDA (20 tubes), which confirmed the scaling basis for the PCCS. Integral tests were performed at the GIRAFFE and PANDA tests facilities. Both were full height simulations of the Simplified Boiling Water Reactor (SBWR), with different aspect ratios. PANDA is scaled to a system scale of 1:25 and GIRAFFE to a system scale of 1:400; that is, the volumes, flow areas, and power are scaled by these ratios for the SBWR. PANDA also simulated possible asymmetrical effects within the drywell and wetwell with two vessels for each region, situated a distance apart, corresponding to the diameter of the SBWR wetwell annulus. The ESBWR/SBWR relationship is discussed in Section 3.0 of this report.

For this phase of the ESBWR preapplication review, the staff's assessment of compliance with Section 52.47(b)(2)(i)(A)(3) is limited to the TRACG code for LOCAs only. The above regulations require that GENE provide data sufficient to assess the TRACG computer code, which is used to analyze ESBWR plant behavior in LOCAs. The staff expects GE to submit

additional topical reports related to the applicability of TRACG to ESBWR transients, including anticipated transient without scram (ATWS) and stability in October and November 2004. These topics are excluded from the scope of this review.

### 3.0 TECHNICAL EVALUATION

The GENE TRACG code is a proprietary methodological development based on the TRAC-BD1 code developed jointly by the NRC and GENE at the Idaho National Engineering Laboratory. The code has models and correlations that were developed at the commercial expense of GENE and are, thus, considered to be proprietary. The staff reviewed and approved the TRACG code for application to anticipated operational occurrences (AOO) in the current operating fleet of BWR/2-6s. The AOOs include the increase and decrease in heat removal by the secondary system, decrease in reactor coolant flow rate, reactivity and power distribution anomalies, and increase and decrease in reactor coolant inventory, all with reactor scram. The TRACG code was also reviewed and approved for application to prediction of the initial peak pressure for ATWS in the current operating fleet of BWRs.

The requirements for a realistic methodology in 10 CFR 50.46 are somewhat different than those for a prescriptive methodology in that more realistic models can be used and a measure of the uncertainty in the code must be determined. Various means of achieving an estimate of uncertainty are available. GENE has chosen to follow the basic Code Scaling Applicability and Uncertainty (CSAU) approach outlined in NUREG/CR-5249, Reference 5. While the CSAU approach defines the process by which uncertainty analysis is performed, it leaves room for the applicant to determine the exact statistical methodology to be applied. In both the AOO application of TRACG and the ATWS application, GENE chose to apply a Normal Distribution One-Sided Upper Limit statistical methodology. The approach taken for application of TRACG to the ESBWR LOCA event is somewhat different. A description of the methodology will be found in Section 3.14 of this SER.

#### ESBWR Safety System Overview

GENE submitted the ESBWR design description, Reference 15, in support of the review of the applicability of TRACG to ESBWR. The staff did not perform a detailed review of this document. The following descriptions are offered due to the unique nature of the systems and equipment not in use in the current commercial fleet of BWRs in the United States. The layout of the ESBWR safety systems are illustrated in Figure 3.0.1 in Section 8 of this report.

**Editorial Note:** In this report numerical values and their units are reported as received from the applicant. Conversions of units are provided for the convenience of the reader.

#### 3.0.1 Gravity-Driven Cooling System

The Gravity-Driven Cooling System (GDCCS) is a low-pressure coolant injection system. The GDCCS and the Automatic Depressurization System (ADS) comprise the ECCS for the ESBWR. The GDCCS consists of three separate GDCCS pools, which are located in the upper containment

(with the pool bottom at about 33 ft above the top of active fuel), and piping with squib valves and check valves to connect the pools to the reactor pressure vessel (RPV). The gas space of each GDCS pool is individually connected to the wetwell (WW) gas space above the SP via a pipe, and the GDCS pools are completely isolated from the drywell (DW).

During a LOCA, cooling water drains from the GDCS pools to the RPV when it is nearly depressurized, so that the gravity driving head of the GDCS pools is sufficient to overcome the pressure difference between the RPV and the wetwell. The RPV depressurization is initially due to the break flow and is further enhanced by the ADS actuation (which by itself is a large-break LOCA), which occurs when the water level in the downcomer drops to 5.547 m (18.2 ft) above the top of active fuel (TAF).

The GDCS is passive in its actions in that no external alternating current (AC) electrical power source or operator action is necessary. Once the injection valves have opened, they remain open and are not capable of being closed or overridden by operator action.

An additional function of the GDCS is to provide cooling water to the drywell floor during a hypothetical severe accident. Note that the evaluation of severe accidents is outside the scope of the ESBWR preapplication review.

### 3.0.2 Passive Containment Cooling System

The PCCS is the ultimate heat sink of the reactor and containment systems during a design-basis accident (DBA), such as a LOCA. It maintains containment cooling for up to 72 hours after initiation of a LOCA, in which core decay heat arrives in the containment in the form of steam. The PCCS keeps the containment pressure below its design pressure of 413.7 kPa (60 psia) without using active safety systems. The PCCS consists of four low-pressure condensers submerged in a large pool of water (IC/PCCS pool) located outside and above the drywell. The inlet of the condensers is always open to the drywell. Steam or a steam/nitrogen mixture (the ESBWR containment is nitrogen-inerted during normal operation) enters a PCCS condenser via a steam inlet line in the drywell and the steam is condensed inside the vertical tubes of the condenser. Pool water outside of the condenser tubes boils off and the steam produced is vented to the atmosphere. Condensate inside the condenser tubes drains into a condensate drain tank that is connected to the RPV with a check valve and a squib valve in between. Noncondensable gas (which may include some uncondensed steam) is vented below the surface of the SP. The PCCS inlet lines, drain lines, and vent lines are always open.

### 3.0.3 Isolation Condenser System

The Isolation Condenser System (ICS) removes decay heat for the transients involving main steam line isolation and reactor scram. It is a passive, high-pressure system that has four isolation condenser loops as part of the reactor coolant pressure boundary. Each loop has an isolation condenser submerged in a large pool of water (IC/PCCS pool) located outside and above the drywell. Steam produced by the core decay heat rises in the core and flows through the chimney region and steam separators and dryers before it enters the ICS supply lines. The

steam is condensed inside the vertical condenser tubes, and the condensate drains into the RPV downcomer annulus and flows into the core to repeat the cycle. As the pool water outside the condenser tubes boils off, the steam produced is vented to the atmosphere. During normal operation, the ICS is in a ready-standby mode with all the steam supply lines fully open and all the drain lines closed with valves. When the main steam lines are isolated and the reactor is scrammed, the ICS is activated by the opening of the valves on the condensate drain lines. Each ICS condenser also has a vent line that is automatically operated to vent the noncondensable gas (produced by radiolytic decomposition of water) below the SP surface. The vent line can also be opened manually by the operator.

Unlike the GDCS, the ICS is not part of the ECCS and is the only safety related system that is not an engineered safety feature. As a result, no credit is taken in GE's analyses for ICS operation during a LOCA. Some of the integral system tests involving the concurrent operation of ICS and PCCS indicate that ICS operation tends to reduce the peak pressures of the RPV and containment. However, the design and testing of the ICS are not part of the ESBWR preapplication review.

#### 3.0.4 Automatic Depressurization System

The ADS provides a rapid depressurization of the RPV. Activation allows the GDCS to provide coolant injection into the RPV during a LOCA. The ADS activates automatically when the water level in the downcomer drops to 5.547 m (18.2 ft) above the TAF by opening the SRVs and Depressurization Valves (DPVs) in groups. The only difference between the ESBWR ADS and the ADS of current operating BWRs is that the ESBWR DPVs discharge into the drywell.

#### 3.0.5 Depressurization Valve

A DPV is a squib-type valve that remains fully open after the activation. Full-size testing of the DPV was successfully conducted by GENE to demonstrate its operation and reliability. However, the design and testing of the DPV are not part of the ESBWR preapplication review.

#### 3.0.6 Vacuum Breaker

The Vacuum Breaker (VB) prevents the wetwell pressure from exceeding the drywell pressure by a specified value. It is a large check valve located between the drywell and the wetwell gas space. The VB is normally closed and will open only when the wetwell pressure has exceeded the drywell pressure by the specified value. GENE has conducted full-size VB tests to demonstrate its operation and reliability. However, technical evaluation of the VB testing program is not part of the ESBWR preapplication review.

#### 3.0.7 Biased-Open Check Valve

A biased-open check valve is installed on each of the GDCS injection lines to the RPV. This type of check valve is designed to remain slightly open when there is no pressure difference across it. In addition, it can be magnetically opened or closed by an external direct current

(DC)-driven torque motor (for testing valve operation). The biased-open check valve by itself is not unique, but magnetically linking to a DC-torque motor is a unique design. However, technical evaluation of the check valve design and operation is not part of the ESBWR preapplication review.

### 3.0.8 Squib Valve

A squib valve is installed on each of the GDCS injection lines to the RPV. The valve is leakproof during normal ESBWR operation. After opening, the squib valve will remain fully open. This kind of squib valve is similar to, but smaller than, the DPV (which has been tested at full size). Technical evaluation of the squib valve design and operation is not part of the ESBWR preapplication review.

### ESBWR/SBWR Relationship

The ESBWR design relies heavily on the integral systems and component test data developed for the SBWR. Justification is therefore needed for using the SBWR test data to qualify the TRACG code for ESBWR applications.

The ESBWR is basically a larger (4000 MWth) version of the SBWR (2000 MWth). Both designs have passive safety systems and components that will activate in a LOCA. Designs of the IC, DPV, VB, biased-open check valve, and squib valve are identical for both ESBWR and SBWR. However, a PCCS condenser in the ESBWR has about 35 percent more condenser tubes (at the same tube diameter, length, and pitch) and capacity than the PCCS in the SBWR.

From a LOCA perspective, the major difference between these two designs is that in the ESBWR, the GDCS pool gas space is connected to the wetwell gas space, while it is connected to the drywell in the SBWR. This design change provides additional gas space (during and after GDCS draining to the RPV) to accommodate the wetwell pressure in the ESBWR during a LOCA. As a result, the overall wetwell and drywell pressures may be lower in the ESBWR than in the SBWR for the same LOCA. There are also other differences. The ESBWR has a 10 foot active core compared to a 9 foot core in the SBWR. The ESBWR has a condensate drain tank in the drywell to collect condensate from the PCCS condenser, and the drain tank is connected to the RPV. In the SBWR, the PCCS condensate drains to the RPV via the GDCS pools in the drywell. The ESBWR has four larger (35 percent more tubes and capacity) PCCS condensers compared to three PCCS condensers in the SBWR. The ESBWR has four IC units (same size) compared to three IC units in the SBWR.

No new phenomena are expected to be introduced from the design differences between the ESBWR and SBWR.

### CSAU Based Technical Evaluation

The CSAU methodology, discussed in References 5 through 8, consists of 14 steps contained within three elements. The first element include steps 1 through 6 and determines the event

specifications and code capabilities. The scenario modeling specifications are identified and compared against code capabilities to evaluate the applicability of the code to the specific plant and accident scenario. Code limitations are noted during Element 1.

The second element in the methodology includes steps 7 through 10 and assesses the capabilities of the code by comparison of calculations against experimental data to determine code accuracy, scale-up capability, and appropriate ranges over which parameter variations need to be considered in sensitivity studies.

The third element in the methodology consists of steps 11 through 14 and individual contributors to uncertainty, such as plant input parameters, state, and sensitivities, are calculated, collected, and combined with biases and uncertainties into a total uncertainty.

## **Element 1— Event Specifications and Code Capability**

### **3.1 Step 1—Scenario Selection**

The processes and phenomena that can occur during an accident or transient vary considerably depending on the specific event being analyzed. GENE has identified the LOCA and containment response in the ESBWR as the events to which the methodology under review will be applied. Application of the methodology to transients has not been considered in this review.

Reference 11, Table 2.4-2 indicates that the GDCS line break (GDLB) results in the lowest static head in the chimney of the three break locations examined, i.e., in the GDCS line, the main steam line, and the bottom drain line. At the design certification stage, GENE will need to provide supporting analyses for a spectrum of break locations to demonstrate that there is no core uncover for the possible break locations. Should core uncover occur, review of the TRACG code will be revisited to determine the adequacy of the applicable models and correlations.

The staff notes this is the first application that has been reviewed in which one single code is used to analyze the entire reactor coolant system/safety systems/containment as a single calculation.

GENE is consistent with this step in the CSAU approach.

### **3.2 Step 2—Nuclear Power Plant Selection**

The dominant phenomena and timing for an event can vary significantly from one nuclear power plant design to another. GENE has specified the nuclear power plant (NPP) applicability for the methodology under review to be the advanced passive BWR design ESBWR.

GENE is consistent with this step in the CSAU approach.

### **3.3 Step 3—Phenomena Identification and Ranking**

The behavior of an NPP undergoing an accident or transient is not influenced in an equal manner by all phenomena that occur during the event. A determination needs to be made to establish those phenomena that are important for each event and various phases within an event. Development of a Phenomena Identification and Ranking Table (PIRT) establishes those phases and phenomena that are significant to the progress of the event being evaluated.

Important phenomena for LOCAs in the ESBWR have been identified in two PIRTs—LOCA/ECCS and LOCA/containment. The PIRT for LOCA/ECCS includes all the high-ranked and medium-ranked phenomena in the RPV, main steam lines, and ICS, including system interactions. The PIRT for LOCA/Containment covers all the high-ranked and medium-ranked phenomena in the drywell, wetwell, GDCS, PCCS, DPVs, VBs, main vents (between the drywell and wetwell), and SRV quenchers. Both top-down and bottom-up processes were conducted by a team of experts to obtain these phenomena, which were later used for TRACG assessment. A diagram of these processes is shown in Figure 3.3.1.

The two PIRTS were further evaluated and revised according to the results of the scaling analysis. The revision either confirmed or downgraded, with few exceptions, the ranking of some high-ranked phenomena. The exceptions were the addition of the mass flow through the break during the GDCS injection phase and long-term cooling phase of the LOCA, mass flow through the SRVs/DPVs during the GDCS injection phase of the LOCA, flashing/redistribution in the control rod guide tube region, and flashing in the downcomer annulus during the GDCS injection phase of the LOCA to the high-ranked phenomena.

The staff identified a weakness in the PIRT that needs to be corrected in the ESBWR design certification application. The PIRT in the application needs to include the long-term cooling phase of the LOCA. Since the long-term cooling phase is not expected to introduce any new phenomena that were not reviewed at the preapplication phase, and since the long-term cooling phase is highly design dependent, the staff concluded that the addition of the long-term cooling phase to the LOCA/ECCS PIRT is not necessary at the preapplication phase. Should new phenomena be found to occur during the long-term cooling phase, the appropriate models and correlations in the TRACG code will be revisited by the staff.

GENE is consistent with this step in the CSAU approach, but needs to include the long-term cooling phase in the PIRT for the ESBWR design certification review.

#### 3.4 Step 4—Frozen Code Version Selection

The version of a code, or codes, reviewed for acceptance should be “frozen” to ensure that after an evaluation has been completed, changes to the code do not impact the conclusions and that changes occur in an auditable and traceable manner. GENE has specified that the TRACG04 code, which is under configuration control, was used for the ESBWR LOCA application. GENE performed the initial assessments with the TRACG02A code and then transitioned to the TRACG04 code. GENE submitted all affected assessment cases using the TRACG04 code. The staff has reviewed the assessment cases and has determined that they are acceptable.

GENE is consistent with this step in the CSAU approach.

### 3.5 Step 5—Provision of Complete Code Documentation

This step is to provide documentation on the frozen code version such that evaluation of the code's applicability to postulated transient or accident scenarios for a specific plant design can be performed through a traceable record. GENE has provided the necessary documentation through submittal of ESBWR-specific documentation, SBWR-specific documentation, and reference to code documentation in the possession of the staff from the previous review of the TRACG code reported in References 1 and 2. The staff reviews of References 1 and 2 are discussed in References 3 and 4.

The staff review of the documentation, most notably References 9 and 10, disclosed numerous errors and omissions which GENE has committed to address in a revised TRACG model description topical report. This should be submitted prior to submission of the design certification application for the ESBWR design. The documentation supporting the application of TRACG to the ESBWR design, the scaling, and the testing programs is found in References 11 through 17.

GENE is consistent with this step in the CSAU approach.

### 3.6 Step 6—Determination of Code Applicability

An analysis code used to calculate a scenario in an NPP should use many models to represent the thermal-hydraulics and components. Those models should include the following four elements:

1. *Field equations*—provide code capability to address global processes.
2. *Closure equations*—provide code capability to model and scale particular processes.
3. *Numerics*—provide code capability to perform efficient and reliable calculations.
4. *Structure and Nodalization*—address code capability to model plant geometry and perform efficient and accurate plant calculations.

The TRACG code application to the ESBWR plant design is in two areas—the reactor coolant system response to a LOCA, and the containment system response to the LOCA. The use of a single thermal-hydraulic computer code for both simulations couples the two systems. Previous analyses of NPP response to LOCAs have made use of separate, independent computer codes for these two systems. The staff review and evaluation of the TRACG code will address the application of the code to each of these systems. In each case, the appropriateness of the code modeling of the above elements will be addressed.

#### 3.6.1 ESBWR TRACG LOCA Applicability

TRACG employs a two-fluid model for two-phase flow. It solves six conservation equations for both the liquid and gas phases, along with phasic constitutive relations for closure. In addition, a boron transport equation and a noncondensable gas mass equation are solved. The spatially discretized equations are solved by donor-cell differencing in staggered meshes in one, two, or three dimensions.

TRACG employs basic component models as building blocks to construct physical models for intended applications. Such an approach renders it a very general and flexible tool to simulate a wide variety of systems. The components that are modeled include pipe, pump, valve, tee, channel, jet pump, steam separator, steam dryer, vessel, upper plenum, heat exchanger, and break and fill as boundary conditions.

#### 3.6.1.1 Thermal-Hydraulics Model

TRACG employs a two-fluid model for two-phase flow. It solves six conservation equations for both the liquid and gas phases, along with phasic constitutive relations for closure. In addition, a boron transport equation and a noncondensable gas mass equation are solved. The spatially discretized equations are solved by donor-cell differencing in staggered meshes in one, two, or three dimensions. TRACG is used for both reactor vessel and containment. However, the current version of the model description report, Reference 10, does not address the phenomena occurring in the containment making it necessary to also use Reference 9 for that material.

The model equations are presented with assumptions. The three dimensional formulation has mixing terms to account for turbulent mixing and molecular diffusion. This is a good feature, but the mixing model is qualitative and has not been qualified. The critical flow model and counter-current flow limit (CCFL) models are applied to the velocity field calculated from the field equations. The code formulation resets the velocities to conform to these models. It is important that when velocities are reset, the mass balance is maintained.

The action of steam flowing upward can impede the downward flow of cooling water and lead to the counter-current flow condition. GENE has assessed the TRACG CCFL model with data from the CSHT test facility. Comparisons, Reference 34, for liquid temperatures near saturation, versus TRACG demonstrate that the code provides excellent agreement for saturated liquid. Agreement with subcooled liquid is excellent with steam flow rates which are less than the condensation capacity. For flow rates greater than the condensation capacity, the average deviation between liquid downflow predicted by TRACG is within the measurement error. Accordingly, the staff concludes that TRACG adequately predicts saturated CCFL and subcooled CCFL breakdown.

#### 3.6.1.2 Heat Conduction

TRACG solves the heat conduction equation for the fuel rods (in cylindrical geometry) and for structural materials (in slab geometry) in the system. The latter has either a lumped slab model or a one-dimensional slab model.

The strengths of the TRACG heat conduction model are the sophisticated transient gap conductance model and the implicit solution method that couples the heat transfer between the fuel rod and the coolant by iteration. The staff concludes that TRACG appropriately provides for solution of heat conduction.

#### 3.6.1.3 Flow Regime Maps

A two-fluid formulation relies upon models for estimating interfacial transfer rates for mass, momentum, and energy. The models for interfacial processes, in turn, rely on the shape and size of the interface. The common practice is to develop flow regime maps to identify the distinct regime for two-phase distribution. The knowledge of the flow regime allows the code to select applicable correlations for transport processes.

The flow regime maps are generally two-dimensional maps between void fraction and mass flux. TRACG has used this approach to identify the two-phase flow regimes. It also has correlations for entrainment for dispersed flow regimes.

The staff questioned a lack of definitions and GENE has committed to incorporate the missing definition for  $E_r$ , and new equations for the transition criterion between churned turbulent and annular flow, including the drift velocity term, in the next revision of Reference 10.

#### 3.6.1.4 Models and Correlations

The list of constitutive models covers all important phenomena that may occur in a BWR, SBWR, or ESBWR. The unified flow regime map is a strong point. TRACG models and correlations consist of models for interfacial shear, wall friction and form losses, critical flow, two-phase level tracking, interfacial heat transfer, and wall heat transfer.

The interfacial shear model was derived from the drift flux model using available experimental data at steady state. The models are based on current state-of-the-art technology and have been assessed with a large database covering the range of conditions that are expected in the reactor. The code uses a critical Weber number criterion for estimating interfacial area density or bubble/droplet diameter. However, there are differences in the way this approach is used for interfacial momentum and heat transfer in bubbly flow and droplet flow. The interfacial shear is assessed, Reference 34, through the capability of TRACG to predict void fraction data including single tube data, rod bundle data, and data for large hydraulic diameters. The test conditions used in assessment cover both adiabatic tests, where there is no effect of heat transfer on the void fraction, and heated tests. The tests cover a wide range of flow conditions with pressure, flow rate, and inlet subcooling varied. Comparisons between TRACG and test data from sources such as the FRIGG and Christensen tests show calculations to be within the measurement error for the tests. The staff concludes this demonstrates acceptable capability to predict interfacial shear.

The wall friction and form losses are important for predicting single- and two-phase flows. The code has standard models consisting of Moody curves for single-phase flow and a two-phase

multiplier based on the Chisholm correlation. Similarly, there is a standard model for form losses for abrupt area changes. The staff recognizes that simplifying assumptions are often necessary or expedient in computer code simulation of two-phase flow phenomena. However, the induced errors due to simplifying assumptions should be understood. GENE has determined those errors in the assumption of consistent wall friction and form loss partitioning between phases through code assessments using data from the FRIGG, Christensen, Wilson, and Bartolomei test programs, Reference 34. In all assessment cases, the prediction-measurement standard deviation was shown to be on the order of the measurement error. In addition, wall friction assessments have been performed using data from the ATLAS facility over a range of flow conditions. The prediction-measurement comparisons show a calculated error rate on the order of the measurement error. The staff concludes these assessments demonstrate acceptable capability to predict wall friction and form loss.

Critical flow is calculated using coarse-mesh nodalization and semi-empirical approximation for choking criteria. The critical flow model also allows for choking in the presence of noncondensable gases. The critical flow model in TRACG has been assessed against data from the Marviken critical flow tests, Pressure Suppression Test Facility (PSTF), and the Edwards test. The Edwards test and the PSTF tests are small scale tests and the Marviken tests are large scale tests. Comparisons of TRACG versus the Marviken tests showed a distinct drop in discharge flow at the transition from liquid blowdown to two-phase blowdown. In each blowdown period the measured and predicted mass flows were in good agreement, with the predicted bounding the measured. Timing of the transition were also in good agreement. The predicted mass flows were generally conservative compared with the data in the smaller scale tests. Comparison of TRACG predictions versus data from tests in different scale test facilities show that TRACG generally overpredicts the data and is therefore conservative. The critical flow model is detailed, well defined, and acceptable for predicting choked flow.

A two-phase level may exist in the bypass, lower plenum, downcomer, chimney, drywell, and wetwell. The two-phase level-tracking model invokes some approximations for the void fraction above and below the mixture level that may not be accurate if significant voiding occurs below the mixture level. Furthermore, the model uses an arbitrary cutpoint  $\alpha_{cut}$  and  $\alpha_{cut}$  for level detection. A level is detected when the  $\alpha_{cut}$  is reached. It is further assumed that void fraction above the level is the same as the void fraction in the cell above the level, and the void fraction below the level is the same as that of the cell below the cell with the level. Level position can then be computed. The model has been assessed with Pressure Suppression Test Facility (PSTF) level swell tests. Comparisons of predicted versus measured level indicate that TRACG was generally able to predict the measured level to an accuracy consistent with the measurement uncertainty. Sensitivity studies were also performed on nodalization, convergence ratio, and time step size. Little sensitivity was found in the studies. The staff concludes that level swell is adequately modeled in TRACG as evidenced by the code predictions falling within the experimental measurement uncertainty.

Vapor generation or flashing is an important phenomenon for any depressurization transient such as a LOCA. The vapor generation is predicted by energy balance at the interface, where

the differences in heat fluxes result in phase change. TRACG has a mechanistic model for interfacial heat transfer that depends upon interfacial area and the shape of the interface. The interface is defined on the basis of flow regime. The model has been assessed with a variety of tests. TRACG predictions were reasonable, indicating that the models are applicable to LOCAs. Staff request for additional information (RAI 54) concerns limits on different characteristics in bubbly flow (and also droplet flows), such as the upper limit on bubble size and number density. RAI 57 concerns interfacial area in stratified flows for which TRACG predicts a much larger interfacial area than the smooth interface. As is the case with all thermal-hydraulic system codes today, there is an inconsistency in interfacial area used for momentum transfer and heat transfer in bubbly and droplet flows.

Wall heat transfer was rated high in many components during a LOCA in the GENE PIRT. TRACG has a very detailed model based on the boiling curve. The model has standard heat transfer regimes—single-phase liquid or vapor, nucleate boiling, critical heat flux, transition boiling, film boiling, and condensation with and without the effect of noncondensibles. There are correlations for transitions between different heat transfer regimes, such as the minimum stable film boiling temperature. The correlations for different regimes are standard correlations from the literature. However, for critical heat flux, TRACG has a proprietary correlation, the General Electric Critical Quality Boiling Length correlation (GEXL), based on the critical quality concept for normal flows, and which uses a modified Zuber correlation for low flows and flow reversal. The GEXL correlation has been approved by NRC for specific fuel designs. The GEXL correlation is expected to be qualified through experimental data for the ESBWR-specific fuel bundle. The code has been assessed with a variety of tests that have become the standards for assessing wall heat transfer. The assessments include THTF tests for film boiling heat transfer, CSHT tests that include thermal radiation heat transfer, and THTF tests for boiling transition, as well as ATLAS critical power data. The staff concludes the breadth and accuracy of the assessment cases demonstrates acceptable capability for TRACG to predict wall heat transfer.

TRACG has a rewet model for post-critical heat flux (CHF) heat transfer. The rewet model is not well described and should be expanded in the revised report.

#### 3.6.1.5 Component Models

TRACG employs basic component models as building blocks to construct physical models for intended applications. Such an approach renders it a very general and flexible tool to simulate a wide variety of systems. The components that are modeled include pipe, pump, valve, tee, fuel channel, jet pump, steam separator, steam dryer, vessel, upper plenum, heat exchanger, and break and fill as boundary conditions. However, a turbine model for balance of plant (BOP) simulation is missing. The heat exchanger model contains some simplifying approximations that may not be appropriate for simulating the isolation condenser or the condenser in BOP. However, GENE is not using the heat exchanger model for simulating either the PCCS or the ICS. On the positive side, TRACG has very sophisticated upper plenum, steam separator, and steam dryer models.

However, since the steam separator is not considered important in the GENE PIRT, it is modeled by a simple semi-empirical model. The model is based on the assumption that the vapor core has solid body rotation and the thin film has azimuthal velocity decaying as the inverse of the square root of the radial position. The model has four constants that are determined by comparing the prediction with the full-scale performance data.

#### 3.6.1.6 Gap Conductance

All section and equation references in the following discussion of Gap Conductance are found in Reference 10.

Section 7.5.2, Fuel Pellet Gap Conductance, describes the thermal conductance model for the gap between the fuel pellet and the cladding of a fuel rod. Section 7.5.3, Cladding Perforation, describes the model that predicts the perforation of the fuel rod cladding.

The review of Sections 7.5.2 and 7.5.3 has resulted in a number of RAIs (68-87). This is due mainly to insufficient documentation of model descriptions in Reference 10. It is understood that the dynamic gap models in TRACG are consistent and similar to the SAFER/GESTR models previously approved by the NRC and also reviewed in the TRACG application for AOOs, Reference 3. The scope of Reference 10, in terms of documentation, is clear from the statement in Section 1.2 of the report that says, "This document is intended to be a complete, stand-alone description of TRACG." The main objective of the review of Sections 7.5.2 and 7.5.3 is not to reevaluate the technical validity of the dynamic gap models, but rather to evaluate the adequacy of the model description and the implementation and integration of the models in TRACG.

The review has resulted in a number of RAIs that suggest the need to provide more detailed description of the models. The following is a list of areas that need better documentation.

1. proper identification of reference for each equation
2. provide basis for determining the values of model constants
3. more detailed description of model parameters
4. proper identification and definition of variables in model equations.

The TRACG transient gap conductance model is comparable to the model in SAFER, Reference 30, that has been reviewed and approved by NRC. The TRACG gap conductance model is also consistent with another NRC-reviewed and approved code, GESTR-LOCA. The initialization of the TRACG gap conductance model is done by retrieving data calculated by GESTR-LOCA using fuel pellet exposure and power as inputs. The model equations are presented in Section 7.5.2 without reference to their sources. An example is Equation (7.5-7) that is similar to the Ross and Stoute model and yet no reference was cited for the model.

The gap conductance is modeled as the sum of the contributions from radiation heat transfer (Section 7.5.2.1), thermal conduction through the gas mixture in the asymmetric radial gap (Section 7.5.2.2), and conduction through the fuel/cladding contact spots (Section 7.5.2.3). The conductance of the gas in the radial gap depends on the effective gap size, and accounts for the asymmetric radial displacement of cracked pellet wedges (Section 7.5.2.4). The contact conductance depends on the size of the gap after accounting for fuel and cladding thermal expansion (Section 7.5.2.5). Section 7.5.2.6 discusses the implementation and initialization of the gap conductance model, including the determination of the gap gas composition (Section 7.5.2.6.1) and the initial gap size (Section 7.5.2.6.2). The assessment of the gap conductance models is briefly described in Section 7.5.2.7.

The radiation heat transfer between the fuel pellet and cladding is modeled by a conventional radiation heat transfer coefficient with separate thermal emissivities for the pellet and clad surface.

The conductance across the gas gap is calculated as the gas gap thermal conductivity divided by an effective gap modified for temperature jump at the gas-solid interface and the effect of discontinuous gas gap due to contact spots. The gas in the gap is composed of helium and fission gas. An effective thermal conductivity is calculated for the gap gas. The helium pressure, composition of the fission gas, and the relative amount of xenon and krypton in the fission gas are all obtained from the GESTR fuel files.

After cladding perforation, the gas conductivity is adjusted to reflect the presence of a stoichiometric mixture of steam and hydrogen from metal-water reaction. The constants in the equation for the gas conductivity in a perforated fuel rod are TRACG input constants.

The contact pressure ( $P_c$ ) is zero when the hot gap size is greater than or equal to zero. In this context the hot gap size is defined as,

$$\text{Hot gap size} = R_{ci} - R_{fo}$$

The initial interaction ( $I_i$ ) is determined from Equation 7.5-30, while the hot outer fuel radius ( $R_{fo}$ ) and the hot cladding inner radius ( $R_{ci}$ ) are calculated from Equations 7.5-25 and 7.5-26, respectively.

The model for the effective gap size ( $R_{eff}$ ) accounts for the thermal expansion of the fuel pellet and the cladding. It also takes into consideration the effects of cladding hoop stress and plastic strain on the gap size.

The  $R_{fo}$  is calculated as the sum of the reference fuel outer radius ( $R_{ref}$ ) and differential growth from thermal expansion.  $R_{ref}$  is calculated as a function of the exposure history and the linear heat generation rate (LHGR) used to accumulate that exposure. It does not vary with time during the transient and is evaluated in Equation 7.5-31 at an initial reference temperature ( $T_{ref}$ ).

The calculation of the hot clad inner radius considers the effects of thermal expansion and hoop stress. Different models are used if the cladding has begun to yield or has perforated.

The interface between GESTR-LOCA and TRACG is discussed in relation to the initialization of the transient gap model implemented in TRACG. TRACG depends on GESTR-LOCA to provide the steady-state conditions for the dynamic gap model. The documentation did not discuss the variables that are passed from the TRACG thermal-hydraulic and neutronic calculations to the gap model. A brief discussion of the coupling between the gap model and the rest of TRACG was provided by GENE.

The ratio of krypton to xenon ( $F_{kr}$ ) is a built-in constant in the GESTR model and cannot be set through input. For typical TRACG applications, the fraction of additional fission gas released  $F_r$  is selected to have a value of  $[[ \quad ]]$ . If a prolonged temperature increase were expected, a larger fraction would be appropriate.

Given the initial total gap conductance ( $h_g$ ) from the GESTR-LOCA output, the initial gap size ( $R_{eff,i}$ ) and the initial contact pressure ( $P_{ci}$ ) are calculated by solving Equation 7.5-7  $[[ \quad ]]$ .

GENE's response to RAI 79 is the only documented information provided that verifies the TRACG implementation of the gap model against the SAFER model. This comparison of gap conductance calculated by TRACG and SAFER shows that the results are indeed comparable.

The TRACG cladding perforation model needs cladding hoop stress and cladding temperature inputs from the code calculation. The fuel rod cladding hoop stress is a function of the difference between the fuel rod internal gas pressure and the external coolant pressure. Section 7.5.3.1 discusses the calculation of the cladding hoop stress and the internal gas pressure. The contribution of the plenum gas temperature to the overall internal gas pressure is discussed in Section 7.5.3.2. The utilization of the hoop stress and cladding temperature in the rod perforation model is outlined in Section 7.5.3.3. The assessment of the perforation model is discussed in Section 7.5.3.4.

The internal gas pressure is calculated by considering gas in the volume along the length of the fuel column and the gas in the fuel rod plenum. Outputs from GESTR-LOCA are used to calculate the initial fuel column volume to temperature ratio.  $[[ \quad ]]$

$[[ \quad ]]$ . The perforation model applies to any point along the length of the fuel rod and is not limited just to the point of peak LHGR (RAI 80). The use of  $[[ \quad ]]$

$[[ \quad ]]$  is explained in the response to RAI 82 as leading to a conservative overestimation of the cladding hoop stress. The staff concludes that this use of the NRC-approved GESTR-LOCA method to set initial steady-state conditions is acceptable. In addition, the resulting cladding hoop stress is conservatively predicted.

The use of the same subscript 'f' in Equation 7.5-35 to refer to two different materials, gas in fuel column and fuel pellet, is confusing. In response, GENE has agreed to update the next version of the documentation.

The cladding average temperature at the maximum LHGR axial position is used in calculating the growth in the volume of the fuel gas plenum in a transient due to thermal expansion. An empirical factor of  $[[ \quad ]]$  is used to account for the fact that the temperature change considered at the maximum LHGR axial position overestimates the length-averaged temperature change for the whole fuel column.

The plenum gas temperature is calculated separately from the gas temperature in the gap of the fuel column.

Rod perforation is evaluated in the following sequence:

TRACG calculates cladding hoop stress and cladding temperature. A curve in Reference 10, Figure 7.5-5, gives the cladding rupture stress as a function of the cladding temperature. Cladding plastic deformation is assumed to commence at a cladding temperature  $[[ \quad ]]$  below the perforation temperature.

1. Plastic strain is assumed to occur when the cladding hoop stress exceeds the cladding rupture stress corresponding to a cladding temperature  $[[ \quad ]]$  above the current cladding temperature.
2. The cladding strain is calculated by multiplying the strain ratio obtained from Figure 7.5-6 by the strain at rupture. The strain ratio is shown in Reference 10, Figure 7.5-6, as a function of the perforation temperature minus the cladding temperature. It varies from  $[[ \quad ]]$  percent at a delta T of  $[[ \quad ]]$  to 100 percent at a delta T of  $[[ \quad ]]$ . The rupture strains were determined from experimental data.

Elastic strain is recovered when a cladding perforation occurs. This has a small impact on the gap size because the irrecoverable plastic component of the total strain is much larger than the elastic strain.

The TRACG gap perforation model is comparable to the model in SAFER, a code previously reviewed and approved by NRC. The cladding rupture stress and plastic strain are based on experimental data and have been reviewed. GENE's response to RAI 79 has demonstrated that the fuel gap models in Sections 7.5.2 and 7.5.3 calculated transient gap responses that agree very well with those calculated by SAFER/GESTR.

The description of the TRACG dynamic gap model will be updated by GENE by incorporating all responses to the RAIs in the approved version of Reference 10, thereby providing a level of detail consistent with a stand-alone document.

#### 3.6.1.7 Neutron Kinetics Model

For LOCA application, TRACG uses core power as input as a table with power as a function of time. The table is generated with their neutronic calculation. A comparison with American Nuclear Society (ANS) 5.1 (1994) is shown and results compare very well after 4 seconds when decay power dominates. The model is conservative as it predicts higher power than the standard for the first 4 seconds when fission power is still continuing. The kinetics model has been assessed through comparisons with SPERT reactivity insertion test data. The staff finds these test data to be acceptable for assessment and sufficient accuracy has been demonstrated to find the TRACG neutron kinetics model acceptable.

#### 3.6.1.8 Numerics

TRACG numerics are a significant improvement over its predecessor TRAC-BD1/MOD1. As a default, TRACG employs fully implicit integration for hydraulic equations. For time-domain stability analyses, TRACG uses an optional explicit integration because the implicit integration may suppress real physical oscillations. The fully implicit integration is accomplished by means of a predictor-corrector iterative technique. The detail of the explicit integration is not described and should be included in the upcoming revised report along with time step control criteria.

TRACG solves the heat conduction equations by implicit integration. The heat transfer coupling between the heat conduction and coolant hydraulics is also treated implicitly via an iterative technique. This implicit coupling represents a significant improvement over commonly used explicit coupling, which may incur an error on the phase shift and amplitude in a thermally induced oscillation.

Once again, the time step control algorithms are not described for heat conduction and need to be included in the revised documentation.

#### 3.6.1.9 Thermodynamic and Material Properties

The thermodynamic properties used in TRACG are calculated from polynomial fits to steam table data for water and from the ideal gas law for the noncondensable gases. The thermodynamic property routines cover a very wide range of pressures ( $1.0 \text{ Pa} < P < 45 \text{ MPa}$ ) and temperatures ([liquid]  $273.15 \text{ K} < T_l < 714 \text{ K}$ , and [vapor]  $273.15 \text{ K} < T_v < 3000 \text{ K}$ ). Separate liquid and vapor property fits are given along with their fitting constants. The accuracies or uncertainties of these property routines have been mentioned, and it is an improvement from the previous version of TRACG documentation.

The material properties used in TRACG are based on the "GE Material Properties Handbook," which is an extensive library of temperature-dependent properties of nuclear fuel ( $\text{UO}_2$ , zircaloy cladding, zirconium oxide, heater rod insulator, and boron nitride insulator) and structure materials (stainless steel 304 and 316, carbon steel, Inconel 600, and concrete). The accuracies or uncertainties of these material property routines are not stated, and should be clearly stated and referenced in the revised report.

#### 3.6.1.10 Summary

TRACG is a detailed best-estimate BWR transient analysis code, Reference 10. It is based on a two-fluid thermal-hydraulic model for the reactor vessel, primary coolant system and containment, and three-dimensional neutron kinetics model for the reactor core. The modular approach used makes it a general-purpose system code with unnecessary assumptions and approximations minimized as practicable. However, the state of the art does not permit it to eliminate all the important assumptions and approximations necessary at the present time. Assessment of TRACG models has been performed against an adequate data base, and the results have been shown to be sufficiently accurate, generally within the measurement error or standard deviation, to demonstrate that the TRACG models are capable of representing the phenomena anticipated to occur in an ESBWR LOCA event.

### 3.6.2 ESBWR TRACG Containment Applicability

TRACG will be used for the calculation of the containment pressure and temperature response. The RPV will also be modeled to provide the boundary conditions needed for the containment analysis, and to provide the mass and energy releases into the containment following a LOCA or main steam line break (MSLB). The entire transient will be calculated by TRACG, starting with the postulated LOCA, and including the blowdown, GDCS, and long-term PCCS phases. GENE has taken an approach for qualification and application of TRACG for the ESBWR containment analysis which includes an evaluation of the TRACG models against appropriate test data representative of the ESBWR design. In addition, the approach also includes some elements of a CSAU methodology to define the important phenomena (PIRT), to identify the uncertainties in the TRACG models, and to define the sensitivity of the containment peak pressure to these parameters.

GENE is following a bounding application approach for the containment analysis. Modeling assumptions in the TRACG application bound several key phenomena. [[

]] This conservative TRACG model is used to perform the analysis of the ESBWR containment response. A "nominal" analysis is obtained by setting the other model parameters and plant initial conditions to their expected values. A "bounding" analysis is obtained by setting these other model parameters and plant initial conditions to conservative values to maximize the calculated containment pressure response. A comparison of the bounding and nominal calculations can be used to indicate the margin inherent in the bounding calculation. The bounding calculation will be used to demonstrate margins to the design limits and will be the basis for review of the containment design during the design certification review to demonstrate compliance with GDC 16, 38, and 50.

To ensure a complete PIRT evaluation, the entire spectrum of events was considered by GENE, including events with less limiting conditions than the design basis case with no auxiliary power. The approach used by GENE focused on the design basis cases, in terms of equipment and systems available. This led to the most severe consequences and the greatest challenges to the analytical models in modeling the phenomena. While there are some differences in the assumptions made for the evaluation of different breaks, these were not important in

determining the phenomenological progression of the LOCA or the importance of various parameters. The limiting LOCA from the perspective of margin to core uncover is a large liquid line (GDCS line) break. The limiting LOCA from the perspective of containment pressure is the MSLB. Chapter 6 of the Design Certification Document will include the entire matrix of calculations for postulated pipe rupture locations and single failures.

### 3.6.2.1 Containment Components

The containment is modeled with TRACG as a combination of a three-dimensional vessel component in conjunction with one-dimensional components, such as pipes, tees, and valves. All these components utilize the same conservation equations and constitutive correlations. The following addresses the correlations for wall heat transfer, interfacial heat transfer, wall shear, and interfacial shear.

BWR containments utilizing the pressure suppression principle have similar components. The ESBWR containment is similar in concept to the Mark III and ABWR containments, in that a horizontal vent system is employed to transfer blowdown energy from the drywell to the SP. In addition, the ESBWR design is equipped with a PCCS for long-term decay heat removal.

A schematic of the ESBWR containment and the corresponding TRACG computer code representation can be found in Reference 11.

The TRACG computer code employs all of the physical models needed for analyzing traditional BWR designs (i.e. drywell, pressure suppression system, including vents connecting drywell and wetwell and the VB check valves), and also employs models for the passive containment safety systems (i.e., the PCCS which transfers the drywell energy to the outside atmosphere and designed primarily for the long term containment cooling). In addition, the code is capable of analyzing the behavior of the GDCS which couples the behavior of RPV and containment. In ESBWR the PCCS is totally independent from the GDCS and its pools.

TRACG will be used to perform design basis containment LOCA analysis for the entire transient (i.e., starting with the postulated LOCA and including the blowdown, GDCS, and long-term PCCS phases). In general, the code was developed to perform best-estimate calculations. However, TRACG does not have specific models for multidimensional (3-D) effects like mixing and stratification, thus limiting the code's capability to correctly calculate several key containment phenomena, i.e., the [[

]]. Therefore, to address these phenomena the code is to be used in a conservative mode by performing "bounding" calculations, i.e., by setting the values of appropriate parameters to maximize the calculated containment pressures and temperatures.

The staff has reviewed the proposed approach and concluded that it satisfies the NRC guidelines specified in Section 6.2.1 of the SRP with regard to calculated wetwell and drywell peak pressure and temperature, and, therefore, is acceptable.

The following contains a brief description of TRACG containment models.

#### 3.6.2.1.1 Drywell

The drywell is composed of an upper drywell, bounded by the drywell head, top slab, containment walls, and the diaphragm floor separating it from the wetwell. The upper drywell constitutes the largest portion of the drywell volume. A break in the main steam line as well as the opening of the DPVs would discharge flow into this region. The annulus region of the drywell comprises the region between the RPV and the inner wall of the wetwell horizontal vent duct system. A break in the GDCS line would be expected to discharge flow into this region. The lower drywell is a separate region that is connected to the drywell annulus by 10 vents of 1.2 m outside diameter (OD). Liquid discharged into the upper drywell or the annulus region (e.g., from a broken GDCS line connected to a GDCS pool) will drain into the lower drywell. A break in the bottom drain line would discharge flow to the lower drywell.

The drywell is modeled as a two-dimensional (axisymmetric) region, with [[ ]] in the upper drywell and [[ ]] in the annular and lower drywell regions. This allows natural circulation patterns to develop, if calculated, [[ ]]. The three-dimensional conservation equations for mass, momentum, and energy are applied in this region.

#### 3.6.2.1.2 Wetwell

The wetwell consists of the suppression pool and the wetwell gas space. The wetwell is bounded by the diaphragm floor on top, containment outer wall, and wetwell inner wall on the sides and the floor of the containment. During blowdown, flow from the SRVs is directed to the SP and quenched via the SRV discharge lines. Flow from the LOCA break and DPVs is directed from the drywell to the SP and quenched via the SP horizontal vent system. Any flow through the passive containment cooling (PCC) vents is also discharged to the SP.

##### Wetwell Gas Space

The wetwell gas (steam and noncondensibles) space is also represented by multidimensional cells. Typically, [[ ]] rings and [[ ]] axial levels are employed in the TRACG model. This would allow for natural circulation in this region. The flow regimes in this region will be the same as in the drywell— single-phase gas, dispersed droplets resulting from entrainment from the suppression pool, and a condensate film on the walls. The models involved in the calculation include turbulent shear between cells, noncondensable distribution, wall friction, interfacial friction, wall heat transfer, fogging and interfacial heat transfer, and heat transfer at the SP interface. These models are discussed in the next section.

##### Suppression Pool

The SP is also represented by multidimensional cells. [[ ]] rings and [[ ]] axial levels are used to represent the pool. The major phenomena of interest for the SP include steam

condensation with or without noncondensable presence, temperature distribution, thermal stratification, and pool two-phase level.

#### 3.6.2.1.3 GDCS Pools

Three separate GDCS pools are located in the upper containment and are isolated from the drywell. During the GDCS phase of the post-LOCA transient, the GDCS pools discharge into the RPV downcomer, following the opening of squib valves and check valves in the four divisionally separated GDCS lines. In the ESBWR configuration, the GDCS pools do not receive condensate from the PCC units.

Following an initiating event, the GDCS is activated by rapid opening of the squib valves allowing water flow into the RPV. Typically, the GDCS pools are about 50 percent drained down in about an hour, and will still be partially filled at the end of 72 hours following a DBA.

The GDCS pools are also modeled as part of the containment model. In practice, two pools are represented, with one accounting for the volume of two of the three pools. The main phenomenon of interest for the GDCS pool is the pool level and the associated inventory of water in the pool. The two-phase level model is also applicable here. Heat transfer at the pool surface is modeled analogously to that for the SP.

#### 3.6.2.1.4 Passive Containment Cooling Pools

The four PCC pools are located outside (above) the containment. Each contains a PCC unit. The four pools are interconnected with each other and with the IC pools.

The pools are represented as part of the 3-D TRACG region, partitioned into the IC and PCC pools. The pools are allowed to communicate with each other at the bottom and the top. [[ ]]. The

pools are modeled with [[ ]] rings each and with [[ ]] axial levels. Heat transfer occurs from the PCC headers and tubes to the water in the pools. Pool side heat transfer is calculated either by a [[ ]] for boiling heat transfer or by single phase convection to liquid [[ ]] for subcooled conditions.

#### 3.6.2.1.5 Passive Containment Cooling Units

The ESBWR has four PCC heat exchanger units. Each is comprised of two-module drum and tube heat exchangers using horizontal upper and lower drums connected with a multiplicity of vertical tubes (336 tubes per module). Two identical modules are coupled to form one PCC heat exchanger unit. The PCC units are represented by one-dimensional components simulating the inlet piping, headers, condenser tubes, condensate discharge lines, and vent

lines. One-dimensional forms of the mass, momentum, and energy equations are applicable. Heat is transferred through the walls of the tubes and headers to the respective pools. Heat transfer inside the tubes is calculated using the [[ ]].

The PCCS can operate in two distinct modes—a condensation mode and a pressure differential mode. In the condensation mode, the steam is condensed in the vertical tubes and the condensate is drained from the lower drum to the individual unit's drain tank. In the pressure differential mode, the flow through the PCC heat exchangers is caused by a drywell-wetwell pressure difference. Since the PCC vent line outlet is about 0.9 m higher than the outlet of the upper horizontal drywell/wetwell LOCA vents, the flow path through the PCCS is the preferred path for most of the long-term, post-accident conditions. In any case, noncondensibles and uncondensed steam are vented to the suppression pool.

#### 3.6.2.1.6 Horizontal Vent System

The ESBWR has 30 horizontal vents between the drywell and the SP. There are 10 vertical flow channels each containing three horizontal vents attached to a vertical vent pipe. The top row of horizontal vents is approximately 0.9 m below the bottom of the PCC vents. The remaining two rows of vents are each vertically separated by 1.37 m.

The horizontal vents are represented by a [[ ]]. The vent component is shown in more detail in Figure 9.6 in Reference 11.

#### 3.6.2.1.7 GDCS Equalizing Lines

Four GDCS equalizing lines (one per division) connect the SP to the RPV downcomer. During the long-term cooling phase of the post-LOCA transient, the squib valves in these lines will open if the level in the downcomer drops to 1 m above the top of the active fuel and a time delay of 30 minutes has elapsed.

The equalizing lines are represented by a [[ ]]. The correlations used for wall friction and singular losses are the same as used for the horizontal vents.

#### 3.6.2.1.8 Vacuum Breakers

The ESBWR has three VBs connecting the upper drywell to the wetwell gas space. The VBs will open when the pressure in the wetwell is higher than that of the drywell by a specified value.

The VBs are represented by one-dimensional VALVE components. VBs are lumped together as one component. The VBs are triggered open at a set negative pressure differential between the drywell and wetwell. They will close at a lower value of the pressure differential. The VBs transport flow from the wetwell gas space to the drywell at conditions corresponding to the cell in the wetwell gas space to which they are connected. The correlations used for the singular losses are the same as for the horizontal vents.

#### 3.6.2.1.9 TRACG Physical Models

##### Heat Transfer Modes



For the condensation mode, a Nusselt condensation correlation can be used with multiplicative factors for shear enhancement and degradation by noncondensibles. The Nusselt correlation is expressed in Equations 6.6-66 and 6.6-67. In these equations, the liquid film Reynolds number is calculated based on the condensate flow rate per unit perimeter of surface and the liquid viscosity. However, the recommended (default) TRACG method is the [[ ]]. As a lower bound, when the noncondensable fraction is below about [[ ]], the [[ ]] correlation is available. [[ ]].

For interfacial heat transfer at the pool interface, the interfacial heat transfer coefficients on the vapor and liquid sides of the interface are defined by Equation 6.5-28. The [ ]], is used to calculate degradation of heat transfer at the pool surface due to noncondensable gases.

The staff reviewed the applicability of the wall heat transfer correlations and found them to be acceptable for modeling of the ESBWR containment behavior for the following reasons. Except for the [[ ]] correlation, the employed heat transfer models are widely used and accepted in the scientific and engineering practices. The [[ ]] correlation was developed specifically for PCCS-like conditions based on limited, small scale experiments. As applied in the TRACG methodology, the [[ ]] correlation was successfully tested against SBWR-specific experiments performed at the PANTHERS and PANDA test facilities. The comparison with the test data was favorable, at least on a global parameters level. Therefore, the staff finds the heat transfer models to be acceptable.

Also, the staff reviewed the applicability of the [[ ]] correlation to the ESBWR interfacial heat transfer at the pool interface. The staff acknowledges that interfacial heat transfer in general is a complex phenomenon and the available physical models are subject to substantial uncertainties. Since the sensitivity study performed by GENE indicates that this phenomenon has a relatively small effect on the peak containment pressure, the staff finds the TRACG interfacial heat transfer at the pool interface to be acceptable. This interfacial heat transfer model may be replaced with a more appropriate model for design certification analyses. (See Section 3.6.2.3, "Phenomena Identification and Ranking," Item WW4: Free Surface Condensation/Evaporation, and Section 4.0 "Confirmatory Items," Item 16.)

### Vent Clearing Model

The rising drywell pressure forces the steam and nondensifiable gas mixture to flow through the vertical flow channels into the horizontal vent piping, pushing the water through the horizontal vents. As the water level drops in the vertical section to "uncover" a horizontal vent row, the vents in each row will be opened to allow flow of steam and noncondensable gas to the suppression pool. This phenomenon is referred to as "vent clearing." Vent clearing terminates the initial pressure rise in the drywell, as the pressure is relieved by the vent discharge to the SP. The vents can clear during the early blowdown. As the blowdown flow rate decreases, the water level in the vertical pipes will rise to cover each row of vents. Eventually, the top row is also covered and flow will persist only through the PCC vents. Following vent clearing, the wetwell gas space pressurizes as the noncondensibles from the drywell are purged into that volume. The drywell pressure is maintained higher than the wetwell by an amount corresponding to the PCC vent submergence.

In the prediction of vent clearing and the associated drywell and wetwell pressure histories, the following phenomena are important:

#### **Level Tracking in the Vertical Vent Pipes**

The one-dimensional component level tracking model described in Reference 10, Section 6.4 is employed in the vertical pipe that is connected to the three horizontal vents.

#### **Vent Flow Regime**

The flow regime in the vents is single-phase liquid, until the vent begins to uncover when it transitions rapidly to bubbly flow. The flow to the vent is "donor celled" at the upstream conditions in the vertical pipe. TRACG calculates a transition from stratified to dispersed flow based on the instability of the interface (Reference 10, Equation 5.1-23).

#### **Pressure Drop Correlations**

The single-phase friction factor is obtained from Reference 10, Equation 6.2-2. The Reynolds number is calculated based on the axial velocity in the cell and the hydraulic diameter of the cell. The pressure drop in the vent is actually dominated by the inlet and exit form loss coefficients. A two-phase multiplier will be applied for wall friction as shown in Reference 10, Equation 6.2-5. For singular losses, Reference 10, Equations 6.2-7 and 6.2-8 are applicable.

#### **Vent Back Pressure**

As the vent discharges vapor into the suppression pool, it will tend to move the liquid in the pool above the vent upwards as it expands. The inertia of this liquid tends to create a back-pressure effect, reducing the discharge flow, and affecting the drywell pressure after vent clearing. This effect is accounted for in the TRACG momentum equation. The liquid mass in the inner ring immediately above the discharge location accelerates upwards as the vapor expands into the pool.

## **Model Assessment**

The vent clearing model in TRACG has been assessed by comparison against data from PSTF. Reference 10, Figure 7.11-5 shows a schematic of the facility. In the 5703 series tests, the drywell was connected by a set of three full-scale Mark III horizontal vents to an eight degree simulation of the Mark III suppression pool. A rupture disk in the blowdown pipe simulated the break of a main steam line, and a venturi downstream of the rupture disk set the size of the simulated break. The blowdown flow, the vent flow and the drywell and wetwell pressure were monitored.

Reference 10, Figure 7.11-6 shows a comparison of the measured and predicted drywell pressures for Test 5703-1. Figure 7.11-7 shows a comparison of the measured and calculated vent flow rates. Figure 7.11-6 shows that TRACG follows the drywell pressure rate accurately until the time of vent clearing at 0.8 seconds. TRACG also calculates the time of vent clearing correctly, as seen from Figure 7.11-7. Following the onset of vent clearing, TRACG undercalculates the vent flow, and the drywell pressure increases to a higher value than seen in the data. The discrepancy is due to large vapor bubbles rapidly transiting through the top part of the vent at the inception of vent uncover. This flow regime is not captured by TRACG. A higher calculated two-phase inertial pressure drop in this transient phase delays the increase in the vent flow, and introduces a lag in the calculated transient response. Subsequent to this period, the transient is captured adequately by TRACG.

The staff did not review details of the TRACG vent clearing model. Instead, the staff reviewed the provided comparison between the TRACG calculation and the PSTF test data and finds the comparison to be consistent with the staff's previous evaluations of the BWR pool dynamic analyses, and therefore, to be acceptable.

### Break flow

Critical flow through the break is calculated using the model evaluated in Section 3.6.1.4 of this document. For the reasons set forth in that section, the staff finds this model to be acceptable.

### Noncondensable Distribution

TRACG has mass continuity equations for multiple species of noncondensibles in addition to steam (Reference 10, Equation 3.1-14). A noncondensable species is treated as a perfect gas and its properties are specified in terms of the gas constant,  $R$  and the specific heat  $C_p$ , (Reference 10, Section 6.6.1 1). The noncondensable gas (or mixture of gases) has the same temperature and velocity as the steam in a given cell. The partial pressure of the noncondensable is calculated based on the temperature and mass of the gas in a cell (Ideal Gas Law). Dalton's law (Reference 10, Equation 3.1-17) relates the partial pressures of steam and noncondensibles to the total pressure. Note that the steam need not be at saturation conditions corresponding to its partial pressure.

The TRACG model for molecular diffusion of noncondensibles driven by concentration gradients is not used. Noncondensibles are transported by bulk convection. Diffusion effects will be

small for nitrogen and air. Transport by diffusion could be more significant for hydrogen. Buoyancy effects are not treated at a local level (i.e., steam and noncondensibles have the same velocity in a cell). However, buoyancy effects will be accounted for on a global level. For example, if a light noncondensable is injected into a cell, a natural circulation pattern will develop between adjacent rings, and lighter fluid will rise to the upper regions.

The distribution of noncondensibles calculated by TRACG was assessed through comparisons against data from the GIRAFFE and PANDA facilities. Based on these comparisons, GE recognized limitations in TRACG's capability to adequately predict mixing and distribution of noncondensable gases. A bounding analysis approach is proposed for the ESBWR analysis. The staff agrees with GENE's conclusions and, since it is conservative, accepts the proposed bounding approach.

#### Wall Friction Correlations

The flow regime in the drywell is mostly single-phase gas. In some cells, a dispersed droplet high void fraction regime may exist. This corresponds to cells where liquid from the break or from the GDCS pool with a broken line is falling to the lower regions of the drywell. In some cells, a liquid film can form on the wall because of condensation. The single-phase friction factor is obtained from Equation 6.2-2, Reference 10. The Reynolds number is calculated based on the axial velocity in the cell adjacent to the wall and the hydraulic diameter of the cell in the direction of the wall. In case a two-phase flow regime is present, a two-phase multiplier will be applied as shown in Equation 6.2-5, Reference 10.

Similarly, the flow regime at the inlet to the PCC is single-phase vapor and/or gas mixture. Due to condensation, a liquid film forms inside the vertical tubes. The exit conditions consist of a draining liquid film and a gas mixture that is rich in noncondensibles. The single-phase friction factor is obtained from Equation 6.2-2, Reference 10. The Reynolds number is calculated based on the axial velocity in the cell and the hydraulic diameter of the cell. In the condensing region, a two-phase multiplier will be applied as shown in Equation 6.2-5, Reference 10.

The staff reviewed the employed model and finds it to be acceptable, since expected flow regimes are either single- or two-phase.

#### Turbulent Shear Between Cells

The TRACG model for turbulent shear between cells at cell boundaries is not being used since the nodalization employed ensures the presence of a wall surface in every cell and such nodalization ensures that no flowing gas is in contact with another stream of gas. All flows in the drywell are driven by buoyancy and wall shear.

The staff reviewed the employed model and finds it to be acceptable.

#### Interfacial Shear Correlations

For the droplet flow regime, the models described in Section 6.1.5, Reference 10, will be employed to calculate the interfacial shear between vapor and droplets. For cells with wall liquid films, the annular flow correlations in Section 6.1.4, Reference 10, are used.

The staff reviewed the employed model and, since the model includes all expected two-phase flow regimes, finds it to be acceptable.

#### Interfacial Shear Correlations

For cells with wall liquid films, the annular flow correlations in Section 6.1.4, Reference 10, are used.

The staff reviewed the employed model and finds the correlations used to be appropriate for the expected flow regimes and, therefore, to be acceptable.

#### Fogging of Drywell Vapor

Heat transfer from the vapor in a cell will result in cooling of the vapor. If the temperature drops below the saturation temperature of the steam corresponding to its partial pressure, condensation will occur. Generally, in this situation a cold wall will be present in the cell. A liquid film will form on the surface because of condensation. This will typically be the dominant form of condensation in the cell. However, if the bulk temperature drops below the saturation temperature, a small amount of liquid droplets will be formed (fogging) by condensation of steam on the airborne impurities. In this situation, a droplet flow regime will exist. Interfacial heat transfer between droplets and vapor will be calculated as per Section 6.5.5, Reference 10. Interfacial shear between the droplets and steam is calculated using the models in Section 6.1.5, Reference 10.

In general, heat transfer from the vapor is more likely to lead to condensation on the walls. Fogging is more likely to occur as a result of adiabatic expansion of steam from pressures higher than 30 bar.

The staff reviewed the employed model for fogging in the drywell and finds it to be acceptable because the pressure in the drywell is expected to remain well below 30 bar, and the effects of fogging on heat transfer in the drywell is not significant.

### Condensation of Vapor Bubbles

In the presence of noncondensibles, the bubbles will include steam and noncondensibles. The partial pressure of steam and noncondensibles will be calculated as stated earlier. The interfacial heat transfer from the liquid to the vapor is calculated according to Equations 6.5-8, and 6.5-9, Reference 10. There is no degradation in heat transfer due to the presence of noncondensibles. Humboldt Bay, Reference 21, and Bodega Bay, Reference 22, large-scale data show complete condensation of the vapor in the suppression pool. All of the liquid and vapor entering the pool from the vent system remained in the pool.

The staff reviewed the employed model and finds it to be acceptable because a sensitivity study performed by GENE indicates that this phenomenon has a relatively small effect on the peak containment pressure. This interfacial heat transfer model may be replaced with a more appropriate model for design certification analyses. (See Section 3.6.2.3, "Phenomena Identification and Ranking," Item WW4: Free Surface Condensation/Evaporation, and Section 4.0 "Confirmatory Items," Item 16.)

### Pool Temperature Distribution

[[

]]. Figure 7.11-3, Reference 10, shows the results from a number of large-scale tests. The measured temperature at the top of the pool has been compared with calculations using the empirical model described above. All data are predicted either well or conservatively.

The limitations of TRACG to adequately predict pool temperature distribution based on a first principle approach is recognized by GENE. The staff agrees with this assessment. The staff reviewed the proposed empirical model and, since it is conservative, finds it to be acceptable.

### Pool Level

The two-phase level model described in Section 6.4, Reference 10, is used to calculate the pool level. The liquid and vapor side interfacial heat transfer coefficients are calculated with Equation 6.5-28, Reference 10. [[

]].

The staff reviewed the employed model and finds the correlation used appropriate for the expected thermodynamic conditions. Further, the correlation is acceptable because a sensitivity study performed by GENE indicates that this phenomenon has a relatively small effect on the peak containment pressure. This interfacial heat transfer model may be replaced with a more appropriate model for design certification analyses. (See Section 3.6.2.3,

“Phenomena Identification and Ranking,” Item WW4: Free Surface Condensation/Evaporation, and Section 4.0 “Confirmatory Items,” Item 16.).

### 3.6.2.2 Large Main Steam Line Break Description

The important features of the transient resulting from a large break in the main steam line are described for each phase of the accident.

#### 3.6.2.2.1 Blowdown Period

This period is characterized by a rapid depressurization of the RPV through the break, SRVs and DPVs. The steam blowdown from the break and DPVs pressurizes the drywell, forcing a mixture of steam and noncondensable gases through, and then clearing, the main containment vents and the PCCS vents. The steam is condensed in the SP and the noncondensable gas collects in the wetwell gas space above the SP.

For the MSLB, the blowdown flow quickly increases the drywell pressure to the scram setpoint, and a control rod scram occurs. The high velocities in the steam line initiate closure of the main steam line isolation valves (MSIVs) and the reactor isolates in 3 to 5 seconds. This trip also opens the IC drain valves, but no credit is taken in the design basis analysis for heat removal by the ICS. High drywell pressure isolates several other systems, including the containment atmosphere control system purge and vent, the fuel and auxiliary pool cooling system, the high and low conductivity sumps, the fission product sampling system, and the reactor building heating, ventilating, and air conditioning (HVAC) exhaust.

Loss of feedwater and flow from the break cause the RPV water level to drop. Without external makeup, the Level 1 (L1) trip will be reached in about 6 minutes. (During this period, the ICS, if available, would be removing energy and reducing pressure and break flow.) After a 10-second delay to confirm the L1 condition, the ADS logic starts a timed sequential opening of the SRVs, DPVs and the GDCS injection valves. The SRVs open in several stages to stagger SRV line-clearing loads in the suppression pool and to minimize the RPV level swell. Blowdown through the break, the SRVs, and the DPVs causes a level swell in the RPV. The two-phase level in the RPV downcomer decreases at the end of the blowdown period, when GDCS injection begins.

In the containment, the steam entering the drywell increases its pressure, opening the main containment vents and sweeping most of the drywell noncondensable gas through the main vents, through the SP, and into the wetwell gas space. (Depending on the location of the break, a substantial portion of the noncondensables in the lower drywell region may remain in that region and bleed out slowly later in the transient). During the blowdown phase of the transient, the majority of the blowdown energy is transferred into the SP by condensation of the steam flowing through the main vents. The increase in the drywell pressure causes flow through the PCCS, which also absorbs part of the blowdown energy. Based on GENE’s response to staff RAI 314.2, about 15 percent of the blowdown energy is absorbed by the PCCS with most of the energy being absorbed in the SP. The ADS, activated by the measured RPV downcomer level, opens the SRVs and the DPVs, and augments the steam flow to the SP and drywell, respectively. The blowdown period of the accident lasts about 10 minutes.

### 3.6.2.2.2 GDCS Period

This period begins when the pressure difference between the RPV and the wetwell is small enough to enable flow from the GDCS pools to enter the RPV. This is the period during which the GDCS pools drain their inventory. Depending on the break, the pools are drained in between 1 and 6 hours. The GDCS flow fills the RPV to the elevation of the DPVs (below the main steam line) break and then the excess GDCS flow spills over into the drywell. The GDCS period is characterized by condensation of steam in the RPV and drywell, depressurization of the RPV and drywell, and the possible openings of the vacuum breakers, which returns noncondensable gas from the wetwell gas space to the drywell.

Quenching of voids in the core by the GDCS flow reduces the steam outflow from the RPV to the drywell. Once the GDCS flow begins, the drywell pressure begins to decrease. The decrease in drywell pressure stops the steam flow through the PCCS and main vents. This pressure decrease may be sufficient to open the VBs between the drywell and the wetwell gas space. Draining of the GDCS pools also helps to reduce the containment pressure as more wetwell volume becomes available for the noncondensibles in the wetwell gas space. Once GDCS flow begins to spill from the RPV into the drywell, the drywell pressure drops further and additional VBs may open. If the VBs open, some of the noncondensable gas in the wetwell gas space will return to the drywell through the VBs. The GDCS period of the transient continues until the water level in the GDCS pools equalizes with the collapsed level in the downcomer of the RPV and the decay heat is able to overcome the subcooling of the GDCS inventory in the RPV. Then, the drywell pressure rises and flow is reestablished through the PCCS. The PCCS heat removal capacity, even while recycling noncondensable gas back to the wetwell, is sufficient to condense the steam generated by decay heat without reopening the main vents. This period of the accident is expected to last for less than 1 hour.

### 3.6.2.2.3 Long-Term Cooling Phase

During this period, the noncondensable gas that reentered the drywell through the VBs is returned to the wetwell. Condensate from the PCCS is recycled back into the RPV through the PCCS drain tank in the drywell. The most important part of the LOCA transient for the RPV response is the blowdown period and the early part of the GDCS period when the RPV is reflooded and inventory restored. For some breaks (e.g., bottom drain line break (BDLB)), the equalizing line from the SP to the RPV may open during the long-term cooling period to provide the RPV an additional source of makeup water if the water level in the downcomer falls to 1 meter above the elevation of the TAF. For the containment, the blowdown phase determines the initial pressurization. During the GDCS phase, the pressure levels off and decreases as the GDCS flow to the RPV first shuts off steaming from the RPV and later spills over into the drywell, condensing steam in the drywell. At the end of the GDCS phase, noncondensibles that returned to the drywell because of VB openings are returned to the wetwell gas space, and the PCCS assumes the decay heat load.

After the drywell pressure transient initiated by the GDCS flow is over, the drywell pressure reaches equilibrium slightly above the wetwell gas space pressure. The MSLB is the limiting break in terms of containment pressure and temperature, as most of the noncondensibles are

swept out from the drywell into the wetwell in the initial blowdown phase. This part of the containment transient is similar to that for the GDLB. However, unlike the GDLB, the steam generated by the decay heat is condensed in the PCCS and all of it is returned to the RPV via the PCCS drain tanks. Thus, there is no long-term drop in the downcomer and chimney water levels due to boiloff. A larger amount of water inventory is retained inside the RPV and a smaller amount in the lower drywell.

### 3.6.2.3 Phenomena Identification and Ranking

The critical safety parameters for the containment/LOCA analyses are the peak pressures and temperatures in the drywell and wetwell of the containment. These safety parameters are the criteria used to judge the performance of safety systems (the PCCS) and the margins in the design (to the allowable design pressure and temperature).

The short-term drywell pressure response is governed by energy deposition from the break flow and the DPV discharge flow. Energy removal from the drywell is through the main vent flow, the PCCS flow, and from condensation on walls and internal structures. The pressure difference necessary for clearing of the main vents controls the initial pressure increase in the drywell. Energy deposition in the wetwell is through the main vent flow, and flow through the SRV quenchers and PCCS vent lines. Thermal stratification of the SP is a key factor in determining how this energy is distributed within the SP; it sets the SP surface temperature and, therefore, the temperature and steam partial pressure in the wetwell gas space.

Another key parameter controlling the short-term wetwell pressure response is the extent to which the noncondensibles (nitrogen) initially in the drywell are purged to the wetwell during the initial blowdown. The design of the containment should also account for the hydrodynamic loads due to SP swell, SRV line air clearing, condensation oscillations, and chugging. TRACG is not used in the design process for this purpose. Empirical models that are based on extensive test data will be employed for the design certification review.

The long-term containment response is primarily controlled by the heat removal by the PCCS. The ability of the PCCS to purge noncondensibles and its performance in the presence of noncondensibles are key issues. The rates of drywell and wetwell energy addition and removal become progressively smaller in the long-term transient. The energy deposition in the wetwell is due to the PCCS vent flow and any steam leakage from the drywell that bypasses the PCCS. Energy removal from the wetwell is through heat transfer in the gas space (at the pool interface and walls) and condensation on the wetwell walls.

The PCCS performance may be affected by the noncondensibles distributions in the drywell. Overcooling of the drywell by the PCCS or by cold water spillover from the RPV can result in the drywell pressure falling below the wetwell pressure. Cold water could be added by flow from a broken GDCS line or spillover from the break after the GDCS fills the RPV to the break or DPV elevation. This will cause the VBs to open, bringing noncondensibles back to the drywell.

Model biases and uncertainties for the containment/LOCA application of TRACG were assessed by GENE, as described below, for the key high-ranked phenomena. These assessments were

typically performed as comparisons between separate effects test data and TRACG calculations performed with the "best estimate" modeling use of the code. The biases and uncertainties indicated by the data comparisons are used to establish ranges for TRACG parameters and correlations. These ranges are implemented through special inputs designated as "PIRT multipliers."

**BR1: Break Flow**

The determining phenomenon for this PIRT parameter is the critical flow. [[

]]. The bias and standard deviation were developed by GENE from the combined data set. [[

]].

**MV1: Main Vent Flow**

**MV3: Main Vent Clearing**

The determining phenomenon for the main vent flow is the irreversible pressure loss (mainly at the vent entrance). Vent clearing is controlled by the inertia of the water initially in the vent line. In Reference 16, the short-term peak drywell pressure was shown to be always conservatively overpredicted by TRACG, and variations of the vent line loss coefficient and inertia did not have a significant effect on the long-term drywell pressure. In response to staff RAI 301, GENE stated that the SBWR and ESBWR vent designs are identical and the SBWR studies are applicable to the qualification of TRACG for the ESBWR. [[

]].

**DW1: Flashing/Evaporation in Drywell**

The basic phenomena associated with this PIRT parameter are flashing of the liquid discharged through the break and evaporation of the liquid accumulated on the drywell floor. The controlling model in TRACG for this phenomenon is the interfacial heat transfer between the liquid and gas phases. Past GENE experience with TRACG has shown very little sensitivity to this parameter [[ ]]. In response to staff RAI 300, GENE clarified that the past experience was based on SBWR studies, Reference 19.

**SQ1: SRV Flow**

The determining phenomenon for the SRV flow is the critical flow, and the uncertainty as discussed for BR1 is used for this PIRT parameter.

**DW2: Drywell Heat Sources and Sinks**

The basic phenomena for this PIRT parameter are condensation and wall/structure heat transfer, which is controlled by conduction and free convection. TRACG uses the [[ ]] for the calculation of the condensation on the walls. Degradation due to the presence of noncondensibles is modeled as a correction factor based on the ratio of the partial pressure of the noncondensibles to total pressure. This model was developed for condensation in tubes. Since the uncertainties in DW2 are for condensation on flat surfaces, and the database used is basically for tube configurations, the uncertainties need to be modified for the ESBWR type geometries. In response to staff RAI 300, GENE clarified that the database used was based on the SBWR studies, Reference 19. A GENE comparison of the normalized average heat transfer coefficient predicted by TRACG with three commonly used models for flat plates showed that the TRACG model agreed well with the Dukler model (for laminar and low end turbulent flow conditions). For film Reynolds numbers larger than 20,000, TRACG predictions fell between the predictions from the Seban and the Colburn models. GENE noted that at such high Reynolds numbers, the heat transfer is conduction controlled and the condensation heat transfer coefficient has a very small effect on the overall heat transfer rate. The TRACG calculations fall between the predictions from the two flat plate condensation models, however the distribution and the deviations for these two models are not known. GENE decided to increase the maximum standard deviation for the tube data by [[ ]] to account for the spread of the flat plate correlations. The free convection correlation used in TRACG compares with data for  $Gr Pr > 4.1 \times 10^4$  within [[ ]]. However, the data for turbulent convection at identical conditions can vary by as much as [[ ]]. This means that, unless the correlation is based on a wide range of data, there could be as much as [[ ]] uncertainty in the model. Therefore, GENE allows the free convection heat transfer coefficient to vary [[ ]] of the nominal value with a uniform distribution. Because the free convection model in TRACG compares favorably with data for  $Gr Pr > 4.1 \times 10^4$  within [[ ]], widening the variation to [[ ]] based on turbulent convection data is conservative. Limiting the lower value to [[ ]] adequately covers the uncertainty, and addresses the non-realistic zero heat transfer if the lower value was set to [[ ]].

**DW3: 3-D Effects in Drywell**

The basic phenomena associated with this PIRT parameter are noncondensable gas stratification and buoyancy/natural circulation. As discussed in Section 3.6.2.4 of this report, a bounding modeling approach is used for the calculations in all cases. In this approach, [[

]].

**DW4: Condensation on Reactor Outflow**

This PIRT parameter represents the condensation of drywell steam due to the overflow of the subcooled GDCS liquid to the drywell from the RPV. The main effect of steam condensation due to GDCS flow is in the RPV, and steam condensation in the containment from the reactor outflow is small. There are no separate effects or integral tests to define this uncertainty. GENE performed bounding calculations by varying the PIRT multiplier on the interfacial heat transfer coefficient (PIRT91) by [[ ]]. The TRACG runs were performed for the SBWR base case that was used for the uncertainty calculations. PIRT multiplier PIRT91 was set to [[ ]] in the drywell nodes containing the broken steam line and also the nodes adjacent to it. GENE found the effect of this change on the thermodynamic conditions in the drywell and the wetwell was negligible. [[ ]].

**WW1: Condensation/Evaporation of Main Vent Discharge**

**WW2: Condensation/Evaporation of SRV Discharge**

The wetwell condensation/evaporation PIRT parameters are controlled by the interfacial heat transfer in the SP. GENE noted that the TRACG model for condensation in the SP does not include any degradation due to the presence of noncondensibles. A large body of experimental data generated by GENE to evaluate the performance of the pressure suppression pool have shown that all the steam discharged into the pool through the main vents will be condensed. No steam channeling was observed based on the measured wetwell gas space pressure. These tests include experiments as early as those performed for the Humboldt Bay reactor, Reference 22, and Bodega Bay reactor, Reference 23. Mark II (4T), Reference 24, pressure suppression confirmatory tests were also performed by GENE. TRACG sensitivity studies have also shown complete condensation of steam within the pool even with substantial changes in the magnitude of the interfacial heat transfer. Therefore, GENE concluded that the total condensation below the pool surface is insensitive to variation in the interfacial heat transfer [[ ]].

**WW3: Condensation/Evaporation of PCCS Vent Discharge**

This wetwell condensation/evaporation PIRT parameter is controlled by the interfacial heat transfer in the SP, as discussed above for WW1 and WW2. However, the PCCS vent submergence in the SP is less than that for either the main vents or the SRV quenchers. In response to RAI 314.1, GENE evaluated the adequacy of vent submergence to preclude steam being added to the wetwell air space. Any steam not condensed by the PCCS that enters the SP should be condensed within the SP. Based on the TRACG calculations, GENE determined that a small amount of steam entering the PCCS during the blowdown period would not be condensed in the PCCS and would enter the SP. After clearing out the noncondensibles above the steam line break location in the first few seconds, the flow through the PCCS is essentially

all steam until 10 minutes into the transient. The amount of steam entering the PCCS, and the PCCS performance was found to be within the test data base from the PANTHERS tests. GENE referenced a paper, "Experimental Investigation of Condensation and Mixing During Venting of Steam/Non-Condensable Gas Mixture into a Pressure Suppression Pool," by C. De Walsche and F. de Cachard, ICONE-8565, Proceedings of ICONE 8, 8th International Conference on Nuclear Engineering, April 2-6, 2000, Baltimore, MD, USA, to address the adequacy of the vent submergence to preclude steam release to the wetwell air space. This investigation covered the conditions expected in the ESBWR, and the test data showed that the steam was fully condensed in all the tests, even with shallow submergences, until the pool temperature got to a few degrees below saturation. At typical subcooling, the steam was condensed at a distance of 10 to 15 cm ( $L/D = 3$  to  $4$ ) above the vent discharge. GENE provided a simple argument that condensation will be complete for a pipe of a different size at the same  $L/D$  or less when the mass flux is the same. Also, for the time frame of interest, the main vents are open. The mixing in the SP will be far greater than that for a PCCS vent discharging into a quiescent pool. This will help with the condensation of the steam, resulting in a more efficient process. Based on available test data, GENE concluded that any steam entering the SP through the PCCS vent, based on the design presented for this review, will be condensed within the SP during the blowdown period of the accident.

The actual design configuration of the PCCS vent system, especially the vent submergence, may influence the amount of steam condensed in the SP. Therefore, during the design certification review, the staff will confirm that steam entering the SP through the PCCS vent, as designed, will perform as expected to condense steam entering the SP.

#### **WW4 : Free Surface Condensation/Evaporation**

The interfacial heat transfer at the free surface controls this PIRT parameter phenomenon. To evaluate the sensitivity of the containment response to the variation of the free surface interfacial heat transfer, the results of one of the PANDA containment tests were used by GENE. Variation of the PIRT7 multiplier, which affects the liquid side interfacial heat transfer [[ ]], did not affect the TRACG predictions. GENE therefore concluded that the free surface condensation is insensitive to the liquid side interfacial heat transfer. The steam in the wetwell gas space is superheated and has to be cooled to the saturation temperature before condensation can occur. Since no condensation is occurring, variation of the liquid side interfacial heat transfer coefficient is not expected to affect the overall heat transfer to the wetwell gas space.

The PIRT multiplier should affect the vapor side heat transfer. GENE studied this by varying the vapor side interfacial heat transfer and comparing the predicted wetwell gas space temperature to the results of PANDA Test M3, Reference 16. The objective was to find the appropriate multiplier on the interfacial heat transfer coefficient (PIRT7), which would result in prediction of the PANDA results. The TRACG interfacial heat transfer when increased by a factor of [[ ]], predicts the correct heat transfer between the pool and wetwell gas space. GENE concluded that this was probably due to a larger than calculated surface area, either from a wavy interface or from entrained droplets. Increasing PIRT7 beyond [[ ]] did not affect the predicted wetwell gas space temperature. Since a value of PIRT7 equal to

[[ ]] resulted in the best agreement with the data, it is used as the nominal TRACG value [[ ]].

The staff could not identify the correlation form used for the interfacial heat transfer at the free surface. In response to staff RAI 306.1, GENE stated that the correlation is for free natural convection in air above a horizontal surface and came from Reference 25, Table 7-2, and is given as  $h = 0.22(T)^{1/3}$  in British units (This equation is taken from Reference 18 and is generally used for free convection above a heated plate or below a cooled plate.) This correlation was then modified by GENE to simulate natural free convection in a medium other than air by [[ ]].

[[ ]]. In the current version of TRACG, there is a conversion error in translating this equation into SI units. The leading coefficient was converted to SI as 1.027, when it should have been 1.52. TRACG assumed [[ ]]

h = [[ ]], at about [[ ]], resulting in TRACG using the equation form h = [[ ]], in SI units, for the interfacial heat transfer at the free surface.

GENE stated that in the fourth edition of Holman, Table 7-2, the coefficient has been reduced slightly with the equation in SI units being  $h = 1.43(T)^{1/3}$ . [[ ]]

[[ ]], then the TRACG should be using the equation form  $h = [[ ]]$ , in SI units. GENE concluded that the error in the equation as used is less than 0.2 percent, based on the revised equation and a different value for the thermal conductivity of air. The staff accepts this approach and notes that GENE will be replacing this model with an appropriate model for design certification. The correction will be made in the next revision of Reference 10.

To account for noncondensibles, the interfacial heat transfer rate is multiplied by what GENE refers to as the [[ ]]. In response to staff RAI 306.2, GENE stated that the precise origin of the tabulated values that are referred to as the [[ ]] factors is not known. GENE believes that these values were obtained by merging the separate results from [[ ]]. The tabulated values in the code are used to degrade the condensation heat transfer at the free surface between the mixture and vapor regions when a water level is predicted in a TRACG cell. The [[ ]]

[[ ]] form shows the same trend as either the [[ ]], Reference 27, or the [[ ]] degradation forms as the air mass fraction becomes smaller. However the [[ ]] form gives less degradation than either the [[ ]] or the [[ ]] forms. Some difference is expected since [[ ]] is based on a flat surface, while [[ ]] and [[ ]] are based on flow inside tubes. The degradation becomes less important as the pressure is increased. For general TRACG applications, the higher [[ ]] curve corresponds to higher pressures and temperatures, and GENE concluded that this form was appropriate for the ESBWR calculations. The [[ ]] is intended for use as a best estimate (unbiased) correlation for stratified mixture-vapor surfaces corresponding to a water level. GENE used the same uncertainly factors as developed for the [[ ]] for this PIRT parameter.

A sensitivity study was performed by GENE varying the PIRT multiplier on the vapor side interfacial heat transfer at the surface from [[ ]]. The effect of this variation was to

change the peak containment pressure by [[ ]]. The use of the current interfacial heat transfer model in the containment/LOCA calculation does not have an appreciable effect on the calculated peak containment pressure. Based on the low sensitivities to significant changes in the interfacial heat transfer coefficient at the vapor-liquid interface, GENE concluded, and the staff agrees, that the current model is adequate for the analysis of the ESBWR containment. However, GENE has committed to replace this model with an appropriate correlation for design certification.

**WW5: Heat Sources/Sinks**

This PIRT parameter phenomenon is controlled by condensation and wall/structure heat transfer. The uncertainties are the same as the values established for DW2.

**WW6: 3-D Effects in Suppression Pool**

The basic phenomenon associated with this PIRT parameter is the stratification in the SP. Temperature stratification in the pool is important, since it will affect the heat transfer to and from the wetwell gas space, which will then affect the containment temperature and pressure response. SP stratification data from large-scale tests have shown that the condensed steam from the main vent discharge heats that portion of the SP above the vent. Based on TRACG sensitivity studies (discussed in Section 3.6.2.4), a bounding model was developed by GENE [[ ]].

**WW7: 3-D Effects in Wetwell Gas Space**

TRACG predictions of the PANDA test with leakage flow (PANDA Test M6/8) (NEDC-32725P) showed that without [[ ]], the wetwell gas space remained [[ ]], unlike the test data. The wetwell cell receiving leakage flow from the drywell remained [[ ]] than the other cells, which remained [[ ]]. GENE needed to [[ ]] to reproduce the measured temperature response (Section 3.6.2.4 of this report). A similar method has been used to [[ ]] in the ESBWR wetwell gas space model. This was accomplished by [[ ]]. This approach produces much [[ ]] and is used for conservatism in modeling the 3-D effects in the wetwell gas space for design basis calculations.

**PC1: Mass Flow into PCCS**

The basic phenomenon controlling the mass flow into the PCCS is the pressure drop in the PCCS inlet line, as indicated by the term  $k/A^2$ . As part of the TRACG qualification effort, the measured PCCS overall pressure drops from the PANTHERS tests have been compared by GENE to the predictions by TRACG, Reference 16. The PANTHERS facility is a full-scale

representation of the SBWR PCCS with close simulation of the inlet and vent lines. Using the test results, the absolute error, bias, and standard deviation for  $k/A^2$  was determined for use in TRACG ESBWR calculations. Since the ESBWR PCCS inlet line is identical to the SBWR PCCS inlet line, the staff finds using the SBWR data for the variation in  $k/A^2$  in the analyses to be acceptable.

**PC2: Condensation on the PCCS Primary Side**

Condensation in the PCCS tubes is modeled with the [[ ]] in TRACG, and accounts for degradation in the condensation due to the presence of noncondensibles, as discussed under DW2. This model has been compared with a wide range of steam and steam air data. However, for the more limited range of conditions encountered in the ESBWR, the best source of comparisons are the full scale PANTHERS data. [[ ]]

]].

**PC3: PCCS Secondary Side Heat Transfer**

The PCCS secondary side heat transfer is controlled by the nucleate pool boiling phenomenon, which is modeled by the [[ ]], Reference 28, in TRACG. Comparisons with prototypical PANTHERS data, Reference 16, have shown good agreement between the measured and predicted heat transfer coefficients. Uncertainties in the wall conduction are also included in this PIRT parameter. The PANTHERS tests were carried out with clean tubes and did not include the effect of crud formation that may occur with continued PCCS operation. The nucleate boiling heat transfer coefficients are large and the heat transfer across the PCCS wall is mainly controlled by conduction. Therefore, uncertainties in wall thickness or crud formation will control the heat transfer. The maximum thickness of the crud was calculated by GENE for the design basis fouling factor and was introduced into the model through an increased PCCS tube wall thickness. Based on a design basis fouling factor of [[ ]], an equivalent inconel thickness of [[ ]] was calculated to represent the thermal resistance due to crud. TRACG calculations for the ESBWR will be made with a bounding input assumption that the wall thickness is equivalent to the design limit for crud formation.

**PC5: Parallel PCCS Unit Effects**

Variations in performance of one of the PCCS due to variations in mass flow rates could result from differences in the PCCS inlet line friction. Since the inlet line resistance of each PCCS was allowed to vary independently, the uncertainties in this parameter are covered by the uncertainties specified for PC1, above.

**PC8: Purging of Noncondensibles**

Uncertainties in purging of noncondensibles through the PCCS are covered by the bounding modeling approach developed for the drywell 3-D effects (DW3).

### DWB1: Wetwell-to-Drywell Leakage

The major paths for leakage between the drywell and wetwell are the possible leakage through the VBs and the electrical penetrations. The design limit of  $A/k = 1 \text{ cm}^2$  ( $0.155 \text{ in}^2$ ) will be used as the uncertainty range for this PIRT parameter. Testing of the VBs has shown that the leakage from an area corresponding to  $A/k = 1 \text{ cm}^2$  ( $0.155 \text{ in}^2$ ) is conservative. The effective flow area corresponding to the maximum acceptable leakage rate for the VBs is  $0.02 \text{ cm}^2$  ( $0.0031 \text{ in}^2$ ). The test data, Reference 29, even after considerable cycling and aging, show that the leakage is much smaller than the amount that would be obtained from a  $0.02 \text{ cm}^2$  ( $0.0031 \text{ in}^2$ ) flow path ( $0.06 \text{ cm}^2$ , or  $0.0093 \text{ in}^2$ , for three VBs). Therefore, a  $1 \text{ cm}^2$  ( $0.155 \text{ in}^2$ ) leakage area is a bounding limit for the leakage path. It is more than 16 times the maximum design leakage through the VBs.

### VB1: Vacuum Breaker Mass Flow Rate

For this PIRT parameter, the VB loss coefficient was calculated from the results of the full flow VB tests, Reference 29. Two sets of tests performed with a 120 mm disc stroke were used for this purpose. The first test was performed with air at 293 K (76.73 F) and 98.8 kPa (14.33 psi), and the second test at a temperature of 303 K (85.73 F) and 98.9 kPa (14.34 psi). The measured pressure drop and volumetric flow rate were used to calculate the values of  $k/A^2$  for all the tested differential pressures to develop an average value for  $k/A^2$  and a standard deviation. The uncertainties in the valve opening and closing pressures were determined by GENE from the curves provided in Reference 29 and are [[ ]] for the opening pressure, and [[ ]] for the closing pressure, with a uniform distribution.

### RPV2: RPV Steam Generation

The basic phenomena affecting RPV2 include decay heat and mixing of GDCS flow as it enters the RPV. TRACG calculates the decay heat with a nominal curve of energy release as a function of time, which approximates the American National Standards Institute (ANSI)/ANS-5.1-1979 standard entitled, "American National Standard for Decay Heat Power in Light Water Reactors." In this standard, values are provided for decay heat power from fission products from fissioning of the major fissionable nuclides present in light-water reactors (LWRs), (i.e.,  $U^{235}$  and  $Pu^{239}$  thermal and  $U^{238}$  fast) and methods are prescribed for evaluating the total fission product decay heat power from the data given for these specific fuel nuclides. The decay heat curve becomes a function of the fuel design, depletion environment, and power history. The variations in decay heat due to the above effects are small, and a generic curve is defined by GENE to cover all locations with little loss in accuracy. The parameters used to generate this generic curve for LOCA analysis have been chosen to be representative of the ESBWR core being analyzed. The details of the derivation as well as the calculation of the uncertainties are described in Reference 30. The magnitude of the uncertainty used for decay heat is a function of time after the accident and has a one-sigma value of approximately [[5]] percent.

### DPV1: DPV Mass Flow

The determining phenomenon for the DPV mass flow is the critical flow and the uncertainty as specified for BR is used for this PIRT parameter.

#### 3.6.2.4 Phenomena Treated with a Bounding Approach

Some phenomena identified by GENE in the PIRT process as being important to the ESBWR Containment/LOCA response are not calculated with TRACG "best estimate" models. These phenomena include the distribution of noncondensable gases in the drywell, the temperature distribution in the wetwell gas space, and the thermal stratification of the SP. Sensitivity studies were performed by GENE to quantify the potential effect of each of these phenomena and to bound their effects on the peak calculated containment pressure.

##### 3.6.2.4.1 Suppression Pool Stratification

The SP stratification model used in TRACG [[

]]. This modeling results in behavior consistent with observations in several small-scale tests (References 31, and 32). GENE has also shown this approach to be a conservative model for determining the pool surface temperature based on full-scale and scaled pressure suppression condensation tests simulating the RPV blowdown for a LOCA with energy addition to the SP from the main horizontal vents (Reference 16). Without this [[ ]] model in TRACG, the SP becomes [[ ]] and the three-dimensional cells used to model the pool [[ ]] at approximately 1 hour after the start of the LOCA.

The SP model uses [[ ]] axial levels with [[ ]] radial rings in each level and is modeled as a TRACG VSSL (vessel) component. The VSSL component is also used to model the ESBWR drywell, wetwell, and RPV. The top most level represents the [[ ]]. The next lower level includes [[ ]]. The model for the [[ ]] (see WW4 in Section 3.6.2.3) is used at this location. The next level down includes [[ ]]. The remaining [[ ]] levels include the [[ ]]. To generalize and automate SP stratification, [[

]]. In response to staff RAI 321, GENE also described the effects of the SRV quenchers on how the SP stratification model functions. The quenchers at the end of the SRV lines are located in the [[ ]]. Initially, there is flow through all three of the horizontal main vents for the large steam line break. While there is flow through all vents, the TRACG model allows the flow [[ ]]. As the blowdown flow decreases, the level in the main vent rises, sequentially closing off the horizontal rows of vents. [[

]].

As discussed in GENE's response to staff RAI 321, in general, there will also be flow through the SRV quenchers during a LOCA. The same logic is used to treat the flow from the SRVs. Because the SRVs discharge into the lowest level, [[ ]] as long as there is flow through the SRVs. This source of flow and energy into the SP results in good mixing within the entire SP. When the SRV flow ceases, the [[ ]]

]]. Typically, SRV flow will continue after the bottom two rows of horizontal vents have closed. [[ ]]

]].

To illustrate this [[ ]] model, GENE provided the results of the LOCA transient for the SBWR with and without the [[ ]] model to show the SP temperature predictions for the first 5000 seconds. For the case without the model, within the first hour, the [[ ]]. The calculation using the [[ ]] model shows the temperatures at different pool levels rising and then becoming constant [[ ]]. After the top-most horizontal vent closes at around 1000 seconds, [[ ]]. The effect of this model is to force the temperature in the upper layers of the SP to be about [[ ]] higher than if the SP were well mixed.

The SP temperature predictions using this stratification model have been compared by GENE to the SP temperature measurements from the PSTF, Reference 16. These comparisons show that the predicted temperatures near the SP surface bound the measured temperatures. With this stratification model, the ESBWR calculation for the liquid temperatures in the cells that contain the pool surface, which are in contact with the wetwell gas space, are bounded. This ensures that the wetwell gas space pressure, and therefore the containment pressure, will not be under predicted.

#### 3.6.2.4.2 Wetwell Gas Space Stratification

Wetwell gas space stratification was identified by GENE in the PIRT as a phenomenon potentially important for the containment response. Sensitivity studies were performed by GENE to investigate the effects of wetwell gas space stratification. TRACG modeling features to address the wetwell gas space stratification were developed by GENE and are used for the bounding modeling approach.

The wetwell gas space is the region of the wetwell above the SP surface. It has a total volume of about 4500 m<sup>3</sup> (151,853 ft<sup>3</sup>). The wetwell gas space is bounded on top by the diaphragm floor, which separates the wetwell and drywell, on the inside by the vent wall between the wetwell and drywell, and on the outside by the wall between the wetwell and the outer containment wall. The wetwell gas space is reasonably open, with a few side-wall gratings and pipes. In the wetwell ceiling, structural members, which are part of the diaphragm floor, run radially across the wetwell between the inner and outer walls. They extend down from the ceiling approximately 1 meter. While they should not inhibit natural circulation caused by temperature differences between the inner and outer walls, they could enhance stratification from any leakage flow from the VBs that are located in the diaphragm floor. The energy balance on the wetwell gas space, particularly during the long-term phase of the LOCA, is an important part of modeling the ESBWR containment, since it directly affects the containment response. If there is a net heating of the gas space and its pressure increases, the pressure throughout the containment is increased. If there is a net cooling of the gas space, its pressure is reduced, which lowers the containment pressure.

In the ESBWR Containment/LOCA model, the wetwell gas space is modeled with [[ ]] axial levels and [[ ]] radial rings, for a total of [[ ]] cells. (These are the same [[ ]] levels as discussed in Section 3.6.2.4.1, above.) The cells in the [[ ]] are in contact with the suppression pool. The inside cells contact the vent wall and the outside cells contact the outer containment wall. The upper cell on the inside, near the vent wall, receives drywell-to-wetwell flow, used to model leakage through the VBs. [[

]]. The basis for choosing this relatively simple arrangement was experience gained by GENE from PANDA post-test analyses. This showed that the [[ ]] wetwell gas space model provided the best prediction of the wetwell vapor temperatures for most of the PANDA tests.

Double-sided heat slabs are attached to cells in all levels of the wetwell gas space and SP to represent the vent wall and the outer containment wall. Due to the limited ability of TRACG to model condensation on horizontal surfaces, that part of the diaphragm floor which is not covered on the drywell side by the GDCS pools has been included with the inner (vent wall) heat slab. In response to staff RAIs 298 and 307.1, GENE acceptably addressed the treatment of the diaphragm floor and heat transfer to horizontal surfaces as discussed below.

Most of the heat slabs in the ESBWR containment wall (volume boundaries) are vertical surfaces. Non-wall heat structures inside the drywell and wetwell are conservatively ignored. The horizontal heat slabs are the drywell and SP basemats, the diaphragm floor, and the drywell top slab. The two basemats are covered with water and will not see any direct condensation, and are conservatively not modeled in the calculations. The diaphragm floor in the wetwell gas space is not expected to be a condensing surface and is also conservatively not modeled. The remaining two horizontal surfaces in the drywell are the diaphragm floor (not part of the GDCS pools) and the drywell top slab. The drywell top slab is conservatively not modeled. The diaphragm floor, which is not part of the GDCS pools, transfers energy from the drywell to the wetwell gas space during the transient. To model this heat conduction, the diaphragm floor is modeled as part of a vertical structure. The vertical wall between the drywell and wetwell includes the diaphragm floor area and assumes the wall thickness is the same as

that for the diaphragm floor. GENE expected this simplification in the modeling to have a small impact on the containment response, as the heat slabs have a small impact on both the short-term and long-term drywell pressure. A sensitivity study was performed by GENE to study the impact of this vertical heat slab modeling, in response to staff RAI 298. In this study, the area of the vertical heat slab between the drywell and wetwell were increased by [[ ]]. The impact on the calculated long-term containment pressure was a change of [[ ]].

In the TRACG documentation, it is stated that the [[ ]] correlation, Reference 33, is available as an option for a lower bound for condensation. Use of this correlation would be consistent with guidance provided in the SRP. As set forth below, in response to staff RAI 307.2, GENE addressed the application of the [[ ]] correlation and the overall impact of wall heat structures on the containment pressure response.

The [[ ]] correlation is not used in the base case calculations. However, for licencing analyses, the [[ ]] correlation will be used if the Uchida correlation rate is less than that from the [[ ]]. Results of the sensitivity study performed by GENE show that the impact of using this option on the long-term drywell pressure is small. The vertical heat slabs have a small impact on both the short-term and long-term drywell pressure. Sensitivity studies were performed by GENE by changing the surface areas of the vertical heat slabs in the drywell-wetwell wall and the wetwell outer wall. The impact on the long-term drywell pressure was [[ ]] for a 25 percent increase in the heat slab areas in the drywell-wetwell wall. The impact on the long-term drywell pressure was [[ ]] for a 25 percent decrease in the heat slab areas in the wetwell outer wall, and [ ] for essentially no heat slabs in the wetwell outer wall. The impact of the condensation model on the peak calculated drywell pressure is small.

GENE referenced sample results for the SBWR to illustrate the effects of the wetwell gas space stratification model. GENE expects the trends to be similar for the ESBWR due to the similarity of the hardware configurations. Without the model to [[ ]] stratification in the wetwell gas space, temperatures predicted by the TRACG SBWR model showed only a few degrees of stratification at 72 hours, the end of the long-term transient. The cells in the upper level were about [[ ]] above those in the lower level. All of the wetwell cells were initially heated by compression as the noncondensable gas was transferred from the drywell. This was followed by some initial cooling from the walls and then a general heating trend was seen in the calculation. Cells in the lower level remained near the SP temperature while the upper level cells heated up. Results from PANDA Test M6/8, where a conservative leakage flow (compared to the GENE design requirement) was tested, showed stratification of the upper region of the wetwell gas space. Based on these test results, a bounding model was developed by GENE for use in TRACG to account for the effect of this temperature stratification in the wetwell gas space.

[[ ]]. The lower cells still remain closely coupled to the SP temperature. The upper cells are cooled in the early portion of the transient, but the effect is less than seen without this model and the cell receiving leakage flow heats up significantly by the end of the transient. The other cell is cooled



The sensitivity studies performed by GENE showed that rearrangement of the drywell and removal of all dead-ended components results in a significant initial holdup of the drywell noncondensibles for the steam line break. However, the overall effect on the final drywell pressure after 72 hours was on the order of [[ ]]. Also, the loss coefficient used to represent the drywell vents, when varied over a wide range, had very little effect on the final containment pressures and temperatures, on the order of [[ ]].

The more significant factor in determining the containment pressure response is the location of the break discharge into the drywell. The discharge location for the steam line break was progressively lowered from the upper most cell in the drywell (the base case) to the lowest level in the drywell. Based on these GENE sensitivity studies, the break located in the lower drywell clears all the noncondensibles quickly. An MSLB located near the top of the drywell results in a slower transport of the noncondensibles from the lower drywell. This results in a longer time over which the performance of the PCCS is degraded by noncondensibles. The maximum pressure was obtained for the break location at the top of the drywell, resulting in a pressure prediction about [[ ]] higher than for a break in the lower drywell. This is the location to be used for containment/LOCA design basis calculations.

#### 3.6.2.5 Plant Parameters and Ranges for Application

Specific inputs for containment/LOCA calculations will be specified with internal GENE procedures, which are used by GENE to control the application of engineering computer programs for licencing analyses. The specific code input will be developed in connection with the design certification application and the development of the application-specific procedure. GENE provided a limited general discussion of how input is treated with respect to quantifying the impact on the calculated results. As such, it serves as a basis for the staff's understanding of the expected development of the application-specific procedures for design certification.

The TRACG code inputs can be divided into four broad categories—geometry inputs, model selection inputs, initial condition inputs, and plant parameters inputs. For each type of input, it is necessary to specify the value for the input. If the calculated result is sensitive to the input value, then it is also necessary to quantify the uncertainty in the input.

The geometry inputs are used to specify lengths, areas, and volumes. Uncertainties in these quantities are due to measurement uncertainties and manufacturing tolerances. These uncertainties usually have a much smaller impact on the results than do other uncertainties associated with the modeling simplifications. When this is not the case, the specific uncertainties can usually be quantified in a straightforward manner.

Geometries are also used to develop spatial nodalization. Spatial nodalization includes modeling simplifications such as the lumping together of individual elements into a single model component. For example, several similar main vent pipes may be lumped together and simulated as one pipe. An assessment of these kinds of simplifications, along with the sensitivities to spatial nodalization, is included in the GENE qualification reports (Reference 34 and Reference 16). With respect to the model used for the containment/LOCA calculations,

only GENE SBWR- and ESBWR-specific separate and integral test comparisons have been used to qualify the modeling (nodalization).

Model selection inputs are used to select the features of the model to be used for the intended application. Once established, these inputs are fully specified in the procedure for the application and will not be changed.

GENE has made a distinction between initial conditions and plant parameters. Initial conditions are considered to be those key plant inputs that determine the overall steady-state nuclear and hydraulic conditions prior to the transient. These are inputs that are essential to determining that the steady-state condition of the plant has been established. Plant parameters are reserved for such things as protection system setpoints and valve capacities that influence the characteristics of the transient response but which do not (when properly prescribed) have an impact on steady-state operation. The staff accepts these distinctions for the purpose of the analysis of the ESBWR design. GENE did not identify any plant parameters as important for this TRACG evaluation study.

#### 3.6.2.5.1 Plant Initial Conditions Used for Calculations

The plant operating conditions represent initial conditions for the TRACG calculations and have an important effect on the calculated response of the containment. The range of allowable initial conditions is governed by plant operating guidelines and, for containment response calculations, it is assumed that the plant will be operated within these guidelines. In a typical calculation, initial conditions in the containment are assumed to be at steady-state, and at limiting pressures and temperatures. The RPV is assumed to be operating at maximum power, and, for a given feedwater flow and temperature, the RPV steam flow, the initial temperatures and pressures, and vessel internal flows are selected to obtain steady state conditions. Initial RPV power is set at 100 percent of rated power for the base case calculation. Experience with similar BWR containment systems has shown that rated power produces the most limiting containment response. The only exception is a break from hot standby, which is typically included in a containment response evaluation. For this accident, it is assumed that the plant was at full power operation, is scrammed and isolated, and the SP is heated by SRV operation to the maximum pool temperature limit before the break occurs. This break can, for some plants, be limiting because of the high initial pool temperature.

The following parameters were used for the base case and bounding case calculations performed by GENE in support of the TRACG application review.

Reactor Power Level—[[  
]]. The analyses performed at the design certification stage will be performed consistent with the power level and appropriate measurement uncertainty.

RPV Level—[[

]].

RPV Pressure—[[

]].

PCCS Pool Level—The initial PCCS pool level was determined from the minimum water inventory above the top of the condenser tubes. Since the IC, PCCS, and other pools on that level of the containment building are connected, the initial PCCS pool level is the minimum allowed for plant operation and is, therefore, a conservative basis for this parameter. [[

]].

PCCS/IC Pool Temperature—[[

]]. GENE considers this a reasonable value for the

pools that are outside the containment.

Wetwell Gas Space Relative Humidity—[[

]]. GENE considers this to be a

reasonable value for the relative humidity in this closed volume exposed to the SP.

Drywell Relative Humidity—[[

]].

Drywell Pressure—[[

]].

Drywell and Wetwell Temperatures—[[

]].

Suppression Pool and GDCS Pool Temperatures—[[

]].

Suppression Pool and GDCS Pool Levels—[[

]].

### 3.6.2.5.2 Results for ESBWR Main Steam Line Break LOCA

The MSLB causes the fastest short term pressurization of the ESBWR drywell. It results in minimum drain-down of the GDCS pools because of the elevation of the break, and hence a smaller wetwell gas space volume in the long term. The steam line break discharging at the top of the drywell also results in a slower clearing out of the noncondensibles in the lower drywell degrading the PCCS for a longer time. All these factors lead to the highest containment pressure for the MSLB.

### 3.6.2.5.3 Baseline Results for Containment Analysis

The RPV and containment were initialized at their base case conditions. Four PCCSs are available with a total rated capacity of 54 MW. A crud thickness assumed on the tube walls corresponded to the design basis fouling factor of [[

]]. No credit was assumed for the ICs. A leakage path was assumed between the drywell and wetwell with an equivalent area of 1 cm<sup>2</sup> (0.155 in<sup>2</sup>).

Apart from the conservative modeling assumptions common to all TRACG containment analysis [[ ]], the other models were set at their mean values as determined by GENE for the uncertainties in the high-ranked PIRT parameters.

Following the postulated LOCA, the drywell pressure increased rapidly leading to clearing of the PCCS and main vents. The initial pressure rise turns over when the GDCS initiates at about 600 seconds. Vacuum breaker openings occur as the steam production drops off as a result of GDCS injection. Subsequently, decay heat overcomes the subcooling of the GDCS water and steaming resumes. The drywell pressure levels off and remains well below the design pressure of 60 psia (413.69 kPa). The peak drywell pressure for this case was [[ ]]. It took about [[ ]] for the noncondensibles to be cleared from the bottom of the drywell. At the end of 72 hours, the PCCS pool level has dropped to about halfway down the tubes. However, this is still sufficient for effective heat transfer. The level in the GDCS pools reaches an equilibrium with the RPV downcomer level, which is at the elevation of the steam line. After the first [[ ]], the PCCSs are able to remove the decay heat. When the PCCS heat removal exceeded the decay heat generation, there is a drop in the drywell pressure to a value below the wetwell pressure. This leads to a temporary cessation of steam flow to the PCCS. The VBs then open and some noncondensibles are returned to the drywell, and the PCCS heat removal increases as the steam flow from the drywell resumes. Initially, all elevations in the SP heat from the main vent and SRV discharge. After the main vents and SRVs close, only the upper levels are impacted by the PCCS vent discharge. For the first [[ ]], the decay heat exceeds the PCCS heat removal capacity and the SP surface temperature increases until it levels off at about [[ ]]. The pool surface temperature directly affects the wetwell pressure through the partial pressure of the steam.

There is an early peak in SP temperature to [[ ]] from the adiabatic compression of the drywell gas into the wetwell gas space. Afterward, the gas in contact with the wetwell and SP walls cools down. The cell receiving the leakage flow from the drywell locally heats up higher than the rest of the wetwell as a result of the wetwell gas stratification model. However, all temperatures remain below the wetwell temperature design limit of [[ ]]. The temperature initially peaks to [[ ]] as the drywell is pressurized from the steam discharge from the break. This temperature is below the short term temperature limit of [[ ]]. In the long term, the temperature remains below [[ ]].

#### 3.6.2.5.4 Bounding Results for Containment Analysis

The initial conditions used for this analysis were set to their bounding case values. Four PCCSs were available with a total rated capacity of 54 MW. No credit was assumed for the ICs. A leakage path was assumed between the drywell and wetwell with an equivalent area of 1 cm<sup>2</sup> (0.155 in<sup>2</sup>). In addition to the conservative modeling assumptions common to all TRACG containment analysis [[ ]], other models were ranged in the conservative direction to maximize the calculated containment pressure, as determined by GENE for the uncertainties in the high ranked PIRT parameters.

The drywell pressure for this calculation peaked at [[ ]]. For the bounding case [[ ]], it took longer for the PCCS to assume the full decay heat load. The SP surface temperature also reached a slightly higher value of about [[ ]].

The peak drywell pressure for the bounding case was below the design limit of 60 psia (413.69 kPa). The margin to the design limit for the pressure increase (based on absolute pressure) is [[ ]] percent. The base case peaked at [[ ]], a margin of [[ ]] percent. Both of these cases assumed a design basis fouling factor on the PCCS tubes corresponding to end-of-life conditions. For the base case without this fouling factor, the peak drywell pressure was calculated to be [[ ]] percent margin.

The wetwell gas space temperature results were similar to the base case. The early peak in temperature to [[ ]] was due to adiabatic compression of the drywell gas into the wetwell gas space. Afterward, the gas in contact with the wetwell and SP walls cools down. [[ ]]

[[ ]] all temperatures remain below the wetwell temperature design limit of 250 F (394.3 K). The drywell temperature initially peaked to [[ ]] as the drywell was pressurized from the steam discharge from the break. This temperature is below the short term temperature limit of 340 F (444.3 K). In the long term, the temperature is about [[ ]].

### 3.6.2.6 Summary of Containment/LOCA Application Methodology

The Commission's regulations in 10 CFR 52.47(b)(2)(i) provide that:

Certification of a standard design which ... utilizes simplified, inherent, passive, or other innovative means to accomplish its safety functions will be granted only if

(A)(1) The performance of each safety feature of the design has been demonstrated through either analysis, appropriate test programs, experience, or a combination thereof;

(2) Interdependent effects among the safety features of the design have been found acceptable by analysis, appropriate test programs, experience, or a combination thereof; [and]

(3) Sufficient data exist on the safety features of the design to assess the analytical tools used for safety analyses over a sufficient range of normal operating conditions, transient conditions, and specified accident sequences, including equilibrium core conditions[.]

The ESBWR uses the PCCS to maintain the containment pressure and temperature below their respective design limits during DBA LOCAs, including MSLBs. In support of design certification, GENE has performed both separate and integral tests of the PCCS to characterize its performance over the ranges of conditions expected to occur in the ESBWR during these accidents.

Analytical comparisons of the PCCS test data performed by GENE using existing TRACG correlations [[

]] have shown that these correlations are adequate to model the PCCS performance during these DBAs. The calculations show that TRACG tends to predict comparable performance as seen in the tests, only with a slightly higher pressure. This is a conservative property of TRACG for containment performances analyses, i.e., the test data show that the PCCS will perform slightly better than predicted by TRACG.

During the review, the staff determined that the interfacial heat transfer correlation used in TRACG to model the liquid to gas heat transfer for the SP to wetwell interface was not adequate. However, GENE performed sensitivity studies varying the interfacial heat transfer rate over a wide range and found that there was very little sensitivity in the calculated peak pressure to the interfacial heat transfer. GENE will replace this model with an appropriate model for design certification. (See Section 3.6.2.3, "Phenomena Identification and Ranking," Item WW4: Free Surface Condensation/Evaporation, and Section 4.0 "Confirmatory Items," Item 16.)

To support design certification, GENE has stated that it will use a bounding application approach for the containment analysis that will encompass the uncertainties associated with

several key phenomena. [[

]]. This conservative approach will be used to account for limitations in TRACG to handle these phenomena, as demonstrated through comparison of TRACG calculations performed by GENE, with and without the models for these phenomena, to applicable test data. The resulting design basis calculations will therefore contain conservatism consistent with the guidance in SRP Section 6.2.1, "Containment Functional Design," and SRP Section 6.2.1.C, "Pressure-Suppression Type BWR Containments." GENE has also stated that it will include drywell to wetwell bypass leakage in the design basis calculations, also consistent with SRP 6.2.1.C.

The bounding application model will also include a conservative treatment of heat transfer to containment structures. Most horizontal surfaces are neglected. Nonstructural surfaces, such as piping and grating, are also neglected. Sensitivity studies performed by GENE showed that the overall importance of the heat structure was low in determining the peak pressure response. The major heat removal process is the transfer of the blowdown energy to the SP. After about [[ ]], the PCCS is able to remove the decay heat for the duration of the accident and maintain the SP temperature within acceptable limits. GENE states that the resulting design basis calculations will therefore contain additional conservatism consistent with the guidance in SPR Section 6.2.1, "Containment Functional Design," and SRP Section 6.2.1.C, "Pressure-Suppression Type BWR Containments."

With respect to the model used for the containment/LOCA calculations, only GENE SBWR- and ESBWR-specific separate and integral test comparisons have been used to qualify the modeling (nodalization) and containment performance-related mass and heat transfer correlations. While there is no compelling reason to believe the models have not been adequately validated for specific use for the ESBWR, the staff believes that additional confirmatory validation studies should be performed by GENE based on widely accepted containment tests.

During the staff's earlier review of the SBWR work that GENE relies on for the ESBWR, Reference 50, the staff noted that GENE had not evaluated more traditional integral containment tests such as the Marviken tests, the Carolinas Virginia Tube Reactor test 3 without sprays, and the Battelle- Frankfurt Model Containment tests C-13 and C-15, for MSLBs. In response to staff RAI 317.1, GENE agreed to perform assessments of TRACG to model containment performance against integral test data that is publicly available for International Standard Problems where the test facilities and tests are well defined. The tests to be analyzed will be specified later, and the analysis will be completed during the design certification review.

The staff also requested that GENE provide a plan and schedule to assess the ability of TRACG to model containment performance against additional separate effects tests. Separate effects tests that should be considered include the Wisconsin Flat Plate condensation tests, (References 36, 37, and 38). In response to staff RAI 317.2, GE agreed to perform assessments of TRACG to model containment performance against separate effects test data that are publicly available for International Standard Problems where the test facilities and tests are well defined. The tests to be analyzed will be specified later, and the analysis will be completed during the design certification review.

Based on the foregoing, the staff has determined that the TRACG computer program, in combination with the bounding modeling approach developed by GENE to address potential weaknesses in TRACG and to ensure a conservative peak containment pressure calculation, is adequate for ESBWR containment performance analyses in support of design certification after the above noted code improvements are made. As set forth above, the base case and bounding calculations performed by GENE for this review demonstrate that TRACG is acceptable for use in design certification of the ESBWR design.

GENE is consistent with this step in the CSAU approach.

## **Element 2—Assessment and Ranging of Parameters**

### **3.7 Step 7—Establish Assessment Matrix**

The Test and Analysis Program Description (TAPD) provides an integrated plan to address the experimental and analytical work needed for analyzing ESBWR performance for normal operations, transients, DBAs, stability, and ATWS conditions in support of ESBWR design certification. A major product of all these activities is the assessed TRACG code for ESBWR analysis. The preapplication review focuses on the review of the TRACG code for LOCA and containment analysis only.

Experimental data from a number of separate effects tests with generic applications (for operating plants as well as ESBWR), integral systems tests and component tests performed for SBWR and ESBWR, and BWR plant operation were used to assess the TRACG code for ESBWR LOCA analysis.

#### **3.7.1 Testing Program**

The TAPD provides an integrated plan to address the experimental and analytical work needed for analyzing ESBWR performance for normal operations, transients, DBAs, stability, and ATWS conditions in support of ESBWR design certification. A major product of all these activities is the “qualified” TRACG code for the ESBWR analysis. As stated earlier, this preapplication review focuses on LOCA applicability of TRACG to the ESBWR design. As a result, test data and TRACG qualification for operational transients, ATWS, and stability are excluded. An overview of the interactions between the TAPD and other activities is shown in Figure 3.7.1.1.

Experimental data from a number of basic and separate effects tests with generic applications to operating BWRs and the ESBWR, and full-size component tests and integral systems tests performed specifically for the SBWR and ESBWR, and BWR plant operation have been used to qualify the TRACG code for the ESBWR LOCA analyses. The following is a summary of the test data (excluding the basic tests) used to qualify the TRACG code initially for the SBWR, and now for the ESBWR LOCA applications. The facilities described were designed and scaled based on the SBWR design. The facilities have been reviewed by the staff for applicability to the ESBWR design. The staff conclusions regarding applicability are based on review of the test objectives, test descriptions, and phenomena represented. The staff conclusions are presented in the form of assessment of the strengths, weaknesses, and evaluation of each of

the facilities. This assessment references the SBWR design as well as the ESBWR design since the facilities were originally designed relative to the SBWR. The ESBWR/SBWR relationship has been previously discussed in Section 3.0 of this report.

### 3.7.1.1 Full-Size Component Tests

#### 3.7.1.1.1 PANTHERS/PCC Tests

A full-size PCCS condenser for the SBWR was tested under this program.

- Test Objectives
  - (1) Demonstrate that the prototype PCC heat exchanger for the SBWR is capable of performing as designed with respect to heat rejection (component performance).
  - (2) Provide a sufficient database to confirm the adequacy of TRACG to predict the quasi-steady heat rejection performance of a prototype PCC heat exchanger over a range of air (simulant for nitrogen in the SBWR containment) flow rates, steam flow rates, operating pressures, and superheat conditions that span and bound the SBWR (and ESBWR) range.
  - (3) Determine and quantify any differences in the effects of noncondensable gas buildup in the PCC heat exchanger tubes between lighter-than-steam and heavier-than-steam gases (concept demonstration).

- Test Description

A full-size PCC condenser of the SBWR consists of two identical modules, and each module consists of a top header, a number of vertical condenser tubes, and a bottom header. The PANTHERS/PCC tests provided data for a full-size, two-module PCCS condenser submerged in a pool of water. Although the tests focused on the performance of a PCCS condenser for the SBWR, the data are applicable to a PCCS condenser in the ESBWR, which has the same condenser tube diameter, length, and pitch as the condenser tested in PANTHERS for the SBWR. The only difference is that the PCCS condenser in the ESBWR has about 35 percent more tubes than in the SBWR. As a result, an ESBWR PCC condenser is expected to have a heat removal rate about 35 percent higher than what was measured in the PANTHERS/PCC condenser.

PANTHERS/PCC testing was performed as a joint effort by GENE, Ansaldo, European Nuclear Energy Association, and Ente Nazionale per l'Energia Elettrica at Societa Informazioni Esperienze Termoidrauliche (SIET) in Piacenza, Italy. The test facility consisted of a prototype PCC unit originally designed to represent the SBWR, a steam supply, an air supply, and vent and condensate volumes sufficient to establish PCC thermal-hydraulic performance. The heat exchanger was a prototype unit, built by

Ansaldo using prototype procedures and prototype materials. The PCC pool had the appropriate water volume for a prototypical PCC unit.

For the steady-state performance tests, the facility was purged with steam and placed in a condition where steam or an air/steam mixture was sent to the PCC, and the flows of the condensate and vented gases were measured. Once steady-state conditions were established, data were collected for a period of approximately 15 minutes. Ninety-seven steady-state tests were performed, including the steam only tests with either saturated or superheated steam. Test conditions covered the entire range of the PCC inlet flow rates and pressures expected in the SBWR.

Transient tests were conducted by first establishing steady-state conditions and then either varying the water level in the PCC pool or allowing the unit to fill up from an injection of noncondensable gases with the vent line closed off by a blind flange.

- Phenomena

Phenomena investigated are the overall PCC heat removal rate, pool water level effect on the PCC performance, mass flow rate into PCC, condensation inside the tubes with or without the presence of noncondensable gases, pool side heat transfer, parallel PCC tube effects, and parallel PCC modules effects.

### Strengths

Full-size component tests have been conducted with the test parameters covering those expected in the SBWR (and in the ESBWR, after a 35 percent increase in the PCC heat removal rate as tested to account for approximately 35 percent increase in the number of condenser tubes) during LOCAs.

Test results demonstrate that a prototype PCC heat exchanger for the ESBWR is capable of performing as designed with respect to heat rejection, and provide a sufficient database to confirm the adequacy of TRACG to predict the quasi-steady heat rejection performance of a prototype heat exchanger over a range of air (as a simulant for nitrogen in the containment) flow rates, steam flow rates, operating pressures, and superheat conditions that cover the expected ranges of values of the parameters for the ESBWR.

### Weaknesses

- (1) A large number of the tests were conducted at a pressure higher than the expected containment pressure in the ESBWR during a LOCA, such as an MSLB, a GDLB, or a BDLB. However, there are also lower-pressure data to bracket the expected range of the containment pressure in the ESBWR. The tests could have been better planned to conduct more tests at the expected containment pressures in a LOCA.
- (2) Temperature measurements were made at the inside and outside walls of four condenser tubes. But there were no measurements of the bulk gas temperature inside these tubes. The heat transfer coefficient inside a tube cannot be derived from the test data. There were no measurements for mass flow rate and noncondensable gas concentration at the inlet of a condenser tube where tube wall temperatures were measured. As a result, a correlation between the heat transfer coefficient and the fluid velocity cannot be derived from the test data.
- (3) Documentation of the test results could have been more clearly written.

### Evaluation

Since the PCC tested at PANTHERS/PCC is equivalent to a full-size PCCS condenser in the SBWR, no scaling analysis is necessary and the test data provide a global heat removal rate of a full-size condenser in the SBWR. The PANTHERS/PCC data have confirmed that a PCCS condenser in the SBWR is capable of a heat removal rate of 10 MW (or higher depending on the inlet conditions) as designed. For the ESBWR, the heat removal rate of a PCCS condenser

is expected to be around 13.5 MW (with 35 percent more condenser tubes than the one tested at PANTHERS/PCC).

However, the PANTHERS/PCC tests were not designed to provide local thermal-hydraulic parameters, such as the heat transfer coefficient, mass flow rate, and noncondensable gas concentration, inside a condenser tube.

In conclusion, the PANTHERS/PCC test data cover a broad range of the SBWR and ESBWR parameters including inlet pressure, total mass flow rate, and total noncondensable gas concentration to confirm the PCC heat removal rate under various LOCA conditions. The PANTHERS/PCC data are acceptable as a valid database to qualify the TRACG code for the global heat removal rate of a PCCS condenser under the expected LOCA conditions in the ESBWR.

#### 3.7.1.1.2 PANTHERS/IC Tests

An IC unit consists of two identical modules, each module consisting of a top header, a number of vertical condenser tubes, and a bottom header. The PANTHERS/IC tests provide data for one full-size module (half) of the IC condenser submerged in a pool of water. Note that an IC in the ESBWR is identical to the IC in the SBWR which was tested in the PANTHERS/IC tests.

- Test Objectives
  - (1) Demonstrate that the prototype IC heat exchanger is capable of performing as designed with respect to heat rejection.
  - (2) Provide a sufficient database to confirm the adequacy of TRACG to predict the quasi-steady heat rejection performance of a prototype IC heat exchanger over a range of operating pressures that span and bound the ESBWR range.
  - (3) Demonstrate the startup of the IC unit under anticipated transient conditions.
  - (4) Demonstrate the capability of the IC design to vent noncondensable gases and to resume condensation following venting.

- Test Description

PANTHERS/IC testing was performed at SIET in Piacenza, Italy. The facility consisted of a prototype IC module, a steam supply vessel simulating the SBWR reactor vessel, a vent volume, and associated piping and instrumentation sufficient to establish IC thermal-hydraulic performance.

The IC tested was one module of a full-scale, two-module vertical tube heat exchanger designed and built by Ansaldo. Only one module was tested because of the high energy rejection rate of the IC unit, and inherent limitations of facility and steam supply size. The IC was a prototype unit, built using prototypical procedures and prototypical

materials. The SBWR has six modules (three heat exchanger units). The IC was installed in a water pool having one half the appropriate volume for one SBWR IC assembly.

For the steady-state tests, the steam supply to the steam vessel was regulated such that the vessel pressure stabilized at the desired value. A constant water level was maintained in the pressure vessel by draining condensate back to the power plant. Data were acquired for a period of approximately 15 minutes. Then the steam supply was increased or decreased to gather data at a different operating pressure, or testing was terminated. In all cases, flow into the IC was natural circulation driven, as is the case for the SBWR.

As with the PCC tests, transient tests were conducted by first establishing steady-state conditions, and then either varying the water level in the IC pool or allowing the unit to fill up from an injection of noncondensable gases. The gases were subsequently purged through vent lines located on both the lower and upper headers.

- Phenomena

Phenomena investigated included the IC heat removal rate, pool water level effect on the IC performance, mass flow rate into the IC, and pool side heat transfer.

#### Strengths

Full-size component tests were conducted with the test parameters covering those expected in the ESBWR during both normal and accident conditions. Since the IC tested has one of the two identical modules of a full-size IC, a scaling analysis is not necessary and the test data are directly applicable to an IC in the ESBWR (which has twice the heat removal rate compared to the IC tested at PANTHERS/IC).

#### Weaknesses

- (1) Temperature measurements were made at the inside and outside walls of eight condenser tubes, but there were no measurements of the bulk gas temperature inside these tubes. As a result, the heat transfer coefficient inside the tubes cannot be derived from the test data. There were no measurements of the mass flow rate and noncondensable gas concentration at the inlet of a condenser tube where tube wall temperatures were measured. As a result, a correlation between the heat transfer coefficient and the fluid velocity cannot be derived from the test data.
- (2) There are some concerns regarding the IC structural design and startup for LOCA conditions, which are beyond the scope of this preapplication review. However, they are raised in the evaluation below as an issue that needs to be addressed in the application for certification of the ESBWR design.
- (3) Documentation of the test results could have been more clearly written.

## Evaluation

The IC tested at PANTHERS/IC was one module of a full-scale, two-module IC in the ESBWR, therefore no scaling analysis is necessary. Test results demonstrate that a prototype IC module is capable of performing as designed with respect to heat rejection and provide a database for TRACG qualification regarding the quasi-steady heat removal rate of an IC. The PANTHERS/IC data are acceptable as a valid database to qualify the TRACG code for the IC global heat removal rate.

However, the test results do not sufficiently demonstrate a startup of the IC under anticipated transient and accident conditions. Loud booms were heard during the IC startup testing. Preliminary investigation suggested that it was caused by the fast opening of the IC drain valve and possible interaction between the trapped water and incoming steam flow in the horizontal section of the IC inlet line. This was supported by a follow-up IC startup test in which the IC drain valve opening time was increased to better simulate the plant conditions and the IC inlet line was drained. However, further investigations are needed to conclusively determine the cause of the water hammer and confirm the means to prevent it (e.g., by changing the hardware design of the IC inlet line or the startup procedure). This is an issue to be resolved for the ESBWR design certification.

Furthermore, the PANTHERS-IC testing was terminated when leakages were detected in the IC upper header. As a result, the leakage issue was never resolved, and it is an IC structural integrity issue that needs to be resolved for the ESBWR design certification.

### 3.7.1.1.3 Depressurization Valve Tests

Full-size DPV tests were conducted at the Wyle Laboratory in the United States.

- Test Objectives  
Demonstrate reliable operation of the DPV.
- Phenomena  
Mass flow rate in a DPV was not measured because the tests focused on the successful opening of the DPV.

Full-size testing of the DPV was conducted by GENE to demonstrate its operation and reliability. However, the design and testing of the DPV are not part of the ESBWR preapplication review.

### 3.7.1.1.4 Vacuum Breaker Tests

Full-size VB tests were conducted at a GENE facility in the U.S.

- Test Objectives

Demonstrate reliable operation of the VB.

- Phenomena

Opening pressure and closing pressure of a VB were measured.

GENE has conducted full-size VB tests to demonstrate its operation and reliability. However, technical evaluation of the VB testing program is not part of the ESBWR preapplication review.

### 3.7.1.2 Integral Systems Tests

Integral systems tests were conducted at three test facilities — GIST, GIRAFFE, and PANDA.

#### 3.7.1.2.1 GIST Tests

- Test Objectives

- (1) Demonstrate the technical feasibility of the GDCS concept.
- (2) Provide a sufficient database to confirm the adequacy of TRACG to predict GDCS flow initiation times, GDCS flow rates, and RPV water levels.

- Test Description

The Gravity-Driven Integrated Systems Tests (GIST) focused on the GDCS performance for maintaining core cooling in a LOCA and were performed by GENE in San Jose, California, in 1988. The GIST facility was a section-scaled simulation of the 1987 SBWR design configuration, with a 1:1 vertical scale and a 1:508 horizontal area scale of the RPV and containment volumes. Because of the 1:1 vertical scaling, the tests provided real-time response of the 1987 SBWR pressures and temperatures.

The GIST test program included the effects of various plant conditions on GDCS initiation and performance. The GIST facility consisted of four pressure vessels—the RPV, upper Drywell, lower Drywell, and the wetwell. The wetwell included the GDCS fluid. The RPV included internal structures, an electrically heated core, and bypass and chimney regions.

The GIST facility modeled the SBWR plant behavior during the late stage of the RPV blowdown. The tests were started with the RPV at 791 kPa (100 psig) and continued until the GDCS flow initiated and flooded the RPV. Four types of tests were conducted—MSLB, GDLB, BDLB, and no break scenario (e.g., loss of feedwater). All these tests lasted from 600 to 1210 seconds. Twenty-nine integral systems tests were conducted.

- Phenomena

Integral systems response of the RPV and containment during the late blowdown phase and GDCS injection phase of LOCAs was investigated.

### Strengths

Unlike the PANDA M-series and GIRAFFE tests, GIST tests were obtained in a facility that was based on an older SBWR design without a separate GDCS pool. Instead, the elevated SP also served as the GDCS coolant source. In this aspect, the GIST design is closer to the ESBWR.

Three kinds of LOCAs were tested in GIST — the MSLB, GDLB, and BDLB. Sensitivity studies have shown that these breaks can be expected to bracket other LOCAs in terms of break sizes, locations, and coolant flow. Nineteen LOCA tests were conducted, which included eight MSLB tests, four GDLB tests, and seven BDLB tests. For the same kind of LOCA (e.g., MSLB), initial test conditions were varied among the reactor vessel water level, SP level, and the number of GDCS injection lines operational. The figure of merit, the critical safety parameter, for the GIST tests was the minimum downcomer water level.

The tests have demonstrated technical feasibility of depressurizing the RPV to sufficiently low pressures below the static head of an elevated pool of water in the containment, enabling coolant injection to the core.

### Weaknesses

There were two phenomenon distortions caused by design limitations. First, GIST used two vertical pipes as the replacement for the annular downcomer of the reactor vessel between the lower plenum and the upper plenum above the core. Asymmetrical behavior was observed during part of the tests that revealed a two-phase or frothy mixture in one downcomer pipe and phase separation (low-void water in the bottom with steam above) in another downcomer pipe. This kind of asymmetry is not expected to occur in the annular vessel downcomer of the ESBWR since it does not have the separation as with the test facility's separate downcomer pipes. Second, a single standpipe was installed above the upper plenum of the RPV, where periodic percolation was found to exist during part of the tests, which led to periodic variations in the RPV pressure. However, these distortions are not expected to invalidate the overall integral systems behavior observed in the GIST tests.

### Evaluation

The GIST tests have demonstrated technical feasibility of the GDCS concept, which involves RPV depressurization to allow coolant injection to the vessel from an elevated pool of water in the containment. Despite the phenomenological distortions described above, the overall GDCS performance providing coolant to a depressurized RPV remains valid as shown in the GIST tests for a broad spectrum of LOCAs. The GIST data are acceptable as a valid database to

qualify the TRACG code for the late blowdown and early GDCS injection phase of the LOCAs, including the MSLB, GDLB, and BDLB.

#### 3.7.1.2.2 GIRAFFE Helium Tests

- Test Objectives

- (1) Demonstrate the operation of a passive containment cooling system with the presence of a lighter-than-steam noncondensable gas, including demonstrating the process of purging noncondensable gases from the PCC.
- (2) Provide a database to confirm the adequacy of TRACG to predict SBWR containment system performance in the presence of a lighter-than-steam noncondensable gas, including potential systems interaction effects.
- (3) Provide a tie-back test, which includes the appropriate quality assurance documentation, to repeat a previous GIRAFFE test.

- Test Description

GIRAFFE/helium tests were performed as a joint effort by GE and Toshiba in Kawasaki City, Japan. The GIRAFFE facility is a large-scale, integral system test facility designed to exhibit post-LOCA thermal-hydraulic behavior similar to the SBWR systems that are important to long-term containment cooling following a LOCA.

The global volume scaling of the facility is approximately 1:400, with a nominal height scaling of 1:1. The SBWR components simulated in the facility are the RPV, PCCS, GDCS, drywell, wetwell, and the connecting piping and valves. Five separate vessels represent the SBWR RPV, drywell, wetwell, GDCS pools, and the PCCS pool. The facility was equipped with one PCC, approximately scaled to represent the three SBWR PCCS condensers. Electric heaters provided a variable power source to simulate the core decay heat and the stored energy in the reactor structures.

For the helium series tests, once the test initial conditions were established, all control (except for the decay of RPV power and helium injection, if called for) was terminated, and the GIRAFFE containment was allowed to function without operator intervention (except that the VB was operated manually to simulate automatic operation in SBWR and minor wetwell microheater power adjustments were made to compensate for facility heat losses).

- Phenomena

Integral systems response of the RPV and containment during the long-term cooling phase of LOCAs was investigated.

#### Strengths

Four tests were conducted to demonstrate the PCCS operation with the presence of a lighter-than-steam noncondensable gas (using helium as a substitute for hydrogen gas) and a heavier-than-steam noncondensable gas (nitrogen). Test H1 was the base case test with the initial test conditions based on TRACG calculations for the SBWR during the long-term cooling phase at 1 hour after the break initiation (RPV initial pressure at 295 kPa or 42.8 psia). Test H2 was a repeat of Test H1 but with helium to replace nitrogen in the drywell. Test H3 was a variation of Test H1 by replacing some steam in the drywell with helium. Test H4 was similar to Test H1 but with a constant helium injection into the drywell.

In addition, two other MSLB tests, Tests T1 and T2, were conducted with nitrogen as the only noncondensable gas in the containment. The initial nitrogen concentrations were much higher than those in helium tests, but the tests were initiated at lower RPV and containment pressures.

### Weaknesses

- (1) Heat loss was a concern in the GIRAFFE facility, which was tall and thin. Electric microheaters were installed to wrap around the metal walls of the drywell, wetwell, and GDCS pool, which were covered with an insulation material. Microheater power for each component was determined during the shakedown tests to compensate for the heat loss. Since the microheater power could not fully compensate for the heat loss, the RPV electric heater power was raised above the scaled decay heat to further compensate for the heat loss in the facility with microheaters on. But this provision could not eliminate the local heat loss in the lower drywell, for which the heat loss was found to be significant. The heat loss could introduce some local distortions in the test data.
- (2) There were only two noncondensable gas sampling locations in the drywell — one at the top of the drywell and the other at the very bottom of the drywell located in the lower drywell where the local heat loss was significant. The heat loss at the bottom sampling location could somewhat distort the noncondensable gas behavior in the drywell. This problem was compounded with the scarcity of the noncondensable sampling locations. For the wetwell gas space, there was only one noncondensable gas sampling location. However, unlike the lower drywell, the wetwell wall heat loss was found to be insignificant. The scarcity of the noncondensable gas sampling locations and the heat loss problem at the lower drywell tended to reduce the quality of the containment noncondensable gas distribution data.
- (3) All the GIRAFFE helium tests (including tests T1 and T2) focused on the long-term cooling phase of the MSLB and did not include the late blowdown phase and GDCS phase. One of the tests should have been selected as a typical MSLB test to cover the late blowdown phase, GDCS phase, and the long-term cooling phase, which is within the capability of the GIRAFFE facility. The lack of a typical MSLB test starting at the late blowdown phase was a weakness of this test program.

### Evaluation

The GIRAFFE helium tests have demonstrated the PCCS performance to maintain containment cooling during the long-term cooling phase of the MSLB, which is the most critical LOCA to

challenge the containment. The impact on the PCCS performance has been investigated for both heavier-than-steam (nitrogen gas) and lighter-than-steam (helium gas) noncondensable gases present in the containment under various test conditions.

Because of the heat loss at the lower drywell, noncondensable gas distribution in the drywell is distorted by having a much higher noncondensable concentration (due to local steam condensation) than expected in the lower drywell. Furthermore, since there were only two noncondensable sampling locations in the drywell and only one in the wetwell gas space, extra efforts are needed to interpret the data and use the data to qualify the TRACG code regarding the noncondensable gas distributions in the containment. Nevertheless, there were many measurements on pressures, temperatures, and water levels that are sufficient to explain the containment response with the presence of the heavier-than-steam and lighter-than-steam noncondensable gases.

The GIRAFFE helium tests were based on the SBWR design, which is very similar to the ESBWR design in terms of the RPV and containment phenomena expected in a LOCA. Furthermore, there aren't any new phenomena introduced as a result of the design changes from the SBWR to the ESBWR. In view of the above, the staff concludes that the GIRAFFE helium tests provide a valid database to qualify the TRACG code for the long-term cooling phase of a LOCA involving both lighter-than-steam and heavier-than-steam noncondensable gases, although a careful examination of all the data was necessary.

#### 3.7.1.2.3 GIRAFFE Systems Interactions Tests

- Test Objectives

Provide a database to confirm the adequacy of TRACG to predict the SBWR ECCS performance during the late blowdown phase and GDCS injection phase of a LOCA, with specific focus on potential systems interaction effects.

- Test Description

A series of four transient systems tests was conducted to provide an integral systems database for potential systems interaction effects in the late blowdown phase and GDCS injection phase. All four tests involved liquid breaks—three GDLBs and one BDLB. Tests were performed with and without the ICS and PCCS in operation, and with two different single failures.

The post-LOCA thermal-hydraulic behavior (especially the RPV pressure transient and water level transient), the GDCS injection characteristics, and possible systems interactions were investigated in the tests. The test facility modeled the whole containment system of the SBWR. The SBWR components modeled in the facility were the RPV, ICS, GDCS, PCCS, drywell, wetwell, and the connecting piping and valves.

Major portions of the SBWR containment (drywell, wetwell, and GDCS pool, as well as IC pool and PCCS pool) were modeled using separate vessels.

The PCC unit was the same as that used for the GIRAFFE Helium Tests and consisted of a steam box, heat transfer tubes, and a water box. The PCC had three heat transfer tubes corresponding to the scaled volume. The heat transfer tubes were full height, and the internal tube flow area was almost the same as the scaled SBWR flow area. One scaled IC was mounted above the drywell vessel. The IC had three tubes, two of which were plugged in order to reduce the heat transfer surface of the unit. This single condenser represented two IC condensers found in the SBWR.

Testing followed a methodology very similar to that used in the PANDA tests and GIRAFFE helium tests. Once the initial conditions for a given test were established, all controls (except for the decay of RPV power) were terminated. The GIRAFFE RPV and containment were allowed to function without operator intervention, mirroring the Standard Safety Analysis Report (SSAR) assumptions for the SBWR. The GDCS pool-to-drywell flow was manually terminated at 1 hour in the GDCS break cases to avoid an inappropriate emptying of the pool. This was necessary since a single pool in GIRAFFE simulated the three SBWR pools, only one of which would have pool-to-drywell flow.

Manually stopping GDCS flow to the drywell in GIRAFFE simulated the end of draining for that one pool in the SBWR and maintained the simulation of flow from the remaining pools to the RPV.

- Phenomena

Integral systems responses of the RPV and containment in the late blowdown phase and GDCS injection phase of the GDLB and BDLB were measured. By comparing two similar GDLB tests with and without the PCCS and ICS operation, interactions between the PCCS/ICS and GDCS were assessed. Phenomena associated with the integral systems tests were investigated.

### Strengths

Four integral systems tests were conducted to assess the GDCS performance in maintaining a covered core with and without the operation of the ICS and PCCS. Two kinds of LOCAs were investigated with break locations below the main steam line elevation—GDLB and BDLB. Test GS1 was for a GDLB without the operation of the PCCS and ICS assuming a DPV failure (failed to open upon demand). Test GS2 was similar to Test GS1 but with the operation of the PCCS and ICS. Test GS3 was a BDLB with the operation of the PCCS and ICS assuming a DPV failure. Test GS4 was a GDLB with the operation of the PCCS and ICS assuming a valve failure on a GDCS injection line. These tests complemented the GIRAFFE helium tests for which only the MSLB was investigated. Potential interactions between the GDCS operation and the PCCS/ICS operation were assessed.

### Weaknesses

- (1) The GIRAFFE heat loss problem, discussed in the GIRAFFE helium tests, was also present in the GIRAFFE systems interaction tests. Although electric microheaters were used around the drywell, wetwell, and GDCS pool, and the RPV heater power was increased beyond the scaled decay heat to compensate for the heat loss, the heat loss problem could not be fully eliminated. For instance, the local heat loss in the lower drywell was found to be significant. The heat loss could introduce some distortions in the test data.
- (2) GIRAFFE/systems interactions tests lasted only two hours, which were not long enough to lead to the potential opening of the equalizing lines to provide SP water to the RPV. As a result, the equalizing line mass flow, which is a high-ranked phenomenon in the LOCA/Containment PIRT, was not observed in the test data.

### Evaluation

In all four tests conducted, the GDCS injection ran smoothly without noticeable flow oscillations. It performed well to keep the core covered and maintain core cooling. Comparing Tests GS1 and GS2, the PCCS/ICS operation had no adverse impact on GDCS performance and led to a lower containment pressure as expected. Operation of the ICS significantly reduced the steam flow available to the PCCS except for the initial 200 to 300 seconds.

The GIRAFFE helium tests were based on the SBWR design, which is very similar to the ESBWR design in terms of the RPV and containment phenomena expected in a LOCA. Furthermore, there aren't any new phenomena introduced as a result of the design changes from the SBWR to the ESBWR. Accordingly, the staff concludes the GIRAFFE systems interactions tests provide a valid database to qualify the TRACG code for the late blowdown phase and GDCS injection phase of a LOCA.

#### 3.7.1.2.4 PANDA M-Series Tests

- Test Objectives
  - (1) Provide a sufficient database to confirm the capability of TRACG to predict SBWR containment system performance, including potential systems interaction effects.
  - (2) Demonstrate startup and long-term operation of a passive containment cooling system.
- Test Description

PANDA M-series tests were performed as a joint effort by GENE and the Paul Scherrer Institute (PSI) in Wuerenlingen, Switzerland. The test facility was a large-scale integrated containment structure which was a 1/25 volumetric, full-height, scaled model of the SBWR containment. It was a modular facility with separate pressure vessels representing the RPV, drywell, wetwell, and GDCS pool. The facility was equipped with three scaled PCC heat exchangers and one IC unit (scaled from two SBWR IC units), each with a separate pool of water. Electrical heaters were used in the RPV to simulate decay heat and the thermal capacitance of the RPV walls and internals in the SBWR. The test facility also had interconnecting piping arrangements needed to conduct the MSLB tests. The tests were started at an equivalent condition from about 1040 seconds (transition from the GDCS injection phase to the long-term cooling phase) to about 3600 seconds (beginning of the long-term cooling phase) after the initiation of the MSLB in the SBWR. The duration of a test was up to 20 hours.

When the initial conditions for a given test were established, all controls were terminated except for automatic control of the wetwell-to-drywell VB position and the electric heater simulation of the RPV structure stored energy release and core decay heat power. The PANDA containment was then allowed to function without operator intervention, consistent with the SSAR assumptions for the SBWR. The only exceptions to the procedure described above were for tests M3A and M3B, which included operator action to maintain PCC pool level, and test M6/8 during which the operator established a drywell-to-wetwell flow path (bypass leakage) and later valved the IC unit out of service.

- Phenomena

Integral systems response of the RPV, drywell, and wetwell was investigated for the late GDCS injection phase and long-term cooling phase of a MSLB LOCA. PCCS performance for maintaining containment cooling was assessed.

### Strengths

PANDA was a "large" test facility at a scale of 1/25 of the SBWR. It had all the necessary components to conduct the integral systems tests to investigate the long-term cooling phase of a DBA, namely the MSLB accident that is most challenging to the containment.

The PANDA M-series tests consisted of 10 integral systems tests for the MSLB that covered a broad spectrum of test conditions expected in the SBWR. Except for test M9, these tests focused on the long-term cooling phase of the MSLB (occurring at about 1 hour after break initiation). Test M9 included both the late GDCS injection phase (with the initial test conditions based on 1040 seconds after the break initiation in the SBWR) and the long-term cooling phase of a LOCA. These tests have demonstrated successful operation of the PCCS for maintaining adequate containment cooling under various MSLB conditions in a large test facility.

### Weaknesses

- (1) PANDA M-series tests were designed to focus on the MSLB accident that is the most challenging LOCA to the containment. There was no lower drywell in PANDA, and consequently the GDLB and the BDLB could not be tested. Potential opening of the GDCS equalizing lines (expected to occur during the long-term cooling phase of the BDLB) to provide SP water to the RPV could not be investigated.
- (2) The volume of the GDCS pool was much smaller than the scaled volume, and consequently there was an insufficient amount of water to cover the entire spectrum of the GDCS injection phase. As a result, the long-term cooling phase and only a portion of the GDCS injection phase of the MSLB LOCA were investigated in the PANDA tests.
- (3) Large oscillations occurred in the main steam line mass flow rates, when the water level in the RPV was high (close to the top of the chimney). The flow oscillations were greatly reduced if the initial RPV water level was at a low level (several meters below the top of the chimney). The flow oscillations might have been caused by design distortions in PANDA (e.g., lack of core inlet orifices, fuel assemblies, steam separators, dryers, and multiple fuel assemblies in the RPV), although they did not prevent the PCCS from maintaining containment cooling.

### Evaluation

The PANDA test facility had all the necessary components to conduct the integral systems tests for a design-basis LOCA such as the MSLB. The M-series tests covered a broad spectrum of the test parameters expected in the SBWR (which are similar to the ESBWR test parameters) to investigate the long-term cooling phase of a LOCA. The PCCS performed well, and maintained adequate containment cooling in the MSLB test. Drywell air was purged to the wetwell via the PCCS. There was a smooth transition from the GDCS injection phase to the long-term cooling phase. The VB openings in a test did not significantly affect the global drywell and pressure response, in comparison to a similar test without the VB openings.

Although the PANDA M-series data are for the MSLB test conditions, the containment phenomena in the long-term cooling phase of other LOCAs, such as the GDLB and BDLB, are generally similar to those of the MSLB (with an exception to be discussed below). This is because before the start of the long-term cooling phase (with variations in the starting time that is LOCA-dependent), the RPV has depressurized from the ADS actuation and the GDCS injection has become insignificant. However, there is one exception. As stated in the "Weaknesses" above, the potential opening of the GDCS equalizing lines (expected to occur during the long-term cooling phase of the BDLB) to provide SP water to the RPV cannot be investigated in PANDA. Nevertheless, the physical process (as well as code modeling) for the SP injection to the RPV is similar to that for the GDCS injection to the RPV (in PANDA test M9). The lack of the PANDA data on the SP injection to the RPV is a deficiency in the test data, but not a critical one.

As stated earlier, the PANDA M-series tests were based on the SBWR design, which is very similar to the ESBWR design in terms of the RPV and containment phenomena expected in a LOCA. Furthermore, no new phenomena were introduced as a result of the design changes from the SBWR to the ESBWR. Equally important, the phenomena observed in the PANDA M-series tests are generally understood and seem to be reasonable. For instance, the addition of relatively cold water at room temperature to the PCC pools temporarily enhances the overall PCC heat removal rate and can lead to VB opening. But this does not significantly affect the overall behavior of the drywell and wetwell pressures.

In conclusion, the PANDA M-series tests provide a valid database to qualify the TRACG code for the long-term cooling phase of a LOCA relevant to the ESBWR LOCA analyses.

#### 3.7.1.2.5 PANDA P-Series Confirmatory Tests

- Test Objectives
  - (1) Reinforce the existing database to confirm the adequacy of TRACG to predict the ESBWR containment performance, including potential systems interaction effects.
  - (2) Confirm the performance of the ESBWR containment configuration with the GDCS gas space connected to the wetwell gas space.

- Test Description

PANDA is a large-scale integral test facility originally designed to model the long-term cooling phase of a LOCA for the SBWR. It has all the major components, including the RPV, drywell, wetwell, and a GDCS pool. The RPV was equipped with electrical heaters and heater controls to simulate decay heat and the release of RPV stored energy. The facility included all three scaled PCC heat exchangers and one IC unit and their associated water pools. Other components represented in PANDA include VBs between the drywell and the wetwell, and the equalizing lines between the SP and the RPV.

The RPV was represented by a single vessel in PANDA, while the drywell and wetwell were represented by two pairs of vessels, connected by large pipes. This double-vessel arrangement permitted investigation of spatial distribution effects within the containment volumes. The water in the RPV was heated by a bank of controlled electrical heaters that could be programmed to match the decay heat curve. Main steam lines conveyed boiloff steam from the RPV to the two drywell vessels. The PCC and IC inlet lines were connected to the drywell and RPV, respectively. Drain lines from the lower headers of the PCC and IC units returned condensate to the RPV. Vent lines from the lower headers of the PCCs and the upper and lower headers of the IC were at prototypical submergences in the SP. VBs were located in the lines connecting the drywell and wetwell gas spaces. PANDA had the capability to valve out one of the main steam lines, the IC and individual PCCs. It also had the capability to inject noncondensable gas (air

or helium) into the drywell over a prescribed time period during the post-LOCA transient tests.

In the original PANDA/SBWR configuration (for the PANDA M-series tests), the GDCS gas space was connected to the drywell. A major modification of PANDA for the ESBWR was to connect the GDCS gas space to the wetwell gas space. This ESBWR design feature provided a larger volume for the noncondensable gases that are purged from the drywell to the wetwell during the blowdown phase and therefore reduced the containment pressure. In its original configuration for the SBWR, PANDA was a 1/25 volume scaled, full-height representation of the SBWR primary system and containment. As configured for the P-series tests for the ESBWR, the PANDA facility is a full-height representation of the ESBWR containment at a nominal volumetric scale of 1:45. The piping interconnecting the PANDA vessels was scaled (primarily with the use of orifice plates) to produce the same pressure loss as the corresponding ESBWR piping. The three PANDA PCC units were approximately equivalent to the four ESBWR PCC units, and the one PANDA IC unit was about 10 percent underscaled relative to the four ESBWR IC units.

- Phenomena

Integral systems response of the RPV, drywell, and wetwell was investigated for the late GDCS injection phase and the long-term cooling phase of the MSLB. PCCS performance for maintaining containment cooling was assessed.

#### Strengths

The PANDA P-series tests were based on the ESBWR design, in which the GDCS pool is isolated from the drywell and its gas space is connected to the wetwell gas space instead of the drywell, as in the SBWR, and the PCCS drain lines were connected to the RPV instead of the GDCS pool, as in the SBWR. This was a minor deviation from the ESBWR design, in which a PCCS drain line is connected to a condensate drain tank that is connected to the RPV. The P-series tests consisted of eight integral systems tests for the MSLB (which is the most challenging LOCA to the containment) to investigate the containment response and phenomena during the long-term cooling phase under various initial and boundary conditions. PCCS performance was successfully demonstrated to maintain containment cooling. Various containment phenomena were investigated. The changes noted made the PANDA-P tests consistent with the ESBWR design with minor deviations.

#### Weaknesses

- (1) Like the PANDA M-series tests, the PANDA P-series tests were conducted in the same facility except with modifications necessary to conform to the ESBWR design as stated earlier. There was no lower drywell, and other LOCAs with a lower break location such as the GDLB and the BDLB could not be tested. Potential openings of the GDCS equalizing lines (expected to occur during the long-term cooling phase of the BDLB) to provide SP water to the RPV were not investigated.

- (2) Unlike the ESBWR, the two vertical main vent pipes between the PANDA drywell and wetwell were exposed to the wetwell gas space. There was drywell gas condensation inside the main vent pipes surrounded by the relatively colder wetwell gas. As a result, the wetwell gas temperature increased. This is a non-prototypical phenomenon not expected in the ESBWR, because all of the vertical main vent pipes in the ESBWR are located inside an annular concrete wall between the drywell and wetwell and are not exposed to the wetwell gas. Because of this non-prototypical condensation, PANDA test operators had to isolate the main vent pipes (by closing valves) from the drywell at 11 hours after initiation of the P1 test. The main vent gas condensation in the P1 test was nonprototypical and caused by a design distortion in PANDA.
- (3) The PCC pools in PANDA were much smaller than the scaled volume. For tests longer than about 35,000 seconds (9.7 hours), the PCC condenser tubes were uncovered unless water was added to the pool from an outside source.

### Evaluation

The PANDA facility has all the necessary components to conduct the integral systems tests for a design-basis LOCA such as the MSLB. The P-series tests covered a broad spectrum of the test conditions expected in the ESBWR to investigate the long-term cooling phase of a LOCA. The PCCS performed well, and maintained adequate containment cooling in the MSLB tested. The transition was smooth from the late GDCS injection phase to the long-term cooling phase. Injection of a noncondensable gas (using either air as a simulant of nitrogen or helium as a simulant of hydrogen) to the drywell degraded the PCC performance. Depending on the amount of the noncondensable gas injected, it seems that the PCCS was capable of purging it from the drywell to the wetwell.

At a low decay heat equivalent to several hours into the MSLB, the test data suggest that the PCCS is capable of maintaining containment cooling even when the PCC condenser tubes are substantially uncovered.

Although the PANDA P-series data are for the MSLB application, the containment phenomena in the long-term cooling phase of other LOCAs, such as the GDLB and BDLB, are generally similar to those of the MSLB (with an exception discussed below). This is because prior to the start of the long-term cooling phase, the RPV has depressurized from the ADS actuation. However, there is one exception. As stated in the "Weaknesses" above, the potential opening of the GDCS equalizing lines (expected to occur during the long-term cooling phase of the BDLB) to provide SP water to the RPV could not be investigated in PANDA. Nevertheless, the physical process (as well as code modeling) for the SP injection to the RPV is similar to that for the GDCS injection to the RPV (in PANDA test P2). This is a potential question to be reviewed at the design certification stage since it is a long term cooling item.

As stated in the "Weaknesses" above, some of the data have revealed distortions, e.g., temperature rise in the wetwell gas space due to nonprototypical heating from the gas flow in the vertical main vent pipe until it was valved out. However, these distortions are not

expected to change the overall containment behavior. The phenomena observed in the PANDA P-series tests are generally understood and seem to be reasonable. For example, when a VB opened, some of the wetwell noncondensable gas flowed to the drywell and degraded the PCC performance. As a result, the drywell pressure first rose and eventually leveled off when the pressure difference between the drywell and the wetwell was sufficient to overcome the PCC vent submergence and vent pipe flow resistance. As expected, main vents cleared (to vent the drywell gas directly into the wetwell) when there was insufficient heat removal in the PCCS as a result of either the absence of one PCC unit (out of a total of three) or noncondensable gas injection to the drywell during a test.

Comparing the counterpart tests between the PANDA P-series and M-series, it reveals that the drywell and wetwell pressures in a P-series test were several psi lower than in a similar M-series test. This favorable comparison supports the statement that the design change made for the ESBWR (by connecting the GDCS pool gas space to the wetwell instead of connecting it to the drywell as in the SBWR) is a design improvement, because the wetwell gas space increases as the GDCS pools drain to the RPV. The larger the wetwell gas space, the smaller the wetwell pressure rise from the same amount of noncondensable gas that fills the containment during the normal operation.

In conclusion, based on the above, the PANDA P-series tests provide a valid database to confirm the qualification of the TRACG code for the long-term cooling phase of a LOCA relevant to the ESBWR LOCA analyses.

#### Summary of the ESBWR Component and Integral Systems Testing Programs

The full-size component test data from the PANTHERS/PCC and PANTHERS/IC test programs cover the range of the operational conditions expected in the design-basis LOCAs in the ESBWR. These data are deemed to be adequate for validating the TRACG code regarding the PCCS and ICS performance in the ESBWR (with the understanding that a PCCS condenser in the ESBWR has approximately 35 percent more heat removal capability compared to the PANTHERS/PCC condenser and an ICS condenser has twice the heat removal capability as the single-module PANTHERS/IC condenser).

The integral systems test data from the GIST, GIRAFFE helium, GIRAFFE systems interactions, PANDA M-series, and PANDA P-series testing programs as a whole cover a range of the late blowdown phase, GDCS phase, and long-term cooling phase of the accidents. Strengths and weaknesses of the individual testing program are identified and evaluated. The staff understands the phenomena revealed in the data and concludes that the weaknesses (including some phenomenon distortions) in general do not invalidate the overall reactor vessel and containment response in a LOCA. The combined data from the GIST, GIRAFFE, and PANDA integral systems tests cover the LOCA phenomena and processes defined in the PIRTs for the late blowdown phase, GDCS phase, and long-term cooling phase.

It should be pointed out that each integral systems test provides a set of "valuable" data on the time-dependent, thermal-hydraulic response of its RPV, drywell, and wetwell with the operation of the GDCS, PCCS, or ICS in a LOCA. In order for the TRACG code to properly simulate the

test, the code must have technically-sound conservation equations including the constitutive package and numerics. As a result, the data of an integral systems test are useful for assessing a code against the test for the specific test configuration and initial and boundary conditions. However, to link the integral systems test data to the ESBWR response in a LOCA, an adequate scaling analysis is needed to demonstrate the applicability of the test data to the ESBWR response. Otherwise, a satisfactory TRACG simulation of the integral systems test data should not be used as an indication of a satisfactory TRACG simulation of the ESBWR LOCA response. Review of the GENE scaling analysis is found in Section 3.10 of this report.

Comparing the similar PANDA M-series and P-series tests reveals that a design change introduced in the ESBWR by connecting the gas space of the GDCS pools to the wetwell (instead of the drywell as in the SBWR) seems to be an improvement, because it leads to a lower containment pressure.

Scaling analyses performed by GENE have shown that the test facilities were scaled properly for their intended purpose. All the test facilities meet the top-down scaling criteria. However, the power-to-volume scaling approach introduces scaling distortions related to structural heating/cooling, aspect ratio, and geometrical complexity. These distortions were identified and evaluated by GENE. GENE concluded that they did not exclude the essential phenomena expected to occur in the ESBWR design and that the experimental results are appropriate for TRACG qualification.

The distortions, as identified by GENE, were due to heat transfer from RPV structures, heat transfer to and from the drywell and wetwell structures, and drywell 3-D effects, including drywell mixing, noncondensable gas stratification, and buoyancy/natural circulation. GENE has developed bounding models to address these 3-D effects such that TRACG is able to adequately predict these effects. GENE concluded that the data from the GIRAFFE and the PANDA facilities can be used for scale-up to the ESBWR through the TRACG code. Based on this evaluation, GENE also concluded that the TRACG model used for the containment/LOCA evaluation is conservatively biased.

The staff has reviewed and evaluated the test programs performed initially in support of the GENE SBWR design and finds the testing to be applicable to the ESBWR design, based on the PIRT and scaling analysis found in Section 3.10 of this report. Based on the design description for the ESBWR provided in Reference 15, the staff concludes that no further testing in support of the thermal hydraulic behavior of the design is necessary. Should significant changes be made to the design as described in Reference 15, the staff will reevaluate that conclusion.

### 3.7.2 Staff Calculations

The use of a single code for both the reactor coolant system performance and containment performance triggered the thought that an independent calculation with a containment-specific code would provide a check on this dual use approach. The staff decided to initiate model development and use of the CONTAIN code as a means of performing an independent confirmatory calculation for comparison with the TRACG results.

In addition, the staff decided to also perform confirmatory calculations using its own audit code, TRACE. Through each of these confirmatory analyses it would be possible for the staff to determine whether or not the TRACG results were reasonably representative of the ESBWR response. The staff did not perform a full assessment of its own codes against all of the assessment cases used in the TRACG assessment. Sufficient assessment has been performed, however, to ascertain the performance characteristics of the staff supported codes.

### 3.7.2.1 Staff Independent Analyses and TRACG ESBWR Input Model Review

#### 3.7.2.1.1 Confirmatory Analysis Scope and Review Approach

The GENE ESBWR design, although developed from the ABWR and operating BWR technology, has several unique features developed during the smaller SBWR design effort—the use of a long chimney on top of the core to enhance in-vessel natural circulation, the venturi type nozzle at the GDCCS injection line, the ADS using DPVs, ECCS injection from the GDCCS pools, and containment cooling by the PCCS system. These new features pose challenges to the modeling capabilities of the TRACG code, which is used to model containment phenomenon as well as the reactor coolant system behavior. As a part of the review process, the staff performed a series of independent analyses to evaluate the TRACG code's capability to model these new features.

The ESBWR PIRT and TAPD, Reference 12, have identified many important physical phenomenon. The staff developed a confirmatory analysis matrix to examine the following list of major code modeling features, which are important to analyze the system response of this reactor during a LOCA event.

- in-vessel chimney two-phase flow
- critical flow through the break during blow-down
- mass and energy discharge from the reactor pressure vessel to the containment
- mass and energy transfer in wetwell pool.

Based on the examination of separate effect models, the GDLB LOCA and the MSLB LOCA case were examined using both TRACG and NRC independent audit codes TRACE/CONTAIN. Table 3.7.2.1 lists the calculation matrix and a brief description of the purposes. The staff performed 11 sets of calculations.

Table 3.7.2.1 Confirmatory Calculation Matrix

#	Case Descriptions	Computer Code Used By Staff	Comparison With	Examined TRACG Features
1	Ontario Hydro Steady State Test	TRACG	Ontario Hydro Test Data	Two-phase flow in the chimney partition. Void fraction distribution.

2	Critical Flow Model Examination	TRACG	Edwards Pipe Test Data	Critical flow through the break.
3	Kinetic Energy Deposition Verification	TRACG	Hand Calculation	Energy conservation through the break into the containment.
4	Suppression Pool Energy Deposition	TRACG	PSTF Test	Mass & energy transfer from drywell to wetwell.
5	Gravity Preservation	TRACG	Hand Calculation	Gravity head calculation.
6	Main Steam Line LOCA With Full Feed Water	TRACG	GENE Bounding Calculation	Examine the peak containment pressure and temperature.
7	Main Steam Line LOCA Base Case	TRACG	GENE Base Case Calculation	Staff independent analysis verifying GENE's calculation.
8	GDCS Line LOCA Base Case	TRACG	GENE Base Case Calculation	Staff independent analysis verifying GENE's calculation.
9	Main Steam Line LOCA Base Case	TRACG, CONTAIN TRACE/ CONTAIN	GENE Base Case Calculation	Evaluate short term containment pressure and temperature responses, long term PCCS cooling.
10	GDCS Line LOCA Base Case	TRACE/ CONTAIN	GENE Base Case Calculation	Evaluate short term ECCS performance and long term cooling.
11	Bottom Drain Line LOCA Base Case	TRACG	GENE Base Case Calculation	Evaluate long term chimney collapsed water level and core heatup

### 3.7.2.1.2 Separate Effect Model Evaluation

#### Two-Phase Flow In Chimney Partition

The ESBWR uses chimney partition plates to divide the space in the chimney region into many small square flow channels. Each chimney partition has up to 16 fuel bundles including the corresponding bypass area to provide the inlet flow. The void fraction distribution in the chimney partition has a strong influence on the core flow as the core flow depends on the net gravity driving head between the downcomer and chimney/core regions. In order to examine

the void distribution in the chimney region, Ontario Hydro Technologies in Canada performed 61 cm diameter vertical tube two-phase flow tests, references 11 and 16. The tests covered the pressure range between 2.8 MPa and 6.4 MPa, the temperature range between 230 °C and 280 °C and the void fraction range between 80 percent and 50 percent. The Multi-beam Gamma Ray Attenuation Technique was used to measure the void fraction radial distribution. The test results showed that the void fraction radial distribution was relatively flat and the average void fractions calculated from the axial pressure drop data were found to be in good agreement with those obtained using the Gamma Densitometer.

For the low pressure and low mass flux flow condition, data from Wilson's and Bartolomei's experiments were used to benchmark the TRACG code, Reference 16. In Wilson's test, steam was bubbled through saturated water in a vertical pressure vessel 0.48 m in diameter and 3.66 m high. The Bartolomei tests were performed in a thick-walled vertical pressure vessel, 1.22 m in diameter and about 5 m tall. Water was heated by high pressure hot water coils inside the vessel. The test covers the pressure range up to 4.6 MPa, with the vapor flux between 0.04–0.1 m/s and the void fraction varying from 12 percent to 20 percent.

GENE performed TRACG calculations to verify the code's capability to calculate the axial void fraction and pressure drop for all three tests. The staff examined the TRACG input model for the Ontario Hydro Test facility and independently ran the TRACG code. Figure 3.7.2.1, in Section 8 of this report, shows the calculated void fraction versus test data. The TRACG calculated void fraction closely followed the transient void fraction measured during the test. Therefore, the staff concluded that TRACG has demonstrated its capability to accurately calculate the void fraction and the pressure drop. Accordingly, the uniform radial void fraction distribution in the chimney partition is a reasonable assumption to model the two-phase flow in that region.

### **Critical Flow Model Verification**

The choked flow rate through the break determines the pressurization rate of the containment and the two-phase water level in the chimney. The accuracy of the model significantly affects the outcome of the LOCA evaluation and the containment peak pressure and temperature analyses. TRACG uses the equilibrium critical flow model based on a semi-empirical approximation of the choking criteria derived from the general one-dimensional, two-phase fluid field equations. From the input, a user can turn on the choke option at any given cell face. GENE has validated the model using several tests and experimental data.

The Edwards Pipe blowdown test has been used as a standard for evaluating critical flow models for rapid depressurization. The test section for this experiment consisted of a 4.096 m long horizontal pipe, with an inner diameter of 0.073 m, filled with liquid, heated, and pressurized to 7.0 MPa. The saturation pressure corresponding to the initial liquid temperature was about 2.4 MPa. At time zero, a glass plate covering the end of the pipe was broken, and the pipe depressurized through the open end of the pipe in approximately 0.6 seconds. As this test covers the choked flow for subcooled liquid and saturated two-phase mixture, it was selected as the confirmatory case to evaluate the TRACG critical flow model.

A TRACG model consisting of a FILL component, a 20-cell horizontal PIPE component, and a BREAK component were used to simulate the test. The results show the critical flow model was turned on at the outlet cell face of the PIPE component during the blowdown.

Figure 3.7.2.2, in Section 8 of this report, shows the comparison between the measured void fraction and the TRACG results. Good agreement between these two sets was observed. The measured pipe internal pressure and the TRACG results are shown in a similar trend. This confirmatory analysis case verifies not only the capability to calculate the choked flow, but also the interfacial heat transfer and other physical models.

Therefore, this case further demonstrates that TRACG has the capability to accurately calculate the critical (choked) flow through a break.

### **Kinetic Energy Deposition**

Historically, the TRAC series of codes eliminated the kinetic energy term from the energy equations through algebraic manipulations involving the momentum equation. In that form, the flow work in the energy equation was of a nonconserving form, and energy balance errors could occur. This simplified approach has been identified as one obstacle when the TRAC series of codes are used to model the interaction between the RPV and the containment during the blowdown phase. With this deficiency, a computer code may significantly underestimate the energy discharge into the containment during a LOCA, thus resulting in nonconservative containment peak pressure and temperature predictions.

TRACG avoids this problem by retaining the kinetic energy term in the energy equations for both the vapor and liquid phases. The internal energy and the kinetic energy are lumped in both time and spacial derivatives. Therefore, the kinetic energy of the break flow transported into the containment during the blowdown period should be preserved. In order to verify the proper implementation of the kinetic energy convection in TRACG code, a simple test problem was developed. As shown in Figure 3.7.2.4, in Section 8 of this report, a straight horizontal PIPE component with a flow area of  $0.5 \text{ m}^2$  and a length of 0.6 meter is modeled. An orifice with a flow area of  $1.0\text{E-}3 \text{ m}^2$  is located in the middle of the pipe. Two BREAK components set up the pressure boundary conditions at 5 MPa and the entire pipe is filled with saturated stagnant water. Then, the pressure of one of the BREAK components ramps down to atmospheric pressure within 50 seconds. The choked flow through the orifice is stabilized around 80 seconds. The vapor and liquid flowing through the orifice reach the speed of sound. After passing through the orifice, both vapor and liquid slow down and the kinetic energy is converted into fluid internal energy.

If the code properly conserves the energy and accurately models the kinetic energy conversion, the inlet and outlet total enthalpy and work should be identical. This TRACG case was run to 100 seconds and all the system variables are stabilized. A hand calculation was performed to

the RPV to the containment, which is essential to model the ESBWR containment pressurization during a LOCA.

### **Suppression Pool Mass and Energy Transfer**

One of the major containment phenomena is SP steam condensation. TRACG was developed primarily for modeling vessel internal flow and heat transfer. It was not intended to be used for containment analysis. In order to model suppression pool mass and energy transfer, a special modeling approach was used. As shown in Figure 3.3-1 of Reference 11[[

]].

During the MSLB LOCA, as the blowdown flow decreases, the level in the main vent rises, sequentially closing off the horizontal rows of vents. When the flow stops in each of the lower two rows of horizontal vents, the fluid in that level of the pool is [[

]]. This modeling approach has been developed largely based on the PSTF test documented in Reference 16. Therefore, the PSTF full-scale vent test case (5803 series) was selected as the basis to examine TRACG's capability to model the SP condensation.

The TRACG model consists of a VESSEL component, combined with several one-dimensional components. The VESSEL component was used for both the drywell and wetwell, with the top level used to represent the drywell volume. The geometry of the PSTF 8-degree section of the suppression pool was preserved in TRACG modeling using a sector of the outer two rings of the VESSEL component. The TRACG result is shown in Figure 3.7.2.8a in Section 8 of this report. The temperature of Volume 5 of the VESSEL model is compared with the measured test data. It is confirmed that TRACG overpredicts the measured temperature profile by approximately 5 °C. Thus, the result confirms that the PSTF assessment was reasonably done and the nodalization developed through the PSTF assessment is applicable to the ESBWR configuration.

### **Gravity Head Preservation**

The ESBWR TRACG GDCS line LOCA model used a 3-D VESSEL component to model both the RPV and the containment. As shown in Figure 2.7-1 of Reference 11, the VESSEL component is divided into [[ ]] radial rings and [[ ]] axial levels. The bottom [[ ]] levels model the reactor vessel and vessel internals, while levels [[ ]] model the containment, including the drywell, GDCS pools, SP, and PCCS drain tanks. Within the 3-D vessel

component, all containment volumes have an arbitrary higher elevation than their real elevations. As the gravity driving head is the dominant force to inject the GDCS pool water into the RPV, it becomes a concern whether the gravity head has been correctly calculated using this modeling approach. A further evaluation of the TRACG code concluded that if two cells within a 3-D VESSEL component only interact with each other through another 1-D component, then the actual elevation difference between two cells must be reflected by the gravity terms defined by the connecting 1-D component.

In order to verify this code feature, a TRACG test problem was set up to examine the flow through a "U" tube with two pools connecting with each end of the PIPE component. As shown in Figure 3.7.2.5, in Section 8 of this report, a 3-D VESSEL component has two pools. One is located at level 2 and ring 1; another is located at level 4 and ring 4. Both pools have the same initial water level and cell center pressure. The top of level 3 is assumed sealed with a zero axial flow area. The two pools are connected by a 5 cell "U" tube. The split of the 3-D vessel component into two volumes with two identical pools should have zero flow rate through the connecting TRACG 1-D PIPE component. The TRACG calculation results show that the flow through the 1-D PIPE is very close to zero. The two pools have the same actual elevations with respect to the "U" tube PIPE component, although they appear to be at different elevations within the 3-D VESSEL component. Therefore, the ESBWR ECCS model preserves the gravity head and the actual elevations with the 1-D component solver.

In addition, this test problem demonstrates that the TRACG code can correctly pass the 3-D cell pressure to the connecting 1-D component cell for a given 1-D connection relative elevation with respect to the 3-D cell bottom cell face.

#### 3.7.2.1.3 Integral Effect Evaluation Using TRACG

GENE submitted two TRACG base input decks for the staff to review, the GDCS LOCA ECCS evaluation model and the MSLB LOCA containment evaluation model. The GDCS line LOCA ECCS model evaluates the effectiveness of the gravity-driven injection and calculates the PCT, minimum water level above the core, and the containment responses. The MSLB LOCA containment model predicts the containment peak pressure and temperature. The staff ran both cases with TRACG04 independently and examined the input and the output of the analysis.

#### GDCS Line Break LOCA

The GDLB scenario is a double-ended guillotine break of a GDCS drain line. There are three GDCS pools in the ESBWR containment, supplying four divisions of GDCS to the vessel. Each drain divides into two branches before entering into the pressure vessel. Each branch has a check valve followed by a squib-operated injection valve, and finally a nozzle in the vessel wall to limit the blowdown flow in case of a break. The GDCS break is assumed to occur in one branch, between the squib-operated valve and the nozzle entering the vessel. GENE has demonstrated that the GDCS line LOCA is the most limiting case to challenge the ECCS system driven by gravity and the pressure difference between the wetwell and the reactor pressure vessel.

In order to model the in-vessel fluid flow and the distribution in detail, GENE developed a specific TRACG model to evaluate the effectiveness of the ECCS injection. As shown in Figure 2.7-1 of Reference 17, a 2-D TRACG VESSEL component is used to model both the RPV and the containment. The first [ ] levels model the reactor vessel, while levels [ ] model the containment. The radial nodalization is primarily determined based on in-vessel component physical structures. There are a total of [ ] rings with the [ ] inner rings for the reactor core region and [ ]. [ ] TRACG CHAN components are used to model the core with the hot channel located in the first ring, which has a bundle power peaking factor of 1.4791. The radial direction flow area [ ] are set to zero to model the lumped 1-D two-phase flow through the chimney partitions. Above the upper plenum, [ ]. The main steam lines, DPVs, SRVs, and main steam isolation valves are modeled using typical TRACG PIPE, TEE, and VALVE components.

The containment is modeled with the same radial nodalization which is determined by the reactor vessel radial dimensions. Therefore, the TRACG VESSEL cell volume fractions and flow area fractions are set to significantly greater than 1.0 to preserve the total fluid volume in each containment level. The axial elevations from level [ ] reflect the physical geometry boundary. [ ]

[ ] The GDCS pools are modeled by [ ] The PCC and IC heat exchanger are modeled by PIPE and TEE components. The vertical PIPE, with constant external heat transfer coefficients and outside temperatures, represents the heat exchanger tube bundles.

The staff examined the TRACG input model and independently performed the GDLB LOCA calculation. The results were found identical to what were documented in Reference 11. Several code features and modeling practices are evaluated in detail and documented below.

### Core Power Model

Although the TRACG code has the capability to model the core power history during a LOCA using its 3-D kinetics model, only the power versus time table with a fixed axial power distribution was used for both ECCS LOCA and containment LOCA analysis. GENE indicated in response to RAI 4 and RAI 325 that GENE has calculated the core power history considering both decay heat and fission power after the scram signal. GENE used its NRC-approved method, SAFER-GESTR, Reference 30, to calculate decay heat with the following improvements:

- decay heat from fission products were updated to conform with the ANSI/ANS-5.1-1994 standard, Reference 39, which the staff previously approved in Reference 3
- the fuel cycle parameters were conservative, bounding values rather than nominal values
- two-sigma data uncertainty from the standard was used

- new, more conservative evaluations of miscellaneous actinides and structural activation products were used.

Even though the method to generate the decay heat table is acceptable, the base GDCS LOCA model assumes the scram at time zero, when the break occurs, without considering the lag between the high drywell pressure signal and the scram. In response to the staff's concern, GENE estimated a scram delay of [ ] and performed a sensitivity study assuming full power operation during the delay of the scram. The analysis shows that the Level 1 trip occurs at about [ ] earlier than the baseline case. The resulting minimum static collapsed water level in the shroud only dropped [ ] during the first 2000 seconds into the LOCA.

In addition, the staff found that the base case did not include a 2 percent power measurement uncertainty which was later included in GENE sensitivity cases.

Therefore, the staff concluded that the TRACG code has the capability of modeling the core power history for ESBWR LOCA evaluation. During the design certification review stage, the ECCS baseline model should justify the scram delay time and the power measurement uncertainty. In addition, the quick closure of the MSIVs while control rods are being inserted may increase the total core power due to void collapse. At the design certification stage, GENE should evaluate the effects of void collapse for GDLB and BDLB LOCA cases.

### **Minimum Water Level Inside The Chimney Partition**

TRACG models the chimney region with [ ]. The localized void fraction in different chimney partitions is smeared away. This averaging assumption is employed by the TRACG 3-D VESSEL two-phase level tracking algorithm to calculate the two-phase water level location in the chimney during the GDCS LOCA transient. For those chimney partitions above high power bundles, it is expected that the void fraction in the chimney is different from the averaged value and the baseline model may predict nonconservative minimum water level above the core.

In response to the staff's concern, GENE performed additional parametric analysis to examine the effect of the bundle power distribution on the minimum chimney water level. GENE set the radial power peaking factor of [ ] fuel bundles [ ]. The other radial peaking factors were [ ] for [ ] bundles feeding the chimney region [ ] for the [ ] feeding the chimney region [ ]. The results demonstrated that the minimum static head calculated by the baseline model is greater than that calculated in the parametric study. The base model overestimated the minimum static head [ ], which is [ ] percent of the margin in the static head. In addition to the impact on the minimum static head, GENE observed enhanced two-phase flow through the hot channel due to additional two-phase driving head in the chimney partition, the so-called "drafting" effect.

Independently from GENE, the staff performed a TRACG run using a different but conservative approach to analyze the two-phase flow in the chimney partition above the hot channel. Instead

of lumping all the fuel bundles in ring 1 into one channel component with the maximum radial power peaking factor, a PIPE component representing 1/4 of a regular chimney partition is connected with the hot channel and the upper plenum. It was conservatively assumed that the bypass flow does not join the channel outlet flow. The results showed a reduction of the minimum chimney static head and the "drafting" effect.

In conclusion, the staff believes that TRACG code and the baseline GDCS LOCA model are able to predict the average static water head in the chimney partition. Nodalization studies will be necessary at design certification to calculate the minimum water level in the chimney partition.

### **Hot Channel High Void Fraction Flashing**

Based on the GDLB LOCA analysis, GENE states that the ESBWR core would never be uncovered during a LOCA since the two-phase water level is always above the top of active fuel region, and no core heatup, no dryout, and no boiling transition would occur. Staff independent analysis identified that the hot channel, which was modeled by CHAN0011, experienced high void fraction flow for a period of 30 seconds starting from 400 seconds into the LOCA event. The maximum channel inlet and outlet void fractions were [[ ]] and [[ ]] respectively, while the void fraction in the heated region was about [[ ]]. Figure 3.7.2.6, in the figures section of this report, shows the hot channel outlet void fraction during the transient. The staff was concerned with the possibility that the ESBWR core experiences boiling transition, and that film boiling may cause core heatup. Consequently, the staff requested additional analyses from GENE to identify the maximum duration for which the hot channel experiences high void fraction flashing and the minimum thermal margin.

In response to the staff's request, GENE analyzed three additional LOCA cases, MSLB LOCA, GDCS LOCA, and BDLB LOCA, with conservative assumptions of 102 percent of rated power prior to the break and delayed scram time. As opposed to the baseline model, the TRACG input models defined all the fuel bundles inside ring 1 as the hot channel.

The staff agrees with GENE that a hot channel "drafting" effect does exist. However, defining all of the fuel bundles in ring one as the hot channel would overestimate the effect and the results may tend to be nonconservative. The staff requested further justification. GENE modified TRACG04 and performed the GDCS LOCA base case analysis. The newly calculated minimum thermal margin is shown in Figure 3.7.2.7 in Section 8 of this report. The minimum value of the thermal margin is above 2.0 throughout the transient, demonstrating that film boiling does not occur. Based on these calculations, the staff agrees with GENE that no core heatup is predicted during a LOCA event.

### **GDCS Pool Over Pressure**

According to the ESBWR design, the GDCS pool gas space is connected with the SP gas space through three large-diameter vent pipes. Therefore, the pressure should be equalized during normal operation. However, an examination of the GDCS LOCA baseline calculation revealed that the TRACG code calculated a higher GDCS pool gas space pressure than the SP

pressure due to the simplified GDCS pool nodalization. The unrealistic pressure results in a higher initial inventory of air in the GDCS gas space, which causes slightly higher GDCS air space pressure during the GDCS phase of injection. GENE examined the input model and indicated that this is caused by the coarse nodalization of the GDCS pool. For the TRACG code, if there is a water level in the cell that is higher than the cell center, the pressure will be correctly calculated at the cell center, accounting for the static head above the cell center. The cell center pressure will be higher than the pressure in the gas space above the level by that static head. Since in TRACG the gas space pressure above the water level in the cell is the same as the cell center pressure, it is overestimated. The initial noncondensable volume at the top of the GDCS pool is of the order of 80 m<sup>3</sup>. The error in the initial noncondensable inventory in the GDCS pool is of the order of 10 percent of the total mass in the 80 m<sup>3</sup> volume. The wetwell gas space volume is of the order of 4500 m<sup>3</sup>. Thus, the fractional error in the total noncondensable inventory in the wetwell gas space plus the GDCS pool is negligible.

Therefore, the staff agrees that TRACG acceptably calculates the cell center pressure and the overestimation of the noncondensable mass in the GDCS pool can be resolved using a different nodalization. The additional amount of noncondensable gas mass is negligible comparing the total amount of initial noncondensable gas mass in the wetwell and GDCS pool air space.

#### **Wetwell and GDCS Pool Connecting Vent Pipe Model**

There are three vertical vent pipes connecting GDCS pool gas space with the wetwell gas space. The TRACG GDCS LOCA model lumps two GDCS pools [ [ ]], and the third pool, which has a broken GDCS injection line, is modeled by a separate volume. Two TRACG PIPE components, PIPE42 and PIPE43, are used to model the vent pipes. The staff found that the volume and the flow area of these two PIPE components are identical, however one of them should be twice as large as the other. Considering a very small pressure difference between the GDCS air space and the wetwell, this modeling practice does not affect the results significantly. However, during the design certification stage, correct vent pipe volume should be used.

#### **PCCS Pool Modeling**

Instead of explicitly modeling the PCCS and ICS pool on top of the drywell, GENE models the heat transfer between the PCCS tube bundle external surface and the pool with a constant heat transfer coefficient and a constant temperature. Although the initial pool temperature is 316.5 K (110°F), the bundle surface bulk fluid temperature is set to 378 K (220°F). During the blowdown period, which is between 0 and 600 seconds into the transient, the dominant mass and heat transfer is steam condensation inside the SP. The impact of PCC operation on the drywell pressure and the wetwell pressure is negligible. Therefore, GENE believes that it is not important to realistically model the heat transfer between the pool and the PCCS heat exchanger. During GDCS injection, since the noncondensibles have been largely swept into the wetwell and the pressure is strongly affected by the VB operation, PCCS operation also does not significantly affect the course of GDCS injection. After the GDCS injection, the pool temperature gradually increases to the saturation temperature and the assumption of 378 K (220°F) for the fluid temperature is acceptable. [The assumption of a constant heat transfer

coefficient is reasonable for the first 2000 seconds while the PCCS heat exchanger is covered.] For transients beyond 2000 seconds, the heat transfer coefficient is subject to change when the condenser tubes are gradually uncovered due to pool boiloff.

Therefore, the staff concludes that the current PCCS pool modeling approach for the first 2000 seconds of ECCS LOCA evaluation is reasonable. During the design certification stage, if the ECCS evaluation model is used beyond 2000 seconds, additional VESSEL levels need to be added on [[ ]], and the pool needs to be modeled in the same fashion as it is done for the containment/LOCA model.

### MSLB LOCA Analysis Using TRACG Code

As described in Section 3.7.2.1.2 of Reference 11, GENE used [[ ]] component to model the entire ESBWR containment and the RPV for containment LOCA analysis, as shown in Figure 3.7-1 of Reference 11. The reactor vessel was coarsely modeled by [[ ]] and [[ ]] levels. [[ ]].

The model includes the DPV lines and SRV lines. The drywell to wetwell vents are modeled by several TEE components and VALVE components.

The staff independently ran the TRACG code with the MSLB LOCA model and produced the same results as what was submitted in Reference 11. The following two modeling features are examined in detail.

### **Heat Structure Modeling**

The ESBWR RPV is made of carbon steel with a thickness of approximate 184 mm. Outside the steel vessel there is an air gap of 250 mm, and then the reflective type of thermal shield with a thickness of 90 mm. Further out stands the 160 mm thick vessel shield which is made of low alloy structural steel. In order to model heat conduction through these structures, GENE's MSLB containment/LOCA base deck defined a [[ ]] thick heat structure around the RPV. The thermal properties are assumed to be uniform across the heat structure. The inner surface of the heat structure is assumed to have an initial temperature equal to the vessel internal fluid temperature. GENE performed a parametric study, replacing the [[ ]] heat structure with a thickness of [[ ]], that demonstrated there was a nonphysical heat sink effect. However, the impact on peak drywell pressure was found to be small, with a pressure increase of [[ ]]. Therefore, the staff agrees that the [[ ]] heat structure does not significantly alter the peak pressure prediction. However, during the design certification stage, the separation of the vessel shield, the reflective thermal insulation layer, and the air gap from the lumped heat structure is considered necessary.

### **Feedwater Mass And Energy Discharge**

In Section 2.2.1.2 of Reference 11, GENE defines the MSLB LOCA scenario. It was assumed that the feedwater pump is tripped and the feedwater flow is lost after the break. From the perspective of LOCA ECCS performance evaluation, the assumption leads to a conservative PCT evaluation as it reduces the available coolant inventory. For containment analysis, the feedwater carrying the feedwater heater train stored energy significantly increases the mass and energy discharge through the break into the containment. The assumption of the loss of feedwater flow used by GENE for the current design is nonconservative, resulting in underestimation of the maximum containment pressure and temperature. The feedwater flow assumption should be justified at the design certification phase.

In order to examine the impact of the feedwater system mass and energy discharge into the RPV, the staff independently performed a sensitivity study using a bounding assumption for the feedwater mass and energy discharge. Without detailed design information for the feedwater heater train, the staff assumed that the feedwater injection lasts for 600 seconds and the temperature ramps down linearly from the initial feedwater temperature to the saturation temperature at the containment design pressure limit. The calculation was done using the baseline MSLB LOCA model. The result is shown in Figure 3.7.2.8 in Section 8 of this report. The peak drywell pressure of [[ ]] occurs about [[ ]] into the transient and is greater than the bounding value calculated by GENE in Reference 11, [[ ]]. Consequently, GENE performed additional analyses in response to the staff's concern. GENE assumed that the hot water residing in the feedwater heater system (98,144 kg, 215,917 lb) prior to the LOCA is injected into the RPV [[ ]]. Using the baseline MSLB model, GENE predicted a [[ ]] peak drywell pressure increase. The results show the feedwater mass and energy release during the MSLB LOCA increases the peak drywell pressure by about [[ ]]. There is also a possibility that the wetwell volume is flooded and the noncondensable gas is purged to the drywell. Should significant amounts of noncondensable gas be discharged into the drywell volume, the PCCS performance may be degraded.

Without detailed feedwater heater system design information, both the staff and GENE had to make assumptions about the mass and energy discharge from the feedwater heater system. The bounding containment peak pressure and temperature will be evaluated during the design certification stage after the feedwater heater system design is finalized. If the evaluation indicates that the code application range is exceeded or that a new scenario, such as wetwell flooding, has not been examined during the preapplication stage, the staff may choose to review the TRACG code for its new use.

#### Bottom Drain Line Break LOCA Analysis Using TRACG Code

The BDLB is one of the three design basis LOCA scenarios defined by GENE. The initial short term scoping analysis performed by GE indicated that the GDLB is the most limiting case in terms of the minimum chimney collapsed water level. Therefore, GENE did not include the BDLB LOCA case in Reference 11. Concerned about the long term ECCS behavior during a BDLB break event, the staff requested an analysis of the BDLB LOCA case up to 72 hours as RAI 183. GENE responded to this RAI and performed the long term BDLB LOCA analysis using the MSLB LOCA model with break location changes. GENE found that the bypass region was uncovered at about 7 hours. The staff therefore requested the TRACG base input model for the

BDLB LOCA case for independent verification. After the input model was submitted, the staff independently ran the TRACG code with the BDLB LOCA model and produced the same results as were submitted by GE in response to RAI 183. The following two issues are discussed in detail.

### **Possible Core Uncovery And Heat Up**

The staff's major concerns are potential core uncovery during the long term cooling stage of the BDLB LOCA and the potential for subsequent core heatup. The staff found that the calculated minimum collapsed water level in the chimney is zero around 7 hours into the transient for the base case and confirmed that the water level in the bypass region dropped below the TAF. However, the in-channel two-phase level did not drop below TAF. As shown in Figure 3.7.2.35 in Section 8 of this report, the top node of the average channel component active fuel region experienced a maximum void fraction of about 65%. Except for the bypass region, the core remains covered.

Although the average channel remains covered during the entire transient and there is no core heatup, the calculated zero minimum chimney water level is not consistent with GENE's determination that the GDCS LOCA case is the most limiting case for ECCS evaluation. In addition, the base case does not differentiate the hot channel from the core average channel. It is unknown whether the hot channel is subject to dryout. Therefore, GENE performed sensitivity studies of collapsed water level versus lower drywell volume. Their calculations indicated that, with a 200 m<sup>3</sup> volume reduction in the lower drywell volume, the ECCS system could provide sufficient coolant to flood the drywell to the elevation of 1 meter above TAF. For the GDCS LOCA case, the minimum collapsed water level in the chimney region is 1.84 m throughout the entire 72 hours of the transient. Therefore, GENE has demonstrated that with a revised lower drywell volume, the ECCS will have the capability to prevent core uncovery and core heatup for all three design basis LOCA scenarios. More detailed evaluation will be performed by the staff performed during the design certification stage to verify that the core remains covered for the final ESBWR design configuration.

### **Modeling Application Procedures**

For the ECCS performance evaluation during the long term cooling stage, GENE has performed BDLB and GDCS LOCA analyses with both the reference design and with the reduced drywell volume configuration. GENE demonstrated that there was sufficient collapsed water level above the core with the reduced drywell volume for the GDCS and BDLB cases. The BDLB case eventually relied on ECCS injection through the suppression pool equalizing line to maintain the level. It was observed that the collapsed water level is sensitive to the pressure balance between the reactor pressure vessel, drywell and wetwell. However, all the long term phenomenon were analyzed using the CONTAINMENT LOCA model documented in Ref. 11, which was specifically tailored to maximize the containment pressure and temperature. At this point, GENE has not demonstrated that the CONTAINMENT LOCA model and relevant application procedures are applicable to the ECCS long term performance evaluation and no uncertainty analysis has been done to quantify the minimum water level. Therefore, for the design certification, appropriate TRACG application procedures should be developed to

conservatively calculate the collapsed water level in the chimney above the hot channel for the three break locations, MSLB, BDLB and GDLB. The procedures and the associated uncertainty analysis methodology should be applicable to both short term and long term LOCA events (up to 72 hours).

### 3.7.2.2 CONTAIN

Staff predictions of the behavior of the GENE ESBWR containment design following an MSLB were obtained using the CONTAIN computer code. These predictions were compared with the GENE predictions from the TRACG baseline containment analysis presented in Reference 11. In order to compare the CONTAIN containment thermodynamic predictions with the TRACG containment predictions from GENE, the mass and energy releases obtained from the TRACG code, up until the time cooling water is determined to enter the RPV, were used as input for the CONTAIN containment analysis. It should be noted that the TRACG analysis includes models of the primary system and containment. During this initial period, choked flow is expected to exist at the break location. Consequently, the break flow during this time is not dependent on containment pressure conditions. During this initial time period, the TRACG calculated mass and energy flows through the DPVs and the SRVs were also provided as input into CONTAIN.

After the initial time period when the break mass and energy conditions were input into CONTAIN, the CONTAIN analysis uses an RPV volume to calculate the mass and energy releases to the containment. The thermodynamic conditions for the RPV at the transition time from choked flow were obtained from the TRACG calculations. Consequently, the CONTAIN code could calculate the mass and energy flowrate from the RPV to the containment through the break, the DPVs and the SRVs. Based on their setpoint actuation conditions, the DPVs were determined by TRACG to open during the initial time period when the mass and energy flow is input into CONTAIN. Consequently, the DPVs are assumed to be fully open at the end of the initial time period; however, SRV operation after the initial time period is determined by the pressure dependent valve operating characteristics input into CONTAIN.

Three CONTAIN models were used to analyze the ESBWR containment. One model divides the drywell into five vertical volumes, a second model divides the drywell into ten volumes, and a third model uses a single drywell volume. The results from the three models are presented in order to provide a sensitivity assessment for noncondensable gas redistribution in the ESBWR containment and the resulting effects on drywell-wetwell vacuum breaker operation, and to assess the PCCS heat exchanger long-term heat removal performance.

For the model with one drywell volume, the volume of the drywell is equal to the sum of the volumes of the five drywell volumes. Similarly, for the CONTAIN model with ten drywell volumes, the volumes of the drywell volumes are half of those used in the five volume model .

The initial containment conditions for the three CONTAIN input models are consistent with the conditions specified for the TRACG containment analysis baseline results described in Reference 11. The CONTAIN modeling is also consistent with the TRACG containment model. Specific characteristics of this model are listed below.

- (1) The ten vents between the drywell and suppression pool are modeled as a single volume with one entrance interface and three exit interfaces to the suppression pool at the three horizontal exit elevations.
- (2) Three GDCS pools are modeled. A valve in the GDCS line between each tank and the RPV is opened at 539 seconds after the MSLB. The time at which this valve opens is obtained from the TRACG analysis. Flow from each GDCS tank to the RPV is determined by CONTAIN using flow path junctions.
- (3) The PCCS heat exchangers are available and operational during and after the initial blowdown period. A flow path representing the PCCS gas vent line connects the top of the outlet plenum and the wetwell suppression pool. The CONTAIN model will account for the condensation of steam flowing out of the PCCS gas vent line as a result of contact with the suppression pool. Water condensed in the PCCS heat exchangers is directed to the PCCS outlet plenum volume. A flow path connects the outlet plenum to the drain tank volume. Flow can exist from the drain tank to the RPV volume after the valve between the drain tank and the RPV opens at 519.66 seconds. The time at which this valve opens is obtained from the TRACG analysis. Consistent with the GENE assumptions for the TRACG baseline containment analysis, four PCCS heat exchangers are assumed available. The CONTAIN model has the ability to perform analyses assuming the availability of three or four PCCS heat exchangers.
- (4) Condensation in the interior surface of the PCCS heat exchanger tubes is calculated using the CONTAIN heat and mass transfer model, which accounts for the presence of noncondensable flow in the steam flow. The condensed liquid is added to the outlet plenum using the CONTAIN "filmflow" calculation, which tracks the condensation film thickness on the inner tube surfaces. The outer surfaces of the PCCS tubes are placed in contact with a constant temperature sink, equivalent to the boiling temperature in the cooling pool, with an input boundary condition heat transfer coefficient of 4500 W/(m<sup>2</sup>-K) to simulate boiling conditions on the PCCS tube exterior. The PCCS heat exchanger model is consistent with the CONTAIN model described in Reference 41 which was developed for use with the GENE SBWR and compared against GIRAFFE test results.

This calculation method does not allow for the determination of the PCCS cooling pool conditions within the CONTAIN calculations. Consequently, the reduction of the water level in the cooling pool was calculated external to the CONTAIN calculations. However, the water level calculation uses the heat removal rates calculated by the CONTAIN code. Specifically, the cooling pool water mass loss was calculated using the following equation, which assumes that all the heat added to the cooling pool by the PCCS heat exchangers will result from pool boiling.

$$m_{\text{pool boiling}} = Q_{\text{to cooling pool}} / ( h_g \text{ (at 373.15 K) } - h_f \text{ (at 316.5 K) } )$$

The saturated vapor enthalpy,  $h_g$ , is obtained for the saturation conditions of 100 °C at 1 atmosphere which is equivalent to outside atmosphere conditions. The liquid enthalpy,  $h_f$ , is determined at the initial water temperature of the PCCS cooling pool.

- (5) The drywell-wetwell VBs are modeled as one lumped pressure dependent flow path. Consistent with the assumptions in the TRACG containment model for the GENE baseline analysis, the current analysis assumes the availability of three VBs; however, the CONTAIN input model can be run assuming the availability of two or three VBs.
- (6) During the initial time period after the MSLB, i.e. before 517 seconds, the break mass and energy are added to the break drywell volume using a source table. The break mass and energy release is obtained from the TRACG analysis. After the initial time period, the break blowdown is calculated by CONTAIN using a flow path junction from the RPV volume.
- (7) The mass and energy flow from the DPVs during the initial time period before 517 seconds are added to the appropriate drywell volume using a source table. The mass and energy releases are obtained from the TRACG analysis and reflect that code's determination of setpoint conditions and actuation delays. After the initial time period, the mass and energy flow through the DPVs are calculated by CONTAIN using a flow path junction to the RPV volume.
- (8) The SRV flows during the initial time period are obtained from the TRACG analysis. The mass and energy flows are added to the corresponding CONTAIN SRV discharge piping volume modeled in CONTAIN using a source table. After the initial time period, flows through the SRVs are determined by a pressure dependent flow junction modeled in CONTAIN.
- (9) Heat slabs have been added to the CONTAIN input using the surface areas, thicknesses, and material definitions contained in the TRACG model. The outer wall atmospheric boundary temperature and heat transfer coefficient were also obtained from the TRACG model.
- (10) Natural convection is used in the CONTAIN analysis to calculate heat transfer coefficients for all structures in the containment volumes by setting the forced convection velocity equal to zero. Forced convection is allowed, however, inside the PCCS heat exchanger tubing.
- (11) The procedure for calculating RPV vapor formation presented in Reference 41 represents an upper end calculation of long-term containment response. This approach was used because the previous version of the CONTAIN code did not have the ability to calculate boiling conditions such as are present in the RPV. Consequently, after the initial time period, which lasts 517 seconds, vaporization in the RPV is calculated assuming the maximum amount of vaporization due to decay heat addition. The vaporization in the RPV volume is set equal to:

$$m = q_{\text{decay heat}} / ( h_g(\text{at } 3 \times 10^5 \text{ Pa}) - h_f(\text{at } 316.5 \text{ K}) ).$$

The steam enthalpy value is assumed at a typical long-term containment pressure of  $3 \times 10^5$  Pa. The liquid enthalpy is assumed consistent with the GDCS pool temperature

of 316.5 K (110 °F). This mass and energy release rate is added to the RPV volume in a source table. At the same time, liquid mass is removed from the RPV pool at 316.5 K (110 °F) to preserve mass and energy balance. Flows from the RPV to the drywell break volume are calculated for both the break and DPV flow paths. Similarly, flow from the RPV through the SRVs are calculated by CONTAIN using the pressure dependent flow paths.

The analyses using the CONTAIN models with five or ten drywell volumes were run assuming that vapor formation in the RPV starts at 517 seconds as indicated above. The analysis using a single volume drywell was executed assuming a delay in the generation of vapor in the RPV volume. The vapor was assumed to stop being generated between 600 and 1500 seconds; during that time the decay heat is added directly to the water in the RPV. This assumption was made to approximate the delay in vapor flow from the break that was predicted by the GE TRACG model, which contains a detailed two-phase model of the RPV. The delay in vapor generation is believed to be attributed to the cooling effect of the GDACS flow entering the RPV. The delay in vapor generation also provides a greater possibility for drywell-wetwell vacuum breaker operation resulting from steam condensation in the drywell. A single drywell volume also results in a more uniform concentration of noncondensable gas than the multi-volume drywell models. With the multi-volume drywell models, the noncondensable gas is calculated to accumulate in the lowest elevation dead-ended drywell volumes.

- (12) Consistent with the GENE TRACG containment model, the CONTAIN input has included a bypass flow path of  $1 \times 10^{-4} \text{ m}^2$  between the drywell and wetwell.
- (13) During the performance of the ESBWR analyses using all three CONTAIN models, numerical solution problems were encountered with the gaseous flow connection between the drywell and the PCCS drain tank. In the ESBWR design, the top of the PCCS drain tank is fully open to the drywell. Unfortunately, because of limitations in the CONTAIN numerical solution, the code would "stall" and stop execution if the full flow area of 2 to 3  $\text{m}^2$  was input. The solution could only be successfully executed if this flow area was set equal to zero or a small value.

#### 3.7.2.2.1 Results

The ESBWR containment analysis for an MSLB, performed by GENE using the TRACG computer code, has been compared to MSLB analyses performed by the staff using the CONTAIN computer code.

#### **Comparison of CONTAIN and TRACG Predictions**

This section compares the results of the three CONTAIN analyses to each other and to the results reported by GE using TRACG.

Pressure Predictions - The drywell and wetwell pressures predicted by the CONTAIN five and ten drywell volume models are very close in value, however, these results differ from the one

drywell volume CONTAIN analysis results. It is interesting to note that containment pressures for the five and ten drywell volume CONTAIN models are predicted to be lower than the TRACG calculation. In contrast, the containment pressures for the one drywell volume exceed the TRACG results in the short-term, but drop below the TRACG predictions in the long-term. The multi-volume drywell models provide a better model of the temperature variations which can occur in the tall drywell compartment.

The multi-volume approach can also account for noncondensable gas distribution effects in the containment. Concerns regarding noncondensable gas distribution were the primary reason for performing a one-volume drywell analysis. The one-volume drywell model would produce a uniform noncondensable gas distribution in the drywell and could affect the distribution of the noncondensable gas in the drywell and wetwell. In fact, the one-volume drywell model resulted in the transfer of almost all the drywell nitrogen to the wetwell early in the calculations; whereas, in the five and ten drywell volume models, nitrogen accumulated in the wetwell and the lower drywell volumes.

It should be noted that the one-volume drywell analysis with an RPV vaporization delay did predict a drop in drywell pressure below wetwell pressure resulting in drywell-wetwell vacuum breaker operation. However, when a vaporization delay was introduced into the multi-volume drywell models, the drywell pressure did not fall below the wetwell pressure and vacuum breaker operation was not predicted.

All CONTAIN analyses predicted lower long-term pressure than TRACG even though tabular inputs for break, DPV and SRV flows obtained from TRACG were used by CONTAIN for the short-term, 0 to 517 second, period. After the short-term period, the "best estimate" assumptions for mass and energy releases were used to calculate the CONTAIN mass and energy releases. However, the CONTAIN analyses did not employ many of the conservative modeling assumptions used in TRACG, nor was CONTAIN able as accurately model the boiling heat transfer in the RPV liquid region and the PCCS cooling pools as TRACG. The differences between the CONTAIN and TRACG results may be due, in part, to the "forced" models activated to produce a conservative TRACG analysis. [[

]].

The staff finds it difficult to draw conclusions at this time regarding long-term behavior based on comparison of the two codes. The differences in capability are significant and call for different approaches to modeling the ESBWR with TRACE or CONTAIN at the design certification stage. The staff conclusion that the TRACG pressure predictions are conservative is not altered by the CONTAIN predictions due to the lack of CONTAIN's ability to adequately model boiling in the RPV liquid region and in the PCCS cooling pool, and the lack of ability to model suppression pool temperature.

Temperature Predictions - The CONTAIN model with one drywell volume predicts short-term drywell temperatures close to the TRACG predictions. The CONTAIN models with five and ten drywell volumes predict a maximum drywell temperature higher than those predicted by TRACG. Because of mixing flows in the ten drywell volume models, the elevated drywell temperature is predicted to decrease in magnitude while the high drywell temperature for the

five drywell volume case remains elevated in the long-term. The temperature prediction for the CONTAIN analysis with a single drywell volume results in an artificially low temperature due to mixing. It should be noted that all the CONTAIN analyses predict lower long-term drywell temperatures than TRACG.

The wetwell in the CONTAIN analysis models was modeled as one volume. The wetwell gas temperatures predicted by the five and ten drywell volume CONTAIN models are very close in value. The wetwell gas temperature predicted by the one drywell volume CONTAIN analysis is lower, but follows the same basic shape. The short-term wetwell gas temperatures for the five and ten drywell volume models are closer to the TRACG predictions. However, all the CONTAIN analyses predict lower long-term wetwell gas temperatures than TRACG.

The wetwell suppression pool temperature predicted by the five and ten drywell volume CONTAIN models are close in value. The one drywell volume CONTAIN analysis predicts lower suppression pool temperatures because CONTAIN assumes that the SP is completely mixed and cannot calculate pool temperature gradients. All the CONTAIN long-term suppression pool temperature predictions are lower than those predicted by TRACG.

The differences between the CONTAIN and TRACG predictions are affected by the previously discussed modeling assumptions used in running TRACG with the staff conclusion stated in the previous discussion of the pressure predictions equally applicable here.

Nitrogen Distribution - The five and ten drywell volume CONTAIN models predict nitrogen accumulation in the lowest drywell volumes where the liquid pool collects. The nitrogen accumulations in the wetwell predicted by these two analyses are also close in value. As expected, the one drywell volume CONTAIN model predicts a larger nitrogen accumulation in the wetwell because a single drywell volume does not allow volume for nitrogen accumulation. Consequently, the single drywell volume model responds to the stop in RPV vaporization in the one drywell volume CONTAIN model with a larger drop in drywell pressure due to condensation resulting in a subsequent vacuum breaker operation. As previously stated, when a vaporization delay was introduced into the multi-volume drywell models, the drywell pressure did not fall below the wetwell pressure and vacuum breaker operation was not predicted.

The TRACG analysis predicts vacuum breaker operation throughout the calculated MSLB transient. This effect is most strongly affected by the previously mentioned modeling assumptions used in running TRACG with the staff conclusion stated in the previous discussion of the pressure predictions equally applicable here.

Flow to the RPV - The five and ten drywell volume CONTAIN analyses predict similar flows from the GDCS to the RPV, as evidenced by the drop in GDCS water level elevation, and which differ from the GDCS flows predicted for the one drywell volume model. All the CONTAIN analyses predict a slower drop in GDCS water level elevation than TRACG, and thus CONTAIN predicts GDCS flow to the RPV at a smaller rate than TRACG.

The flow from the PCCS drain tank to the RPV predicted by the five and ten drywell volume CONTAIN models, as evidenced by the PCCS drain tank elevation change, are about the same.

However, the PCCS water level for the one drywell volume CONTAIN model is different, implying a different condensation and heat removal rate in the PCCS heat exchangers.

The differences in GDCS and PCCS flow to the RPV could be affected by the previously mentioned TRACG modeling assumptions.

PCCS Heat Removal - The heat removal via the PCCS heat exchanger predicted by the five and ten drywell volume CONTAIN models are very close. The one drywell volume CONTAIN model predicts that the PCCS will remove more heat in the short-term, but the CONTAIN prediction approaches the values predicted by the multi-volume drywell models in the long-term when the PCCS heat removal approaches the decay heat addition. All the CONTAIN models predict a smaller short-term PCCS heat removal than TRACG. In the long-term, TRACG predicts a slightly larger PCCS heat removal than the CONTAIN models.

The CONTAIN models assume free convection on structural surfaces by specifying a zero surface velocity for all surfaces except the inner PCCS heat exchanger surface. Therefore, a free convective, condensing heat transfer coefficient is used on most containment structural surfaces. The PCCS heat exchanger is allowed to account for forced convection effects to determine a forced convective, condensation heat transfer coefficient. In contrast, the TRACG modeling assumptions include the presence of forced convective flow on heat structure surfaces. Consequently, the TRACG heat structures would be expected to heat up faster than the CONTAIN structures. The larger long-term structural heat removal in CONTAIN could result in a lower calculated PCCS heat load. This could account for the slight differences in long-term PCCS heat removal calculated by the CONTAIN models and TRACG. However, the short-term TRACG calculated PCCS heat removal is larger than that calculated by CONTAIN, implying that the overall heat transfer coefficient predicted in the TRACG for the PCCS heat exchanger is larger than that calculated for CONTAIN PCCS heat exchanger using a forced convection heat transfer coefficient. The difference in PCCS heat removal can be related to differences in the overall heat exchanger heat transfer modeling in CONTAIN and TRACG. The condensing heat transfer correlation used in TRACG for the inner tube surface could be different from the one used in CONTAIN. Additionally, the differences between the CONTAIN and TRACG PCCS heat removal may be affected by the differences in heat transfer modeling between the outer surface of the PCCS heat exchanger tubes and the cooling pool. CONTAIN assumes a constant boiling type heat transfer coefficient of  $4500 \text{ W}/(\text{m}^2\text{-K})$  with a constant temperature sink equivalent to the boiling temperature in the cooling pool; in contrast, the TRACG code employs an internal boiling heat transfer model with code calculated cooling pool thermodynamic conditions.

#### 3.7.2.2.2 Overall CONTAIN Conclusions

Overall, based on examination of the behavior of CONTAIN, the staff notes that noncondensable gases take longer to get to the wetwell than predicted by TRACG, resulting in a tendency to predict a higher initial drywell pressure, and a slower pressurization of the wetwell compared with the behavior of TRACG. Between about 600 seconds and 2000 seconds, the CONTAIN and TRACG calculations agree very well.

### 3.7.2.3 TRACE/CONTAIN

TRACE and CONTAIN were first coupled using the Exterior Component Interface (ECI) logic of TRACE to analyze the LOCA containment response of the Westinghouse AP1000 reactor design, which utilizes either a sockets-based or shared memory-based protocol for handling all interprocess communication. In this coupling scheme, TRACE functions as the master process and spawns CONTAIN as a child process. The time step size and edit frequency are controlled by TRACE and communicated to CONTAIN. The boundary conditions, initial conditions, and output variables communicated between TRACE and CONTAIN are specified by the user in a separate input file which is read by a new interface routine added to CONTAIN. This design gives the user flexibility to choose the precise variables to be communicated based on the need for a particular transient.

Several improvements related to ESBWR modeling were later added to the TRACE/CONTAIN coupling interface logic. The first of these was the ability to handle noncondensable flow to and from the RPV modeled by the TRACE code. The second improvement was the ability to handle bi-directional flow between TRACE and CONTAIN, permitting a two-phase mixture to flow from TRACE to CONTAIN and a single-phase liquid to flow from a CONTAIN pool to TRACE. Additional minor improvements which were made include (1) the ability to specify multiple TRACE mass/enthalpy sources to the same CONTAIN cell, (2) improved types of mass/enthalpy sources (e.g., single-phase liquid, single-phase vapor with or without noncondensibles, and two-phase mixture with or without noncondensibles), (3) the ability to handle flow reversals and provide the correct donoring, (4) the ability to handle the situation where a CONTAIN modeled pool completely drains, (5) functionality to allow the time step to be limited by the CONTAIN user-input maximum time step size, (6) error checking the input, and (7) the ability to utilize any TRACE numerical scheme.

The current time advancement logic utilized in TRACE/CONTAIN is explicit in nature, whereby CONTAIN is advanced first, followed by TRACE. In this scheme, CONTAIN uses the previous time step mass flow and enthalpy to compute new time pressure and temperature boundary conditions which are then passed to TRACE prior to the start of TRACE's time step advancement.

#### 3.7.2.3.1 GDCS Line Break LOCA Analysis Using Coupled TRACE and CONTAIN Codes

In addition to using the TRACG code to perform independent analyses, the staff analyzed the limiting GDCS LOCA case using NRC's independent codes, TRACE and CONTAIN. TRACE is used to model the RPV and relevant piping systems. CONTAIN models the entire ESBWR containment and PCCS system. The analysis was performed by running the TRACE and CONTAIN codes in a coupled mode.

#### Steady State Model

The steady-state ESBWR TRACE model was developed by converting the GENE ESBWR TRACG input deck into the TRAC-BF1 format. A TRACG input deck modeling only the reactor

vessel was first extracted from the TRACG GDCS LOCA baseline model. A steady state calculation was performed and demonstrated that the control system was fully functional to maintain the downcomer water level. A PERL script was executed to convert the input model into the TRAC-BF1 format. Therefore, NRC's TRACE model is almost identical to the TRACG input model.

The TRACE vessel nodalization for the ESBWR model is shown in Figure 3.7.2.9 in Section 8 of this report. The vessel is divided into [[ ]] and [[ ]] radial rings, with dimensions indicated on the figure. The three inner rings in the vessel correspond to the steam generation region, and the fourth outer ring corresponds to the vessel downcomer. The level in the downcomer is maintained by a controller on the feedwater flow, which enters the vessel near the top of level 16. The target value for the downcomer level is set at 20.6916 m above the vessel bottom, or 13.2518 m above the TAF.

[[ ]] CHAN components [[ ]] are used to model the reactor core; CHAN [[

]]. Each CHAN component is based on a GE-12 fuel bundle and is modeled using [[ ]] axial cells, [[ ]] of which correspond to the active fuel region. This model is illustrated in Figure 3.7.2.10 in the figures section of this report. Both the water rods and part length fuel rods are explicitly modeled using the TRACE advanced fuel channel model.

The nominal power for the ESBWR core is 4000 MW, and the TRACE model uses point kinetics with reactivity feedback to calculate the core power. The axial power distribution used for each CHAN component is shown above in Figure 3.7.2.10 in Section 8 of this report. The power component modeled in TRACE also includes a scram table and decay heat data. The scram table is designed to insert all of the negative reactivity (-0.2175 k/k) into the core over a period of 2.8 seconds following receipt of the scram signal.

The chimney region of the ESBWR vessel is separated among the [[ ]] and spans axial levels [[ ]]. Levels [[ ]] comprise the mixing section below the inlet to the separators. The separators are currently modeled using [[ ]] SEPD components (SEPD 80–82), one for each radial ring. The simple separator model is utilized here, where the liquid carryover and vapor carryunder qualities are both set to zero. The dryer region above the separators is modeled at [[ ]], with the steam dome comprising [[ ]]. The inlet to the steam lines is modeled at a position of 1.015 m above the bottom of [[ ]].

The steam lines themselves are modeled with two trains, one representing one line and one representing three lines, as illustrated in Figure 3.7.2.11 in Section 8 of this report. TEE 83 and 84 connect to the vessel and correspond to the steam inlet, and both include a branch for 1 DPV and 3 DPVs, respectively. Connecting to TEE 83 and 84 are TEE 88 and 89, respectively, both of which include a branch for the SRVs. Connecting to TEE 88 and 89 are VALVE 94 and 95, respectively, which represent the "in board" MSIV and are followed by the

“out board” MSIV modeled by VALVE 85 and 86, respectively. VALVES 85 and 86 come into a single steam manifold, modeled by TEE 96, which leads to TEE 87, which models the direction of steam flow to the first stage of the turbine or the turbine bypass.

The CONTAIN model used for the TRACE/CONTAIN LOCA analysis was developed based on the model used in the CONTAIN stand-alone analysis described in Section 3.7.2.2 of this report. The nodalization of the model with elevations is shown in Figure 3.7.2.12 in Section 8 of this report. There were 21 cells used to model the ESBWR containment building, five of which were used for the drywell. One cell each was used for the PCCS upper and lower plenum, and six cells were used for the PCCS tubes. The PCCS pool, PCCS drain line, wetwell, and wetwell vent pipes were modeled with one cell each. An additional cell (Cell 10) was used to provide the atmospheric condition for the PCCS pool.

The connections to the TRACE model are highlighted in red in Figure 3.7.2.12 in Section 8 of this report. BREAKs 41-43, which represent the DPV boundaries, are connected to the upper drywell of the CONTAIN model (Cell 2). BREAKs 44 and 45, which represent the SRV boundaries, connect to the SRV discharge pipes modeled by Cell 7 and Cell 8, respectively. BREAKs 66 and 67, which represent the wetwell boundary for the GDCCS tanks, are both connected to the wetwell modeled by Cell 6. And lastly, BREAKs 98 and 99, which represent the GDLB, are both connected to the portion of the drywell modeled with Cell 3.

### Steady State Results

A few key parameters from the steady-state calculation performed with TRACE were compared against results obtained with TRACG, and also against design values, where available. This comparison, which examined steam dome pressure, feedwater temperature and flow rate, downcomer level and flow rate, core inlet subcooling, and core exit void fraction is shown in Table 3.7.2.2. The steam dome pressure and the downcomer water level match the TRACG results very well since these parameters were target values for the steady-state control system. The feedwater flow, however, was not a target value, but still matched well with both the TRACG result and the design value.

Table 3.7.2.2 Comparison of Steady-State Key Parameters.

Key Parameter	Units	TRACE Value	TRACG Value	Design Value	% Deviation
Steam Dome Pressure	Pa	7.16085e6	7.161418e6	7.171e6	-7.39e-3
Feedwater Temperature	K	488.12	488.1	488.75	0.0
Feedwater Flow	kg/sec	2161.2	2161.0	2160.0	9.25e-3

Downcomer Flow	kg/sec	11530.7	11767.8	11833.3	-2.015
Downcomer Level	m	19.4903	19.4916		-6.67e-3
Core Inlet Subcooling	k	13.51	12.85		5.136
Core Exit Void Fraction		0.7493	0.7594		-1.330

The downcomer flow rate (or core flow rate), the core inlet subcooling, and the core exit void fraction also agree very well between the two codes. Even though the TRACE and TRACG codes use different numerical integration schemes and physics packages, only 1% difference in core exit void fraction is observed. The largest relative difference occurs with the core inlet subcooling, which is only 0.66 K (1.19 °F). The slightly different core inlet subcooling results in about 2% difference in the total core flow rate. The comparison of steady state results confirmed that TRACG is capable of calculating the correct initial conditions for the current ESBWR reference design.

#### GDCS Line Break Model

The GDCS system contains three tanks, one of which provides flow to two 200 mm lines. The other two tanks each provide flow to one 200 mm line. Each of the four lines branches off into two 150 mm lines, giving eight branches into the reactor vessel. On each of the eight GDCS branches, a squib valve and a check valve are present. A diagram of this system is shown in Figure 3.7.2.13 in Section 8 of this report. As indicated in the figure, the assumed break in the GDCS line occurs between the check valve and the vessel wall on one of the four branches coming from the first GDCS pool. Also noted in the figure, one of the squib valves in one of the four lines from the other two tanks is assumed to fail to open, which will be taken into account in the TRACE model.

The TRACE nodalization for the GDLB LOCA, which is based on the diagram previously discussed, is shown in Figure 3.7.2.12 in Section 8 of this report. The two GDCS tanks that are not associated with the break are lumped into a single tank, which is modeled with TEE 77. This TEE connects to VALVE 78, which represents only three GDCS check valves since one squib valve has an assumed failure. Connected to the top of TEE 77 is a vent line modeled by PIPE 76, which connects to the wetwell boundary modeled by BREAK 67.

The other GDCS tank is modeled by TEE 71, which uses PIPE 70 to connect to the wetwell boundary, modeled by BREAK 66. It should be noted that BREAKs 66 and 67 both receive their boundary conditions from the same wetwell volume. TEE 71 connects to TEE 72, which is used to branch into two GDCS lines. TEE 72 connects to VALVE 73 on one end, which represents one GDCS check valve on the broken line, and VALVE 74 on the other, which represents two intact GDCS check valves. VALVE 73 connects to BREAK 98, which corresponds to the drywell

to which the GDLB will blow down. BREAK 99 is the vessel-side break component and is connected to the vessel via PIPE 75. BREAKs 98 and 99 both dump mass and energy to, and receive pressure/temperature boundary conditions from, the same drywell location.

The initiation of the GDLB comes at time zero of the LOCA transient. One second after the break occurs, the turbine is isolated by closing both in-board MSIVs (VALVEs 94 and 95) and both outboard MSIVs (VALVEs 85 and 86). One second later, the feedwater pumps trip, causing the feedwater pumps to coast down. The reactor receives the confirmed scram signal 6.05 seconds into the event and begins to insert the control rods over a period of 2.8 seconds. The vessel will continue to drain until the L1 setpoint is reached, and the ADS sequence is initiated. All information concerning the sequence of events was taken from References 1 and 15.

The control system used for the ADS sequence controls the flow area of the SRVs (VALVEs 92 and 93) and the trip status of the DPVs (VALVEs 58, 90, and 91) and GDCS valves (VALVEs 73, 74, and 78). The control logic for the ADS sequence is based on the L1 level setpoint. Once the L1 setpoint is hit, the SRVs begin to open in stages following a 10-second delay to confirm the L1 condition. The first stage of the DPVs are then tripped open 45 seconds after receipt of the confirmed L1 condition. One hundred and fifty seconds following the confirmed L1 condition, the GDCS check valves begin to open once the upstream pressure is less than the downstream pressure. The GDCS LOCA analysis proceeds for 2000 seconds, at which point the downcomer level is near the top of the chimney region.

#### GDCS Line Break Results

The GDLB case was run for 2000 seconds, which encompassed the initial blowdown period and the GDCS period. In order to establish a direct comparison between the TRACG analysis results and TRACE/CONTAIN results, the TRACG power-time table is used to model the total reactor core power in TRACE. It is assumed that the reactor is scrammed at time zero due to high drywell pressure. When the downcomer level drops below the Level 2 (L2) set point, a trip signal isolates the steam lines and opens the isolation condenser drain valves. As in the TRACG analysis, no credit is taken for heat removal by the IC. After L2, the downcomer water level continues to decrease, and, without external makeup, the Level 1 (L1) setpoint is reached. After a 10-second delay to confirm the L1 condition, the ADS logic starts the timed sequential opening of the depressurization and injection valves. Four SRVs open first with the remaining eight SRVs opening in two stages to stagger SRV line clearing loads in the SP and to minimize downcomer level swell. Similarly, the opening of the DPVs is delayed 45 seconds. Ten seconds after the last DPV opens, the GDCS injection valves are opened. In the TRACE model, only one valve component is used to model the functional features of both the squib valve and the check valve on each GDCS injection line. Therefore, the GDCS flow does not begin to refill the vessel and the downcomer until the pressure drop opens the check valve. After the GDCS injection starts, both the downcomer and the chimney collapsed water levels start to recover. When the two-phase water level reaches the break, the GDCS flow spills back into the drywell. It is predicted that the GDCS water flow is sufficient to raise the downcomer two-phase level above the break until the pools empty, after which the level drains back to the

break elevation. Figures 3.7.2.15 to 3.7.2.23 in Section 8 of this report depict the major parameters of the system.

### **Break Flow**

The mass flow rate through the GDLB is shown in Figure 3.7.2.15. Both codes predict the same trend of the mass flow rate. At the beginning of the transient, the mass flow rate increases due to increasing dome pressure. After the ADS opens all of the SRVs and DPVs, the break flow rate drops. From 650 to 950 seconds, both codes calculate very small mass flow through the break due to the pressure equalization between the vessel and the drywell. After 1200 seconds the flow from the GDSC spills through the break, and the calculated mass flow rates by both codes are almost identical.

### **Vessel Steam Dome Pressure**

Figure 3.7.2.16 shows the steam dome pressure calculated by the TRACG and TRACE/CONTAIN codes. Both codes predict the initial pressure rise due to the MSIV closure after the break. The dome pressure rises until the downcomer L1 trip activates the ADS system. Both the TRACE/CONTAIN and the TRACG predictions reach the L1 trip about 310 seconds into the transient. After the ADS activates, both codes predict the rapid depressurization and a nearly identical long term pressure trend.

### **Collapsed Water Level**

The collapsed water levels in the downcomer and the chimney partition are shown in Figures 3.7.2.17 and 3.7.2.18. While there are differences in the downcomer water level calculated by the two codes for the early stage of the GDSC injection due to the different containment wetwell pressure, the trends of the downcomer water level prediction are almost identical. Both codes predict that the minimum water level in the downcomer is lower than the TAF. TRACE/CONTAIN predicts a slightly lower minimum water level in the downcomer. The collapsed water level in the chimney decreases at different times consistent with the ADS opening times. The lowest water level remains 1.95 meters above the TAF. Both codes predict a similar trend of level increase following GDSC injection, indicating that the ECCS is capable of preventing core uncover.

### **Drywell Pressure**

The upper drywell total pressure and the noncondensable partial pressure are shown in Figure 3.7.2.19. Both codes predict that most of the noncondensibles in the drywell are purged into the wetwell during the early blowdown. The same trend of pressure stabilization is observed. The total pressure difference between the TRACG and TRACE/CONTAIN results is about 0.75 bar, with the TRACG code predicting a higher pressure at about 670 seconds. The difference appears to be caused by different nodalization schemes used for the two codes.

### **Wetwell Pressure**

Figure 3.7.2.20, indicates that the total pressure in the wetwell increases primarily due to the transfer of noncondensibles through the drywell to wetwell vents. The dominant mass transfer through the wetwell liquid is the noncondensable gases which accumulate in the wetwell air space. The TRACG code predicts higher pressure (by about 0.75 bar) at about 670 seconds.

### **Drywell and Wetwell Temperature**

The difference in these two codes is demonstrated clearly in the calculated drywell and wetwell air space temperature, shown in Figure 3.7.2.21. TRACG predicts a 50 K (90 °F) degree higher wetwell air space temperature than does TRACE/CONTAIN. The major difference may be due to the code internal physics packages, e.g, for calculating interfacial heat transfer and pool water surface condensation. Also contributing to the difference is the nodalization schemes used for the two calculations. While the TRACG nodalization partitions the wetwell air space into [ ] nodes, the TRACE/CONTAIN nodalization represents the wetwell by one node. TRACG calculates different air space temperature in different nodes. Although the temperature distributions in the containment are different, the pressure distributions in different containment compartments is similar.

### **GDCS Injection Mass Flow Rate**

A significant feature of the ESBWR ECCS design is the use of a gravity driven cooling system. Figure 3.7.2.22 shows the total GDCS injection mass flow rate. The magnitude and the trend of the TRACG and TRACE predictions are almost identical, with the exception of a shift in the timing of the injection. This timing difference is caused by the different wetwell pressure, confirming not only that the ESBWR gravity driven ECCS system can be expected to function as intended, but also that the TRACG code is capable of realistically modeling the ECCS performance during the GDCS LOCA.

### **Core Peak Cladding Temperature**

The requirement of limiting the PCT to 2200 °F is clearly stated in 10 CFR 50.46. Figure 3.7.2.23 shows the PCT calculated by both TRACG and TRACE/CONTAIN. The PCT peaks at approximately 590 K (602 °F) in the early stage of the blowdown. After the ADS actuation, the PCT drops to about 420 K (296 °F). Both codes predict almost identical trends and maximum peaks, confirming that the ESBWR ECCS system is capable of maintaining core cooling during the blowdown and GDCS injection periods.

## **Staff Findings And Conclusions**

Through the comparison of the ESBWR GDCS LOCA response as calculated with the TRACG and TRACE/CONTAIN codes, the staff has observed the following—

- (1) The Automatic Depressurization System is important to reduce the system pressure to equalize it with the drywell pressure so that GDCS injection can maintain the in-vessel water level. TRACG is capable of predicting the ADS actuation timing.
- (2) Although the TRACG code may tend to overpredict the temperature and pressure in the containment, it is still be able to predict the physical timing of GDCS injection initiation and the injection mass flow rate.
- (3) The chimney collapsed water level remains above the core with significant margin (1.9 m for the base case). The reactor core remains covered and the PCT remains significantly below the regulatory limit of 2200 °F.
- (4) The two codes, TRACG and TRACE/CONTAIN, using different models, correlations and numerical solution techniques, produce very similar predicted behavior of the ESBWR design for the first 2000 seconds of the GDCS LOCA. The similarity of the comparisons of the major parameters, described above, increases confidence in the capability of the TRACG code to support analytical needs at the design certification phase.
- (5) Although significant differences exist between the TRACE/CONTAIN and TRACG codes in modeling containment behavior during the GDCS LOCA, the similarity of the predicted containment behavior supports the conclusion that the TRACG code is able to predict the first order effects in the containment response and has sufficient accuracy for this application.

#### 3.7.2.3.2 MSLB LOCA Analysis Using Coupled TRACE and CONTAIN Codes

The coupled TRACE and CONTAIN code suite was again selected to analyze the MSLB LOCA. Unlike the specific approach GENE used to maximize the containment pressurization rate and the special treatment of the suppression pool model, the staff used the same containment and reactor vessel model to perform the analysis. The advantage of using a single set of reactor and containment models is that the model is not biased for either ECCS evaluation or containment integrity evaluation. The detailed reactor vessel model can also more accurately predict mass and energy releases through the break and provide a more detailed thermal-hydraulic solution in the vessel.

##### TRACE/CONTAIN Model Modifications

The MSLB model, and the sequence of events, are similar to those described for the GDCS LOCA case in the previous section. The GDCS line model is the same as that shown in Figure 3.7.2.14, in Section 8 of this report, except that the break between the vessel and one of the GDCS valves was removed. Specifically, PIPE 75, BREAK 98, and BREAK 99 are not modeled, and VALVE 73 connects directly to the vessel.

As for the steam line modeling, it is the same as that shown in Figure 3.7.2.25, in Section 8 of this report, with the exception that a double-ended break in one steam line is modeled between the vessel and TEE 83. A diagram of the break is shown in Figure 3.7.2.25 in Section 8 of this report. BREAKs 36 and 37 connect to the upper drywell volume of the CONTAIN model. No significant containment model change is made except that the break location was moved to the upper drywell volume.

### MSLB LOCA Calculation Results

The sequence of the MSLB LOCA events is very similar to the GDCS LOCA. At the break initiation, the blowdown flow quickly increases the drywell pressure to the scram set point, and a control rod scram occurs. The high velocities in the main steam line initiate the closure of the MSIVs and the reactor is isolated within 3-5 seconds. For the base case, the feedwater system is assumed to be unavailable to make up the coolant loss. The downcomer water level quickly reaches the L1 setpoint and triggers the actuation of the ADS system. Because of quick depressurization through the main steam line as well as the ADS, the reactor vessel pressure drops much faster than it does in the GDCS LOCA, resulting in earlier GDCS injection initiation. In the containment, the steam entering the drywell quickly raises the pressure, opening the main containment vents and sweeping most of the drywell noncondensable gas through the main vents. During the blowdown phase of the transient, the majority of the blowdown energy is transferred into the suppression pool by condensation of the steam flowing through the main vents. This increases the pressure of the wetwell and GDCS pool air space. During the early GDCS injection period, the GDCS flow reaches its peak mass flow rate and the cold water collapses the void in the reactor pressure vessel. Because of a limitation of the CONTAIN model, the MSLB simulation stops at 2000 seconds into the transient. Figures 3.7.2.25 to 3.7.2.34 in Section 8 of this report depict the major parameters of the system.

### **Vessel Steam Dome Pressure**

Figure 3.7.2.26 in Section 8 of this report shows the steam dome pressure calculated by the TRACG and TRACE/CONTAIN codes. Both codes predict the same trend of the depressurization process.

### **Break Flow**

The mass flow rate through the MSLB is shown in Figure 3.7.2.25 in Section 8 of this report. Both TRACG and TRACE/CONTAIN predict the same trend in the mass flow rate. However, between 0 and 600 seconds, TRACE/CONTAIN predicts higher oscillatory break mass flow rate. This is mainly caused by the high entrainment in the vessel steam dome and main steam line, while the upstream steam quality calculated by TRACG is much higher. The integrated coolant discharge for the two codes does not differ significantly, thus giving confidence in the prediction of both codes.

### **Drywell Pressure**

The upper drywell total pressures calculated by both TRACG and TRACE/CONTAIN are shown in Figure 3.7.2.28 in Section 8 of this report. The peak pressure calculated by TRACG during the first 2000 seconds is much higher than that calculated by TRACE/CONTAIN. However, it is still below the design limit. The difference in the calculations appears to be caused by different nodalization schemes used for the two codes with the result that the TRACE/CONTAIN calculation tends to predict more mixing than TRACG.

### **Wetwell Pressure**

Similar to the drywell pressure prediction, TRACG predicts a higher wetwell pressure peak value. As shown in Figure 3.7.2.29 in Section 8 of this report, the wetwell pressure calculated by TRACG peaks at about 550 seconds. The TRACE/CONTAIN peak value is much lower, demonstrating that TRACG is possibly more conservative in terms of calculating the wetwell pressure load.

### **Drywell and Wetwell Temperature**

As shown in Figure 3.7.2.32 in Section 8 of this report, TRACG again predicts higher drywell and wetwell air space temperatures. This is again due to the different nodalization schemes used with the code input models. The drywell and wetwell temperatures are from the "hottest" cell in the drywell and the wetwell. Using the peak temperature values in the drywell and wetwell, the staff finds that the temperatures are lower than the design limit. Figure 3.7.2.33 in Section 8 of this report shows the wetwell liquid temperature. For the cell down stream of the highest vent in the wetwell, TRACG and TRACE/CONTAIN predict almost identical liquid temperatures.

### **Collapsed Water Level**

The collapsed water level in the chimney partition is shown in Figures 3.7.2.31 in Section 8 of this report. The chimney collapsed water level for TRACE/CONTAIN for the GDCS and MSLB LOCA cases are compared. It is observed that the lowest chimney collapsed water level is similar for both GDCS and MSLB LOCA cases. The level starts to rise after the GDCS injection is initiated. There is significant liquid inventory in the chimney to prevent core uncover.

### **GDCS Injection Mass Flow Rate**

Both codes predict very similar GDCS injection mass flow rates. As shown in Figure 3.7.2.32 in Section 8 of this report, both the trend and the maximum peak values are in good agreement. As does the GDCS LOCA case, the MSLB case demonstrates that TRACG is capable of modeling the early GDCS injection.

### **Core Peak Cladding Temperature**

Unlike the TRACG GDCS LOCA model, the MSLB LOCA model uses [[ ]] to model the entire reactor core. Without a hot channel component, no peak cladding temperature can be obtained from the TRACG MSLB LOCA calculation for comparison.

Therefore, Figure 3.7.2.34 in Section 8 of this report shows only the PCT calculated by TRACE/CONTAIN. It is observed that no heat up occurs, and that the entire core is well cooled.

#### Staff Findings And Conclusions

Through the comparison of the ESBWR MSLB LOCA responses using the TRACG and TRACE/CONTAIN codes, staff has observed the following—

- (1) During the first 2000 seconds of the MSLB LOCA, TRACG predicts higher drywell and wetwell pressures and temperatures than does TRACE/CONTAIN. The pressures and temperatures are all below the design limits.
- (2) The calculated MSLB chimney collapsed water level is generally much higher than that of the GDCS LOCA case. This confirms GENE's position that the GDCS break is more limiting for ECCS evaluation. Again, the level remains above the core with significant margin. The reactor core remains covered and the PCT remains significantly below the regulatory limit of 2200 °F.
- (3) The two codes, TRACG and TRACE/CONTAIN, using different models, correlations and numerical solution techniques, produce very similar predicted behavior of the ESBWR design for the first 2000 seconds of the MSLB LOCA. The similarity of the comparisons of the major parameters described above, increases confidence in the capability of the TRACG code to support independent analytical needs of the design certification process.
- (4) Significant differences exist between the TRACE/CONTAIN and TRACG codes in modeling the containment behavior during the MSLB LOCA. However, the similarity of the predicted containment behavior supports the conclusion that the TRACG code is able to predict the first order effects in the containment response and has sufficient accuracy for this application.

GENE is consistent with this step in the CSAU approach.

#### 3.8 Step 8—NPP Nodalization Definition

References 1 and 11 discuss the tradeoffs in determining an adequate NPP nodalization. GENE developed guidelines for the ESBWR nodalization in such a manner as to remove, as far as possible, nodalization as a contributor to calculational uncertainty. The nodalization strategy applied by GENE takes into consideration basic geometric considerations, experience with nodalization used in prior studies for the operating fleet of BWRs, nodalization for the various SBWR test facilities, and qualification studies in Reference 16. In addition, GENE relied on standard nodalization developed in assessment cases against separate and integral effects tests. Nodalization studies were performed in assessing the test data to establish the level of detail necessary to represent the important phenomena. The standard nodalization for modeling the ESBWR design was also used for the SBWR design.

GENE is consistent with this step in the CSAU approach.

### 3.9 Step 9—Definition of Code and Experimental Accuracy

Simulation of experiments developed from Step 7 using the NPP nodalization from Step 8 provides checks to determine code accuracy. The differences between the code calculated results and the test data provide bias and deviation information. Code scale-up capability can also be evaluated from separate effects data, full-scale component tests data, plant test data, and plant operating data, where available. Overall code capabilities are assessed from integral systems test data and plant operational data. These assessments were performed as part of the SBWR qualification of the TRACG methodology documented in References 11, 13, and 16. The assessments have been extended to the ESBWR based on the similarity of the designs, which results in no new phenomena being expected in the ESBWR.

GENE is consistent with this step in the CSAU approach.

### 3.10 Step 10—Determination of Effect of Scale

Various physical processes may give different results as components or facilities vary in scale from small to full size. The effect of scale must be included in the quantification of bias and deviation to determine the potential for scale-up effects.

GENE uses the Hierarchical Two-Tier Scaling (H2TS) process. One of the key elements of the H2TS approach is the identification of the important physical phenomena governing a process. Generally, the phenomena will be identified and ranked in importance by a group of experts. The results of this effort are documented in a PIRT. The H2TS approach consists of a “top-down” method, which is a system scaling analysis used to derive scaling groups and establish a scaling hierarchy, and a “bottom-up” method, which focuses on the important processes and introduces similitude to assure that the scaled test data is applicable to the prototype. The H2TS approach is described by Zuber (Reference 49). However, the top-down system scaling does not replace, but rather provides a rational framework for the bottom-up scaling.

#### **Evaluation of GENE Scaling**

GENE adopted the H2TS approach for the ESBWR. The LOCA serves as the basic event for the scaling analysis. Since the importance of the governing phenomena changes as the event unfolds, GENE defined four accident phases (shown in Figure 3.10.1 in Section 8 of this report) which span the accident, namely, late blowdown, GDCS initiation, GDCS phase, and PCCS phase. The early blowdown period is not significant for passive safety system performance and is ignored. The primary test facilities scaled for SBWR and ESBWR testing can simulate decay power levels starting at approximately one hour after the initiation of the accident. Since a key issue is PCCS performance, the scaling is directed at the “late blowdown phase extending into the long-term cooling phase.” The long-term cooling phase is unique to the SBWR and ESBWR containment because of the substitution of passive for active cooling systems.

GENE begins their scaling efforts with a PIRT. The top-down scaling approach complements the PIRT by identifying the important phenomena during each accident phase based on non-dimensionalization of the governing equations. The global momentum and energy conservation equations used are based on the lumped-parameter approach. The bottom-up scaling considers the individual phenomena at a local level.

### 3.10.1 Top Down Scaling

#### Methodology Description

The system was divided into several large volumes. The equations of energy and mass balance developed for a generic volume were then applied to each of these volumes at different time periods during the transient. The equations were made non-dimensional and the resulting non-dimensional coefficients were defined as the  $P_i$ 's to represent the relative importance of the participating phenomena.

#### Evaluation Metrics

In this section, we define the objectives of a scaling analysis for code assessment and use that definition to evaluate how the GENE ESBWR scaling report demonstrates that the objectives have been accomplished. General and specific comments are made about yet unresolved questions and issues with the content of the aforementioned report.

#### Criterion

In the Scaling Report, Reference 46, the objective is defined as "to show that the test facilities properly 'scale' the important phenomena and processes identified in the ESBWR PIRT and/or provide assurance that the experimental observations from the test programs are sufficiently representative of ESBWR behavior for use in qualifying TRACG for ESBWR design basis calculations." The staff accepts the objective as stated.

The main objective of integral scaled facilities is to capture not only the component behavior but also their dynamic interactions as a complete system. To a certain extent, the GENE report acknowledges this in the executive summary, where it states that "A comprehensive experimental program was carried out to demonstrate the thermal-hydraulic performance of these passive systems and their components." While one cannot expect that any of the scaled facilities represent a simulation of the prototype, for completeness, they must at least exhibit the same kind of interactions between components and subsystems as expected of the prototype. It is up to the scaling analysis, therefore, to determine how relevant these interactions are. System interactions are not explicitly called out in the PIRT as phenomena. They are, however, an integral part of the transient and determine the sequence of events that define the beginning of a phase, the end of a phase, and what process controls the state of the system during that phase.

#### The Approach

In general, the reactor system is divided into subsystems for which governing equations are developed. The governing equations are made non-dimensional by referring all variables to a set of norms or reference parameters (including a reference time), according to the purpose of the analysis. The intent of this process is to obtain non-dimensional parameters. The non-dimensional coefficients of these equations, the system Pi's, contain information about how the different components of the system interact, and which of these many interactions dominates the transient behavior during a given phase.

During each transient, the system state and its configuration changes as the transient progresses from one phenomenologically distinct phase to the next. In each of these phases there will be a process or a set of competing processes that define the beginning and the end of the phase, and therefore its reference time. The general approach needs to be repeated for each system configuration and each reference time.

It is difficult to prescribe the level of system detail that the top-down scaling should reach. In one extreme, one could assume that the entire reactor system is one comprehensive volume, and conduct the analysis accordingly. The result would be simple and of limited value. Another approach is to go into as much detail as possible, without invoking multi-dimensional effects or the local distribution of a phenomenon. The latter would likely result in a system representation that varies from phase to phase of the transient, as the system configuration varies (valves open and close, tanks empty or fill).

GENE selected an in-between approach and identified the major system volumes as the components, all represented, in principle, by the same equations of energy and mass conservation. It appears that the momentum equations of the connecting lines or paths are neglected as having no dynamic contribution. Furthermore, Reference 46, Section 6.2 cites previous efforts— "results from the SBWR work showed that there are no significant interactions in the SBWR system or the related tests and no new Pi numbers resulted." What the SBWR study found is that the lines and connecting paths have very fast response times compared to other simultaneous processes, and that they contribute enough damping so as to suppress oscillations. In the same section (6.2), the last paragraph suggests that the analysis conducted for SBWR was not carried out for ESBWR because they are "similar enough." In both SBWR and ESBWR, the volumes do interact because they are connected. Part of the difference between these two systems is in the connecting paths between volumes.

The statement in Reference 46, Section 6.3 "these equations are applied to the specific regions of the ESBWR" raised the question that interactions were ignored in the GENE approach. Even when there are two or three volumes actively participating and interacting with each other, the volumes are dealt with independently. The volume equations (mass and energy) have terms that represent inflows and outflows. In most cases, these are not external inputs to the reactor system, but result from gradients between connecting volumes and, therefore, are not independent variables. A single volume equation can neither capture nor describe this system behavior, and is insufficient to draw conclusions about that behavior. It is likely that the two or three volumes involved are interdependent and can be represented by a single equation.

However, the equation used by GENE in its analysis is not capable of demonstrating this. In fact, there seems to be no analysis of system interactions at all.

#### Closeout of Top Down Scaling for the GDCS Transition Phase

In response to staff RAIs, GENE addressed the deficiencies in the top down scaling with a subsequent revision of the GENE scaling analysis using new equations that account for the interactions between volumes. The system Pi's that resulted from the revised analysis were significantly different than the system Pi's from the non-interacting equations. GENE successfully applied the equations to the "GDCS Transition Phase" which is the onset of GDCS injection and the time period when the minimum vessel inventory occurs. They showed that the experiments behave qualitatively the same as their scaling model and the TRACG ESBWR model.

#### Specific Comments On Application of Top Down Scaling to Long Term Cooling

The proposed representation of the ESBWR system, provided in Figure 3.10.1 in Section 8 of this report, is an approximation for the formulation of the top-down scaling relationships. The ESBWR system encompasses two major energy sinks—the SP and the PCCS pool. The SP is the primary sink in the initial portion of the transient. The PCCS pool takes over in the long-term portion of the transient.

The view of GENE is influenced by the behavior of current generation reactors. In responding to RAI 283, GENE stated, "It is important to understand that in any pressure suppression containment system, the long-term containment pressure is dominated by the wetwell air space response, not by the drywell." The staff disagrees with this because, in the long term, the wetwell cannot serve as a sink unless one postulates that the containment pressure can increase indefinitely. The functionality of the SP as a sink will decrease as the heat transferred to the PCCS pool becomes the leading process in the long-term portion of the transient. The system interactions between the drywell and wetwell will determine the distribution of the noncondensibles. These processes may be verified by analysis of appropriate long-term tests that were performed in the PANDA facility.

The transition from heat deposition in the wetwell to heat deposition in the PCCS pool is a fundamental element of the ESBWR system. In current reactors, reliance is on active heat removal from the SP resulting in the functional statement quoted from RAI-283. However, this is not the case for the ESBWR and, therefore, the energy partition between the wetwell and the PCCS pool must be represented in the initial formulation of the top-down scaling. By limiting the representation to a single volume system with only one pool, as shown in Figure 3.10.1 in Section 8 of this report, implicit assumptions on the system behavior are imposed and important terms are removed from the governing equations. A more inclusive representation of the system would consider two equations for the vessel (similar to Reference 46, Equations 3.1-6 and 3.1-7), two equations for the wetwell, and one equation for the pressure in the drywell connected to the PCCS pool saturation condition via appropriate heat transfer through the PCCS. This heat transfer would also be a function of the noncondensable distribution dictated

by the wetwell governing equations. Such a system of five governing equations would enable a proper representation of the system interactions that GENE has represented by two equations.

Another approach would be to consider the various portions of the transient with different representations of the system. This would require an *a priori* knowledge of the energy partition in the various sinks. In previous scaling efforts, this approach has been successful because significant knowledge of system behavior was available from integral test programs at different scales. Nonetheless, significant difficulties had to be circumvented to properly transition from short-term transients to their long-term states.

Additionally, one could argue that in the long term, the cumulative effect of the heat removal by the massive containment structures will result in lower pressures. Lower pressures in turn would result in lower density of the noncondensibles. This means that larger volumes would be necessary to completely segregate them or that a more active participation of the noncondensibles in the heat transfer at the PCCS should be incorporated into the analysis. Appropriate tests and analyses will clarify this issue. Therefore, it would be desirable to include the structural contribution to heat removal in the formulation of the top-down scaling as well. This could be accomplished with appropriate terms in the drywell and wetwell pressure equations.

The staff recognizes the deficiencies in the submitted scaling analysis regarding the system interactions, the energy partition between the SP and PCCS pools, and the effect of containment structures. Consequently, the ESBWR responses to various accident scenarios may be subject to additional uncertainties that will be reviewed during the design certification stage.

### 3.10.2 Bottom-Up Scaling

#### Methodology Description

Bottom up scaling is used to look at specific processes important to system behavior in more detail. For the ESBWR, the bottom-up scaling process is described in Section 3 of the TAPD Report, Reference 12, and Section 7.6 of the Scaling Report, Reference 46. As noted on page 3-1 of Reference 12, the ESBWR bottom-up process relies heavily on the SBWR study documented in References 47 and 48. The bottom-up process is similar for the SBWR and ESBWR. There is a significant difference, however, between the bottom-up scaling discussions for the SBWR and ESBWR.

The ESBWR TAPD Report, Reference 12, page 3-3, identifies 46 highly ranked phenomena needing detailed evaluation. A summary of the detailed evaluations is given in Section 3.3 of Reference 12. The bottom-up process for the SBWR is described in Section 3 of Reference 48. For the SBWR, a total of 79 phenomena called for detailed evaluation, as discussed on page 3-2 of Reference 48. For both the SBWR and ESBWR, the evaluations make reference to the relevant test reports and provide the basis for acceptability of the data for TRACG qualification.

Bottom-up scaling of SBWR specific phenomena is described in some detail in Section 3 of Reference 47. The governing equations and similarity variables describing each phenomenon are presented and discussed. For The ESBWR, bottom-up scaling is reduced to consideration of just four processes as discussed in Section 7.6 of Reference 46. Three of these phenomena are dismissed as not being of significant interest. Only PCC and IC behavior are stated to be of significant interest. GENE states that full height testing of PCC and IC behavior has been conducted for the SBWR in PANDA, GIRAFFE, and PANTHERS, and that a detailed data base for low-pressure condensation heat transfer in the presence of noncondensibles is provided by the Massachusetts Institute of Technology and University of California at Berkeley single tube tests. The bottom-up scaling for PCC and IC behavior in the ESBWR is stated to be the same as for the SBWR. This is the only bottom-up scaling item addressed specifically for the ESBWR. While additional highly ranked items are discussed for the SBWR, there is not enough information to determine whether the available data cover the range expected for the prototype.

#### Evaluation

The non-dimensional coefficients, or Pi groups, identified in the top down scaling are more complex than the more traditional similarity parameters derived in the study of physical phenomena such as the Reynolds number and Prandtl number. Evidence of this complexity is the fact that a characteristic system time is an integral part of these Pi groups, and also that they come in sets of two or more. The Pi groups are derived from the macroscopic analysis of distinct elements of the system that accounts for the way in which the elements interact and exchange mass, energy, or both, with each other and with the environment. These Pi groups are a useful tool to determine what processes or mechanisms dominate the behavior for each particular system. They can also be used to assess if two different systems can be expected to have similar behavior. However, the similarity can only be guaranteed *a priori* if the two systems have identical Pi groups. If the Pi group values are different, further analysis is necessary to assess the similarity between the different systems. The most important part of this further analysis is the verification that the data—and code calculation for the test facility—exhibit the same trends, magnitudes, and variations in non-dimensional space. The other aspect of this analysis is the evaluation of local phenomena to ensure that while the systems are expected to be similar in their macroscopic behavior, the local phenomena (bottom-up) support this expectation by producing the same regime. This invokes the more traditional non-dimensional groups, such as Reynolds, Prandtl, and Biot numbers, which correspond to the local processes not captured by the top down formulation of the system equations. The GENE scaling report, in its original version, is very weak in this area because it does not produce these analyses. Instead, it relies on an arbitrary range of Pi groups for similarity assessment. During the review process, GENE abandoned the arbitrarily defined range and conducted a rigorous analysis for the GDCS injection period of an ESBWR LOCA.

As a further observation, the systems test facilities are scaled and designed in such a way that little data was obtained regarding multi-dimensional phenomena. Analysis of the system test data is based on a lumped-parameter approach that eliminates multi-dimensional spatial variations. As such, the tests do not provide sufficient data to credit multi-dimensional effects. Since the data are not suitable to qualify TRACG to predict multi-dimensional effects, TRACG is not used to credit multi-dimensional effects in the ESBWR analysis.

### 3.10.3 Scaling Conclusion

The staff concludes that GENE demonstrated that there are relevant and sufficient data to qualify TRACG in its simulation of the phase for which the scaling analysis was completed. The phase for which this has been done, the GDACS injection phase, is indeed the most important period of the transient. Conservative, bounding analyses have been employed for the remainder of the LOCA events. The rigor of the analyses is not at issue, but rather the completeness of the analysis. As a part of this review, the staff has determined that it is acceptable for GENE to perform a rigorous scaling analysis limited to the most important phase of the LOCA event, and in terms of the most critical variable (core collapsed water level), thereby demonstrating that the scaling analysis tools are correct while the detailed scaling analysis itself may be incomplete. GENE has been fully responsive to the staff concerns regarding the scaling analysis and methodology.

## **Element 3—Sensitivity and Uncertainty Analysis**

### 3.11 Step 11—Determination of the Effect of Reactor Input Parameters and State

The purpose of this step is to determine the effect that variations in the plant operating parameters have on the uncertainty analysis. Plant process parameters characterize the state of operation and are controllable by the plant operators to a certain degree. The design basis ECCS/LOCA analyses were performed assuming loss of the preferred electric power, and assuming that the non-ECCS vessel inventory control systems, specifically, the feedwater system, the ICS and the control rod drive system are not credited. In addition, the plant initial conditions, which are anticipated from the operating fleet of BWRs and the test programs to have the greatest influence on the minimum core/chimney mixture level, were selected for the evaluation of uncertainties.

GENE is consistent with this step in the CSAU approach.

### 3.12 Step 12—Performance of NPP Sensitivity Calculations

Sensitivity calculations are performed to evaluate methodology sensitivity to various operating conditions that arise from uncertainties in the reactor state at the initiation of the transient, in addition to sensitivity to plant configuration. Sensitivity studies were performed for the GDLB for the plant conditions found to have the greatest influence on the minimum core/chimney mixture level. The base case was defined to minimize the drywell pressurization. All perturbations were found to be small with the minimum static head occurring at slightly different times in the transient. The bounding calculations were performed using the combination of parameters that resulted in the minimum static head in the chimney.

GENE is consistent with this step in the CSAU approach.

### 3.13 Step 13—Determination of Combined Bias and Uncertainty

The individual uncertainties resulting from code models of important phenomena, scale effects, and NPP input parameter variations should be combined to obtain an overall bias and uncertainty. The CSAU approach does not prescribe the manner in which the individual biases and uncertainties are to be combined. Regulatory Guide 1.157, Reference 8, suggests that a one-sided upper statistical limit calculated at the 95 percent probability level for the primary safety parameters is preferred. Lack of core heatup in the ESBWR analyses suggests a statistical analysis of the PCT would not be the best metric for acceptable performance. The approach taken by GENE is to perform [[

]]. The staff finds the GENE approach acceptable due to confirmation of the GENE results through staff calculations performed independently.

In addressing the containment analysis application of TRACG, GENE has stated that a rigorous statistical calculation is not performed. [[

]].

GENE is consistent with this step in the CSAU approach

### 3.14 Step 14—Determination of Total Uncertainty

Previous uses of the TRACG methodology have made use of Normal Distribution One-Sided Upper Tolerance Limit statistics to assess the uncertainty in the analyses. Application of the code to the ESBWR advanced passive system design relies on a very different approach to uncertainty since all preliminary calculations indicate the core remains covered and does not heat up. Uncertainty evaluation is done in this case using a much simpler [[  
]]. This approach does not make any claims on variation of parameters, but does claim to provide a limiting-case evaluation.

The specific plant conditions ranged and their limits are as identified in the following table, however, no plant parameter uncertainties have been considered.

Table 3.14.1  
Uncertainty Considerations

Quantity	Control of Initial Condition	Range of Conditions	Consideration of Uncertainty about the Initial Conditions
[[			



			]]

Unlike prior reviewed and approved applications of the TRACG methodology, the application of TRACG to the ESBWR LOCA event does not utilize a rigorous statistical methodology to combine uncertainties. The model and plant parameters (indicated in Table 1) are determined through sensitivity studies. [[

]]. The calculation result is considered successful based on the minimum static head in the chimney, thus indicating the core remains covered and there is no heatup of the fuel.

Additionally, the containment response is evaluated by a bounding calculation in [[

]]. The bounding calculation is compared to the design conditions to establish that sufficient margin exists to the containment design pressure and temperature.

The staff notes that no previous "realistic" plant evaluation has incorporated the reactor coolant system and containment system into a single computer code calculation. Doing so raises a question as to whether or not the uncertainty analysis that is performed to assess uncertainties in the 10 CFR 50.46 acceptance criteria should also include uncertainties in the containment aspect of the calculation. The current GENE TRACG hybrid analysis applies a pseudo uncertainty analysis, as discussed previously, to the reactor coolant system alone. The containment system is treated in a bounding way as also discussed previously. The question of performing a combined uncertainty analysis should be examined more closely at the design certification stage. This view is strengthened by a statement made by GENE in response to a staff RAI. GENE stated, "The precise origin of the tabulated values that are referred to as the [[ ]] is not known. There is reason to believe...that these values were obtained by merging the separate results from [[ ]]." Using data of unknown provenance for design basis calculations is questionable. This is especially troubling since the [[ ]] data is the least conservative of the available curves in the literature. If the containment portion of the calculation is being performed as a bounding calculation, then the more conservative models of [[ ]] would be more appropriate to use. At the design certification phase, GENE should perform the analyses for the ESBWR using the appropriate models and supportable data bases.

GENE is not consistent with this step in the CSAU approach for the LOCA/ECCS application of the TRACG code, but the staff finds the GENE method acceptable in light of the predicted lack of core uncover. Should it be found during the design certification review of the ESBWR system that core uncover does occur, the staff will revisit the method of uncertainty combination and statistical methodology for the LOCA/ECCS application.

#### 4.0 CONFIRMATORY ITEMS

In the course of conducting the review of TRACG for applicability to the ESBWR LOCA, several items were identified as needing confirmation at the design certification stage. These items do not affect the applicability or capability of the code, but do address the response of the plant design, and adequacy of the documentation.

- 1) The PIRT at the design certification stage should include the long-term cooling phase of the LOCA since the long-term cooling phase is highly design dependent. Should it be found that unreviewed phenomena occur during the long-term cooling phase, the appropriate models and correlations in the TRACG code will be revisited by the staff.
- 2) During the design certification review, the staff will verify that the TRACG application procedures conservatively calculate the collapsed water level in the chimney above the hot channel for the three break locations, MSLB, BDLB and GDLB.

Reference 11, Table 2.4-2 indicates that the GDLB results in the lowest static head in the chimney of the three break locations examined, the GDCS line, the main steam line, and the bottom drain line. At the design certification stage, GENE will need to provide supporting analyses for a spectrum of break locations to demonstrate that there is no core uncover for the possible break locations. Should core uncover occur, review of the TRACG code will be revisited to determine the adequacy of the applicable models and correlations

The procedures should be applicable to both short term and long term LOCA events (i.e., up to 72 hours).

- 3) GENE has committed to incorporate the missing definition for  $E_r$ , and new equations for the transition criterion between churned turbulent and annular flow, including the drift velocity term in updated code model description documentation.
- 4) The description of the TRACG model, Reference 10, will be updated to reflect all current models and correlations, thereby providing a level of detail consistent with a stand-alone document.
- 5) Further investigations are needed to conclusively determine the sound in the PANTHERS-IC testing that may have been due to water hammer, and to confirm its prevention in the ESBWR (e.g., by changing the hardware design of the IC inlet line or the startup procedure).
- 6) The PANTHERS-IC testing was terminated when leakages were detected in the IC upper header. As a result, the leakage issue was never resolved, and is an IC structural integrity issue that needs to be resolved for the ESBWR design certification.
- 7) During the design certification review stage, the ECCS baseline model should include the scram delay time and the 2 percent power measurement uncertainty.

- 8) During the design certification stage, separate modeling of the vessel shield, the reflective thermal insulation layer, and the air gap from the lumped heat structure will be necessary.
- 9) Nodalization studies will be necessary at design certification to calculate the minimum water level in the chimney partition.
- 10) The assumption of the loss of feedwater flow used by GENE is not conservative. Therefore the existing GENE MSLB model and the current analysis approach underestimates the maximum containment pressure and temperature. At the design certification phase, this should be resolved.
- 11) Without detailed feedwater heater system design information, both the staff and GENE had to make assumptions about the mass and energy discharge from the feedwater heater system. The staff believes that the bounding containment peak pressure and temperature need to be evaluated during the design certification stage after the feedwater heater system design is finalized. If the evaluation indicates that the code application range is exceeded or a new scenario, such as wetwell flooding, has not been examined during the preapplication stage, the staff may choose to review the TRACG code for such new use.
- 12) The quick closure of the MSIVs while control rods are being inserted may increase the total core power due to void collapse. At the design certification stage, GENE should evaluate the effects of void collapse for the GDCS and BDLB LOCA cases.
- 13) During the staff's earlier review of the SBWR, work that GENE relies on for the ESBWR, the staff noted that GENE had not evaluated more traditional integral containment tests such as the Marviken tests, the Carolinas Virginia Tube Reactor test 3 without sprays, and the Battelle- Frankfurt Model Containment tests C-13 and C-15, for MSLBs. In response to staff RAI 317.1, GENE agreed to perform assessments of TRACG to model containment performance against integral test data that is publicly available for International Standard Problems where the test facilities and tests are well defined. The tests to be analyzed will be specified later, and the analysis will be completed during the design certification review.

The staff also requested that GENE provide a plan and schedule to assess the ability of TRACG to model containment performance against additional separate effects tests. Separate effects tests that should be considered include the Wisconsin Flat Plate condensation tests, (References 36, 37, and 38). In response to staff RAI 317.2, GENE agreed to perform assessments of TRACG to model containment performance against separate effects test data that is publicly available for International Standard Problems where the test facilities and tests are well defined. The tests to be analyzed will be specified later, and the analysis will be completed during the design certification review.

- 14) GDCS gas space and the wetwell vent should be modeled correctly during the design certification stage.

- 15) During the design certification review, if the ECCS evaluation model is used beyond 2000 seconds, additional VESSEL levels need to be added on top of the existing [[ ]], and the pool needs to be modeled in the same fashion as is done for containment/LOCA modeling.
- 16) Prior to submission of the final design analyses in support of design certification, GENE should perform a review of the appropriateness of the [[ ]] factors and the liquid/vapor interface heat transfer used in the containment modeling.
- 17) Prior to performing the final design analyses at the design certification stage, GENE should perform a thorough evaluation of the ESBWR design records and TRACG ESBWR model development records to substantiate that the TRACG models and correlations are consistent with the final design requirements and intended application.
- 18) At the design certification stage, GENE should examine further whether or not an uncertainty analysis can be performed on the combined reactor coolant system/containment system calculation rather than treating the containment aspect of the ECCS LOCA calculation in a bounding way. The uncertainty analysis methodology should be applicable to both short term and long term LOCA events (i.e., up to 72 hours).
- 19) The actual design configuration of the PCCS vent system, especially the vent submergence, may influence the amount of steam condensed in the SP. Therefore, during the design certification review, the staff will confirm that steam entering the SP through the PCCS vent, as designed, will perform as expected to condense steam entering the SP.
- 20) This safety evaluation is based on the 4000 MWth ESBWR reference design as described in Reference 15. At the design certification stage, GENE should demonstrate that the reference design as described in Reference 15 has not been altered in such a way as to affect the staff's conclusions of this report. Significant changes in the design that challenge the conclusions of this report will result in the staff reevaluating the applicability of the TRACG code.

## 5.0 CONCLUSIONS

### Test Program

The **full-size component** test data from the PANTHERS/PCC and PANTHERS/IC testing programs cover the range of the operational conditions expected in the design-basis LOCAs in the ESBWR. These data are deemed to be adequate for validating the TRACG code regarding the PCCS and ICS performance in the ESBWR, with the understanding that a PCCS condenser in the ESBWR has approximately 35 percent more heat removal capability compared to the PANTHERS/PCC condenser and an ICS condenser (with two identical modules of tubes) has

twice the heat removal capability as the PANTHERS/IC condenser (with only one module of tubes).

The **integral systems** test data from the GIST, GIRAFFE helium, GIRAFFE systems interactions, PANDA M-series, and PANDA P-series test programs as a whole cover a range of the late blowdown phase, GDCS phase, and long-term cooling phase of the accidents. Strengths and weaknesses of the individual test programs are identified and evaluated. The staff has reviewed the test programs and results and concludes that the weaknesses (including some phenomenon distortions) in general do not invalidate the overall reactor vessel and containment response in a LOCA shown by TRACG. The combined data from the GIST, GIRAFFE, and PANDA integral systems tests are generally expected to cover the LOCA phenomena and processes defined in the PIRTs for the late blowdown phase, GDCS phase, and long-term cooling phase.

The GENE test programs, as set forth in detail above, lack an integral test facility in the ESBWR configuration, and the PCCS tests are not full scale to the ESBWR design. These weaknesses in the test data will increase overall uncertainty in plant calculations. However, the design certification analysis is not anticipated to result in uncovering of the ESBWR core during a LOCA based on the margin demonstrated in the calculated results.

#### Independent Analyses

The staff's independent analyses of the reactor coolant system and containment behavior under a LOCA, using the GENE TRACG code and the staff's TRACE/CONTAIN code, indicate that beyond 600 seconds, TRACG and TRACE/CONTAIN provide consistent results. While differences occur in the short time period within 600 seconds, the codes indicate the same trends and predict the same phenomena. At this time, those differences can not be fully explained as the TRACE code is still in the developmental stage and has not yet been fully assessed.

#### Scaling

The staff concludes that GENE demonstrated that there are relevant data sufficient to qualify TRACG in its simulation of the phase for which the scaling analysis was completed. The phase for which this has been done, the GDCS injection phase, is indeed the most important period of the transient. Conservative, bounding analyses have been employed for the remainder of the LOCA event. The rigor of the analyses is not at issue, but rather the completeness of the analysis. As a part of this review, the staff has determined that it is acceptable for GENE to perform a rigorous scaling analysis limited to the most important phase of the LOCA event, and in terms of the most critical variable (core level), thereby demonstrating that the scaling analysis tools are correct while the scaling analysis itself may be incomplete. GENE has been fully responsive to the staff concerns regarding the scaling analysis and methodology.

#### Uncertainty Analysis

The staff concludes, based on review of the GENE uncertainty analysis, that GENE is not consistent with this step in the CSAU methodology approach for the LOCA/ECCS application of the TRACG code. However, as set forth in Section 3.14 above, the staff finds the GENE method acceptable in light of the margins in the design as indicated in the predicted lack of core uncover and heatup. Should it be found during the design certification review of the ESBWR system that core uncover does occur, the staff will revisit the method of uncertainty combination and the associated statistical methodology for the LOCA/ECCS application.

#### Assumptions

The assumption of the loss of feedwater flow used by GENE for the current stage in the design is not conservative, resulting in underestimation of the maximum containment pressure and temperature. Although there is adequate margin in the prediction of containment pressure and temperature, the feedwater flow assumption needs to be justified at the design certification phase.

#### TRACG Applicability and Overall Conclusion

The staff concludes, based on the above discussion, that TRACG, including the application methodology, is an acceptable evaluation model for ESBWR Loss-of-Coolant Accident analyses as presented in NEDC-33083P, *TRACG Application for ESBWR*. The staff therefore concludes that TRACG is acceptable for referencing during the design certification review of the ESBWR, provided the conditions specified in this safety evaluation are met. Section 4 of this report identifies those items that should be addressed at the design certification stage as part of the application of TRACG to the ESBWR design.

#### NRC Criteria

If the NRC's criteria or regulations change so that its conclusions about the acceptability of the report are invalidated, GENE or the applicant referencing the report, or both, will be expected to revise and resubmit its respective documentation, in accordance with 10 CFR 52.47, or submit justification for the continued effective applicability of the report without revision of the respective documentation.

## 6.0 ACRONYMS

ABWR	Advanced Boiling Water Reactor
AC	Alternating Current
ADS	Automatic Depressurization System
ANS	American Nuclear Society
ANSI	American National Standards Institute
AOO	Anticipated Operational Occurrence
ATWS	Anticipated Transient without Scram
BDLB	Bottom Drain Line Break
BOP	Balance of Plant
BWR	Boiling Water Reactor
CCFL	Counter-Current Flow Limit
CHF	Critical Heat Flux
CSAU	Code Scaling Applicability and Uncertainty
DBA	Design Basis Accident
DC	Direct Current
DPV	Depressurization Valve
DW	Dry Well
ECCS	Emergency Core Cooling System
ECI	Exterior Component Interface
ESBWR	Economic Simplified Boiling Water Reactor
GDC	General Design Criteria
GDCS	Gravity-Driven Cooling System
GDLB	GDCS Line Break
GE	General Electric Company
GENE	General Electric Nuclear Energy
GEXL	General Electric Critical Quality Boiling Length Correlation
GIST	Gravity-driven Integral Systems Test
H2TS	Heirarchical Two-Tiered Scaling
HVAC	Heating, Ventilation and Air Conditioning
IC	Isolation Condenser
ICS	Isolation Condenser System
KSP	Kuhn-Schrock-Peterson
LHGR	Linear Heat Generation Rate
LOCA	Loss-of-Coolant Accident
MCPR	Minimum Critical Power Ratio
MSIV	Main Steam Isolation Valve
MSLB	Main Steam Line Break
NPP	Nuclear Power Plant
OD	Outside Diameter
PCC	Passive Containment Cooling
PCCS	Passive Containment Cooling System
PCT	Peak Cladding Temperature
PIRT	Phenomena Identification and Ranking Table
PSTF	Pressure Suppression Test Facility

QA	Quality Assurance
RAI	Request for Additional Information
RPV	Reactor Pressure Vessel
SBWR	Simplified Boiling Water Reactor
SER	Safety Evaluation Report
SIET	Societa Informazioni Esperienze Termoidrauliche
SP	Suppression Pool
SRP	Standard Review Plan
SRV	Safety Relief Valve
SSAR	Standardized Safety Analysis Report
TAF	Top of Active Fuel
TAPD	Testing and Analysis Program Description
VB	Vacuum Breaker
V-S	Vierow-Schrock
WW	Wet Well

## 7.0 REFERENCES

1. NEDE-32906P, Rev. 0, *TRACG Application for Anticipated Operational Occurrences (AOO) Transient Analyses*, January 2000.
2. NEDE-32906P Supplement 1, *TRACG Application for Anticipated Transient Without Scram Transient Analysis*, September 2002.
3. Safety Evaluation Report by the Office of Nuclear Reactor Regulation for NEDE-32906P, *TRACG Application for Anticipated Operational Occurrences (AOO) Transient Analyses*, June 2002.
4. Safety Evaluation Report by the Office of Nuclear Reactor Regulation for NEDE-32906P, Supplement 1, *TRACG Application for Anticipated Transient Without Scram Transient Analyses*, August 2003.
5. NUREG/CR-5249, *Quantifying Reactor Safety Margins: Application of Code Scaling Applicability, and Uncertainty Evaluation Methodology to a Large-Break, Loss-of-Coolant Accident*, December 1989.
6. Draft Regulatory Guide, DG-1120, *Transient and Accident Analysis Methods*, U.S. NRC, December 2000.
7. Draft Standard Review Plan, Section 15.0.2, *Review of Analytical Computer Codes*, U.S. NRC, December 2000.
8. Regulatory Guide 1.157, *Best-Estimate Calculations of Emergency Core Cooling System Performance*, May 1989.
9. NEDE-32176P, Rev. 1, *TRACG Model Description*, February 1996.
10. NEDE-32176P, Rev. 2, *TRACG Model Description*, December 1999.
11. NEDC-33083P, *TRACG Application for ESBWR*, November 2002.
12. NEDC-33079P, *ESBWR Test and Analysis Program Description, Supplement 1 - Discussion of PIRT Parameters*, August 2002.
13. NEDC-33080P, *TRACG Qualification for ESBWR*, August 2002.
14. NEDC-33081P, *ESBWR Test Report*, August 2002.
15. NEDC-33084P, Revision 1, *ESBWR Design Description*, August 2003.
16. NEDC-32752P, *TRACG Qualification for SBWR*, August 2002.

17. NEDC-32606P, *SBWR Testing Summary Report*, August 2002.
18. McAdams, W. H., *Heat Transmission*, 3d ed., McGraw-Hill Book Company, Inc., New York, 1954.
19. NEDE-32178P, Rev.1, *Application of the TRACG Model to SBWR Licensing Safety Analysis*, 1998.
20. Kuhn, S. Z., V. E. Schrock, and P. F. Peterson, *Final Report on U. C. Berkley Single Tube Condensation Studies*, University of California, Berkley Report UCB-NE-4201, August 1994.
21. Robbins, C. H., *Tests of the Humboldt Bay Pressure Suppression Containment*, GEAP-3596, November 1960.
22. *Pressure Suppression Test Program*, PG&E, Bodega Bay Atomic Power Unit 1 Exhibit 1, Preliminary Hazards Summary Report, December 1962.
23. NEDE-13442P-01, *Mark II - Pressure Suppression Test Program*, May 1976.
24. NEDM-13377, *Mark III Confirmatory Test Program*, Phase I - Large Scale Demonstration Tests, Test Series 5701 through 5703, October 1974.
25. Holman, J. P., *Heat Transfer*, 3<sup>rd</sup> Edition, McGraw-Hill Book Company, Inc., New York, 1972.
26. Collier, J. G., *Convective Boiling and Condensation*, McGraw-Hill Book Company, Inc., New York, 1972.
27. NEDC-32301, *Single Tube Condensation Test Program*, March 1994.
28. Forster, H. K., and N. Zuber, *Dynamics of Vapor Bubbles and Boiling Heat Transfer*, AIChE Journal, pp 531-535, 1955.
29. COMPRES Report ED45913, *SBWR Vacuum Breaker (VB) Prototype Experimental Qualification General Test Report*, October 1994.
30. NEDE-23785-PA, Rev. 1, *The GESTR-LOCA and SAFER Models for the Evaluation of the Loss-of-Coolant Accident, Volume III: SAFER/GESTR Application Methodology*, October 1984.
31. Fujii, T., et al., *Experimental Study of Performance of a Hybrid Baffle Plate for the Water Wall Type Passive Containment Cooling System*, Nuclear Technology, Vol. 112, October 1985.

32. Kataoka, Y., et al., *Thermal-Hydraulic Characteristics and Heat Removal Capability of Containment Cooling System with External Water Wall*, Nuclear Science and Technology, 27[9], pp 802-814, September 1990.
33. Uchida, H., A. Oyama, and M. Togo, *Evaluation of Post-Incident Cooling Systems of Light Water Power Reactors*, Third International Conference on the Peaceful Uses of Atomic Energy, Vol. 13, Geneva, Switzerland, 1964.
34. NEDE-32177P, Rev. 2, *TRACG Qualification*, January 2000.
35. *Containment Configuration Data Book*, 25A5044, Rev. 1, November 1992.
36. Huhtiniemi, I. K., and M. L. Corradini, *Condensation in the Presence of Noncondensable Gases*, Nuclear Engineering Design, 141, pp 429-446, 1993.
37. Siddique, M., *The Effects of Noncondensable Gasses on Steam Condensation Under Forced Convection Conditions*, MIT, January 1992.
38. Lian, K., *Experimental and Analytical Study of Direct Contact Condensation of Steam and Water*, MIT, May 1991.
39. ANSI/ANS-5.1, Decay Heat Standard, 1994.
40. NEDC-33082P, *ESBWR Scaling Report*, December 2002.
41. Tills, J., *Letter Report on the CONTAIN SBWR Plant Assessment*, Sandia National Laboratory, June 19, 1994.
42. Murata, K. K., et al, *Code Manual for CONTAIN 2.0: A Computer Code for Nuclear Reactor Containment Analysis*, Sandia National Laboratory, NUREG/CR-6533, June 1997.
43. Tills, J., *Letter Report on PCCS Modeling for SBWR*, Sandia National Laboratory, March 1994.
44. Tadios, E. L., *CONTAIN Model for the GIRAFFE Passive Heat Removal Test Facility*, Sandia National Laboratory, June 29, 1995.
45. Tills, J., *Analysis of the GE PANTHERS Tests Using the CONTAIN Code*, Sandia National Laboratory, June 20, 1996.
46. NEDC-33082P, Rev. 0, *ESBWR Scaling Report*, December 2002.
47. NEDC-32288P, Rev. 1, *Scaling of the SBWR Related Tests*, October 1995.
48. NEDC-32391P, Rev. 1, *SBWR Test and Analysis Program Description*, April 1995.

49. NUREG/CR-5809, *A Hierarchical, Two-Tiered Scaling Analysis*, November 1991.
50. Letter from T.R. Quay, USNRC, to J.E. Quinn, *GE Nuclear Energy, Staff Review of GE's Report NEDC-32288P, Revision 1, Scaling of SBWR Related Tests Related to Containment Area*, April 24, 1996 (Accession No. 9906030224).

#### Technical Evaluation Reports

51. Barber, D. A., *ESBWR LOCA Confirmatory Analysis*, Task Order 29, Information Systems Laboratories, Inc., October 2003.
52. Han, J., *ESBWR PIRT, Test and Analysis Program Description, and Full-Size Component Testing Programs and Integral Testing Programs*, NRC Office of Nuclear Regulatory Research, October 2003.
53. Krotiuk, W., *Scoping Analysis of a Main Steam Line Break in the GE ESBWR Containment Using CONTAIN*, NRC Office of Nuclear Regulatory Research, November 2003.
54. Rohatgi, U. S., L. Cheng, and J. Jo, *TRACG Model Description, NEDE-32176P, Rev. 2*, Brookhaven National Laboratory, October 2003.
55. Cheng, L., J. Jo, and U. S. Rohatgi, *TRACG Qualification, NEDE-32177P, Rev. 2*, Brookhaven National Laboratory, October 2003.
56. Jo, J., U. S. Rohatgi, and L. Cheng, *TRACG Qualification for ESBWR, NEDE-33080P, Rev. 0*, Brookhaven National Laboratory, October 2003.
57. Cheng, L., J. Jo, and U. S. Rohatgi, *TRACG Application for ESBWR, NEDE-33083P*, October 2003.
58. Staudenmeier, J., et al., *ESBWR TAPD, PIRT, Scaling, and Testing*, NRC Office of Nuclear Regulatory Research, January 2004.

Requests for Additional Information

<b>Author</b>	<b>Description</b>	<b>Date</b>
A. Cubbage	Request for Additional Information Letter No. 1 Related to ESBWR Pre-application Review	May 16, 2003
A. Cubbage	Request for Additional Information Letter No. 2 Related to ESBWR Pre-application Review	May 20, 2003
A. Cubbage	Request for Additional Information Letter No. 3 Related to ESBWR Pre-application Review	May 30, 2003
A. Cubbage	Re-issuance of Request for Additional Information Letter No. 4 Related to ESBWR Pre-application Review	July 25, 2003
A. Cubbage	Request for Additional Information Letter No. 5 Related to ESBWR Pre-application Review	July 17, 2003
A. Cubbage	Request for Additional Information Letter No. 6 Related to ESBWR Pre-application Review	July 17,2003
A. Cubbage	Request for Additional Information Letter No. 7 Related to ESBWR Pre-application Review	July 30, 2003
A. Cubbage	Re-issuance of Request for Additional Information Letter No. 8 Related to ESBWR Pre-application Review	August 19,2003
L. Fields	Re-issuance of Request for Additional Information Letter No. 9 Related to ESBWR Pre-application Review	September 11, 2003

GENE Responses to Requests for Additional Information

<b>Author</b>	<b>Title/Description</b>	<b>Document Date</b>
A. Rao	Responses to Request for Additional Information (RAI) numbers (9, 16-24, 113-143, 213, 214, 234, 236, 257, 258, 266, 275, 276, 279 and 281) for ESBWR Pre-application Review.	July 31,2003
A. Rao	Response to Request for Additional Information Numbers (187, 190, 191, 195, 202, 220, 225, 231, 232, 272, 296, 297, 327, 334-338, 345, 347, 349-359, 371-376, 378, & 379) for ESBWR Pre-Application Review.	August 8,2003

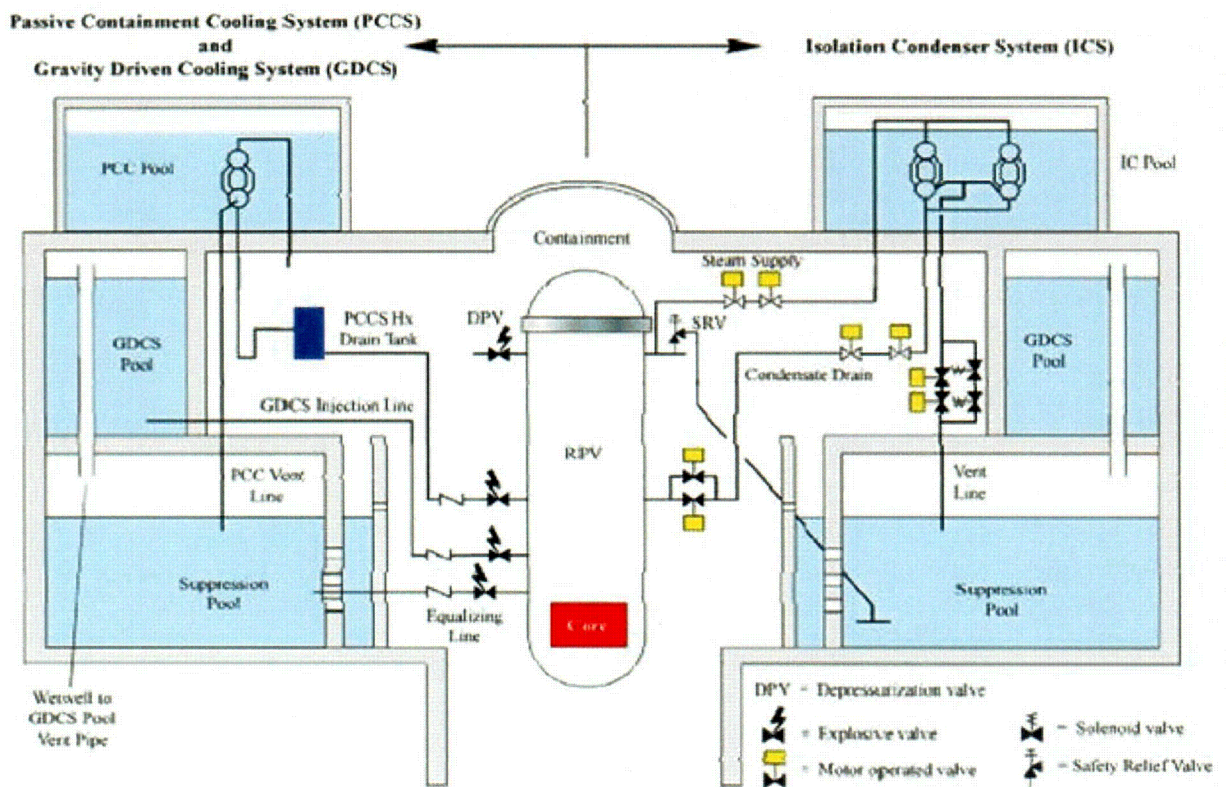
A. Rao	Response to Request for Additional Information (RAI) numbers (13, 14, 28-30, 33, 34, 36-44, 46, 49-53, 55, 57-59, 61-64,66, 68,69, 72-76, 78, 80, 81, 83-85, 88, 93, 96, 98, 99, 102-104, 107, 108, 110-112, 147-150, 153-158, 163, 165,166, 168-175, 178-182, 185, 186, 188, 189, 192-194, 196-201, 203-212, 215-219, 221-224, 226-230, 233, 235,237-256, 263, 265, 267-270,273, 274, 278, 280, 283-285, 287-289, 291, 300, 302, 303, 318, 320, 322, 328, 332, 340-344, 348, 361, 362, 364-370, 377, 386,407, 409-413) for ESBWR Pre-application Review.	August 18, 2003
A. Rao	Response to Request for Additional Information (RAI) numbers (7 and 8) for ESBWR Pre-application Review.	August 15, 2003
S. Delvin	Response to Request for Additional Information Numbers (1-5, 10-12, 25-27, 31, 32, 144-146, 151, 152, 160, 167, 177, 262, 277, 290, 294, 308, 312-315, 346, 360, 363, 380, 381, 383-385, & 389-405) for ESBWR Pre-Application Review.	August 20, 2003
A. Rao	Response to Request for Additional Information Numbers (161, 162, 164, 176, 183, 184, 286, 292, 293, 295, 301, 323, 325, 339, & 382) for ESBWR Pre-Application Review.	August 22, 2003
A. Rao	Re-transmittal of Response to Request for Additional Information (RAI) numbers (6, 15, 35, 45, 47, 48, 60, 65, 67, 77, 89-92, 94, 95, 97, 105, 159, 264, 271, 298, 299, 304,305, 307, 310 317,321, 324, 326, 329, 331, 387, 388, 406, and 408) for ESBWR Pre-application Review.	September 5, 2003
S. Delvin	Response to Request for Additional Information (RAI) 330 for ESBWR Pre-application Review.	September 3, 2003
S. Delvin	Response to Request for Additional Information (RAI) Nos. (54, 79, 100, 101, 109, 259, 282, 309, 311, 333, and 383) for ESBWR Pre-Application Review.	September 5, 2003
A. Rao	Response to Request for Additional Information (RAI) numbers (7, 8, 106 and 177) for ESBWR Pre-application Review.	September 12, 2003
A. Rao	Response to Request for Additional Information (RAI) numbers (70, 71, 82, 86,87,316, and 318) for ESBWR Pre-application Review.	September 16, 2003
A. Rao	Response to Request for Additional Information (RAI) numbers (25, 306, and 319) for ESBWR Pre-application Review.	September 18, 2003

A. Rao	Response to Request for Additional Information (RAI) Number 56 for ESBWR Pre-Application Review.	September 19, 2003
S. Delvin	Response to Request for Additional Information (RAI) numbers (306 and 339) for ESBWR Pre-application Review.	September 24, 2003
S. Delvin	Response to Request for Additional Information (RAI) numbers (7 and 8) for ESBWR Pre-application Review – Supplementary Information.	October 2, 2003
S. Delvin	Response to Request for Additional Information (RAI) numbers (117.2, 306, 314.1, 322, 323.4, 329, and 406) for ESBWR Pre-application Review - Supplementary Information	October 13, 2003
S. Delvin	Response to Request for Additional Information (RAI) numbers (15, 259, 286, and 292) for ESBWR Pre-application Review - Supplementary Information.	October 20, 2003
A. Rao	Response to Request for Additional Information (RAI) numbers (322 and 406) for ESBWR Pre-application Review - Supplementary Information	October 23, 2003
A. Rao	Response to RAI 339 - Supplementary information	November 3, 2003
S. Delvin	Response to RAI 406 additional supplementary information	November 4, 2003
S. Delvin	Response to Request for Additional Information (RAI) on Scaling Responses for ESBWR Pre-application Review – Additional Supplementary Information.	November 6, 2003
S. Delvin	Response to Request for Additional Information (RAI) on Model LTR NEDE-32176 (Rev 1 and 2) and RAI number (330.4) for ESBWR Preapplication Review – Additional Supplementary Information.	November 7, 2003
S. Delvin	Response to Request for Additional Information (RAI) Number (25) for ESBWR Pre-application Review – Additional Supplementary Information. (Errata to TRACG qualification for ESBWR)	November 12, 2003
S. Delvin	Response to Request for Additional Information (RAI) Number (406) for ESBWR Pre-application Review – Additional Supplementary Information.	November 14, 2003

S. Delvin	Response to Request for Additional Information (RAI) Number (406) for ESBWR Pre-application Review – Supplementary Information regarding Identification of changes to TRACG04.	November 19, 2003
S. Delvin	Response to Request for Additional Information (RAI) number (330.4) for ESBWR Pre-application Review – Additional Supplementary Information Regarding TRACG Input Deck for PSTF Test 5807-29.	November 21, 2003
R. Gamble	Response to Request for Additional Information (RAI) No. 183 for ESBWR Pre-application Review - Supplementary Information.	March 1, 2004
R. Gamble	Response to Requests for Additional Information (RAIs) Related to TRACG Calculations for the GDCS Line Break.	March 3, 2004
R. Gamble	Response to RAI No. 183 for ESBWR Pre-application Review - Supplementary Information With Revised Calculation.	March 16, 2004
R. Gamble	Response to Request for Additional Information (RAI) Number 183 for ESBWR Pre-application Review - Supplementary Information with Parametric Long-Term Calculation for GDCS Line Break	April 12, 2004
R. Gamble	Update of ESBWR TRACG Application Cases for NEDC-33083P Using the 9-Apr-2004 Program Library Version of TRACGO4	June 2, 2004
R. Gamble	Update of ESBWR TRACG Qualification for NEDC-32725P and NEDC-33080P Using the 9-Apr-2004 Program Library Version of TRACGO4	June 2, 2004
R. Gamble	Response to Additional RAIs on ESBWR PCCS Modeling for TRACG Calculations	June 18, 2004
R. Gamble	Description of Changes in TRACG4 Between Original Version and April 9, 2004 Program Library Version	July 7, 2004
R. Gamble	Response to Additional RAIs on TRACG Calculations for GDCS Line Break	July 9, 2004

8.0 FIGURES

Figure 3.0.1 ESBWR Layout  
(Note: Figure is not to scale)



C-01

PIRT Process

Top-Down Process Bottom-Up Process

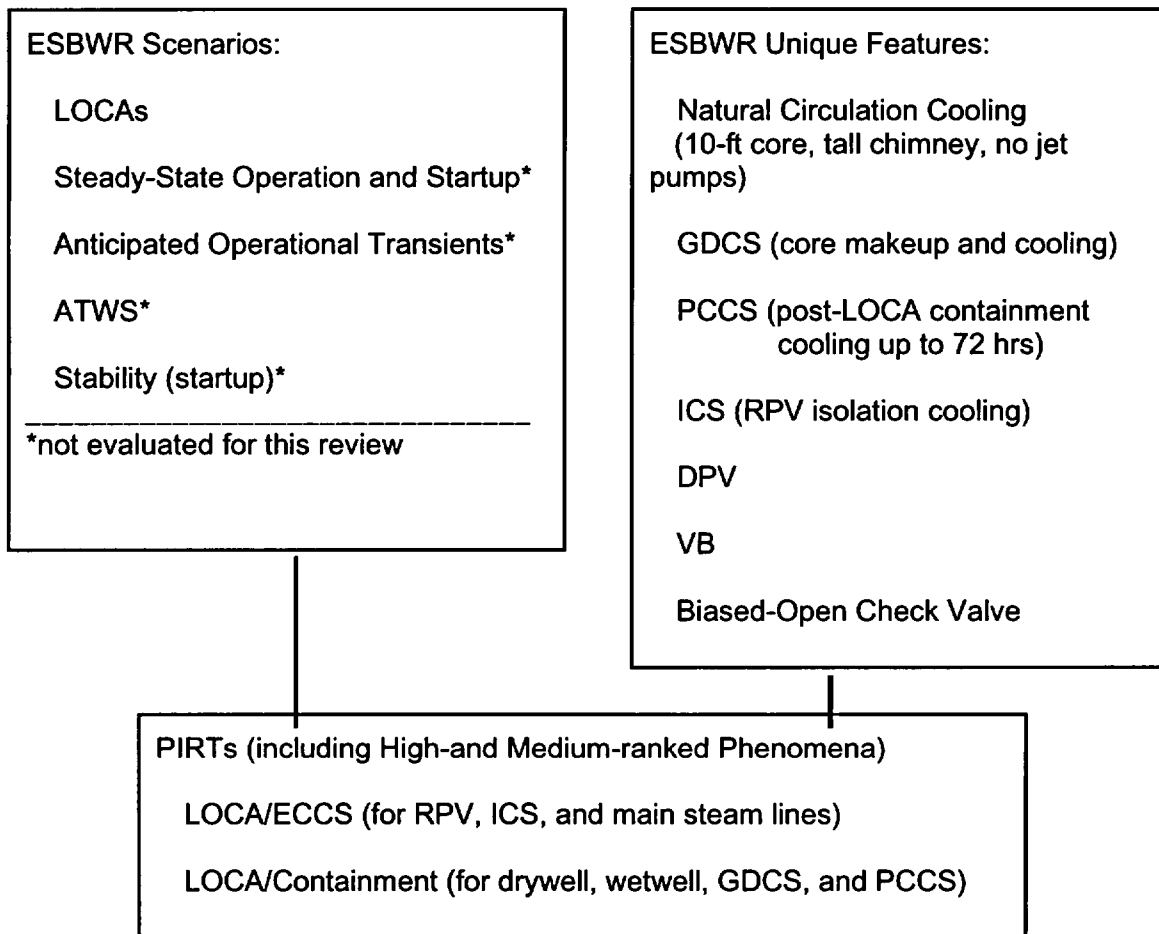


Figure 3.3.1 - PIRT Process

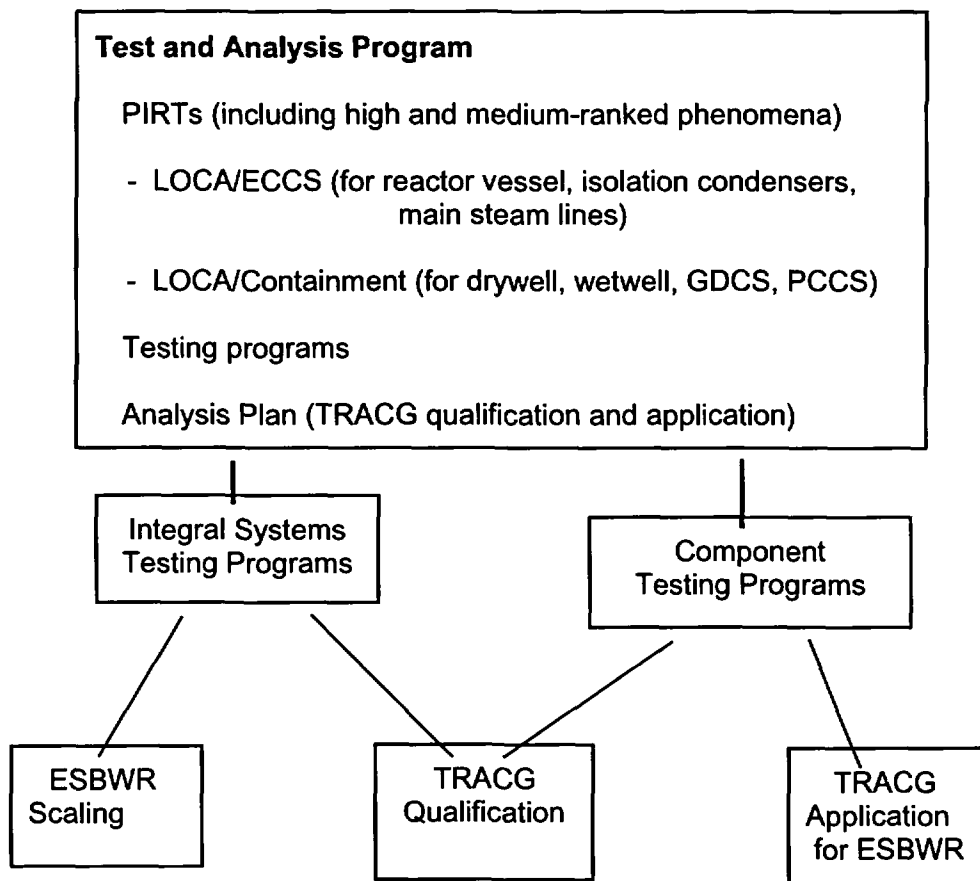


Figure 3.7.1.1 - Test and Analysis Program

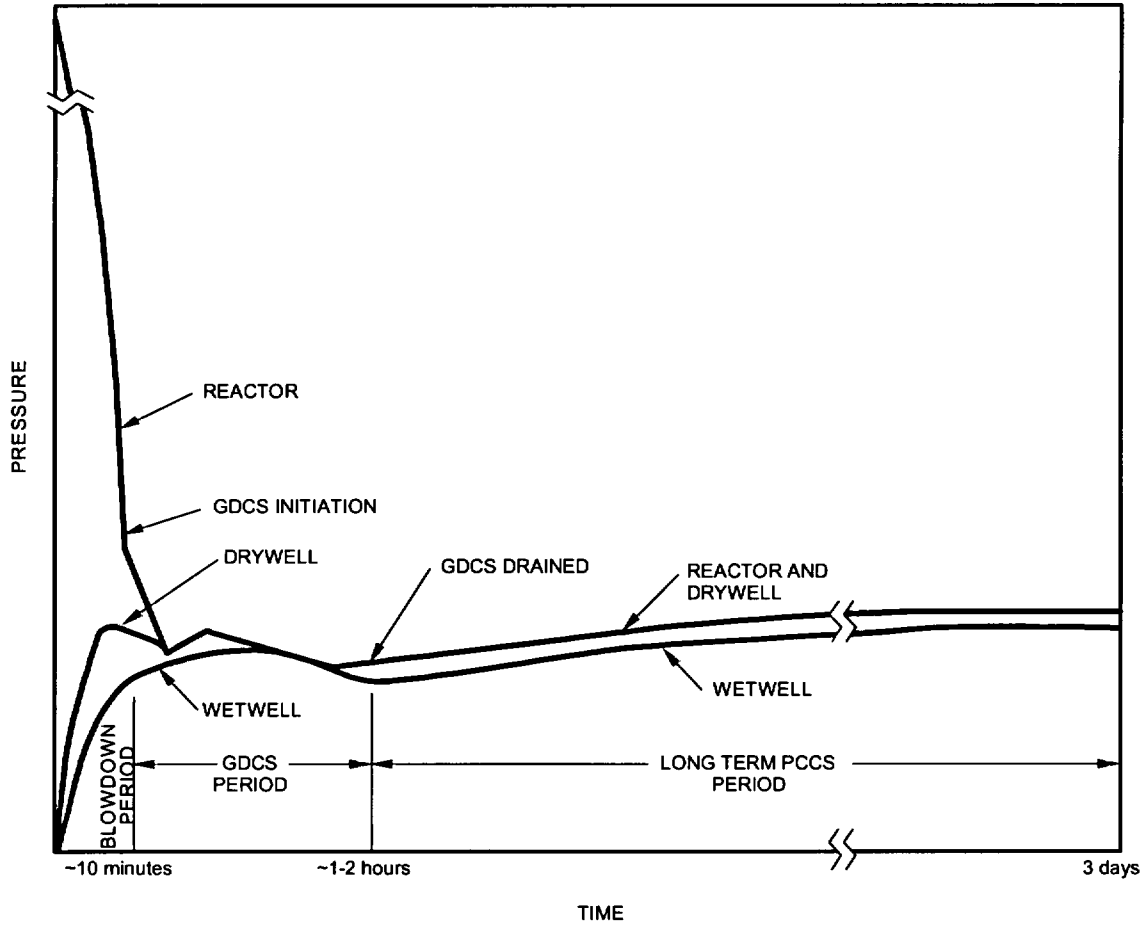


Figure 3.10.1 Time Phases of LOCA Event

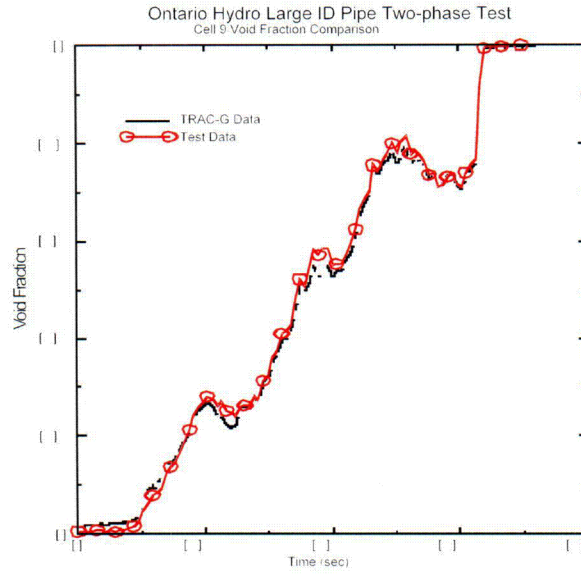


Figure 3.7.2.1 Ontario Hydro Large Pipe Two-phase Flow Testing - Void Fraction

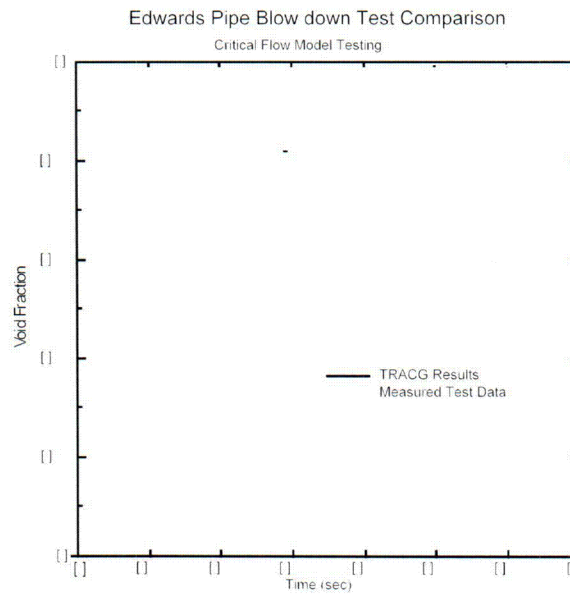


Figure 3.7.2.2 Edwards Pipe Blow Down Test - Void Fraction.

C-02

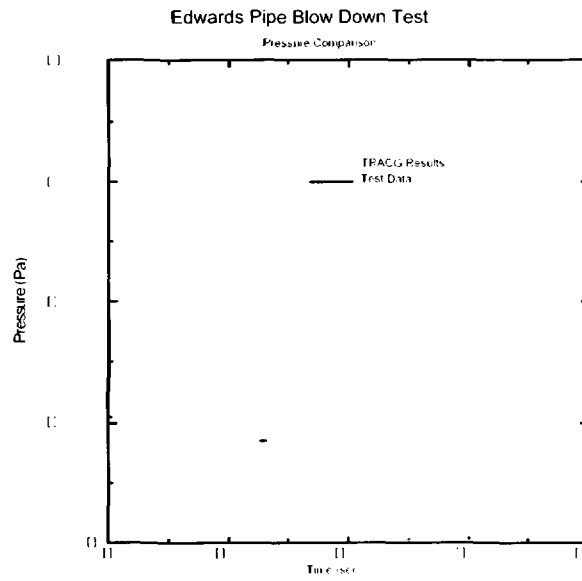


Figure 3.7.2.3 Edwards Pipe Blow Down Test - Pressure

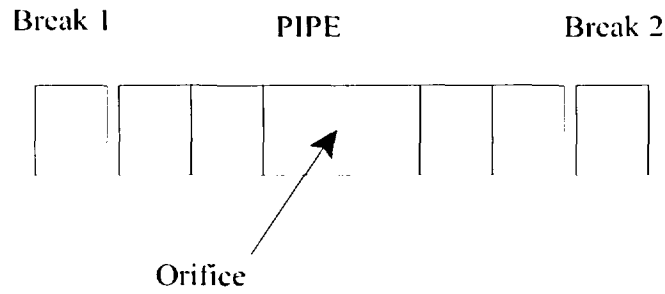


Figure 3.7.2.4 Kinetic Energy Verification Test Problem Nodalization

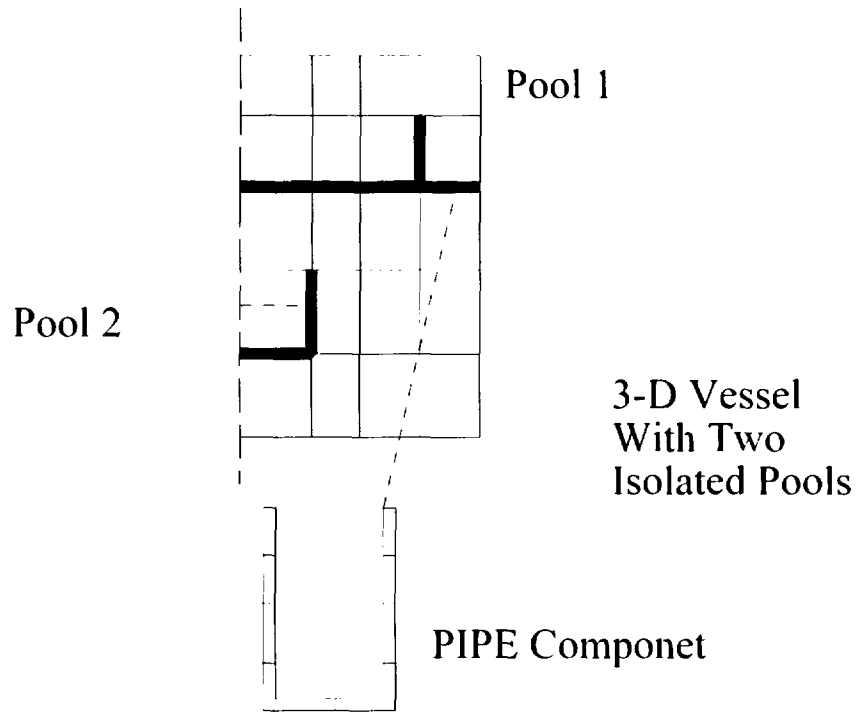


Figure  
3.7.2.5

Gravity Head Preservation Verification Test.

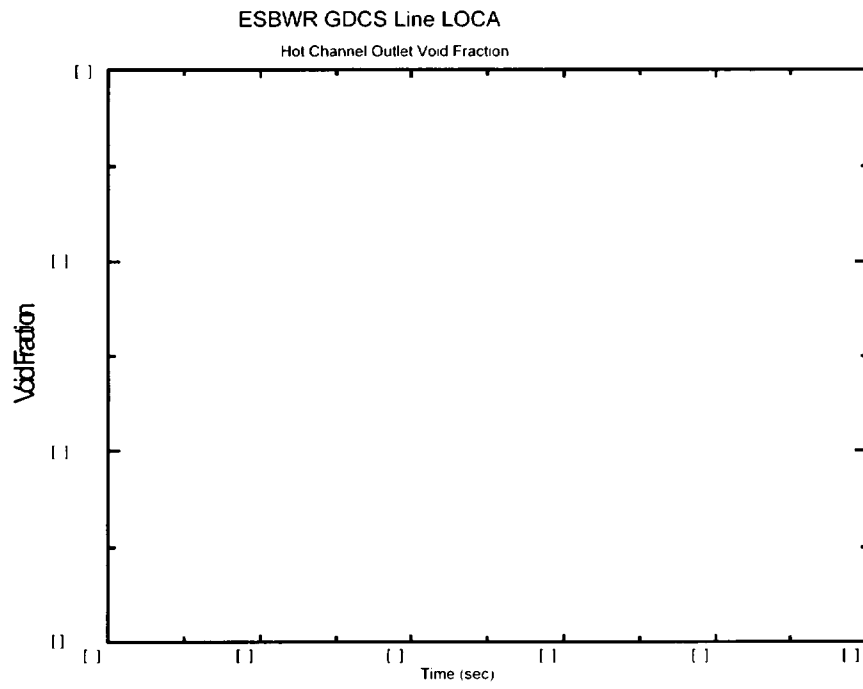


Figure 3.7.2.6 Hot Channel Void Fraction During Blowdown.

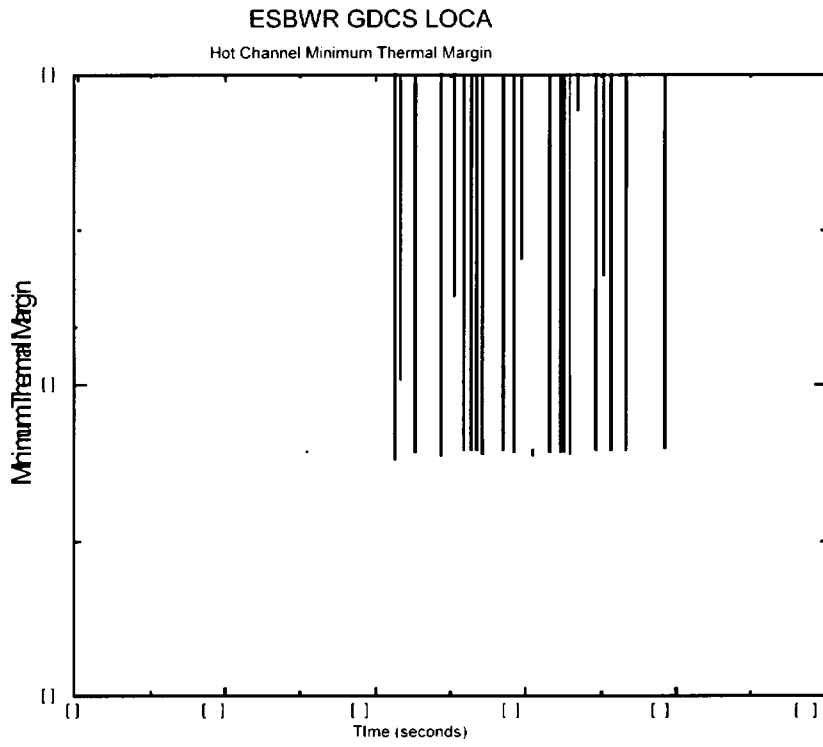


Figure 3.7.2.7 Hot Channel Minimum Thermal Margin During GDCS Line Break LOCA.

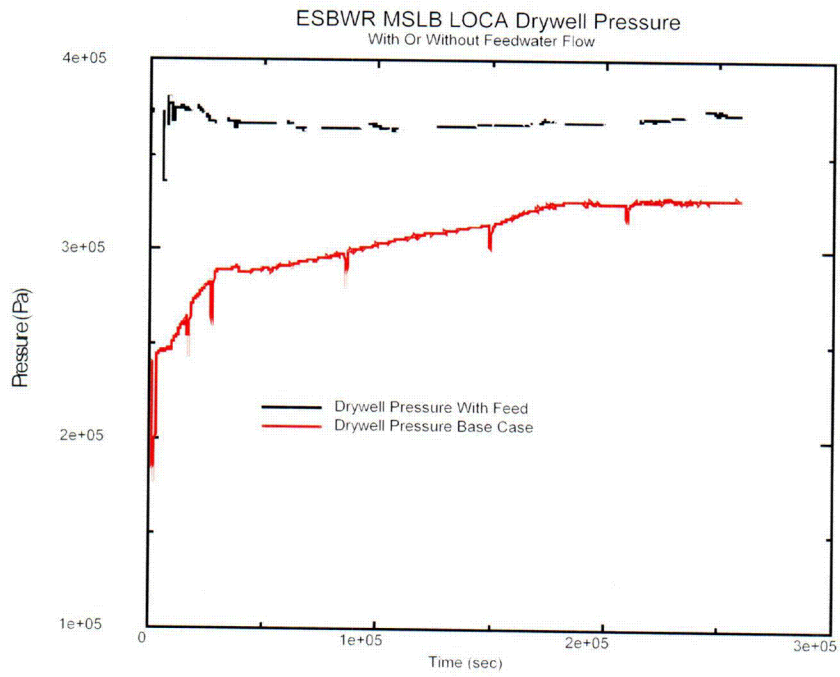


Figure 3.7.2.8 Drywell Pressure With or Without Feedwater Mass And Energy.

C-03

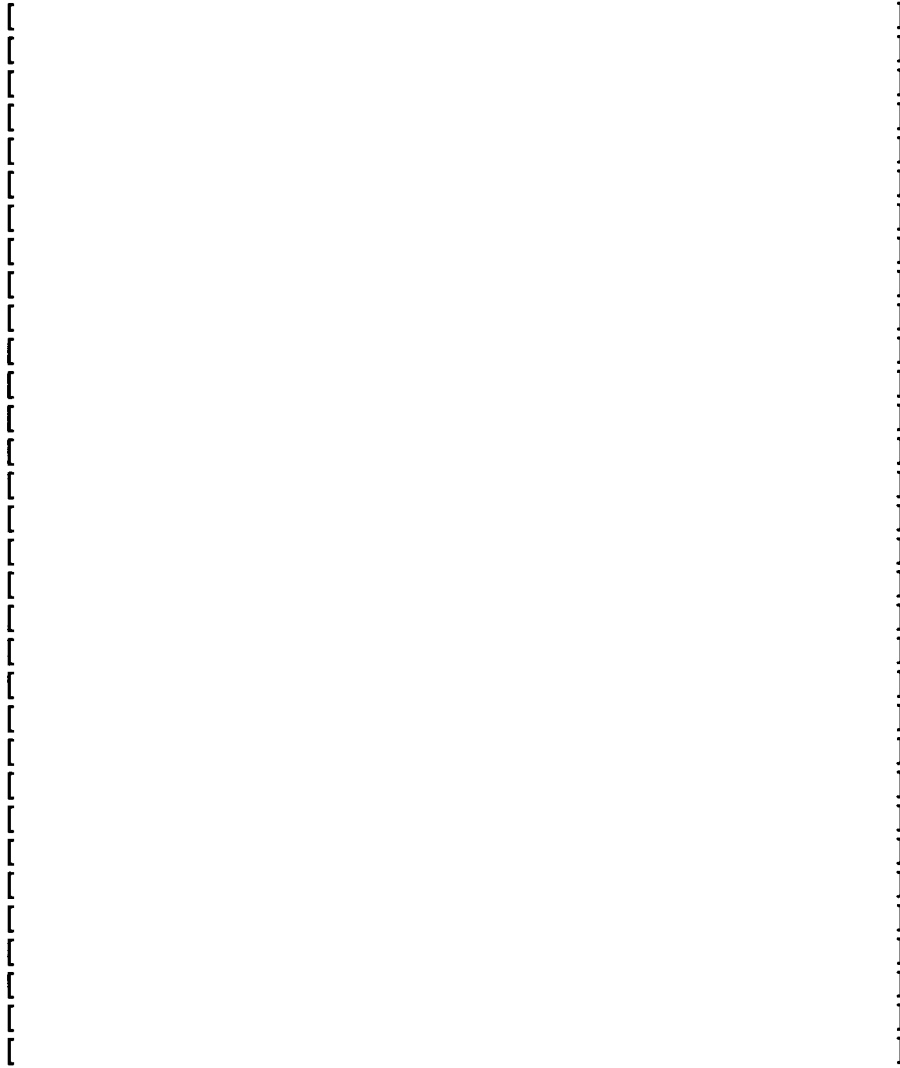


Figure 3.7.2.9 : TRACE ESBWR Reactor Vessel Model

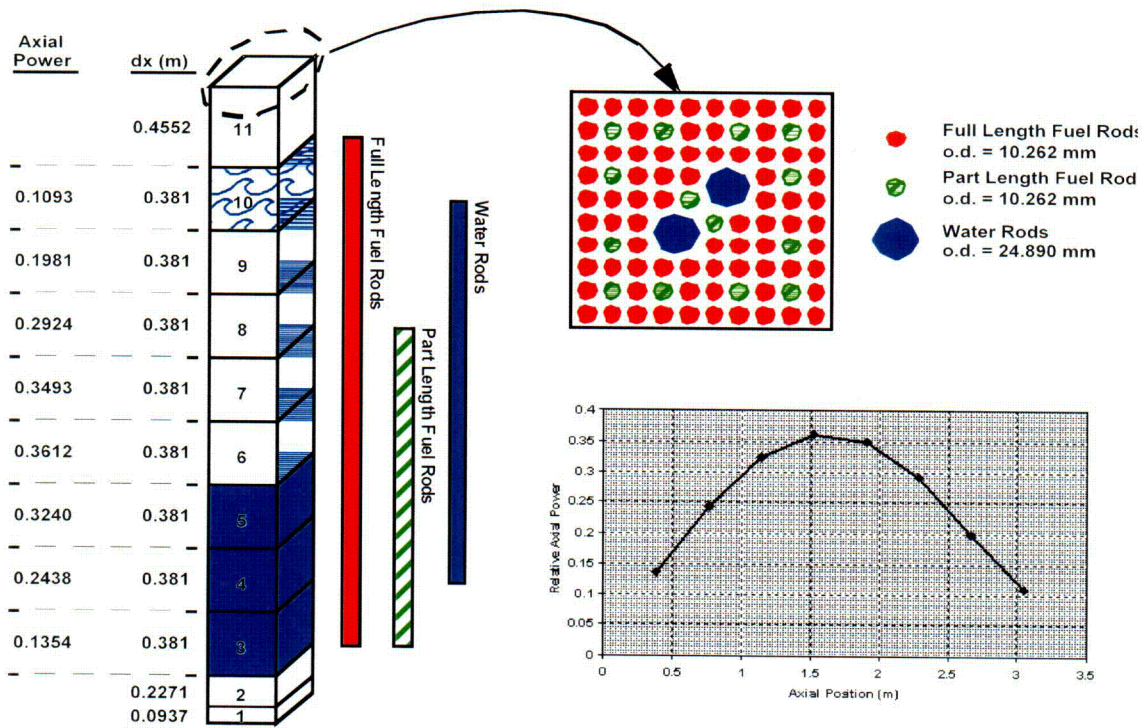


Figure 3.7.2.10 TRACE Fuel Channel Model.

C-04

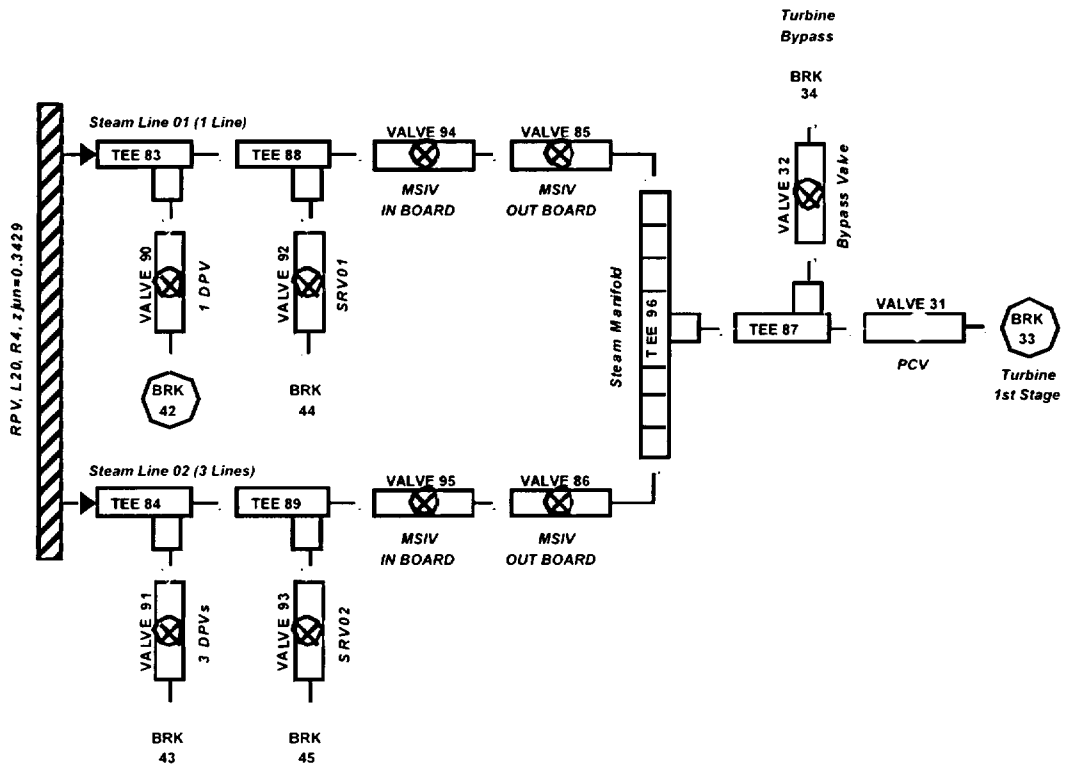


Figure 3.7.2.11 TRACE ESBWR Main Steam Line.

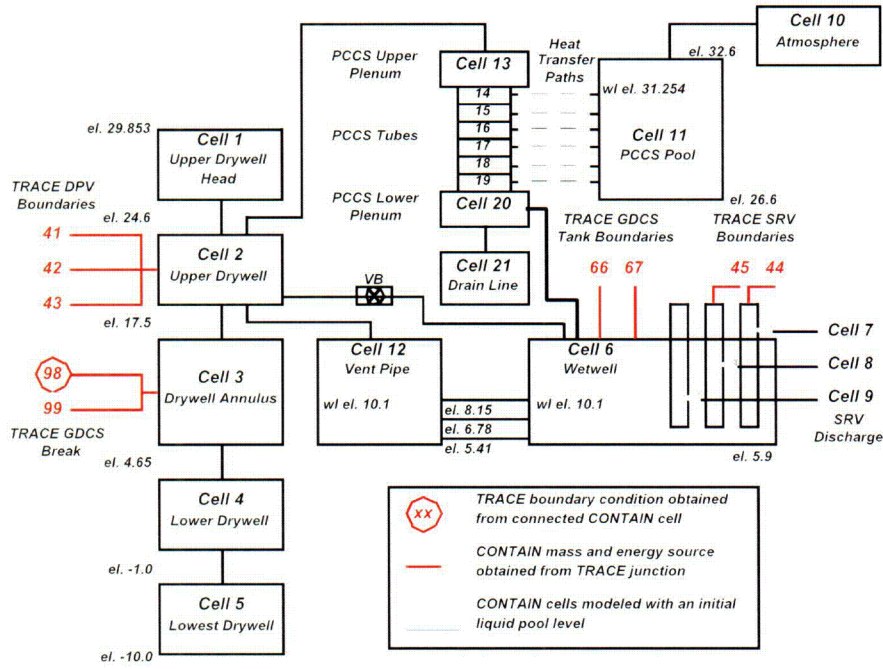


Figure 3.7.2.12 TRACE ESBWR Containment Model

C-05

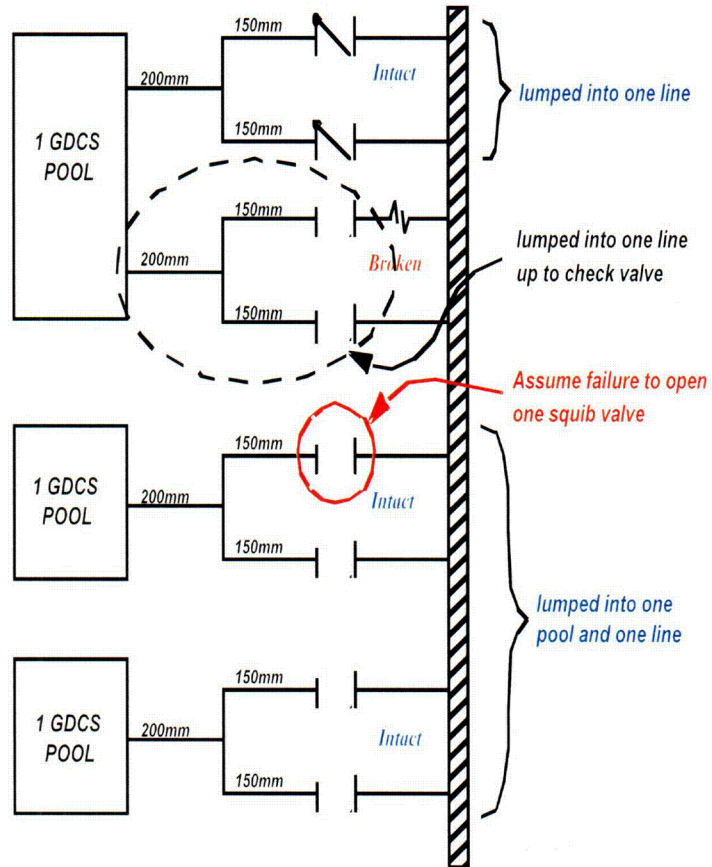


Figure 3.7.2.13 GDCS Line Break Model.

C-06

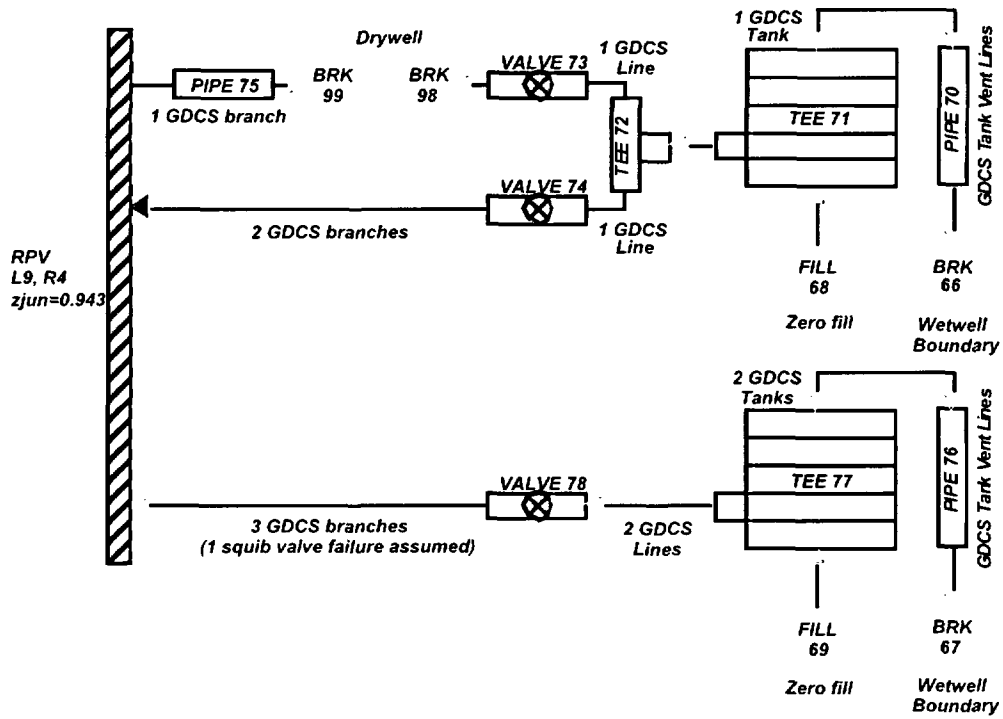
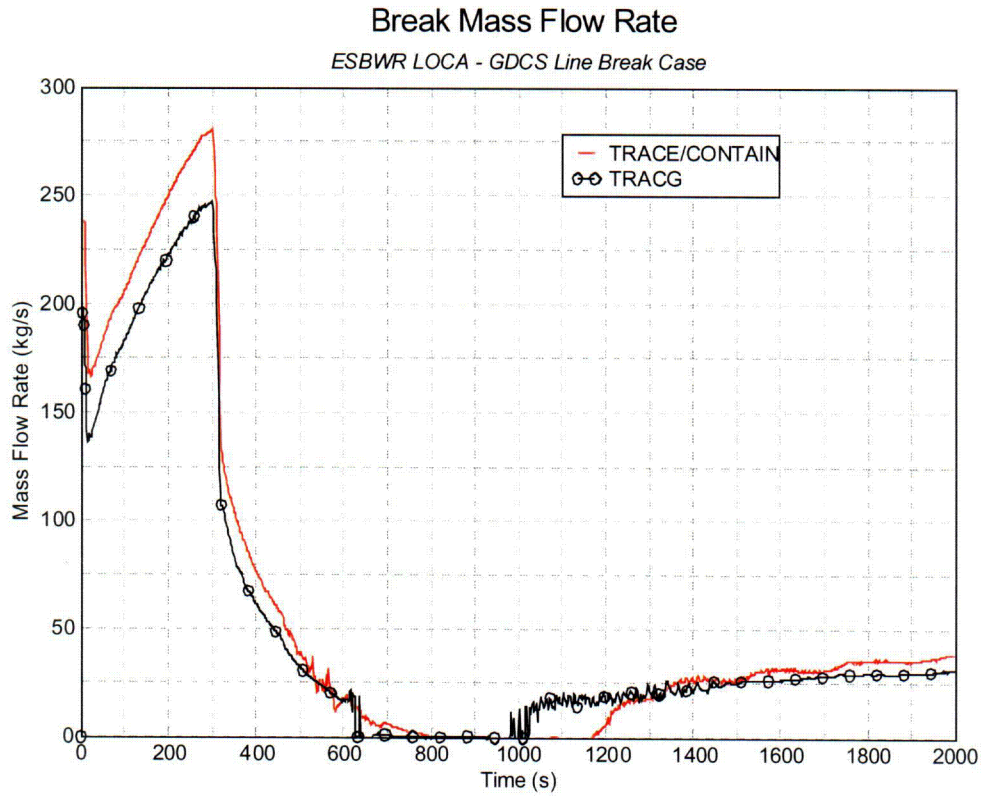


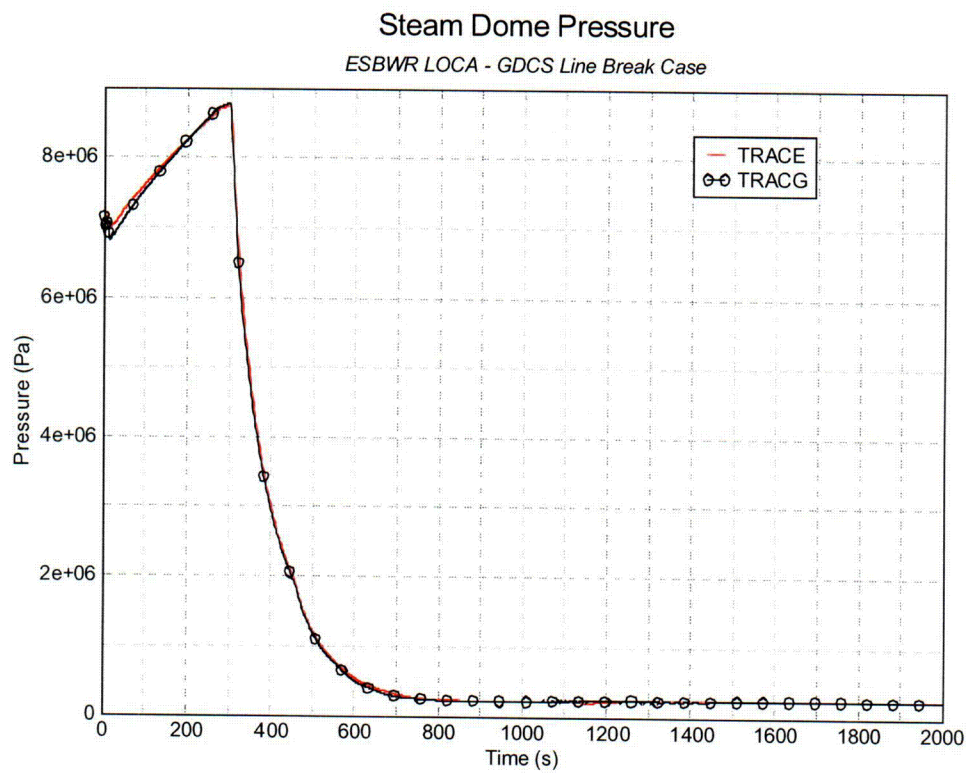
Figure 3.7.2.14 Nodalization of GDCS for the GDCS line Break LOCA Case.



Sat Aug 14 10:05:58 2004

Figure 3.7.2.15 GDCS Line Break Mass Flow Rate.

C-07



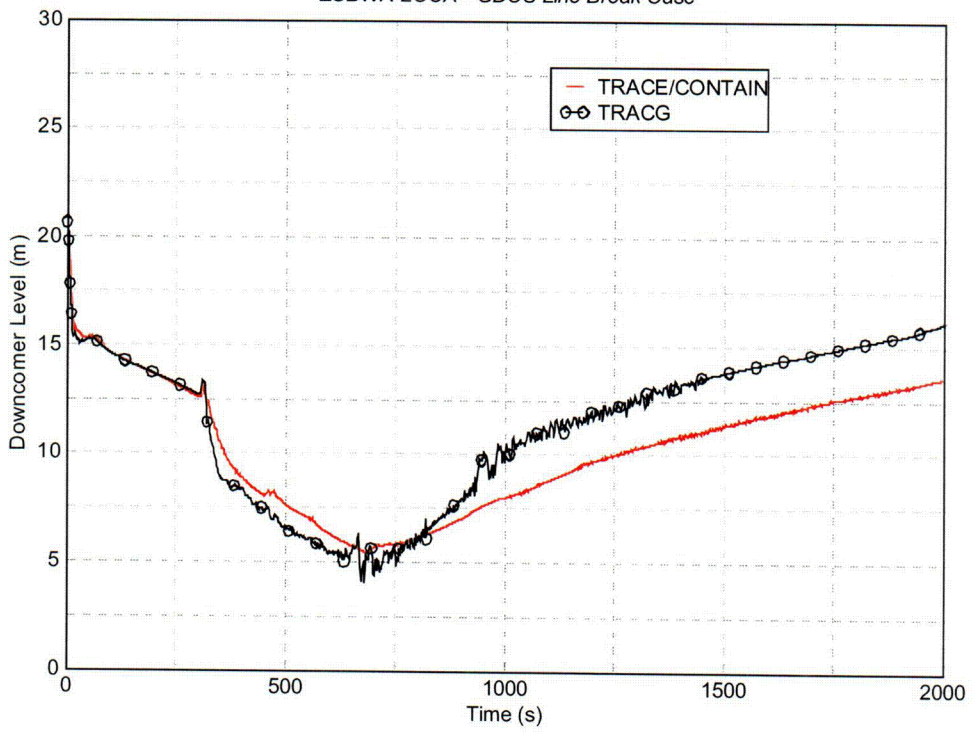
Tue Aug 10 11:57:23 2004

Figure 3.7.2.16 GDCS Line Break Dome Pressure.

C-08

### Downcomer Collapsed Liquid Level

ESBWR LOCA - GDCS Line Break Case



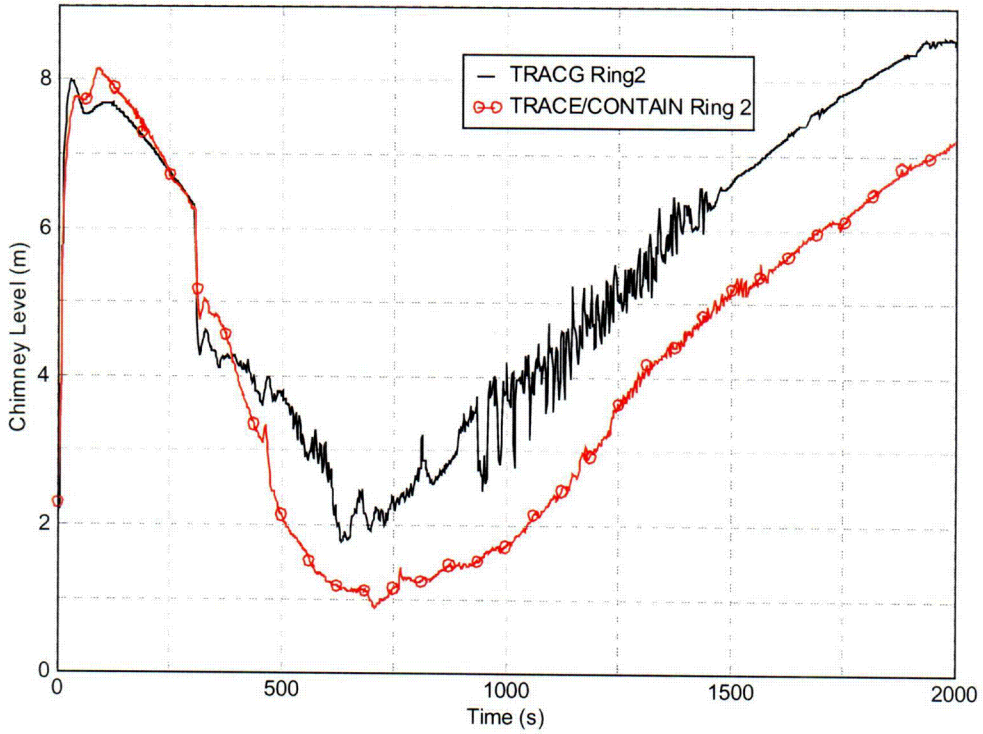
Tue Aug 10 12:06:02 2004

Figure 3.7.2.17 Downcomer Water Level.

C-09

### Chimney Collapsed Liquid Level

ESBWR LOCA - GDCS Line Break Case

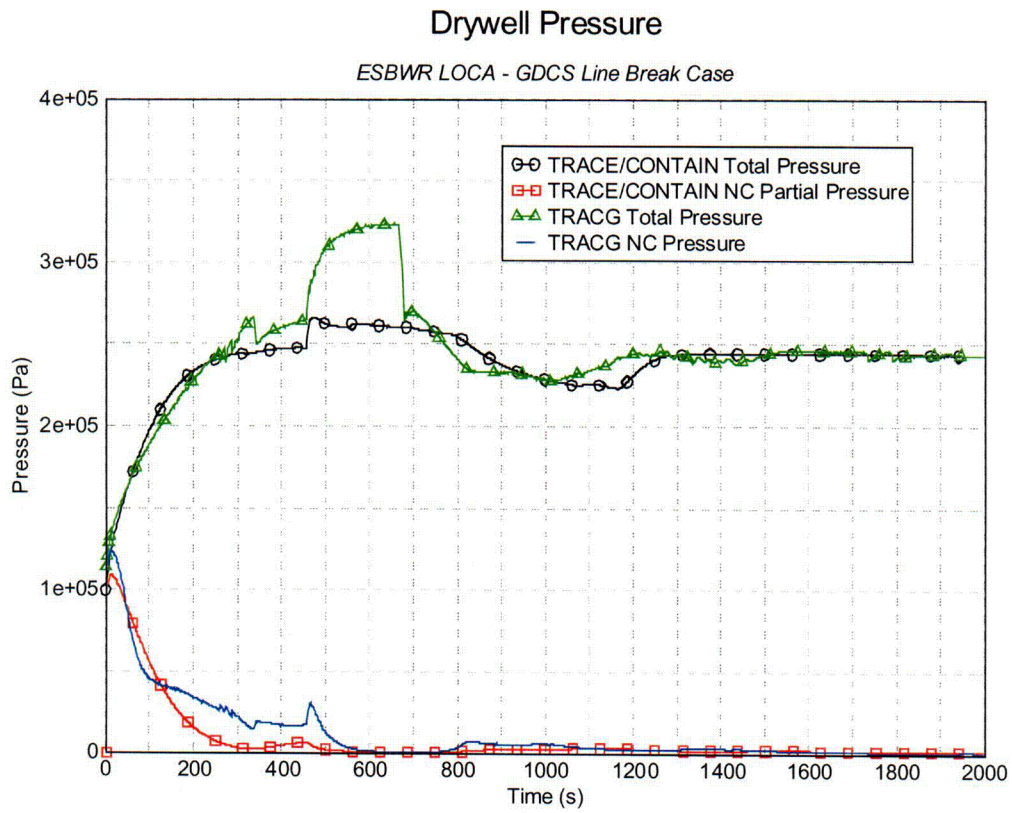


Tue Aug 10 12:15:53 2004

Fig

Figure 3.7.2.18 Collapsed Water Level in the Chimney.

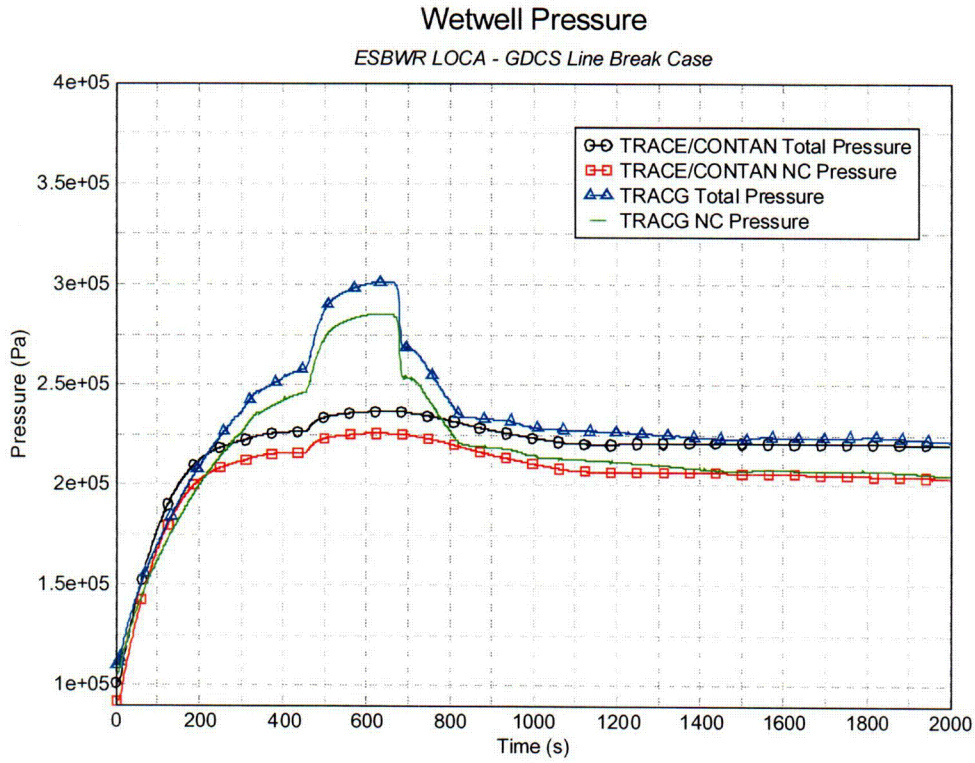
C-10



Sat Aug 14 10:12:59 2004

Figure 3.7.2.19 Drywell Total Pressure and Non-Condensable Partial Pressure.

C-11

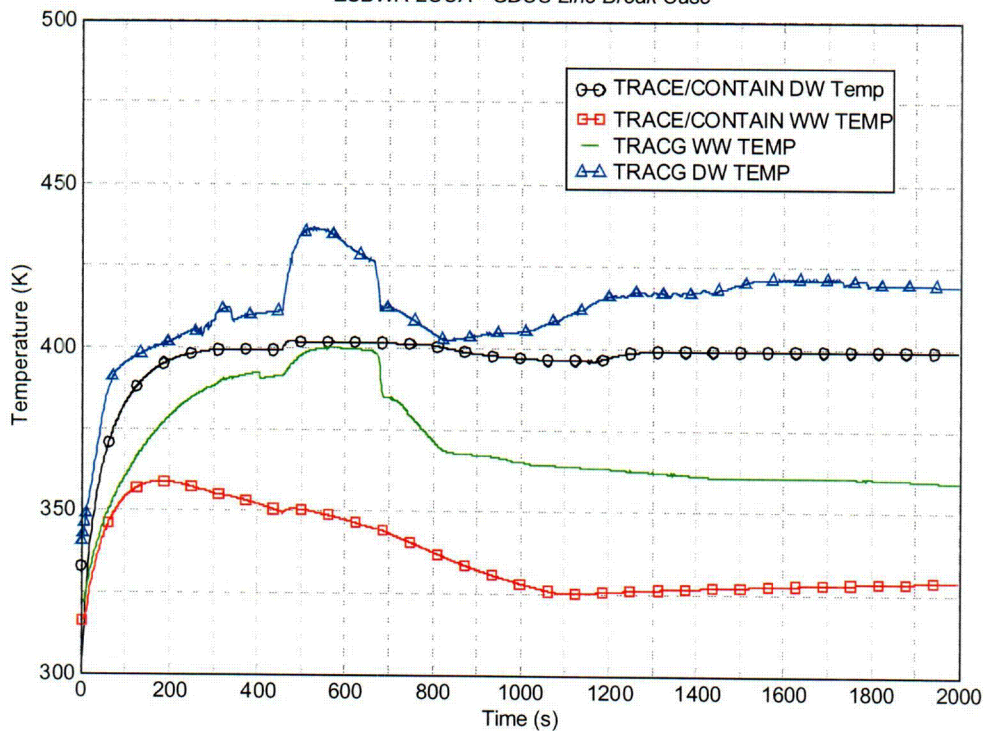


Sat Aug 14 10:20:14 2004

Figure 3.7.2.20 Wetwell Total Pressure and Non-Condensable Partial Pressure.

### Drywell and Wetwell Gas Temperature

ESBWR LOCA - GDCS Line Break Case



Sat Aug 14 11:26:48 2004

Fig

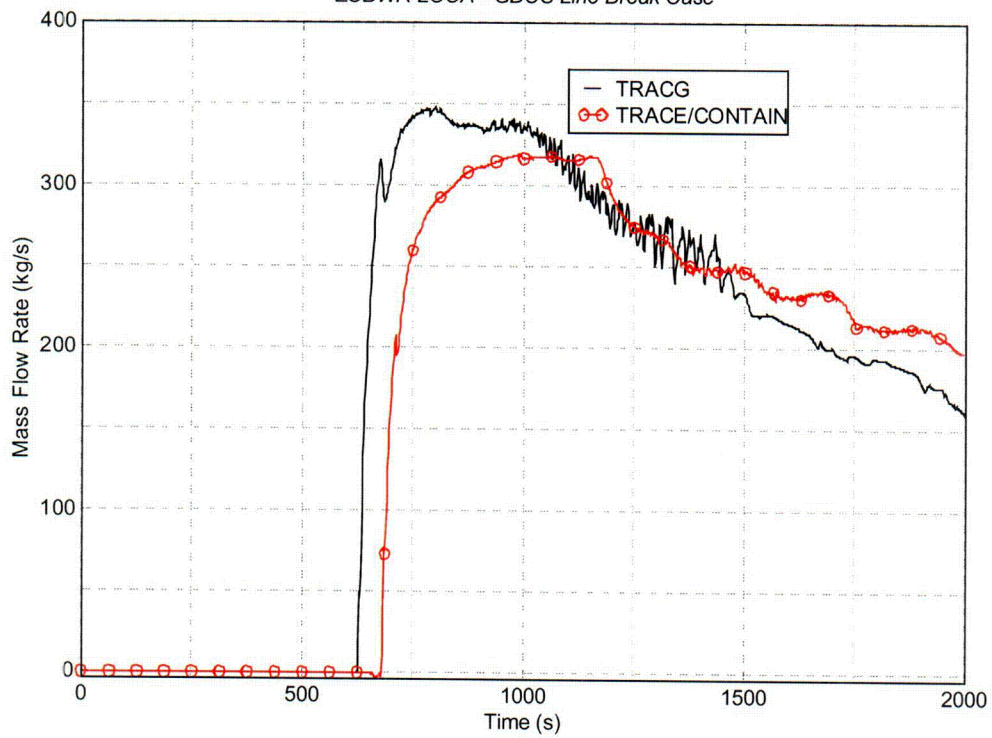
3.7.2.21 Drywell and Wetwell Atmosphere Temperature.

ure

C-13

### Total GDCS Injection Mass Flow Rate

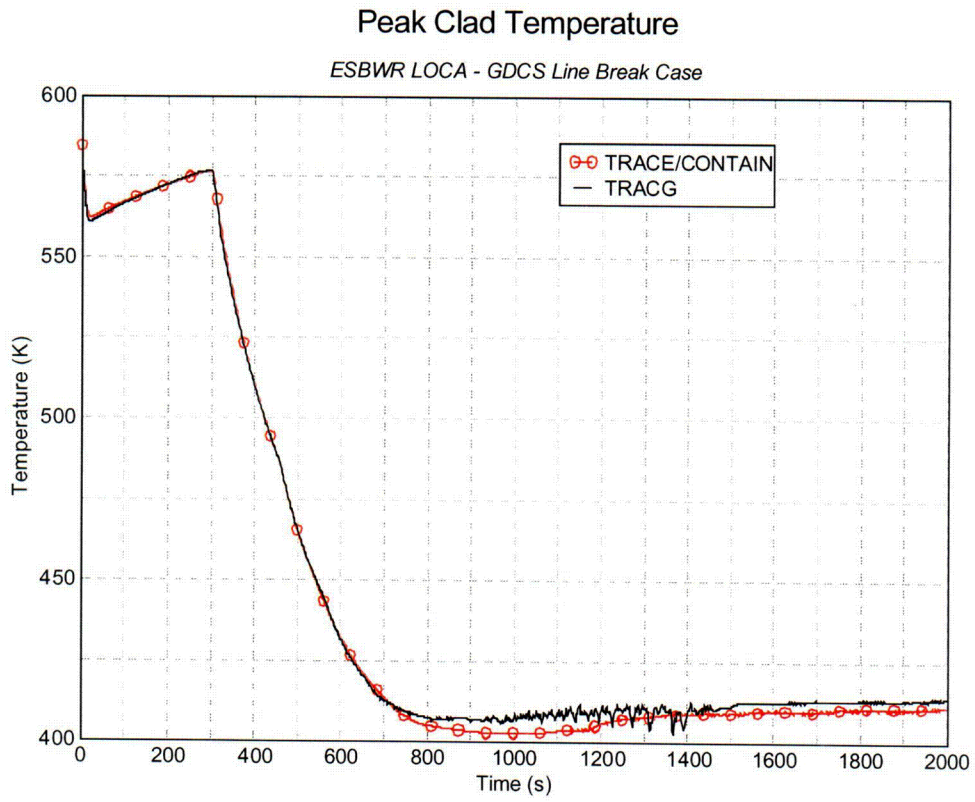
ESBWR LOCA - GDCS Line Break Case



Fri Aug 13 10:41:06 2004

Figure 3.7.2.22 GDCS Mass Flow Rate

C-14



Fri Aug 13 11:09:01 2004

Fig

3.7.2.23 Peak Cladding Temperature

re

C-15

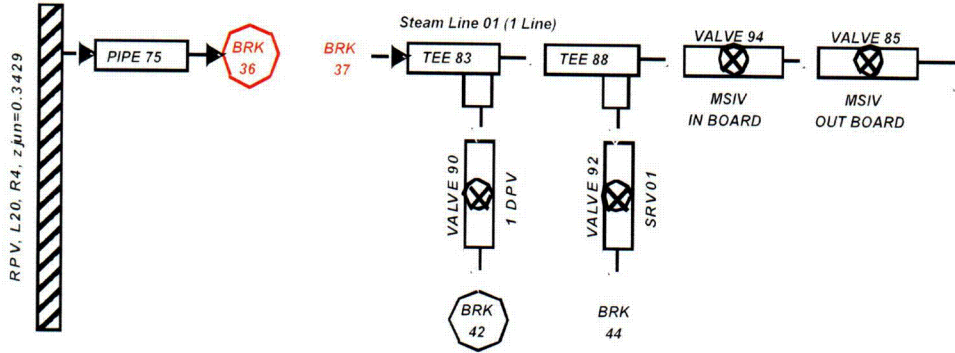
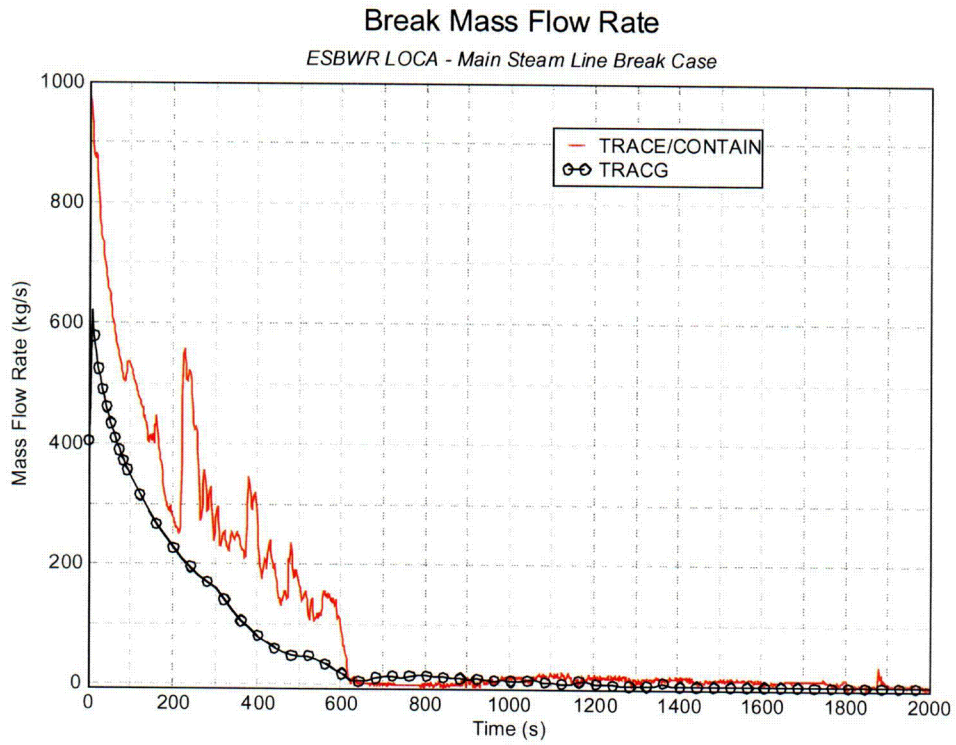


Figure 3.7.2.24 MSLB Broken Steam Line Nodalization.

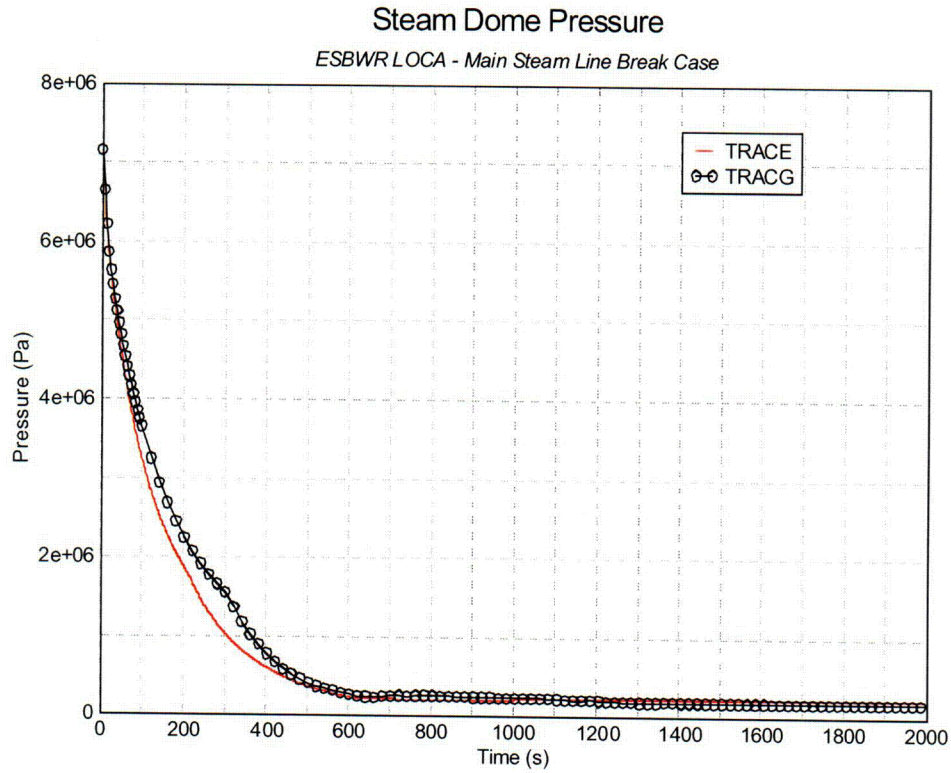
C-16



Sat Aug 14 12:05:25 2004

Figure 3.7.2.25 MSLB Break Mass Flow Rate.

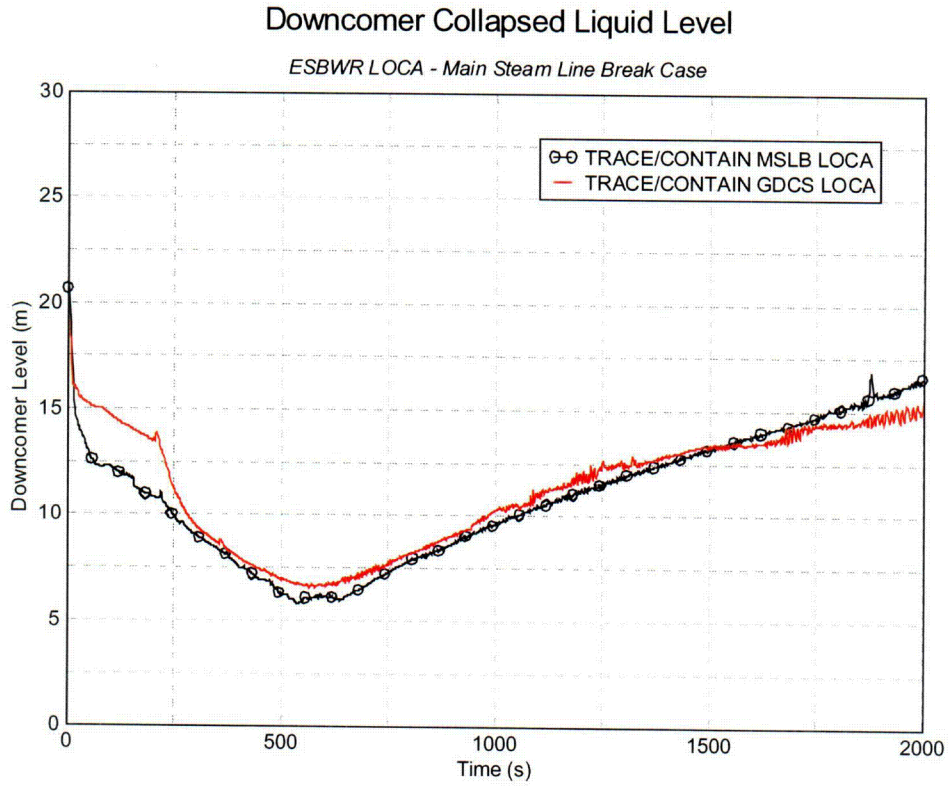
C-17



Sat Aug 14 12:20:35 2004

Figure 3.7.2.26 MSLB Steam Dome Pressure.

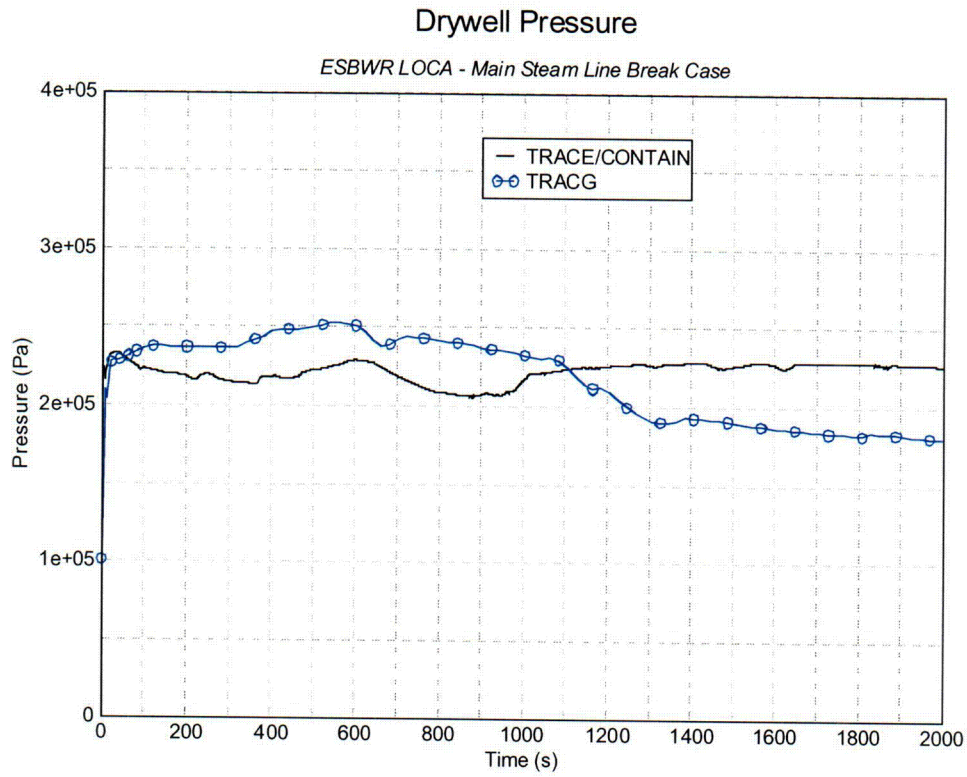
C-190



Sat Aug 14 12:40:53 2004

Figure 3.7.2.27 MSLB and GDCS LOCA Downcomer Water Level.

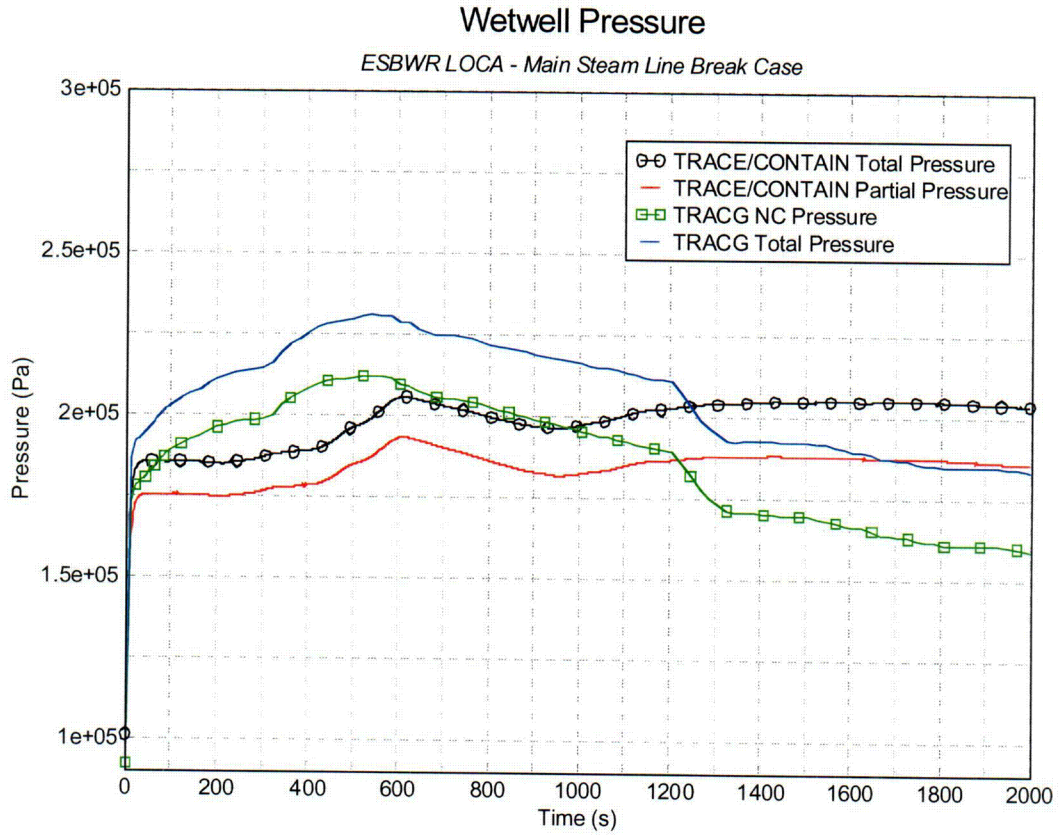
C-19



Sat Aug 14 12:50:54 2004

Figure 3.7.2.28 MSLB Drywell Total Pressure.

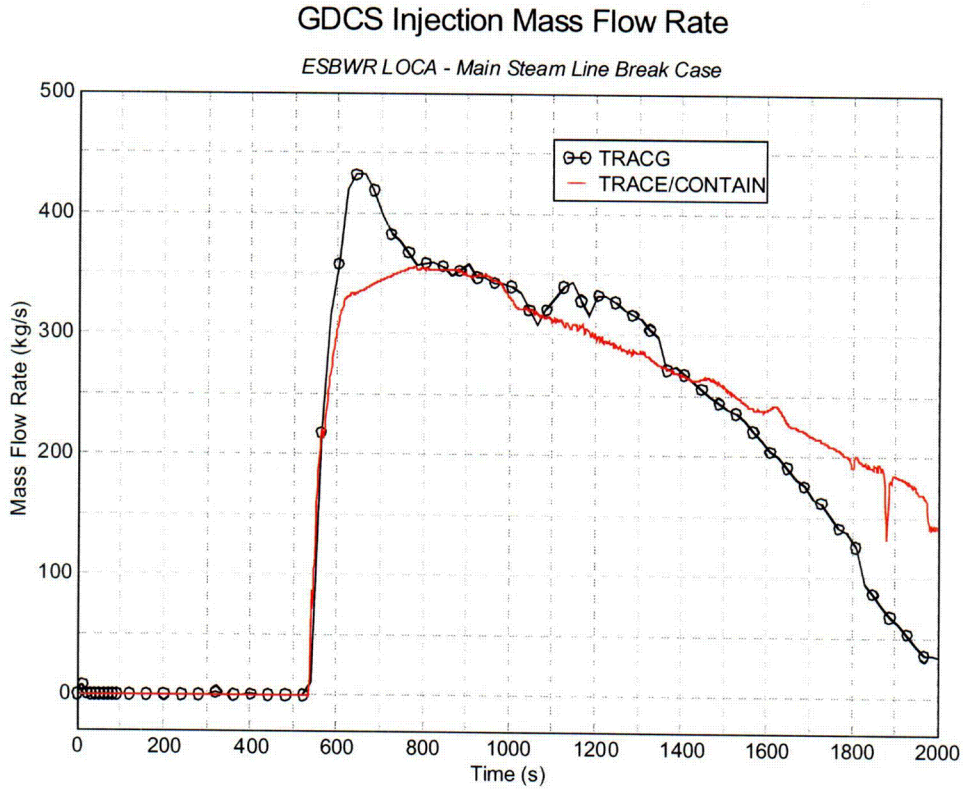
C70



Sat Aug 14 13:18:17 2004

Figure 3.7.2.29 MSLB Wetwell Total Pressure And Noncondensable Partial Pressure.

c-21



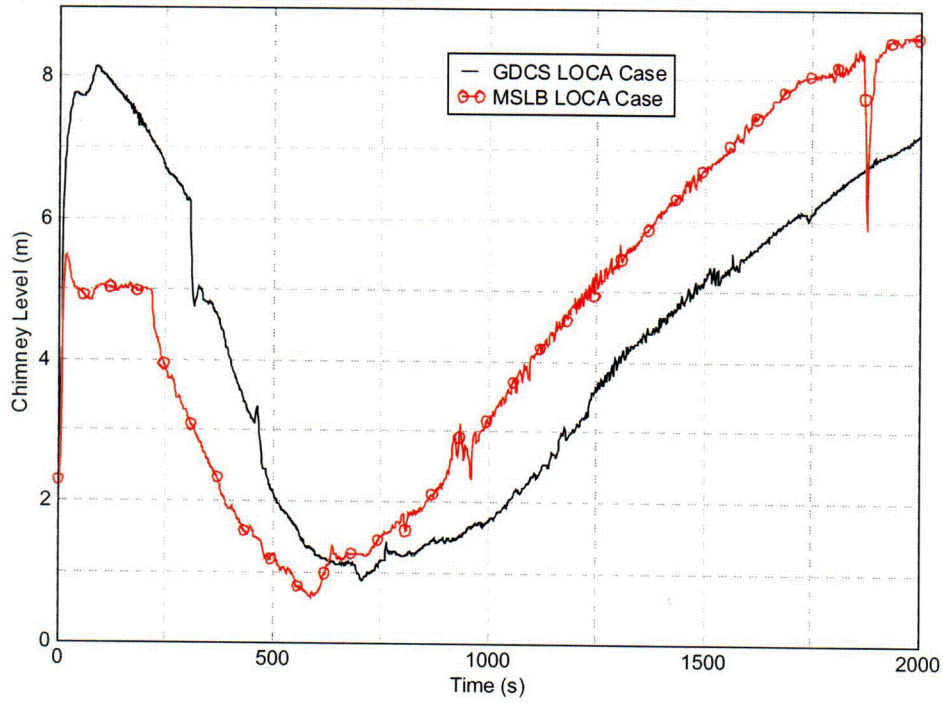
Sat Aug 14 13:56:49 2004

Figure 3.7.2.30 MSLB GDCS Line ECCS Injection Mass Flow Rate.

C-22

### Chimney Collapsed Liquid Level

ESBWR LOCA - MSLB&GDCS Break Case



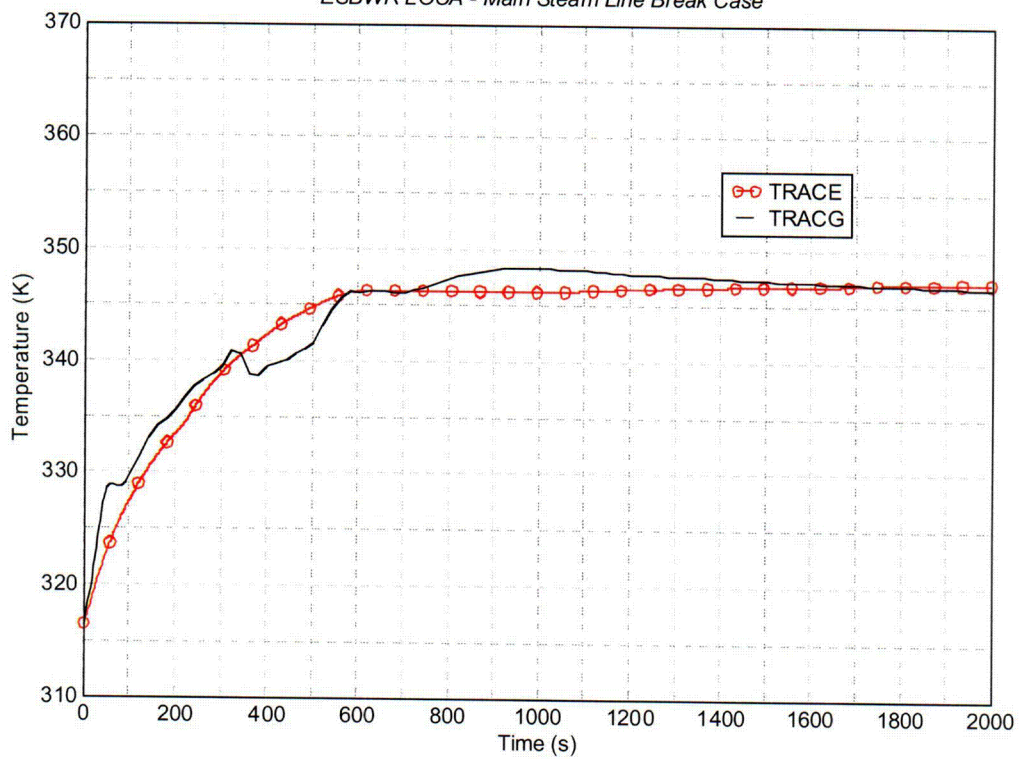
Sat Aug 14 14:13:00 2004

Figure 3.7.2.31 MSLB and GDCS LOCA Chimney Collapsed Water Level

C-23

### Wetwell Liquid Temperature

ESBWR LOCA - Main Steam Line Break Case



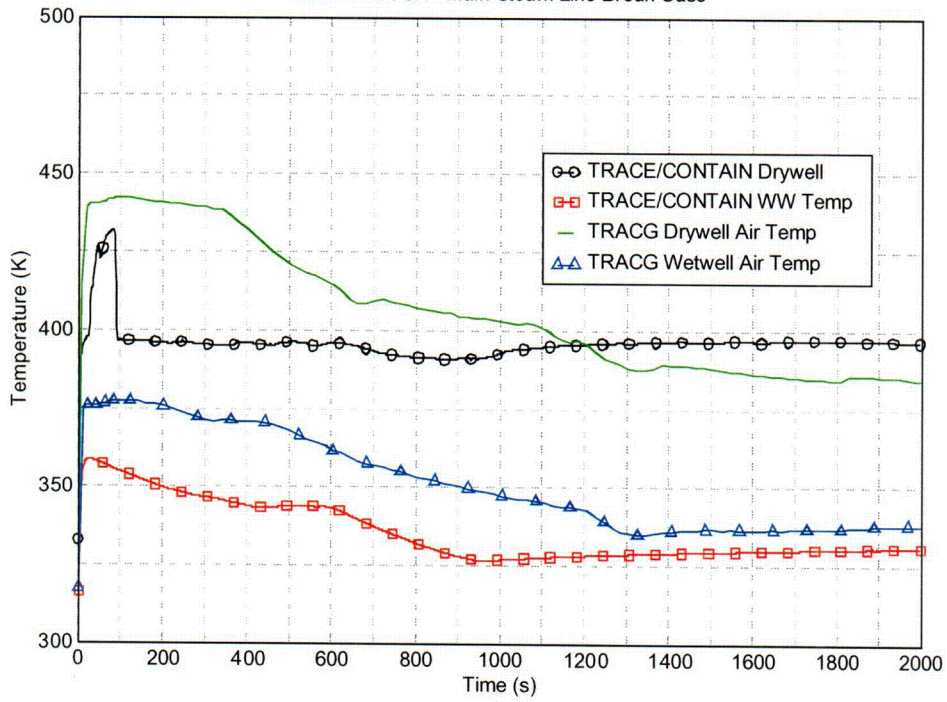
Sat Aug 14 14:21:39 2004

Figure 3.7.2.32 MSLB LOCA Wetwell Liquid Temperature.

C-24

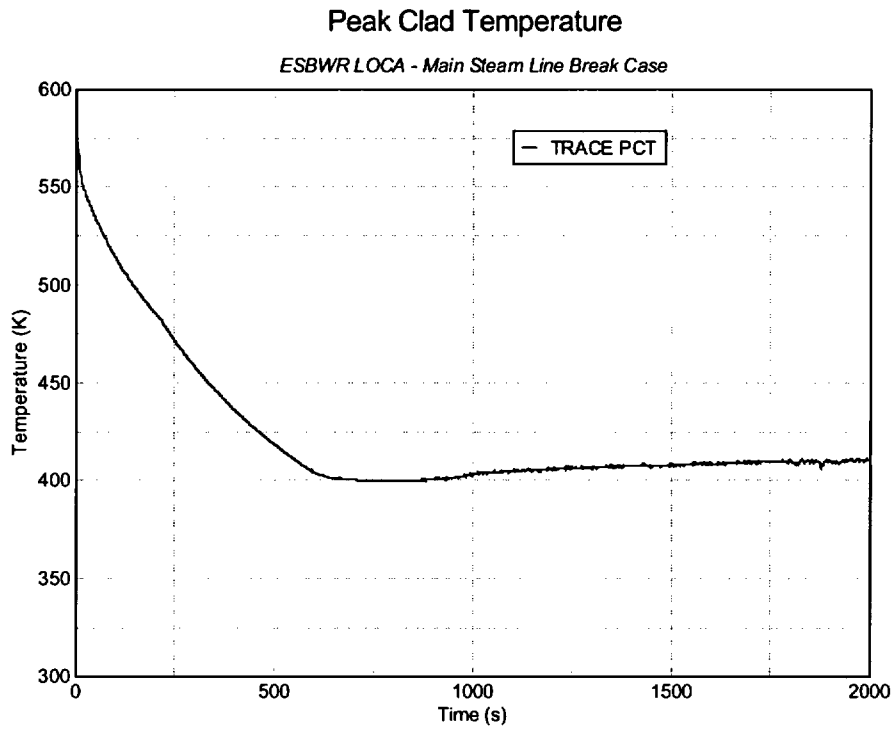
### Drywell and Wetwell Gas Temperature

ESBWR LOCA - Main Steam Line Break Case



Sat Aug 14 14:36:18 2004

Figure 3.7.2.33 MSLB LOCA Drywell And Wetwell Vapor Temperature.



Sat Aug 14 14 02:36 2004

Figure 3.7.2.34 MSLB LOCA Peak Cladding Temperature. Figure

### GE ESBWR Bottom Drain Line Break Core Average Channel Void Fraction

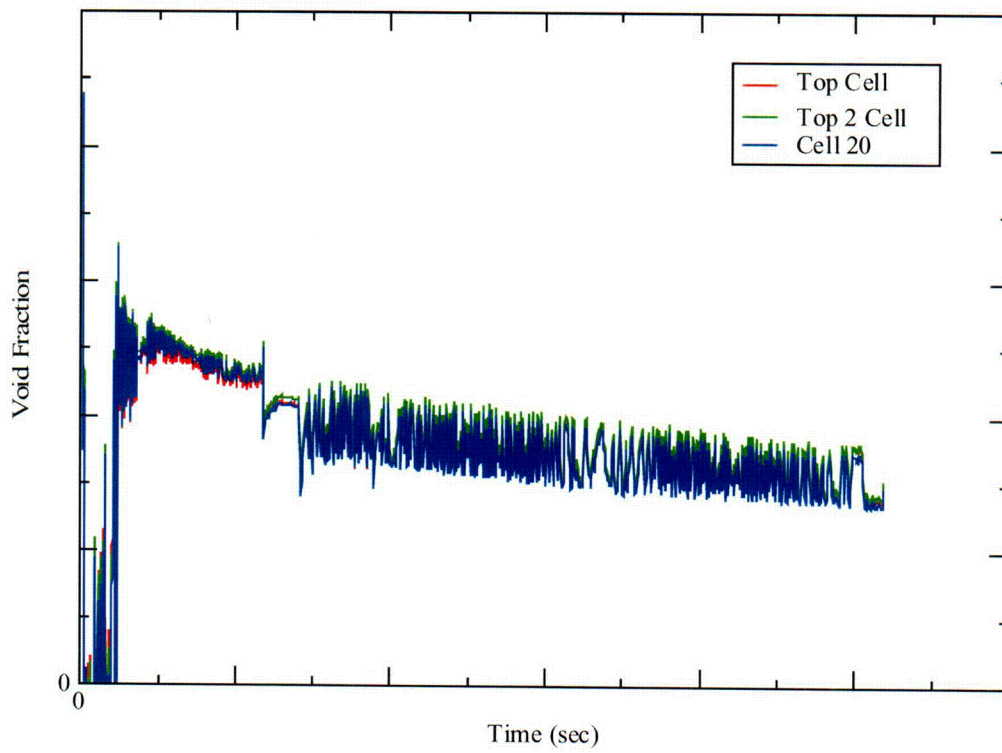


Figure 3.7.2.35 BDLB LOCA Core Average Channel Void Fraction.

C-26

## Table of Contents

	Page
<b>1. INTRODUCTION</b>	<b>1-1</b>
<b>1.1 Background</b>	<b>1-1</b>
<b>1.2 Summary</b>	<b>1-2</b>
1.2.1 ECCS/LOCA Application	1-2
1.2.2 Containment/LOCA Application	1-3
1.2.3 AOO Application	1-3
<b>1.3 Scope of Review</b>	<b>1-4</b>
<b>2. ECCS/LOCA ANALYSIS</b>	<b>2-1</b>
<b>2.1 Licensing Requirements and Scope of Application</b>	<b>2-1</b>
2.1.1 General Requirements	2-1
2.1.2 Specific 10CFR50.46 Licensing Acceptance Criteria for ECCS Performance	2-1
2.1.3 Analysis Requirements	2-1
2.1.4 Standard Review Plan (SRP) Guidelines (NUREG 800)	2-2
2.1.5 Proposed Application Methodology	2-2
2.1.5.1 Conformance with Regulatory Guide 1.157	2-2
2.1.5.2 Conformance with CSAU Methodology	2-28
2.1.6 Implementation Requirements	2-32
2.1.7 Review Requirements For Updates	2-33
2.1.7.1 Updates to TRACG Code	2-33
2.1.7.2 Updates to Fuel Rod Thermal Mechanical Model for ECCS/LOCA Application	2-33
2.1.7.3 Updates to TRACG Model Uncertainties	2-33
2.1.7.4 Updates to TRACG Application Method	2-34
2.1.7.5 Cycle Specific Uncertainties in Safety Parameters	2-34
2.1.8 Range of Application	2-34
<b>2.2 Phenomena Identification and Ranking</b>	<b>2-35</b>
2.2.1 LOCA Transient Response	2-35
2.2.1.1 GDCS Line Break	2-36
2.2.1.2 Main Steamline Break	2-38
2.2.1.3 Small Breaks	2-39
2.2.1.4 Non-Design Basis LOCAs	2-39
2.2.2 Composite List of Identified Phenomena and Interactions	2-40
<b>2.3 Applicability of TRACG to ESBWR ECCS/ LOCA</b>	<b>2-47</b>
2.3.1 Model Capability	2-47
2.3.2 Model Assessment Matrix	2-47

## Table of Contents (cont'd)

	Page
<b>2.4 Model Uncertainties and Biases</b>	<b>2-58</b>
2.4.1 Model Parameters and Uncertainties	2-58
2.4.2 Effects of Nodalization	2-64
2.4.3 Effects of Scale	2-65
2.4.3.1 RPV Level	2-65
2.4.3.2 Scale-up of Level Changes	2-65
2.4.4 Sensitivity to PIRT Parameters	2-66
2.4.4.1 Scoping ECCS/LOCA Break Spectrum Analysis	2-66
2.4.4.2 Sensitivity Study on PIRT Parameters	2-67
2.4.4.3 Sensitivity Study on Interactions between ECCS and Containment	2-67
<b>2.5 Application Uncertainties and Biases</b>	<b>2-86</b>
2.5.1 Input	2-86
2.5.2 Plant Conditions Used for Base Line Calculations	2-87
2.5.3 Uncertainties in Plant Parameters/Initial Conditions	2-87
2.5.4 Sensitivity to Plant Parameters/Initial Conditions	2-87
<b>2.6 Combination of Uncertainties</b>	<b>2-91</b>
2.6.1 Specific Application Process	2-91
<b>2.7 Results for ECCS/LOCA Analysis</b>	<b>2-92</b>
2.7.1 Nominal ECCS/LOCA Analysis	2-92
2.7.1.1 TRACG Nodalization for ESBWR ECCS/LOCA Analysis	2-92
2.7.1.2 Results for Baseline ECCS/LOCA Analysis	2-92
2.7.2 Bounding ECCS/LOCA Analysis	2-101
2.7.2.1 Analysis Assumptions	2-101
2.7.2.2 Bounding Analysis Results	2-101
<b>2.8 Summary of ECCS/LOCA Application Methodology</b>	<b>2-106</b>
<b>3. CONTAINMENT/LOCA ANALYSIS</b>	<b>3-1</b>
<b>3.1 Licensing Requirements and Scope of Application</b>	<b>3-1</b>
3.1.1 Licensing Acceptance Criteria for Containment/LOCA Performance	3-1
3.1.2 Analysis Requirements	3-3
3.1.3 Standard Review Plan (SRP) Guidelines (NUREG 800)	3-3
3.1.4 Proposed Application Methodology	3-3
3.1.5 Implementation Requirements	3-4
3.1.6 Review Requirements For Updates	3-4
3.1.6.1 Updates to TRACG Code	3-4

## Table of Contents (cont'd)

	Page
3.1.6.2 Updates to TRACG Application Method	3-5
3.1.7 Range of Application	3-5
<b>3.2 Phenomena Identification and Ranking</b>	<b>3-6</b>
3.2.1 LOCA Transient Response	3-6
3.2.1.1 Containment Response for the GDCS Line Break	3-7
3.2.1.2 Main Steamline Break	3-9
3.2.1.3 Small Breaks	3-11
3.2.2 Composite List of Highly Ranked Phenomena and Interactions	3-11
<b>3.3 Applicability of TRACG to Containment/LOCA</b>	<b>3-18</b>
3.3.1 Model Capability	3-18
3.3.1.1 Phenomena Treated with a Bounding Approach	3-18
3.3.2 Model Assessment Matrix	3-23
<b>3.4 Model Uncertainties and Biases</b>	<b>3-36</b>
3.4.1 Model Parameters and Uncertainties	3-36
3.4.2 Effect of Scale	3-43
<b>3.5 Plant Parameters and Ranges for Application</b>	<b>3-48</b>
3.5.1 Input	3-48
3.5.2 Plant Initial Conditions Used for Base Line Calculations	3-49
3.5.2.1 Plant Initial Conditions Not Varied	3-49
3.5.2.2 Plant Conditions ranged to a Bounding Value for Sensitivity Studies	3-50
<b>3.6 Application Procedure for Containment Analysis</b>	<b>3-52</b>
<b>3.7 Results for ESBWR Main Steamline Break LOCA</b>	<b>3-53</b>
3.7.1 TRACG Nodalization for Containment Analysis	3-53
3.7.2 Baseline Results for Containment Analysis	3-55
3.7.3 Bounding Results for Containment Analysis	3-65
<b>3.8 Summary of Containment/LOCA Application Methodology</b>	<b>3-73</b>
<b>4. TRANSIENT ANALYSIS</b>	<b>4-1</b>
<b>4.1 Licensing Requirements and Scope of Application</b>	<b>4-1</b>
4.1.1 10CFR50 Appendix A	4-1
4.1.2 Standard Review Plan Guidelines (NUREG 800)	4-1
4.1.3 Proposed Application Methodology	4-2
4.1.3.1 Conformance with CSAU Methodology	4-2

**TABLE OF CONTENTS (CONT'D)**

	Page	
4.1.4	Implementation Requirements	4-3
4.1.5	Review Requirements For Updates	4-4
4.1.5.1	Updates to TRACG Code	4-4
4.1.5.2	Updates to TRACG Model Uncertainties	4-4
4.1.5.3	Updates to TRACG Statistical Method	4-4
4.1.5.4	Updates to Event Specific Uncertainties	4-4
4.1.6	AOO Scenario Specification	4-5
4.1.7	Nuclear Power Plant Selection	4-5
<b>4.2</b>	<b>Phenomena Identification and Ranking</b>	<b>4-6</b>
4.2.1	ESBWR AOO Classes	4-6
4.2.1.1	Fast Pressurization Events	4-6
4.2.1.2	Slow Pressurization Events	4-7
4.2.1.3	Decrease in Reactor Coolant Inventory	4-7
4.2.1.4	Decrease in Moderator Temperature	4-7
4.2.1.5	Generator Load Rejection Event Description	4-7
4.2.2	Phenomena Identification and Ranking Table (PIRT) for AOOs	4-9
<b>4.3</b>	<b>Applicability of TRACG to Transient Analysis</b>	<b>4-13</b>
4.3.1	Model Capability	4-13
4.3.2	Model Assessment Matrix	4-16
<b>4.4</b>	<b>Model Uncertainties and Biases</b>	<b>4-21</b>
4.4.1	Model Parameters and Uncertainties	4-21
4.4.2	Effects of Nodalization	4-32
4.4.3	Effects of Scale	4-32
<b>4.5</b>	<b>Application Uncertainties and Biases</b>	<b>4-33</b>
4.5.1	Input	4-33
4.5.2	Initial Conditions	4-34
4.5.3	Plant Parameters	4-35
<b>4.6</b>	<b>Combination of Uncertainties</b>	<b>4-37</b>
4.6.1	Recommended Approach for Combining Uncertainties	4-37
4.6.1.1	Order Statistics (OS) Method – Single Bounding Value	4-37
4.6.1.2	Normal Distribution One-Sided Upper Tolerance Limit	4-39
4.6.1.3	Advantages of Recommended Method	4-40
4.6.2	Implementation of Statistical Methodology	4-40
4.6.2.1	Conformance with Design Limits	4-41
4.6.3	Determination of OLMCPR	4-41
4.6.3.1	Details of Process of OLMCPR Calculation	4-42

**Table of Contents (cont'd)**

	Page
<b>4.7 Demonstration Calculations for ESBWR AOOs</b>	<b>4-46</b>
4.7.1 Baseline Analysis	4-46
4.7.1.1 Load Rejection No Bypass (LRNB) Baseline Analysis	4-46
4.7.1.2 Feedwater Controller Failure (Maximum Demand at 150% of Rated)	4-47
4.7.1.3 Main Steamline Isolation Valve (MSIV) Closure	4-47
<b>4.8 Summary of TRACG Application to ESBWR AOOs</b>	<b>4-65</b>
<b>5. REFERENCES</b>	<b>5-1</b>

## List of Tables

	Page
Table 2.1-1 Code Scaling, Applicability and Uncertainty Evaluation Methodology	2-29
Table 2.2-1 LOCA Scenario with Diesel Generators Available - Additional Systems Functional	2-42
Table 2.2-2 LOCA Scenario with Offsite Power & Diesel Generators Available	2-42
Table 2.2-3 Composite List of Highly Ranked Phenomena for ECCS/LOCA	2-43
Table 2.3-1 High Ranked ESBWR ECCS/LOCA Phenomena AND TRACG Model Capability Matrix	2-48
Table 2.3-2 Separate Effects Tests for Highly Ranked Phenomena for TRACG Qualification for ESBWR – ECCS/LOCA	2-50
Table 2.3-3 Component Tests for Highly Ranked Phenomena for TRACG Qualification for ESBWR – ECCS/LOCA	2-52
Table 2.3-4 Integral System Tests for Highly Ranked Phenomena for TRACG Qualification for ESBWR – ECCS/LOCA	2-54
Table 2.3-5 BWR Plant Data for Highly Ranked Phenomena for TRACG Qualification for ESBWR – ECCS/LOCA	2-56
Table 2.4-1 Parameters Governing High Ranked PIRT Phenomena	2-69
Table 2.4-2 Summary of Scoping Break Spectrum Analysis – Minimum Static Head inside Chimney	2-70
Table 2.4-3 TRACG PIRT Parameters ranged for ECCS/LOCA Sensitivity Study	2-71
Table 2.5-1 Significant Input Variables to the Loss-of-Coolant Accident Analysis	2-88
Table 2.5-2 Plant Variables with Nominal And Sensitivity Study Values	2-89
Table 3.2-1 Highly Ranked PIRT Phenomena for ESBWR Containment/ LOCA	3-13
Table 3.3-1 High Ranked ESBWR Containment/LOCA Phenomena and TRACG Model Capability Matrix	3-24
Table 3.3-2 Separate Effects Tests for Highly Ranked Phenomena for TRACG Qualification for ESBWR - Containment	3-26
Table 3.3-3 Component Tests of Highly Ranked Phenomena for TRACG Qualification for ESBWR - Containment	3-28
Table 3.3-4 Integral System Tests for Highly Ranked Phenomena for TRACG Qualification for ESBWR - Containment	3-30
Table 3.3-5 Effect of Break Discharge Location on the Containment Pressure	3-32
Table 3.4-1 Uncertainties in Highly Ranked PIRT Parameters for Containment/LOCA	3-44
Table 3.5-1 Plant Initial Conditions Considered in the Containment Sensitivity Study	3-51
Table 3.7-1 Model Parameters for Bounding Case	3-66
Table 4.1-1 Code Scaling, Applicability and Uncertainty Evaluation Methodology	4-3
Table 4.2-1 Composite List of Highly Ranked Phenomena for ESBWR Transients	4-11
Table 4.3-1 High Ranked ESBWR Phenomena and TRACG Model Capability Matrix	4-14
Table 4.3-2 Qualification Matrix for High Ranked Phenomena for ESBWR Transients	4-17
Table 4.4-1 High Ranked Model Parameters for AOO analysis	4-31
Table 4.5-1 Key Plant Initial Conditions	4-35
Table 4.5-2 Analytical Scram Speeds for ESBWR	4-36

**List of Tables (cont'd)**

	Page
Table 4.7-1 Sequence of Events for LRNB Transient	4-48
Table 4.7-2 Sequence of Events for FWCF Event	4-49
Table 4.7-3 Sequence of Events for MSIV Closure Transient	4-50

## List of Figures

	<b>Page</b>	
Figure 2.2-1	ESBWR Passive Safety Features	2-45
Figure 2.2-2	Phases of the LOCA Transient	2-46
Figure 2.2-3	GDCS Line Break - Chimney and Downcomer Two-Phase Levels vs. Time	2-46
Figure 2.4-1	Void Fraction Deviations for Tests Applicable to Regions with Large Hydraulic Diameter	2-72
Figure 2.4-2	Sensitivity of TRACG Prediction of Average Void Fraction in EBWR Test Facility to PIRT Multiplier on Interfacial Drag Coefficient	2-73
Figure 2.4-3	Probability Distribution for Multiplier on Interfacial Drag Coefficient	2-74
Figure 2.4-4	Void Fraction Deviations for Toshiba Void Fraction Tests	2-75
Figure 2.4-5	Sensitivity of TRACG Prediction of Toshiba Void Fraction to PIRT Multiplier on (Co-1)	2-76
Figure 2.4-6	Sensitivity of TRACG Prediction of Toshiba Void Fraction PIRT Multiplier on Entrainment Coefficient, $\eta$	2-76
Figure 2.4-7	Fractional Error in Modified Zuber Critical Heat Flux Correlation	2-77
Figure 2.4-8	Comparison of the Predicted and Measured Two-Phase Level Histories for Marviken Test 24	2-78
Figure 2.4-9	Comparison of the Predicted and Measured Two-Phase Level Histories for Marviken Test 15	2-79
Figure 2.4-10	Deviation in Level Change Versus the Hydraulic Diameter for Separate Effects and Integral Facilities	2-80
Figure 2.4-11	GDCS Line Break with GDCS Injection Valve Failure – Two-phase Level inside Chimney	2-81
Figure 2.4-12	GDCS Line Break with GDCS Injection Valve Failure – Collapsed Level (Static Head) inside Chimney	2-82
Figure 2.4-13	Chimney Static Head Sensitivity to Uncertainties in TRACG PIRT Parameters (See Table 2.4-3)	2-83
Figure 2.4-14	PCT Sensitivity to Uncertainties in TRACG PIRT Parameters (See Table 2.4-3)	2-84
Figure 2.4-15	Chimney Static Head Sensitivity to TRACG Simulation of DW Noncondensable Holdup	2-85
Figure 2.5-1	Chimney Static Head Sensitivity to Plant Parameter Uncertainties	2-90
Figure 2.7-1	TRACG Nodalization of ESBWR RPV and containment for ECCS/LOCA Analysis	2-94
Figure 2.7-2	TRACG Nodalization of ESBWR Steam Line System	2-95
Figure 2.7-3	TRACG Nodalization of ESBWR IC, DPV and Feedwater Systems	2-96
Figure 2.7-4	RPV Pressure Response (Base Case)	2-97
Figure 2.7-5	RPV, Drywell and Wetwell Pressure Response (Base Case)	2-98
Figure 2.7-6	Two-Phase Levels in Downcomer and Inside Core Shroud (Base Case)	2-99
Figure 2.7-7	Two-Phase Level and Static Head In Chimney (Base Case)	2-100
Figure 2.7-8	RPV Pressure Response (Bounding Case)	2-102

**List of Figures (cont')**

	Page
Figure 2.7-9 RPV, Drywell and Wetwell Response (Bounding Case)	2-103
Figure 2.7-10 Two-Phase Levels in Downcomer and Inside Core Shroud (Bounding Case)	2-104
Figure 2.7-11 Two-Phase Level and Static Head In Chimney (Bounding Case)	2-105
Figure 3.2-1 Main Steam Line Break Vessel and Containment Pressures (Typical)	3-16
Figure 3.2-2 Main Steam Line Break Decay Heat and PCCS Heat Removal (Typical)	3-17
Figure 3.3-1 Wetwell Gas Space and Pool Showing TRACG Nodalization	3-33
Figure 3.3-2 Suppression Pool Temperatures With and Without Forced Stratification (SBWR)	3-34
Figure 3.3-3 Wetwell Gas Space Temperatures Without Forced Stratification (SBWR)	3-35
Figure 3.3-4 Wetwell Gas Space Temps – Restricted Mixing between Top Layer and Lower Layer (SBWR)	3-35
Figure 3.4-1 Comparison of PANDA Test M3 Wetwell Airspace Temperature with TRACG Predictions for WW1 Pressure.	3-47
Figure 3.7-1 TRACG Nodalization for ESBWR Containment Analysis	3-54
Figure 3.7-2 Containment Pressure Response (Base Case)	3-57
Figure 3.7-3 Drywell Noncondensable Partial Pressures (Base Case)	3-58
Figure 3.7-4 3 PCC Pool Level (Base Case)	3-59
Figure 3.7-5 GDCS Pool Level (Base Case)	3-60
Figure 3.7-6 PCCS Heat Removal vs. Decay Heat (Base Case)	3-61
Figure 3.7-7 Suppression Pool Temperatures (Base Case)	3-62
Figure 3.7-8 Wetwell Gas Space temperature Response (Base Case)	3-63
Figure 3.7-9 Drywell Temperature Response (Base Case)	3-64
Figure 3.7-10 Containment Pressure Response (Bounding Case)	3-67
Figure 3.7-11 PCCS Heat Removal vs. Decay Heat (Bounding Case)	3-68
Figure 3.7-12 Suppression Pool Temperatures (Bounding Case)	3-69
Figure 3.7-13 Drywell Pressure Response vs. Design Limit	3-70
Figure 3.7-14 Wetwell Gas Space Temperature Response (Bounding Case)	3-71
Figure 3.7-15 Drywell Temperature Response (Bounding Case)	3-72
Figure 4.4-1 Void Coefficient Normalized %Bias and %Standard Deviation [3]	4-23
Figure 4.6-1 Schematic Process for Combining Uncertainties	4-39
Figure 4.6-2 Generic DCPR/ICPR Uncertainty Development	4-43
Figure 4.6-3 NRSBT Determination	4-43
Figure 4.6-4 GESAM Calculation Procedure for Analytical Determination of OLMCPR	4-45
Figure 4.7-1 Pressure response for LRNB Transient	4-51
Figure 4.7-2 Neutron Flux Response for LRNB Transient	4-52
Figure 4.7-3. Downcomer Two-Phase Level Response for LRNB Transient	4-53
Figure 4.7-4 Bundle Power Response for LRNB Transient	4-54
Figure 4.7-5 Bundle Inlet Flow for LRNB Transient	4-55
Figure 4.7-6 Downcomer Level Response for FWCF Transient	4-56
Figure 4.7-7 Pressure Response for FWCF Transient	4-57
Figure 4.7-8 Neutron Flux response for FWCF Transient	4-58

**List of Figures (cont'd)**

	Page
Figure 4.7-9 Bundle Power Response for FWCF Transient	4-59
Figure 4.7-10 Bundle Inlet Flow Response for FWCF Transient	4-60
Figure 4.7-11 Pressure Response for MSIV Closure Transient	4-61
Figure 4.7-12 Neutron Flux Response for MSIV Closure Transient	4-62
Figure 4.7-13 Downcomer Level for MSIV Closure Transient	4-63
Figure 4.7-14 IC Steam Flow for MSIV Closure Transient	4-64

# 1. INTRODUCTION

## 1.1 Background

TRACG is a General Electric (GE) proprietary version of the Transient Reactor Analysis Code (TRAC). TRACG uses advanced realistic one-dimensional and three-dimensional methods to model the phenomena that are important in evaluating the operation of BWRs. Realistic analyses performed with TRACG have been used previously to support licensing applications in different areas, including transients otherwise known as an Anticipated Operational Occurrences (AOO), and pipe breaks referred to by the acronym ECCS/LOCA (Emergency Core Cooling Systems/Loss of Coolant Accident). Recently, the application of TRACG for Anticipated Operational Occurrences (AOOs) for operating BWRs has been approved by the NRC [3].

TRAC was originally developed for pressurized water reactor (PWR) analysis by Los Alamos National Laboratory, the first PWR version of TRAC being TRAC-P1A [4]. The development of the BWR version of TRAC started in 1979 in close cooperation between GE and Idaho National Engineering Laboratory. The objective of this cooperation was the development of a version of TRAC capable of simulating BWR LOCAs. The main tasks consisted of improving the basic models in TRAC for BWR applications and in developing models for specific BWR phenomena and components. This work culminated in the middle 1980's with the development of TRACB04 at GE [[5],[6],[7],[8],[9],[10],[11]] and TRACG-BD1/MOD1 at INEL [12]. Due to the joint development, these versions were very similar. In the earlier stages, General Electric (GE), the United States Nuclear Regulatory Commission (NRC) and the Electric Power Research Institute (EPRI) jointly funded the development of the code. A detailed description of these earlier versions of TRAC for BWRs is contained in References 12 through 14.

## 1.2 Summary

The TRACG computer code is used to perform licensing analysis of the ESBWR. This report presents the methodology for application of TRACG to the ESBWR. TRACG is specifically used for the following four categories of analyses:

1. ECCS/LOCA
2. Containment/LOCA
3. Anticipated transients with scram (AOO)
4. Anticipated transients without scram (ATWS)

### 1.2.1 ECCS/LOCA Application

LOCA events (Section 2) are analyzed to establish the reactor system response, including the calculation of the chimney level and Peak Cladding Temperature (PCT). Because there is no core uncover for any break size or location, local cladding oxidation and core-wide cladding oxidation do not need to be evaluated. This application specifically addresses TRACG capabilities to ensure that TRACG is a qualified model for evaluating margins to the acceptance criteria for ECCS performance stated in 10CFR50.46. The application report defines the application process and demonstrates that TRACG analyses can be used for ECCS/LOCA licensing calculations. The application process includes the quantification of uncertainties that are applied to the realistic nominal results of TRACG analyses, resulting in a “licensing calculation”.

### **1.2.2 Containment/LOCA Application**

TRACG is utilized for the calculation of the containment pressure and temperature transient (Section 3). The application methodology will be used to demonstrate that the containment and its associated systems can accommodate, without exceeding the design leakage rate and with sufficient margin, the calculated pressure and temperature conditions resulting from any loss-of-coolant accident.

### **1.2.3 AOO Application**

This document describes the application methodology for AOOs (Section 4) that is in compliance with licensing limits. AOO events are analyzed to establish the reactor system response, including the calculation of the Operating Limit Minimum Critical Power Ratio (OLMCPR). TRACG capabilities are addressed to ensure that TRACG is a qualified model for the evaluation of margins to acceptable fuel design limits and reactor coolant pressure boundary design conditions. This application report extends the approved TRACG application methodology for AOO analysis to the ESBWR. Uncertainties are quantified and will be applied to the realistic nominal results of TRACG analyses. The licensing criteria to be satisfied is that less than 0.1% of the fuel rods are expected to experience a boiling transition for the most severe AOO.

Some of these uncertainties are fuel type dependent. Therefore, periodic changes in the statistical analysis will be required as core design changes. The statistical analysis process is defined in this report and criteria to be used to change this analysis are provided.

The overall analysis approach followed is consistent with the Code Scaling Applicability and Uncertainty (CSAU) analysis methodology [28]. Conformance with CSAU methodology is demonstrated in Section 4.1.3.1.

### **1.3 Scope of Review**

The Licensing Topical Reports NEDE-32176P, TRACG Model Description [1]; NEDE-32177, TRACG Qualification [2]; NEDC-32725, TRACG Qualification for SBWR Volumes 1 and 2, [24] and NEDC-33080, TRACG Qualification for ESBWR [25] are incorporated by reference as part of the review scope.

## 2. ECCS/LOCA ANALYSIS

### 2.1 Licensing Requirements and Scope of Application

#### 2.1.1 General Requirements

The *General Design Criteria (GDC) for Nuclear Power Plants* are stipulated in Appendix A to Part 50 of 10CFR. The applicable GDC is GDC 35, which requires each BWR to be equipped with an emergency core cooling system (ECCS) that refills the vessel in a timely manner to satisfy the requirements of the regulations for ECCS performance given in 10 CFR Part 50, §50.46 and Appendix K to 10CFR50 [17]. GDC 35 also requires redundant ECCS components to be provided to adequately cool the core during a LOCA. 10CFR100 [18] specifies mitigation of radiological consequences of an accident. Guidance is also provided in 10CFR 50.34 (*Contents of Applications; Technical Information*).

#### 2.1.2 Specific 10CFR50.46 Licensing Acceptance Criteria for ECCS Performance

The specific 10CFR50.46 licensing acceptance criteria for ECCS performance are as follows:

1. The calculated maximum fuel element cladding temperature shall not exceed 2200°F.
2. The calculated total local oxidation of the cladding shall nowhere exceed 17% of the total cladding thickness before oxidation.
3. The calculated total amount of hydrogen generated from the chemical reaction of the cladding with water or steam shall not exceed 1% of the hypothetical amount that would be generated if all the metal in the cladding cylinders surrounding the fuel, excluding the cladding surrounding the plenum volume, were to react.
4. Calculated changes in core geometry shall be such that the core remains amenable to cooling.
5. After any calculated successful initial operation of the ECCS, the calculated core temperature shall be maintained at an acceptably low value, and decay heat shall be removed for the extended period of time required by the long-lived radioactivity.

#### 2.1.3 Analysis Requirements

The calculational framework used for evaluating the ECCS in terms of core behavior is called an evaluation model. It includes one or more computer programs, the mathematical models used, the assumptions and correlations included in the program, the procedure for selecting and treating the program input and output information, the specification of those portions of the analysis not included in computer programs, the values of parameters, and all other information necessary to specify the calculation procedure. The evaluation model must comply with the acceptance criteria for ECCS given in 10CFR50.46 and Appendix K to 10CFR50. The evaluation model must have been previously documented and reviewed and approved by the NRC staff.

On September 16, 1988, the NRC staff amended the requirements of §50.46 and Appendix K so that these regulations reflect the improved understanding of ECCS performance obtained through

the extensive research performed since the promulgation of the original requirements in January 1974. Paragraph 50.46 (a)(1) now permits the use of a realistic evaluation model. It also requires that the uncertainty in the realistic evaluation model be quantified and considered with the applicable limits in Paragraph 50.46 (b) listed above, so that there is a high probability that the criteria will not be exceeded. Regulatory Guide 1.157 [16] describes models, correlations, data, model evaluation procedures, and methods that are acceptable to the NRC staff for a realistic or best-estimate calculation of ECCS performance during a LOCA and for estimating the uncertainty in that calculation. Both the NRC and ACRS have stated that the CSAU methodology [15] is in full compliance with Regulatory Guide 1.157. Compliance of the GE methodology for ECCS/LOCA analysis with Regulatory Guide 1.157 is demonstrated in Section 2.1.5.1. Conformance with the CSAU process is shown in Section 2.1.5.2.

#### **2.1.4 Standard Review Plan (SRP) Guidelines (NUREG 800)**

The NRC guidelines for review of ECCS/LOCA safety analysis are identified in Section 15.6.5 of the SRP [19], *Loss-of-Coolant Accidents Resulting from Spectrum of Postulated Piping Breaks within the Reactor Coolant Pressure Boundary*. A draft Section 15.0.1, *Review of Analytical Computer Codes*, is currently undergoing NRC review.

#### **2.1.5 Proposed Application Methodology**

TRACG is a complete transient thermal-hydraulic model, and it will be used to calculate the entire LOCA transient for both the vessel and containment.

TRACG calculates the PCT, local oxidation and core-wide oxidation. Thus, conformance with Criteria 1 through 3 of 10CFR50.46 is demonstrated by the TRACG analysis results. As discussed in Reference 88, conformance with Criterion 4 (coolable geometry) is demonstrated by conformance to Criteria 1 and 2. The bases and demonstration of compliance with Criterion 5 (long term cooling) are documented in Reference 88, and are usually not affected by the TRACG ECCS/LOCA analysis.

##### **2.1.5.1 Conformance with Regulatory Guide 1.157**

The proposed application methodology using TRACG for ESBWR ECCS/LOCA analyses complies with all the requirements of Regulatory Guide 1.157, "Best-Estimate Calculations of Emergency Cooling System Performance" [16]. This section shows how these requirements are addressed on a point-by-point basis.

The regulatory guide describes models, correlations, data, model evaluation procedures, and methods that are acceptable to the NRC staff for meeting the requirements for a realistic or best-estimate calculation of ECCS performance during a LOCA and for estimating the uncertainty in that calculation. It also provides a description of the acceptable features of best-estimate computer codes and acceptable methods for determining the uncertainty in the calculations. The guide lists TRAC-BWR as an acceptable code for best-estimate calculations of ECCS performance. Both the NRC and ACRS have stated that the CSAU process [15] is in full compliance with the Regulatory Guide and is acceptable under the provisions of Paragraph 50.46(a)(1) for use of a realistic evaluation model. The GE methodology follows the CSAU

steps (see next section). Thus, the GE methodology should be acceptable with respect to the requirements of Regulatory Guide 1.157. Nevertheless, in this section the features of the GE methodology are compared with the required features in the regulatory positions in Regulatory Guide 1.157.

**Regulatory Position 1: Best-Estimate Calculations**

<b>Staff Position</b> Licensees may use TRAC-PWR, TRAC-BWR, RELAP5, COBRA and FRAP codes	<b>GE Process</b> TRACG, a derivative of TRAC-BWR, is used.	<b>Evaluation</b> TRACG shares the same structure and field equations as TRAC-BF1. The bulk of the constitutive relations are the same [1]. Differences are listed in Appendix A of Reference 1. TRACG is in the family of acceptable codes.
Licensee must demonstrate that the code and models used are acceptable and applicable to the specific facility over the intended operating range.	Description of models [1] and qualification [2],[24],[25] demonstrate applicability. Range of test data and qualification requirements are specified in these documents.	Range of models and correlations reviewed by NRC in TRACG Model Report [1]. Model acceptability demonstrated through qualification against test data and reviewed by NRC as part of TRACG Qualification [2].
Licensee must quantify uncertainty in the specific application.	Uncertainty is quantified in the application report for ECCS/LOCA application.	Uncertainty obtained from integral comparisons and bounded by combination of individual uncertainties. Meets CSAU and Reg. Guide requirements.
The model should be compared with applicable experimental data and should predict the mean of the data.	TRACG has been compared against a wide range of applicable data and generally predicts mean of data [2],[24],[25].	TRACG is intended to predict mean of data. Bias and uncertainty in predictions are quantified in Qualification Reports.
Effects of all important variables should be considered.	Capability to treat important phenomena is shown in PIRT Section 2.2 of this report.	TRACG considers all important LOCA parameters.

**Staff Position**

Best-estimate code should be compared with applicable experimental data (e.g., separate effects tests and integral simulations of LOCAs) to determine overall uncertainty and bias

**GE Process**

Comparisons made in Model Report [1] and Qualification Reports [2],[24],[25] for separate effects and integral tests.

**Evaluation**

Requirements satisfied.

**Regulatory Position 2: Considerations for Thermal-Hydraulic Best-Estimate Codes**

**2.1.1 Numerical Methods**

<b>Staff Position</b>	<b>GE Process</b>	<b>Evaluation</b>
Sensitivity studies and evaluations of the uncertainty introduced by noding should be performed.	ESBWR nodalization is justified through qualification studies and sensitivity studies in the SBWR Qualification Report [24].	Reg. Guide requirements satisfied.
Effect of time step size should be investigated.	Time step is determined internally by TRACG (Section 8.2.4 of Reference 1). Maximum time step has been varied in calculations to show insensitivity [2].	Insensitivity to time step size demonstrated in the range of time steps sizes used for the calculations.

**2.1.2 Computational Models**

<b>Staff Position</b>	<b>GE Process</b>	<b>Evaluation</b>
Separate flow fields for different fluid phases and calculation of nonequilibrium between phases may be required.	TRACG has separate field equations for the vapor and liquid phases and calculates individual phasic velocities and temperatures [1, Section 3.1.2].	The adequacy of the TRACG field equations and constitutive relations has been validated by extensive comparisons against separate effects data for void fraction and heat transfer [2, Sections 3.1 and 3.2].

**Regulatory Position 3: Best-Estimate Code Features**

**3.1 Initial and Boundary Conditions and Equipment Availability**

**Staff Position**

Most limiting initial conditions expected over the life of the plant should be used.

**GE Process**

Most limiting operating conditions (power/flow, pressure, exposure, etc.) have been determined.

**Evaluation**

Limiting operating conditions are used in analysis.

The calculations should be performed over the spectrum of possible break sizes up to a full double-ended break of the largest pipe. Effects of longitudinal splits with the split area equal to twice the cross-sectional area of the pipe should be included.

The full spectrum of breaks is analyzed. The split break evaluation has no specific consideration of break geometry; the conditions upstream of the break are determined by flow from both sides of the break location.

The break spectrum is analyzed to identify the case leading to the minimum chimney static head (no core heatup).

Other boundary and initial conditions (equipment availability, control systems and operator actions) should be based on plant technical specification limits.

Trips such as scram, MSIV closure, ADS opening, etc., are assumed to occur based on technical specification limits. Instrument setpoints and equipment performance are set to their analytical limits. The LOCA analysis takes no credit for non-safety systems to mitigate the accident. When the expected operation of a non-safety system can cause the results to be more severe (e.g., bypass valve pressure regulation), it is considered.

Analytical values corresponding to the technical specification limits are used, accounting for uncertainties. No credit is taken for non-safety systems or for mitigating operator actions.

<p><b>Staff Position</b> Single failure and loss of onsite and offsite power should be considered.</p>	<p><b>GE Process</b> Loss of preferred power is assumed. Sensitivity to all single failures is considered.</p>	<p><b>Evaluation</b> Process conforms to Reg. Guide and Appendix A of 10 CFR 50.</p>
------------------------------------------------------------------------------------------------------------	--------------------------------------------------------------------------------------------------------------------	------------------------------------------------------------------------------------------

**3.2 Sources of Heat During a LOCA**

**3.2.1 Initial Stored Energy of the Fuel**

<p><b>Staff Position</b> The steady-state temperature distribution and stored energy in the fuel should be calculated on a best-estimate basis.</p>	<p><b>GE Process</b> Because the stored energy is dependent on the plant operating history at the time of LOCA, a design basis operating trajectory is used to calculate this parameter.</p>	<p><b>Evaluation</b> Reasonable approach, considering operating states.</p>
<p>An acceptable model should recognize the effects of fuel burnup, fuel pellet cracking and relocation, cladding creep, and gas mixture conductivity.</p>	<p>The GESTR [27] model includes all of these effects. The TRACG dynamic gap conductance model (Section 7.5.2 of Reference 1) is initialized by GESTR.</p>	<p>GESTR has been separately reviewed and accepted for use by the NRC staff [27].</p>
<p>The model must be checked against several sets of relevant data.</p>	<p>The GESTR model has been extensively compared with irradiated BWR fuel data [27].</p>	<p>GESTR has been separately reviewed and accepted for use by the NRC staff [27].</p>

**3.2.2 Fission Heat, 3.2.3 Decay of Actinides, 3.2.4 Fission Product Decay Heat**

<b>Staff Position</b>	<b>GE Process</b>	<b>Evaluation</b>
<p>The heat from radioactive decay of actinides, including neptunium and plutonium generated during operation, as well as isotopes of uranium, should be calculated in accordance with fuel cycle history.</p>	<p>Heat from radioactive decay of actinides, including neptunium and plutonium, as well as isotopes of uranium, is included in the calculation.</p>	<p>The model used is in compliance with Reg. Guide requirements.</p>
<p>The heat generation from radioactive decay of fission products should be calculated in accordance with the 1979 ANS standard.</p>	<p>The heat generation from radioactive decay of fission products is calculated in accordance with the ANS standard. A generic curve is calculated to characterize the core average response for reference values of fuel exposure, depletion power density, irradiation time, fuel enrichment, and void fraction. Uncertainties due to variations in the operational parameters listed above, as well as due to measurements, are considered.</p>	<p>Calculations are made in accordance with the 1979 ANS Standard. The average core decay heat history is slightly conservative for most operating conditions. Sensitivities to variations in voids, enrichment and operating history are shown in Appendix B of Reference 21.</p>

**3.2.5 Metal-Water Reaction Rate**

**Staff Position**

The metal-water reaction rate should be calculated with a best-estimate model. For rods calculated to rupture, oxidation of the inside of the cladding should be calculated.

Below 1900°F, model should be checked against appropriate data. It should recognize the effects of steam pressure, pre-oxidation of cladding, deformation during oxidation and internal oxidation from both steam and UO<sub>2</sub> fuel.

Above 1900°F, Cathcart's data is acceptable.

**GE Process**

The Cathcart correlation (Equation 6.6-136 of Reference 1) is used at all temperatures. The model is also used on the inside surface of the cladding if the fuel rod perforates.

The Cathcart correlation is used. This will tend to be conservative at temperatures below 1900°F. Effects of internal oxidation from UO<sub>2</sub> and steam pressure effects are not included.

The Cathcart correlation is used.

**Evaluation**

Acceptable model is used. Metal-water reaction is of no importance for ESBWR, as PCTs are low (no cladding heatup). Metal-water reaction is negligible below 1700°F.

Conservative, but acceptable model is used.

In conformance with Reg. Guide position.

### 3.2.6 Heat Transfer from Reactor Internals

**Staff Position**

Heat transfer from piping, vessel walls and internal hardware should be calculated in a best-estimate manner.

**GE Process**

TRACG models pipe and vessel walls as well as internal hardware as “heat slabs”. Conduction through the slabs is modeled as 1-D process across the slab with radial nodalization of the walls [1, Section 4]. Geometrical complexity (at penetrations, etc.) is not simulated, but masses and surface areas of the structures are preserved. Heat transfer coefficients correspond to the fluid regimes in contact with the heat slabs. Single-phase convection to liquid or vapor, subcooled and nucleate boiling and condensation are modeled [1, Section 6.6].

**Evaluation**

Heat transfer from reactor internals is modeled in a best-estimate manner consistent with a system code representation, to assure that that heat releases to the fluid are calculated accurately. Calculations of integral experiments (TLTA, FIST, GIRAFFE/SIT) show good comparisons for pressure response and voiding in the lower plenum. The uncertainty in this parameter is largely in the value of the heat transfer coefficients. Sensitivity studies have been made on the heat transfer coefficients as part of the uncertainty study in Section 2.4.4.

### 3.3 Reactor Core Thermal/Physical Parameters

#### 3.3.1 Thermal Parameters for Swelling and Rupture of the Cladding and Fuel Rods

**Staff Position**

The model should calculate fuel cladding swelling and rupture resulting from the temperature distribution in the cladding and from the pressure difference between the inside and outside of the cladding, both as a function of time.

**GE Process**

TRACG calculates swelling and rupture based on an empirical fit to experimental data for BWR size fuel rods. The cladding strain is a function of the cladding temperature and the hoop stress (Section 7.5.3.3 of Reference 1).

**Evaluation**

Requirements are met. TRACG model for cladding swelling is empirically based, rather than true best estimate. No fuel cladding swelling will occur in ESBWR LOCA as the core is always covered.

**Staff Position**

The degree of swelling and rupture should be taken into account in the calculation of gap conductance, cladding oxidation and embrittlement, hydrogen generation, and heat transfer and fluid flow outside of the cladding.

The calculation of fuel and cladding temperatures as a function of time should use values of gap conductance and other thermal parameters as functions of temperature and time.

The calculation of the swelling of cladding should take into account spatially varying cladding temperatures, heating rates, anisotropic material properties, asymmetric deformation of cladding, and fuel rod thermal and mechanical parameters.

**GE Process**

The change in gap size affects the gap conductance calculation (Section 7.5.2.5 of Reference 1). Cladding oxidation and hydrogen generation are functions of the cladding surface area. Changes in cladding embrittlement are not calculated by TRACG. While the effects of the area change on the flow outside the rod can be handled by TRACG, the analysis does not account for this effect. Experimental data have shown insensitivity to this effect.

TRACG has a dynamic gap conductance model (Section 7.5.2 of Reference 1) which accounts for changes in gap conductance, plenum temperature, rod internal pressure and thermal properties with time.

TRACG simulates the fuel rod with axial and radial nodes. The calculation of cladding swelling accounts for spatial variations in temperatures and heating rates. Asymmetric effects are accounted for empirically through the use of data.

**Evaluation**

See above. Cladding embrittlement is not calculated in TRACG. Requirements for coolable geometry are met by meeting criteria on PCT and oxidation. No fuel cladding swelling will occur in ESBWR LOCA as the core is always covered.

The TRACG gap conductance model meets the requirements of the Reg. Guide.

TRACG model for cladding swelling is empirically based and meets Reg. Guide requirements. No fuel cladding swelling will occur in ESBWR LOCA as the core is always covered.

**3.3.2 Other Core Thermal Parameters**

**Staff Position**

Physical and chemical changes in in-core materials (e.g., eutectic formation, phase change, etc.) should be included as necessary.

**GE Process**

TRACG does not model physical and chemical changes in in-core materials.

**Evaluation**

These phenomena are not significant for ESBWR LOCAs, and their treatment is not necessary.

**3.4.1 Break Characteristics and Flow**

**Staff Position**

The critical flow model should consider the fluid conditions at the break location, upstream and downstream pressures, and break geometry.

**GE Process**

The TRACG critical flow model (Section 6.3 of Reference 1) accounts for break conditions (subcooled, two-phase, steam), and upstream and downstream pressures. Break geometry can be treated with the use of discharge coefficients.

**Evaluation**

Split and double-ended breaks can be analyzed. The TRACG model is empirically based but accounts for all relevant parameters and has been shown to be accurate by extensive comparisons to data.

The uncertainties and bias of the model should be stated, as well as the range of applicability.

The uncertainty and bias for the TRACG critical flow model have been quantified (Section 6.3.6 of Reference 1).

TRACG model meets Reg. Guide requirements.

### 3.4.2 ECC Bypass

**Staff Position**

ECC bypass during the blowdown phase of a LOCA should be calculated in a best estimate manner. One-dimensional models justified through analysis and data are acceptable.

**GE Process**

TRACG models “flooding” or CCFL type of phenomena through a Kutateladze type of correlation (Section 6.1.7.2 of Reference 1). The correlation used in TRACG is conservative for predicting ECC bypass in the downcomer (Section 6.1.7.4 of Reference 1).

**Evaluation**

The ECC bypass phenomenon is important for PWRs, but is not significant for BWRs (Section 6.1.7.4 of Reference 1). Therefore, a conservative model is acceptable for BWR analysis. Also, in the ESBWR, the GDCS flow enters the vessel at the end of blowdown.

### 3.5 Noding Near the Break and ECCS Injection Point

**Staff Position**

Sufficient sensitivity studies should be performed on the noding and other important parameters to ensure calculations provide realistic results.

**GE Process**

Sensitivity to nodalization near the break and ECC injection point has been studied. Nodalization is consistent between test facilities and ESBWR in these regions. Uncertainties in other parameters are considered as part of the PIRT parameter uncertainty study.

**Evaluation**

Process meets Reg. Guide requirements.

### 3.6 Frictional Pressure Drop

**Staff Position**

The frictional pressure drop in pipes and other components should be calculated using models that include variation of friction factor with Reynolds number and effects of two-phase flow effects on friction.

The gravitational, friction and acceleration components of pressure drop should be consistently calculated.

Model should be checked against experimental data and the bias and uncertainty should be stated.

**GE Process**

Wall friction is calculated with a fit to the Moody curves as a function of Reynolds number and surface roughness (Section 6.2.1.3 of Reference 1). The two-phase multiplier is a modified Chisholm multiplier (Section 6.2.1.4 of Reference 1).

The terms in the phasic momentum equations are consistently formulated and calculated (Section 3 of Reference 1).

The frictional pressure drop models in TRACG have been extensively compared with experimental data for tubes and bundles (Section 6.2.1.6 of Reference 1). Estimates of the mean bias and uncertainty are also given in the same section.

**Evaluation**

Models are in conformance with Reg. Guide requirements.

Most data comparisons are for total pressure drop. Since the void fraction is compared against other data, these comparisons are checks on the consistency of the pressure drop components.

Models are in conformance with Reg. Guide requirements.

### 3.7 Momentum Equation

#### Staff Position

The momentum equation should include terms for: 1) temporal change in momentum, 2) momentum convection, 3) area change momentum flux, 4) momentum change due to compressibility, 5) pressure loss resulting from wall friction, 6) pressure loss resulting from area change, and 7) gravitational acceleration.

Technical basis should be demonstrated with data and analysis.

#### GE Process

The momentum equations are formulated for each phase and contain all the relevant terms (Section 3.1.2 of Reference 1 for the differential form; Sections 3.2.1.1 and 3.2.2.1 of Reference 1 for the difference form).

The validity of the momentum equations is demonstrated by comparisons with pressure drop, void fraction and critical flow data (Sections 3.5, 3.1 and 3.4 of Reference 2).

#### Evaluation

Equations for separate phase flows are used with the appropriate interfacial terms.

The momentum equations represent best-estimate models and are adequately qualified against test data.

### 3.8 Critical Heat Flux

#### Staff Position

Best-estimate models developed from appropriate steady-state or transient experimental data should be used for calculating CHF.

#### GE Process

TRACG uses the best-estimate GEXL correlation for calculation of CHF (Section 6.6.6.1 of Reference 1). The GEXL correlation is based on an extensive database for steady-state CHF in BWR rod bundles. At low flow conditions, a modified Zuber correlation is used (Section 6.6.6.1 of Reference 1).

#### Evaluation

The correlations cover the range of LOCA conditions. The correlations have been validated for time varying conditions that exist in operational transients and LOCAs (Sections 3.2.1 and 5.1.2 of Reference 2).

The boiling length correlation is known to be accurate over a large range of lengths and covers the 10 ft active core height of the ESBWR. A larger value of uncertainty (5% vs. 3.2%) is assumed for the analysis.

Return to nucleate boiling is allowed if justified by local fluid and surface conditions.

TRACG allows a return to transition boiling if the wall temperature is below  $T_{min}$  and the local quality is less than the critical quality. Nucleate boiling is restored when the wall temperature is less than  $T_{CHF}$ .

The TRACG model has been validated against test data from BWR rod bundles (Sections 5.1.2, 5.2.3 and 3.6.2 of Reference 2-11). No fuel heatup will occur in ESBWR LOCA as the core is always covered.

Technical basis should be demonstrated with data and analysis.

The TRACG CHF model has been extensively qualified for transient conditions simulating LOCAs [2].

The TRACG model is in conformance with the requirements of the Reg. Guide.

### 3.9 Post-CHF Blowdown Heat Transfer

#### Staff Position

A model for post-CHF heat transfer should:

- a. Be checked against an acceptable set of relevant data.
- b. Recognize effects of liquid entrainment, thermal radiation, and thermal nonequilibrium, low and high mass flow rates, low and high power densities and saturated and subcooled inlet conditions.

#### GE Process

TRACG calculates post-dryout heat transfer in two regimes: (1) dispersed droplet flow at high flow and qualities, and (2) inverted annular flow at low flow rates and low qualities. These heat transfer regimes are described in Sections 6.6.9 and 6.6.10 of Reference 1. Liquid entrainment is considered. The TRACG model allows for unequal temperatures for the two phases. The radiation model is described in Section 6.6.12 of Reference 1. The Bromley correlation for low quality film boiling has been compared against a range of bundle reflooding data (Section 6.6.9.3 of Reference 1).

#### Evaluation

The correlations cover the range of expected LOCA conditions. The correlations have also been validated against appropriate data. No fuel cladding heatup will occur in ESBWR LOCA as the core is always covered

<b>Staff Position</b>	<b>GE Process</b>	<b>Evaluation</b>
<p>Correlations for heat transfer from uncovered fuel bundles should:</p> <ul style="list-style-type: none"> <li>a. Be checked against an acceptable set of relevant data.</li> <li>b. Recognize the effects of radiation and of laminar, turbulent and transition flows.</li> </ul>	<p>The correlations used in the uncovered portion of the bundle are described in Section 6.6.10 of Reference 1. The single-phase steam correlation includes the laminar, turbulent and transition regimes. Additionally, the effects of droplets are accounted for through the Sun-Tien-Gonzalez correlation (Equation 6.6-49). The radiation heat transfer model is described in Section 6.6-12 of Reference 1.</p>	<p>The models are in conformance with the requirements of the Reg. Guide. Comparisons with core spray cooling data are shown in Section 6.6.10.3 of Reference 1. No fuel cladding heatup will occur in ESBWR LOCA as the core is always covered</p>
<p>Uncertainties and bias in the models for post-CHF heat transfer should be stated.</p>	<p>Applicability and uncertainty and bias in the low and high void fraction film boiling regimes are provided in Sections 6.6.9.3 and 6.6.10.3 of Reference 1.</p>	<p>Reg. Guide requirements have been satisfied.</p>

### 3.10 Pump Modeling

#### Staff Position

The characteristics of rotating primary system pumps should be derived from a best-estimate dynamic model that includes momentum transfer between the fluid and the rotating member, with variable speed as a function of time. The model for two-phase flow should be verified by comparison to applicable data.

#### GE Process

The governing equations for the pump are given in Section 7.2.1 of Reference 1. The momentum equation for the pump component includes a term for the momentum transfer from the rotating member to the fluid. Homologous curves are used to characterize the pump head and torque as a function of the fluid volumetric flow and pump speed. To account for the two-phase effects on pump performance, degradation factors based on data are applied.

#### Evaluation

There are no primary system pumps in ESBWR.

### 3.11 Core Flow Distribution During Blowdown

#### Staff Position

The core flow through the hottest region (no larger than one fuel bundle) should be calculated as function of time. Calculations should account for any crossflow between regions.

#### GE Process

The high power bundle is modeled as a separate region in TRACG.

#### Evaluation

This requirement is aimed at PWR analysis. Because of the BWR configuration with zircaloy channels surrounding each bundle, there is no crossflow between bundles.

### 3.12 Post-Blowdown Phenomena

#### 3.12.1 Containment Pressure

#### Staff Position

The containment pressure used for evaluating effectiveness during the post-blowdown phase of a LOCA should be best-estimate and include the effects of containment heat sinks.

#### GE Process

The containment is explicitly modeled for LOCA analysis and includes the effects of heat sinks in the containment. Additionally, sensitivity studies have been made with respect to containment pressure.

#### Evaluation

Reg. Guide requirements met.

**3.12.2 Calculation of Post-Blowdown Thermal Hydraulics for Pressurized Water Reactors**

Not Applicable

**3.12.3 Steam Interaction with ECC Water in Pressurized Water Reactors**

Not Applicable

**3.12.4 Post-Blowdown Heat Transfer for Pressurized Water Reactors**

Not Applicable

**3.13 Convective Heat Transfer Coefficients for BWR Rods Under Spray Cooling**

**Staff Position**

Following the blowdown period, convective heat transfer coefficients should be determined based on the calculated fluid conditions and heat transfer modes.

During the period following lower plenum flashing, but prior to ECC initiation, heat transfer models should include steam cooling or two-phase flow convection.

**GE Process**

TRACG applies convective heat transfer coefficients following blowdown corresponding to the calculated heat transfer regime. The heat transfer selection logic is shown in Section 6.6.2 of Reference 1.

TRACG applies convective heat transfer coefficients following blowdown corresponding to the calculated heat transfer regime. The heat transfer selection logic is shown in Section 6.6.2 of Reference 1. Steam cooling, nucleate boiling and film boiling are considered.

**Evaluation**

The TRACG models have been extensively qualified [2],[24] for tests simulating jet pump BWRs and ESBWR.

TRACG models for post lower plenum flashing heat transfer phenomena are best-estimate and meet the Reg. Guide requirements.

**Staff Position**

Following ECC initiation, but prior to reflooding, heat transfer models should account for rod-to-rod variations in heat transfer.

After the two-phase level reaches the level under consideration, a best-estimate heat transfer model should be used. This model should include the effects of any flow blockage.

Thermal hydraulic models that do not consider multiple channels should be compared with experimental data or more detailed calculations to ensure that all important phenomena are adequately calculated.

**GE Process**

Best-estimate correlations are used for steam/droplet cooling (Section 6.6.10 of Reference 1), and rod-rod, and rod-channel radiative heat transfer with an absorbing medium (Section 6.6.12 of Reference 1). TRACG spray heat transfer models have been validated against spray cooling tests (Section 6.6.10.3 of Reference 1).

TRACG applies convective heat transfer coefficients following blowdown corresponding to the calculated heat transfer regime. The heat transfer selection logic is shown in Section 6.6.2 of Reference 1. Typically, the modified Bromley correlation (Section 6.6.9 of Reference 1) would be used at low void fractions.

Multiple channels are modeled in TRACG.

**Evaluation**

TRACG has the required models.

These effects are not important for ESBWR, as there is no core uncover.

Effects of flow blockage due to swelling of cladding are not considered in TRACG other than as an increase in surface area of the fuel rod cladding. Experimental data [56] have shown minor sensitivity to even large amounts of flow blockage. No fuel cladding swelling or flow blockage will occur in ESBWR LOCA as the core is always covered and well cooled.

Comparison with data from the 30° Steam Sector Test Facility (Section 5.4 of Reference 2) has shown the capability of TRACG to model the multi-channel phenomena seen in the refill/reflood phase of a BWR.

**3.14 BWR Channel Box Under Spray Cooling**

**Staff Position**

Following the blowdown period, heat transfer from the channel box and wetting of the channel box should be determined based on the calculated fluid conditions on both sides of the channel box and should make use of best-estimate rewetting models that have been compared with applicable experimental data.

**GE Process**

TRACG applies convective heat transfer coefficients following blowdown corresponding to the calculated heat transfer regime on either side of the channel box. The heat transfer selection logic is shown in Section 6.6.2 of Reference 1. TRACG employs a quench front propagation correlation (Section 6.6.13 of Reference 1), which is a fit to the two-dimensional conduction solution. These models have been extensively validated against core spray cooling data[54],[2].

**Evaluation**

Reg. Guide requirements met.  
No fuel cladding heatup will occur in ESBWR LOCA as the core is always covered. There are no core spray systems in ESBWR.

**3.15 Special Considerations for a Small-Break LOCA in Pressurized Water Reactors**

Not Applicable

**3.16 Other Features of Best-Estimate Codes**

**Staff Position**

**Completeness:**  
Comparisons of the overall calculations to integral experiments should be performed to ensure that important phenomena can be predicted.

**GE Process**

Comparisons of TRACG predictions against integral experiments are shown in Section 5 of Reference 2 and in Volume 2 of Reference 24. An overall assessment of TRACG capabilities to predict this data is shown in Reference 24.

**Evaluation**

The integral test comparisons show that all major LOCA phenomena are captured by TRACG.

**Data Comparisons:**

Individual models should be compared against data. Uncertainty and bias in models should be evaluated.

Comparisons of TRACG against separate effects data are shown in Sections 3.1 through 3.9 of Reference 2 and in Volume 1 of Reference 24.

The separate-effects test comparisons show that the individual models in TRACG predict separate-effects phenomena correctly.

**Regulatory Position 4: Estimation of Overall Computational Uncertainty**

**4.1 General**

**Staff Position**

The calculational uncertainty should include the uncertainty due to individual models (“code uncertainty”), experimental data, boundary and initial conditions, fuel behavior and simplifying assumptions.

**GE Process**

Uncertainties due to individual models, boundary and initial conditions and fuel behavior are accounted for explicitly. Some boundary and initial conditions are chosen conservatively. Experimental data were selected for comparisons based on adequate accuracy in the experiments. Deviations between data and calculations implicitly include experimental uncertainties. Effects of simplifying assumptions are implicit in comparisons with integral tests.

**Evaluation**

The required uncertainty components are accounted for.

A 95% probability level is acceptable for comparing best-estimate predictions to the applicable limits of Paragraph 50.46(b) of 10CFR50.

Calculations are intended to bound the 95th percentile value of the minimum chimney static head

Meets Reg. Guide requirements.

**4.2 Code Uncertainty**

**Staff Position**

**GE Process**

**Evaluation**

It will be necessary to evaluate the code's predictive ability over several time intervals.

The entire transient is considered in the evaluation rather than a single value.

Meets Reg. Guide requirements.

**4.3 Other Sources of Uncertainty**

**Staff Position**

Uncertainties associated with boundary and initial conditions (initial power, pump performance, valve actuation times and control systems operational) should be accounted for. It is acceptable to limit the variables to conservative bounds.

Uncertainties in fuel parameters such as fuel conductivity, gap width, gap conductivity and peaking factors should be accounted for in the uncertainty analysis.

**GE Process**

Sensitivity studies have been performed to assess the effect of changes in boundary and initial conditions. Many variables have been set to conservative values (technical specification limits).

Uncertainties in the fuel conductivity, gap width and conductance are treated as individual model uncertainties contributing to the uncertainty in the fuel rod stored energy. Uncertainties in the peaking factor are included in the initial conditions.

**Evaluation**

Meets Reg. Guide requirements.

Meets Reg. Guide requirements.

**4.4 Statistical Treatment of Overall Computational Uncertainty**

<b>Staff Position</b>	<b>GE Process</b>	<b>Evaluation</b>
<p>Justification should be provided for the assumed parameter distributions and ranges.</p>	<p>Justification for the assumed parameter distributions and ranges is provided in Section 2.4.</p>	<p>This corresponds to the CSAU step on ranging of the parameters under Step 4.</p>
<p>The evaluation of PCT at the 95% level need only be performed for the limiting break. Justification must be provided that the overall calculational uncertainty at the limiting condition bounds that at the other conditions.</p>	<p>Calculations are performed for the limiting break. See discussion above regarding the lack of impact on PCT.</p>	<p>The requirements of the Reg. Guide are met.</p>

### 2.1.5.2 Conformance with CSAU Methodology

The TRACG LOCA application methodology also addresses all the elements of the NRC-developed Code Scaling, Applicability and Uncertainty (CSAU) evaluation methodology. The CSAU methodology is documented in the report *Quantifying Reactor Safety Margins, Application of Code Scaling, Applicability, and Uncertainty Evaluation Methodology to a Large-Break Loss-of-Coolant Accident* [15]. The CSAU report describes a rigorous process for evaluating the total model and plant parameter uncertainty for a nuclear power plant calculation. Further details on the CSAU methodology are contained in the NRC-issued Regulatory Guide 1.157. The CSAU methodology incorporates the elements of phenomena identification and ranking, documentation of models, assessment against Systems Effects Tests (SETs) and Integral System Tests (ISTs) for the key phenomena, and quantification of uncertainties due to the models, scaling and plant parameters. In the CSAU process, the model uncertainty is derived from the propagation of individual model uncertainties through code calculations; experimental comparisons are used as a check on the derived uncertainty. This process will be followed with TRACG, but for the ESBWR a simpler bounding approach will be used to combine uncertainties.

The CSAU methodology consists of 14 steps, as outlined in Table 2.1- 1.

**Table 2.1- 1. CODE SCALING, APPLICABILITY AND UNCERTAINTY EVALUATION METHODOLOGY**

<b>CSAU Step</b>	<b>Description</b>	<b>Addressed In</b>
1	Scenario Specification	Section 2.1.5.2
2	Nuclear Power Plant Selection	Section 2.1.5.2
3	Phenomena Identification and Ranking	Section 2.2
4	Frozen Code Version Selection	Reference [1]
5	Code Documentation	References [1,2,24,25,26]
6	Determination of Code Applicability	Section 2.3
7	Establishment of Assessment Matrix	Section 2.3.2
8	Nuclear Power Plant Nodalization Definition	Section 2.4.2
9	Definition of Code and Experimental Accuracy	Reference [1,2,24]
10	Determination of Effect of Scale	Section 2.4.3
11	Determination of the Effect of Reactor Input Parameters and State	Section 2.5
12	Performance of Nuclear Power Plant Sensitivity Calculations	Section 2.6,2.7
13	Determination of Combined Bias and Uncertainty	Section 2.6,2.7
14	Determination of Total Uncertainty	Section 2.6,2.7

The 14 CSAU steps are summarized in the following paragraphs. The objectives for each step are addressed by indicating how they will be addressed in this report.

#### **1. Specify scenario.**

The LOCA scenarios include the full range of pipe breaks analyzed for the ESBWR. Further, the scenarios are differentiated for large and small breaks and by the location of the break. Typical ESBWR LOCA scenarios are described in Section 2.2.1. For LOCAs, the transient has been divided into the *Blowdown*, *GDCS* and *Long Term PCCS* phases. Of these only the first two are relevant for ECCS/LOCA considerations. The subdivision into phases allows reduction of the analysis to only those processes and components that are important during each phase.

## 2. Select nuclear plant.

The Nuclear Power Plant (NPP) which is the basis for this application report is the 4000 MWt ESBWR described in detail in the ESBWR Design Description [23].

## 3. Identify and rank phenomena.

All processes and phenomena that occur during an event do not equally influence plant behavior. The most cost efficient, yet sufficient, analysis reduces all candidate phenomena to a manageable set by identifying and ranking the phenomena with respect to their influence on the primary safety criteria. The phases of the events and the important components are investigated. The processes and phenomena associated with each component are examined. Cause and effect are differentiated. After the processes and phenomena have been identified, they are ranked with respect to their effect on the primary safety criteria for the event. A phenomena identification and ranking table (PIRT) is established to guide the subsequent uncertainty quantification. The PIRTs for ECCS/LOCA are developed in Reference 29 and reported in Section 2.2.

## 4. Select frozen code.

TRACG04A is the frozen code selected for the analysis. TRACG02A was the code frozen for AOO analysis. The only major model additions to create TRACG04A are the axial conduction controlled quench front model, PANAC11 physics and I/O changes. An earlier version of TRACG04 was used for the majority of the validations presented in the SBWR TRACG Qualification Report [24]. The recent additions in TRACG04A should have no impact on the earlier qualification. This has been confirmed by running spot checks on the SBWR qualification cases. All aspects of management, control, maintenance, testing and documentation of the code are governed by internal procedures (see Section 2.5.1).

## 5. Document code.

The details of the models are contained in the *TRACG Model Description* LTR [1]. A summary description of the TRACG assessment is provided in Section 2.3.2. Details are contained in the *TRACG Qualification* LTRs [2], [24], [25]. This report describes the application process. The User' Manual [26] provides guidance on the use of the code.

## 6. Determine code applicability.

To demonstrate *applicability*, one must begin with *capability*. Capability to calculate an event for a nuclear power plant rests on four elements: (1) conservation equations, which provide the code capability to address global processes; (2) constitutive correlations and models, which provide code capability to model and scale particular processes; (3) numerics, which provide code capability to perform efficient and reliable calculations; and (4) structure and nodalization, which address code capability to model plant geometry and perform efficient and accurate plant calculations. All four elements must be considered when evaluating the code capability for a specific application. Code

capability is only one aspect needed to demonstrate that the code is applicable. *Applicability* also implies that the capability of the code has been demonstrated by actually applying the code in the intended manner and then qualifying the results. The capability of TRACG to model phenomena that are important to ESBWR simulations has been addressed in Table 2.3-1 in Section 2.3.1. *Qualification* aspects have also been addressed in Section 2.3.2.

#### **7. Establish assessment matrix.**

The determination of uncertainty for a computer code must be based on a sufficient data set, which necessarily will include both separate and integral effects tests and available plant data. The assessment matrix must cover all phenomena and components that were identified and ranked important in the PIRT for the selected events for the nuclear power plant. The LOCA PIRTs are documented in Section 2.2. The assessment coverage of the PIRTs is summarized in Table 2.3-2 through Table 2.3-5.

#### **8. Define nodalization for plant calculations.**

The plant model must be nodalized finely enough to represent both the important phenomena and design characteristics of the nuclear power plant but coarsely enough to remain economical. In principle, nodalization can be treated as an individual contributor to code uncertainty; however, quantification of nodalization uncertainty can be very costly. Thus, the preferred path is to establish a standard nodalization based on the assessment against separate and integral effects tests. Nodalization studies have been performed in assessing this test data in order to determine the level of detail necessary to represent the important phenomena and then consistent levels of detail have been applied to establish standard noding schemes for the ESBWR. The standard ESBWR nodalization for TRACG for ECCS/LOCA applications is defined based on the qualification and is described in *TRACG Qualification* for SBWR [24].

#### **9. Determine code and experiment uncertainty.**

Simulations against experiments are used to determine the code accuracy. Comparisons to separate effects tests are used to quantify the uncertainty in the individual models and correlations. Typically, experimental uncertainty is inherent in these comparisons and is not separated out. Quantification of the uncertainties in the model parameters is discussed in Section 2.4.1. The impact on the primary safety parameters for the nuclear power plant can be determined by varying the inputs to the individual models by a specified amount (e.g.  $\pm 1 \sigma$ ). The overall uncertainty of the code in simulating the important phenomena for ECCS/LOCA is addressed fully in Section 2.4.

#### **10. Determine effects of scale.**

The differences for similar physical processes, at scales up to and including full scale, should be evaluated to establish a statement of potential scaling effects. For TRACG, this has been done by evaluating the experimental basis for the individual models and

correlations against full-scale plant conditions, by performing qualification against separate-effects tests, integral effects tests at different scales and full-scale plant data (where plant data exist), and by using a plant nodalization based on the qualification studies. Specific evaluations for ECCS/LOCA are addressed in Section 2.4.3.

#### **11. Determine effects of plant operating conditions.**

Uncertainties in the nuclear power plant simulations may result from uncertainties in plant operating state at the initiation of the LOCA or in plant process parameters. For example, the plant power distribution is a function of burnup history and control rod pattern prior to the transient. For the ESBWR, these uncertainties are accounted for by using analytical limits for parameters that influence ECCS/LOCA response (Section 2.5.3).

#### **12. Perform plant sensitivity calculations.**

Nuclear power plant calculations for a given event are used to determine the code's output sensitivity (in the primary safety criteria parameters) to various plant operating conditions that arise from uncertainties in the reactor state at the initiation of the transient event or in plant process parameters. Similarly, nuclear power plant calculations are used to address the uncertainties introduced by the code models and correlations. In this manner, the sensitivities of the safety-related quantities to these parameters are evaluated individually or collectively. The sensitivity studies for ECCS/LOCA are documented in Section 2.4.4.

#### **13. Combine biases and uncertainties.**

In this step, all the biases and uncertainties are combined into an overall bias and uncertainty. There are different techniques that can be used, as discussed in Section 2.6. Because there is no core heatup for the ESBWR for LOCAs, a bounding approach has been adopted. The results of the ECCS/LOCA analysis are shown in Section 2.7.

#### **14. Determine total uncertainty.**

The statement of total uncertainty for the code for ESBWR ECCS/LOCA analysis is given in terms of the difference between the bounding and nominal results.

##### **2.1.6 Implementation Requirements**

The implementation of TRACG into actual licensing analysis is contingent on completion of the following implementation requirements:

- Review and approval by the NRC of:
  1. The uncertainties documented in Section 2.4.
  2. The bounding process for analyzing ECCS/ LOCA described in Section 2.6.

- Analysis for the ESBWR LOCA break spectrum and the overall biases and uncertainties to be applied to the limiting LOCAs are included in this report. The acceptance criteria (PCT, local oxidation and core-wide oxidation) are automatically met as long as the core remains covered. Demonstration of core coverage is based on application of the application processes described in Section 2.6. These results demonstrate compliance with the acceptance criteria (Section 2.7).

The criteria for updating the overall bias and uncertainty in subsequent plant cycles are discussed in more detail in Section 2.7.

### **2.1.7 Review Requirements For Updates**

In order to effectively manage the future viability of TRACG for ESBWR ECCS/LOCA licensing calculations, GE proposes the following requirements for upgrades to the code to define changes that (1) require NRC review and approval and (2) that will be on a notification basis only.

#### **2.1.7.1 Updates to TRACG Code**

Modifications to the basic models described in Reference 1 may not be made for ECCS/LOCA licensing calculations without NRC review and approval.

Changes in the numerical methods to improve code convergence may be used in ECCS/ LOCA licensing calculations without NRC review and approval, as long as the cumulative effect of these changes on the calculated PCT is less than 50<sup>0</sup> F. These changes will be subject to reporting under the requirements of 10CFR50.46.

Features that support effective code input/output may be added without NRC review and approval.

#### **2.1.7.2 Updates to Fuel Rod Thermal Mechanical Model for ECCS/LOCA Application**

The NRC-approved GESTR/LOCA model [27] has been used to initialize the TRACG calculations in this application report. The NRC may approve updates to the fuel rod model in the future. In this event, the updated fuel rod model may be used for the same purpose in ECCS/ LOCA licensing calculations without NRC review and approval as long as the safety parameters of PCT, local oxidation and core-wide oxidation are not impacted compared to the model used in this LTR (i.e. the core remains covered at all times). A typical ECCS/ LOCA calculation for the limiting break will be performed and the results of the comparison will be transmitted for information.

#### **2.1.7.3 Updates to TRACG Model Uncertainties**

New data may become available with which the specific model uncertainties described in Section 2.4 may be reassessed. If the reassessment results in a need to change specific model uncertainty, the specific model uncertainty may be revised for ECCS/ LOCA licensing calculations without NRC review and approval as long as the process for determining the uncertainty is unchanged. These changes will be subject to reporting under the requirements of 10CFR50.46.

#### **2.1.7.4 Updates to TRACG Application Method**

Revisions to the TRACG application method described in Section 2.6 may not be made for ECCS/LOCA licensing calculations without NRC review and approval.

#### **2.1.7.5 Cycle Specific Uncertainties in Safety Parameters**

Biases and uncertainties in the minimum two-phase level in the chimney are developed for the ESBWR plant using the process described in this report. This process will be implemented for the first operating cycle for the ESBWR. The magnitudes of these biases and uncertainties may change for future core designs and do not require NRC review and approval. The values of the uncertainties will be transmitted to the NRC for information if the margin to core uncover is significantly impacted.

#### **2.1.8 Range of Application**

The intended application is ECCS/LOCA analysis as required by 10CFR50.46 for ESBWR. This covers the entire spectrum of break sizes and locations. The break could be initiated anywhere in the operating domain for an ESBWR operating at or below the technical specification limits. Equipment out of service or performance relaxations can also be analyzed. The application range includes, but is not restricted to:

- Initial, transition, and equilibrium cores
- ADS valve out of service
- Feedwater heater out of service
- MSIV out of service
- Feedwater temperature reduction

## 2.2 Phenomena Identification and Ranking

The critical safety parameters required by 10 CFR 50.46 for ECCS/ LOCA are peak cladding temperature (PCT), maximum cladding oxidation, maximum hydrogen generation, coolable geometry and long-term cooling. Additional intermediate safety parameters include the downcomer level and two-phase mixture level inside the core shroud. These safety parameters are the criteria used to judge the performance of the safety systems and the margins in the design. It is expected that only the two-phase level inside the shroud is relevant for the ESBWR because the core does not uncover for any LOCA. The values of the critical safety parameters are determined by the governing physical phenomena. To delineate the important physical phenomena, it has become customary to develop Phenomena Identification and Ranking Tables (PIRTs). PIRTs are ranked with respect to their impact on the critical safety parameters. For example, the two-phase level inside the shroud is determined by the reactor vessel inventory and inventory distribution between the various vessel regions, core power generation, core flow etc.

All processes and phenomena that occur during a LOCA do not equally influence plant behavior. The most cost efficient, yet sufficient, analysis reduces all candidate phenomena to a manageable set by identifying and ranking the phenomena with respect to their influence on the critical safety parameters. The phases of the events and the important components are investigated. The processes and phenomena associated with each component are examined. Cause and effect are differentiated. After the processes and phenomena have been identified, they are ranked with respect to their effect on the critical safety parameters for the event. The identification of important phenomena for the ESBWR was done in two ways: (1) a Top-Down process based on analyses and sensitivity studies, and (2) a Bottom-Up process based on examination of individual design features [29].

Section 2.2.1 describes representative TRACG calculations that established the scenarios of various LOCA events. The descriptions stress the phenomenological evolution of the transients. The scenarios are then reviewed by interdisciplinary teams to identify each thermal-hydraulic phenomenon that plays a role in the analysis, and to rank all of them in terms of "importance"; that is, degree of influence on the figure of merit (e.g., two-phase level inside the core shroud). Section 2.2.2 reports the results of the phenomena ranking from References 29 and 24.

### 2.2.1 LOCA Transient Response

Chapter 6 of the SSAR will include the entire matrix of calculations for postulated pipe rupture locations and single failures. For a complete PIRT evaluation, the entire spectrum of events must be covered, including analyses with less limiting conditions than the design-basis case with no auxiliary power. The approach followed in this study was to focus initially on the design basis cases, in terms of the equipment and systems available. This led to the most severe consequences and the greatest challenges to the analytical models in modeling the phenomena. The next step was to examine the possible interactions with other systems that might be available, even though they are not classified as engineered safeguard features for the event. To facilitate understanding, a large break in the Gravity-Driven Cooling System (GDCS) line has been chosen to illustrate the sequence of events during the LOCA. The sequence of events is

similar for all the LOCA events, particularly after initiation of the GDCS flows, when the vessel and containment transients are coupled. While there are some differences in the assumptions made for analysis of the different breaks, these are not very important in determining the phenomenological progression of the LOCA or the importance of various parameters. The limiting LOCA from the perspective of margin to core uncover is a large liquid line (GDCS line) break; from the viewpoint of containment pressure, it is likely to be the large steamline break. A schematic of the ESBWR passive safety systems is shown in Figure 2.2-1.

The overall LOCA sequence can be divided into three periods: blowdown period, GDCS period and the long-term cooling PCCS period. These periods are shown in Figure 2.2-2. The **Blowdown period** is characterized by a rapid depressurization of the vessel through the break, safety relief valves (SRVs) and depressurization valves (DPVs). The steam blowdown from the break and DPVs pressurizes the drywell, clearing the main containment vents and the PCCS vents. First, noncondensable gas and then steam flows through the vents and into the suppression pool. The steam is condensed in the pool and the noncondensable gas collects in the wetwell air space above the pool. At about 500 seconds, the pressure difference between the vessel and the wetwell is small enough to enable flow from the GDCS pools to enter the vessel. This marks the beginning of the **GDCS period**, during which the GDCS pools drain their inventory. Depending on the break size and location, the pools are drained in between 2000 and 7000 seconds. The GDCS flow fills the vessel to the elevation of the break, after which the excess GDCS flow spills over into the drywell. The GDCS period is characterized by condensation of steam in the vessel and drywell, depressurization of the vessel and drywell and possible openings of the vacuum breakers, which returns noncondensable gas from the wetwell airspace to the drywell. The decay heat eventually overcomes the subcooling in the GDCS water added to the vessel and boiloff resumes. The drywell pressure rises until flow is reestablished through the PCCS. This marks the beginning of the **Long-term PCCS cooling period**. During this period, the noncondensable gas that entered the drywell through the vacuum breakers is returned to the wetwell. Condensate from the PCCS is recycled back into the vessel through the PCCS drain tank in the drywell.

The most important part of the ECCS/LOCA transient for vessel response is the blowdown period and the early part of the GDCS period when the vessel is reflooded and inventory restored. For some breaks (e.g. bottom drain line break), the equalization line from the suppression pool to the reactor vessel may open during the long-term cooling period (after more than 24 hours) to provide the vessel an additional source of makeup water if the water level in the downcomer falls to 1m above the elevation of the top of active fuel.

### 2.2.1.1 GDCS Line Break

The GDCS line break scenario is a double-ended guillotine break of a GDCS drain line. There are three GDCS pools in the ESBWR containment, supplying four divisions of GDCS to the vessel. Each drain divides into two branches before entering into the pressure vessel. Each branch has a check valve followed by a squib operated injection valve and finally a nozzle in the vessel wall to control the blowdown flow in case of a break. The check valve prevents backflow from the vessel to the pool. The GDCS break is assumed to occur in one branch, between the squib-operated valve and the nozzle entering the vessel. Additional assumptions for the LOCA

analysis include a simultaneous loss of auxiliary power and no credit for the on-site diesel generators. The only AC power assumed available is that from battery powered inverters.

- **Blowdown Period** — At break initiation, the assumed simultaneous loss of power trips the generator, causing the turbine bypass valves to open and the reactor to scram. The bypass valves close after 6 seconds. No credit is taken for this scram or the heat sink provided by the bypass. The power loss also causes a feedwater coastdown. Drywell cooling is lost and the control rod drive (CRD) pumps trip. The blowdown flow quickly increases the drywell pressure to the scram setpoint.

High drywell pressure isolates several other functions, including the Containment Atmosphere Control System (CACCS) purge and vent, Fuel and Auxiliary Pool Cooling System (FAPCS), high and low conductivity sumps, fission product sampling, and reactor building Heating, Ventilating and Air Conditioning (HVAC) exhaust.

Loss of feedwater and flow out the break cause the measured water level in the downcomer to drop past the Level 3 (L3) scram setpoint. The “measured” or “sensed” downcomer level corresponds to the static head in the downcomer above the lower instrument tap used for the wide range level instrument. This setpoint will scram the reactor if it has not already scrambled on high drywell pressure. The scram will temporarily increase the rate of measured downcomer level drop and the Level 2 (L2) trip will quickly follow the L3 trip. This trip will isolate the steamlines and open the isolation condenser (IC) drain valves, but no credit is taken in the safety analysis for heat removal by the IC. After L2, the rate of decrease in the downcomer sensed level will slow and, without external makeup, the Level 1 (L1) trip will be reached, but not for several minutes. During this delay, the IC, if available, would be removing energy and reducing pressure and break flow. After a 10-second delay to confirm the L1 condition, the Automatic Depressurization System (ADS) logic will start a timed sequential opening of depressurization and injection valves. Four SRVs (one on each steamline) open first. The remaining eight SRVs open in two stages to stagger SRV line clearing loads in the suppression pool and minimize downcomer level swell. Similarly, opening of the depressurization valves (DPVs) is delayed 45 seconds. Two DPVs on the main steamlines open first, followed by two stages of two additional DPVs. The remaining two DPVs open after an additional delay. Blowdown through the break and the SRVs and DPVs causes a level swell in the downcomer and chimney, which collapses at the end of the blowdown period, with the GDCS injection. Ten seconds after the last DPV opens, the GDCS injection valves are opened. When the GDCS injection valves first open, the hydrostatic head from the pool plus the wetwell pressure (GDCS pools are located in the wetwell) is not sufficient to open the check valves and GDCS flow does not begin immediately. When the GDCS check valves do open, the cold GDCS water further depressurizes the vessel.

**GDCS Period** — The GDCS flow begins refilling the vessel and the downcomer two-phase level rises. When the two-phase level reaches the break, the GDCS flow spills back into the drywell. For the GDCS break, the flow of GDCS water is sufficient to raise the downcomer two-phase level above the break, until the pools empty, then the level drains back to the break elevation. Inside the core shroud, the two-phase level in the chimney also decreases after

depressurization, but is restored after the GDCS refills the vessel. Figure 2.2-3 shows the expected chimney and downcomer two-phase levels during the first 2000 s of the transient. The two-phase level swell during the initial blowdown and opening of the SRVs and DPVs is not visible in the figure (note the level drop and then rise during the GDCS period as the vessel is refilled).

For the GDCS break, the reactor core does not uncover, so there is no cladding heatup above the initial operating temperature. In evaluating the “importance” of various phenomena in the PIRT process, the phenomena associated with cladding heatup (e.g., radiation heat transfer, metal-water reaction) are unimportant, while phenomena associated with the two-phase level inside the core shroud (e.g., decay heat, energy release from heat slabs) are comparatively important.

The LOCA scenario develops slowly for the ESBWR. The accident detection system logic functions almost instantaneously, but thereafter, the time scales are measured in hours rather than seconds. The chimney two-phase level (Figure 2.2-3) dips briefly about 10 minutes into the LOCA due to void collapse following GDCS injection. For the GDCS line break, the minimum chimney level ( $> 1$  m above the top of the core) occurs at about 10 to 12 hours after the break. At this point in time, the core void fraction is very small, and the chimney and downcomer levels are almost the same. This slow response, which is due to the large volume of water in the reactor vessel and GDCS pools, makes the LOCA a very slow moving event from the reactor systems and operator response standpoint.

For the ECCS/LOCA transient response, the primary interaction with the containment is in the determination of the GDCS initiation time. The wetwell pressure will also decrease as the GDCS pools drain, thus slowing down the rate of injection slightly. The minimum two-phase level in the chimney occurs shortly after the GDCS starts to inject. Subsequently, there is no effect of the containment boundary conditions on the ECCS/LOCA transient.

### 2.2.1.2 Main Steamline Break

In this subsection, the important features of the transient resulting from a large break in the main steamline are described. The emphasis is on those features that are different from the GDCS line break scenario.

- **Blowdown Period** — At break initiation, the blowdown flow quickly increases the drywell pressure to the scram setpoint, and a control rod scram occurs. The high velocities in the steamline initiate closure of the Main Steamline Isolation Valves (MSIVs) and the reactor isolates in 3 - 5 seconds. This trip also opens the Isolation Condenser (IC) drain valves, but no credit is taken in the safety analysis for heat removal by the IC. High drywell pressure isolates several other systems, including the Containment Atmosphere Control System (CACs) purge and vent, Fuel and Auxiliary Pool Cooling System (FAPCS), high and low conductivity sumps, fission product sampling, and reactor building Heating, Ventilating and Air Conditioning (HVAC) exhaust.

Loss of feedwater and flow from the break cause the vessel water level to drop. Without external makeup, the Level 1 (L1) trip will be reached in about 6 minutes. During this period,

the IC, if available, would be removing energy and reducing pressure and break flow. After a 10-second delay to confirm the L1 condition, the Automatic Depressurization System (ADS) logic starts a timed sequential opening of depressurization and injection valves. The SRVs open in several stages to stagger SRV line clearing loads in the suppression pool and to minimize vessel level swell. The sequence of opening of the DPVs and the GDCS injection valves is similar to that for the GDCS line break described earlier. However, because of the large steam break, the vessel depressurizes faster and GDCS injection begins earlier than for the GDCS line break. Blowdown through the break, the SRVs, and the DPVs causes a level swell in the vessel. The two-phase level in the downcomer decreases at the end of the blowdown period, when GDCS injection begins.

- ***GDCS Period*** — The GDCS flow begins refilling the vessel and the downcomer two-phase level rises. When the two-phase level reaches the elevation of the open DPVs, the GDCS flow spills back into the drywell. Inside the core shroud, the two-phase level in the chimney also decreases after depressurization, but is restored after the GDCS refills the vessel. The minimum two-phase level in the chimney is of the order of 3 m above the top of the core; there is substantial margin to core heatup.

### 2.2.1.3 Small Breaks

The thermal hydraulic phenomena that characterize the small breaks in the ESBWR are very similar to those for the large steamline break. This is because once the downcomer level drops below the Level 1 set point, the reactor is automatically depressurized through the SRVs and DPVs. For small breaks (depending on the size and location), it may take several minutes before the reactor is scrammed on low water level (Level 3), and still longer before the ADS is actuated. For a steamline break having an area equivalent to 2% of the main steamline cross-sectional area, the measured downcomer water level will boil off to reach Level 1 in about one hour. During this period, the break flow exceeds the condensing capacity of the PCCS and results in clearing the top row of horizontal vents. This results in energy addition to the portion of the suppression pool above the top vents, and increases the pool surface temperatures. The ESBWR incorporates an ADS trip on high suppression pool surface temperature in conjunction with a high drywell pressure to mitigate this effect.

### 2.2.1.4 Non-Design Basis LOCAs

The discussion to this point has focused on LOCA scenarios with design basis assumptions. The consequences of relaxing these assumptions towards a “best estimate scenario” and considering the availability of non-safety systems are examined in this subsection.

#### ***Single Failures:***

In the ESBWR, the active component failures considered are the failure of a valve in the GDCS line to open and the failure of a DPV to open. Scenarios without failures have been analyzed. With no failures, design margins are increased. No new thermal-hydraulic phenomena or interactions are introduced because the differences relate simply to the number of GDCS lines available (quantity of GDCS flow) or the number of DPVs available for depressurization (amount of steam blowdown flow and rate of depressurization). Tests with

both types of single failure and ones without any failure were included in the LOCA simulations performed in the GIST facility.

***Isolation Condenser Operation:***

For LOCA analysis, the IC is not treated as an engineered safety feature and no credit is taken in the safety analysis for its operation. The valve in the condensate return line will open in a realistic scenario. This increases the vessel liquid inventory before ADS and reduces the steam load on the containment. LOCA scenarios with the IC operational have been included in the consideration of important phenomena in Sections 2.1.1 through 2.1.3. These phenomena include the IC condensation efficiency, steam quenching in the reactor vessel downcomer, and interactions between the IC steam flow and the steam flow through the DPVs on the same nozzle.

***Diesel Generators Available:***

Additional non-safety systems become available when the diesel generators start up (Table 2.2-1). Only the Control Rod Drive System in its high-pressure injection mode is initiated automatically. This system injects water through the feedwater line into the downcomer. The Fuel and Auxiliary Pool Cooling System (FAPCS) will also be available to the operator with the diesels operational. FAPCS isolates automatically on high drywell pressure. The operator can override the isolation manually. The FAPCS has several modes of operation. It can be aligned to function initially in the Low Pressure Coolant Injection (LPCI) mode. When core cooling is established, the FAPCS can serve as a Suppression Pool cooling system. Interactions between the FAPCS and the passive safety systems (GDCCS/PCCS) are uniformly beneficial and increase LOCA margins [29].

***Offsite Power Available:***

Table 2.2-2 shows that the primary additional water makeup systems available with offsite power are the condensate and feedwater systems. Numerous auxiliary systems such as fuel pool cooling, drywell coolers, and drywell sump drain pumps would also be available. With feedwater and offsite power available, the accident becomes a relatively mild event. After scram on high drywell pressure, the feedwater maintains normal downcomer water level for an extended period of time even for large breaks. This allows the operator to initiate a controlled depressurization of the reactor. The water spilling out of the reactor collects in the lower drywell. For large breaks, the sump drain pumps will not be able to keep up with the break discharge. Eventually, water spills into the wetwell through the spillover holes in the pipes connected to the horizontal vents. The feedwater will be throttled back or turned off as the water level rises in the wetwell.

## **2.2.2 Composite List of Identified Phenomena and Interactions**

The composite list of highly ranked phenomena and interactions for ECCS/LOCA primarily considers single failure scenarios and those with the Isolation Condenser available. Multiple failures have been excluded. A more detailed explanation of what the phenomena are and the basis for the judgment on their relative importance is provided in the ESBWR TAPD and Supplement 1 of the TAPD report [29].

Table 2.2-3 is a list of highly ranked phenomena for ECCS/ LOCA. A relatively large number of phenomena in this table are “generic”; that is, common for all BWRs.

While the base LOCA scenario does not claim credit for the Isolation Condenser, the Isolation Condenser can be expected to operate and have a beneficial effect on the transient by retaining vessel inventory during the blowdown phase. Because each Isolation Condenser unit consists of two modules coming off a single riser, and as many as four units could be in operation, interactions between modules and units are possible (XL1). The interaction between the system depressurization rate and GDCS affects GDCS timing and the minimum liquid inventory during the transient. This interaction has been designated XL3. It is a subset of Interaction XL4, which is the integral system response of the reactor vessel and containment during the late blowdown period, assuming the Isolation Condensers are available.

**Table 2.2-1. LOCA Scenario with Diesel Generators Available -  
Additional Systems Functional**

<b>Symptom</b>	<b>Action(s)</b>
Loss of normal AC	Diesel Generator starts
	FMCRD run-in backs up hydraulic scram
Low water level L2	CRD initiates in high pressure injection mode
Above actions are automatic, no operator action necessary. Actions below require operator intervention.	
Low water level L3	FAPCS LPCI mode, injection through FW system
High pool temperature	FAPCS Pool cooling mode, if adequate core cooling. Operator action required to over-ride system isolation.
Low water level < L1 per EPG	External water source
Containment pressure high or T dw > Technical Specifications LCO	DW Cooler
GDCS Pool level < NWL - 0.5m (2 of 3 pools)	Trip CRD pumps

**Table 2.2-2. LOCA Scenario with Offsite Power & Diesel Generators Available**

<b>Symptom</b>	<b>Action(s)</b>
Low water level L3	FW and condensate injection
Pressure > normal setpoint	Turbine bypass valves

**Table 2.2-3. Composite List of Highly Ranked Phenomena for ECCS/LOCA**

--

**Table 2.2-3 Composite List of Highly Ranked Phenomena for ECCS/LOCA (Continued)**

---

--

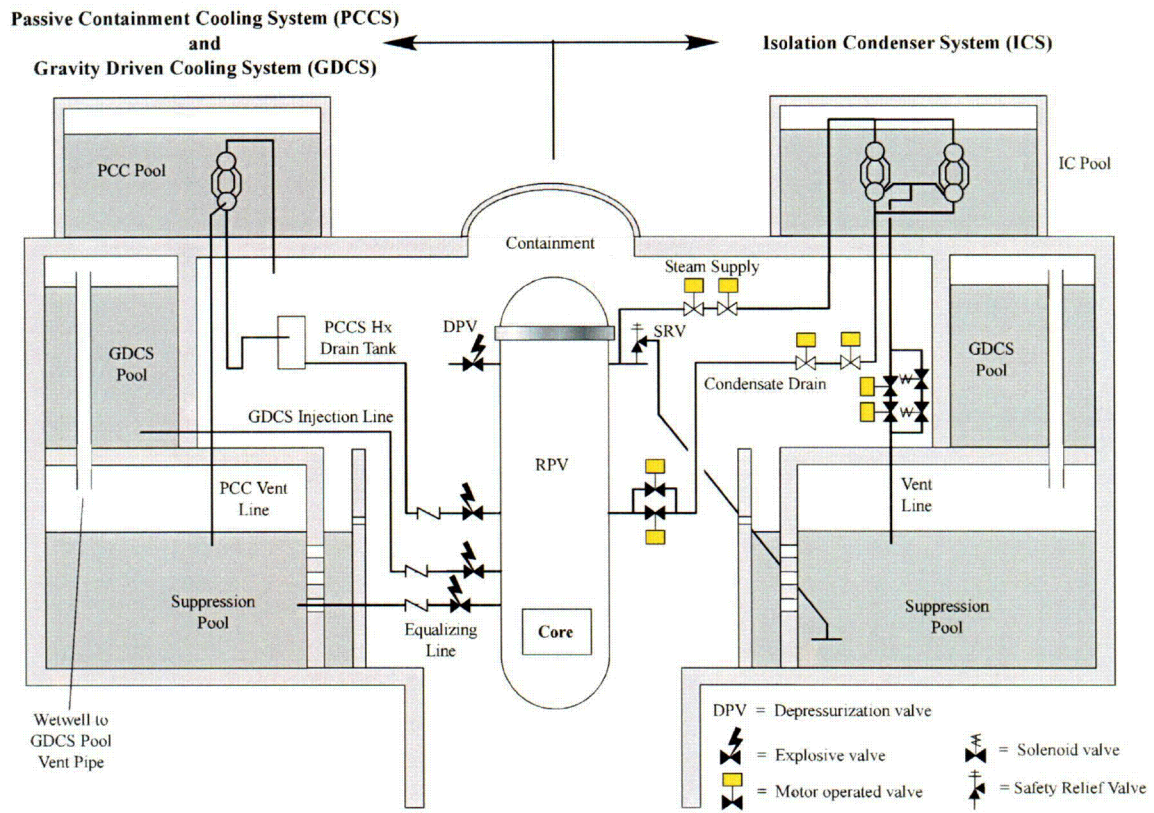
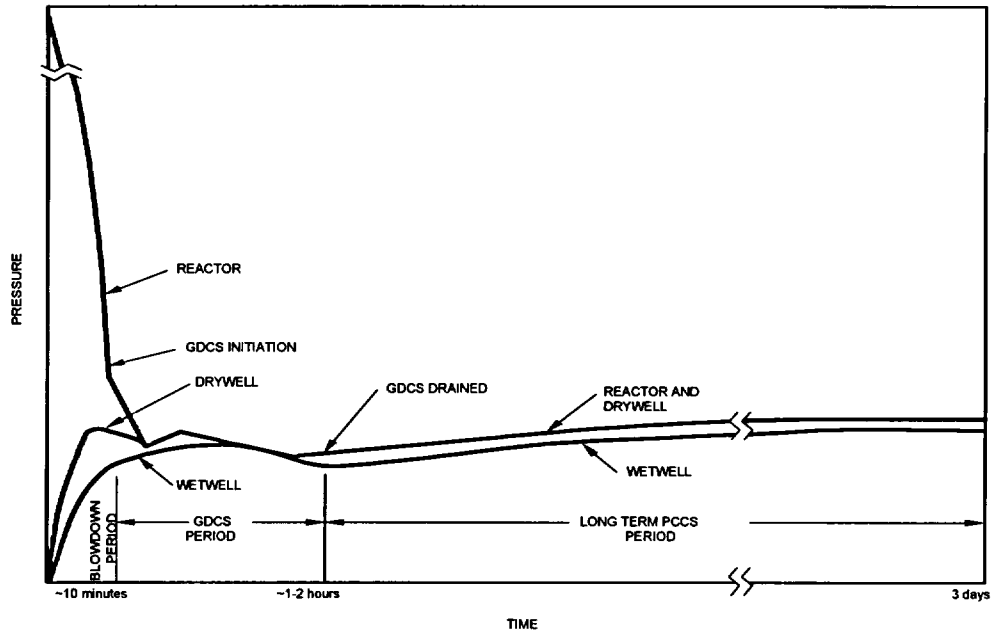


Figure 2.2-1 ESBWR Passive Safety Features

C-27



**Figure 2.2-2 Phases of the LOCA Transient**

**Figure 2.2-3. GDCS Line Break - Chimney and Downcomer Two-Phase Levels vs. Time**

## **2.3 Applicability of TRACG to ESBWR ECCS/ LOCA**

The objective of this section is to demonstrate the applicability of TRACG for the analysis of LOCAs in ESBWR. To accomplish this purpose, the capability of the TRACG models to treat the highly ranked phenomena and the qualification assessment of the TRACG code for ECCS/ LOCA applications is examined in the next two subsections.

### **2.3.1 Model Capability**

The capability to calculate an event for a nuclear power plant depends on four elements:

- Conservation equations, which provide the code capability to address global processes.
- Correlations and models, which provide code capability to model and scale particular processes.
- Numerics, which provide code capability to perform efficient and reliable calculations.
- Structure and nodalization, which address code capability to model plant geometry and perform efficient and accurate plant calculations.

Consequently, these four elements must be considered when evaluating the applicability of the code to the event of interest for the nuclear power plant calculation. The key phenomena for each event are identified in generating the PIRTs for ECCS/LOCA application, as indicated in Section 2.2. The capability of the code to simulate these key phenomena is specifically addressed, documented, and supported by qualification in References 2 and 24.

Important BWR phenomena have been identified and TRACG models have been developed to address these phenomena as indicated in Table 2.3-1. For each model, the relevant elements from the Model Description LTR [1] are identified. The Interactions listed in Table 2.2-3 have not been included in Table 2.3-1 because the calculation of system interactions does not involve any new models beyond those needed for the individual phenomena. Table 2.3-1 shows that TRACG has models for all the highly ranked phenomena for ECCS/LOCA.

### **2.3.2 Model Assessment Matrix**

For each of the governing BWR phenomena, TRACG qualification has been performed against a wide range of data. In this section, the qualification basis is related to the phenomena that are important for ECCS/LOCA. This is a necessary step to confirm that the code has been adequately qualified for the intended application.

The list of highly ranked phenomena for ECCS/LOCA is cross-referenced to the qualification basis. Data from separate effects tests (Table 2.3-2), component tests (Table 2.3-3), integral system tests (Table 2.3-4) and plant data (Table 2.3-5) have been used to qualify the capability of

TRACG to model the phenomena. The tables show that highly ranked phenomena for ESBWR ECCS/LOCA are well covered by TRACG assessment.

**Table 2.3-1**  
**HIGH RANKED ESBWR ECCS/LOCA PHENOMENA AND TRACG MODEL**  
**CAPABILITY MATRIX**



**Table 2.3-1 High Ranked ESBWR ECCS/LOCA Phenomena and TRACG Model Capability Matrix (Continued)**



**Table 2.3-2**

**Separate Effects Tests for Highly Ranked Phenomena for TRACG Qualification for ESBWR – ECCS/LOCA**

**Table 2. 3-2 (continued)**  
**Separate Effects Tests for Highly Ranked Phenomena for TRACG Qualification for ESBWR – ECCS/LOCA**

**Table 2.3-3**  
**Component Tests for Highly Ranked Phenomena for**  
**TRACG Qualification for ESBWR – ECCS/LOCA**



**Table 2.3-3 (cont'd)**  
**Component Tests for Highly Ranked Phenomena for**  
**TRACG Qualification for ESBWR – ECCS/LOCA**

**Table 2.3-4**  
**Integral System Tests for Highly Ranked Phenomena for TRACG Qualification for ESBWR**  
**– ECCS/LOCA**



**Table 2.3-4 (cont'd)**  
**Integral System Tests for Highly Ranked Phenomena for**  
**TRACG Qualification for ESBWR – ECCS/LOCA**



**Table 2.3-5**

**BWR Plant Data for Highly Ranked Phenomena for TRACG Qualification for ESBWR – ECCS/LOCA**

**Table 2.3-5 (cont'd)**  
**BWR Plant Data for Highly Ranked Phenomena for**  
**TRACG Qualification for ESBWR – ECCS/LOCA**

---

## 2.4 Model Uncertainties and Biases

Model biases and uncertainties for LOCA application of TRACG are assessed as described below for each of the high ranked phenomena identified in Section 2.2. The assessments are typically performed on the basis of comparisons between separate effects test data and TRACG calculations performed with the best-estimate version of the code. The biases and uncertainties indicated by the data comparisons are used to establish probability density functions (PDFs) for TRACG parameters and correlations. These are implemented into TRACG through special input parameters designated as “PIRT multipliers”. The correspondence between the PIRT multiplier inputs and the models they modify is shown in Table 2.4-3. Biases are compensated by appropriate choice of the mean value of the PIRT multiplier and uncertainties are accommodated by choosing PDFs to represent the standard deviation of the data comparisons. In general, no attempt is made to separate out the uncertainty in the data comparisons for the possible effect of measurement errors; i.e. measurement uncertainties are implicitly included in the standard deviation of the data comparisons. There are some parameters affecting the high ranked phenomena for which no applicable test data are available. For these cases, the PIRT model uncertainty is chosen on the basis of engineering judgment and comparisons with similar parameters for which data are available. In some instances, the parameter was found to have little impact on the figure of merit for the LOCA calculation (e.g., two-phase level inside the core shroud) and it was possible to use a conservative estimate of the uncertainty. The results of this evaluation are summarized in Table 2.4-1.

### 2.4.1 Model Parameters and Uncertainties

This section discusses the biases and uncertainties in the TRACG parameters and correlations that have a potential effect on each of the high-ranked phenomena listed in Table 2.2-3. As in Table 2.2-3, the presentation is organized by plant region, starting with the lower plenum and ending with the steamline. Under the heading of each phenomenon, the applicable TRACG parameters and correlations are identified, the sources of the test data and the statistical characteristics of the deviations between TRACG calculations and the test data are described and the choice of the PDF is explained. The results of the evaluation are summarized in Table 2.4-1. In addition, the sensitivity of the calculated mixture level inside the shroud is discussed in Section 2.4.4.2.

#### Lower Plenum





















**Table 2.4-1. Parameters Governing High Ranked PIRT Phenomena**

**Table 2.4-2. Summary of Scoping Break Spectrum Analysis – Minimum Static Head inside  
Chimney**

**Table 2.4-3. TRACG PIRT Parameters ranged for ECCS/LOCA Sensitivity Study**



**Figure 2.4-1 Void Fraction Deviations for Tests Applicable to Regions with Large Hydraulic Diameter**



**Figure 2.4-2. Sensitivity of TRACG Prediction of Average Void Fraction in EBWR Test Facility to PIRT Multiplier on Interfacial Drag Coefficient**

**Figure 2.4-3. Probability Distribution for Multiplier on Interfacial Drag Coefficient**



**Figure 2.4-4. Void Fraction Deviations for Toshiba Void Fraction Tests**

**Figure 2.4-5. Sensitivity of TRACG Prediction of Toshiba Void Fraction to PIRT Multiplier on  $(C_0-1)$**

**Figure 2.4-6. Sensitivity of TRACG Prediction of Toshiba Void Fraction PIRT Multiplier on Entrainment Coefficient,  $\eta$**

**Figure 2.4-7. Fractional Error in Modified Zuber Critical Heat Flux Correlation**

**Figure 2.4-8. Comparison of the Predicted and Measured Two-Phase Level Histories for Marviken Test 24**

**Figure 2.4-9. Comparison of the Predicted and Measured Two-Phase Level Histories for Marviken Test 15**

**Figure 2.4-10. Deviation in Level Change Versus the Hydraulic Diameter for Separate Effects and Integral Facilities**

**Figure 2.4-11. GDCS Line Break with GDCS Injection Valve Failure – Two-phase Level inside Chimney**

**Figure 2.4-12. GDCS Line Break with GDCS Injection Valve Failure – Collapsed Level (Static Head) inside Chimney**

**Figure 2.4-13. Chimney Static Head Sensitivity to Uncertainties in TRACG PIRT Parameters (See Table 2.4-3)**

**Figure 2.4-14. PCT Sensitivity to Uncertainties in TRACG PIRT Parameters (See Table 2.4-3)**

**Figure 2.4-15. Chimney Static Head Sensitivity to TRACG Simulation of DW  
Noncondensable Holdup**

## 2.5 Application Uncertainties and Biases

### 2.5.1 Input

Specific inputs for ECCS/LOCA calculations are specified via internal procedures, which are the primary means used by GE to control application of engineering computer programs. The specific code input will be developed in connection with the application LTR and the development of the application specific procedure. This section will be limited to a more general discussion of how input is treated with respect to quantifying the impact on the calculated results. As such, it serves as a basis for the development of the application specific procedures.

Code inputs can be divided into four broad categories: (1) geometry inputs; (2) model selection inputs; (3) initial condition inputs; and (4) plant parameters. For each type of input, it is necessary to specify the value for the input. If the calculated result is sensitive to the input value, then it is also necessary to quantify the uncertainty in the input.

The geometry inputs are used to specify lengths, areas and volumes. Uncertainties in these quantities are due to measurement uncertainties and manufacturing tolerances. These uncertainties usually have a much smaller impact on the results than do other uncertainties associated with the modeling simplifications. When this is not the case, the specific uncertainties can usually be quantified in a straightforward manner.

Individual geometric inputs are the building blocks from which the spatial nodalization is built. Another aspect of the spatial nodalization includes modeling simplifications such as the lumping together of individual elements into a single model component. For example, several similar fuel channels may be lumped together and simulated as one fuel channel group. An assessment of these kinds of simplifications, along with the sensitivities to spatial nodalization, is included in the *qualification reports* [2], [24].

Model selection inputs are used to select the features of the model that apply for the intended application. Once established, these inputs are fully specified in the procedure for the application and will not be changed.

A distinction has been made in this document between *initial conditions* and *plant parameters*. Obviously, when specified in absolute units, the initial rated conditions for a nuclear power plant are specific to the plant and thus have been considered as plant parameters in some documents. In this document, *initial conditions* are considered to be those key plant inputs that determine the overall steady-state nuclear and hydraulic conditions prior to the transient. These are inputs that are essential to determining that the steady-state condition of the plant has been established.

The name *plant parameter*, on the other hand, is reserved for such things as protection system setpoints, valve capacities that influence the characteristics of the transient response but which do not (when properly prescribed) have an impact on steady-state operation.

### **2.5.2 Plant Conditions Used for Base Line Calculations**

Based on prior experience, it is assumed for design basis ECCS/LOCA analyses that the preferred electric power is lost simultaneously with the initiation of LOCA. As a further conservatism, the ESBWR design analyses do not take credit for non-ECCS vessel inventory control systems including, specifically, the Feedwater System, the Isolation Condenser System and the Control Rod Drive system. The significant plant input variables used for the base line ECCS analyses are given in Table 2.5-1.

**Table 2.5-1. Significant Input Variables to the Loss-of-Coolant Accident Analysis**

**Table 2.5- 1. Significant Input Variables to the Loss-of-Coolant Accident Analysis  
(Continued)**

**Table 2.5-2. Plant Variables with Nominal And Sensitivity Study Values**

**Figure 2.5-1. Chimney Static Head Sensitivity to Plant Parameter Uncertainties**

## 2.6 Combination of Uncertainties

In order to determine the total uncertainty in predictions with a computer code, it is necessary to combine the uncertainties due to model uncertainties (CSAU Step 9), scaling uncertainties (CSAU step 10), and plant condition or state uncertainties (CSAU Step 11). Various methods have been used to combine the effects of uncertainties in safety analysis. All these approaches are within the framework of the CSAU methodology, since the CSAU methodology does not prescribe the approach to be used.

NRC Regulatory Guide 1.157 for use of best-estimate models for LOCA analysis defines acceptable model features and application procedures. The guide states that a one-sided upper statistical limit (OSUSL) can be calculated at the 95% probability level for the primary safety parameters. In addition, the statistical methodology should be provided and justified.

## **2.7 Results for ECCS/LOCA Analysis**

In this Section, TRACG results are presented for ECCS/LOCA analysis for the ESBWR. The results include:

1. Nominal TRACG analyses for the limiting break,
2. Bounding analysis in accordance with the process defined in Section 2.6.1.

### **2.7.1 Nominal ECCS/LOCA Analysis**

A baseline analysis was performed for the GDCS line break with a failure of one GDCS injection valve to open. This was determined to be the limiting LOCA in Section 2.4.4. The plant initial conditions are specified in Table 2.5-1.



**Figure 2.7-1. TRACG Nodalization of ESBWR RPV and containment for ECCS/LOCA Analysis**

**Figure 2.7-2. TRACG Nodalization of ESBWR Steam Line System**

**Figure 2.7-3. TRACG Nodalization of ESBWR IC, DPV and Feedwater Systems**

**Figure 2.7-4. RPV Pressure Response (Base Case)**

**Figure 2.7-5. RPV, Drywell and Wetwell Pressure Response (Base Case)**

**Figure 2.7-6. Two-Phase Levels in Downcomer and Inside Core Shroud (Base Case)**

**Figure 2.7-7. Two-Phase Level and Static Head In Chimney (Base Case)**



**Figure 2.7-8. RPV Pressure Response (Bounding Case)**

**Figure 2.7-9. RPV, Drywell and Wetwell Response (Bounding Case)**

**Figure 2.7-10. Two-Phase Levels in Downcomer and Inside Core Shroud (Bounding Case)**

**Figure 2.7-11. Two-Phase Level and Static Head In Chimney (Bounding Case)**

## **2.8 Summary of ECCS/LOCA Application Methodology**

This report has defined an application methodology that meets the licensing requirements for ECCS /LOCA analysis for the ESBWR.

The requirements to be met and the scope of application were identified in Sections 2.1. Phenomena important for ECCS/LOCA analysis for ESBWR were identified in Section 2.2. Section 2.3 justified the applicability of TRACG for ECCS/LOCA analysis. Model and plant parameters and their ranges were established in Sections 2.4 and 2.5. A bounding application approach was proposed in Section 2.6. Results with this bounding approach were presented for the limiting GDCS line break in Section 2.7 and shown to have large margin to core uncover.

Hence, conformance to design limits such as PCT and oxidation is assured.

### 3. CONTAINMENT/LOCA ANALYSIS

#### 3.1 Licensing Requirements and Scope of Application

The NRC Standard Review Plan, NUREG-0800 [19], presents the responsibilities and guidelines for the NRC's reviews of nuclear power plants. The sections of the Standard Review Plan (SRP) that are relevant to the TRACG analysis for the ESBWR are Section 6.2.1 covering the containment functional design. The specific elements of these sections of the SRP that are relevant to ESBWR applications of TRACG are presented in this section of this report. These guidelines, in general, require the use of methods that have been reviewed and approved by the NRC. The TRACG Model Description NEDE-32176P, TRACG Qualification NEDE-32177, TRACG Qualification for SBWR Volumes 1 and 2, NEDC-32725, and TRACG Qualification for ESBWR NEDC-33080 are incorporated by reference as part of the review scope.

##### 3.1.1 Licensing Acceptance Criteria for Containment/LOCA Performance

The NRC guidelines for review of Containment/LOCA safety analysis are identified in Section 6.2.1, *Containment Functional Design*, of the SRP [19]. Two statements from the introduction of this section relate directly to the TRACG analyses of the ESBWR Containment/LOCA response:

- “The containment structure must be capable of withstanding, without loss of function, the pressure and temperature conditions resulting from postulated loss-of-coolant, steam line or feedwater line break accidents.”
- “GDC (General Design Criteria) 50, among other things, requires that consideration be given to the limitations in defining accident phenomena, and the conservatism of calculational models and input parameters, in assessing containment design margins.”

Guidelines which are more specific to BWR pressure suppression containments are identified in SRP Section 6.2.1.1.C, *Pressure-Suppression Type BWR Containments*. Although this section of the SRP covers Mark I, II, and III pressure-suppression containments, it has been used as the basis for the review of the ABWR containment safety analysis by the NRC. The ESBWR containment design has evolved from the Mark III and ABWR containments. Therefore, these guidelines can be considered as the applicable basis for the review of the ESBWR containment analysis. The following statements from SRP Section 6.2.1.1.C are quoted directly in an attempt to summarize the NRC's review approach and requirements as they relate to ESBWR Containment/LOCA pressure and temperature response analysis using TRACG.

## I. AREAS OF REVIEW

“1. The temperature and pressure conditions in the drywell and wetwell due to a spectrum (including break size and location) of loss-of-coolant accidents.”

“5. The capability of the containment to withstand the effects of steam bypassing the suppression pool.”

“7. The effectiveness of static {ESBWR Passive Containment Cooling System} and active {not relevant to ESBWR} heat removal systems.”

“12. The evaluation of analytical models used for containment analysis.”

## II. ACCEPTANCE CRITERIA

CSB {Containment Systems Branch of NRC} accepts the containment design if the relevant requirements of General Design Criteria 4, 16, 38, 50, and 53 are complied with. The relevant requirements are as follows:

GDC 16 and 50, as they relate to the containment being designed with sufficient margin, require that the containment and its associated systems can accommodate, without exceeding the design leakage rate and with sufficient margin, the calculated pressure and temperature conditions resulting from any loss-of-coolant accident.

Specific criterion or criteria that pertain to design and functional capability of BWR pressure-suppression type containments are indicated below:

If an analytical model other than the General Electric Mark III analytical model is used, the model should be demonstrated to be physically appropriate and conservative to the extent that the General Electric model has been found acceptable. In addition, it will be necessary to demonstrate its performance with suitable test data in a manner similar to that described above.

For Mark III plants at the construction permit stage, containment design pressure should provide at least a 15% margin above the peak calculated containment pressure, and the design differential pressure between drywell and containment should provide at least a 30% margin above the peak calculated differential pressure.

GDC 38 requires that a Containment Heat Removal system to remove heat from the reactor containment shall be provided. The system safety function shall be to reduce rapidly, consistent with the functioning of other associated systems, the containment pressure and temperature following any LOCA and maintain them at acceptably low levels.

The other containment acceptance criteria are related to missile and pipe whip protection (GDC 4), periodic inspections (GDC 53), containment dynamic loads, allowable bypass leakage rates,

design leakage rate, containment negative pressures, external pressures, SRV in-plant tests, local suppression pool temperature limits during SRV discharges, and instrumentation for post-accident monitoring. These criteria are not relevant to this TRACG application method since they are addressed by other analytical methods and/or procedures.

### **3.1.2 Analysis Requirements**

The calculational framework used for evaluating the containment systems in terms of pressure and temperature behavior is called an evaluation model. It includes one or more computer programs, the mathematical models used, the assumptions and correlations included in the program, the procedure for selecting and treating the program input and output information, the specification of those portions of the analysis not included in computer programs, the values of parameters, and all other information necessary to specify the calculation procedure. The evaluation model must comply with the acceptance criteria for Containment/LOCA described in Section 3.1.1. The evaluation model must have been previously documented and reviewed and approved by the NRC staff.

### **3.1.3 Standard Review Plan (SRP) Guidelines (NUREG 800)**

The NRC guidelines for review of LOCA Containment safety analysis are identified in Section 6.2.1 of the SRP [19], covering the containment functional design.

### **3.1.4 Proposed Application Methodology**

### **3.1.5 Implementation Requirements**

The implementation of TRACG into actual licensing analysis is contingent on completion of the following implementation requirements:

- Review and approval by the NRC of:
  - The TRACG models used for containment analysis
  - The bounding process for analyzing containment/LOCA described in Section 3.6.
- Analysis for the ESBWR LOCA break spectrum that demonstrates compliance with the acceptance criteria (Section 3.7)

### **3.1.6 Review Requirements For Updates**

In order to effectively manage the future viability of TRACG for ESBWR Containment/LOCA licensing calculations, GE proposes the following requirements for upgrades to the code to define changes that (1) require NRC review and approval and (2) that will be on a notification basis only.

#### **3.1.6.1 Updates to TRACG Code**

Modifications to the basic models described in Reference 1 may not be made for containment/LOCA licensing calculations without NRC review and approval.

Changes in the numerical methods to improve code convergence may be used in containment/LOCA licensing calculations without NRC review and approval, as long as differences in the results are less than 5% in design margin.

Features that support effective code input/output may be added without NRC review and approval.

### **3.1.6.2 Updates to TRACG Application Method**

Revisions to the TRACG application method described in Section 3.6 may not be made for containment/LOCA licensing calculations without NRC review and approval.

### **3.1.7 Range of Application**

The intended application is containment/LOCA analysis as required by Chapter 6 of the SAR for ESBWR. This covers the entire spectrum of break sizes and locations. The break could be initiated anywhere in the operating domain for an ESBWR operating at or below the technical specification limits.

## 3.2 Phenomena Identification and Ranking

The critical safety parameters for containment/LOCA are the peak pressures and temperatures in the drywell and wetwell of the containment. These safety parameters are the criteria used to judge the performance of the safety systems and the margins in the design. The values of the critical safety parameters are determined by the governing physical phenomena. To delineate the important physical phenomena, it has become customary to develop Phenomena Identification and Ranking Tables (PIRTs). PIRTs are ranked with respect to their impact on the critical safety parameters. For example, the pressure inside the wetwell is determined by the blowdown flow, noncondensable transport from the drywell, suppression pool stratification, and PCCS heat removal.

All processes and phenomena that occur during a LOCA do not equally influence containment behavior. The most cost efficient, yet sufficient, analysis reduces all candidate phenomena to a manageable set by identifying and ranking the phenomena with respect to their influence on the critical safety parameters. The phases of the events and the important components are investigated. The processes and phenomena associated with each component are examined. Cause and effect are differentiated. After the processes and phenomena have been identified, they are ranked with respect to their effect on the critical safety parameters for the event. The identification of important phenomena for the ESBWR was done in two ways: (1) a Top-Down process based on analyses and sensitivity studies, and (2) a Bottom-Up process based on examination of individual design features [29].

Section 3.2.1 describes representative TRACG calculations that established the scenarios of various LOCA events. The descriptions stress the phenomenological evolution of the transients. The scenarios are then reviewed by interdisciplinary teams to identify each thermal-hydraulic phenomenon that plays a role in the analysis, and to rank all of them in terms of “importance”; that is, degree of influence on the figure of merit (e.g., wetwell pressure). Section 3.2.2 reports the results of the phenomena ranking from References 29 and 24.

### 3.2.1 LOCA Transient Response

Chapter 6 of the SSAR will include the entire matrix of calculations for postulated pipe rupture locations and single failures. For a complete PIRT evaluation, the entire spectrum of events must be covered, including analyses with less limiting conditions than the design-basis case with no auxiliary power. The approach followed in this study was to focus on the design basis cases, in terms of the equipment and systems available. This led to the most severe consequences and the greatest challenges to the analytical models in modeling the phenomena. To facilitate understanding, a large break in the Gravity-Driven Cooling System (GDCCS) line and a large break in a main steamline have been chosen to illustrate the sequence of events during the LOCA. The sequence of events is similar for all the LOCA events, particularly after initiation of the GDCCS flows, when the vessel and containment transients are coupled. While there are some differences in the assumptions made for analysis of the different breaks, these are not very important in determining the phenomenological progression of the LOCA or the importance of

various parameters. The limiting LOCA from the perspective of margin to core uncover is a large liquid line (GDCS line) break; from the viewpoint of containment pressure, it is likely to be the large steamline break.

The overall LOCA sequence can be divided into three periods: blowdown period, GDCS period and the long-term cooling PCCS period. These periods are shown in Figure 2.2-2. The ***Blowdown period*** is characterized by a rapid depressurization of the vessel through the break, safety relief valves (SRVs) and depressurization valves (DPVs). The steam blowdown from the break and DPVs pressurizes the drywell, clearing the main containment vents and the PCCS vents. First, noncondensable gas and then steam flows through the vents and into the suppression pool. The steam is condensed in the pool and the noncondensable gas collects in the wetwell air space above the pool. At about 500 s, the pressure difference between the vessel and the wetwell is small enough to enable flow from the GDCS pools to enter the vessel. This marks the beginning of the ***GDCS period***, during which the GDCS pools drain their inventory. Depending on the break, the pools are drained in between 1 and 6 hours. The GDCS flow fills the vessel to the elevation of the break, after which the excess GDCS flow spills over into the drywell. The GDCS period is characterized by condensation of steam in the vessel and drywell, depressurization of the vessel and drywell and possible openings of the vacuum breakers, which returns noncondensable gas from the wetwell airspace to the drywell. The decay heat eventually overcomes the subcooling in the GDCS water added to the vessel and boiloff resumes. The drywell pressure rises until flow is reestablished through the PCCS. This marks the beginning of the ***Long-term PCCS cooling period***. During this period, the noncondensable gas that entered the drywell through the vacuum breakers is returned to the wetwell. Condensate from the PCCS is recycled back into the vessel through the PCCS drain tank in the drywell.

The most important part of the LOCA transient for the vessel response is the blowdown period and the early part of the GDCS period when the vessel is reflooded and inventory restored. For some breaks (e.g. bottom drain line break), the equalization line from the suppression pool to the reactor vessel may open during the long-term cooling period to provide the vessel an additional source of makeup water if the water level in the downcomer falls to 1m above the elevation of the top of active fuel. For the containment, the blowdown phase determines the initial pressurization. During the GDCS phase the pressure levels off and decreases as the GDCS first shuts off steaming from the vessel and later spills over into the drywell, condensing steam in the drywell. At the end of the GDCS phase, noncondensibles that returned to the drywell because of vacuum breaker openings are returned to the wetwell gas space, and the PCCS assumes the decay heat load.

### **3.2.1.1 Containment Response for the GDCS Line Break**

Containment response calculations assume loss of all AC power except that available from battery powered inverters, reactor power at 102% of rated power and no credit for IC operation. The single failure used is the failure to open a squib valve in one of the GDCS pool drain lines. Initial conditions are containment normal operating pressure and temperature, with the suppression pool at its maximum allowable operating temperature.

- **Blowdown Period** — The blowdown for the GDCS line break occurs from the vessel side of the broken line. The break flow is initially a liquid blowdown, and after the downcomer two-phase level falls below the GDCS line elevation, the break becomes a vapor blowdown. The ADS, activated by the measured downcomer level, opens the SRVs and the DPVs. The flashing liquid (and later, steam) entering the drywell increases its pressure, opening the main containment vents and the PCCS vents. Most of the drywell noncondensable gas is swept through the main vents, the suppression pool and into the wetwell airspace. The steam flow through the vents is condensed in the suppression pool. During the blowdown phase of the transient, the majority of the blowdown energy is transferred into the suppression pool through the main vents. Within the pool, temperature stratification occurs, with the blowdown energy being absorbed primarily in the region above the open vents. The increase in drywell pressure also establishes flow through the PCCS, which absorbs part of the blowdown energy. After the DPVs have opened, the GDCS squib valves open about 150 s following the L1 signal. This causes the pool side of the broken line to drain the inventory of the one affected GDCS pool into the containment. The check valve keeps the vessel from blowing down through the unbroken branch of the GDCS line. For the GDCS break, this period of the accident lasts less than 10 minutes. The peak containment pressure in the short term is primarily set by the compression of the noncondensibles initially in the drywell into the wetwell vapor space. The controlling parameters are the ratio of the drywell to wetwell vapor volumes, and the temperature at the top of the suppression pool, which sets the steam partial pressure.
- **GDCS Period** — Once the vessel pressure drops below the pressure on the GDCS pool side of the check valves in the unbroken GDCS lines, the GDCS pools begin to empty their inventory into the vessel. The subcooled GDCS water quenches the core voids, stopping the steam flow from the vessel. The GDCS flow refills the vessel to the elevation of the break and then spills over into the drywell. Spillover from the break into the drywell begins at about 20 minutes into the accident and continues throughout the GDCS period of the accident. Once the GDCS flow begins, the drywell pressure peaks and begins to decrease. The decrease in drywell pressure stops the steam flow through the PCCS and main vents. The drop in drywell pressure is sufficient to open the vacuum breakers between the drywell and the wetwell airspace several times. As the GDCS pools empty, the effective wetwell gas space volume increases because the GDCS pools are connected to the wetwell gas space. The containment pressure is thereby reduced. Once the GDCS flow begins to spill from the vessel into the drywell, the drywell pressure drops further and additional vacuum breaker openings occur. Some of the noncondensable gas in the wetwell airspace is returned to the drywell through the vacuum breakers. The GDCS period of the transient continues until the GDCS pools empty and the decay heat is able to overcome the subcooling of the GDCS inventory in the vessel. Then, the drywell pressure rises and flow is re-established through the PCCS. The PCCS heat removal capacity, even while recycling noncondensable gas back to the wetwell, is sufficient to handle the steam generated by decay heat and the main vents are not reopened. Any uncondensed steam condenses and deposits its latent heat in the

portion of the suppression pool above the outlet of the PCCS vent. This period of the accident is expected to last approximately 1 to 2 hours for the GDCS line break.

- **Long-Term PCCS Period** — After the drywell pressure transient initiated by the GDCS flow is over, the drywell pressure settles out, slightly above the wetwell airspace pressure. A drywell-to-wetwell pressure difference is established which is sufficient to open the PCCS vent and drive the steam generated by decay heat through the PCCS. By between 6 to 8 hours, the PCCS heat removal increases to nearly equal the decay heat power. During this final period of the transient, drywell pressure may rise slowly. This results from a slow increase in the wetwell airspace pressure, due to the assumed leakage flow between the drywell and wetwell airspace. Without the leakage, the containment pressure remains nearly constant or decreases slightly during the long-term period of the transient.

The LOCA scenario develops slowly for the ESBWR. The accident detection system logic functions almost instantaneously, but thereafter, the time scales are measured in hours rather than seconds. Containment response is gradual, with substantial margin to the design pressure even 72 hours after the break. This slow response permits well-considered, deliberate operator actions.

### 3.2.1.2 Main Steamline Break

In this subsection, the important features of the transient resulting from a large break in the main steamline are described. The emphasis is on those features that are different from the GDCS line break scenario.

- **Blowdown Period** — At break initiation, the blowdown flow quickly increases the drywell pressure to the scram setpoint, and a control rod scram occurs. The high velocities in the steamline initiate closure of the Main Steamline Isolation Valves (MSIVs) and the reactor isolates in 3 - 5 s. This trip also opens the Isolation Condenser (IC) drain valves, but no credit is taken in the safety analysis for heat removal by the IC. High drywell pressure isolates several other systems, including the Containment Atmosphere Control System (CACs) purge and vent, Fuel and Auxiliary Pool Cooling System (FAPCS), high and low conductivity sumps, fission product sampling, and reactor building Heating, Ventilating and Air Conditioning (HVAC) exhaust.

Loss of feedwater and flow from the break cause the vessel water level to drop. Without external makeup, the Level 1 (L1) trip will be reached in about 6 minutes. During this period, the IC, if available, would be removing energy and reducing pressure and break flow. After a 10-second delay to confirm the L1 condition, the Automatic Depressurization System (ADS) logic starts a timed sequential opening of depressurization and injection valves. The SRVs open in several stages to stagger SRV line clearing loads in the suppression pool and to minimize vessel level swell. The sequence of opening of the DPVs and the GDCS injection valves is similar to that for the GDCS line break described earlier. However, because of the large steam break, the vessel depressurizes faster and GDCS injection begins earlier than for

the GDCS line break. Blowdown through the break, the SRVs, and the DPVs causes a level swell in the vessel. The two-phase level in the downcomer decreases at the end of the blowdown period, when GDCS injection begins.

In the containment, the steam entering the drywell increases its pressure, opening the main containment vents and sweeping most of the drywell noncondensable gas through the main vents, through the suppression pool, and into the wetwell airspace. (Depending on the location of the break, a substantial portion of the noncondensibles in the lower drywell region may remain in that region and bleed out slowly later in the transient). During the blowdown phase of the transient, the majority of the blowdown energy is transferred into the suppression pool by condensation of the steam flowing through the main vents. The increase in drywell pressure causes flow through the PCCS, which also absorbs part of the blowdown energy. The ADS, activated by the measured downcomer level, opens the SRVs and the DPVs and augments the steam flow to the suppression pool and drywell, respectively. This period of the accident lasts less than 10 minutes.

- ***GDCS Period*** — The GDCS flow begins refilling the vessel and the downcomer two-phase level rises. When the two-phase level reaches the elevation of the open DPVs, the GDCS flow spills back into the drywell. Inside the core shroud, the two-phase level in the chimney also decreases after depressurization, but is restored after the GDCS refills the vessel. The minimum two-phase level in the chimney is of the order of 3 m above the top of the core; there is substantial margin to core heatup.

Quenching of voids in the core by the GDCS flow reduces the steam outflow from the vessel to the drywell. Once the GDCS flow begins, the drywell pressure peaks and begins to decrease. Figure 3.2-1 shows the RPV, drywell and wetwell pressure response for the first 12 hours of the accident. The decrease in drywell pressure stops the steam flow through the PCCS and main vents. This pressure decrease may be sufficient to open the vacuum breakers between the drywell and the wetwell airspace. Draining of the GDCS pools helps to reduce the containment pressure as more wetwell volume becomes available for the noncondensibles in the wetwell gas space. Once GDCS flow begins to spill from the vessel into the drywell, the drywell pressure drops further and additional vacuum breakers may open. If the vacuum breakers open, some of the noncondensable gas in the wetwell airspace will return to the drywell through the vacuum breakers. The GDCS period of the transient continues until the water level in the GDCS pools equalizes with the collapsed level in the downcomer of the reactor pressure vessel and the decay heat is able to overcome the subcooling of the GDCS inventory in the vessel. Then, the drywell pressure rises and flow is re-established through the PCCS. The PCCS heat removal capacity, even while recycling noncondensable gas back to the wetwell, is sufficient to transfer the steam generated by decay heat without reopening the main vents. This period of the accident is expected to last for less than one hour. Figure 3.2-2 shows the PCCS heat removal during the first 12 hours of the transient. Also shown is the decay heat.

- **Long-Term PCCS Period** — After the drywell pressure transient initiated by the GDCS flow is over, the drywell pressure settles out, slightly above the wetwell airspace pressure. The Main Steamline break is the limiting break in terms of containment pressure and temperature, as most of the noncondensibles are swept out from the drywell into the wetwell in the initial blowdown phase. This part of the containment transient is similar to that for the GDCS line break. However, unlike the GDCS line break, the steam generated by the decay heat is condensed and all of it is returned to the vessel via the PCCS Drainage Tank. Thus, there is no long-term drop in the downcomer and chimney water level due to boiloff. A larger amount of water inventory is retained inside the vessel and a smaller amount in the lower drywell.

### 3.2.1.3 Small Breaks

The thermal hydraulic phenomena that characterize the small breaks in the ESBWR are very similar to those for the large steamline break. This is because once the downcomer level drops below the Level 1 set point, the reactor is automatically depressurized through the SRVs and DPVs. For small breaks (depending on the size and location), it may take several minutes before the reactor is scrammed on low water level (Level 3), and still longer before the ADS is actuated. For a steamline break having an area equivalent to 2% of the main steamline cross-sectional area, the measured downcomer water level will boil off to reach Level 1 in about one hour. During this period, the break flow exceeds the condensing capacity of the PCCS and results in clearing the top row of horizontal vents. This results in energy addition to the portion of the suppression pool above the top vents, and increases the pool surface temperatures. The ESBWR incorporates an ADS trip on high pool surface temperature in conjunction with high drywell pressure to mitigate this effect.

### 3.2.2 Composite List of Highly Ranked Phenomena and Interactions

Table 3.2-1 shows the Phenomena Identification and Ranking Table (PIRT) that was developed for ESBWR Containment/LOCA analysis.

The short-term drywell pressure response is governed by energy deposition by break flow and DPV discharge flow (DPV1 in Table 3.2-1). Energy removal from the drywell is through main vent (MV1) and PCCS flow (PC1), and condensation on walls and internal structures. The pressure difference required for clearing of the main vents controls the initial pressure increase in the drywell. Energy deposition in the wetwell is through the main vent flow (WW1), and flow through the SRV quenchers (WW2) and PCC vent lines (WW3). Thermal stratification of the suppression pool (WW6) is a key factor in determining how this energy is distributed within the pool; it sets the pool surface temperature and, therefore, the temperature and steam partial pressure in the wetwell gas space.

Another key parameter controlling the short-term wetwell pressure is the extent to which the noncondensibles (nitrogen) initially in the drywell are purged to the wetwell in the initial blowdown (DW3). The design of the containment must also account for the hydrodynamic loads due to pool swell, SRV line air clearing, condensation oscillations and chugging (TRACG is not

used in the design process for this purpose. Empirical models are employed, which are based on extensive test data).

The long-term containment response is controlled primarily by the heat removal by the PCCS (PC2 and PC3). The ability of the PCCS to purge noncondensibles and its performance in the presence of noncondensibles are key issues (PC2 and PC5). The rates of drywell and wetwell energy addition and removal become progressively smaller in the long-term transient. The energy deposition in the wetwell is due to the PCC vent flow and any steam leakage from the drywell that bypasses the PCCS (DWB1).

Energy removal from the wetwell is through heat transfer in the gas space (at the pool interface and walls) and condensation on the wetwell walls (WW4 and WW5). The PCCS performance may be affected by the noncondensable distributions in the drywell (DW3). Overcooling of the drywell by the PCCS or by cold water spillover from the RPV can result in the drywell pressure falling below the wetwell pressure. Cold water could be added by flow from a broken GDCS line or spillover from the break after the GDCS fills the RPV to the break elevation (DW4). This will cause the vacuum breakers to open, bringing noncondensibles back to the drywell (VB1). The interaction between the RPV and the containment (RPV2) has been included in Table 3.2-1.

**Table 3.2-1. Highly Ranked PIRT Phenomena for ESBWR Containment/ LOCA**

<b>Governing Phenomena for Containment/LOCA</b>					
		<b>Containment / LOCA (Focus: Containment Pressure)</b>			
		<b>Phase</b>	<b>Blowdown</b>	<b>GDCS</b>	<b>Long Term</b>
	<b>Phenomena</b>	<b>Basic Phenomena</b>	<b>Rank (H=High, M=Medium)</b>		
<b>BR</b>	<b>Region: break (focus: energy addition to drywell)</b>				
BR1	Mass Flow	Critical Flow	H		
		Friction	H		
		Entrainment	H		
<b>MV</b>	<b>Region: main vent (focus: energy addition to suppression pool)</b>				
MV1	Mass flow	Void fraction/entrainment	H		
		Friction	H		
MV3	Vent clearing time		H		
<b>SQ</b>	<b>Region: SRV quenchers (focus: energy addition to suppression pool)</b>				
SQ1	Mass Flow	Void fraction entrainment	H		
		Critical flow	H		
		Friction	H		
<b>DW</b>	<b>Region: drywell (focus: pressure, temperature, noncondensable distribution)</b>				
DW1	Flashing/evaporation	Interfacial heat transfer	H		
DW2	Heat sources/sinks	Condensation	H		
		Degradation of condensation	H		
DW3	3-D effects	Phase separation	H		
		Noncondensable stratification	H	H	H
		Buoyancy/natural circulation			H
DW4	Condensation on reactor outflows	Condensation		H	

Table 3.2-1 (Contd.)

Highly Ranked PIRT Phenomena for ESBWR Containment/ LOCA

Governing Phenomena for Containment/LOCA					
		Containment/ LOCA (Focus: Containment Pressure)			
		Phase	Blowdown	GDCS	Long Term
	Phenomena	Basic Phenomena	Rank (H=High, M=Medium)		
<b>WW</b>	<b>Region: wetwell (focus: pressure, pool and gas temperature)</b>				
WW1	Condensation/evaporation of main vent discharge	Interfacial heat transfer	H		
		Degradation by non-condensibles	H		
WW2	Condensation/evaporation of SRV discharge	Interfacial heat transfer	H		
WW3	Condensation/evaporation of PCC vent discharge	Interfacial heat transfer	H		H
		Degradation by non-condensibles			H
WW4	Free surface condensation/evaporation	Interfacial heat transfer			H
		Degradation by non-condensibles			H
WW5	Heat sources/sinks	Condensation	H		H
WW6	Pool mixing and stratification	Stratification/thermal plumes	H		H
WW7	3-D effects in gas space	Mixing, entrainment into jets	H		H
		Buoyancy/natural circulation			H
		Stratification of noncondensibles			H
<b>PC</b>	<b>Region: PCCS (focus: energy removal)</b>				
PC1	Mass flow into PCC	Friction			H
PC2	Condensation on primary side	Interfacial heat transfer		H	H
		Degradation by N/C		H	H
		Shear enhancement		H	H
PC3	Secondary side heat transfer	Natural circulation			H
PC5	Parallel PCC unit effects	Friction			H
		Void fraction			H

Table 3.2-1 (Contd.)

Highly Ranked PIRT Phenomena for ESBWR Containment/ LOCA

Governing Phenomena for Containment/LOCA					
			Containment/ LOCA (Focus: Containment Pressure)		
		Phase	Blowdown	GDCS	Long Term
	Phenomena	Basic Phenomena	Rank (H=High, M=Medium)		
PC8	Purging of noncondensibles			H	H
<b>DWB</b>	<b>Region: DW/WW Boundary</b>				
DWB1	Leakage	Friction			H
<b>VB</b>	<b>Region: vacuum breakers (focus: noncondensible distribution)</b>				
VB1	Mass flow	Friction			H
<b>EQ</b>	<b>Region: equalizing line</b>				
EQ1	Equalizing line mass flow	Friction			H
<b>RPV</b>	<b>Region: reactor pressure vessel (focus: steam flow/energy addition to drywell)</b>				
RPV2	RPV steam generation		H		
<b>DPV</b>	<b>Region: depressurization valves (focus: energy addition to drywell)</b>				
DPV1	Mass flow	Critical flow	H		
<b>XC</b>	<b>Interaction</b>				
XC2	Potential system interaction: IC/PCC units, GDCS etc.			H	H
XC6	Light noncondensibles DW/PCCS/WW				H
XC7	Early containment response (DW, WW, MV)		H		
XC8	Interaction PCC/MV		H	H	H

DW, WW & VESSEL PRESSURES

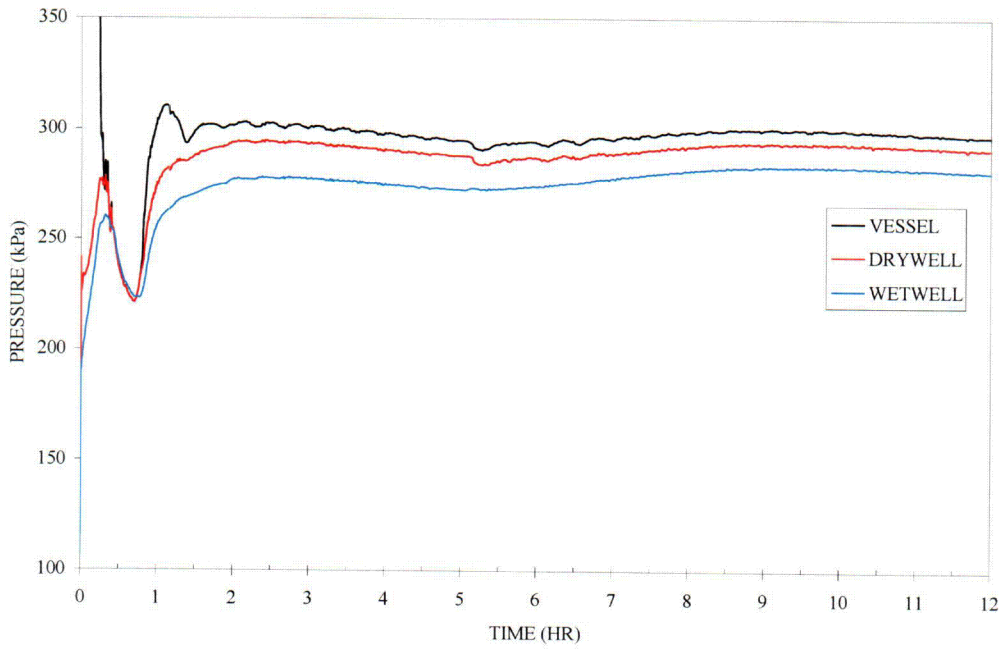
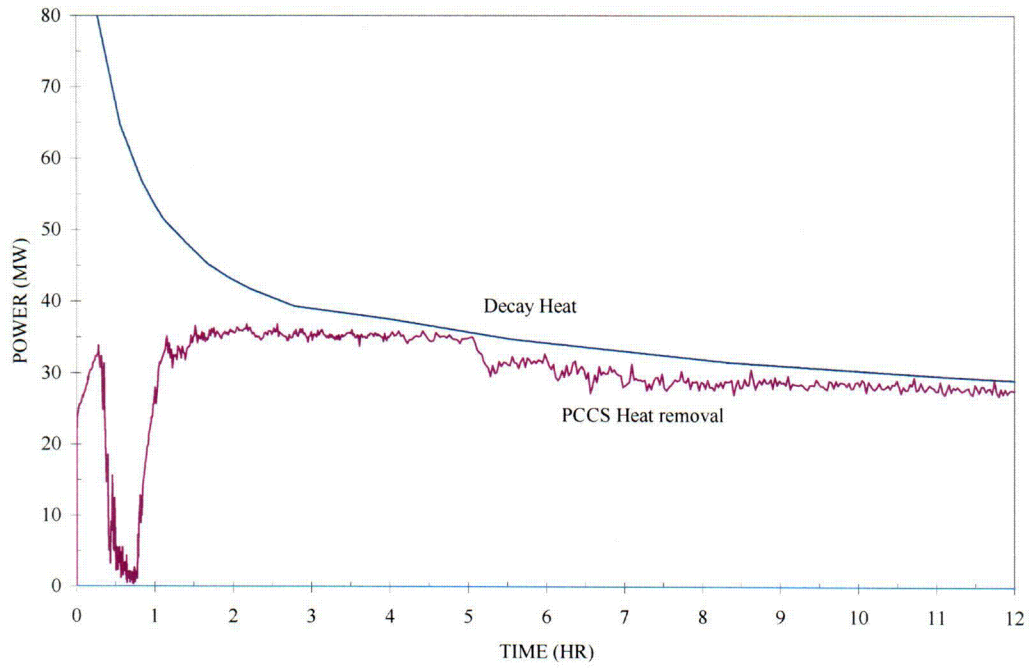


Figure 3.2-1 : Main Steam Line Break Vessel and Containment Pressures (Typical)



**Figure 3.2-2 Main Steam Line Break Decay Heat and PCCS Heat Removal (Typical)**

### **3.3 Applicability of TRACG to Containment/LOCA**

The objective of this section is to demonstrate the applicability of TRACG for the analysis of LOCAs in ESBWR. To accomplish this purpose, the capability of the TRACG models to treat the highly ranked phenomena and the qualification assessment of the TRACG code for containment/ LOCA applications is examined in the next two subsections.

#### **3.3.1 Model Capability**

The capability to calculate an event for a nuclear power plant depends on four elements:

- Conservation equations, which provide the code capability to address global processes.
- Correlations and models, which provide code capability to model and scale particular processes.
- Numerics, which provide code capability to perform efficient and reliable calculations.
- Structure and nodalization, which address code capability to model plant geometry and perform efficient and accurate plant calculations.

Consequently, these four elements must be considered when evaluating the applicability of the code to the event of interest for the nuclear power plant calculation. The key phenomena for each event are identified in generating the PIRTs for containment/LOCA application, as indicated in Section 3.2.2. The capability of the code to simulate these key phenomena is specifically addressed, documented, and supported by qualification in References 2 and 24.

Important BWR containment phenomena have been identified and TRACG models have been developed to address these phenomena as indicated in Table 3.3-1. For each model, the relevant elements from the Model Description LTR [1] are identified. The Interactions listed in Table 3.2-1 have not been included in Table 3.3-1 because the calculation of system interactions does not involve any new models beyond those needed for the individual phenomena. Table 3.3-1 shows that TRACG has models for most highly ranked phenomena for containment/LOCA. The remaining phenomena are treated in a bounding way in the TRACG models as detailed below.

##### **3.3.1.1 Phenomena Treated with a Bounding Approach**





|

|



### **3.3.2 Model Assessment Matrix**

For each of the governing BWR phenomena, TRACG qualification has been performed against a wide range of data. In this section, the qualification basis is correlated to the phenomena that are important for containment/LOCA. This is a necessary step to confirm that the code has been adequately qualified for the intended application.

The list of highly ranked phenomena for containment/LOCA is cross-referenced to the qualification basis. Data from separate effects tests (Table 3.3-2), component tests (Table 3.3-3), and integral system tests (Table 3.3-4) have been used to qualify the capability of TRACG to model the phenomena. The tables show that TRACG has been adequately qualified for the calculation of ESBWR containment phenomena.

**Table 3.3-1**  
**HIGH RANKED ESBWR CONTAINMENT/LOCA PHENOMENA AND TRACG**  
**MODEL CAPABILITY MATRIX**







**Table 3.3-2 Separate Effects Tests for Highly Ranked Phenomena  
for TRACG Qualification for ESBWR – Containment (continued)**

**Table 3.3-3**  
**Component Tests of Highly Ranked Phenomena for**  
**TRACG Qualification for ESBWR - Containment**

**Table 3.3-3 Component Tests of Highly Ranked Phenomena for  
TRACG Qualification for ESBWR - Containment (Continued)**

**Table 3.3-4**  
**Integral System Tests for Highly Ranked Phenomena for**  
**TRACG Qualification for ESBWR - Containment**

**Table 3.3-4 Integral System Tests for Highly Ranked Phenomena for  
TRACG Qualifications for ESBWR - Containment (Continued)**

**Table 3.3-5. Effect of Break Discharge Location on the Containment Pressure**

	<b>Location of the Break Discharge into the DW</b>	<b>Peak Drywell Pressure (psia)</b>
Baseline Case *	Middle of Level 10 **	47.7
Sensitivity Study Case 1	Top of Level 8	44.6
Sensitivity Study Case 2	Top of Level 6	44.6
Sensitivity Study Case 3	Top of Level 1	44.0

\* Baseline case described in Section 3.7.2

\*\* See Figure 3.7-1, TRACG nodalization for ESBWR containment analysis.

**Figure 3.3-1. Wetwell Gas Space and Pool Showing TRACG Nodalization**

**Figure 3.3-2. Suppression Pool Temperatures With and Without Forced Stratification (SBWR)**

**Figure 3.3-3. Wetwell Gas Space Temperatures Without Forced Stratification (SBWR)**

**Figure 3.3-4 -Wetwell Gas Space Temps – Restricted Mixing between Top Layer and Lower Layer (SBWR)**

### 3.4 Model Uncertainties and Biases

Model biases and uncertainties for containment application of TRACG are assessed as described below for the key high ranked phenomena identified in Section 3.2. The assessments are typically performed on the basis of comparisons between separate effects test data and TRACG calculations performed with the best-estimate version of the code. The biases and uncertainties indicated by the data comparisons are used to establish ranges for TRACG parameters and correlations. These ranges are implemented through special inputs designated as “PIRT multipliers”. Correspondence between these input parameters and the phenomena that they affect is shown in Table 3.4-1. Biases are compensated by appropriate choice of the mean value of the PIRT multiplier and uncertainties are accommodated by choosing probability density functions (PDFs) to represent the standard deviation of the data comparisons. In general, no attempt is made to separate out the uncertainty in the data comparisons for the possible effect of measurement errors; i.e. measurement uncertainties are implicitly included in the standard deviation of the data comparisons. There are some parameters affecting the high ranked phenomena for which no applicable test data are available. For these cases, the PIRT uncertainty is chosen on the basis of engineering judgment and comparisons with similar parameters for which data are available. In some instances, the parameter was found to have little impact on the figure of merit for the containment calculation (e.g., containment pressure) and it was possible to use a conservative estimate of the uncertainty. For several key parameters bounding models are used as described in Section 3.3.1.1. The results of this evaluation are summarized in Table 3.4-1.















**Table 3.4-1. Uncertainties in Highly Ranked PIRT Parameters for Containment/LOCA**

NEDO-33083-A



**Figure 3.4-1 Comparison of PANDA Test M3 Wetwell Airspace Temperature with TRACG Predictions for WW1 Pressure.**

## 3.5 Plant Parameters and Ranges for Application

### 3.5.1 Input

Specific inputs for containment/LOCA calculations are specified via internal procedures, which are the primary means used by GE to control application of engineering computer programs. The specific code input will be developed in connection with the application LTR and the development of the application specific procedure. This section will be limited to a more general discussion of how input is treated with respect to quantifying the impact on the calculated results. As such, it serves as a basis for the development of the application specific procedures.

Code inputs can be divided into four broad categories: (1) geometry inputs; (2) model selection inputs; (3) initial condition inputs; and (4) plant parameters. For each type of input, it is necessary to specify the value for the input. If the calculated result is sensitive to the input value, then it is also necessary to quantify the uncertainty in the input.

The geometry inputs are used to specify lengths, areas and volumes. Uncertainties in these quantities are due to measurement uncertainties and manufacturing tolerances. These uncertainties usually have a much smaller impact on the results than do other uncertainties associated with the modeling simplifications. When this is not the case, the specific uncertainties can usually be quantified in a straightforward manner.

Individual geometric inputs are the building blocks from which the spatial nodalization is built. Another aspect of the spatial nodalization includes modeling simplifications such as the lumping together of individual elements into a single model component. For example, several similar main vent pipes may be lumped together and simulated as one pipe. An assessment of these kinds of simplifications, along with the sensitivities to spatial nodalization, is included in the *qualification reports* [2], [24].

Model selection inputs are used to select the features of the model that apply for the intended application. Once established, these inputs are fully specified in the procedure for the application and will not be changed.

A distinction has been made in this document between *initial conditions* and *plant parameters*. Obviously, when specified in absolute units, the initial rated conditions for a nuclear power plant are specific to the plant and thus have been considered as plant parameters in some documents. In this document, *initial conditions* are considered to be those key plant inputs that determine the overall steady-state nuclear and hydraulic conditions prior to the transient. These are inputs that are essential to determining that the steady-state condition of the plant has been established.

The name *plant parameter*, on the other hand, is reserved for such things as protection system setpoints and valve capacities that influence the characteristics of the transient response but which do not (when properly prescribed) have an impact on steady-state operation. No plant parameters are important for this study.

### **3.5.2 Plant Initial Conditions Used for Base Line Calculations**

The plant operating conditions represent initial conditions for the TRACG calculations and affect the long-term containment response. Initial conditions have an important effect on the calculated response of the containment. The range of allowable initial conditions is governed by plant operating guidelines and, for containment response calculations, it is assumed that the plant will be operated within these guidelines. In a typical calculation, initial conditions in the containment are assumed to be at steady-state, and at limiting pressures and temperatures. The RPV is assumed to be operating at maximum power and, for a given feedwater flow and temperature, the RPV steam flow, the initial temperatures and pressures and vessel internal flows are selected to obtain steady state conditions. Initial RPV power is set at 100% of rated power for the baseline calculation. Experience with similar BWR containment systems have shown that rated power produces the most limiting containment response. The only exception is a break from hot standby, which is typically included in a containment response evaluation. For this accident, it is assumed that the plant was at full power operation, is scrammed and isolated and the suppression pool is heated by SRV operation to the maximum pool temperature limit before the break occurs. This break can, for some plants, be limiting because of the high initial pool temperature. Because of the availability of the IC system following reactor isolation for the ESBWR, this break is not a concern. This is because the RPV can be depressurized without added heat load to the suppression pool.

The initial plant conditions that affect the containment response are summarized in Table 3.5-1. Some plant conditions were varied for the bounding calculation while others were maintained at nominal conditions. The basis for selection of the plant conditions to vary is discussed below.

#### **3.5.2.1 Plant Initial Conditions Not Varied**

Plant conditions that provided bounding initial conditions for the containment/LOCA analysis or conditions that would not be expected to change with normal plant operation were not varied. They included:

**3.5.2.2 Plant Conditions ranged to a Bounding Value for Sensitivity Studies**

**Table 3.5-1****Plant Initial Conditions Considered in the Containment Sensitivity Study**

<b>No.</b>	<b>Plant Parameter</b>	<b>Nominal Value</b>	<b>Bounding Value</b>
1	RPV Power	100%	102%
2	WW relative humidity	100%	100%
3	PCC pool level	4.8m	4.8m
4	PCC pool temperature	110F (316.5K)	110F (316.5K)
5	DW Pressure	14.7 psia (101.3kPa)	16.0 psia (110.3kPa)
6	DW Temperature	115F (319.3K)	115F (319.3K)
7	WW Pressure	14.7 psia (101.3kPa)	16.0 psia (110.3kPa)
8	WW Temperature	110F (316.5K)	110F (316.5K)
9	Suppression pool Temp.	110F (316.5K)	110F (316.5K)
10	GDCS pool temperature	110F (316.5K)	110F (316.5K)
11	Suppression pool level	5.45m	5.50m
12	GDCS pool level	6.70m	6.75m
13	DW relative humidity	20%	20%
14	RPV pressure	1040 psia (7.17 MPa)	1055 psia (7.274 MPa)
15	RPV Water Level	NWL	NWL+0.3m

### **3.6 Application Procedure for Containment Analysis**

### **3.7 Results for ESBWR Main Steamline Break LOCA**

The main steamline break causes the fastest pressurization of the ESBWR drywell in the short term. It results in minimum drain-down of the GDCS pools because of the elevation of the break, and hence a smaller wetwell gas space volume in the long term. The steamline break discharging at the top of the drywell also results in a slower clearing out of the noncondensibles in the lower drywell, resulting a degraded PCCS for a longer time. All these factors lead to the highest containment pressure for the main steamline break.

#### **3.7.1 TRACG Nodalization for Containment Analysis**

**Figure 3.7-1. TRACG Nodalization for ESBWR Containment Analysis**

### 3.7.2 Baseline Results for Containment Analysis

The RPV and containment were initialized at the base conditions shown in the Nominal Value column of Table 3.5-1. Four PCCs are available with a total rated capacity of 54 MW. A crud thickness is assumed on the tube walls corresponding to a design basis fouling factor of  $0.000045 \text{ m}^2\text{-K/W}$  or an equivalent additional inconel wall thickness of 0.65 mm (Section 3.4.1). No credit is assumed for the ICs. A leakage path was assumed between the drywell and wetwell with an equivalent area of  $1 \text{ cm}^2$ .

Apart from the conservative modeling assumptions common to all TRACG containment analysis (suppression pool stratification, wetwell gas space stratification and a break location at the top of the drywell), the other models were set at the mean values of the ranges shown in Table 3.4-1.

|



**Figure 3.7-2. Containment Pressure Response (Base Case)**

**Figure 3.7-3. Drywell Noncondensable Partial Pressures (Base Case)**

**Figure 3.7-4. 3 PCC Pool Level (Base Case)**

**Figure 3.7-5. GDCS Pool Level (Base Case)**

**Figure 3.7-6. PCCS Heat Removal vs. Decay Heat (Base Case)**

**Figure 3.7-7. Suppression Pool Temperatures (Base Case)**

**Figure 3.7-8. Wetwell Gas Space temperature Response (Base Case)**

**Figure 3.7-9. Drywell Temperature Response (Base Case)**

### **3.7.3 Bounding Results for Containment Analysis**

**Table 3.7-1. Model Parameters for Bounding Case**

**Figure 3.7-10. Containment Pressure Response (Bounding Case)**

**Figure 3.7-11. PCCS Heat Removal vs. Decay Heat (Bounding Case)**

**Figure 3.7-12. Suppression Pool Temperatures (Bounding Case)**

**Figure 3.7-13. Drywell Pressure Response vs. Design Limit**

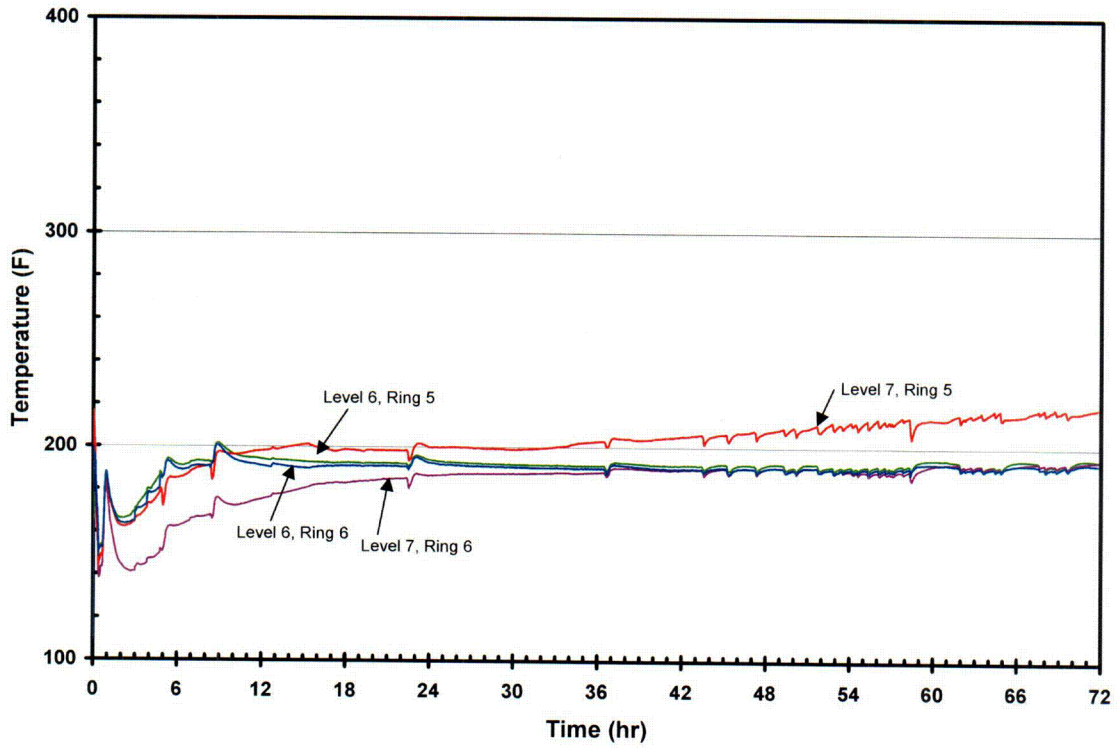


Figure 3.7-14. Wetwell Gas Space Temperature Response (Bounding Case)

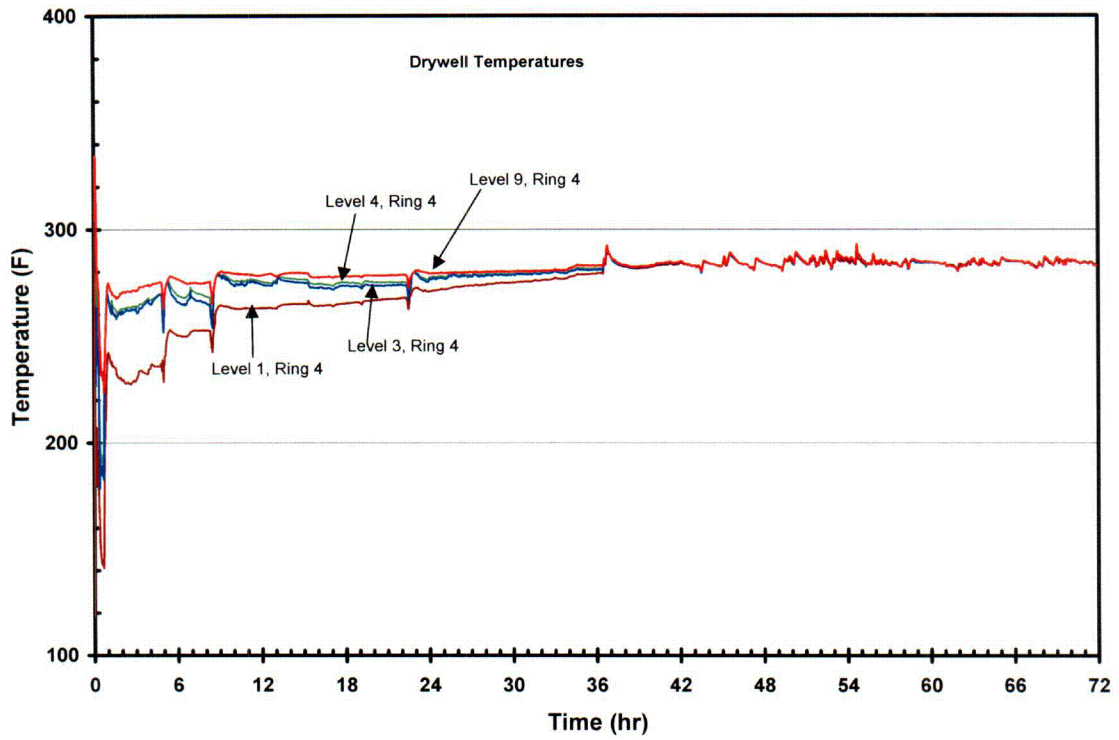


Figure 3.7-15. Drywell Temperature Response (Bounding Case)

### **3.8 Summary of Containment/LOCA Application Methodology**

This report has defined an application methodology that meets the licensing requirements for containment /LOCA analysis for the ESBWR.

The requirements to be met and the scope of application were identified in Sections 3.1. Phenomena important for containment/LOCA analysis for ESBWR were identified in Section 3.2. Section 3.3 justified the applicability of TRACG for containment/LOCA analysis. Model and plant parameters and their ranges were established in Sections 3.4 and 3.5. A bounding application approach was proposed in Section 3.6. Results with this bounding approach were presented for the limiting main steamline break in Section 3.7 and shown to have adequate margin to the design limit.

## 4. TRANSIENT ANALYSIS

### 4.1 Licensing Requirements and Scope of Application

#### 4.1.1 10CFR50 Appendix A

The *General Design Criteria for Nuclear Power Plants* are stipulated in Appendix A to Part 50 of 10CFR. Anticipated Operational Occurrences are classified as transient events of moderate frequency. The Standard Review Plan for events in this classification states that the “acceptance criteria are based on meeting the requirements of the following regulations” and then defines the acceptance criteria “as it relates” to the general design criteria (GDC). NRC approval of licensing methods used for AOO analysis implies that the methods are capable of assessing an AOO transient response “as it relates” to the GDC.

#### 4.1.2 Standard Review Plan Guidelines (NUREG 800)

The NRC guidelines for review of anticipated operation occurrences (AOOs) are identified in Section 15 of the Standard Review Plan (SRP) [19].

The AOO scenarios (incidents of moderate frequency) applicable to ESBWR that can be analyzed using TRACG are listed with the corresponding SRP section.

Section	Event
15.1.1 - 15.1.4	Decrease in feedwater temperature, increase in feedwater flow, increase in steam flow, and inadvertent opening of a steam generator relief or safety valve.
15.2.1 - 15.2.5	Loss of external load; turbine trip; loss of condenser vacuum; closure of main steam isolation valve (BWR); and steam pressure regulator failure (closed).
15.2.6	Loss of non-emergency AC power to the station auxiliaries.
15.2.7	Loss of normal feedwater flow.

In addition to the events given above, there are others such as the rod withdrawal errors (Section 15.4.1.3) and fuel misloading errors (Section 15.4.7) that are analyzed with the steady-state three-dimensional core simulator PANACEA [78]. Control rod drop accidents (Section 15.4.9) are currently considered incredible events for the Fine Motion Control Rod Drives (FMCRDs) and are dispositioned generically. GE has used TRACG to perform realistic calculations for control rod drop accidents but this application is not included in the scope of the current submittal.

### **4.1.3 Proposed Application Methodology**

The methodology for this application of TRACG to ESBWR is identical to that approved by the NRC for BWR/2-6 AOOs [3].

#### **4.1.3.1 Conformance with CSAU Methodology**

The application methodology using TRACG for ESBWR AOO transient analyses addresses all the elements of the NRC-developed CSAU evaluation methodology [15]. The CSAU report describes a rigorous process for evaluating the total model and plant parameter uncertainty for a nuclear power plant calculation. The rigorous process for applying realistic codes and quantifying the overall model and plant parameter uncertainties appears to represent the best available practice.

The CSAU methodology as documented in Reference 15 consists of 14 steps, as outlined in Table 4.1-1, which also shows where these steps are addressed for the current TRACG application.

**Table 4.1-1  
CODE SCALING, APPLICABILITY AND UNCERTAINTY EVALUATION METHODOLOGY**

<b>CSAU Step</b>	<b>Description</b>	<b>Addressed In</b>
1	Scenario Specification	Section 4.1.6
2	Nuclear Power Plant Selection	Section 4.1.7
3	Phenomena Identification and Ranking	Section 4.2
4	Frozen Code Version Selection	Reference [1]
5	Code Documentation	Reference [1]
6	Determination of Code Applicability	Section 4.3
7	Establishment of Assessment Matrix	Section 4.3.2
8	Nuclear Power Plant Nodalization Definition	Section 4.4.2
9	Definition of Code and Experimental Accuracy	Reference [2],[24],[25]
10	Determination of Effect of Scale	Section 4.4.3
11	Determination of the Effect of Reactor Input Parameters and State	Section 4.5
12	Performance of Nuclear Power Plant Sensitivity Calculations	Section 4.6
13	Determination of Combined Bias and Uncertainty	Section 4.6
14	Determination of Total Uncertainty	Section 4.6

**4.1.4 Implementation Requirements**

The implementation of TRACG into actual licensing analysis is contingent on completion of the following implementation requirements:

- Review and approval by the NRC of:
  - The modeling uncertainties documented in Section 4.4.
  - The statistical process for analyzing AOOs described in Section 4.6.
- ESBWR implementation using best-estimate modeling to consider sensitivities due to initial condition and plant parameters described in Sections 4.5.2 and 4.5.3.

Specific operating limits derived or comparison with acceptance criterion (peak pressure, water level, and fuel thermal/mechanical) will be based on application of the statistical application processes described in Section 4.6.

#### **4.1.5 Review Requirements For Updates**

In order to effectively manage the future viability of TRACG for AOO licensing calculations, GE proposes the following requirements for upgrades to the code to define changes that (1) require NRC review and approval and (2) that will be on a notification basis only.

##### **4.1.5.1 Updates to TRACG Code**

Modifications to the basic models described in Reference 1 may not be used for AOO licensing calculations without NRC review and approval.

Updates to the TRACG nuclear methods to ensure compatibility with the NRC-approved steady-state nuclear methods (e.g., PANAC11) may be used for AOO licensing calculations without NRC review and approval as long as the  $\Delta$ CPR/ICPR, peak vessel pressure, and minimum water level shows less than 1 sigma deviation difference compared to the method presented in this LTR. A typical AOO in each of the event scenarios will be compared and the results from the comparison will be transmitted for information.

Changes in the numerical methods to improve code convergence may be used in AOO licensing calculations without NRC review and approval.

Features that support effective code input/output may be added without NRC review and approval.

##### **4.1.5.2 Updates to TRACG Model Uncertainties**

New data may become available with which the specific model uncertainties described in Section 4.4 may be reassessed. If the reassessment results in a need to change specific model uncertainty, the specific model uncertainty may be revised for AOO licensing calculations without NRC review and approval as long as the process for determining the uncertainty is unchanged.

The nuclear uncertainties (void coefficient, Doppler coefficient, and scram coefficient) may be revised without review and approval as long as the process for determining the uncertainty is unchanged. In all cases, changes made to model uncertainties done without review and approval will be transmitted for information.

##### **4.1.5.3 Updates to TRACG Statistical Method**

Revisions to the TRACG statistical method described in Section 4.6 may not be used for AOO licensing calculations without NRC review and approval.

##### **4.1.5.4 Updates to Event Specific Uncertainties**

Event specific  $\Delta$ CPR/ICPR, peak pressure, and water level biases and uncertainties will be developed for AOO licensing applications based on a reference fuel type. These biases and

uncertainties do not require NRC review and approval. The generic uncertainties will be transmitted to the NRC for information.

#### **4.1.6 AOO Scenario Specification**

The transient scenarios are those associated with anticipated operational occurrences (AOOs) in ESBWR. The following AOO transient events groups are specifically included:

1. Pressurization events, including: turbine trip without bypass, load rejection without bypass, feedwater controller failure increasing flow, downscale failure of pressure regulator, main steam line isolation valve closure without position scram. This grouping includes all events in SRP Section 15.2.1 - 15.2.5 that apply to BWRs. The feedwater controller failure increasing flow is in Section 15.1.1 - 15.1.4 but can also be considered a pressurization transient. The loss of auxiliary power is in SRP Section 15.2.6.
2. Depressurization events, including: upscale failure of pressure regulator. The upscale failure of pressure regulator is in SRP Section 15.1.1 - 15.1.4.
3. Cold water events, including: loss of feedwater heating. The loss of feedwater heating (decrease in feedwater temperature) is in SRP Section 15.1.1 - 15.1.4. This grouping includes all events in SRP Section 15.5.1 - 15.5.2 that apply to BWRs.
4. Level transient events such as partial or complete loss of feedwater. This grouping includes all events in SRP Section 15.2.7 that apply to BWRs.

#### **4.1.7 Nuclear Power Plant Selection**

The intended application in this report is for the ESBWR plant.

## 4.2 Phenomena Identification and Ranking

The critical safety parameters for AOO transients are minimum critical power ratio (MCPR), fuel thermal-mechanical margins, downcomer water level and peak reactor pressure vessel (RPV) pressure. These are the criteria used to judge the performance of the safety systems and the margins in the design. The values of the critical safety parameters are determined by the governing physical phenomena. To delineate the important physical phenomena, it has become customary to develop phenomena identification and ranking tables (PIRTs). PIRTs are ranked with respect to their impact on the critical safety parameters. For example, the MCPR is determined by the reactor short-term response to transients. The coupled core neutronic and thermal-hydraulic characteristics govern the neutron flux, reactor pressure, core flow and downcomer water level transients.

Section 4.2.1 describes representative scenarios for ESBWR AOOs. The descriptions stress the phenomenological evolution of the transients. The scenarios provide a background for the listing and ranking of phenomena that go into the PIRT. Section 4.2.2 reports the results of the phenomena ranking from Reference 29.

### 4.2.1 ESBWR AOO Classes

The PIRTs for anticipated transients were synthesized from consideration of the phenomena involved in various classes of events.

#### 4.2.1.1 Fast Pressurization Events

These are the limiting pressurization events. Principal figures of merit on which “importance” is defined are critical power (MCPR) and reactor pressure.

- ***Turbine Trips*** — initiated by trip of turbine stop valves from full open to full closed. Analyzed with bypass valves functional, and with bypass failure.
- ***Generator Load Rejection*** — initiated by fast closure of turbine control valves from partially open position to full-closed. This event is analyzed with bypass valves functioning, and with bypass failure. The turbine control valves may be initially at the same position (full arc turbine admission) or at different positions (partial arc turbine admission).
- ***Loss of AC Power*** — Similar to load rejection; however, bypass valves are assumed to close after 6 seconds due to loss of power to condenser circulating water pumps.
- ***Main Steamline Isolation Valve (MSIV) Closure*** — In this case, the scram signal on valve position is further in advance of complete valve closure. This effectively mitigates the shorter line length to the vessel available as a compression volume.
- ***Loss of Condenser Vacuum*** — This event is similar to the Loss of AC Power and a Turbine Trip with Bypass. Because a turbine trip occurs at a higher vacuum setpoint than the bypass valve isolation, the bypass valves are available to mitigate the initial pressure increase.

#### 4.2.1.2 Slow Pressurization Events

These are analyzed principally to ensure that they are bounded by the fast pressurization events. MCPR and reactor pressure determine “importance.”

- *Pressure Regulator Downscale Failure* — Simultaneous closure of all turbine control valves in normal stroke mode. The triplicated fault tolerant control system prevents any single failure from causing this and makes its frequency below the anticipated abnormal occurrence category.
- *Single Control Valve Closure* — This event could be caused by a hydraulic failure in the valve or a failure of the valves rotor/actuator.

#### 4.2.1.3 Decrease in Reactor Coolant Inventory

Loss of feedwater flow is characteristic of this category of transient. The IC maintains downcomer water level. Reactor water level in the downcomer is the principal figure of merit on which “importance” is defined.

#### 4.2.1.4 Decrease in Moderator Temperature

These events challenge MCPR and stability, which are the figures of merit on which “importance” is defined:

- Loss of Feedwater Heating — initiated by isolation or bypass of a feedwater heater.
- Feedwater Controller Failure — hypothesizes an increase in feedwater flow to the maximum possible with all four feed pumps operating at maximum speed. This event is similar to turbine trip but with more severe power transient due to colder feedwater.

To determine the phenomena important in modeling anticipated transients, the sequence of events and system behavior for each class of events should be understood. To provide an example of this, the sequence of events for a fast pressurization transient is discussed below. For this class of transients, important phenomena are those affecting the MCPR and reactor pressure.

#### 4.2.1.5 Generator Load Rejection Event Description

A fast pressurization event will occur due to the fast closure of the turbine control valves (TCVs), which can be initiated when electrical grid disturbances occur which result in significant loss of electrical load on the generator. Closure of the turbine stop valves is initiated by the turbine protection system. The valves are required to close rapidly to prevent excessive overspeed of the turbine-generator rotor.

At the same time, the turbine stop or control valves are signaled to close, and the turbine bypass valves are signaled to open in the fast opening mode. The bypass valves are fully open only slightly later than the turbine valves are closed, and can relieve more than one-third of rated steam flow to the condenser, greatly mitigating the transient. The bypass valves also use a triplicated digital controller. No single failure can cause all turbine bypass valves to fail to open on demand. The worst single failure can only cause one turbine bypass valve to fail to open on demand.

The closing time of the TCVs is short relative to the sonic transit time of the steamline, so their closure sets up a pressure wave in the steamlines. When the pressure wave reaches the vessel steam dome, the flow rate leaving the vessel effectively undergoes a step change. The area change entering the steam dome partially attenuates the pressure wave, propagating a weaker pressure disturbance down through the chimney and downcomer, increasing the vessel pressure, and reducing voids in the core. The void-reactivity feedback results in an increase in the neutron flux. A reflection of the pressure wave also travels back toward the turbine, producing an oscillation in flow and pressure in the steamlines.

Concurrent with closure of the turbine control valves, a scram condition is sensed by the reactor protection system. A turbine stop valve position less than approximately full open triggers a scram, as does the low hydraulic fluid pressure in the turbine control valve solenoids that start their fast closure mode. The ESBWR digital multiplexed Safety System Logic Control (SSLC) will initiate a scram when any two turbine stop valves are sensed as closing, or any two turbine control valves are sensed as fast closing.

The core reactivity is decreased by the control blade insertion and increased by the decrease in core voids and increase in inlet flow. The net effect may be either an immediate shutdown of the reactor and decrease in neutron flux (in cases where there are control blades partially inserted in high worth areas of the core) or a short period of increased reactivity and neutron flux followed by shutdown (in the safety analysis case where there are no control blades initially inserted, and a slower bounding CRD scram insertion time is assumed.)

In the case where the neutron flux undergoes a transient increase, the energy deposition in the fuel pellet will increase clad heat flux. The minimum value of critical power ratio during this transient is found to occur in the upper part of the bundle.

Eventually, as the blades are fully inserted, the reactor is driven subcritical, power drops to decay heat levels, and clad temperature equilibrates near saturation temperature.

The vessel pressure increase is terminated by the bypass valve opening. The downcomer water level drops below the feedwater sparger and sprays subcooled water into the steam dome. This quenching of vapor also helps to terminate the pressure increase. If the bypass and feedwater systems are assumed to be unavailable, the duration of increased pressure would be long enough to initiate the isolation condenser.

In the ASME overpressure protection analysis, the Isolation Condenser is not considered, causing the pressure to slowly increase to the SRV opening pressure. The pressure increase is terminated immediately with SRV activation, and the maximum vessel pressure occurs at the vessel bottom. The overpressure protection case conservatively assumes the first scram signal to fail, and scram on neutron flux terminates the power increase in both turbine valve closure and the MSIV closure events.

The downcomer water level response in pressurization events is driven by the transfer of water from the downcomer to core and chimney caused by the collapse of voids in the core and chimney regions. The sensed water level decreases rapidly below the L3 low water scram setpoint. The feedwater

system flow increases fast enough to prevent the L2 setpoint being reached in high frequency events (events where feedwater and bypass valves are available). The feedwater control system will demand maximum feedwater flow for approximately one minute, until normal downcomer water level is restored. Without feedwater, the downcomer level drop will progress to L2, initiating the IC, isolating the MSIVs and transferring the CRD system to high-pressure injection mode. The IC can independently maintain the downcomer water level near the L2 setpoint. CRD high-pressure injection will cause the downcomer water level to slowly recover to above normal, and then automatically trip off.

#### 4.2.2 Phenomena Identification and Ranking Table (PIRT) for AOOs

A table was developed to identify the phenomena that govern ESBWR AOO transient responses in Reference 29. The transient events have been categorized into three groups: (1) pressurization events; (2) depressurization events; and (3) cold water insertion events. For each event type, the phenomena are listed and ranked for each major component in the reactor system. The ranking of the phenomena is done on a scale of high importance to low importance or not applicable, as defined by the following categories:

- *High importance (H)*: These phenomena have a significant impact on the primary safety parameters and should be included in the overall uncertainty evaluation. The table for High ranked phenomena has been extracted from Reference 29 and is shown in Table 4.2-1. An example of such a parameter would be the *void coefficient* for a pressurization event (C1AX in Table 4.2-1). The void coefficient determines the amount of reactivity change due to void collapse during the transient.
- *Medium importance (M)*: These phenomena have insignificant impact on the primary safety parameters and may be excluded in the overall uncertainty evaluation. An example of such a parameter would be *flashing in the core* for a depressurization event. Vapor production due to fuel heat transfer dominates the effect of flashing in the core.
- *Low importance (L) or not applicable (N/A)*: These phenomena have no impact on the primary safety parameters and need not be considered in the overall uncertainty evaluation. An example of such phenomenon would be *lower plenum stratification* during a pressurization event. The pressurization event happens so quickly that even if there were significant thermal stratification in the lower plenum, it could not impact the critical parameters before the event was over.

The PIRT serves a number of purposes. First, the phenomena are identified and compared to the modeling capability of the code to assess whether the code has the necessary models to simulate the phenomena. Second, the identified phenomena are cross-referenced to the qualification basis to determine what qualification data are available to assess and qualify the code models and to determine whether additional qualification is needed for some phenomena. As part of this assessment, the range of the PIRT phenomena covered in the tests is compared with the corresponding range for the intended application to establish that the code has been qualified for the highly ranked phenomena over the appropriate range.

Finally, uncertainties in the modeling of the highly ranked PIRT phenomena are carefully evaluated, and then combined through a statistical process, to arrive at the total model uncertainty. In this third stage, one may find that some highly ranked phenomena do not contribute significantly to the overall uncertainty even when conservative values for the individual phenomena uncertainties are used. It is at this stage that one can determine how individual uncertainties influence the total uncertainty so that the effort can be focused on establishing the uncertainties for those phenomena that have the greatest impact on the critical safety parameters. These uncertainties will be more fully developed later in this report.

**Table 4.2-1 Composite List of Highly Ranked Phenomena for ESBWR Transients**



**4.2-1 Composite List of Highly Ranked Phenomena for ESBWR Transients (Continued)**

### **4.3 Applicability of TRACG to Transient Analysis**

The objective of this section is to demonstrate the applicability of TRACG for the analysis of anticipated transient events in ESBWR. To accomplish this purpose, the capability of the TRACG models to treat the highly ranked phenomena and the qualification assessment of the TRACG code for AOO applications is examined in the next two subsections.

#### **4.3.1 Model Capability**

The capability to calculate an event for a nuclear power plant depends on four elements:

- Conservation equations, which provide the code capability to address global processes.
- Correlations and models, which provide code capability to model and scale particular processes.
- Numerics, which provide code capability to perform efficient and reliable calculations.
- Structure and nodalization, which address code capability to model plant geometry and perform efficient and accurate plant calculations.

Consequently, these four elements must be considered when evaluating the applicability of the code to the event of interest for the nuclear power plant calculation. The key phenomena for each event are identified in generating the PIRTs for the intended application, as indicated in Section 4.2.2. The capability of the code to simulate these key phenomena is specifically addressed, documented, and supported by qualification in References 2 and 24.

Important ESBWR phenomena have been identified and TRACG models have been developed to address these phenomena as indicated in Table 4.3-1 for the high ranked phenomena. The models are identified so that they may be easily correlated to the model description sections.

**Table 4.3-1**  
**High Ranked ESBWR Phenomena and TRACG Model Capability Matrix**





### **4.3.2 Model Assessment Matrix**

The qualification of TRACG models is summarized in Table 4.3-2. For each of the governing ESBWR phenomena, TRACG qualification has been performed against a wide range of data. In this section, the qualification basis is related to the phenomena that are important for the intended application. This is a necessary step to confirm that the code has been adequately qualified for the intended application.

The list of High ranked phenomena is cross-referenced to the qualification basis in Table 4.3-2. Data from separate effects tests, component tests, integral system tests and plant tests as well as BWR plant data have been used to qualify the capability of TRACG to model the phenomena.

**Table 4.3-2**  
**QUALIFICATION MATRIX FOR HIGH RANKED PHENOMENA FOR ESBWR TRANSIENTS**



NEDO-33083-A

NEDO-33083-A



## **4.4 Model Uncertainties and Biases**

Overall model biases and uncertainties for a particular application are assessed for each high ranked phenomena by using a combination of comparisons of calculated results to: (1) separate effects test facility data, (2) integral test facility test data, (3) component qualification test data and (4) BWR plant data. Where data is not available, cross-code comparisons or engineering judgment are used to obtain approximations for the biases and uncertainties. Some medium ranked phenomena have also been included where it was felt the effects were not negligible. For some phenomena that have little impact on the calculated results, it is appropriate to simply use a nominal value or to conservatively estimate the bias and uncertainty.

The phenomena for ESBWR AOO transients have already been identified and ranked, as indicated in Section 4.2. For the high ranked phenomena, the bases used to establish the nominal value, bias and uncertainty for that parameter are documented in Section 4.4.1. Also, the basis for the selection of the probability density function used to model the uncertainty is provided in Section 4.4.1. The bias and uncertainty are implemented in TRACG through special input parameters designated as "PIRT multipliers".

### **4.4.1 Model Parameters and Uncertainties**

This section discusses the uncertainties associated with each item from Table 4.2-1 (list of highly ranked parameters). Some medium ranked parameters have also been included. The results are summarized in Table 4.4-1.



**Figure 4.4-1. Void Coefficient Normalized %Bias and %Standard Deviation [3]**















**Table 4.4-1**  
**High Ranked Model Parameters for AOO analysis**



## 4.5 Application Uncertainties and Biases

### 4.5.1 Input

Specific inputs for each transient event are specified via internal procedures, which are the primary means used by GE to control application of engineering computer programs. The specific code input will be developed in connection with the application LTR and the development of the application specific procedure. This section will be limited to a more general discussion of how input is treated with respect to quantifying their impact on the calculated results. As such, it serves as a basis for the development of the application specific procedures.

Code inputs can be divided into four broad categories: (1) geometry inputs; (2) model selection inputs; (3) initial condition inputs; and (4) plant parameters. For each type of input, it is necessary to specify the value for the input. If the calculated result is sensitive to the input value, then it is also necessary to quantify the uncertainty in the input.

The geometry inputs are used to specify lengths, areas and volumes. Uncertainties in these quantities are due to measurement uncertainties and manufacturing tolerances. These uncertainties usually have a much smaller impact on the results than do other uncertainties associated with the modeling simplifications. When this is not the case, the specific uncertainties can usually be quantified in a straightforward manner. For example, consider the 2% channel flow area uncertainty that is considered as part of the Safety Limit MCPR (SLMCPR). This uncertainty is determined from the manufacturing tolerances on the inner dimensions of the channel box and the outer diameter of the fuel and water rods. It is known that neglecting this uncertainty causes the calculated SLMCPR value to be non-conservative by no more than 0.0015. Even though channel flow area is considered to be *important*, the impact associated with the uncertainty in this parameter is small.

Individual geometric inputs are the building blocks from which the spatial nodalization is built. Another aspect of the spatial nodalization includes modeling simplifications such as the lumping together of individual elements into a single model component. For example, several similar fuel channels may be lumped together and simulated as one fuel channel group. An assessment of these kinds of simplifications, along with the sensitivities to spatial nodalization, is included in the *TRACG Qualification* [2].

Model selection inputs are used to select the features of the model that apply for the intended application. Once established, these inputs are fully specified in the procedure for the application and will not be changed.

A distinction has been made in this document between *initial conditions* and *plant parameters*. Obviously, when specified in absolute units, the initial rated conditions for a nuclear power plant are specific to the plant and thus have in some documents been considered as plant parameters. In this document we consider *initial conditions* to be those key plant inputs that determine the overall steady-state nuclear and hydraulic conditions prior to the transient. These are inputs that are essential to determining that the steady-state condition of the plant has been established. Initial conditions parameters and the uncertainties associated with them are addressed in Section 4.5.2.

The name *plant parameter*, on the other hand, is reserved for such things as protection system setpoints, valve capacities and stroke times, and scram characteristics that influence the characteristics of the transient response but which do not (when properly prescribed) have an impact on steady-state operation. Plant parameters and the uncertainties associated with them are addressed in Section 4.5.3.

#### 4.5.2 Initial Conditions

*Initial conditions* are those conditions that define a steady-state operating condition. Initial conditions for a particular transient scenario are specified in the procedure for the application. For example, the procedure may specify that the calculation be performed at the end-of-cycle exposure at 100% of rated power and flow using a power and exposure distribution that has been obtained from a prescribed process.

Initial conditions may vary due to the allowable operating range or due to uncertainty in the measurement at a give operating condition. The plant Technical Specifications and Operating Procedures provide the means by which controls are instituted and the allowable initial conditions are defined. At a given operating condition, the plant's measurement system has inaccuracies that also must be accounted for as an uncertainty. The key plant initial conditions are identified in Table 4.5-1.

The analyses performed must maintain consistency with the allowed domains of operation. The impact of the initial condition on the results are characterized in the following manner:

- The results are sensitive to the initial condition and a basis for the limiting initial condition cannot be established. Future plant analyses (e.g., the reload licensing analyses) will consider the full allowable range of the initial condition.
- The results are sensitive to the initial condition and a basis for the limiting initial condition can be established. Future plant analyses (e.g., the reload licensing analyses) will consider the parameter to be at its limiting initial condition.
- The results are not sensitive to the initial condition and a nominal initial condition will be assumed for the parameter.

Each initial condition is monitored through the use of plant sensors or simulated prediction. Because of instrument or simulation uncertainty, the plant condition may vary from the indicated value. The results are characterized in the following manner:

- The results are sensitive to the uncertainty in the initial condition and the uncertainty in the initial condition will be included in the statistical analysis.
- The results are not sensitive to the uncertainty in the initial condition and the uncertainty does not need to be accounted for.

The impact of the total uncertainty in initial conditions must also be quantified for the critical safety parameters such as  $\Delta\text{CPR}/\text{ICPR}$ , peak vessel pressure and water level. Some of these uncertainties

may already be considered by other means. The evaluation, which addresses the characterization, is contained in this section.

**Table 4.5-1**  
**KEY PLANT INITIAL CONDITIONS**

### **4.5.3 Plant Parameters**

A *plant parameter* is defined as a plant-specific quantity such as a protection system setpoint, valve capacity or stroke time, or a scram characteristic, etc. *Plant parameters* influence the characteristics of the transient response and have essentially no impact on steady-state operation, whereas *initial conditions* are what define a steady-state operating condition.

For each plant parameter, a conservative value corresponding to the *analytic limit* is defined. The analytic limit (AL) is the value used for the transient licensing analyses. In many cases, the value used for the AL can be related to a plant Technical Specifications, since most of the plant parameter values that are important for AOO transient responses are related to processes that are controlled by the plant Technical Specifications. These parameters may be periodically measured at the plants to

assure compliance with the Technical Specifications. Performance and uncertainties for the processes that the Technical Specifications are designed to control are based on manufacturing specifications, performance data, as well as required surveillance. A Technical Specification value will usually be in terms of a maximum or minimum acceptable value that bounds the entire population of values that are measured at the plant.

The Technical Specifications values may be used to define the analytic limits used for the licensing analyses. The original licensing basis specified bounding Technical Specifications values for most of the plant parameters. This is one acceptable way by which conservatism can be added to a “best estimate” methodology. Another option for establishing plant parameters is to establish an uncertainty in the parameter. For example, the NRC has accepted (AOO analysis *Option B* for operating plants) a faster scram speed when used together with considerations of the uncertainties in the scram speeds. This approach is supported by surveillance procedures at the plant, whereby the scram times are measured. The uncertainty in the scram times is then accounted for in the AOO analyses as part of the statistical methodology.

GE procedures will define the critical Operating Parameters for Licensing (OPL) for transient analysis. It serves as a guide for generating plant parameter data to be used for licensing. This procedure addresses Technical Specifications items as well as other items that are important to the severity of transients.

The reactor scram is the most effective plant system for mitigating the severity of a transient. The plant Technical Specifications provide surveillance requirements to ensure control rod operability and scram times. The scram times used for the analysis depend on the type of transient analyzed. Table 4.5-2 shows the analytical scram speed characteristics for the ESBWR. These are based on the ABWR. Because the control rod stroke is shorter, rod motion is slower than for ABWR.

**Table 4.5-2  
ANALYTICAL SCRAM SPEEDS FOR ESBWR**



## **4.6 Combination of Uncertainties**

A proven Monte Carlo technique is used to combine the individual biases and uncertainties into an overall bias and uncertainty. The Monte Carlo sample is developed by performing random perturbations of model and plant parameters over their individual uncertainty ranges. Using the histogram generated by the Monte Carlo sampling technique, a probability density function is generated for code output of the primary safety criteria parameters.

In order to determine the total uncertainty in predictions with a computer code, it is necessary to combine the effects of model uncertainties (CSAU Step 9), scaling uncertainties (CSAU step 10), and plant condition or state uncertainties (CSAU Step 11). Various methods have been used to combine the effects of uncertainties in safety analysis. This section summarizes the method used for combining uncertainties for the AOO application. This is the same approach that has been successfully used and approved for analyses of AOO transients for operating plants [3].

### **4.6.1 Recommended Approach for Combining Uncertainties**

#### **4.6.1.1 Order Statistics (OS) Method – Single Bounding Value**

The Monte Carlo method that has been used in Germany by Gesellschaft für Anlagen-und Reaktorsicherheit (GRS) [83] requires only a modest number of calculations, and automatically includes the effects of interactions between perturbations to different parameters. In the OS method, Monte Carlo trials are used to vary all uncertain model and plant parameters randomly and simultaneously, each according to its uncertainty and assumed probability density function (PDF), and then a method based on the order statistics of the output values is used to derive upper tolerance bounds (one-sided, upper tolerance limits OSUTLs).

An OSUTL is a function  $U = U(x_1, \dots, x_n)$  of the data  $x_1, \dots, x_n$  (which will be the values of an output parameter of interest in a set of Monte Carlo trials), defined by two numbers  $0 < \alpha, \beta < 1$ , so that the proportion of future values of the quantity of interest that will be less than  $U$  is  $100\alpha\%$ , with confidence at least  $100\beta\%$  --- this is called an OSUTL with  $100\alpha\%$ -content and (at least)  $100\beta\%$  confidence level.

The order statistics method, originally developed by Samuel Wilks, produces OSUTLs that are valid irrespective of the probability distribution of the data, requiring only that they be a sample from a continuous PDF. Given values of  $\alpha$  and  $\beta$ , the OSUTL can be defined as the largest of the data values, provided the sample size  $n \geq \log(1 - \beta) / \log \alpha$  [84]. For 95%-content and 95% confidence level, the minimum sufficient sample size is  $n=59$ .

The order statistics method is generally applicable, irrespective of the probability distribution of the data, and requires only that these be like outcomes of independent random variables with a common probability distribution.

If the method is implemented as described above, whereby the sample size (59) was chosen so that the sample maximum is the upper tolerance bound sought (95% content with 95% confidence), then this bound, as a random quantity, has variability that is typical of the maximum of a sample of that size, which can be substantial, and occasionally may yield an overly conservative bound.

To mitigate this variability, one can choose a suitably larger sample size so that the bound sought is now given by the second or third largest sample value. For example, the 95% content with 95% confidence tolerance bound is the third largest observation in a sample of size 124: Just for the sake of illustration, in normal (that is, Gaussian) populations its variability is about one half of the variability of the maximum in a sample of size 59; and in the more heavily-tailed Student's  $t$  distribution with 4 degrees of freedom, the variability of the third largest in a sample of size 124 is about one third of the variability of the maximum in a sample of size 59.

The following table summarizes the sample sizes that are required, when the bound is the largest, the second largest, or the third largest order statistic, all for 95% content and 95% confidence:

Order Statistic	Sample Size
Largest	59
2 <sup>nd</sup> Largest	93
3 <sup>rd</sup> Largest	124

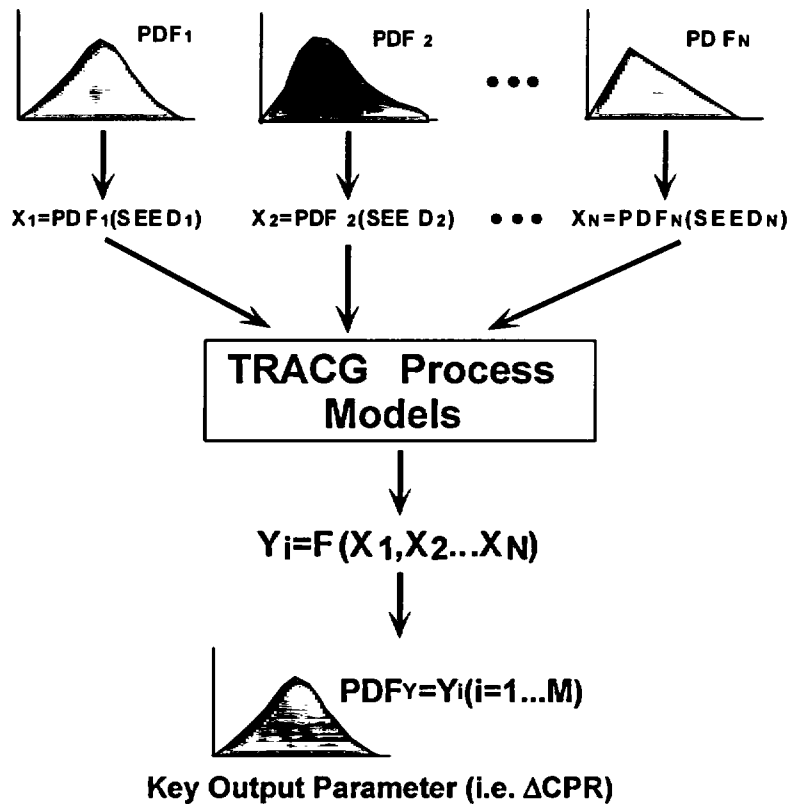


Figure 4.6-1. Schematic Process for Combining Uncertainties

#### 4.6.1.2 Normal Distribution One-Sided Upper Tolerance Limit

If the data that the tolerance bound will be derived from can reasonably be regarded as a sample from a normal (that is, Gaussian) probability distribution, then this normal distribution one-sided upper tolerance limit (ND-OSUTL) is of the form

$$ND - OSUTL_{\alpha,\beta} \equiv \bar{y} + z_{\alpha,\beta} \cdot s$$

where  $\bar{y}$  denotes the average of the outcomes of the TRACG trials, and  $s$  denotes their standard deviation, and the factor  $z_{\alpha,\beta}$  is chosen to guarantee  $100\alpha\%$ -content and  $100\beta\%$  confidence level. Since this factor  $z_{\alpha,\beta}$  depends on the assumption of normality for the data, one must first ascertain whether the data does indeed conform with the Gaussian model, typically using one or several goodness-of-fit tests: for example, Ryan-Joiner's, Shapiro-Wilk's, or Anderson-Darling's. The values of  $z_{\alpha,\beta}$  are tabulated in many statistical textbooks [86] as *factors for one-sided normal tolerance limits*. For example, for a sample of size  $n = 59$ , and a 95% content and a 95% confidence level,  $z_{95,95} = 2.024$ . As the sample size  $n$  increases, this factor approaches 1.645, the 95<sup>th</sup> percentile of the standard normal distribution. Unlike the order statistics method, this ND-OSUTL method does not require specific minimum sample sizes; but

it does require normality. If the data are unlikely to have originated from a normal population, then one should use the order statistics method.

#### **4.6.1.3 Advantages of Recommended Method**

#### **4.6.2 Implementation of Statistical Methodology**

The purpose of this section is (1) to describe the process by which the statistical results will be used to determine the Operating Limit Minimum Critical Power Ratio (OLMCPR), and (2)

establish that fuel thermal/mechanical performance, peak vessel pressure, and minimum water level have acceptable margins to design limits. The application to the latter three is straightforward, and is discussed in the next section. The determination of the OLMCPR is more involved, and is detailed in the subsequent sections.

**4.6.3.1 Details of Process of OLMCPR Calculation**

**Figure 4.6-2. Generic  $\Delta$ CPR/ICPR Uncertainty Development**

**Figure 4.6-3. NRSBT Determination**



**Figure 4.6-4. GESAM Calculation Procedure for Analytical Determination of OLMCPR**

#### **4.7 Demonstration Calculations for ESBWR AOs**

The analyses provided in this Section form the bases for future application of TRACG to ESBWR AOs. TRACG performance is demonstrated on one or more limiting licensing basis events for the scenarios specified in Section 4.2.1. This demonstration includes baseline TRACG analysis for a representative core. Statistical calculations for the various limiting AOs will be performed for the ESBWR for the final core design utilizing the process described in Section 4.6.



**Table 4.7-1. Sequence of Events for LRNB Transient**



**Table 4.7-2. Sequence of Events for FWCF Event**



**Table 4.7-3. Sequence of Events for MSIV Closure Transient**



**Figure 4.7-1. Pressure response for LRNB Transient**

**Figure 4.7-2. Neutron Flux Response for LRNB Transient**

**Figure 4.7-3. Downcomer Two-Phase Level Response for LRNB Transient**

**Figure 4.7-4. Bundle Power Response for LRNB Transient**

**Figure 4.7-5. Bundle Inlet Flow for LRNB Transient**

**Figure 4.7-6. Downcomer Level Response for FWCF Transient**

**Figure 4.7-7. Pressure Response for FWCF Transient**

**Figure 4.7-8. Neutron Flux response for FWCF Transient**

**Figure 4.7-9. Bundle Power Response for FWCF Transient**

**Figure 4.7-10. Bundle Inlet Flow Response for FWCF Transient**

**Figure 4.7-11. Pressure Response for MSIV Closure Transient**

**Figure 4.7-12. Neutron Flux Response for MSIV Closure Transient**

**Figure 4.7-13. Downcomer Level for MSIV Closure Transient**

**Figure 4.7-14. IC Steam Flow for MSIV Closure Transient**

## **4.8 Summary of TRACG Application to ESBWR AOOs**

This report has provided the basis for extending the application methodology that has been approved for operating BWRs for AOOs to the ESBWR.

The requirements to be met and the scope of application were identified in Section 4.1. Phenomena important for AOO analysis for ESBWR were identified in Section 4.2. Section 4.3 justified the applicability of TRACG for ESBWR AOO analysis. Model and plant parameters and their ranges were established in Sections 4.4 and 4.5. A statistical application approach (identical to that approved for operating plants) was proposed in Section 4.6. Sample base line analyses were shown in Section 4.7 for three different pressurization transients to illustrate ESBWR response and demonstrate that it is generally similar to operating plants.

Actual application to the ESBWR SAR calculations will involve repeating the baseline analysis for the final ESBWR core; performing sensitivity studies for model and plant parameters; and performing a statistical analysis in conformance with the process described in Section 4.6.

## 5. REFERENCES

- [1] J. G. M. Andersen, et al., TRACG Model Description, NEDE-32176P, Revision 2, December 1999; Revision 1, February 1996.
- [2] J. G. M. Andersen, et al., TRACG Qualification, NEDE-32177P, Rev. 2, January 2000.
- [3] J. G. M. Andersen, et al.. TRACG Application for Anticipated Operational Occurrences Transient Analysis, NEDE-32906P, January 2000.
- [4] R. J. Pryor, et al., TRAC-P1A, An Advanced Best Estimate Computer Program for PWR LOCA Analysis, Los Alamos Scientific Laboratory, NUREG/CRA-0665, May 1979. J. G. M. Andersen, et al., TRACG Model Description, NEDE-32176P, Rev. 2, December 1999.
- [5] J. G. M. Andersen, K. H. Chu and J. C. Shaug, BWR REFILL/REFLOOD Program Task 4.7 - Model Development, Basic Models for the BWR Version of TRAC, GEAP-22051, NUREG/CR-2573, EPRI NP-2376, April 1983.
- [6] Y. K. Cheung, V. Parameswaran and J. C. Shaug, BWR REFILL/REFLOOD Program Task 4.7 - TRAC BWR Component Models, GEAP-22052, NUREG/CR-2574, EPRI NP-2377, April 1983.
- [7] Md. Alamgir, BWR REFILL/REFLOOD Program Task 4.8 - TRAC-BWR Model Qualification for BWR Safety Analysis, Final Report, GEAP-30157, NUREG/CR-2571, EPRI NP-2377, October 1983.
- [8] J. G. M. Andersen and C. L. Heck, BWR Full Integral Simulation Test (FIST) Program, TRAC-BWR Model Development, Volume 1 - Numerical Methods, GEAP-30875-1, NUREG/CR-4127-1, EPRI NP-3987-1, November 1985.
- [9] K. H. Chu, J. G. M. Andersen, Y. K. Cheung and J. C. Shaug, BWR Full Integral Simulation Test (FIST) Program, TRAC-BWR Model Development, Volume 2 - Models, GEAP-30875-2, NUREG/CR-4127-2, EPRI NP-3987-2, October 1985.
- [10] Y. K. Cheung, J. G. M. Andersen, K. H. Chu and J. C. Shaug, BWR Full Integral Simulation Test (FIST) Program, TRAC-BWR Model Development, Volume 2 - Developmental Assessment for Plant Applications, GEAP-30875-3, NUREG/CR-4127-3, EPRI NP-3987-3, October 1985.

- [11] W. A. Sutherland, Md. Alamgir J. A. Findlay and W. S. Hwang, BWR Full Integral Simulation Test (FIST) Program, Phase II Test Results and TRAC-BWR Model Qualification, GEAP-30876, NUREG/CR-4128, EPRI NP-3988, October 1985.
- [12] D. D. Taylor, et al., TRAC-BD1/MOD1: An Advanced Best Estimate Program for Boiling Water Reactor Transient Analysis, Volumes 1-4, NUREG/CR-3633, Idaho National Engineering Laboratory, April 1984.
- [13] J. A. Borkowski, et al., TRAC-BF1/Mod1: An Advanced Best Estimate Program for BWR Accident Analysis, NUREG/CR-4356, Idaho National Engineering Laboratory, August 1992.
- [14] J. A. Borkowski, et al., TRAC-BF1/Mod1 Models and Correlations, NUREG/CR-4391, Idaho National Engineering Laboratory, August 1992.
- [15] B. Boyack, et al., Quantifying Reactor Safety Margins: Application of Code Scaling, Applicability, and Uncertainty Evaluation Methodology to a Large-Break, Loss-of-Coolant Accident, NUREG/CR-5249, December 1989.
- [16] U.S. NRC Regulatory Guide 1.157, Best-Estimate Calculations of Emergency Core Cooling System Performance, May 1989.
- [17] Code of Federal Regulations, Title 10, Energy, Part 50 -- Domestic Licensing Of Production And Utilization Facilities. Section 50.46 Acceptance Criteria For Emergency Core Cooling Systems For Light-Water Nuclear Power Reactors.; and Appendix K to Part 50 -- ECCS Evaluation Models
- [18] Code of Federal Regulations, Title 10, Energy, Part 100 -- Reactor Site Criteria
- [19] U.S. NRC, Standard Review Plan, NUREG 0800.
- [20] General Electric Standard Application for Reactor Fuel (GESTAR II), NEDE-24011-P-A-13, August 1996.
- [21] B. S. Shiralkar, et al., The GESTR-LOCA and SAFER Models for the Evaluation of the Loss-of-Coolant Accident, Volume III: SAFER/GESTR Application Methodology, NEDE-23785-1-PA, Rev. 1, October 1984.
- [22] J. A. Findlay, et al., SAFER Model for Evaluation of Loss-of-Coolant Accidents for Jet Pump and Non-Jet Pump Plants Volume II: SAFER Application Methodology for Non-Jet Pump Plants, NEDE-30996PA, October 1987.

- [23] ESBWR Design Description, NEDC-33048P, August 2002.
- [24] TRACG Qualification for SBWR, NEDC-32725P, Rev.1, Vol.1 and 2, September 1997.
- [25] TRACG Qualification for ESBWR, NEDC-33080P, Rev.0, August 2002.
- [26] J. G. M. Andersen, C. L. Heck and J. C. Shaug, *TRACG04 User's Manual*, GE-NE-0000-0009-7162 (UM-0136), Rev. 0.
- [27] S.O. Akerlund et al., The GESTR-LOCA and SAFER Models for the Evaluation of the Loss-of-Coolant Accident, Vol. I, NEDO-23785-1-A, February 1985.
- [28] *Quantifying Reactor Safety Margins*, B.E. Boyack et. al, Nuclear Engineering and Design (Parts 1-4), 119, Elsevier Science Publishers B.V. (North Holland), 1990.
- [29] ESBWR Test and Analysis Program Description, NEDC-33079P, August 2002.
- [30] *TRACG Qualification for SBWR*, J.R. Fitch, et al., NEDC-32725P Revision 1, Volumes 1 and 2, August 2002.
- [31] *SBWR Testing Summary Report*, P.F. Billig, et al., NEDC-32606P Revision 0, August 2002.
- [32] V. P. Carey, *Liquid-Vapor Phase-Change Phenomena*, Hemisphere 1992.
- [33] D. R. Liles et al., TRAC-PF/MOD1 Correlations and Models, NUREG/CR-5069, LA-11208-MS, December 1998.
- [34] H. A. Hasanein, A. M. C. Chan, M. Kawaji and Y. Yoshioka, Steam-Water Two-Phase Flow in Large Diameter Vertical Piping at High Pressures and Temperatures, 4<sup>th</sup> JSME/ASME Joint International Conference on Nuclear Engineering, New Orleans, March 1996.
- [35] A. M. C. Chan, *Void Fraction Measurements in Large Diameter Pipes with Thick Metal Walls or Complex Internal Geometries*, Proceedings of the National Heat Transfer Conference, American Nuclear Society, 1992 (pp. 236-244).

- [36] A. M. C. Chan and D. Bzovey, Measurements of Mass Flux in High Temperature High Pressure Steam-Water Two-Phase Flow using a Combination of Pitot Tubes and a Gamma Densitometer, *Journal of Nuclear Engineering and Design*, V. 122, 1990 (pp. 95-104).
- [37] J. F. Wilson, R. J. Grenda and J. F. Patterson, Steam Volume Fraction in a Bubbling Two-Phase Mixture, *Trans. ANS* 4(2), 1961 (pp. 356-357).
- [38] G. G. Bartolomei, V. A. Suvorov and S. A. Tevlin, *Hydrodynamics of Steam Generation in a Two-Circuit Nuclear Power Plant*, *Teploenergetika* 10(1), 1963 (pp. 52-57).
- [39] M. Petrick and E. A. Spleha, Thermal Hydraulic Performance Characteristics of EBWR, ANL 6693, May 1963.
- [40] H. Nagasaka, New Japanese Correlations on Core Cooling and CCFL Characteristics During BWR LOCA, Transactions of the Thirteenth Water Reactor Safety Research Information Meeting, Gaithersburg, MD, October 1985.
- [41] O. Nylund and R. Eklund, OF-64 Results of Void Measurements, FRIGG PM-69, September 1970.
- [42] S. Morooka, T. Ishizuka, M. Iizuka and K. Yoshimura, Experimental Study on Void Fraction in a Simulated BWR Assembly (Evaluation of Cross-Sectional Averaged Void Fraction), *Nuclear Engineering and Design* 114, pp. 91-98 (1989).
- [43] T. Mitsutake, S. Morooka, K. Suzuki, S. Tsonoyama and K. Yoshimura, *Void Fraction Estimation within Rod Bundles Based on Three-Fluid Model and Comparison with X-Ray CT Void Data*, *Nuclear Engineering and Design* 120, pp. 203-212 (1990).
- [44] K. C. Chan, et al., The GESTR-LOCA and SAFER Models for the Evaluation of the Loss-of-Coolant Accident V.II, SAFER-Long Term Inventory Model for BWR Loss-of-Coolant Analysis, NEDE-23785-1-PA, Rev. 1, October 1984.
- [45] J. E. Leonard et al., Calculation of Counter-Current Flow Limiting Conditions in BWR Geometry, NEDE-13430, September 1975.
- [46] B. S. Shiralkar and J. R. Ireland, Backflow Leakage from the Bypass Region for ECCS Calculations, NEDE-23690, October 1977.

- [47] J. P. Walkush, *High Pressure Counterflow CHF*, MIT Report, September 1974.
- [48] V. P. Carey, *Liquid-Vapor Phase-Change Phenomena*, Hemisphere, 1992.
- [49] R. E. Dimenna et al., *RELAP5/MOD2 Models and Correlations*, NUREG/CR-5194 (EGG-2531), August 1988.
- [50] D. C. Groeneveld, S. C. Cheng and T. Doan, *1986 AECL-UO Critical Heat Flux Lookup Table*, Heat Transfer Engineering 7, 1986 (pp. 46-62).
- [51] P.F. Billig, *Simplified Boiling Water Reactor (SBWR) Program Gravity-Driven Cooling System (GDCCS) Integrated Systems Test - Final Report*, GE Nuclear Energy, GEFR-00850, October 1989.
- [52] *GIRAFFE SBWR System Interaction Test Report*, NEDC-32504P, June 1996.
- [53] *Acceptance for Referencing of Licensing Topical Reports, Methodology and Uncertainties for Safety Limit MCPR Evaluations*, NEDC-32601P; *Power Distribution Uncertainties for Safety Limit MCPR Evaluation*, NEDC-32694P; Letter from F. Akstulewicz (NRC) to G. A. Watford (GE) dated March 11, 1999.
- [54] F. D. Shum, et al., *SAFER Model for Evaluation of Loss-of-Coolant Accidents for Jet Pump and Non-Jet Pump Plants, Vol. I, SAFER – Long Term Inventory Model for BWR Loss-of-Coolant Analysis*, NEDE-30996P-A, October 1987.
- [55] B.L. Charboneau, *Overview of TRACBD1/Model Assessment Studies*, NUREG/CR-4428, EGG-2422, November 1985.
- [56] J. E. Leonard, J. D. Duncan, A. S. Rao and R. C. Cipolla, *Emergency Core Cooling Tests of an Internally Pressurized Zircaloy-Clad, 8x8 Simulated BWR Fuel Bundle*, NEDE-20231-P-A, April 1976.
- [57] R. E. Gamble, et al., *Scaling of the SBWR Related Tests*, NEDC-32288P, Revision 1, October 1995.
- [58] ANSI/ANS-5.1-1979 Standard entitled “American National Standard for Decay Heat Power in Light Water Reactors”, 1979.

- [59] T. Fujii, et al., Experimental Study of Performance of a Hybrid Baffle Plate for the Water Wall Type Passive Containment Cooling System, Nuclear Technology, Vol. 112, October 1995.
- [60] Y. Kataoka, et al., Thermal-Hydraulic Characteristics and heat Removal Capability of Containment Cooling System with External Water Wall, Nuclear Science and Technology, 27[9], pp.802-814, September 1990.
- [61] MIT and UCB Separate Effects Tests for PCCS Tube Geometry, "Single Tube Condensation Test Program", NEDC-32301.
- [62] Separate Effect Tests at UCB for PCCS Tube Geometry, NEDC-32310.
- [63] GIRAFFE Passive Heat Removal Testing Program, K. M. Vierow, NEDC-32215P, June 1993.
- [64] SBWR Vacuum Breaker (V.B.) Prototype Experimental Qualification General test Report, COMPES Report ED45913, October 1994.
- [65] C.H. Robbins, Tests of the Humboldt Bay Pressure Suppression Containment, GEAP-3596, November 1960.
- [66] *Pressure Suppression Test Program*, PG&E, Bodega Bay Atomic Power Unit 1 Exhibit 1, Preliminary Hazards Summary Report, December 1962
- [67] Mark II - Pressure Suppression Test Program, NEDE-13442P-01, May 1976.
- [68] Mark III Confirmatory Test Program, Phase I - Large Scale Demonstration Tests, Test Series 5701 through 5703, NEDM-13377, October 1974.
- [69] S.Z. Kuhn, V.E. Schrock, and P.F. Peterson, *Final Report on U. C. Berkeley Single Tube Condensation Studies*, University of California, Berkeley Report UCB-NE-4201, August 1994.
- [70] Thermal Hydraulic Data Report of PANTHERS/PCC Tests, SIET Document No. 00393RP95, Rev.1, January 1996..
- [71] D. Abdollahian et al., *Post-Test Analysis of PANTHERS PCC Tests*, GE Report NEDC-32615P, June 1996.

- [72] *ESBWR Scaling Report*, NEDC-33082, December 2002.
- [73] USNRC Regulation Guide 1.49, *Power Levels of Nuclear Power Plants*, Rev. 1, December 1973.
- [74] USNRC Regulation Guide 1.7, *Control of Combustible Gas Concentrations in Containment Following a Loss-of-Coolant Accident*, Rev. 2, November 1978.
- [75] *Containment Configuration Data Book*, 25A5044, Rev. 1, November 1992.
- [76] *Safety Limit MCPR Evaluation*, NEDC-32601P, Class 3, December 1966.
- [77] G.J. Scatena, and G.L. Upham, *Power Generation in a BWR Following Normal Shutdown or Loss-of-Coolant Accident Conditions*, NEDO-10625, March 1973.
- [78] *Steady State Nuclear Methods*, NEDO-30130-A, April 1985.
- [79] *General Electric Standard Application for Reactor Fuel (GESTAR II)*, NEDE-24011-P-A-13, August 1996.
- [80] *Qualification of the One-Dimensional Core Transient Model for Boiling Water Reactors*, NEDO-24154-P (Supplement 1 – Volume 4).
- [81] P. Saha and N. Zuber, *Point of Net Vapor Generation and Vapor Void Fraction in Subcooled Boiling*, Proceedings of the 5th International Heat Transfer Conference, Tokyo 1974.
- [82] *Application of TRACG to model the SBWR Licensing Safety Analysis*, NEDE-32178P Rev. 1, January 1998.
- [83] H. Glaeser, E. Hofer (GRS-Germany), *Determination of Importance of Uncertain Parameters in Code Applications*, Transactions of the American Nuclear Society, Washington, D.C., November 13-17, 1994, p. 308-309.
- [84] H. A. David, *Order Statistics* (2<sup>nd</sup> edition), John Wiley & Sons, New York, 1969.
- [85] *Power Distribution Uncertainties for Safety Limit MCPR Evaluations*, NEDC-32694P-A, August, 1999.

- [86] D. C. Montgomery, Introduction to Statistical Quality Control, John Wiley and Sons, Inc., 1996.
- [87] General Electric Standard Application for Reactor Fuel (GESTAR II), NEDE-24011-P-A-13, August 1996.
- [88] J. Duncan and P. W. Marriott, *General Electric Company Analytical Model for Loss-of-Coolant Analysis in Accordance with 10CFR50 Appendix K – Volumes 1 and 2*, NEDE-20566-P-A, September 1986.

The folders are in S:\ESBWR\NRC Correspondence\RAIs The MFN letters are in S:\MFN-BB										
NRC RAIs and Allocation by Report										
RAI #	Letter	ESBWR SCALING	ESBWR Test and Analysis Program Description	ESBWR Test Report	SBWR Testing Summary RPT	TRACG Qualification for SBWR	TRACG Application for ESBWR	TRACG Model Description	TRACG Qualification	TRACG Qualification for ESBWR
		NEDC-33082P	NEDC-33079P	NEDC-33081P	NEDC-32606P	NEDC-32725P	NEDC-33083P	NEDE-32176P	NEDE-32177P	NEDC-33080P
1	MFN-03-078						X			
2	MFN-03-078						X			
3	MFN-03-078						X			
4	MFN-03-078						X			
5	MFN-03-078						X			
6	MFN-03-080						X			
7	MFN 03-094 Supplements						X			
8	MFN 03-094 Supplements						X			
9	MFN-03-057						X			
10	MFN-03-078						X			
11	MFN-03-078						X			
12	MFN-03-078						X			
13	MFN 03-070	X								
14	MFN 03-070	X								
15	MFN 03-117supple to 15	X								
16	MFN-03-057	X					X			
17	MFN-03-057						X			
18	MFN-03-057						X			
19	MFN-03-057						X			
20	MFN-03-057						X			
21	MFN-03-057						X			
22	MFN-03-057						X			
23	MFN-03-057						X			
24	MFN-03-057						X			
25	MFN-03-078									X
	MFN 03-100									X
	MFN 03-142									X
26	MFN-03-078						X			
27	MFN-03-078						X			
28	MFN 03-070						X			
29	MFN 03-070						X			
30	MFN 03-070						X			
31	MFN-03-078						X			
32	MFN-03-078							X		
33	MFN 03-070		X							
34	MFN 03-070							X		
35	MFN 03-080							X		

RAI #	Letter	ESBWR SCALING	ESBWR Test and Analysis Program Description	ESBWR Test Report	SBWR Testing Summary RPT	TRACG Qualification for SBWR	TRACG Application for ESBWR	TRACG Model Description	TRACG Qualification	TRACG Qualification for ESBWR
36	MFN 03-070							X		
37	MFN 03-070							X		
38	MFN 03-070							X		
39	MFN 03-070							X		
40	MFN 03-070							X		
41	MFN 03-070							X		
42	MFN 03-070							X		
43	MFN 03-070							X		
44	MFN 03-070							X		
45	MFN 03-080							X		
46	MFN 03-070							X		
47	MFN 03-080							X		
48	MFN 03-080							X		
49	MFN 03-070							X		
50	MFN 03-070							X		
51	MFN 03-070							X		
52	MFN 03-070							X		
53	MFN 03-070							X		
54	MFN 03-082							x		
55	MFN 03-070							X		
56	MFN 03-102							X		
57	MFN 03-070							X		
58	MFN 03-070							X		
59	MFN 03-070							X		
60	MFN 03-080							X		
61	MFN 03-070							X		
62	MFN 03-070							X		
63	MFN 03-070							X		
64	MFN 03-070							X		
65	MFN 03-080							X		
66	MFN 03-070							X		
67	MFN 03-080							X		
68	MFN 03-070							X		
69	MFN 03-070							X		
70	MFN 03-099							X		
71	MFN 03-099							X		
72	MFN 03-070							X		
73	MFN 03-070							X		
74	MFN 03-070							X		
75	MFN 03-070							X		
76	MFN 03-070							X		
77	MFN 03-080							X		
78	MFN 03-070							X		
79	MFN 03-082							x		
80	MFN 03-070							X		
81	MFN 03-070							X		
82	MFN 03-099							X		

RAI #	Letter	ESBWR SCALING	ESBWR Test and Analysis Program Description	ESBWR Test Report	SBWR Testing Summary RPT	TRACG Qualification for SBWR	TRACG Application for ESBWR	TRACG Model Description	TRACG Qualification	TRACG Qualification for ESBWR
83	MFN 03-070							X		
84	MFN 03-070							X		
85	MFN 03-070							X		
86	MFN 03-099							X		
87	MFN 03-099							X		
88	MFN 03-070							X		
89	MFN 03-080								X	
90	MFN 03-080								X	
91	MFN 03-080								X	
92	MFN 03-080								X	
93	MFN 03-070								X	
94	MFN 03-080								X	
95	MFN 03-080								X	
96	MFN 03-070								X	
97	MFN 03-080								X	
98	MFN 03-070								X	
99	MFN 03-070								X	
100	MFN 03-082								X	
101	MFN 03-082								X	
102	MFN 03-070								X	
103	MFN 03-070								X	
104	MFN 03-070								X	
105	MFN 03-080								X	
106	MFN-03-094								X	
107	MFN 03-070								X	
108	MFN 03-070								X	
109	MFN 03-082								X	
110	MFN 03-070								X	
111	MFN 03-070								X	
112	MFN 03-070								X	
113	MFN-03-057									X
114	MFN-03-057									X
115	MFN-03-057									X
116	MFN-03-057									X
117	MFN-03-057									X
	MFN 03-115 supple to 117.2									X
118	MFN-03-057									X
119	MFN-03-057									X
120	MFN-03-057									X
121	MFN-03-057									X
122	MFN-03-057									X
123	MFN-03-057									X
124	MFN-03-057									X
125	MFN-03-057									X
126	MFN-03-057									X
127	MFN-03-057									X
128	MFN-03-057									X

RAI #	Letter	ESBWR SCALING	ESBWR Test and Analysis Program Description	ESBWR Test Report	SBWR Testing Summary RPT	TRACG Qualification for SBWR	TRACG Application for ESBWR	TRACG Model Description	TRACG Qualification	TRACG Qualification for ESBWR
129	MFN-03-057									X
130	MFN-03-057									X
131	MFN-03-057									X
132	MFN-03-057									X
133	MFN-03-057									X
134	MFN-03-057									X
135	MFN-03-057									X
136	MFN-03-057									X
137	MFN-03-057									X
138	MFN-03-057									X
139	MFN-03-057									X
140	MFN-03-057									X
141	MFN-03-057									X
142	MFN-03-057									X
143	MFN-03-057									X
144	MFN-03-078						X			
145	MFN-03-078						X			
146	MFN-03-078						X			
147	MFN 03-070						X			
148	MFN 03-070						X			
149	MFN 03-070						X			
150	MFN 03-070						X			
151	MFN-03-078						X			
152	MFN-03-078						X			
153	MFN 03-070						X			
154	MFN 03-070						X			
155	MFN 03-070						X			
156	MFN 03-070						X			
157	MFN 03-070						X			
158	MFN 03-070						X			
159	MFN 03-080						X			
160	MFN-03-078						X			
161	MFN 03-079						X			
162	MFN 03-079						X			
163	MFN 03-070						X			
164	MFN 03-079						X			
165	MFN 03-070						X			
166	MFN 03-070						X			
167	MFN-03-078						X			
168	MFN 03-070						X			
169	MFN 03-070						X			
170	MFN 03-070						X			
171	MFN 03-070						X			
172	MFN 03-070						X			
173	MFN 03-070						X			
174	MFN 03-070						X			
175	MFN 03-070						X			

RAI #	Letter	ESBWR SCALING	ESBWR Test and Analysis Program Description	ESBWR Test Report	SBWR Testing Summary RPT	TRACG Qualification for SBWR	TRACG Application for ESBWR	TRACG Model Description	TRACG Qualification	TRACG Qualification for ESBWR
176	MFN 03-079						X			
177	MFN-03-078		X							
	NFN 03-094		X							
178	MFN 03-070		X							
179	MFN 03-070		X							
180	MFN 03-070		X							
181	MFN 03-070		X							
182	MFN 03-070		X							
183	MFN 03-079						X			
183 supp	MFN 04-22						X			
183 revised	MFN 04-29						X			
183 supp	MFN 04-39						X			
184	MFN 03-079		X							
185	MFN 03-070		X							
186	MFN 03-070		X							
187	MFN-03-064		X							
188	MFN 03-070		X							
189	MFN 03-070		X							
190	MFN-03-064		X							
191	MFN-03-064		X							
192	MFN 03-070		X							
193	MFN 03-070		X							
194	MFN 03-070		X							
195	MFN-03-064		X							
196	MFN 03-070		X							
197	MFN 03-070		X							
198	MFN 03-070		X							
199	MFN 03-070		X							
200	MFN 03-070		X							
201	MFN 03-070		X							
202	MFN-03-064		X							
203	MFN 03-070		X							
204	MFN 03-070		X							
205	MFN 03-070		X							
206	MFN 03-070		X							
207	MFN 03-070		X							
208	MFN 03-070		X							
209	MFN 03-070		X							
210	MFN 03-070		X							
211	MFN 03-070		X							
212	MFN 03-070		X							
213	MFN-03-057		X							
214	MFN-03-057		X							
215	MFN 03-070		X							
216	MFN 03-070		X							
217	MFN 03-070		X							
218	MFN 03-070		X							

RAI #	Letter	ESBWR SCALING	ESBWR Test and Analysis Program Description	ESBWR Test Report	SBWR Testing Summary RPT	TRACG Qualification for SBWR	TRACG Application for ESBWR	TRACG Model Description	TRACG Qualification	TRACG Qualification for ESBWR
219	MFN 03-070		X							
220	MFN-03-064		X							
221	MFN 03-070		X							
222	MFN 03-070		X							
223	MFN 03-070		X							
224	MFN 03-070		X							
225	MFN-03-064		X							
226	MFN 03-070		X							
227	MFN 03-070		X							
228	MFN 03-070		X							
229	MFN 03-070		X							
230	MFN 03-070		X							
231	MFN-03-064		X							
232	MFN-03-064		X							
233	MFN 03-070		X							
234	MFN-03-057		X							
235	MFN 03-070		X							
236	MFN-03-057		X							
237	MFN 03-070		X							
238	MFN 03-070		X							
239	MFN 03-070		X							
240	MFN 03-070		X							
241	MFN 03-070		X							
242	MFN 03-070		X							
243	MFN 03-070		X							
244	MFN 03-070		X							
245	MFN 03-070		X							
246	MFN 03-070		X							
247	MFN 03-070		X							
248	MFN 03-070		X							
249	MFN 03-070		X							
250	MFN 03-070		X							
251	MFN 03-070		X							
252	MFN 03-070		X							
253	MFN 03-070	X								
254	MFN 03-070	X								
255	MFN 03-070	X								
256	MFN 03-070	X								
257	MFN-03-057	X								
258	MFN-03-057	X								
259	MFN 03-082	X								
260 deleted										
261 deleted										
262	MFN-03-078	X								
263	MFN 03-070	X								
264	MFN 03-080	X								

RAI #	Letter	ESBWR SCALING	ESBWR Test and Analysis Program Description	ESBWR Test Report	SBWR Testing Summary RPT	TRACG Qualification for SBWR	TRACG Application for ESBWR	TRACG Model Description	TRACG Qualification	TRACG Qualification for ESBWR
265	MFN 03-070	X								
266	MFN-03-057	X								
267	MFN 03-070	X								
268	MFN 03-070	X								
269	MFN 03-070	X								
270	MFN 03-070	X								
271	MFN 03-080	X								
272	MFN-03-064	X					X			
273	MFN 03-070	X								
274	MFN 03-070	X								
275	MFN-03-057	X								
276	MFN-03-057	X								
277	MFN-03-078	X								
278	MFN 03-070	X								
279	MFN-03-057	X								
280	MFN 03-070	X								
281	MFN-03-057	X								
282	MFN 03-082	X								
283	MFN 03-070	X								
284	MFN 03-070	X								
285	MFN 03-070	X								
286	MFN 03-079	X								
	MFN 03-117	X								
287	MFN 03-070	X								
288	MFN 03-070	X								
289	MFN 03-070	X								
290	MFN-03-078	X								
291	MFN 03-070	X								
292	MFN 03-079	X								
	MFN 03-117	x								
293	MFN 03-079	X								
294	MFN-03-078	X								
295	MFN 03-079	X								
296	MFN-03-064			X						
297	MFN-03-064			X						
298	MFN 03-080						X			
299	MFN 03-080						X			
300	MFN 03-070						X			
301	MFN 03-079						X			
302	MFN 03-070						X			
303	MFN 03-070						X			
304	MFN 03-080						X			
305	MFN 03-080							X		
306	MFN 03-100							X		
	MFN 03-104 supplem info							X		
	MFN 03-115 supple to 306							X		
307	MFN 03-080							X		

RAI #	Letter	ESBWR SCALING	ESBWR Test and Analysis Program Description	ESBWR Test Report	SBWR Testing Summary RPT	TRACG Qualification for SBWR	TRACG Application for ESBWR	TRACG Model Description	TRACG Qualification	TRACG Qualification for ESBWR
308	MFN-03-078							X		
309	MFN 03-082						X			
310	MFN 03-080						X			
311	MFN 03-082						X			
312	MFN-03-078							X		
313	MFN-03-078							X		
314	MFN-03-078							X		
	MFN 03-115 supple to 314.1									
315	MFN-03-078 mfn-03-117 SUPPLEMENT							X		
316	MFN 03-099							X		
317	MFN 03-080						X			
318	MFN 03-070						X			
	MFN 03-099 ADD INFO						X			
319	MFN 03-100						X			
320	MFN 03-070						X			
321	MFN 03-080						X			
322	MFN 03-070						X			
	MFN 03-115 supple to 322									
	MFN 03-127 supple to 322									
323	MFN 03-079						X			
	MFN 03-115 supple to 323.4									
324	MFN 03-080						X			
325	MFN 03-079						X			
326	MFN 03-080						X			
327	MFN-03-064						X			
328	MFN 03-070						X			
329	MFN 03-080						X			
	MFN 03-115 supple to 329									
330						X	X		X	
330.4 Suppl	MFN 03-141, part 2 table								X	
330.4 Suppl	MFN 03-147								X	
331	MFN 03-080						X			
332	MFN 03-070						X			
333	MFN 03-082						X			
334	MFN-03-064			X	X					
335	MFN-03-064			X	X					
336	MFN-03-064			X						
337	MFN-03-064			X	X					
338	MFN-03-064			X	X					
339	MFN 03-104			X	X					
339 Rev .1	MFN 03-079			X	X					
340	MFN 03-070			X	X					
341	MFN 03-070			X	X					
342	MFN 03-070			X	X					
343	MFN 03-070			X	X					

RAI #	Letter	ESBWR SCALING	ESBWR Test and Analysis Program Description	ESBWR Test Report	SBWR Testing Summary RPT	TRACG Qualification for SBWR	TRACG Application for ESBWR	TRACG Model Description	TRACG Qualification	TRACG Qualification for ESBWR
344	MFN 03-070			X	X					
345	MFN-03-064			X	X					
346	MFN-03-078			X						
347	MFN-03-064			X						
348	MFN 03-070			X	X					
349	MFN-03-064			X						
350	MFN-03-064			X						
351	MFN-03-064			X						
352	MFN-03-064			X						
353	MFN-03-064			X						
354	MFN-03-064			X						
355	MFN-03-064			X						
356	MFN-03-064			X						
357	MFN-03-064			X						
358	MFN-03-064			X						
359	MFN-03-064			X						
	MFN 03-117supple to 259 & 286									
360	MFN-03-078				X					
361	MFN 03-070				X					
362	MFN 03-070				X					
363	MFN-03-078				X					
364	MFN 03-070				X					
365	MFN 03-070				X					
366	MFN 03-070				X					
367	MFN 03-070				X					
368	MFN 03-070				X					
369	MFN 03-070				X					
370	MFN 03-070				X					
371	MFN-03-064				X					
372	MFN-03-064				X					
373	MFN-03-064				X					
374	MFN-03-064				X					
375	MFN-03-064				X					
376	MFN-03-064				X					
377	MFN 03-070				X					
378	MFN-03-064				X					
379	MFN-03-064				X					
380	MFN-03-078				X					
381	MFN-03-078				X					
382	MFN 03-079				X					
383	MFN-03-078				X					
	MFN-03-082				X					
384	MFN-03-078				X					
385	MFN-03-078				X					
386	MFN 03-070				X					
387	MFN 03-080						X			
388	MFN 03-080						X			

RAI #	Letter	ESBWR SCALING	ESBWR Test and Analysis Program Description	ESBWR Test Report	SBWR Testing Summary RPT	TRACG Qualification for SBWR	TRACG Application for ESBWR	TRACG Model Description	TRACG Qualification	TRACG Qualification for ESBWR
389	MFN-03-078				X					
390	MFN-03-078				X					
391	MFN-03-078				X					
392	MFN-03-078				X					
393	MFN-03-078				X					
394	MFN-03-078				X					
395	MFN-03-078				X					
396	MFN-03-078				X					
397	MFN-03-078				X					
398	MFN-03-078				X					
399	MFN-03-078				X					
400	MFN-03-078				X					
401	MFN-03-078				X					
402	MFN-03-078				X					
403	MFN-03-078				X					
404	MFN-03-078				X					
405	MFN-03-078				X					
406	MFN 03-080						X			
	MFN 03-115 suppl to 406									
	MFN 03-127 suppl to 406									
	MFN 03-132 suppl to 406						X			
	MFN 03-144						X			
406 (TRACG Model chan	MFN 03-145	Drop, superceded by MFN 04-069						X		
407	MFN 03-070						X			
408	MFN 03-080						X			
409	MFN 03-070		X							
410	MFN 03-070		X							
411	MFN 03-070		X							
412	MFN 03-070		X							
413	MFN 03-070		X							
Addl suppl on scaling	MFN 03-140	X								
Addl suppl on Model	MFN 03-141							X		
A1	MFN 04-23						X			
A2	MFN 04-23						X			
APP case update	MFN 04-58						X			
QUAL update	MFN 04-59									X
A3	MFN 04-65						X			
TRACG Model changes	MFN 04-69							X		
A4	MFN 04-70						X			
The following responses to information requests have been excluded from the LOCA SER										
1132 bundle core design	MFN 04-63	AOO								
PANAC info	MFN 04-71	AOO								
1132 bundle vessel inter	MFN 04-72	AOO								

RAI #	Letter	ESBWR SCALING	ESBWR Test and Analysis Program Description	ESBWR Test Report	SBWR Testing Summary RPT	TRACG Qualification for SBWR	TRACG Application for ESBWR	TRACG Model Description	TRACG Qualification	TRACG Qualification for ESBWR
PANAC info	MFN 04-77	AOO								
AOO ref inputs	MFN 04-83	AOO								
PANAC info	MFN 04-95	AOO								
TRACG control system	MFN 04-96	AOO								

## NRC RAIs and Responses

### TRACG Application for ESBWR NEDC-33083P

Note: RAI responses including data files that cannot be read on a PC are not included.

Q1. The ESBWR input deck for ECCS/LOCA analysis (Gdl-nl2.inp) defines the axial flow area fractions of all rings at level 23 [[

]]

Is this true? If it is, is it physical? (In file "Gdl-nl2.inp", the following two lines were given:

[[

]] E)

R1. Yes, [[

]] in this case. The baseline case (GDL-NL2.INP) simulates

[[

]] Section 2.4.4.3 discusses the

results of sensitivity study on interactions between ECCS and containment.

Q2. Is the suppression pool spill over line explicitly modeled by both ECCS/LOCA and containment analysis TRAC-G models. If not, please provide an explanation.

R2. The suppression pool spillover pipes are not modeled in both the ECCS/LOCA and Containment/LOCA TRACG input models. The water level in the DW does not reach the spillover hole elevation in the cases presented in the application report.

Q3. Does radius distortion in the TRAC-G ECCS/LOCA model for the containment part affect the 3-D vessel numerical scheme and the overall containment response? (Both the stacked approach and large volume fraction and flow area fraction.) Please provide the explanations regarding the impact on the containment response.

R3. The radius distortion would affect the momentum exchange terms. The impact on the containment response is expected to be very small due to the relatively large radial flow area in the containment and consequently the small magnitude of the velocities and momentum fluxes. This can be seen by examining the pressure drop in the radial direction. Figure 3.1 shows the pressure difference at the top of drywell between the first cell and the fourth cell, for the ECCS/LOCA baseline case. The pressure difference is on the order of [[ ]]. Hence the radius distortions are of no consequence. [[

Figure 3.1

]]

Q4. It was indicated that decay heat table was used to define the core total power history during the GDCS line break LOCA. Is the initial full power operating condition and the subsequent scram considered in the decay heat table? If not, please explain.

R4. The total power table used for the ECCS LOCA calculations is the sum of the fission and decay heat components. The fission power following scram is based on a representative fission power decay used in BWR LOCA analysis. This includes the effects of void reactivity feedback, which can be dominant for a large break. The decay heat table is a fit to the ANS standard. (ANSI/ANS-5.1-1994). The total power table assumes that scram and CRDs start at time 0.0 (baseline case). This assumption is expected to have very minor impact on the key calculated parameter, such as the minimum static head level inside shroud.

For GDCS line break, reactor scrams on high drywell pressure of 2 psid, which occurs at about [[ ]] (Note 1) after the break initiation. The signal response time is [[ ]] and the CRDs start to insert [[ ]] later. The total time between the break initiation and the CRDs first movement is [[ ]] A sensitivity study case was performed to show the impact of the simplified assumption used in the baseline case. In this case, the time scale in the baseline power table is shifted by adding [[ ]] and this case assumes 100% constant power from [[ ]]

Figures 4.1 and 4.2 show the static head inside shroud for the baseline case and the sensitivity study case. For the sensitivity study case, the Level 1 trip occurs at about [[ ]] earlier than the baseline case. This change in timing to L1 is the only significant effect of the delayed scram. After the Level 1 trip, which initiates the GDSCS injection, the responses of the static head inside shroud for these cases are very similar. Figure 4.3 compares the results of these two cases, with a time shift corresponding to the shift of the Level 1 trip timing. This figure shows that these two curves are almost on top of each other, after the Level 1 trip. The minimum static head level for the sensitivity study case is [[ ]] lower than the baseline case. Therefore the impact on ECCS performance margin is minor.

(Note 1: The scram trip time of [[ ]] is calculated from the drywell pressure response in the first [[ ]] of the sensitivity study case.)

[[

Figure 4.1. Baseline case – CRDs start at 0.0 second

Figure 4.2. Sensitivity case – CRDs start at 6.05 seconds.

Figure 4.3. Comparison of Static Head Inside Shroud

]]

- Q5. It is assumed that the PCCS condensate accumulation tank has an initial void fraction of [[ ]] (\*\*\*\*\* ALPN VSSL000129ALPN0 [[ ]] E). [[ ]] Please clarify. If not, what is the impact to the analysis results?
- R5. The current configuration of the PCCS condensate drain tanks are correctly defined in the response to Q 195. The plant design had been evolving and an earlier version indeed had some water in the drain tanks to provide a loop seal. The impact of the assumed water (approximately 10 m3) in the TRACG deck are not expected to impact the analyses. For the ECCS/LOCA analysis the minimum water level is determined by the timing of the GDCS flow and not the size of the GDCS drain tank and flow. Compared to the GDCS pool capacity of [[ ]] (for all three pools), the PCCS condensate drain tank capacity is insignificant. For the Containment/LOCA analysis, the PCCS condensate drain tank has almost no impact, because the containment pressures are determined primarily by the large free air spaces in the drywell [[ ]] and wetwell [[ ]] and GDCS drain down volumes.
- Q6. Is there a matrix of TRACG calculations (Design Record Files) to support TRACG validation, assessment for ESBWR application and ECCS/Transient analyses? If not, please provide a table which lists all the TRACG calculations within the scope of ESBWR pre-application.
- R6. Tables 6-1 and 6-2 summarize the ESBWR TRACG ECCS/LOCA and Containment/LOCA cases within the scope of the ESBWR Application Report (NEDC-33083P).

[[ Table 6-1. Summary of ESBWR TRACG ECCS/LOCA Cases

Table 6-1. (Continued)

Table 6-2. Summary of ESBWR TRACG Containment/LOCA Cases

- Q7 Please explain the process of developing the ESBWR core model for three transient calculations documented in NEDC-33083P, "TRACG Application for ESBWR." More specifically, the core fuel loading pattern, burn-up distribution, control rod insertion pattern, ect.
- Q8 Please provide the ESBWR specific GE-12 fuel bundle design data and F-type control rod data.

**Hypothetical ESBWR Core Design**  
***Response to NRC RAI numbers (7 and 8)***  
***And Analysis Files***

1. BOC\_Exposure.xls
2. BOC\_UH.xls
3. EOC\_Exposure.xls
4. EOC\_UH.xls

1. Introduction

This document describes a hypothetical equilibrium ESBWR core design containing 1020 fuel bundles similar to GE12. This document will be used by the U.S. NRC to setup and perform calculations that can be compared to results obtained from TRACG. Other details regarding ESBWR evaluations are outside the scope of this document.

2. ESBWR F-Lattice Core Design

The purpose of this section is to describe the methods used in the core and fuel design for the ESBWR F-Lattice core. In general, these methods can be used with any standard BWR simulation code.

[[

]]

Figure 2-1, F-Lattice Configuration

[[

]]

Figure 2-2, ESBWR Core Configuration (showing Control Cells)

[[





---

<sup>1</sup> This procedure was benchmarked by comparison with a quarter-core case with the center rod out.

]]

2.1 Hot Excess Reactivity

[[

]]

2.2 Cold Shutdown Margin

[[

]]

2.3 Maximum Linear Heat Generation Rate

[[

]]

2.4 Minimum Critical Power Ratio

[[

]]

2.5 Fuel Cycle Summary

[[

]]

Table 2-1, Fuel Cycle Characteristics  
[[

]]

Table 2-2, Thermal Operating Limits for the Equilibrium Cycle

[[

]]

3 Panacea Wrapups

[[

]]

**Table 3-1 PANACEA Wrapups**

[[

]]

**4 Bundle Designs**

[[

]]

**Table 4-1 Bundle Lattices**

[[

]]

[[

]]

5. Core Design

[[

]]

Table 5-1 General Core Information

[[

]]

[[

]]

6. References

- [1] General Electric Fuel Bundle Designs, NEDE-31152P, Revision 7, June 20

## **Appendix A**

### **Hypothetical ESBWR Bundle Design**

[[





## **Appendix B**

### **PANAC10 Summary “ARK” Edits for Rodded Depletion**

[[



















## **Appendix C**

### **PANAC11 Summary Edits for “Haling” Depletion**

[[

















]]

## **Appendix D**

### **Reference GE12 Design Basis Specifications**

[[



]]

---

**Appendix E**  
**F-Lattice Control Rod Data**

**F-Lattice Control Rod Position**

The distance a control rod is *inserted* into a BWR core is:

$$D = HCR - CRS * (NOTCH / NNOTCH)$$

where NOTCH is the control rod notch position (in notches withdrawn), HCR is the height of a fully inserted rod, CRS is the control rod stroke and NNOTCH is the number of notches in a full stroke. [[ ]]

$$NNOTCH = [[ ]]$$

$$HCR = [[ ]]$$

$$CRS = [[ ]]$$

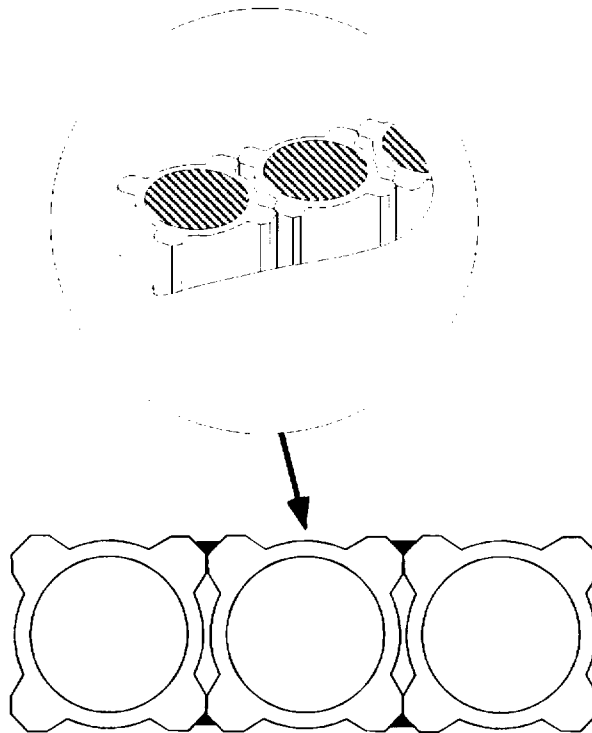
**F-Lattice Control Rod Design Parameters (Marathon Design)**

The following table identifies the differences between the F-Lattice control blade and the original equipment N-Lattice (see reference figure on page D2). The following figure (next page) identifies the further manufacturing details of the F-Lattice Marathon design.

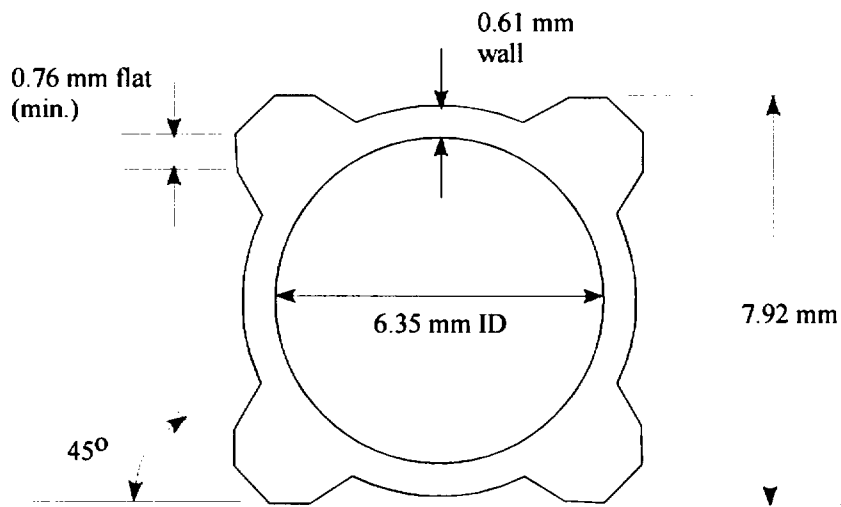
[[

]]

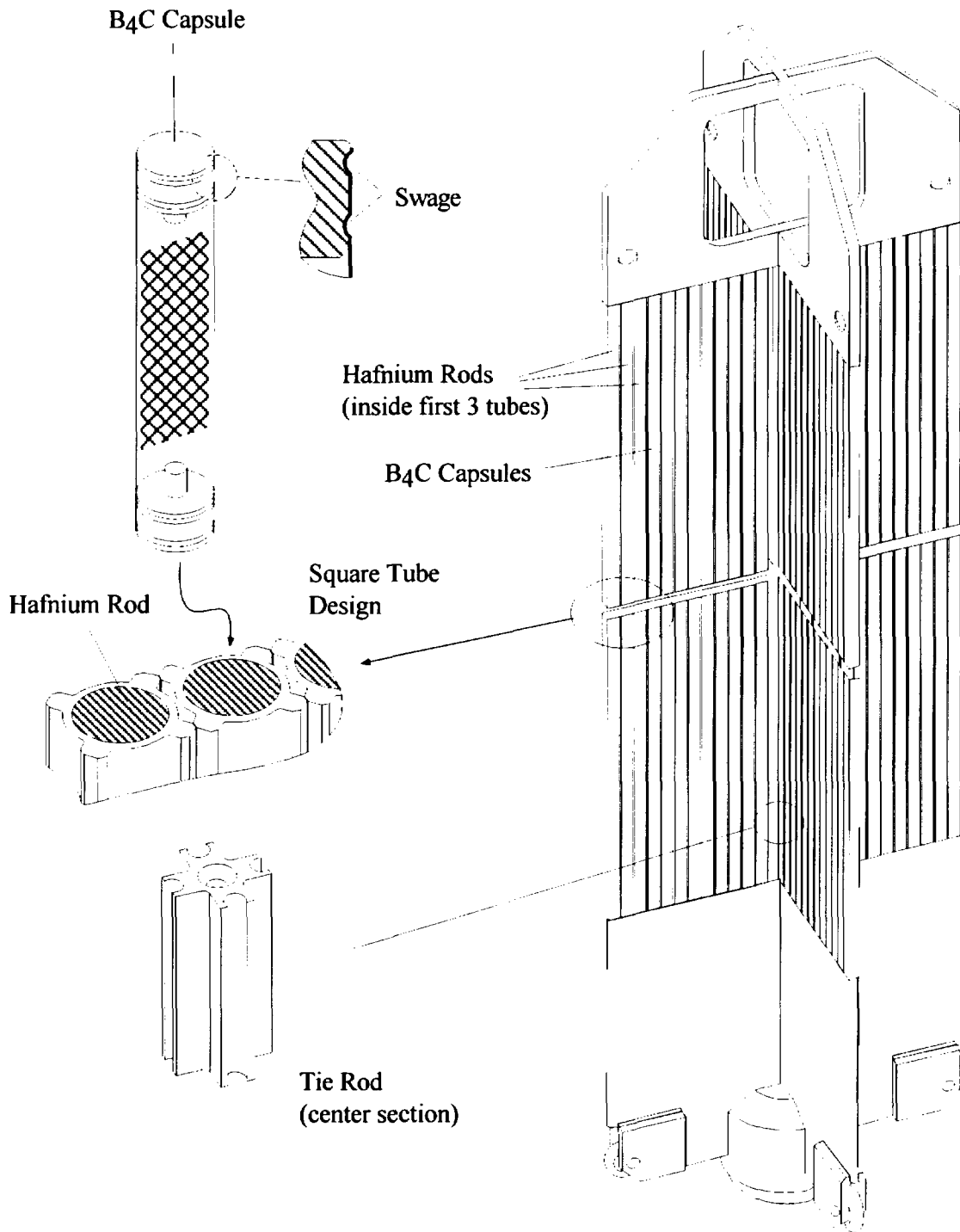
Square Tube  
Design



Welds



The data and calculations provided are preliminary pending detail design.



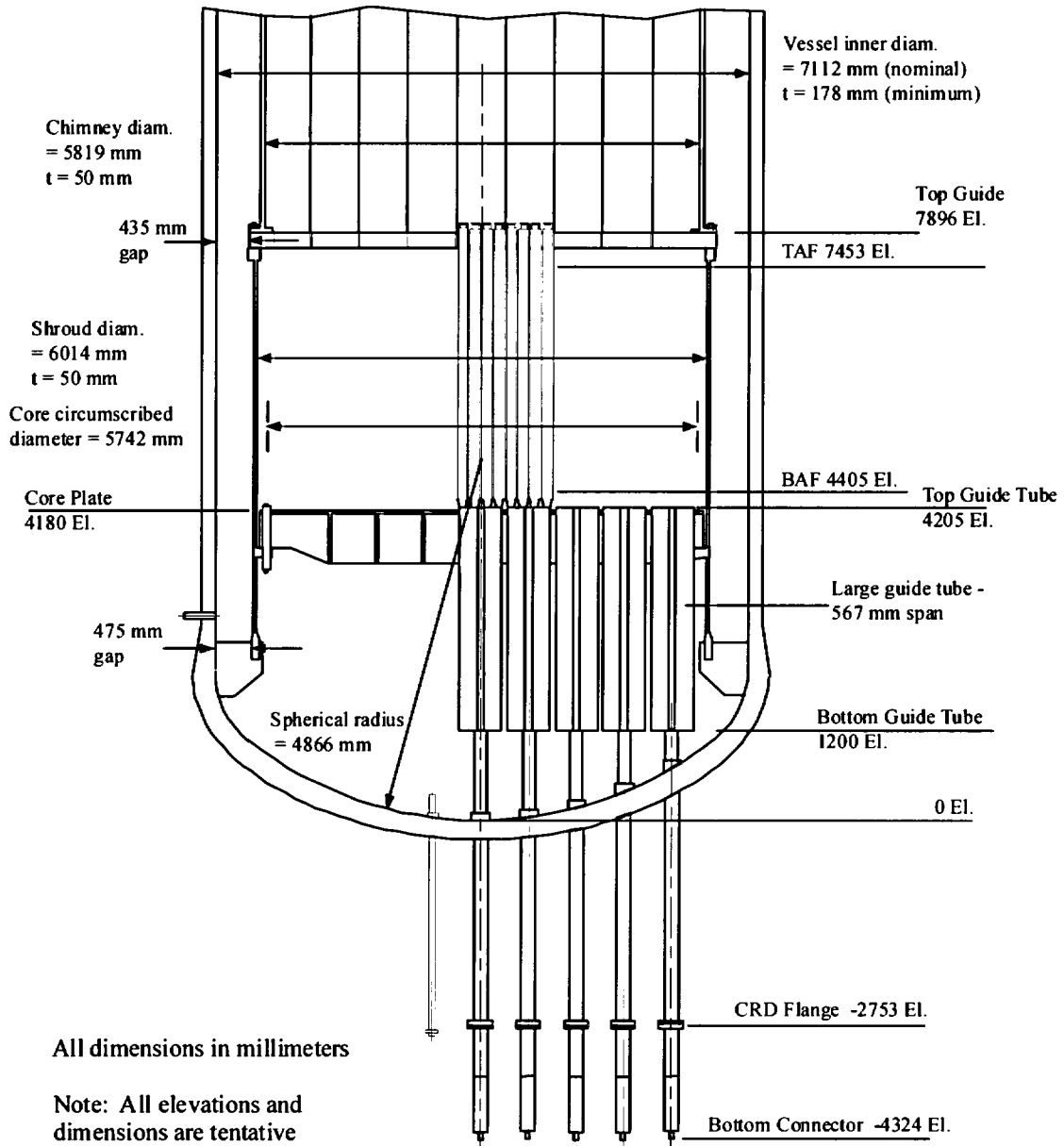
**Marathon Control Rod**

The data and calculations provided are preliminary pending detail design.

- Q9 Please provide a large scale drawing of the ESBWR vessel and the vessel internals with major dimensions and elevations.
- R9. The following figures and table provide the major dimensions and elevations of the ESBWR vessel, internals and containment.

**Figure 9.1. ESBWR Reactor Key Features**

Figure 9.2. ESBWR RPV with 10 ft Fuel



**ESBWR Lower Plenum - 10 ft Fuel**  
 Figure 9.3. ESBWR Lower Plenum with 10 ft Fuel

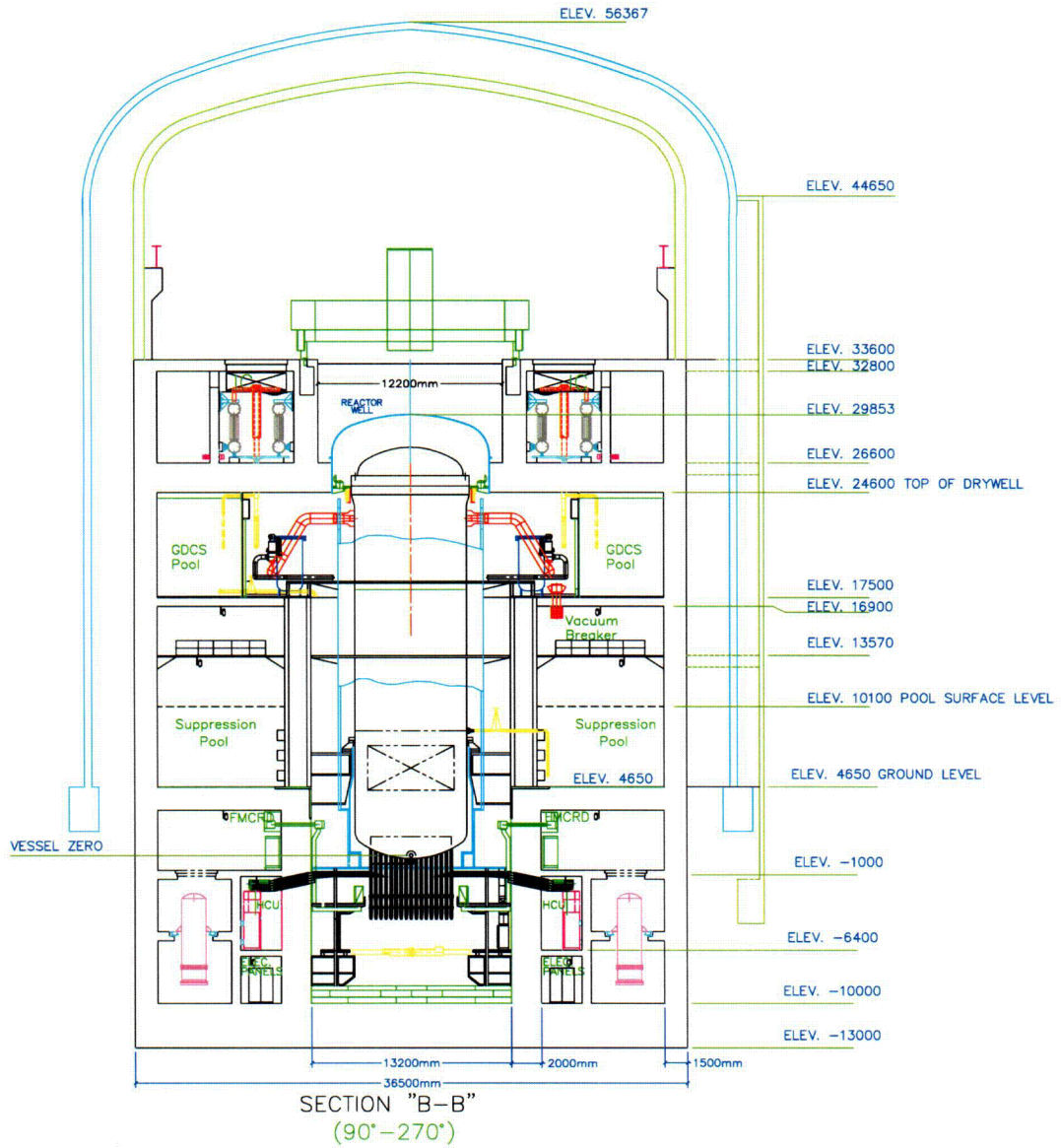


Figure 9.4. ESBWR Sectional View (90° – 270°)

Note: All elevations and dimensions are tentative pending detail design.

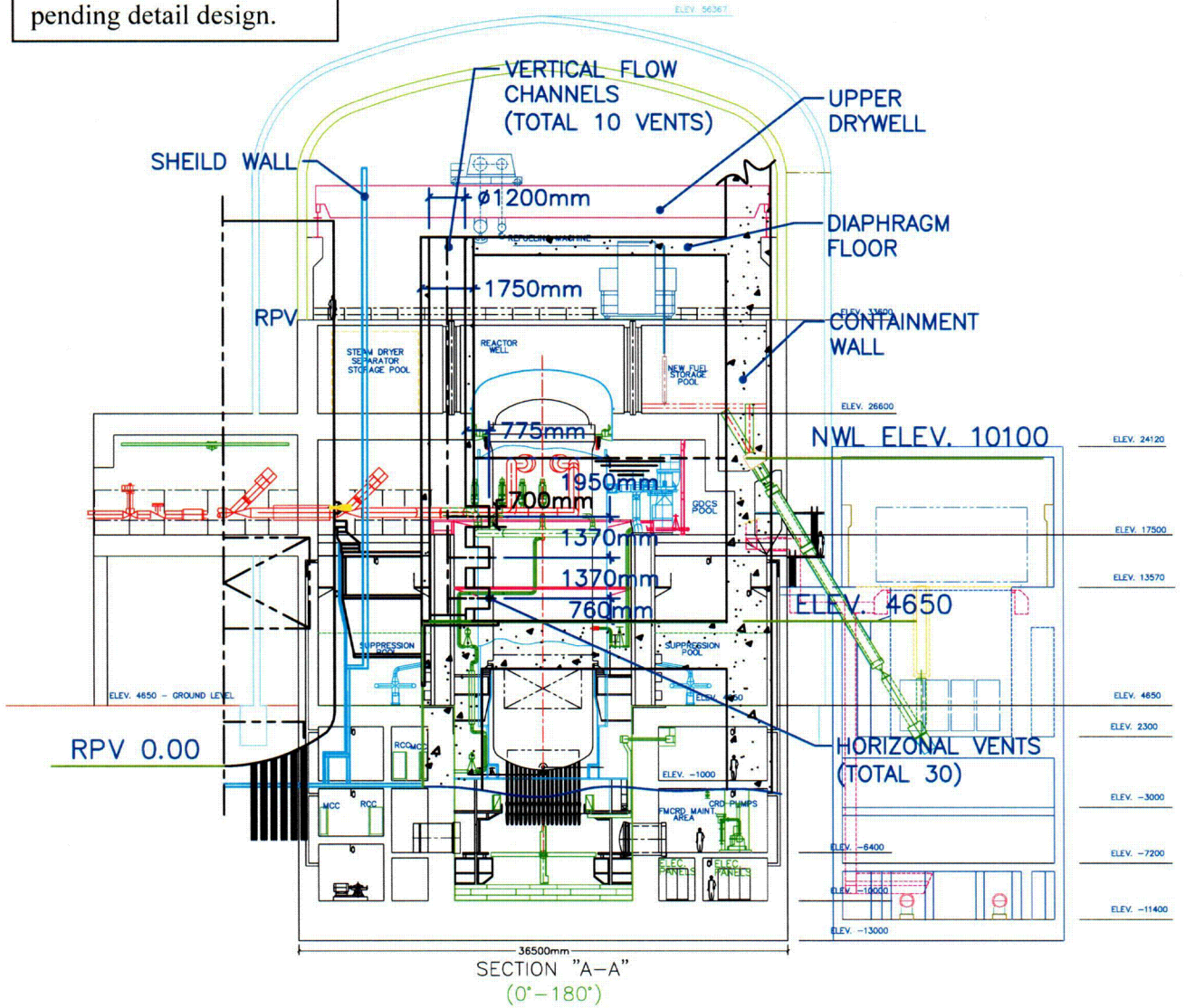


Figure 9.5. ESBWR Sectional View (0° - 180°)

Figure 9.6. ESBWR Horizontal Vent System

Volume #	Description	Free Air Volume (m <sup>3</sup> )
VOLUME 0	Lower Drywell 0	1203.
VOLUME 1	Lower Drywell 1	361.
VOLUME 2	Drywell Annulus	906.
VOLUME 3	Upper Drywell	3947.
VOLUME 4	Upper Drywell Head	259.
VOLUME 5	GDCS Air Space	82.
VOLUME 6	Wetwell Air Space	4504.
		Water Volume (m <sup>3</sup> )
VOLUME 7	GDCS Pool Drainable Water	1480.
VOLUME 8	Suppression Pool	3610.

Table 9.1. Summary of Key Volumes (See Figure 7 for Location)

Figure 9.7. Location of Key Volumes in Table 1

- Q10. For the ECCS/LOCA model, how many PCCS units are lumped into one set of TRAC-G 1-D components? 3 or all 4 of them?
- R10. 4 PCCS units are lumped into one set of TRACG 1-D components in the ECCS/LOCA model.
- Q11. PIPE 42 and PIPE 43 are used to model GDCS air space to wetwell air space vents. However, they have identical volume and flow area. Why?
- R11. For simplification, identical volume and flow area were used for PIPE 42 and PIPE 43 in the ECCS/LOCA model. The pressure difference between the GDCS air space and the wetwell is very small because flows are generally small and resistance is minor. Therefore, the results are not affected by this simplification.
- Q12. The input deck "Mslb-n.inp" has the following input card: "VSSL000101DSTH0  
[[ ]]" Is [[ ]] used to define the vessel wall thickness? If it is, is ESBWR reactor pressure vessel designed to have a thickness of [[ ]] Could you please clarify?
- R12. The double-sided heat slab in the second ring of the VSSL component has a thickness of [[ ]] This double-sided heat slab is used to [[  
]] to model the heat transfer from the RPV inside to the DW air space.
- The impact of this composite wall modeling on the long-term drywell pressure is expected to be small. A parametric study case was performed, replacing the composite wall by carbon steel with thickness of 7.25", which is typical material and thickness for the RPV outside wall. Result of this parametric case shows that the impact on peak drywell pressure is small, about [[ ]]
- Q17. Please add the PCCS vent submergence to "ESBWR Horizontal Vent System" figure. Is the top elevation of the suppression pool gas volume (i.e., lower surface of diaphragm floor between DW and WW) at 16900 mm? And, please provide a figure showing the top view (including azimuthal and radial locations of the 10 vertical vent pipes) of the horizontal vent system with radial dimensions.
- R17. The top elevation of the suppression pool gas volume is at 16900 mm. Figures 17.1 and 17.2 provide additional information on the PCC vent exit and the top view of the vent pipes. For the main steam break case, the suppression pool collapse level following the blowdown is at an elevation of [[ ]] from the RPV bottom.

**Figure 17.1. Horizontal Vent System and PCC Vent Pipe**  
(Note: All elevations and dimensions are tentative pending detail design)

Figure 17.2. Horizontal Vent System (Top View)  
(Note: All dimensions are tentative pending detail design)

- Q18. Please provide a table listing the height (in reference to the inner surface of pool bottom) of Isolation Condenser (IC)/PCCS pools, the normal water level in these pool, the elevation of the top of the condenser tubes (or the bottom elevation of the top header), the normal “total water volume” in the IC/PCCS pools (with the presence of IC and PCC condensers), and the maximum water volume filling to the top of the pools with the presence of IC and PCCS condensers.
- R18. Figure 18.1 shows the height and elevations. The ID of lower and top headers of PCC is [[ ]]. Figure 18.2 shows the water volumes in various pools.

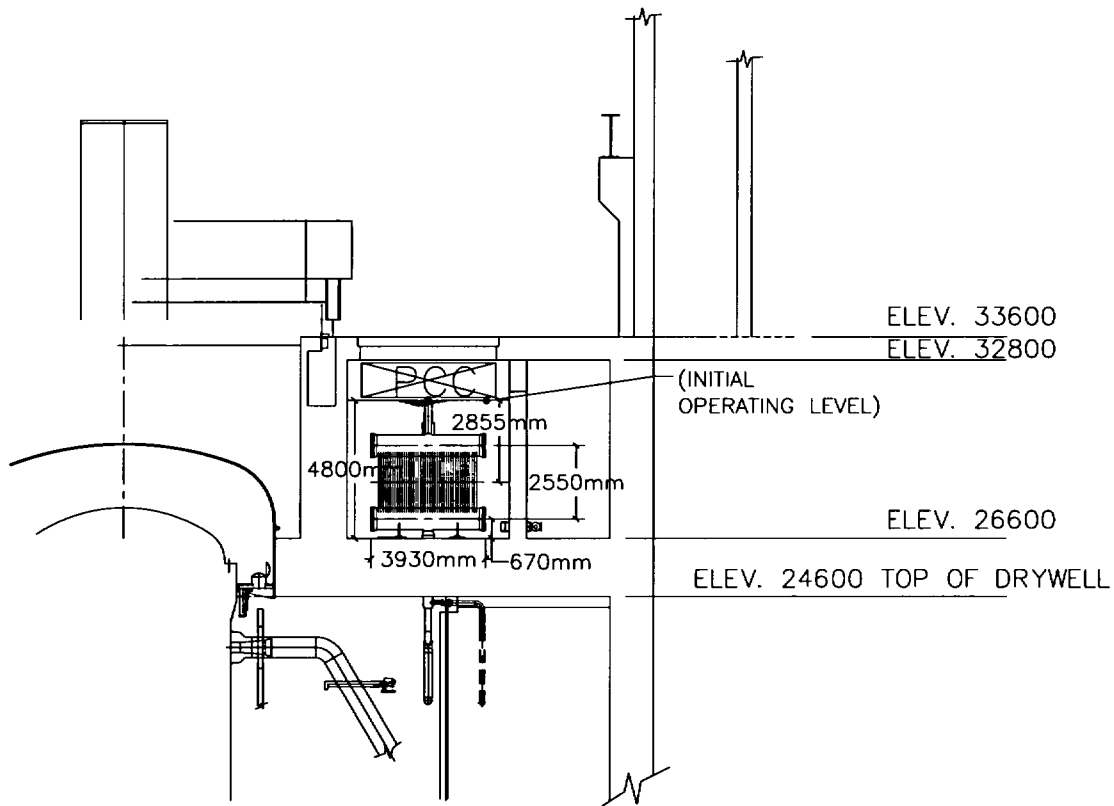


**Figure 18.1. ESBWR PCC Pool**  
**(Note: All elevations and dimensions are tentative pending detail design)**

Figure 18.2. Total Water Volume available for IC/PCC HXs [[ ]]  
(Note: All elevations and dimensions are tentative pending detail design)

- Q19. Does Volume 0 communicate freely with Volume 1 in the “Location of Key Volumes in Table 1,” figure? What is the rationale or advantage to separate these two volumes? Will the loss-of-coolant accident (LOCA) break flow and the condensed steam on the drywell wall fill up Volume 0 first and then Volume 2 next?
- R19. Volume 0 communicates freely with Volume 1. The Vessel Zero elevation is chosen as one of the axial “Levels” in the TRACG nodalization. The free air volumes in Volumes 0 and 1 are calculated accordingly. In the case of LOCA, condensate and liquid from breaks will fill up lower volumes first, in the order of Volume 0, 1 and 2.

- Q20. Please provide a sketch showing how a fuel assembly is supported on the core plate and the various leakage paths between fuel assemblies and the bypass region of the ESBWR.
- R20. Figure 20.1 shows the Standard BWR bypass leakage paths. Figure 20.2 shows “F” lattice bypass leakage paths for ESBWR. Figure 20.3 shows the “F” lattice core plate partial section view, and Figure 20.4 shows “F” lattice core plate isometric – partial section view.

Figure 20.1. Standard BWR Bypass Leakage Paths

Figure 20.2. "F" Lattice Bypass Leakage Paths

Figure 20.3. "F" Lattice Core Plate Partial Section View

Figure 20.4. “F” Lattice Core Plate Isometric – Partial Section View

- Q21. Provide instrumentation diagrams for the RPV that show all the safety-related instrument locations for measuring pressures, temperatures, water levels (or differential pressure), and gas concentrations in the RPV (for initiating reactor scram and containment isolation). Show Levels 0.5, 1, 2, 3, 8, and 9, normal water level, top of active fuel (TAF), and bottom of active fuel (BAF).
- R21. These instrumentation diagrams will be submitted as part of the SAR. The current design information has only been submitted as a reference for review of the analysis methods and testing. The DW and WW instrumentations are design issues and are not part of the current NRC review scope.

Figure 21.1 and Table 21.1 show the RPV levels and setpoints. These values are tentative pending detail design.

Figure 21.1. ESBWR Water Levels

Table 21.1. Summary of ESBWR RPV Levels\*

- Q22. Will Level 9, Level 3, Level 2, Level 1, or Level 0.5 initiate a reactor scram if reactor is not yet scrammed? Please explain the logic for the Level 2 initiation of a joint automatic depressurization system (ADS) inhibit plus standby liquid control system (SLCS) initiation with a concurrent “APRM Not Downscale” signal.
- R22. The reactor will scram and isolate when the water level rises to Level 8 position that is below the Level 9 elevation. Similarly, the reactor will scram when the water level drops to Level 3 position that is above the Level 2 elevation.
- Q23. After Level 1 is confirmed, describe the actuation sequence and time delay of 12 safety relief valves (SRVs), 8 depressurization valves (DPVs), 8 gravity driven cooling system (GDCCS) injection valves, and 4 PCCS drain tank valves.
- R23. The actuation sequence and time delay are summarized in Table 23.1. These values are tentative pending detail design. The SRV distribution is as follow. Each main steam line connects to 3 SRVs. Main steam lines # 1 and # 3 have 1 SRV with 0.0 second delay time and 2 SRVs with 10. seconds delay time. Main steam lines # 2 and # 4 have 2 SRVs with 0.0 second delay time and 1 SRV with 10. seconds delay time.

**Table 23.1. Actuation sequence and delay time for ADS and GDCS valves**

Q24. How many nozzles does the RPV have? What are the inside diameters of each nozzle?

R24. Table 24.1 summarizes the ESBWR RPV nozzles and LOCA break areas.

Table 24.1. Summary of ESBWR RPV Nozzles and LOCA Break Areas

ESBWR RPV Nozzles and LOCA Break Areas

Name	Quantity	Break Area (one)
Main steam nozzle	4	152.4 in <sup>2</sup>
Feedwater nozzle	6	130 in <sup>2</sup>
DPV / IC nozzle	4	<152.4 in <sup>2</sup>
RWCU / SDC nozzle	2	101.6 in <sup>2</sup>
I.C. Return nozzle	4	26.1 in <sup>2</sup>
GDCS nozzle	8	7.07 in <sup>2</sup>
GDCS equalizing nozzle	4	3.14 in <sup>2</sup>
PCCS condensate return nozzle	4	26.1 in <sup>2</sup>
SLC nozzle	2	2.95 in <sup>2</sup>
Bottom drain nozzle	4	3.14 in <sup>2</sup>
Vent nozzle	1	2.95 in <sup>2</sup>
Vibration instrumentation	1	45.7 in <sup>2</sup>
Instrument nozzles (reference leg)	4	2.99 in <sup>2</sup>
Instrument nozzles	12	0.75 in <sup>2</sup>
Seal leak detection nozzle	1	0.21 in <sup>2</sup>
CRD housing nozzle		1.9 in <sup>2</sup>
Incore instrument housing nozzle		3.14 in <sup>2</sup>

Q26. The GE report NEDC-33083P presented main steam line break (MSLB) and gravity driven cooling system line break (GDCSLB) loss of coolant accidents (LOCAs) (Section 3.2.1, Page 3-6), but not a bottom drain line break (BDLB). Is a BDLB LOCA considered less limiting than the other two LOCAs? If yes, please explain.

R26. Yes. BDLB LOCA is considered less limiting than the other two LOCAs. The long-term peak drywell pressure depends on the effective wetwell airspace volume, which is the sum of initial wetwell airspace volume and the GDCS pool draindown volume. For both the BDLB and GDCSLB cases, the entire drainable volume of the GDCS pools will drain down and create larger draindown volume as compared to the MSLB case, resulting in lower drywell pressure. Compared to the GDCSLB, the BDLB cases have milder responses due to smaller liquid break pipe size.

Q27. The isolation condenser system (ICS) has not been considered in the LOCA calculations. Condensate return from ICS may delay opening of the depressurization valves (DPVs). Is this a conservative assumption?

R27. The IC operation has several effects when it operates. It takes some of the steam produced in the vessel and condenses it and returns it to the vessel. The steam condensation has the effect of reducing the vessel pressure faster. The faster initial depressurization reduces inventory loss following ADS operation and possibly results in earlier initiation of the GDCS. Additionally, the IC returns the condensate directly to the vessel. This later effect will have a greater impact and will result in a higher minimum water level during a LOCA.

Although IC operation may delay opening of the DPVs, the net impact of the IC operation is positive. Therefore, not considering IC operation is a conservative assumption.

Q28. The passive containment cooling system (PCCS) performance depends on the pressure difference between drywell (DW) and wetwell (WW) and not having any other path than the PCCS (the only path between them being through the PCCS). A GDCSLB with a single failure of the check valve can potentially create bypass between DW and WW, and compromise the PCCS performance. Please explain why this is not considered or why this is not possible.

R28. Please refer to the simplified system schematic (figure 28.1), which shows that the GDCS suction line is placed in a long, vertical sump that extends several meters below the bottom elevation of the GDCS Pool. The GDCS sump is formed from a heavy-walled stainless steel pipe that runs adjacent to the outer bounding wall of the suppression pool and is structurally supported from this wall. The GDCS injection piping in this region reaches downward to the sump bottom but maintains an appropriate clearance such that inordinate flow entry losses are

avoided. The depth and diameter of the sump are selected to ensure that the necessary residual inventory of water to maintain the loop seal intact and functioning is always present throughout the post-LOCA period.

If the GDCS injection line to the vessel were to break at a non-conservative location and the biased open check valve failed, water would siphon out of that GDCS pool, flooding the lower drywell as designed. The water in the suction line sump would only drain down to the level of the lowest pipe break elevation, leaving water in the sump to provide a seal sufficient to prevent bypass flow from the drywell to wetwell or vice-versa.

ESBWR Gravity-Driven Cooling System - Simplified Schematic Diagram

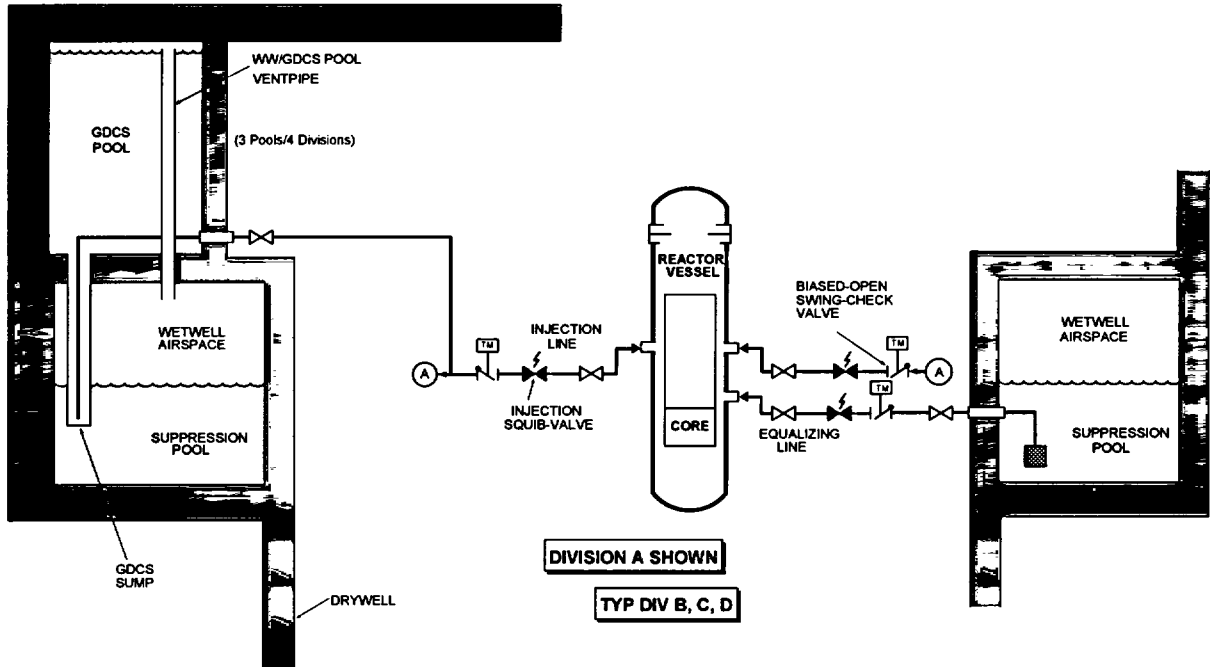


Figure28.1

- Q29. What are possible single failure criteria? Should the failure of vacuum breaker (VB) be considered as a single failure? If not, please explain why not.
- R29. The failure of one out of the three vacuum breakers could be considered highly unlikely (based on an extensive test program) however there is a remote possibility that it would fail and then it would be considered as a single failure if it did not close. This possibility exists but the vacuum breakers are backed up with a manually controlled valve that can close the inlet to any vacuum breaker determined to be open or not fully closed. Refer to Section 3.3.7.3 of Document NEDC-33079P, "Test and Analysis Program Description"
- Q30. Section 3.6, NEDC-33083P, states that a bounding calculation was performed with conservative values of all parameters and initial conditions. Were there any studies performed that the combination of the worst values would generate the conservative results?
- R30. There were no specific studies performed to show that the combination of the worst values would generate the conservative results for ESBWR. However, results from previous studies for SBWR suggested that this approach would generate conservative results.

Uncertainty analysis was performed for the SBWR containment (NEDE-32178P, Sect. 4.3.2) with 59 TRACG trial runs. In these studies, specific uncertainties were defined for a total of [[

]] The difference in the peak containment pressures (results from 72 hours), that is the difference between the highest calculated value in 59 runs and the calculated value with base case conditions (delta containment pressure), is about [[ ]]

The magnitudes of uncertainties and individual perturbations are similar between the SBWR and the ESBWR. It is reasonable to expect that if an uncertainty analysis (59 trial runs) were performed using the full set of 24 TRACG inputs for the ESBWR the calculated delta containment pressure would be comparable to that for the SBWR.

For the ESBWR, a bounding calculation was performed with the combination of the worst values of all operating plant parameters and 6 significant model parameters (a subset of those used in the SBWR 59 trial runs). The difference in the peak containment pressures (delta containment pressure) between the bounding case and the base case is [[ ]] (NEDC-33083P, TRACG Application for ESBWR, Sect. 3.7.3). The ESBWR approach generates delta containment pressure that is [[ ]] than that is calculated by 59 trial runs for the SBWR. Hence, the calculated value is acceptable.

- Q31. The time step sizes sometime influence the results of the calculations. What was the basis of the time step size selection for ESBWR analysis (maximum as well as average)?
- R31. TRACG chooses its time step in accordance with an internal logic that continuously optimizes the accuracy and efficiency of the calculation. The only control imposed by the user is to supply maximum and minimum time step size limits. TRACG will not use a time step larger than the specified maximum and it will stop if its built-in accuracy criteria require it to use a time step smaller than the specified minimum. In addition, the user may divide the analysis time span into segments and vary the specified maximum and minimum time steps from segment to segment. The ESBWR containment calculation uses a maximum time step of [[ ]] for the first hour of the simulation and [[ ]] thereafter. The minimum time step is [[ ]] for the first hour and [[ ]] thereafter. It may also be noted that a time step sensitivity study performed in conjunction with the SBWR TRACG qualification showed no significant sensitivity to the choice of maximum time step [*TRACG Qualification for SBWR*, NEDC-32725P, V. 1, Rev. 1, August 2002, (Appendix B)].
- Q144. Section 2.1.5 (p. 2-2) - Is it the intent of the last sentence of the section to say that TRACG analysis will not be used to demonstrate the conformance of the ESBWR to Criterion 5 (long term cooling) of 10 CFR 50.46? Has the applicability of Reference 88 to the ESBWR been demonstrated with regard to serving as the bases for compliance with Criterion 5?
- R144. Long term cooling will be calculated with TRACG to demonstrate that the core is well cooled in the long term for conformance to Criterion 5. The ESBWR safety systems operate in such a way that the short term cooling is ensured by having a large vessel inventory, which is replenished by the GDCS system (GDCS pool initially and suppression pool in the long term).
- Q145 Section 2.2.1.1 (p. 2-36) and Section 2.2.1.2 (p. 2-38) - What is the sensitivity of the chimney water level to the delay in GDCS flow if the IC is available? Would a delay in GDCS flow or a delay in the opening of the DPV result in significant loss of coolant from the reactor? Would the delays cause a reduction in the amount of coolant available for delivery to the reactor?
- R145. The IC operation has several beneficial effects when it operates. It takes some of the steam produced in the vessel and condenses it and returns it to the vessel. The steam condensation has the effect of reducing the vessel pressure faster. The faster initial depressurization reduces inventory loss following ADS operation and possibly results in earlier initiation of the GDCS. Additionally, the IC returns the condensate directly to the vessel. This later effect will have a greater impact on the calculation and will result in a higher water level.

Q146 Section 2.2.1.4 (p. 2-39) - On p. 2-8, GE claims sensitivity to all single failures is considered and yet for the ESBWR only 2 active component failures (GDCS valve and DPV) were considered. Do these 2 single failure cases bound all other failures?

R146. Section 2.4.4.1 (NEDC-33083P) considers single failure of the following 3 active components (one GDCS injection valve, or one DPV, or one SRV). These failures are expected to bound all other failures as the GDCS capacity available to the vessel will be higher for other failures. This conclusion was also supported by analyses performed for the SBWR Standard Safety Analysis Report (Table 6.3-3).

Q147. Section 2.3.2 (p. 2-47) - Tables 2.3-2 through 2.3-5 did not show any test that assessed the PIRT high ranked phenomenon C23, core pressure drop. Was the assessment done as part of other PIRT phenomena?

R147. [[

]]

Q148. Table 2.3-4 (p. 2-54) - What is the reason for introducing a new PIRT phenomenon C26 in this table? Should the interest be for the critical power for a 10-ft core and not a 9-ft one?

R148. [[

]]

Q149. Section 2.4.4.1 (p. 2-66) - The collapsed level is a measure of liquid inventory, and is the product of mixture level and the liquid fraction. How could the sensitivity to the calculated void fraction be removed when the collapsed rather than the mixture two-phase level is used as the figure of merit to characterize water level above the core in a transient?

R149. [[

]]

Q150. Table 2.4-1 (p. 2-69) - According to Table 2.4-1, burnout correlation, PIRT parameter C13, is a high ranked phenomenon. Why wasn't C13 identified in Table 2.4-3 for sensitivity study? Is the modified-Zuber critical heat flux (CHF) correlation one of the options available for channel component in TRACG?

R150. C13 was not identified in Table 2.4-3 because all TRACG calculations show that the core is covered with two-phase mixture for all cases. No core heatup was calculated due to local critical heat flux.

TRACG evaluates boiling transition with the [[  
]] for the CHAN  
component.

A sensitivity study has subsequently been performed on the Zuber correlation. A multiplier of 0.8 was applied to account for a 20% uncertainty. No core heatup was calculated.

Q151. Table 2.4-3 (p. 2-71) - What should the range of value for PIRT84 be?

R151. There is a typo in Table 2.4-3. The correct range of value for PIRT84 should be [[  
]] This will be corrected in the next revision of the report.

Q152. Section 2.4.4.2 (Figure 2.4-13) - Do "M" and "P" denote the lower and upper bound of the parameter value?

R152. Yes. "M" denotes the lower bound and "P" denotes the upper bound of the parameter value.

Q153. Section 2.4.4.2 (Figure 2.4-13) - Why is it that for some PIRT parameters, e.g. PIRT05 and PIRT84, only positive deviation is observed for both the lower and upper bound values? What is the implication of this deviation to the selection of conservative bounding values for the PIRT parameters? Are the responses of the chimney collapsed level to the uncertainties in the PIRT parameters consistent with the expected behavior of the two-phase system?

R153. [[

]]

- Q154. Section 2.4.4.2 (Figures 2.4-13 and 2.4-14) - The sensitivity studies looked at the responses of the collapsed level and the peak cladding temperature (PCT) to the uncertainties in the PIRT parameters. Figures 2.4-13 and 2.4-14 show that in response to uncertainty in a given PIRT parameter the deviations in collapsed level and PCT do not always go in the same direction (see e.g. PIRT84M and PIRT84P). What is the correspondence between uncertainties in the collapsed level and the PCT? 10 CFR 50.46 defines 5 acceptance criteria for ECCS. How does the chimney collapsed level relate to these 5 acceptance criteria?
- R154. The ESBWR design is such that there is no core uncover during any LOCA scenario (i.e. the chimney collapsed level is always above the top of the core). Under this situation, the PCTs are directly proportional to the differences in liquid saturation temperature corresponding to the slight differences in maximum pressure reached before ADS, and are on the order of 1° K. Hence, there is no correlation between the sensitivities in the chimney collapsed level and the PCT. The 10CFR50.46 criteria are satisfied because the PCT is well below 2200 F. In the absence of any core heatup, the criteria related to PCT, maximum local oxidation, maximum hydrogen generation, coolable geometry and long term cooling are automatically satisfied. The minimum chimney collapsed level criterion is an additional design margin that GE has proposed above and beyond the requirements of 10CFR50.46.
- Q155. Section 2.6 (p. 2-91) - Is it possible in the TRACG calculation to predict a dryout condition in one of the core channels while a two-phase level exists in the chimney? A likely situation when this might happen is when the core flow is low. The modified-Zuber critical heat flux (CHF) correlation is inversely proportional to the void fraction and its value can be much lower than the pool boiling CHF. What is the minimum critical power ratio (CPR) in the bounding base and the sensitivity calculations?

R155. [[

]]

Q156 Section 2.6.1 (p. 2-91) - What is the basis for determining the  $2\sigma$  uncertainty level of the static head in the chimney?

R156. [[

]]

Q157 Section 2.7.1.1 (p. 2-92) - The TRACG nodalization of the ESBWR RPV and containment for ECCS/LOCA analysis was shown in Figure 2.7-1. Where is the suction point of the GDCS? Is there any possibility of draining the GDCS pool through the broken GDCS line creating a bypass flow path between the drywell and wetwell? Was this confirmed by an qualification tests?

R157. Please refer to the response to RAI 28 for a description of the GDCS pool and suction line. The loop seal design principle has been confirmed in other integrated tests but for the GDCS line break and GDCS suction line draining, no qualification test was deemed necessary.

Q158 Section 2.7.2.2 (p. 2-101) - Some of the sensitivity cases have suggested that the net effect of combining uncertainties at the extreme values may not be synergistic. A case in point is the result shown in Figure 2.5-1 where the chimney collapsed level responded in opposite directions to uncertainties in plant parameters individually and when combined. Could there be compensating effects? Are the results of the 'bounding' case bounding? Which case has the lower minimum

chimney collapsed level, the 'bounding case' or sensitivity case PIRT57-P shown in Figure 2.4-13?

R158. Please refer to response to Q153 for the discussions of compensating effects and adequacy of the 'bounding' approach. The 'bounding case' has the lower minimum chimney collapsed level than the sensitivity case PIRT57-P, about 0.31 m lower.

Q159. NEDC-33083P states "A complete description of the ESBWR containment model can be found in Section 8.2 of Reference 24." Reference 24 is NEDC-32725P, "TRACG Qualification for SBWR," Rev. 1, Volumes 1 and 2, September 1997. In comparing Figure 3-7-1 in NEDC-33083P and Figure 8.2-5 in NEDC-32725P, any description in NEDC-32725P would not be fully representative of the ESBWR, because of the differences in ESBWR as compared to the SBWR design. Please provide supplemental information to address this issue.

R159. The key differences between the ESBWR and SBWR containment model are provided in the following.

(a) ESBWR model radial boundaries

Radial boundary	Location	Value (m)
1	Radius of RPV shroud (mid-wall)	[[ ]]
2	RPV inside radius	[[ ]]
3	Intermediate location in DW	[[ ]]
4	Annulus DW outer radius	[[ ]]
5	Intermediate location in WW	[[ ]]
6	Inner radius of containment wall	[[ ]]

(b) PCC Drain Tanks

The ESBWR PCC drain line PIPE84 connects to drain tank TEE62. Top of TEE62 connects to the DW and bottom of TEE62 connects to VLVE44 which returns PCC drain to the RPV. Components TEE62 and VLVE44 are additional components not simulated in the SBWR model.

The ESBWR PCC drain line PIPE46 connects to drain tank TEE63. Top of TEE63 connects to the DW and bottom of TEE63 connects to VLVE45 which returns PCC drain to the RPV. Components TEE63 and VLVE45 are additional components not simulated in the SBWR model.

(c) GDCS pool and airspace

The ESBWR GDCS pools and airspace have no direct connection to the DW.

(d) GDCS airspace and WW connections

PIPE81 and PIPE82 are used to model the connections between the ESBWR GDCS airspace and WW airspace.

(e) SRV modeling

There are a total of 12 SRVs, 3 SRVs for each ESBWR main steam line. VLVE24 models 3 SRVs and VLVE28 models 6 SRVs, from the intact MSLs. The 3 SRVs from the broken MSL were not modeled in the MSL break case.

(f) DPV modeling

There are a total of 8 DPVs, one DPV for each of the MSLs, and 4 DPVs connect to the RPV via the DPV/IC nozzles. VLVE19 models 3 DPVs from the intact MSLs. VLVE12 and VLVE13 represent 2 DPVs each. The DPV from the broken MSL was not modeled in the MSL break case.

Q160. The ESBWR nodalizations presented in Figure 2.7-1 and Figure 3.7-1 are not the same. Please clarify.

R160. The nodalizations for ECCS and Containment analyses are different because the key parameters are different for these analyses. However, the geometries (such as volumes and elevations) are identical in these two nodalizations.

Figure 2.7-1 shows the TRACG nodalization for the ECCS/LOCA analyses. The key parameters for these analyses are the mixture level inside shroud and the peak cladding temperature. The RPV is modeled with more nodes (more levels and rings) to provide detailed responses inside the RPV.

Figure 3.7-1 shows the TRACG nodalization for the Containment/LOCA analyses. The key parameter for these analyses is the containment pressure. The containment is modeled in greater detail with more nodes while the RPV modeling is simplified with fewer nodes.

Q161 It is stated in Section 3.1.4 (Page 3-4) that “the ESBWR pressure transient does not rapidly increase to a peak value from which it must be rapidly reduced. The pressure increases slowly over several hours...”

Q161.1 What about the peak pressure in the DW immediately after the blowdown, before and after the main horizontal vents are cleared? This peak could be higher than the long term pressure (e.g., Figure 2.7-5 vs. Figure 3.7-2.) Please provide a document discussing this initial peak pressure.

R161.1. The ESBWR containment is designed like a typical pressure suppression containment where the drywell initially pressurizes rapidly (1 to 5 seconds) following a pipe break. [[

]] The pressure then increases slowly, as the remaining noncondensibles are cleared from the drywell. This final containment pressure is determined by the amount of noncondensibles transferred to the wetwell airspace and the vapor pressure.

Q161.2 Clearing of horizontal vents in the main vent lines (PIRT MV3) and chugging (partial opening of the top vent) are potentially important to affect the initial noncondensable gas flow into the WW, and the initial DW pressure peak. Please explain how this issue is handled in the analyses, and list any tests used to validate this model.

R161.2. An extensive set of test data has been obtained over the years for the horizontal vent system for both the Mark III and ABWR containments. [[

]]

Q162 It is stated in Section 3.1.4 (Page 3-4) that “The containment pressure is determined by the transport of the noncondensable gases into the drywell, not by heat input to the containment.” Is this statement true only if the PCCS were 100% efficient? The containment pressure is also affected by the heat not removed by the PCCS, which is deposited in the WW water by condensing steam which was not condensed by PCCS, which, in turn, raises the partial pressure of steam in the WW gas space. Is this long-term deposit of heat into WW the ultimate concern for the ESBWR containment and purpose of various tests and evaluations? Please clarify.

R162. As stated in RAI 161, it is indeed true that the containment pressure is determined by a combination of the noncondensibles pressure and steam vapor pressure. However, [[

]] Consequently, the containment pressure is primarily determined by the noncondensable pressure.

Q163. Modeling of WW gas space stratification in Section 3.3.1.1.2 referred to the PANDA modeling experience for basis of having “restricted mixing between layers,” which “produced conservative results for PANDA and is expected to be conservative for ESBWR.”

Q163.1. The PANDA report (NEDC-33080P) does not mention this particular modeling. The PANDA report says in Section 2.6.2.10 that “post-test evaluation of P-series tests demonstrated that TRACG conservatively calculates heatup of the WW gas space.” However, PANDA modeling does not use the “restricted mixing between layers.” Please explain.

R163.1. [[

]]

Q163.2. PANDA results show substantially different trends for the WW gas temperature between the test and analyses for all tests, although the magnitudes are similar. This difference may be magnified in the long-term (PANDA usually ran about 10 hours, while the time period of interest in ESBWR is 72 hours.) Please discuss how the difference in trends is concluded to be conservative.

R163.2. [[

]]

Q164. It is stated that the volumes of drywell were adjusted for “hideout volume” to maximize the effect of noncondensable gas hideout during the blowdown phase of the LOCA.

Q164.1. In Page 3-21, it is stated that the region over the GDCS pools is included in the hideout volume. Since this region is a part of WW, not DW, this seems to be incorrect. Please clarify.

R164.1. The region over the GDCS pools is not part of the DW and is not included in the hideout volume. The statement will be corrected in the next revision of the report.

Q164.2. Please discuss how this hideout volume would affect the initial peak of the DW pressure (adjusting volumes where a large amount of steam is released and compressed should affect the pressure change in the volume.)

R164.2. The initial peak of the DW pressure in the containment analysis is not affected by the modeling of the hideout volume because the total DW volume, including the hideout volume, participates in the pressurization process. The distinguishing feature of the hideout volume is that it retains a higher than average fraction of non-condensable at the end of the initial pressurization transient.

The total DW airspace volume is conserved in the Containment/LOCA analysis. The lower drywell represents the portion of DW below the RPV bottom and is the most significant portion of the hideout volume. The lower drywell is modeled by a one-dimensional component (TEE35, shown in Figure 3.7-1, TRACG Application for ESBWR, NEDC-33083P), which communicates to the bottom of the drywell annulus. This 1-D component participates freely in the pressurization process even though it is labeled as “hideout volume”. The 1-D nodalization used in this component effectively retards the short-term mixing of the noncondensable gases in the lower drywell with the discharged steam in the upper drywell.

Q164.3. Immediately after the blowdown, it is possible that some of the DW noncondensable gases can move to the hideout volumes since the

pressure in the open space volume is higher than these hideout volumes. Preventing these gases from moving to these volumes, the concept of hideout volumes may result in less noncondensable gases in these volumes than in reality, thus less noncondensable gas available to bleed later. Please discuss if this observation is correct.

R164.3. The observation is incorrect insofar as it presumes the pressure in the open-space volume is higher than in the hideout volume. As discussed in the response to 164.2, the entire drywell volume is pressurized equally but the hideout volume is effectively isolated from the short-term mixing processes that allow most of the noncondensable in the open-space region to be entrained by the blowdown steam and transferred to the wetwell. The TRACG containment analysis shows that the lower drywell (TEE35) retains a large mass fraction of noncondensable at the end of the blowdown. The subsequent gradual release of this noncondensable simulates the effect of hideout on long-term PCCS performance.

Q164.4. On Page 3-22, it is stated that, "This loss coefficient was representative of the loss that would be expected through the restriction area connecting the upper and lower drywell." In view of the potential importance of impact on the PCCS of a small amount of noncondensable gas bleeding, this coefficient may be important. Please explain how this coefficient is determined. Were sensitivity studies performed varying this coefficient?

R164.4. The loss coefficient used in the analyses is based on the restriction area connecting the upper and lower drywell in the ESBWR. This loss coefficient is applied at the TEE35 junction which connects to the bottom of the drywell annulus (VESSEL component).

Sensitivity studies for the SBWR were performed to assess the impact of this loss coefficient on drywell noncondensable gas mass. Calculations of drywell noncondensable gas mass during the first 20 hours of the LOCA, with a zero loss coefficient and a loss coefficient that was twice the value used for the nominal case has a small effect on both the bleed-down rate of drywell noncondensable gas and the calculated pressure.

Q165. In Tables 3.3-3 and 3.3-4, some of the highly ranked phenomena are not cross-marked for any tests. Please discuss how these phenomena are validated or qualified for TRACG.

R165. A composite of Tables 3.3-2, 3.3-3 and 3.3-4 (see TAPD, NEDC-33079P) shows that the following highly ranked containment phenomena do not have test coverage:

[[

]]

Q166. How is the nodalization accounted for in the bias calculations?

R166. [[

]]

Q167. Was condensation on the containment walls included in the analysis? While the wall condensation generally helps to keep the containment pressure low, the lost water may not be available in the re-circulation through PCCS, and this may contribute to lowering of the vessel water level eventually, especially the GDCCS break where the water level is relatively close to the top of core. In the GDCCS break, water level is already down to the break elevation. The wall condensation will gradually lose the water in the long-term. In the period of 72 hours, this loss, in combination with loss of some steam (which was uncondensed in the PCCS) to the SP, may not be negligible. Please discuss whether this issue was assessed and its results.

R167. Condensation on the containment walls was included in the analysis. Any water condensed on the walls collects in the lower drywell and then flows through the spillover holes to the suppression pool. The water from the suppression pool then flows back to the vessel through the equalization lines.

The equalization lines (4 lines), connecting the suppression pool and the RPV, provide for long-term coolant boil-off losses to the drywell. The equalization line injection valves will open following a [[ ]] time delay initiated by a Level 1 signal and when the downcomer level reaches 1 m above the TAF. For the GDCS line break, if the downcomer level drops below 1 meter above the TAF, the equalization lines will open and refill the RPV level to 10 meters, the same elevation as the suppression pool level.

Q168. On Page 3-37 (MV1), it is stated that “In Section 5.5 of Reference 24, the short-term peak drywell pressure is shown to be always conservatively overpredicted by TRACG.” Please provide a summary discussion of that finding.

R168. [[

]]

Q169. On page 3-40 (PC1), the bias in  $k/A^2$  was determined “assuming the same values for  $\rho_{\text{mix}}$  and  $m_{\text{mix}}$ .” However, these values are not constants through the PCCS tubes, due to condensation, since the  $\Delta p$  in the equation is overall pressure drop in the PCCS,  $\rho_{\text{mix}}$  and  $m_{\text{mix}}$  should be some kind of average in the tubes, which requires some knowledge of how much steam is condensed along the tubes. Please explain how  $\rho_{\text{mix}}$  and  $m_{\text{mix}}$  are determined in the evaluation of the bias of  $k/A^2$ .

R169. [[

]]

Q170. With respect to PC2 (Page 3-40), the potential degradation of condensation in the PCCS tubes due to continuous bleeding of a small amount of noncondensable gas in a long period may be the single most important issue in the ESBWR containment performance. Yet the documents reviewed do not provide any specific information regarding the degree of degradation. Are there any studies (tests and analyses) showing the degrees of degradation as a function of concentration (and perhaps flow rates) of noncondensable gas in the tubes? Are there any such tests available where a small amount of noncondensable gas (in the order of 1%) is continuously injected to the DW?

R170. [[

]]

Q171. Initial DW and WW temperatures were set at their operating limit, i.e, 110°F (P. 3-49, Section 3.5.2.1). However, the higher initial temperature may results in less noncondensable gas inventory and, thus, may not be conservative. Please discuss this aspect.

R171. Lowering the initial DW and WW temperatures will increase the noncondensable gas inventory.

The long-term DW pressure depends on the amount of noncondensable gas inventory, the suppression pool surface temperature, and the WW temperature. Lowering the initial suppression pool temperature (to be consistent with the initial WW temperature) would reduce the transient WW temperature and suppression pool surface temperature. The DW pressure reduction due to these two factors is more than that by the increased noncondensable gas inventory.

Q172. Table 3.5-1 shows that the bounding value of the suppression pool level is higher than the nominal value. While it may be conservative in terms of the WW gas space available in the later stage of the accident, it may not be conservative in terms of the water inventory above the PCCS vent outlet, which is available to be heated by the uncondensed steam in the bounding calculations. It will also

require a higher  $\Delta p$  (DW-WW) to clear the PCCS vent to the WW pool. Please explain.

- R172. The impact of 5 cm higher initial suppression pool level on the surface temperature is expected to be small.

Figures 3.7-7 (Base Case) and 3.7-12 (Bounding Case) (NEDC-33083P, TRACG Application for ESBWR) show the suppression pool temperature responses. These figures show that (a) [[ ]] of the temperature rises in the top 3 levels (Levels 4, 5 and 6) of the suppression pool occurs during the [[ ]] of the transient, and (b) Levels 4, 5 and 6 are well mixed at the end of this period due to steam flow from the top horizontal vents and PCC vent flow. The PCC vent flow (steam + air) reduces significantly after this time period. From [[ ]] the PCC vent flow contains essentially only air and no significant amount of energy is added to the top layer of the suppression pool.

Uncertainty analysis was performed for the SBWR containment (NEDE-32178P, Sect. 4.3.2) with 59 TRACG trial runs. In these studies, the suppression pool level was varied over a range of 10 cm. A positive correlation coefficient indicated [[ ]] so overall conservative. The slightly higher  $\Delta P$  (DW-WW) to clear the PCCS vent to the WW pool shows no significant impact on the peak containment pressure.

- Q173. Table 3.5-1 shows that the bounding value of the GDCS pool level is higher than the nominal value. While it may be conservative in terms of the WW gas space available in the later stage of the accident, it may not be conservative in terms of the total water inventory available to cool the reactor. Please explain.

- R173. The increased GDCS water volume due to higher initial GDCS pool level is less than 1%, and is expected to have insignificant impact on the reactor cooling.

TRACG calculations show that the core is covered with two-phase mixture for all cases and no core heatup was calculated. The chimney water level recovers shortly after the start of the GDCS flow and the minimum water level does not depend on the amount of GDCS water volume.

- Q174. Section 3.7.2 refers to Figure 2.7-5 for the short term response. However, Figure 2.7-5 presents the result of a GDCS line break, while Section 3.7.2 discusses Main Steam line break. Please clarify.

- R174. Yes, it is an error to refer Figure 2.7-5 for the discussion in Section 3.7.2. The phrase "(For the short term response (2000 s), see Figure 2.7-5)" should be deleted from the 3<sup>rd</sup> paragraph in Section 3.7.2.

- Q175. Figure 3.7-2 shows periodic drops of containment pressure. Please explain whether they are real or numerical and what causes them, and evaluate the impact of these phenomena on the eventual containment pressure.
- R175. The periodic drops of containment pressure are caused by periodic flows of GDCS cold water into the RPV. This phenomenon has no impact on the eventual containment pressure.

Figure 3.7-5 (NEDC-33083P) shows the level in the two GDCS pools. The level in the pools reaches an equilibrium with the RPV downcomer level, which is at the elevation of the steamline. After reaching an equilibrium level, the RPV level drops slowly due to boil-off, and the pressure difference between the RPV and the WW (same as the GDCS air space) reduces slowly as the decay heat decreases. At some time later, the GDCS driving head (GDCS pool pressure + the static head) becomes greater than that for the RPV, and allowing cold GDCS water to flow into the RPV. This sudden addition of cold water into the RPV reduces the steam production. As shown in Figure 3.7-6, the sharp dips in the heat removal indicate periods where the PCC heat removal exceeded the RPV steam production, resulting a drop in the drywell pressure below the wetwell pressure. Subsequently the vacuum breakers open, some noncondensibles are returned to the drywell. The GDCS flow stops shortly after the vacuum breaker opening due to lower GDCS driving head and increased RPV water level. Following the vacuum breaker opening and the stop of GDCS flow, steam production is resumed in the RPV and restores some pressure difference between the RPV and the DW and WW. The GDCS and RPV levels reach another equilibrium at this time.

These periodic drops of containment pressure and opening of vacuum breakers occur several times during the 72 hours transients. Each time some noncondensibles are returned to the drywell. During the period between the periodic drops, these noncondensibles are pushed back into the wetwell by the PCC action. The eventual containment pressure can be determined when all noncondensibles have been pushed into the wetwell, and are not impacted by these periodic drops of containment pressure.

- Q176. Figures 3.7-6 and 3.7-11 show a substantial improvement of PCCS heat removal at about 8 hours. Yet, a substantial amount of noncondensable gases remain in the DW (Figure 3.7-3). Please explain what causes this improvement. The same figures show that the PCCS removes almost 100% of decay heat after 8 hours, yet the containment pressure continues to increase. What is the cause of this pressure increase?
- R176. Figures 3.7-6 and 3.7-11 compare the total heat removal by the PCCS with the decay heat. Figure 3.7-6 shows that the total heat removal capacity increases from [[ ]]. This increase is the result of a reduction of the noncondensable fraction in the inlet flow to the PCCS. The

PCCS takes steam/gas mixture from the upper half of the DW, and Figure 3.7-3 shows that the amount of noncondensable gases in this region is significantly reduced during this time period.

After 8 hours the PCCs are able to remove the DW heat load with some margin to spare. From 8 to 48 hours, the containment pressure continues to increase due to the purging of the noncondensable gases from the lower half of the DW into the WW. During this time period, the noncondensable fraction in the inlet mixture is small and does not prevent the PCCS from removing the entire decay heat load. The DW pressure reaches the maximum value when all noncondensable gases are purged from the DW into the WW.

Q183 Page 2-2 - It seems that "2.2 Analysis of Events" should include two additional events – bottom drain line break (BDLB) and inadvertent automatic depressurization system (ADS). The BDLB is the only break located below the core and leads to the slowest RPV depressurization compared to the MSLB and the GDLB (break at the downcomer annulus above the core). These three LOCAs are expected to bracket other LOCAs in terms of the break sizes, locations, and fluid conditions upstream of the break. TRACG calculations for BDLB are therefore desirable and should cover 72 hours of the transient. Containment response to the BDLB should also be included, because the break flow at such a low elevation is likely to sweep nitrogen gas from the lower DW to the WW and reduce the likelihood of later release of noncondensable gas to PCCS condensers to degrade their performance. As a result, BDLB may provide a lower bound on the containment pressure during the long-term PCCS cooling phase.

R183. The analysis reported in the TRACG Application for ESBWR (NEDC 33083P), includes representative breaks and failures. The SSAR will include a complete set of calculations to cover all breaks and single failures to determine the limiting breaks and single failures for the final design. See also response to RAI 184 on the discussion of the inadvertent ADS actuation event.

The calculations submitted in the Application report (NEDC 33083P) have focused on the early stages of the plant response (about 2000 seconds) because during this time period the plant is undergoing transient changes like vessel depressurization and water injection from the GDCCS. The long-term response (up to 72 hours) is dependent on the long-term equilibrium distribution of the different water inventories (See response to RAI 323.5). Since these inventories are expected to be dependent on the final design to be included in the SSAR, the long-term response of the vessel might be slightly different in the SSAR. However, the attached results show the plant response to the BDL break for the current reference design for the longer time period.

This case shows that there is no core heatup for the entire BDLB transient. The core is covered and remains covered by more than 3 meters of 2-phase mixture after the injection of suppression pool water into the RPV via the equalization lines.

This case assumed a single failure of 1 GDCS injection valve, and used the base case conditions as described in Section 3.7.2 in the ESBWR Application Report (NEDC-33083P). Reactor scram was initiated on Level 3 trip, and reactor power started to shutdown after an appropriate delay time.

Figure 183-1 shows the long-term pressure response. Following the postulated LOCA, the drywell pressure increased rapidly leading to clearing of the PCC and main vents. The DW pressure reaches the first peak with a value of [ ] The pressure decreases when the GDCS starts flowing at about [ ] seconds. Vacuum breaker openings occur as the steam production drops off. The GDCS pools are completely drained in about 2 hours. Subsequently, decay heat overcomes the subcooling of the GDCS water, and steaming resumes. The drywell pressure increases and reaches a 2nd peak with a value of [ ] The long-term DW pressure is significantly lower than that for the MSLB case due to the additional GDCS draindown volume, which is about 2 times larger than that for the MSLB case.

Figure 183-2 compares the two-phase levels in the RPV Chimney, RPV downcomer, Drywell Annulus and Suppression Pool. For the first [ ], the RPV continues to lose water inventory to the DW annulus via the BDL break. Consequently, the RPV water levels drop and the water level in the DW annulus rises. At [ ] after the break, the water from the GDCS pools and the RPV fill the DW annulus to about [ ] The chimney and downcomer levels reach the minimum value of about 7 meters. At this minimum value, the chimney two-phase level drops [ ] At this minimum 2-phase level, the core is still covered with two-phase mixture with adequate cooling. No core heatup was calculated for the entire BDLB transient.

From 6 to 16 hours, BDL break flow reverses direction. A small amount of water flows from the DW annulus into the RPV. The DW annulus level drops slightly with the RPV levels rise accordingly in this period. At [ ] water starts to flow into the RPV from the suppression pool via the equalization lines. The levels in the RPV and DW annulus increase as the results of the initial and subsequent water injections. The water levels reach equilibrium conditions after [ ] following the break. For long-term (from [ ]), the core is covered by more than 3 meters of 2-phase mixture. The pressure dips (Figure 183-1) slightly each time there is significant addition of cold water to the RPV (at about [ ])

[[

Figure 183-1. Containment Pressure Response – BDLB

Figure 183-2. Level Response – BDLB

]]

**Table 1**Supplemental Information on RAI 183

The basedecks for the BDLB transient calculation are enclosed in the attached CD.

The basedecks and files included in the attached CD are summarized in the following table.

Item #	File name	Description
1	BDL_NSS27.INP	Steady-state input deck (ASCII file) for BDL transient.
2	BDL_A9.INP	Input deck (ASCII file) for the BDL transient calculation. The transient calculation restarts from the end of steady-state run "BDL_NSS27".
3	BDL_A9.OUT	Output file (ASCII file) for the BDL transient calculation.
4	BDL_NSS27-input.pdf	PDF file format of Item #1, with page header "GE PROPRIETARY INFORMATION".
5	BDL_A9-input.pdf	PDF file format of Item #2, with page header "GE PROPRIETARY INFORMATION".
6	BDL_A9-output.pdf	PDF file format of Item #3, with page header "GE PROPRIETARY INFORMATION".

Supplemental Response to RAI 183 with Revised Calculation

To address the concerns expressed by NRC staff regarding the long-term water level for the Bottom Drain Line (BDL) break, a parametric calculation has been performed using a revised lower drywell (LDW) volume. As in the previous case (original RAI response), there is no core heatup during the entire BDL break transient. The minimum chimney collapsed level is [[ ]] above the Top of Active Fuel (TAF). (The minimum two-phase level in the chimney is greater than [[ ]] ) After the injection of suppression pool water into the RPV via the equalization lines, the chimney collapsed level rises to an equilibrium value of about [[ ]] above the TAF.

ESBWR design criteria are for the GDCS pools and LDW to be sized such that the drywell can be flooded to the TAF for all break and single failure combinations. At this time GE has not finalized the configuration of the LDW and the interim configuration used in the previous TRACG basedecks GE has submitted did not satisfy this criteria. The initial intention was to leave this as a certification phase activity. However, after discussing the issue with NRC staff, GE has revised the TRACG input decks to meet the stated design criteria now for this parametric study. The final configuration to meet the design criteria will be determined after considering structural analyses, severe accident mitigation, arrangement issues and other design features later this year.

In this parametric calculation, the lower drywell volume in the TRACG model is reduced by [[ ]] (compared to the previous case for the original RAI response). This volume reduction will satisfy the design criteria that the drywell will be flooded to the elevation of ([[ ]]) by the GDCS pool water. This case uses the same conditions as those for the case (Run BDL\_A9) used for the response to RAI 183, i.e., a single failure of 1 GDCS injection valve, and reactor scram on Level 3 trip.

Figure 183S-1 shows the long-term pressure response. Following the postulated LOCA, the drywell pressure increased rapidly leading to clearing of the PCC and main vents. The DW pressure reaches the first peak with a value of [[ ]] at about [[ ]]. The pressure decreases when the GDCS water starts flowing into the RPV at about [[ ]]. Vacuum breaker openings occur as the steam production drops off. The GDCS pools are completely drained in about 3 hours. Subsequently, decay heat overcomes the subcooling of the GDCS water, and steaming resumes. The drywell pressure increases and reaches a 2nd peak with a value of [[ ]] at about [[ ]]. The long-term DW pressure is significantly lower than that for the MSLB case (ESBWR Application Report, NEDC-33083P) due to the additional GDCS draindown volume, which is about 2 times larger than that for the MSLB case.

Figure 183S-2 compares the two-phase levels in the RPV Chimney, RPV downcomer, Drywell Annulus and Suppression Pool. The "0.0" value in Figure 183S-2 corresponds to the RPV bottom 0 elevation. For the first [[ ]], the RPV continues to lose water inventory to the DW annulus via the BDL break. Consequently, the RPV water levels drop and the water level in the DW annulus rises. At approximately 6 hours after

the break, the water from the GDCS pools and the RPV fill the DW annulus to about [[ ]]. The chimney and downcomer 2-phase levels reach the minimum value of about [[ ]], respectively. At this minimum 2-phase level, the core is still covered with two-phase mixture with adequate cooling. No core heatup was calculated for the entire BDLB transient.

From approximately [[ ]], BDL break flow reverses direction. A small amount of water flows from the DW annulus into the RPV as the pressure difference between the RPV and drywell decreases corresponding to the decrease in decay heat. The DW annulus level drops slightly and the RPV levels rise accordingly in this period. At [[ ]], water starts to flow into the RPV from the suppression pool via the equalization lines as the check valves open in these lines. The levels in the RPV and DW annulus increase as the results of the initial and subsequent water injections. The water levels reach equilibrium conditions after [[ ]] following the break. For long-term (from [[ ]]), the core is covered by more than 3 meters of 2-phase mixture. The pressure dips (Figure 183S-1) slightly each time there is a significant addition of cold water to the RPV via the equalization line.

Figure 183S-3 shows the collapsed levels in the RPV Chimney and RPV downcomer. The "0.0" value in Figure 183S-3 corresponds to the RPV bottom 0 elevation. The chimney collapsed level reaches the minimum value of [[ ]] at about 8 hours. At this minimum value, the chimney collapsed level is above the TAF by [[ ]].

The input deck and output file for this parametric calculation are included in the attached CD, and summarized in the following table.

Item #	File name	Description
1	BDL_A10B.INP	Input deck (ASCII file) for the BDL transient. This is a "stand-alone" input deck and no restart dump file is needed for the calculation.
2	BDL_A10B.OUT	Output file (ASCII file) for the BDL transient calculation.
3	BDL_A10B-input.pdf	PDF file format of Item #1, with page header "GE PROPRIETARY INFORMATION".
4	BDL_A10B-output.pdf	PDF file format of Item #2, with page header "GE PROPRIETARY INFORMATION".

[[

Figure 183S-1. Containment Pressure Response – BDLB Revised ]]

[[

Figure 183S-2. Two-phase Level Response – BDLB Revised ]]

[[

Figure 183S-3. Chimney and Downcomer Collapse Levels – BDLB Revised ]]

Supplemental Response to RAI 183  
with Parametric Long-term Calculation for GDCS Line Break

To address the concerns expressed by NRC staff regarding the long-term water level responses after a pipe break, an additional parametric long-term calculation has been performed for GDCS Line Break (GDLB) using a revised lower drywell (LDW) volume. As in the Bottom Drain Line (BDL) break cases (original RAI response), there is no core heatup during the entire (72 hours) GDL break transient. The long term minimum chimney collapsed level is [[ ]] above the Top of Active Fuel (TAF). (The minimum two-phase level in the chimney is greater than [[ ]]) For this case, there is no activation of equalization line valves and no fluid flow between the suppression pool and the RPV.

ESBWR design criteria are for the GDCS pools and LDW to be sized such that the drywell can be flooded to the TAF for all break and single failure combinations. At this time GE has not finalized the configuration of the LDW and the interim configuration used in the previous TRACG basedecks GE has submitted did not satisfy this criteria. The initial intention was to leave this as a certification phase activity. However, after discussing the issue with NRC staff, GE has revised the TRACG input decks to meet the stated design criteria now for this parametric study. The final configuration to meet the design criteria will be determined after considering structural analyses, severe accident mitigation, arrangement issues and other design features later this year.

In this parametric calculation, the lower drywell volume in the TRACG model is reduced by 200 m<sup>3</sup> (compared to the previous BDL case for the original RAI response). This volume reduction will satisfy the design criteria that the drywell will be flooded to the elevation of (TAF+1 m) by the GDCS pool volume. This case simulates the GDCS line break with a single failure of 1 GDCS injection valve on one of the intact GDCS lines. The reactor power scram is initiated on Level 3 trip.

Figure 183S-4 shows the long-term pressure response for the GDCS Line Break (GDLB). Following the postulated LOCA, the drywell pressure increased rapidly leading to clearing of the PCC and main vents. The DW pressure reaches the first peak with a value of [[ ]] The pressure decreases when the GDCS water starts flowing into the RPV at about [[ ]] seconds. Vacuum breaker openings occur as the steam production drops off. The GDCS pools are completely drained in [[ ]] Subsequently, decay heat overcomes the subcooling of the GDCS water, and steaming resumes. The drywell pressure increases and approaches a quasi-constant value of [[ ]] The long-term DW pressure is significantly lower than that for the MSLB case (ESBWR Application Report, NEDC-33083P) due to the additional GDCS draindown volume, which is about 2 times larger than that for the MSLB case.

Figure 183S-5 compares the two-phase levels in the RPV Chimney, RPV downcomer, Drywell Annulus and Suppression Pool. The "0.0" value in Figure 183S-5 corresponds to the RPV bottom 0 elevation. [[

]] Consequently, the RPV water levels drop and the water level in the DW annulus rises. At approximately [[ ]] after the break, the water from the GDCS pools and the RPV fill the DW annulus to about [[ ]]. At this time, the downcomer two-phase level drops below the elevation of the GDCS line break location. From this point on, the RPV continues to loss inventory to DW but at a much slower rate. This is because most of the steam generated by the decay heat is condensed in the PCCS and returned to the RPV, but some of the steam is condensed on the DW walls and collects in the DW annulus. This drywell condensate results in the rise of DW annulus level [[ ]].

At approximately [[ ]] after the break, the chimney and downcomer 2-phase levels drop to about [[ ]], respectively. From this point on these 2-phase levels continue to drop and reach the minimum values of about [[ ]] (or [[ ]] above the TAF) at the end of the transient. For long-term the core is covered, and the 2-phase level is at about [[ ]] above the TAF. There is no core heatup during this 72 hours GDCS Line Break transient.

Figure 183S-6 shows the collapsed levels in the RPV Chimney and RPV downcomer. The "0.0" value in Figure 183S-6 corresponds to the RPV bottom 0 elevation. The RPV downcomer collapsed level reaches the minimum value of [[ ]] at about [[ ]]. This minimum downcomer level is above the Level 0.5 setpoint [[ ]]. The equalization line valves are not activated and the flow path between the suppression pool and the RPV is not opened for this transient. The chimney collapsed level reaches the minimum value of [[ ]] at about [[ ]]. At this minimum value, the chimney collapses level is above the TAF [[ ]].

The input deck and output file for this parametric calculation are included in the attached CD, and summarized in the following table.

Item #	File name	Description
1	GDL_A6.INP	Input deck (ASCII file) for the GDL transient. This is a “stand-alone” input deck and no restart dump file is needed for the calculation.
2	GDL_A6.OUT	Output file (ASCII file) for the GDL transient calculation.
3	GDL_A6-input.pdf	PDF file format of Item #1, with page header “GE PROPRIETARY INFORMATION”.
4	GDL_A6-output.pdf	PDF file format of Item #2, with page header “GE PROPRIETARY INFORMATION”.

[[

Figure 183S-4. Containment Pressure Response – GDLB ]]

[[

Figure 183S-5. Two-phase Level Response – GDLB ]]

[[

Figure 183S-6. Chimney and Downcomer Collapsed Levels – GDLB ]]

- Q272. The report says that PANDA is “heavily instrumented with approximately 560 sensors” (page 5-7). However, it is not clear whether these 560 instruments are sufficient to provide a reliable (with built-in redundancy and cross-checking) mass and energy balance of steam, water, and noncondensable gases in the facility during a test that is consistent with the TRACG model nodalization of all components. Address the effectiveness of the instrumentation in providing a conclusive and detailed representation of these quantities.
- R272. Instrumentation in the PANDA test facility provides measurements of important test parameters related to reactor safety evaluations, namely the DW and WW pressures and temperatures. The facility also underwent pretest characterization testing prior to the two major testing series (M-series and P-series) to determine irreversible line losses and system heat losses. Instrument diagrams (Figures 272.1 and 272.2) showing instrument locations in the PANDA facility vessels and the IC (typical of the PCCs also) are attached. Superimposed on these diagrams are the TRACG nodalizations for the corresponding components. It can be seen that the instrumentation does provide coverage of the important quantities calculated by the code. While no test facility, particularly an integral systems test facility as complex as PANDA, will ever have enough instrumentation to determine all details of its behavior, PANDA does have sufficient instrumentation to meet its experimental objectives, namely to demonstrate the behavior and operation of the passive cooling systems during the long-term cooling phase of the ESBWR LOCA transient and to provide a qualification basis for TRACG.

[[

Figure 272.1. GDCS, DW, WW (SC) and SP Instrumentation Superimposed on TRACG  
Nodalization ]]

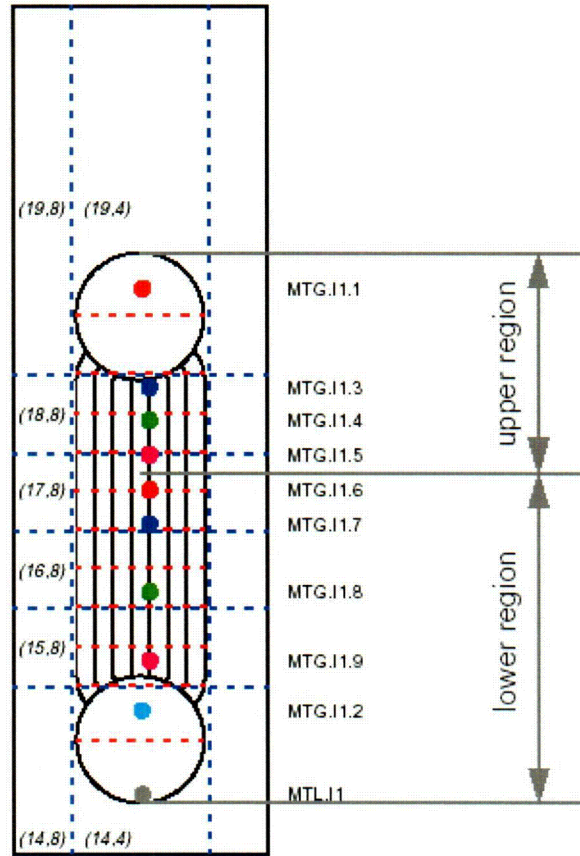


Figure 272.2. IC/PCC Instrumentation Superimposed on TRACG Nodalization

- Q298 On page 3-20 of NEDC-33083P, “TRACG Application for ESBWR,” General Electric (GE) states that because of the limited ability of TRACG to model condensation on horizontal surfaces, part of the diaphragm floor is included in the vent wall heat slab. Mass and heat transfer from horizontal structures differs from mass and heat transfer on vertical structures. Lumping the structures may also effect the definition of the characteristic length used to determine whether the mass and heat transfer process is laminar or turbulent. Describe how the combined heat structure was created, including a discussion of the physical properties (materials, thickness, etc.) and the Biot number (the measure of the thermal internal resistance to the surface film resistance) for each structure and the combined structure to support this model. Provide justification that this model is conservative for this purpose.
- R298. Most of the heat slabs in the ESBWR containment wall (volume boundaries) are vertical surfaces. Non-wall heat structures inside the DW and WW are conservatively ignored. The horizontal heat slabs are the drywell and suppression pool basemats, the diaphragm floor and the drywell top slab. The two basemats are covered with water and will not see any direct condensation. These two basemats were conservatively not modeled in the calculations. The diaphragm floor in the wetwell airspace also is not expected to see any condensation and was conservatively not modeled. The remaining two horizontal surfaces in the drywell are the diaphragm floor (not part of the GDCS pools) and the drywell top slab. The top slab was conservatively not modeled. The diaphragm floor, which is not part of the GDCS pools transfers energy from the DW to the WW airspace during the transient. To model this heat conduction, the diaphragm floor was modeled and accounted for as part of the vertical wall between the DW and WW. The vertical wall between the DW and WW (Levels 6 and 7 in Figure 3.7-1) includes the diaphragm floor area and assumes wall thickness same as that for the diaphragm floor [[ ]]. This simplification in the modeling is expected to have a very small impact on the containment response, as the heat slabs have a very small impact on both the short-term and long-term DW pressure. A sensitivity study was performed to study the impact of this vertical heat slab modeling. In this study, the areas of the vertical heat slab between the DW and WW were [[ ]]. The impact on the calculated long-term containment pressure was a change of [[ ]].
- Q299. On page 3-21 of NEDC-33083P, GE states that certain regions with dead end connections were eliminated but their volumes were maintained in the overall model. This was done to address difficulties in TRACG to control the release of noncondensable gases from these regions. Describe these regions (general location, size, volume, flow path areas, etc.). Are the heat structures associated with these regions included in the model? The calculations are based on a uniform relative humidity in the drywell, with a lower bound value to maximize the noncondensable gases present at the start of the analysis. Are these regions large enough and isolated (by flow restrictions) such that the relative humidity in

these regions could be less than the average resulting in a large inventory of noncondensable gases which could be transported to the wetwell?

R299. Unlike the SBWR design, where the spaces above the GDCS pools were easily identified volumes where the noncondensable gases could accumulate, there are no such large significant volumes with dead end connections in the ESBWR drywell. All other volumes in the drywell are reasonably well connected that the relative humidity and other conditions in any volumes are expected to be uniform. As discussed in RAI 164, the TRACG model does not handle [[  
]] To handle the possible hideout of noncondensable gases in the lower drywell, a simplified volume [[  
]] is used in the ESBWR nodalization.

Q300. In Table 3.4-1 of NEDC-33083P, phenomena identification and ranking table (PIRT) phenomena DW1 and DW4 are identified as "Insensitive." How were these determinations made? PIRT phenomena DW2, DW3 and WW5 are also identified as "Insensitive," based on Reference 82, NEDE-32178P, Rev. 1, "Application of TRACG to Model the SBWR Licensing Safety Analysis," January 1998. Provide a description and the results of the evaluation performed to make these determinations. If DW1 and DW4 were also addressed in NEDE-32178P, include these in the response. (NEDE-32178P is not identified as a report in support of the ESBWR pre-application review.)

R300. [[

II

- Q301 In Table 3.4-1 of NEDC-33083P, PIRT phenomena MV1 and MV3 are identified as “Long-term response insensitive,” based on Reference 24, “TRACG Qualification for SBWR,” NEDC-32725P, Rev. 1 , Vol 2, Section 5.5, September 1997. Is the vent system (pipe length, submergence, flow area, etc.) similar to the SBWR design tested at the Pressure Suppression Test Facility? If not, provided a justification for the values used in the TRACG ESBWR model.
- R301. Both the SBWR and the ESBWR use identical vent systems. The PSTF geometry tested for the Mark III containment is similar to that in the ESBWR. Please refer to RAI 323.8 for further details and discussion. The SBWR vent system was not tested at the Pressure Suppression Test Facility (PSTF).
- Q302. Question was addressed in July 9, 2003, meeting.
- R302. No Response Required.
- Q303. Question was addressed in July 9, 2003, meeting.
- R303. No Response Required.
- Q304. In the PANDA tests (Section 5.7 of NEDC-32725P) it was noted that there was little or no axial stratification in the drywell. However, the TRACG models maintains stratification over the long-term, out to 48 hours (Fig. 3.7-3, NEDC-33083P).

- Q304.1. Explain the mass and heat transport processes in TRACG which sustain this axial stratification. Are there integral or separate effects test which show this sustained axial stratification? How would complete mixing effect the calculated performance on the passive containment cooling system (PCCS) and the containment response to the main steam line break (MSLB) (maintaining a high level of noncondensable gases near the PCCS inlet)?
- R304.1 The PANDA tests have an open drywell geometry, which promotes good mixing. TRACG also calculated good mixing for the PANDA tests and the noncondensibles were quickly swept out of the drywell region into which the steam was injected. In tests where there was a stagnant drywell (i.e. in which the steam was injected in only one of the drywell volumes and the PCCs in the other drywell were not in service), TRACG undercalculated the mixing in the stagnant drywell. In particular, the noncondensibles in the region below the connecting pipe in the stagnant drywell remained in that region in the TRACG calculations, whereas some were swept out in the tests. PANDA did not simulate the restricted lower drywell region, which would not have mixed with the upper drywell.

TRACG transports noncondensibles with the same velocity as the steam; i.e., only one gas phase velocity is calculated. In regions where there are high steam velocities due to the injection of break flow, noncondensibles are quickly swept out with the steam. In regions at the bottom of the vessel, that are not in the primary flow field between the break discharge and exit vents or PCCs, the velocities are low and noncondensable flow may be undercalculated. The circulation velocities are calculated based on the wall friction in the cells in the drywell annulus. Turbulent mixing between cells is not calculated.

The limitations of TRACG with respect to mixing and transport of noncondensibles have been recognized, and the effects analyzed through parametric studies. The issue of complete versus incomplete mixing was dealt with in the studies reported in Table 3.3-5 of NEDC-33083P. The location of the steam line break was artificially varied from axial level 1 through 10 (See Figure 3.7-1 of NEDC-33083P). This was an artifice to vary the mixing of the noncondensibles in the upper drywell. When the break flow was injected in Level 1, the entire upper drywell is well mixed. For break discharge into the higher levels, only the regions above the break location are well mixed. Table 3.3-5 shows a decrease in the peak pressure from [[ ]] as a result of the drywell being completely mixed. Note that most of the decrease is a result of good mixing in the region above the annulus (Level 8 through 10).

The pressure increase in the containment is a consequence of moving the noncondensibles over from the drywell to the wetwell gas space together with an increase in the vapor pressure due to heating of the suppression pool. Beyond 50 hours, all the noncondensibles from the upper drywell have been moved to the wetwell for all cases shown in Table 3.3-5. The energy to the suppression pool due to PCCS heat transfer degradation is minimized for the well mixed case, for which there is a high concentration of noncondensable at the inlet to the PCCS, but for a shorter period of time.

Q304.2. Provide a figure similar to Fig. 3.7-3 for the bounding case analysis.

R304.2. Figure 304-1 shows the Drywell noncondensable partial pressure for the bounding case analysis.

[[

Figure 304-1. Drywell Noncondensable Partial Pressure (Bounding Case)

]]

- Q309 Provide plots similar to Figures 3.7-2 through 3.7-15 in Section 3 of NEDC-33083P for the ECCS/LOCA calculations presented in Section 2 of NEDC-33083P (time frame 0 to 2000 seconds). These plots will provide a means to assess modeling differences, if they exist, between the modeling of containment for core performance versus the modeling of containment for containment performance.
- R309. A set of plots from the ECCS/LOCA case for the Main Steam Line break with one GDSC injection valve failure (Table 2.4-2, NEDC-33083P) is attached here as Figures 309-1 to 309-7. This case uses nominal plant conditions and these figures correspond to those for the Containment/LOCA base case (Figures 3.7-2 to 3.7-9).

It should be mentioned that there are several key nodalizational differences between the ECCS/LOCA and the Containment/LOCA cases. These differences contribute to higher DW pressure (about [[ ]] response for the ECCS/LOCA case for the first few hundred seconds. The longer term response is not impacted.

The ECCS case uses a more detailed nodalization to model the reactor internals (including heat structures and inventory distribution) such as the guide tubes,

shroud wall and steam separators. This detailed modeling of the RPV internals provides better simulation of the RPV response, and calculates a slower depressurization rate for the RPV. The MSL break flow is slightly larger because of the higher RPV pressure and results in a higher DW pressure compared to the Containment case. The Containment case uses a simplified RPV nodalization that does not model the reactor internals. This is the main contributor to the difference in the results. Hence, the ECCS case is judged to be more accurate for the early blowdown response and provides a more realistic time of GDCS initiation.

For the containment case, the initial peak DW pressure following the main vent clearing could be under-estimated by a few psi due to lower break flow as a result of the simplified RPV nodalization. However, this simplification has no impact on the containment design because the maximum DW pressure is determined by the long-term peak pressure, which is higher than the initial peak for the limiting main steam line break case.

Additional differences in the nodalization between the two cases are the main vent modeling and PCC pool temperature. The ECCS case uses [[

]] The Containment case models [[

]] which discharges

horizontally into the suppression pool. A constant PCC pool temperature of [[

]] is assumed for the ECCS case, while the initial PCC pool temperature is [[

]] for the Containment case. The containment model is more representative of the plant in this case. However, these items contribute to only about 1/3 of the DW pressure differences between the ECCS and Containment models seen in the early phase of the transient.

[[

Figure 309-1. RPV and Containment Pressure Responses

**Figure 309-2. Drywell Noncondensable Partial Pressures**

Figure 309-3. GDCS Pool Level

Figure 309-4. PCCS Heat Removal vs. Decay Heat

**Figure 309-5. Suppression Pool Temperatures**

Figure 309-6. Wetwell Gas Space Temperature Response

Figure 309-7. Drywell Temperature Response

]]

- Q310. Provide plots similar to Figures 3-7-2 through 3.7-15 in Section 3 of NEDC-33083P but for the time frame 0 to 500 seconds and for the time frame 0 to 3600 seconds. These plots will provide a means to assess the containment modeling on the short term (blowdown and early gravity driven cooling system (GDCS) injection periods).
- R310. A set of plots from the Containment/LOCA Base Case and Bounding Case is attached here as Figures 310-1 to 310-13.

[[

Figure 310-1. Containment Pressure Response (Base Case)

Figure 310-2. Drywell Noncondensable Partial Pressures (Base Case)

Figure 310-3. PCC Pool Level (Base Case)

Figure 310-4. GDCS Pool Level (Base Case)

Figure 310-5. PCCS Heat Removal vs. Decay Heat (Base Case)

Figure 310-6. Suppression Pool Temperature (Base Case

Figure 310-7. Wetwell Gas Space Temperature Response (Base Case)

Figure 310-8. Drywell Temperature Response (Base Case)

Figure 310-9. Containment Pressure Response (Bounding Case)

Figure 310-10. PCCS Heat Removal vs. Decay Heat (Bounding Case)

Figure 310-11. Suppression Pool Temperatures (Bounding Case)

Figure 310-12. Wetwell Gas Space Temperature Response (Bounding Case)

Figure 310-13. Drywell Temperature Response (Bounding Case) ]]

Q311. Provide a table of the mass flow rate (kg/sec) and energy (J/sec) from the MSLB pipe break into the drywell for the base case (Section 3.7.2 of NEDC-33083P) and the bounding case (Section 3.7.3 of NEDC-33083P). The time between data points should be sufficiently small such that integrating the tabular data would match the integrated values at the time of GDCS injection, and to capture the timing of the suppression pool vents opening and closing and to be useful in performing a CONTAIN audit analysis of the blowdown portion of the accident (data to the onset of GDCS flow is adequate). Also provide the average reactor pressure vessel conditions at the start of GDCS injection - water inventory, steam inventory, average pressure and average temperature, and the times of each trip signal up to GDCS injection.

R311. Tables 311-1 and 311-2 provide the mass flow rate and energy from the MSLB pipe break into the drywell for the base case and bounding case. Figure 311-1 presents break mass flow rate for the two cases. Figure 311-2 presents energy through the break for the two cases.

It should be mentioned that for long-term containment pressure, the SBWR uncertainty analyses (NEDE-32178P Rev.1) showed that a smaller critical flow multiplier results in higher DW peak pressure. Hence, a model parameter of [[ ]] was applied to the critical flow for the bounding case (PIRT84, Table 3.7-1, NDEC-33083P). If the short-term peak pressure were the figure of merit, a multiplier of [[ ]] would have been employed.

Average RPV conditions at or around the start of GDCS injection

**MSLB Base case (at 540 seconds)**

Average RPV pressure = [[ ]] Pa  
 Average temperature = [[ ]] K  
 Water inventory = [[ ]] kg  
 Steam inventory = [[ ]] kg

Trip signal

Power scram at [[ ]] seconds  
 MSIV closure initiated at [[ ]] seconds  
 Level 1 confirmed at [[ ]] seconds

**MSLB Bounding case (at 600 seconds)**

Average RPV pressure = [[ ]] Pa  
 Average temperature = [[ ]] K  
 Water inventory = [[ ]] kg  
 Steam inventory = [[ ]] kg

Trip signal

Power scram at [[ ]] seconds  
 MSIV closure initiated at [[ ]] seconds  
 Level 1 confirmed at [[ ]] seconds

Time (s)	Break Flowrate (kg/s)	Energy (J/s)
----------	-----------------------------	--------------

[[

NEDO-33083-A

]]

Table 311-2. Bounding Case Main Steam Line Break Mass Flow Rate and Energy

[[	Time (s)	Break Flowrate (kg/s)	Energy (J/s)
----	----------	-----------------------------	-----------------

NEDO-33083-A

]]

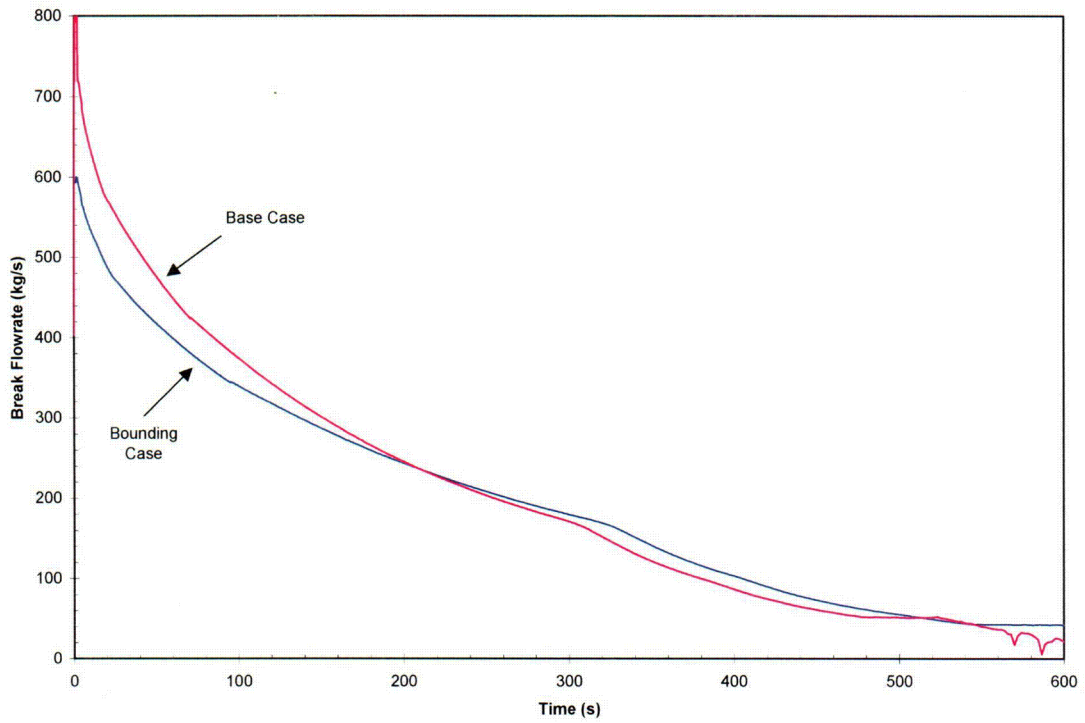


Figure 311-1. Main Steam Line Break Mass Flow Rate

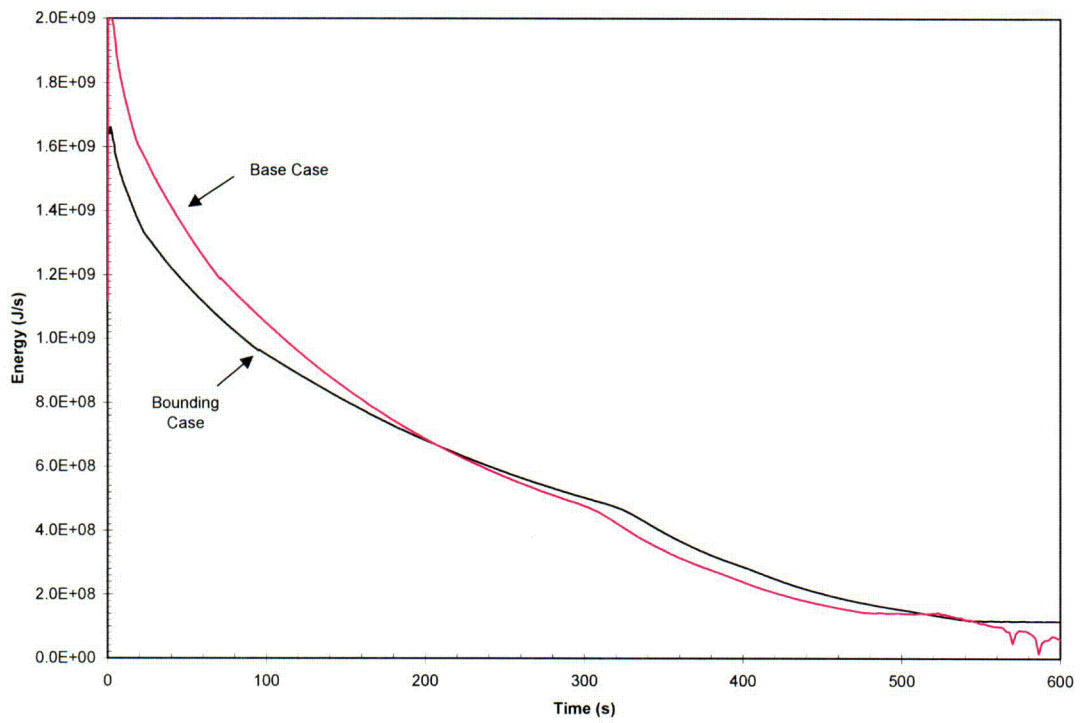


Figure 311-2. Main Steam Line Break Energy

COS

Q317. The TRACG containment models utilize the same conservation equations and constitutive correlations as applied to the reactor system models, i.e., the code, which was initially developed to model the BWR primary coolant system, is currently being used to model the full plant, including the containment. In addition, many of the models have identified errors and uncertainties associated with their use for the containment evaluation. Further the TRACG nodalization models are prescribed to account for additional shortcomings in TRACG to treat some important features, like mixing and stratification in the containment. Some of these prescribed models are based on expected performance (engineering judgement) or the results from small-scale experiment. Typically, containment codes are assessed against a large body of experimental tests (both separate effects and integral tests) designed to address containment performance. In addition, when a new code is proposed for use, an applicant provides a comparison to its currently acceptable code as a benchmark to aid in understanding the results and identifying important features or phenomena in the new methodology.

Q317.1. Provide a plan and schedule to assess the ability of TRACG to model containment performance against integral tests. Integral tests that should be considered include the Marviken tests, the Carolinas Virginia Tube Reactor (CVTR) test 3 without sprays, and the Battelle-Frankfurt Model Containment (BFMC) tests C-13 and C-15 for main steam line breaks. The TRACG results should be assessed against available results from other computer program results (GOTHIC, CONTAIN, etc.).

R317.1. GE agrees to perform assessment of TRACG to model containment performance against integral test data that is publicly available for Standard Problems where the test facilities and tests are well defined. The tests to be analyzed will be specified later, and the analysis will be completed during the design certification phase of the program. GE prefers to compare TRACG calculated results directly to the data rather than to other computed results.

Q317.2. Provide a plan and schedule to assess the ability of TRACG to model containment performance against separate effect tests. Separate effects tests that should be considered include the Wisconsin Flat Plate condensation tests (Huhtiniemi, I.K. and Corradini, M.L., "Condensation in the Presence of Noncondensable Gases," Nuclear Engineering Design, 141, pp.429-446, 1993), M. Siddique, "The Effects of Noncondensable Gases on Steam Condensation Under Forced Convection Conditions," MIT, January 1992, and K. Liang, "Experimental and Analytical Study of Direct Contact Condensation of Steam and Water," MIT, May 1991. The TRACG results should be assessed against available results from other computer program results (GOTHIC, CONTAIN, etc.)

R317.2. GE agrees to perform assessment of TRACG to model containment performance against separate effects test data that is publicly available for Standard Problems where the test facilities and tests are well defined. The tests to be analyzed will be specified later, and the analysis will be completed during the design certification phase of the program. GE prefers to compare TRACG calculated results directly to the data rather than to other computed results.

Q317.3. Provide a plan and schedule to assess TRACG against the previously accepted GE codes used for containment performance evaluations, M3CPT and SHEX. These comparisons need not extend beyond the time of GDCS injection.

R317.3. TRACG comparisons against Mark II and Mark III blowdown tests (which were also the basis of M3CPT assessment) are judged to be sufficient for assessment of TRACG for the blowdown phase of the ESBWR LOCA transient.

Q318 The qualification report for application of TRACG to the ESBWR design indicates that the code version used for the assessment calculations was TRACG02A. The intended code of record is to be version TRACG04. Please confirm and verify that no changes would occur in the calculations when performed with the later version of TRACG. If any changes would occur in the calculated results, submit the corrections to the qualification cases.

R318. [[

]]

**Additional Information provided in response to RAI 318**

The versions of the TRACG code used for the qualification studies reported in TRACG Qualification for SBWR (NEDC-32725P, Rev.1) and TRACG Qualification (NEDE-32177P, Rev.2) were presented in Table 1.2.1 of NEDC-32725P. That table has been used to create the attached Table 318-1. The qualification studies reported in TRACG Qualification for ESBWR (NEDC-33080P) have also been added to the table.

The versions of the TRACG code used in the table are discussed below.

[[



[[

**Table 318-1**  
**Versions of TRACG used for Qualification Studies**

**Table 318-1**  
**Versions of TRACG used for Qualification Studies**  
**(continued)**

**Table 318-1**  
**Versions of TRACG used for Qualification Studies**  
**(continued)**

**Table 318-1**  
**Versions of TRACG used for Qualification Studies**  
**(continued)**

[[

**Figure 318-1: PSTF pressure and level response vs. TRACG04 (ESBWR)**

**Figure 318-2a. TRACG04 (ESBWR) vs. Toshiba CT Void Data at 1.0 MPa and 1390 Kg/m<sup>2</sup>-s**

**Figure 318-2b: TRACG04 (ESBWR) vs. Toshiba CT Void Data at 1.0 MPa and 833 Kg/m<sup>2</sup>-s**

**Figure 318-2c: TRACG04 (ESBWR) vs. Toshiba CT Void Data at 0.5 MPa and 1390 Kg/m<sup>2</sup>-s**

**Figure 318-3: Comparison of TRACG04 (ESBWR) and Time-averaged Data - Average Void Fraction at Nominal Temperature of 280°C**

**Figure 318-4a.: Comparison of Break Flow for Marviken Test 15 with TRACG04 (ESBWR)**

**Figure 318-4b: Comparison of Break Flow for Marviken Test 24 with TRACG04 (ESBWR)**

]]

Q319. The TRAC-BD1 code from which TRACG was derived had an error such that a junction placed other than at the center of a volume would result in an incorrect hydrostatic head. Please confirm that this error does not exist in TRACG.

R319. TRACG does not contain this error. TRACG explicitly accounts for the static head difference in defining the boundary pressure for the 1D components when a junction is not connected to the center of a vessel cell. In addition TRACG contains internal checking of all loops and generates an error message if an elevation mismatch exists. For a loop it is required that:

$$\oint_{\text{Loop}} g dz = 0$$

Q320. The uncertainty analysis methodology for the application of TRACG to AOO events is described very well. Please provide a detailed description of the methodology by which uncertainties are determined for the application of TRACG to the LOCA.

R320. The Application Report sections on ECCS/LOCA and AOOs were compared with a view of providing supplementary information for the ECCS/LOCA section.  
[[

NEDO-33083-A

**KEY PLANT INITIAL CONDITIONS**

NEDO-33083-A

]]

Conformance with 10CFR50.46 criteria requires that:

Peak Cladding Temperature (PCT)	< 1477 K
Peak Local Oxidation ( $\delta$ )	< 17%
Core-wide oxidation ( $\sigma$ )	< 5%

If the absence of core heatup is established with a high level of confidence, these criteria are automatically satisfied.

- Q321. Please augment the discussion presented in Section 3.3.1.1.1 of NEDC-33083P, "TRACG Application to ESBWR," to include the safety relief valves (SRVs). Provide a revised Figure 3.3-1 including the location of the SRV release point into the suppression pool. In the augmented discussion, using the modified figure as a reference; describe what happens in the model as the flow in each main vent stops. For example, when the lower main vent closes, what happens to the interface between the stacked cells (at ring 5 between level 2 and level 3, at ring 6 between level 2 and level 3) as well as what happens to the radial cell interfaces (level 2 between ring 5 and ring 6). Take the discussion through the time when the upper main vent flow stops. What happens to the energy from the SRVs? What cells are considered in the stratification model to account for the SRVs?
- R321. Section 3.3.1.1.1 which discusses the suppression pool stratification model has been supplemented to account for the SRV discharge as shown below to address this RAI. Similarly, Figure 3.3-1 has been modified as shown in the attached figure. **Additions are shown in bold.**

**3.3.1.1.1 Suppression Pool Stratification**

[[

NEDO-33083-A



[[

]]

- Q322. NEDC-33083P, Section 2.2.1.2 defines the Main Steam Line Break (MSLB) LOCA scenario. It assumes that the feedwater flow is not available during the transient. From the emergency core cooling system (ECCS) LOCA evaluation perspective, this assumption leads to conservative ECCS performance evaluation. For containment analysis, it is the common practice to assume that the feedwater flow is available during the LOCA and the injection continues until all the hot water from the feedwater system is consumed. Please provide justification and explain why the feedwater flow is assumed to be cut off during MSLB and why it is conservative to do so.
- R322. For the MSLB containment response analysis, the SAR calculation will assume an appropriate feedwater flow (based on the final design of the feedwater system), consistent with past practice. The calculation performed in NEDC-33083P assumed a simplified feedwater flow coast down in the analysis. It is expected that the assumption of the feedwater flow coast down will have a very limited

impact on the ESBWR MSLB response because the peak containment pressure for this break is determined primarily by the wetwell volume and GDCS pool partial drain down. Since any reasonable addition of feedwater flow will not impact the wetwell airspace and GDCS drain down volume, any impact on the containment pressure is expected to be minimal. The impact of any added energy with the feedwater system is also different (compared to standard BWR's) for the ESBWR as the design has a PCCS system, which would remove any additional energy without significantly heating up the suppression pool.

### **Supplement to RAI 322 Response**

A sensitivity study was performed to assess the impact on containment pressure of injecting all available hot water from the ESBWR feedwater system into the RPV during a LOCA. The Baseline Main Steam Line Break (MSLB) was used in this study. In a sensitivity case, feedwater flow is assumed to be available until all the hot water from the feedwater system is consumed. The results of this study show that the impact on peak drywell pressure is [[ ]].

The Baseline case injected a total of [[ ]] of feedwater [[ ]], or a total volume of [[ ]]. For the sensitivity case, the total hot water volume in the feedwater system (including all the volumes from the feedwater piping and heaters [[ ]) is [[ ]]. To simulate the injection of this additional feedwater mass in the sensitivity case, the TRACG component FILL05 (which simulates the feedwater injection in the TRACG nodalization) is modified as summarized in Table 322.1. The injection velocity is kept constant at the initial value for a period of [[ ]] before the flow coastdown.

Figure 322.1 compares the Feedwater flows between the sensitivity case and the Baseline case. The sensitivity case injected a total of [[ ]], or a total volume of [[ ]].

Figures 322.2 to 322.6 compare the pressures and temperatures in the Drywell and Wetwell between the sensitivity case and the Baseline case.

Table 322.1 Comparison of Feedwater Simulation between  
the Sensitivity and Baseline Cases

**Baseline Case: FILL05 Fill velocity versus time**

[[

]]

**Sensitivity Case: FILL05 Fill velocity versus time**

[[

]]

[[

Figure 322.1 Comparison of Feedwater flow simulations

]]

[[

Figure 322.2 Comparison of Drywell pressures

]]

[[

Figure 322.3 Comparison of Wetwell pressures

]]

[[

Figure 322.4 Comparison of Wetwell Temperatures (Level 7)

]]

[[

Figure 322.5 Comparison of Wetwell Temperatures (Level 6)

]]

[[

]]

Figure 322.6 Comparison of Drywell Temperatures (Level 9)

Q323. For the ECCS LOCA case, in Section 2.6.1 of TRACG application, it is stated that “Drywell model set to minimize containment pressurization rate.” In Section 3.1.4 (Page 3-3), it is indicated that a conservative application approach for containment analysis has been used to model MSLB LOCA containment behavior. GE also pointed out that the TRACG code is not designed to accurately predict containment phenomenon. Specific application procedures are used to apply TRACG to this specific design and different procedures are used to evaluate ECCS and containment responses. Please address the following questions for ECCS LOCA and containment LOCA analysis:

ECCS/LOCA

Q323.1. Does the minimized containment pressurization rate provide a conservative gravity driven cooling system (GDCS) line injection timing and minimum water level prediction? Please explain why.

R323.1. GDCS line injection begins when the combination of the containment (wetwell) pressure and the static head in the GDCS pool is greater than the vessel pressure. [[

]]

Q323.2. List all other detailed modeling procedures and practices to minimize the containment pressurization rate and provide justifications.

R323.2. The major modeling procedure to minimize the containment pressurization rate is [[

]]

Q323.3. In particular, please explain how the wetwell (WW) and drywell (DW) are partitioned into different radial and axial cells and what criteria are used to establish the cell face boundary?

R323.3. The rationale for the nodalization of the SBWR containment model is described in [[

]]

Q323.4. The TRACG physics package is mainly developed based on small and confined space test data. This package has been used to calculate the WW pool condensation, thermal and interfacial heat transfer between the noncondensable gas and WW pool water. Can this physics package provide a conservative two-phase water level in the shroud with the given nodalization?

R323.4. The TRACG models for containment modeling have been discussed at length in responses to RAIs [[

]]

**Supplemental Information for RAI 323.4**

TRACG uses realistic models to calculate the effects of compression of the noncondensibles and heat transfer to the walls on the wetwell gas temperature. A sensitivity study was performed to assess the impact of using a lower bound value for the wetwell gas temperature on the two-phase water level in the RPV chimney. The result shows that the maximum impact is an [[ ]]] delay in the starting time of the GDCS flow, and a reduction of [[ ]]] in the minimum static head in the chimney.

TRACG calculates a peak wetwell gas temperature of [[ ]]] at about [[ ]]], or a short time before the initiation of GDCS flow in the ECCS/LOCA Base case (GDCS line break). This WW gas temperature is reasonable when compared to the lower bound value of [[ ]]] (TRACG calculated suppression pool surface temperature) and the upper bound value of [[ ]]] (calculated by isentropic compression, assuming all noncondensable gases in the WW airspace). A lower WW gas temperature would have the effect of reducing the WW gas pressure, which in turn,

decreases the GDCS driving head and delays the starting time of the GDCS flow. The estimated delay time based on the RPV depressurization response and perfect gas assumption in the wetwell gas space is [[ ]] if the WW gas temperature is set equal to the lower bound value of [[ ]]. A TRACG parametric case was performed with [[ ]] delay on the initiation time of the GDCS flow. The effect was to reduce the minimum static head in the chimney by [[ ]].

Q323.5. Due to the TRACG ECCS/LOCA model containment radial distortion, the staff is not convinced that the distribution of steam and noncondensable gas calculated by the ECCS/LOCA model is inaccurate. Please explain how the long term cooling through passive containment cooling system (PCCS) was affected and why the current application procedure can lead to a conservative minimum water level prediction at about 10 to 11 hours into the transient.

R323.5. The long term minimum water level is determined primarily by [[

]]

Q323.6. For the same reason, have other parts of the containment (WW, GDCS Pool, PCCS) model been set to minimize the prediction of the two-

phase water level above the core? If so, please provide detailed modeling procedures and justifications.

R323.6. See the response above for the final equilibrium level reached.

Q323.7. Have the DW to WW vents been modeled in the same way for ECCS /LOCA as for containment/LOCA? If not, please explain why.

R323.7. [[

]]

#### CONTAINMENT/LOCA

Q323.8. It is stated that a special modeling approach has been used to model WW and DW to WW vents to conservatively calculate the WW temperature and pressure response. This approach appears to be developed based on the TRACG model nodalization for the pressure suppression test facility (PSTF) test. Please explain why the similar nodalization can produce conservative response even though the PSTF geometry dimensions appear to be different from that of the ESBWR WW.

R323.8. [[

]]

Q324 It was stated on page 2-38 of NEDC-33083P that the minimum chimney water level occurs at about 10 to 12 hours after the break. However all the ECCS LOCA cases documented in the report stop at 2000 seconds. Please provide a

conservative GDCS LOCA calculation to demonstrate that the two-phase water level remains above the core beyond 12 hours after the break. When performing the calculation, consider using 102% power, the correct scram time and other conservative assumptions.

- R324. A GDCS LOCA calculation was performed at 102% power with other conservative assumptions. In this case, reactor scram was initiated on High DW pressure, and reactor power started to shutdown after an appropriate delay time. Figure 324-1 shows the comparison of static head in chimney and downcomer collapse level. The core is covered and remains covered by more than [[  
]] of 2-phase mixture for the entire transient (0 ~ 7 hours). Consequently, there is no core heatup. At the end of this transient, the static head in chimney reaches the quasi-steady level of [[  
]] Please refer to RAI 323.5 for additional discussion of level responses beyond 7 hours.

[[

Figure 324-1. Comparison of Static Head in Chimney and Downcomer Collapse Level  
]]

- Q325. What computer code was used to calculate decay heat and core void effects? Has that code been previously reviewed by staff? If so, please provide any relevant references.

R325. The decay heat model for transients and for LOCA evaluations is the same as the model reviewed and approved for SAFER-GESTR (NEDE-23785 Vol. III Appendix B), with the following improvements:

- The decay heat from fission products has been updated from the ANSI/ANS-5.1-1979 standard to the 1994 standard
- The fuel cycle parameters (enrichment, exposure, ect.) were conservative, bounding values rather than nominal values
- Because conservative values were used for the fuel cycle parameters in place of nominal values, the uncertainty terms associated with the nominal values were eliminated, leaving the basic two-sigma data uncertainty from the standard
- New, more conservative evaluations of miscellaneous Actinides and structural activation products provide additional heat

Q326. According to the ESBWR design description, the GDCS pool air space is connected to the suppression pool air space through three large diameter vent pipes. Therefore, the pressure should be equalized during normal operation. However, TRACG calculated a higher GDCS pool air space pressure than the suppression pool pressure due to the simplified GDCS pool nodalization. This unrealistic pressure results in a higher initial inventory of air in the GDCS space. Please explain the effect of this nodalization on the calculated ECCS performance and, ultimately, the minimum chimney two-phase water level.

R326. TRACG uses a staggered mesh in which the momentum equation is integrated from cell-center to cell-center. The cell pressure is calculated at the center of the cell. [[

]]

Q327. It is assumed that the MSLB never occurs outside containment inside the out-board main steam isolation valve. Please explain why.

R327. The issue of pipe breaks between the MSIV and the containment boundary has been addressed previously for BWR's and the resolution has been accepted by the NRC. This issue is addressed in the Safety Analysis Report. The simple answer is that no pipe breaks or cracks are postulated in portions of piping from containment wall to and including the inboard or outboard isolation valves. The piping from the inboard isolation valve out to the outboard isolation valve is what we call "holy pipe". It is designed to very stringent requirements as dictated by the ASME code and as stipulated in the SAR. This piping must have somewhat low stress levels and fatigue usage. Welded attachments are avoided and welds are minimized. The isolation valves are located "as close as practical to the containment wall".

Please see the attached three pages from the ABWR Standard Safety Analysis Report for further details. Similar positions exist for all the operating BWR's licensed by the NRC. Since there is nothing fundamentally different in the ESBWR, the same approach applies to the ESBWR.

Q328. TRACG models the two-phase flow in the chimney using three large 3-D vessel radial rings instead of 1-D pipe components.

Q328.1. Does the 3-D vessel component result in the same flow regime as 1-D pipe components if 1-D components have been used to model the chimney?

R328.1. [[

]]

Q328.2. For the open space above chimney and below the separator inlets, what would be the flow regime there during normal operation? Is it possible that, during the normal full power operation, steam and saturated liquid would tend to separate in this open space and the volume averaging approach may not be valid?

R328.2. [[

]]

Q328.3. TRACG 1-D Pipe component has been validated against Ontario Hydro test data. Does this validation apply to 3-D Vessel component too? How? Does Ontario Hydro test data cover both ESBWR full power operation condition and start-up operation? During the start-up, when the channel outlet void fraction is small (in the bubbly flow regime), is it possible that the void tend to flow preferably in a small region in the chimney or the open space above to form a high void concentration region so that the averaging by TRACG would over-estimate the two-phase natural circulation driving head?

R328.3. [[

]]

Q329. It has been repeatedly stated that the ESBWR has significant margins for LOCA since the calculated two-phase water level by TRACG is always above the top of active fuel. The TRACG 3-D vessel two-phase water level tracking algorithm has been used to calculate the two-phase water level location in the chimney region during GDCS LOCA transient. The underlying assumption of this level tracking algorithm is that within each cell, there are no flow restrictions. However the entire core is not under a single chimney partition. The two-phase water level in the chimney is expected to be vary. The TRACG 3-D vessel model numerically averages the two-phase mixture level in three radial rings. Please provide justification or demonstrate through sensitivity runs that the TRACG code is capable of calculating the minimum two-phase water level considering the chimney partition and bundle power distributions for GDCS LOCA.

R329. The TRACG nodalization used for the ECCS/LOCA analysis employs three vessel rings to represent the large number (~ 60) of chimney cells in the reactor vessel. Each chimney partition cell in the ESBWR receives flow from 16 fuel

bundles (4 x 4 array) and the bypass region associated with those bundles. Thus, the calculated two-phase level in each ring of the TRACG model represents the average of the chimney two-phase levels for all the partition cells represented by that ring. In order to assess the effect of modeling a localized chimney cell above a high-power cluster of 16 bundles, one can examine the sensitivity of the two-phase levels in the three TRACG rings representing chimney cells, each fed by a corresponding group of bundles, to the bundle radial peaking factors. Accordingly, a study was performed to examine the effect of bundle power distribution on the minimum chimney water level.

The baseline case (GDCS line break) was used for the study. The same radial peaking factor was applied to all the bundles in a given ring. The radial peaking factor for all 194 bundles feeding the chimney region in Ring 1 was set equal to 1.43. The other radial peaking factors were 1.00 for the 492 bundles feeding the chimney region in Ring 2 and 0.75 for the 336 bundles feeding the chimney region in Ring 3. The minimum static heads in the chimney regions in Rings 1, 2 and 3 for this parametric case are [[ ]]

The result of this study shows that the impact of assigning a uniform high radial peaking to all the bundles feeding the chimney region in Ring 1 is less than [[ ]] on the chimney minimum static head, or less than [[ ]] of the margin in the minimum static head. Therefore, the TRACG code with the current representation of the ESBWR chimney (Figure 2.7-1) and bundle power distribution is judged to be adequate for calculating the minimum two-phase water level for a GDCS LOCA.

**Supplemental Information for RAI 329**

Additional parametric study was performed to examine the effect of bundle power distribution on the minimum chimney water level. The baseline case (GDCS line break) was used for the study. The same radial peaking factor was applied to all the bundles in a given ring. The radial peaking factor for all 194 bundles feeding the chimney region in Ring 1 was set equal to 1.4791. The other radial peaking factors were 1.00 for the 492 bundles feeding the chimney region in Ring 2 and 0.7263 for the 336 bundles feeding the chimney region in Ring 3. The minimum static heads in the chimney regions in Rings 1, 2 and 3 for this parametric case are [[ ]].

The result of this additional study shows that the impact of assigning a uniform high radial peaking to all the bundles feeding the chimney region in Ring 1 is less than [[ ]] on the chimney minimum static head, or less than [[ ]] of the margin in the minimum static head.

Q330. Please provide the following TRACG input decks:

Q330.1. ECCS/LOCA Bottom drain line LOCA case

Please provide both the pre-test and post-test calculation input decks for Tests 15\_1 and 23\_4 ( Page 4.1-1 of TRACG SBWR qualification for SBWR.)  
Need 1-Tube model and eight tube models.  
Test T12, T13, T11 and T02 input decks

R330.1 The requested input decks were provided to the NRC separately.

Q330.2 MSLB/LOCA case power/time table (TRACG Power Cards) considering delayed scram

Please provide both the pre-test and post-test calculation input decks for Tests 15\_1 and 23\_4. ( Page 4.1-1 of TRACG SBWR qualification for SBWR.)  
Need 1-Tube model and eight tube models.  
Test T12, T13, T11 and T02 input decks

R330.2 The requested input decks were provided to the NRC separately.

Q331. Please provide the material properties and dimensions of the vessel wall, vessel thermal insulation layer, air gap and vessel shield. Justify why these components are lumped into one heat structure.

R331. The following provides the necessary information about the vessel, thermal insulation, and shield wall.

**RPV:**

Wall thickness = Nominal 184 mm (including cladding)

Wall material – Either plate or forgings of SA-533, Grade B, Class 1 for plate and SA-508, Class 3 for forgings

**Insulation:**

Insulation is approximately 90 mm thick of the reflective type, with thin inner sheets separated by air gaps. The insulation stands off from the vessel wall about 250 mm. The average heat transfer coefficient is  $0.907 \text{ W/m}^2\text{K}$

Vessel shield wall is 160 mm thick made of low alloy structural steel.

Please refer to RAI 12 for the answer to part 2. of the question

Q332. On Page 2-36 of NEDC-33083P, it is stated that “There are three GDCS pools in the ESBWR containment, supplying four divisions of GDCS to the vessel.” Based on the ESBWR design description, there is only one division of GDCS for each GDCS pool. Please clarify the total number of divisions from GDCS pools.

R332. The ESBWR Design Description, NEDC-33084P, Section 4.1.2.1, "GDCS Short-Term Subsystem Requirements", states:

The required total RPV injection flow rates, as established by appropriate ECCS analyses, shall be supplied from three separate, non-divisional, GDCS pools via a four-division set of short-term injection piping trains, with one of these three GDCS pools being connected to the RPV via two independent short-term injection piping trains and each of the other two GDCS pools being respectively connected to the RPV via single dedicated remaining short-term injection trains.

There are three (3) pools supplying four (4) divisions of GDCS. Also refer to the schematic shown in Figure 332.1.

ESBWR Gravity-Driven Cooling System - Simplified Schematic Diagram

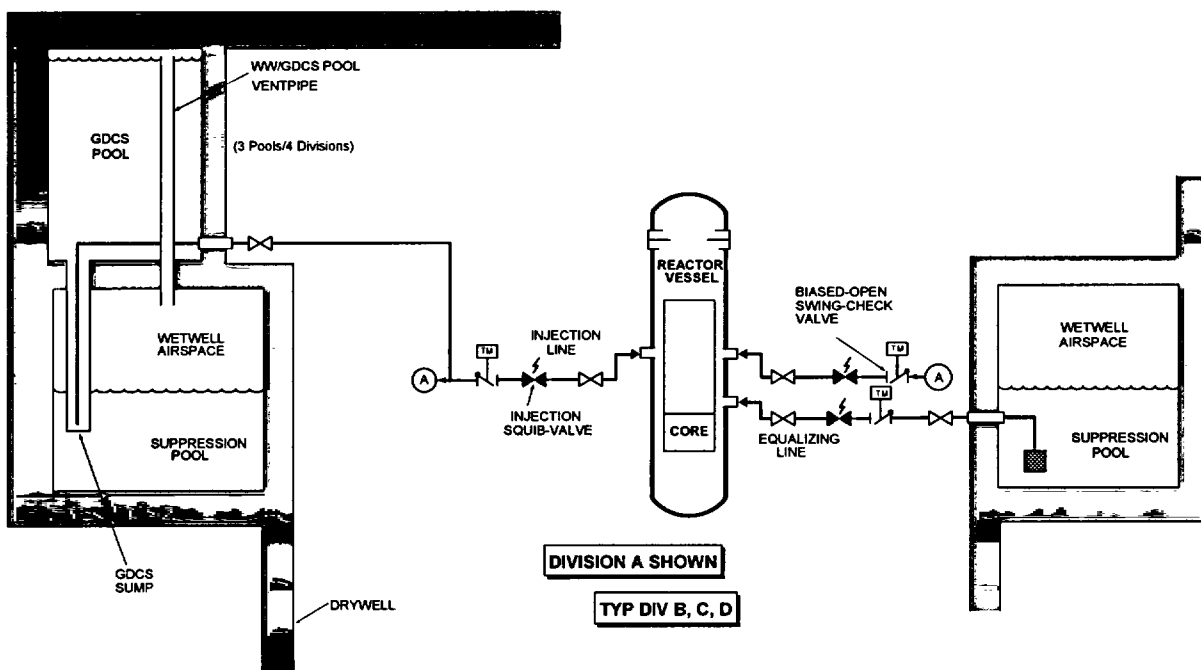


Figure 332.1

Q333. In order to verify the TRACG critical flow model, we have developed and run a simple test problem. It consists of two break components and a pipe component. Two break components define the pressure boundary conditions (73 bar upstream and atmospheric pressure downstream). A pipe with an orifice at the center was initially set to 73 bar through out its entire length. Then, the downstream break is depressurized to atmospheric pressure. The TRACG code predicts choke condition at the orifice. However, the calculated fluid velocity at the choke point is only about 60 meters per second. Usually, the sound speed is expected to have be on the order of 100 - 300 meters per second. Therefore, the calculated choke

flow velocity appears to be lower than the sound speed. Please provide a separate effect test benchmark TRACG deck to assist the staff's further review.

- R333. The sonic velocity varies as a function of stagnation pressure and quality at the choke plane. Both have a strong effect on the velocity of sound in homogenous, equilibrium mixtures (HEM) of steam and water. These relationships are shown in Figure 6.11 on page 146 of Graham Wallis's book One-dimensional Two-phase Flow (McGraw Hill, New York, 1969). Wallis attributes the figure to H. B. Karplus (1958). For convenience, it is reproduced here as Figure 333-1. The figure shows that one should expect that for a pressure of 73 bar (1059 psia) that the HEM sonic velocity is approximately 50 m/s for qualities of 0.05 or lower. At the choke plane where the pressure is lower, the sonic velocity is even lower.

The sonic velocity is discontinuous at qualities of 0.0 and 1.0 corresponding to the transitions between single-phase and two-phase flow. This discontinuity in sonic velocity is due to the discontinuity in the specific heat at constant volume ( $C_v$ ) that occurs at these points. The fact that this will lead to a discontinuity in the sonic velocity is evident from equations (D-10), (D-17) and (D-18) in Appendix D of NEDE-32176P (Rev. 2). This discontinuity is the reason that the sonic velocity can be as much as an order of magnitude lower for low-quality steam-water mixtures than it is for single-phase saturated liquid at the same pressure.

Appendix E of NEDE-32176P (Rev. 2) contains the derivation of the HEM sonic velocity that is used in TRACG. The crux of the problem is to define the compressibility at constant entropy. The simplified form with no noncondensable gas is presented in Eq. (E-40). Free and Spore have obtained the same result (see References 6.3-1 and 6.3-2 cited in NEDE-32176P, Rev. 2). The conclusion is that the fluid velocity of approximately 60 m/s calculated by TRACG at the choke point is a reasonable value.

A proof of the adequacy and applicability of the TRACG critical flow model is the qualification against separate effects critical flow experiments that is documented in Section 3.4 of NEDE-32177P, Rev. 2. The Edwards blowdown problem described in Section 3.4.3 is a good one to consider both because of its simplicity and because it involves critical flow for a wide range of void fractions. Selected calculated results are compared to test data in Figures 3.4-16 and 3.4-17 of NEDE-32177P, Rev. 2. The TRACG input deck for the Edwards blowdown problem is transmitted in the separate ASCII file named "EDWARDS.INP". The corresponding pressure and void fraction data are contained in the ASCII file named "EDWARDS.DAT".

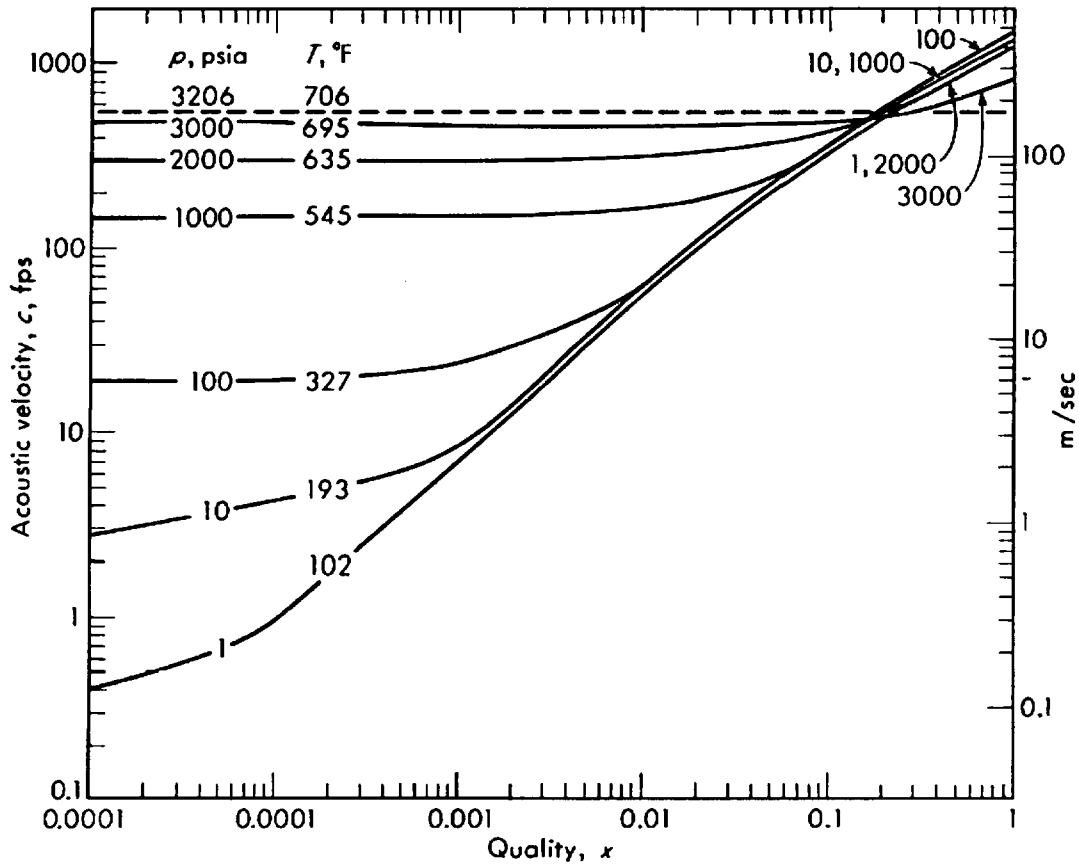


Figure 333-1 Theoretical Sonic Velocity for HEM of Steam and Water

Q387. Pages 2-113 (1st paragraph) and 2-119 (Table 2.6-2). As stated, the initial test conditions for the GIRAFFE/SIT tests approximate the SBWR conditions when the RPV pressure reaches 150 psia.

Q387.1. What was the basis for the initial test conditions in Table 2.6-2?

R387.1. The initial test conditions in Table 2.6.2 were based on TRACG runs for the SBWR. The conditions at 1.034 MPa were selected for the initial conditions of the tests.

Q387.2. Compared to three other GDLB tests, Test GS3 (BDLB) had the highest initial DW and WW pressures, but it had the lowest initial SP water temperature. Why didn't Test GS3 have the highest initial SP temperature?

R387.2. Please see the response to RAI 387.1, which describes the basis for the initial conditions for the tests. [[

]]

**Q388. Page 2-113, last paragraph. As stated, data from Test GS3 were examined to identify any potential systems interactions associated with the IC and PCC operation for a BDLB. How was this done? Was there a similar BDLB test but without the isolation of the ICs and PCCS operation for comparison?**

**R388. [[**

]]

[[

]]

It has been indicated that the ESBWR core would never be uncovered during a loss-of-coolant accident (LOCA) since the two-phase water level is always above the top of active fuel region. The staff performed a confirmatory analysis using TRACG V4.0 and gravity-driven cooling system (GDCCS)/LOCA input deck provided by General Electric (GE). The calculated results show that the hot channel, which is modeled by CHAN0011, experiences high void fraction flow for a period of 30 seconds starting from 400 seconds into the GDCCS/LOCA event. The maximum channel inlet and outlet void fractions are 0.96 and 0.98 respectively, while the void fraction in the heated region is about 93 percent. Therefore, part of the core is uncovered for a short period of time. A tele-conference was held on July 29, 2003, between the NRC staff and GE representatives regarding this issue. The following are GE's verbal positions:

- GE also predicted the same high void flow using TRACG V4.0 code for the GDCS/LOCA case.
- GE believes that [[  
  
]] This is no different from operating BWR LOCA phenomenon.
- GE believes that [[  
  
]] no dryout would occur during the blowdown.
- GE indicated that [[  
  
]] However, [[  
  
]] during the blow-down phase.
- GE believes that the TRACG code has the capability to predict critical heat flux for high void flow in the core and the [[  
  
]] the boiling transition.
- GE believes that the ESBWR fuel rod surface will not experience boiling transition [[  
  
]] occurs during the blowdown.

The staff requests GE to respond to the following questions and provide necessary justifications and technical basis:

- Q406. Three LOCA cases have been analyzed by GE so far. They are the GDCS Line LOCA, Main Steam Line LOCA and bottom drain line LOCA. Please calculate the duration of the hot channel high void flow for all three cases using conservative approaches, i.e, 102 percent initial power level, delayed scram, 2 uncertainty for correlations leading to a higher void fraction and a longer duration of high void flow, hot channel bundle power peaking factors, etc. Please model the chimney partition above the hot channel appropriately.
- R406. Results of the Scoping Break Spectrum Analysis (Table 2.4-2, NEDC-33083P, TRACG Application for ESBWR) show that the GDCS line break with one GDCS injection valve failure is the limiting case. Accordingly, this limiting case was analyzed to determine the duration of the hot channel high void flow. This case was performed with 102% initial power and other conservative assumptions. Reactor scram was initiated on high drywell pressure, and reactor power started to shutdown after an appropriate delay time. The effect of chimney partition above the hot channel was modeled the same way as that discussed in RAI 329. In this extreme case, the radial peaking factor for all the bundles feeding the chimney region in Ring 1 was set equal to 1.43. Results of this case show that the peak



drafting effect. These cases (Cases 1 to 3 in the following Table) were performed with 102% initial power and other conservative assumptions. Reactor scram was initiated on high drywell pressure, and the control rods started to move into the core after an appropriate delay time. The effect of chimney partition above the hot channel was modeled the same way as discussed in RAI 329. In these cases, the radial peaking factor for all the bundles feeding the chimney region in Ring 1 was set equal to 1.4791.

No core heatup was calculated for these three cases. The hot channel peak void fraction and minimum thermal margin during the transient for these cases are summarized in Table 406.1. The high void fraction “window” is shown graphically in the attached figures. Two other cases were re-run with the detailed thermal margin edits for the GDCS Line LOCA without the chimney drafting effect corresponding to the Baseline and Bounding Cases presented in the Application Report (NEDC-33083P, Rev. 0). The results for these cases are also summarized in Table 406.1 (Cases 4 and 5) for comparison. Note that the early thermal margin from the GEXL correlation relates to critical power ratio, while the thermal margin in the later part of the transient from either the Zuber or Biasi correlations refers to critical heat flux ratio. Significant margin to boiling transition ( $\geq 2$ ) is calculated during the high void period of depressurization for all these cases.

Table 406.1 Summary and Comparison of Parametric Case Results

[[

---

]]

[[

Figure 406.1 Window of high channel exit void fraction for Case 1

]]

[[

Figure 406.2 Window of high channel exit void fraction for Case 2

]]

[[

]]

Figure 406.3 Window of high channel exit void fraction for Case 3

[[

Figure 406.4 Window of high channel exit void fraction for Case 4

]]

[[

Figure 406.5 Window of high channel exit void fraction for Case 5

]]

Q407. What is the uncertainty of the modified Zuber critical heat flux correlation? Please calculate the hot channel departure from nuclear boiling ratio (DNBR) through out the entire high void flow condition and demonstrate that adequate margin exists. Please provide justification that the current DNBR calculation is conservative enough to ignore any sub-channel flow effects.

R407. [[

]]

Q408. What is the basis to define the hot channel power peaking factor as [[ ]]? Have any sensitivity analyses been performed to address the impact of the axial power shape and hot rod power peaking factor? If so, please provide the results of the sensitivity analyses.

R408. BWR cores are not restricted to a maximum value of the radial peaking factor. Two thermal limits have to be satisfied: the Peak Linear Heat Generation Rate (PLHGR) for the fuel design and the Minimum Critical Power Ratio (MCPR) for the limiting Anticipated Operating Occurrence (AOO). The specification of these criteria allows the core designer to optimize the fuel design and core operation. [[

]]

QA1 Explain the sudden increase in break flow observed in the TRACG calculation of the GDCS line break at about 540 s (see Figure A-1.1).

RA1 The TRACG calculation for the GDCS line break was performed with just one cell representing the broken GDCS line between the reactor pressure vessel (RPV) and the break location. This cell also accounted for the change in cross-sectional area of the pipe from the area of the venturi throat at the RPV nozzle to the full area of the GDCS line (as shown in the inset figure A-1.1). While this representation was adequate for the early transient, it introduced distortions at low pressure. At about 540 s into the transient, the minimum area at the venturi became unchoked, resulting in a shift to Bernoulli flow at the larger exit flow area. This caused a sudden increase in the break flow. This change was exaggerated by the single cell nodalization.

Normal practice for LOCA calculations is to use several cells (typically [[ ]]) for the break pipe. A second calculation was made in which the break pipe was nodalized into [[ ]] cells. The cross-sectional area of these cells was kept constant, equal to the area of the venturi throat. The results are plotted in Figure A-1.2. It can be seen that there is no longer a sudden change in the flow at 540 s. The drop in flow at 600 s, which is common to both calculations, is due to the two-phase level in the downcomer falling to the elevation of the break. The impact of using the [[ ]] break pipe on the minimum collapsed level in the chimney was [[ ]]m, relative to the greater than 2 m margin to core uncoverly. Figure A-1.3 shows a comparison of the break flow for the two cases ( [[ ]] break pipes). This shows clearly that the sudden increase in break flow in the original calculation is an artifact of the coarse nodalization used.

The calculations for the Safety Analysis Report will be performed with a detailed nodalization of the break region, with at least [[ ]] cells. A break nodalization sensitivity study will also be performed to justify the adequacy of the nodalization used.

[[

**Figure A-1.1: Break flow response for GDCS Line Break with One-Cell Break Pipe**  
]]

[[

**Figure A-1.2: Break flow response for GDCS Line Break with Four-Cell Break Pipe**  
]]

[[

·  
·  
·

**Figure A-1.3: Comparison of Break Flow with One and Four Cell Break Pipes** ]]

QA2 In the TRACG calculation of the GDCS line break LOCA (see below), the level in the chimney was oscillating significantly, followed by a sudden jump. Is this physical?

[[

]]  
RA-2 The oscillations in the chimney level were present in the time period from 900 to 1400 s. During this time period, GDCS water is refilling the core and chimney through the downcomer and lower plenum. Quenching of voids in the core results in an increased static head inside the shroud. Consequently, the flow from the downcomer is reduced. After a transport delay, the void fraction in the core and chimney increases slightly because of the reduced flow. The reduction in static head in the core and chimney produces an increase in the flow from the downcomer, completing a cycle of manometric oscillation between the core/chimney and downcomer. The TRACE calculation also shows oscillatory behavior in this time period.

The TRACG model of the chimney consists of three rings. The plot shown above is for the central ring with the high power bundles. The transient responses of the collapsed level in the chimney for the three rings and for the downcomer are shown in Figures A-2.1 through A-2.4. There are effectively three parallel paths between the downcomer and the core/chimney regions. The oscillations are most noticeable in the central chimney ring, which has the smallest area and the highest power bundles.

As stated above, the oscillations are physical and not numerical in origin. Figure A-2.5 shows details of a 100 second period between 1000 to 1100 s. The mass flow rates in the Ring 1 chimney region are plotted at different elevations. The time period for these manometric oscillations is of the order of 6-7 s, which is reasonable for these U-tube oscillations. Numerical oscillations would have a time period of the order of two time steps ( much less than 1 s). During this time period, the chimney is filling up and the average level in the chimney is below the top. Thus, the mass flux at the exit is zero for the most part with the exception of a few oscillation peaks that result in flow out the top of the chimney.

Later in the transient, the two-phase level in the chimney rises above the top of the partitions and the oscillations in the chimney levels are significantly reduced. As the downcomer level rises still further, the pressure drop imposed on the chimney increases. [[

]]. Rings 2 and 3 are not as significantly affected by flow regime transitions and have a smoother response.

[[

**Figure A-2.1: Collapsed Level in Ring 1 of Chimney**

**Figure A-2.2: Collapsed Level in Ring 2 of Chimney ]]**

[[

Figure A-2.3: Collapsed Level in Ring 3 of Chimney

**Figure A-2.3: Collapsed Level in Ring 3 of Chimney**

**Figure A-2.4: Collapsed Level in Downcomer ]]**

[[

**Figure A2-5: Mass flow oscillations in chimney during refilling phase ]]**

QA3 Provide parametric study case to support the simplified modeling of the PCCS used in the ESBWR TRACG Calculation.

RA3 A parametric case has been performed to evaluate the effect of simplified modeling of the PCC fluid volumes and flow areas on the long-term containment pressure. The result shows that the peak drywell pressure for the case using actual PCCS volumes and flow areas is [[ ]] than that of the case using simplified model.

The reference ESBWR design uses 4 PCCS with a total rated capacity of [[ ]]. The ESBWR PCC has [[ ]] rated capacity than the prototype unit used in the PANTHERS test. The increased capacity in the ESBWR unit is achieved by increasing the total number of PCC tubes by [[ ]] (i.e., from 496 to 672). The headers (steam and water) volumes are also increased accordingly.

The TRACG nodalization for the PCCS used in the ESBWR application cases is as follow. The heated perimeter and the heat transfer area for the PCC condenser tubes are scaled up [[ ]] from those of the prototype unit. However, there are no adjustments in the volumes and flow areas for the headers and the PCC tubes, i.e., same volumes and flow areas as those for the prototype unit. This simplification was based on engineering judgment that the effect of these increased volumes and flow areas on the long-term containment pressure is expected to be small.

A parametric case has been performed to evaluate the effect of these increased volumes and areas on the long-term containment pressure. The nominal Containment/LOCA Analysis (Section 3.7.2 of NEDC-33083P), i.e., baseline case for the Main Steam Line Break, was simulated with simplified modeling of the PCCS (the base case) and with corrected PCCS volumes and flow areas (the parametric case). Both cases were run using the 9-Apr-2004 Version of TRACG04. The effect on the long-term containment pressure is determined by comparing the results from these two cases.

Figures A3-1a and A3-1b show the comparison of long-term containment pressure responses. Figure A3-1a shows the results from the base case without adjustment of PCC cell volumes and flow areas, and Figure A3-1b shows the results from the parametric case with adjustment of PCC cell volumes and flow areas. These figures show good agreement for the transient responses between the base case and the parametric case. The peak drywell pressure levels off and remains well below the design pressure of 60 psia. The peak DW pressure for the parametric case with [[ ]] and flow areas is [[ ]] than that of the base case.

[[

Figure A3-1a. Containment Pressure Response for the Main Steam Line Break (Base Case)

]]

[[

Figure A3-1b. Containment Pressure Response for the Main Steam Line Break Parametric Case, With Corrected PCC Volumes and Flow Areas)

]]

QA4 Explain the sudden increase in SRV flow observed in the TRACG calculation of the GDCS line break at about 320 seconds (see Figure A4-1). If necessary, provide a revised ESBWR TRACG input deck for the GDCS line break analysis.

RA4 The “sudden spikes” in the SRV mass flow (Figure A4-1) and velocity were observed shortly after the SRVs opened fully. This was caused by an input error related to the SRV valve model. The loss coefficient at the valve location for component VLVE92 is modeled as a function of valve opening area, i.e., a data table with loss coefficient versus valve area opening fraction. In this table, loss coefficient became zero when the valve was fully opened. When there is no irreversible loss at the valve location, the flow at the restriction becomes unchoked, resulting in a high flow rate for a short period of time until it is limited by choking at a downstream location.

Normal practice is to use a loss coefficient of 1.0 at locations of large area contractions. The input deck was revised to include the following SRVs modeling changes: (1) replace the valve data table with a constant loss coefficient of 1.0 at the valve location for component VLVE92, and (2) change the loss coefficient of 0.6 to 1.0 at boundary # 7 of components VLVE92 and VLVE93. The impact of the SRVs modeling change on the minimum collapsed level in the chimney was [[ ]], relative to the greater than [[ ]] to the core uncover.

The ESBWR TRACG input deck for the GDCS line break analysis (nominal baseline case) was revised to include two other modifications.

1. The break pipe between the reactor pressure vessel (RPV) and the break location in the drywell (DW) is modeled with 4 cells instead of the earlier single cell. This issue was discussed in RAI A-1. The impact of this modeling modification on the minimum collapsed level in the chimney was [[ ]].

2. The discharge location for the broken GDCS line between the GDCS pool and the DW annulus was corrected.

An error was identified in the ECCS/LOCA input deck for the GDCS line break. This error was related to the discharge location for the broken GDCS line between the GDCS pool and the DW annulus. The broken line discharged to the suppression pool instead of to the DW annulus. Because the ECCS/LOCA cases are run for a short period of time (~2000 sec), the inventories in the drywell and the suppression pool are minimally impacted by the error. A run was made after correcting this input error and the impact on the minimum collapsed level in the chimney was [[ ]].

The revised input deck with the modifications described above was run using the TRACG04 version that was created on 17-Jan-2003 (version sent to NRC). Figure A4-2 shows the SRV mass flow rate at the valve location from component VLVE92. A comparison between Figure A4-1 and A4-2 clearly shows that the sudden increase in SRV flow at about 320 seconds (Figure A4-1) is no longer present when reasonable loss coefficients are input at the valve location.

Figures A4-3 and A4-4 show the comparison of two-phase level and the static head in the chimney. Figure A4-3 shows the results before the 3 input modifications, and Figure A4-4 shows the results after the 3 input modifications. These figures show that the impact of input modifications on the transient responses is minimal. The impact of these combined changes on the minimum collapsed level in the chimney was [[ ]], relative to the greater than 2 m margin to the core uncovery.

The revised input deck was also run using the TRACG04 version that was created on 9-Apr-2004. The transient responses agree well between these two versions of TRACG04. The impact on the minimum collapsed level in the chimney was [[ ]].

The input deck and the output file (using TRACG04 version of 17-Jan-2003) are included in the attached CD, and summarized in the following table.

Item #	File Name	Description
1	GDL-NL2_K2.INP	Input deck (ASCII file) for the GDCS line break. This is a "stand-alone" input deck and no restart dump file is needed for the calculation. This input deck included 3 input modifications.
2	GDL-NL2_K2.OUT	Output file (ASCII file)
3	GDL-NL2_K2-input.pdf	PDF file format of Item # 1, with page header "GE PROPRIETARY INFORMATION"
4	GDL-NL2_K2-output.pdf	PDF file format of Item # 2, with page header "GE PROPRIETARY INFORMATION"

[[

]]

Figure A4-1. SRV Mass Flow Rate from VLVE92 (Case GDL-NL2)

[[

]]

Figure A4-2. SRV Mass Flow Rate from VLVE92 (Case GDL-NL2\_K2, revised input)

[[

Figure A4-3. Two-Phase Level and Static Head in Chimney for the GDCS Line Break  
(Case GDL-NL2)

]]

[[

Figure A4-4. Two-Phase Level and Static Head in Chimney for the GDCS Line Break  
(Case GDL-NL2\_K2, revised input)

]]



remains well below the design pressure of 60 psia. The peak drywell pressure was [[  
]] for the original case, and [[  
]] for the updated calculation.

[[

**Figure 1a. Two-Phase Level and Static Head in Chimney for the GDSC Line Break  
(Original – Fig. 2.7-7 of NEDC-33083P)**

Figure 1b. Two-Phase Level and Static Head in Chimney for the GDCS Line Break  
(Updated) ]]

[[

Figure 2a. Containment Pressure Response for the Main Steam Line Break (Original – Fig. 3.7-2 of NEDC-33083P)

Figure 2b. Containment Pressure Response for the Main Steam Line Break (Updated) ]]

NEDO-33083-A

## **NRC RAIs and Responses**

**ESBWR Scaling Report  
NEDC-33082P**

**Note: RAI responses including data files that cannot be read on a PC are not included.**

**Q13. Test facility insulation / Heat Losses :**

Tests were performed at prototypical temperature and pressure; whereas, test pressure vessel walls were thinner than the actual vessel wall thickness. As a result, heat losses through the vessel wall in the tests are expected to be higher than the prototype, and can result in systematic distortions of test data. The impact and safety significance of distortions needs to be related to the degree of importance of the distorted phenomena. In the Scaling report, there was no discussion presented on the distortions due to heat losses, especially in the GIRAFFE facility testings, where the primary variable of interest is the water level in the reactor pressure vessel (RPV). The staff, therefore, requests that General Electric (GE) assess the impact of heat loss on test data obtained from the facilities, such as GIRAFFE, and explain what was done to offset this potential source of distortion when qualifying the TRACG code.

- R13.** The effects of RPV heat losses in the GIRAFFE/SIT and GIST tests were assessed in the SBWR Scaling Report (NEDC-32288P, Rev 1). The results for these tests can be found in Tables 4.1-11 and 4.1-14 of that report. The analyses found that the heat losses in the SBWR and GIST were negligible while the heat losses in GIRAFFE were on the order of 6% of the decay heat for the late blowdown and GDCS transition phases. The resulting distortion in the overall heat input is small as indicated by the similar values of  $\Pi_q$  for SBWR and the test facilities given in the referenced tables. Therefore the safety significance of the distortions is very small on two counts: 1) the total contribution of the heat losses to the depressurization rate is small; and 2) the distortion in the total sensible energy term, as denoted by  $\Pi_q$ , is also small. As would be expected, the distortion in the sensible energy term,  $\Pi_q$ , is 6%, the same as the decay heat loss.

Because the effects of heat losses were found to be small in the SBWR analyses, the heat losses were grouped together with the decay heat term in the current analyses and report rather than retaining them as separate terms. The effect of the heat losses is still contained in the combined term so heat losses are factored into the assessment of heat loss scaling distortions. See response to RAI 230 for TRACG response.

**Q14. Surface-to-Volume ratio of PCC headers :**

In the 2<sup>nd</sup> paragraph, page 8-5 of the Scaling report (NEDC-33082P), it was stated that because the surface area to volume ratio is increased for the reduced length headers of the passive containment cooling system (PCCS) in the testing facilities (PANDA, PANTHERS), the heat removal through the header walls was increased. The staff realizes that the heat loss in the headers is much less compared to that through the tube walls. However, a higher heat loss through the headers results in increased total heat removal capacity for the PCCS in the tests (non-conservative effect), and this may have an impact on the containment pressure. The staff, therefore, requests that GE provide an estimate as to how a distortion in PCCS heat removal capacity will impact the peak containment pressure.

R14. The additional heat loss through the headers does not have a significant effect on the containment pressure. As noted in Section 7.6 of the ESBWR Scaling Report, the total capacity of the PCC is only important during periods where the demand for heat removal is greater than the maximum capacity of the PCC. For all other periods the PCCs will self regulate to the demand level. An example is given in Figure 14-1 which is the base case TRACG prediction for the ESBWR main steam line break (previously presented as Figure 3.7-6 in NEDC-33083P). Figure 14-1 illustrates that the heat removal demand is greater than the PCC's ability to remove heat for approximately the first eight hours. It is during this interval that increased surface area (i.e. a larger header) would provide additional benefit. Beyond eight hours the PCC has excess heat removal capacity and self-regulates to match the decay heat load. Therefore excess capacity in the header has no influence on the PCC heat removal or the system behavior. To quantify the impact of excess heat removal capability in the PCC, sensitivity cases were performed using TRACG with excess heat removal capacity through the PCC header.

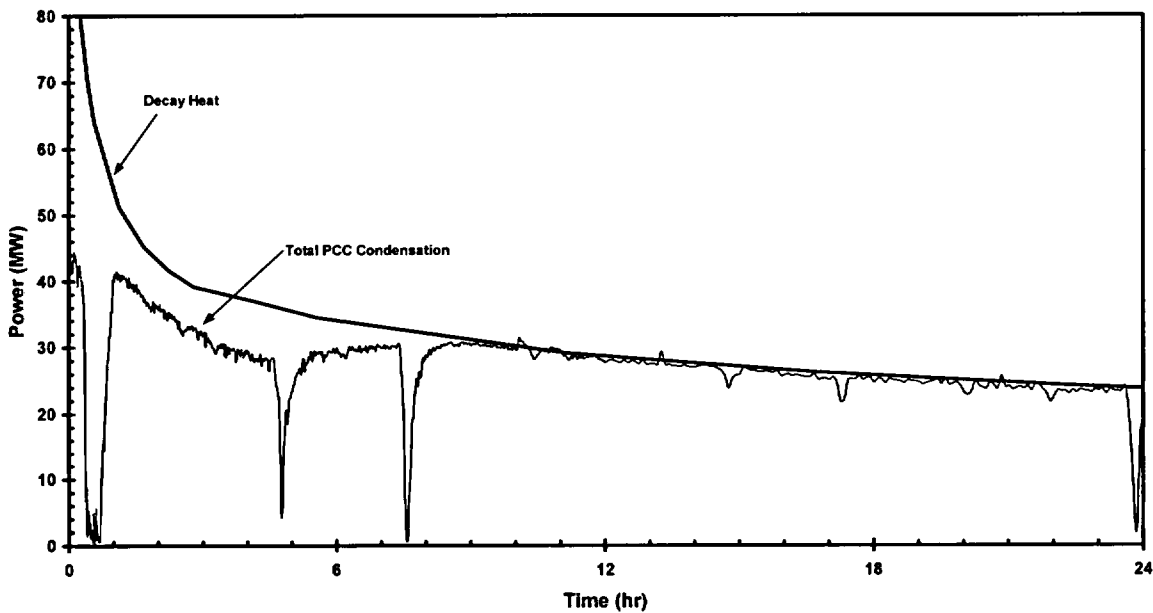


**Figure 14-1 PCC and Decay heat Power for Base Case**

The header heat losses were addressed in detail in the bottom-up scaling results presented in the SBWR scaling report (NEDC-32288P, Rev 1). [[

]] The larger heat loss in PANDA is primarily due to the fact that the surface area of the header endplates is approximately full scale while the number of tubes is scaled to 1:25 of the SBWR. [[

]]

Two TRACG cases were considered for this analysis. The first case modeled a PCC with no header surface area. [[

]] The increased PCC capacity results in a WW pressure decrease. [[

]] As expected, the change in PCC surface area is manifested in small changes in the suppression pool temperature and consequently the wetwell pressure during the first 8 hours, when the decay heat exceeds the PCC heat removal capability. [[

[[

]]

**Figure 14-2 Comparison of Suppression Pool Surface Temperatures for Different PCC Header Heat Losses**

**Figure 14-3 Comparison of Wetwell Pressure for Different PCC Header Heat Losses**

]]

Q15. Absence of a quantitative bottom-up scaling analysis :  
In page 10-2 of the ESBWR Scaling report (NEDC-33082P), the last sentence of 4<sup>th</sup> paragraph states that, "Much of the bottom-up results are borrowed from the SBWR scaling report rather than repeating them in this report." The staff, however, notes that in letter dated May 14, 1996, from NRC to GE, "Staff Review of GE Scaling Report NEDC-32288P, Rev. 1, Scaling of SBWR Related Tests, Related to Reactor Systems Area," it was stated in Items 3 and 4 that, "...while the H2TM approach uses both top-down scaling for systems or components, and bottom-up scaling that focuses on phenomenology, GE's approach provides a quantitative evaluation only on the basis of top-down scaling parameters. The bottom-up approach is discussed in a qualitative fashion in the scaling report, but a quantitative analysis is not presented. The lack of a bottom-up scaling analysis means that there is no explicit link between significant SBWR phenomena, as identified in GE's Phenomena Identification and Ranking Tables (PIRTs) for the SBWR, and the test facility scaling. This failure to link the PIRT and scaling is the major shortcoming of GE's report." In light of the fact that a quantitative bottom-up scaling analysis was not presented in the ESBWR Scaling report, the staff requests GE to submit such an analysis as part of the H2TM approach, clearly demonstrating explicit link between significant ESBWR phenomena, as identified in the PIRT and the test facility scaling.

R15. There are two major portions to the hierarchical two-tiered scaling (H2TS) approach: the first is top-down scaling, which is used to identify processes important to the system behavior; and the second is the bottom-up scaling, used to assess the adequate scaling of processes that are determined to be important from the top-down scaling. Therefore the quantitative top-down scaling presented in the ESBWR Scaling Report and supporting documents can be used to quantitatively confirm or adjust the ranking of PIRT phenomena identified in the TAPD (NEDC-33079P). GE agrees that the linkage between the top-down scaling parameters and PIRT phenomena is not clearly presented and has provided this linkage below, in order to quantify the PIRT rankings.

The set of important phenomena in the ESBWR is very limited, as demonstrated in the attached tables. The table at the end of this RAI response provides the bottom-up parameters associated with these important parameters and comments on their scaling.

### **15.1 Relationship Between PIRT Phenomena and Scaling Groups**

[[

NEDO-33083-A

NEDO-33083-A

NEDO-33083-A

]]

#### **15.4 Summary**

The tables provided in this RAI response provide the requested link between the PIRT parameters and scaling analysis. The PIRT ranking confirmation comes from the top-down scaling rather than the bottom-up scaling. Confirmation of the PIRT rankings are provided in the tables. In addition a summary of the bottom-up phenomena associated with the important PIRT phenomena is provided.

[[

[[ **Figure 15.1-1 Procedure for Validating Highly Ranked PIRT Parameters** ]]

Figure 15.1-2 Flow Chart for Phenomena Affecting the Heat Addition to Drywell Gas Space 11

**[[ Table 15.1-1 Association of PIRT Phenomena with Top-Down Scaling Groups (Reactor Vessel)**

**Table 15.1-1 (cont'd) Association of PIRT Phenomena with Top-Down Scaling Groups (Reactor Vessel)**

---

**Table 15.1-1 (cont'd) Association of PIRT Phenomena with Top-Down Scaling Groups (Reactor Vessel)**

**Table 15.1-1 (cont'd) Association of PIRT Phenomena with Top-Down Scaling Groups (Reactor Vessel)**

]]

**[[ Table 15.1-2 Association of PIRT Phenomena with Top-Down Scaling Groups (LOCA/Containment)**

**Table 15.1-2 (cont'd) Association of PIRT Phenomena with Top-Down Scaling Groups (LOCA/Containment)**

---

**Table 15.1-2 (cont'd) Association of PIRT Phenomena with Top-Down Scaling Groups (LOCA/Containment)**

---

**Table 15.1-2 (cont'd) Association of PIRT Phenomena with Top-Down Scaling Groups (LOCA/Containment)**

---

]]

**Table 15.1-3 Magnitude and Ranking of Top-Down Scaling Groups (LOCA/ECCS)**

]]

**[[ Table 15.1-4 Magnitude and Ranking of Top-Down Scaling Groups (LOCA/Containment)**

NEDO-33083-A

**Table 15.1-4 (cont'd) Magnitude and Ranking of Top-Down Scaling Groups (LOCA/Containment)**

]]

**[[ Table 15.2-1 PIRT Phenomena Added or Deleted for LOCA/ECCS**

]]

**[[ Table 15.2-2 PIRT Phenomena Added or Deleted for LOCA/Containment**

]]

[[

**Table 15.2-3 Validation of Highly Ranked Phenomena for LOCA/ECCS**

**Table 15.2-3 (cont'd) Validation of Highly Ranked Phenomena for LOCA/ECCS**

]]

[[

**Table 15.2-4 Validation of Highly Ranked Phenomena for LOCA/Containment**

**Table 15.2-4 Validation of Highly Ranked Phenomena for LOCA/Containment**

**Table 15.2-4 Validation of Highly Ranked Phenomena for LOCA/Containment**

**Table 15.2-4 (cont'd) Validation of Highly Ranked Phenomena for LOCA/Containment**

**Table 15.2-4 (cont'd) Validation of Highly Ranked Phenomena for LOCA/Containment**

**Table 15.2-4 (cont'd) Validation of Highly Ranked Phenomena for LOCA/Containment**

**Table 15.2-4 (cont'd) Validation of Highly Ranked Phenomena for LOCA/Containment**

]]

If Table 15.3-1 Evaluation of Bottom-up Parameters Associated with High Ranking Processes

]]

**Supplementary Information for RAI 15**

**Supplementary request:**

Provide examples of bottom up phenomena found in the ESBWR experiments that were not expected in the top down scaling of the tests.

Response:Bottom- Up Phenomena seen in Tests but not Considered in Top Down Scaling

	<b>Phenomena</b>	<b>Test</b>	<b>Cause</b>	<b>Disposition</b>
1	“Percolation” phenomenon in RPV upper plenum and standpipe	GIST	Non-prototypical upper plenum with single standpipe	Test facility distortion. Did not affect time-average behavior/ inventory in upper plenum/ core. Not seen in GIRAFFE/SIT tests. TRACG predicted occurrence for GIST, but not for ESBWR.
2	Light gas retention in lower drywell for extended period.	GIRAFFE/ Helium	Non-prototypical heat loss and condensation in lower drywell.	Test facility distortion. Affected containment pressure evolution but not final value. Valid data for PCCS performance with light noncondensibles were obtained.
3	Unequal inlet flows to the three PCC units.	PANDA-M	Small differences between PCC units and/or piping or in inlet conditions to the PCCs.	Possible phenomenon in plant. Does not affect total PCC heat removal. Demonstrated PCC capability to adapt to variable heat load.
4	Condensation in main vents and wetwell heatup.	PANDA-P	Non-prototypical main vent routing through wetwell gas space combined with a high heat load relative to PCC capacity maintained condensation in main vents.	Test facility distortion. Main vent closed off after reflooding of the vents to prevent non-prototypical behavior.
5	Oscillation in steam flow from RPV.	PANDA Test M7	Test started at low RPV level, low drywell temperature and high noncondensable load. RPV downcomer level got low enough (top of shroud) to produce oscillations in level and steaming. Detailed RPV geometry not scaled in PANDA.	Combination of low drywell temperature/low RPV level unlikely to occur in plant. Time-average response was not greatly affected. Free surface separation in PANDA likely aggravated oscillatory behavior when downcomer level got close to top of shroud. Oscillations were calculated

	<b>Phenomena</b>	<b>Test</b>	<b>Cause</b>	<b>Disposition</b>
				with TRACG PANDA model under similar conditions
6	Small flow reversals between RPV and GDCS pools over extended time periods.	PANDA Test P2	After early draining of GDCS pool, small backflow occurred through biased open check valve followed by subsequent draining, in response to RPV to WW pressure difference.	Possible phenomenon in plant, but of no consequence to overall response of containment or RPV. Resulted in one additional opening of vacuum breakers at about two hours from the start of the test.
7	Thermal stratification at top of wetwell gas space due to leakage flow from drywell	PANDA Test M6/8	Higher temperature steam leakage from drywell tended to stratify at top of wetwell	Possible effect in plant. Treated through conservative modeling process in TRACG.

- Q16 Abbreviation error :  
In page 1-1 of the ESBWR Scaling report (NEDC-33082P), 2<sup>nd</sup> line of last paragraph should be “SBWR,” not “ESBWR.”
- R16. GE agrees. The sentence should read “SBWR.” The change will be incorporated into the next revision of the report.

## General Comments for Scaling Report

The report states “The objective of this scaling report is to show that the test facilities properly ‘scale’ the important phenomena and processes identify in the ESBWR PIRT and/or provide assurance that the experimental observations from the test programs are sufficiently representative of ESBWR behavior for use in qualifying TRACG for ESBWR licensing calculations.” Yet there is no such specific demonstration that these objectives were achieved in the report. Throughout the report statements about the “approximate” scale of each facility, and the varying scales of subsystems within the facilities abound. One specific example is the references to PANDA scale being 1:50 (page 1-1) and approximately 1:50 (page 5-6). There seems to be no metric for evaluating if the objective of the report was met. As section 8.1 states “No specific quantitative criterion exists to define what constitutes a well-scaled test.” The next sentence in that paragraph is “A seemingly acceptable criterion that we adopt here is to maintain important phenomena within factor of around three of the prototype.” What does seemingly acceptable mean, and how is this criterion determined? These arbitrary (or at least unjustified) evaluations of results are a repetitive theme throughout the report. Certain phenomena, distortions, physical dimensions or geometry are said to be negligible or unimportant without explanation or reference, as if they were axioms of the trade, obvious to anyone. One example of this is the choice of reference variables on pages 4-4 and 4-5. The report says that “A natural definition for  $\Delta_{hr}$  arises...” There was no such demonstration. Despite the lack of metric, the report goes ahead and concludes (page 8-5) that “the phenomena important to the plant system behavior are well scaled in the test facilities thus providing useful data for TRACG qualification.” The question of data sufficiency does not seem to be addressed directly.

The report refers to some of the non-dimensional coefficients as if they were phenomena and to others as ratios of system variables. In some cases, the ESBWR values are outside the bounds of the experimental space. This means that the experiments do not represent the particular phenomena associated with that non-dimensional coefficient and the data matrix is insufficient. This is the case for the stored energy. How are these phenomena accounted for in the analysis and in the qualification of TRACG?

There is a discussion in the report regarding characteristic times. Some of the times mentioned seem to be the same concept recycled (connecting lines appear associated with multiple time scales) and most of the definitions seem imposed instead of derived. In reality, however, for a complex dynamic system, independent subsystems or components will contribute to the system behavior with their inherent time constant. For example, an emptying tank has an associated time constant, function of its cross sectional area and the outlet resistance to flow. A tank that is filling up by an input flow is not an independent component because its dynamic response is determined by the magnitude of the incoming flow. The comparison of the characteristic times of independent components is the proper way to determine the relative time scales between processes or modes of a dynamic system. It is not clear that this rigorous approach was actually followed. It appears that the generic control volume that was introduced in chapter 3 was used repeatedly to model not only the different facilities, but also the different phases of the

transient. This may explain why all the phases of the transient wound up described by a single first order differential equation in time, as opposed to a system of equations. While this final result may still be valid in most cases, it is not clear if the other dynamic features of these systems were neglected. What is the reasoning to exclude flow paths and multiplicity of tanks in the final description given to each phase? Where is the analysis that shows that all facilities can indeed be described with a single first order equation?

Even though it was mentioned as an objective of the report, the issue of data sufficiency is not clearly addressed. Is the data from these facilities sufficient?

These issues discussed above are addressed specifically in the following questions.

Q253. Section 2.2, page 2-2 - It is stated that for a facility to be perfectly scaled the values of all the PI numbers for prototype and model should be “perfectly matched.” What does “matched” mean? Is it the mathematical meaning of congruency or is it something else?

R253. Perfectly matched refers to “the mathematical meaning of congruency” i.e. the PI groups having the same numerical values when numerical reference values are substituted in. It should be pointed out that this is not a necessary condition for the test facilities in the ESBWR test program. Rather, the ESBWR tests provide data for conditions in which the important phenomena or processes have similar magnitudes to those in the ESBWR so that the TRACG code can be qualified against the data. The code is then used to predict the plant response. This is different than a prototype test, which is used to predict the system behavior by itself. To meet the stated requirements, of providing data for TRACG qualification, the important phenomena and processes as indicated by the PI group magnitudes should be of similar magnitude in the tests and ESBWR. In addition the dominant processes should be the same in the tests and ESBWR.

Q254. The first paragraph in section 2.4 begins the discourse on response times and suggests many options. Each independent dynamic element of the system, each mode, has only one characteristic time associated with its dynamic response. What is the technical basis to suggest alternatives and in what instances were these alternatives proven to work better?

R254. Each element of a system can have several characteristic times. Which one is appropriate is dependent on the process of interest. For example a pipe has characteristic times associated with inertia and a transit time. Which characteristic time is of interest is dependent on what aspect of the system element is being studied and the dynamic behavior of the system as a whole. If the start up of flow due to a sudden change in the boundary conditions is of interest such as the initial clearing of the main vents at the beginning of blowdown, then the inertia time constant is of interest. During the long-term portion of an accident in the ESBWR the pressure boundary conditions evolve so slowly that the conditions in the pipe are quasi-steady and dependent on the pressures in the volumes that it connects. Pipe inertia plays no part in the pipe behavior for these conditions.

The section on time constants was intended to provide background for later discussions on specific time constants used. GE understands the potential for confusion between the terms “time constant” and “characteristic time” in the discussion of pipe transit times, and future revisions of the scaling report will use the appropriate terminology.

Specific selections of time constants for use in the scaling application sections are spelled out in the report. The appropriate reference time selected for each

temporal phase is described in Section 7.3.2. The numerical values of the reference times are reported in the Tables in appendix A.

- Q255. The system representation provided in Fig. 3-1 depicts a single generic volume with a water liquid phase and a multi-component vapor phase. In principle, this is a generic representation of any system. Specifically, how is this treated for the ESBWR design? How does it encompass the various portions of the transient where different components play dominant roles in affecting the overall system behavior?
- R255. Figure 3-1 is a sketch of a generic volume because Section 3 develops the general, or generic, equations for mass, energy and pressure for a volume with gas and liquid. The specific applications are demonstrated in Section 7 for the ESBWR. The specific applications are applied to the test facilities in Section 8. For example the specific form of the equation for liquid mass in the RPV is shown in Figure 7-1. The processes of interest are shown in the sketch of the RPV in that figure. The PI groups shown in the boxes of the figure indicate the individual processes considered. The magnitudes of the processes are shown by the bar chart in the bottom right portion of the Figure. This specialization is repeated for other temporal phases, regions and parameters (e.g. pressure) in subsequent figures. Rather than limiting the equation to processes that are expected to be dominant for the phase, all of the processes are considered and the magnitudes of PI groups indicate if the process is important or not. This same procedure is applied to the test facilities in the figures of Section 8.
- Q256. Section 3.1 - The generic equations derived for this system representation do not include explicitly important terms that are key in assessing the relevance of the various scaling groups. How can one relate the generic scaling groups derived in this report with the ESBWR key phenomena and components?
- R256. The generic equations developed in Section 3 are made specific in Section 7. The specific equation representations in Figures 7-1 through 7-7 show the equations used for each system volume. The sketch in the left portion of each Figure indicates the processes considered and the variable name for each process. See response for RAI 255 also.
- Q257. Section 3.1 - The reader is referred to Figure 3.2-1. There is no such figure in this report.
- R257. The Figure number should be 3-1 rather than 3.2-1. The change will be incorporated into the next revision of the report.
- Q258. Equation 3.1-7 is incorrect. The dimensions of the second term of the right hand side do not match those of the other terms.
- R258. There is a "+" missing between the second and third terms on the right hand side of equation 3.1-7.

The term  $v \sum_k \dot{Q}_k$  should be  $v + \sum_k \dot{Q}_k$ . The change will be incorporated into the next revision of the report.

- Q259 In the formulation of the generic governing equation, two elements require additional documentation:
- Q259.1 The explicit representation of the condensation processes in the PCCS is the key element that links the system to its ultimate heat sink (the PCCS pool). How can the pressure be determined in the intermediate and long-term portion of the transient without the inclusion of this element?
- R259.1 It is true that the PCC links the containment to its ultimate heat sink. The manner in which the PCC heat removal capacity relates to the pressure is indirect, however, by influencing the suppression pool surface temperature. [[

]]

The containment pressure in the intermediate and long term portions of a LOCA is set by the wetwell pressure. The wetwell pressure is equal to the sum of the noncondensable partial pressure and the steam partial pressure. The steam partial pressure is equal to, or very close to, the saturation pressure corresponding to the suppression pool surface temperature for most periods of a LOCA. Therefore the containment pressure is influenced by the surface temperature of the suppression pool.

The dominant cause of the increase in containment pressure is the movement of Nitrogen from the drywell to the wetwell during the initial (blowdown) portion of the transient. The majority of the noncondensable gas moves to the wetwell during the early portion of a transient as a result of blowdown forcing a mixture of steam and noncondensable gas through the main vents and PCC vents. There is a secondary contribution to the pressure increase caused by the increase in suppression pool surface temperature resulting from condensation of steam in the suppression pool during blowdown. A much smaller quantity of noncondensables move through the PCC vent to the wetwell during later periods of the transient as a result of the PCC vent clearing noncondensables from the PCC.

The effect of the PCC is to minimize the quantity of uncondensed steam that enters the suppression pool and thereby minimize the increase in the steam partial pressure in the wetwell gas space. During blowdown, the PCC reduces the quantity of steam that passes through the main vent to the suppression pool. For the intermediate and long-term portions of a transient the PCC has excess heat removal capacity (i.e. it can remove more energy than the load resulting from decay heat). During these periods the PCC self-regulates to the decay heat load by partially filling with noncondensable gas. The effect of differing PCC heat removal capacities is to change the timing when the PCC can accommodate the entire decay heat load and to change the integrated energy that goes into the suppression pool prior to the time when the decay heat load is matched by the PCC capacity.

To appreciate the dominant role of noncondensable transfer for post-LOCA containment pressurization, it is useful to examine the pressurization rate equation as applied to the wetwell during blowdown. The generic nondimensional pressure rate equation is given by equation 6.1-5 of the ESBWR scaling report as,

$$f_2^+ V^+ \frac{dP^+}{dt^+} = \sum_k \Pi_{P,\dot{Q},k} \dot{Q}_k^+ - \Pi_{P,\dot{V}} P^{*+} \frac{dV^+}{dt^+} + \sum_i \Pi_{P,W,h,i} W_i^+ h_i^+ + \frac{P^{*+}}{\rho^+} \sum_i \Pi_{P,mech,i} W_i^+ - V^+ \sum_j \Pi_{P,y,j} \left( f_{1,j}^+ \frac{dy_j^+}{dt^+} \right) \quad (259-1)$$

where the terms in the equation are defined on pages 6-4 and 6-5 of the report. The processes of interest to the WW are shown in Figure 7-7 of the report. The table below shows the reference parameters for the ESBWR during blowdown. The resulting PI groups are shown in the bar chart below the table. [[

NEDO-33083-A

]]

To see how the PCC participates in the containment pressurization transient, we can look at the energy equation for the suppression pool. The generic nondimensional energy equation is given by equation 6.1-3 of the ESBWR scaling report as,

$$M^+ \frac{de^+}{dt^+} = -\Pi_{e,v} P^+ \frac{dV^+}{dt^+} + \sum_k \Pi_{e,\dot{Q},k} \dot{Q}_k^+ + \sum_i \Pi_{e,wh,i} W_i^+ h_i^+ + \frac{P^+}{\rho^+} \sum_i \Pi_{e,mech,i} W_i^+$$

(259-2 )

[[

]]

This PI group for the vents is given by,

$$\Pi_{e,Wh,vents} = \frac{W_{vents} \Delta h_r t_r}{M_o \Delta e_r} \quad (259-4)$$

[[

]]

- Q259.2** The derivation of the vapor generation equation in Appendix B of NEDC-32288P, "SBWR Scaling Report," is referenced to the book of Lahey & Moody. In consulting the reference, there is no trace of such equation. Please provide a detailed basis for the derivation of this crucial result, including any assumptions.
- R259.2** For the derivation of the vapor generation equation see Section 2.4.3 of "Two-Phase Flow in Complex Systems" by Solomon Levy. Equation 2.4.13 of that

reference is for the vapor generation rate and the derivation is described. Future revisions of the report will refer to this alternate reference. For convenience, a copy of the relevant pages is in the attached file

- Q262. The RPV liquid mass equation is derived in Appendix A. The derivation relies on the vapor generation formulation. No distinction is made between the short-term depressurization where the pressure in the RPV is independent of the containment conditions and the long-term transient where the containment pressure affects the vapor evolution in the vessel. Please provide the rationale for deriving equations in a generic form without considering these significant differences in the various portions of the transient.
- R262. The effect of pressure on the RPV liquid mass is implemented through the last term in the liquid mass equation (Equation 3.1-11 of the report). The depressurization of the vessel results in flashing of the liquid and a reduction in liquid mass.

As pointed out in the question, the RPV is decoupled from the containment as a result of the flow being choked during the short-term depressurization (RPV pressure greater than ~90 psia). Therefore the RPV pressure (and therefore liquid mass) are not impacted by the containment pressure during this period. Subsequent to this time, the blowdown flow is no longer choked and there is some interaction between the containment pressure and RPV pressure. However, the containment time constant is orders of magnitude longer than the RPV depressurization time constant due to the thermal capacity of the suppression pool. Therefore the containment pressure is approximately constant during the later portion of RPV blowdown. [[

]]

For periods beyond 800 sec, the effects of pressure changes on vapor generation are negligible, as summarized below. During the period from 800 sec until approximately 1 hour after accident initiation, the liquid in the vessel is subcooled as a result of the subcooled GDCS flow into the vessel. Therefore the RPV liquid will not flash during this period and the pressurization rate is not important to the vapor generation rate. After GDCS injection finishes, the vessel is filled to a level well above the top of the core. The RPV mass is not of significant interest during these long-term periods because the water level in the vessel is so high and changes in mass happen relatively slowly. The parameter of primary interest for safety is, instead, the containment pressure.

However, it is easy to see the potential impact of pressure changes on the RPV mass by considering the Liquid Mass Equation (Eq. 6.1-1 in the report). Losses of mass due to depressurization are captured by the PI group,  $\Pi_{M,\dot{p}2}$ . By setting this PI group equal to 1 we can see the potential change in mass for a given change in pressure,

$$\Pi_{M,\dot{p}2} = \frac{f_{4,o} \Delta P_r M_{f,o}}{h_{fg,o} \Delta M_{f,r}} = 1 \rightarrow \frac{\Delta M_{f,r}}{M_{f,o}} = \frac{f_{4,o} \Delta P_r}{h_{fg,o}} \quad (262-1)$$

The pressure during the long-term period is 2 to 3 bar, so the maximum realistic pressure decrease is ~2 bar. [[

]]

(262-2)

[[

]]

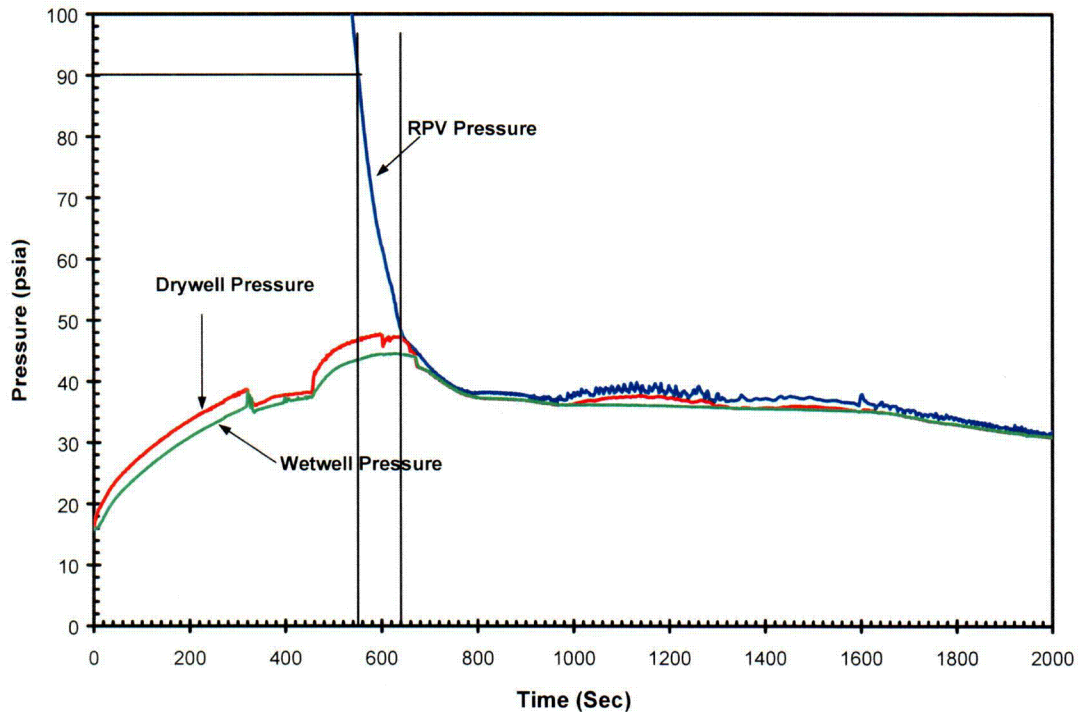


**Figure 2.7-5. RPV, Drywell and Wetwell Pressure Response (Base Case)**

Q263. The system clearly presents a variety of time scales. According to the definition of the volume residence time it follows that, since  $V_r \sim A_r L_r \sim R$ ;  $W_r \sim R$  and  $\rho_r \sim 1$ , the only possible time scale is such that  $t_r \sim 1$  or that there is isochronicity. The report concludes that this is the case. However, it appears that the report, in section 4.6, considers this choice as arbitrary and that there could be other possibilities. Please explain how this apparent degree of freedom is introduced.

R263. For the scaling method used there should be isochronicity,  $t_R \sim 1$ . The confusion seems to arise from the use of upper and lower case r in the subscripts. Lower case r is used to indicate reference values and gives no indication of the ratio of the ESBWR value to the test value. Upper case R is used to indicate the ratio of an ESBWR value to a test facility value.

Section 4.6 discusses several time constants for different processes. The lower case r in these equations indicates that they are reference values. These equations do not indicate any scaling ratios. Application of any of the time constant equations in Section 4.6 to both the ESBWR and test would result in a time constant ratio of  $t_R \sim 1$ .

**Q264** The scaling of vertical piping follows the traditional scaling approach. Particular care should be taken in locating the concentrated losses because the liquid level may or may not be present at these specific elevations of the piping during portion of the transient. Could you elaborate on the representation of the distributed losses with concentrated losses in view of this possibility.

**R264.** The conditions in most of the lines in the plant and facility fall into one of two situations: either there is through flow in the line and the flow is single phase; or, there is little or no flow in the line and the flow is controlled by a balance between driving pressure difference and submergence so that the friction/distributed losses are not important (such as the main and PCC vents). In the first case the location of the distributed loss does not matter since the flow is single phase. In the latter case, the pressure drop associated with friction and distributed losses are negligible. The only time that there is a mixture of gas or vapor and liquid in these lines is when there is no flow or during the short startup transient when liquid is being cleared out of the lines. As was discussed in the SBWR scaling report, flow startup transients are not important to the behavior of the system. The flows in the lines of the ESBWR are controlled by a balance between the driving pressure resulting from the difference in pressure between the two volumes connected by the line and either the friction and distributed losses in the pipe or the submergence losses.

Each of the lines and the importance of the distributed losses in them are discussed in the table below. This is done by temporal phase since the importance of the distributed losses and conditions in the different lines can vary from phase to phase.

Line	Remarks
<b>Long-term phase</b>	
GDCS line	There is no flow in this line in the long-term period
PCCS return line	This line returns condensed liquid from PCC. The rate is determined by PCC condensation rate. The flow rate results from a balance between hydrostatic head and friction losses in the pipe. The elevation difference between the level in the pipe and the RPV will adjust until all of the condensed steam is returned to the vessel. Therefore differences in friction losses will just result in an adjustment in the water level in the pipe. The overall effect on the system is negligible.
RPV to DW (DPVs and/or broken main steam line)	The flow in this path is always gas or steam in the long-term so the location of distributed losses is not important
PCC inlet	The flow in this path is always gas or steam in the long-term so the location of distributed losses is not important.
PCC vent	The small flow rates in the vent lines are controlled by a balance between pressure difference and submergence. Therefore the friction and distributed losses are unimportant.
Main vent	The small flow rates in the vent lines are controlled by a balance between pressure difference and submergence. Therefore the friction and distributed losses are unimportant.
<b>Mid-term phase</b>	
GDCS line	Friction and distributed losses are important since they control the rate of GDCS flow. The pipe is filled with liquid so the location of the losses is not important.
Other lines	Conditions are similar to long-term phase
<b>Blowdown phase</b>	
DPV and MSL	The flow in this path is always gas or steam so the location of distributed losses is not important
SRV	The tests do not cover the startup transient when the vents are cleared at the beginning of blowdown. Subsequent to this the flow is either single phase or there is no flow.
PCC vent/Main vent	The tests do not cover the startup transient when the vents are cleared at the beginning of blowdown. Subsequent to this the flow is either single phase or there is no flow.

Q265. Section 4.2, page 4-4 - It is stated that “A natural definition for  $\Delta_{hr}$  arises  $\frac{1}{4}$ ”  
What is the basis for that statement?

R265. Section 4.2 refers to phase changes at interfaces. The typical energy carried away from these interfaces is given by the difference between the liquid and vapor enthalpies. Therefore the recommended value for enthalpy differences is  $\Delta h_{fg,r}$ . Since prototypical fluids are used in the tests any other selection for  $\Delta h_r$  would result in the same scaling ratio of  $(\Delta h_r)_R \sim 1$ . To avoid any confusion in the future subsequent revisions to the report will be revised to use the term “rational definition” rather than “natural definition”.

It should be noted that this section relates to general equations for system design. In later sections where the equations are applied to specific system elements, the local enthalpy differences are used as reference enthalpy differences in order to assure that the normalized enthalpy differences have magnitudes very close to 1. As a result the confusion described above is eliminated in the specific applications.

- Q266. The second paragraph on page 4-5 states that the flow mass flux due to phase change at the surface of a pool “may depend of the fluid conditions on both sides of the interface.” Under what circumstances is the mass flux independent of the fluid conditions?
- R266. The words “may depend of” should be replaced with “depends on” The change will be incorporated into the next revision of the report.
- Q267. The sentence before equation 4.3-7 in page 4-6 refers to a demonstration in section 4.2 (“it was shown ¼”). There was no such demonstration in section 4.2.
- R267. See answer to question 265. Future revisions of the report will be changed to say that “ $\Delta h_{fg,r}$  is the rational choice for  $\Delta h_r$ ” rather than “it was shown...”.
- Q268. The second paragraph of section 4.4 states that reduced velocities in the models is not important as long as transit times between volumes are small compared to volume fill times. Transit times, or delays, are important when a discontinuity or a signal is carried from one end of the transmission line to the other. In the case of this thermal-hydraulic system, in which the lines are either full of water or steam, it is not clear why a line delay plays any role in the dynamic response of the system. What is the importance of the transit time? What is the basis for these comparative statements between transit times and filling up times?
- R268. Section 4 provides a discussion of general scaling laws for use in test design. Therefore it is not restricted to “this hydraulic system” as stated in the question. When the specific situation present in the ESBWR is considered, the transit times are not important as suggested by the RAI.
- Q269. Page 4-10 has a similar statement that upgrades transit time to the category of time constant and says that it must be compared to other time constants of the system. If transit time depends on the flow, which in turn depends on pressure and hydraulic heads, it is not a constant. Why is this transit time relevant?
- R269. As pointed out in RAI 268, in some cases transit times can lead to delays which can in turn effect the timing of the pressure response of the receiving volume. In cases where the pressure of the receiving volume is important to the flow rate, and therefore transit time, in the pipe, there can be important interactions between the pipe and the receiving volume. For the specific application to the ESBWR the

time constant of the large volumes are much longer than the pipe transit times and there are no interactions. As discussed in the response to RAI 268, the text in this section provides a discussion of general scaling laws. Therefore it is left broad enough to cover instances where the transit time can be important.

- Q270. At the bottom of page 4-10, volume fill time is equated with residence time. Residence time is actually closer to a transit time than to a filling time. This statement needs correction or clarification.
- R270. The use of volume fill time and residence time in this report is consistent with that described in Section 3.4.8 of "An Integrated Structure and Scaling Methodology for Severe Accident Technical Issue Resolution", NUREG/CR-5809, upon which the scaling method is based. However, the wording will be revised in the next revision of the report to minimize any confusion.
- Q271. The second sentence on page 4-11 says "The volume fill time  $t_f$  is the natural scale for subsystems and processes where volume emptying or filling due to mass flows take place." The fill time is not a "natural" characteristic of any vessel because it depends on the magnitude of the input flow. Since the input flow drives the response of the vessel, the vessel is no longer an independent dynamic component and has no characteristic time of its own to contribute. Please clarify your statement in light of the volume fill time not being a truly natural time scale.
- R271. The filling time may not be a "natural" characteristic of the vessel or a time constant of the vessel, however, it is the reference time that will render the non-dimensional time,  $t^+$ , of order 1 for the rate of change of RPV liquid mass equation. It is therefore the reference time used for the GDACS (Reflood) phase in the RPV (see Section 7.3.2 of the report). In future revisions of the report, the text will be revised to eliminate calling this "reference time" a "natural time" or a "time constant".
- Q273. The stored heat in the massive containment structures is not represented in any of the facilities. This may yield conservative peak-pressure evolutions in the short-term. It is not clear whether that stored heat has an effect in the long-term portion of the transient and whether the stored heat affects that long-term noncondensable gas behavior. Provide additional discussion of the effect of stored heat beyond the paragraph 5.5.1.4.
- R273. The containment structures are indeed massive but have very long thermal time constants so they absorb or reject energy slowly. The steel structures in the containment and the portion of the wall surface can absorb energy more rapidly, but this is similar to the steel structures of the test facilities. As discussed in Section 7.5.2.1 and shown in Figure 7-6, the contribution of structures to the drywell pressure evolution is negligible. The contribution of structure stored energy to the wetwell pressure is larger but still small compared to the large

pressure change which results from noncondensable gas accumulation in the WW, as discussed in Section 7.5.2.2 and shown in Figure 7-7.

The comparison of stored energy effects for the ESBWR and tests is shown in Figures 8-6 and 8-7 for the drywell and wetwell respectively. For the PANDA tests the heat entering the structures is scaled fairly well. The heat losses from the vessels in the PANDA facility were similar to the expected rate at which heat would be conducted into the walls of the ESBWR containment. The heat flow into the walls was not scaled as well in the GIRAFFE facility. In the GIRAFFE facility, the walls were fitted with microheaters in order to eliminate any heat losses. Therefore the heat loss in the GIRAFFE wetwell was approximately zero. This is a conservative result since heat loss in the wetwell would tend to reduce the steam partial pressure in the wetwell. The heat loss in the GIRAFFE lower drywell were not compensated for and were fairly large as indicated by the structure heat loss bars in Figure 8-6. As shown heat loss to structures is a small contributor to overall pressure evolution in the drywell. The fact that these heat losses were concentrated in the lower drywell did cause a non-prototypical flow of noncondensibles to the lower drywell. This has been discussed elsewhere (see SBWR Testing Summary Report (NEDC-32606P), Section 4.4.4.3, for example).

Q274. The third paragraph on page 5-10 justifies the steady state test conditions for the PANTHERS PCC with a narrative analysis of time scales of the relevant components. What are the governing equations of these components and the exact values of the corresponding PIs that allow the narrative to be valid? What are the results of the same comparison for the other facilities and the prototype? What is the impact of these differences in their relative standing when it comes to validating the PIRT?

R274. [[

]]

**Q275.** Page 5-2, first sentence - Does it mean the tests or should it say the test facilities?

**R275.** The sentence should read “test facilities.” The change will be incorporated into the next revision of the report.

Q276. The last sentence on the top paragraph of page 5-2 is not clear and should be revised.

R276. The word “area” in this sentence should be “are”. The change will be incorporated into the next revision of the report.

Q277. The bottom paragraph on page 5-3 states that the depressurization created representative thermal-hydraulic conditions in the RPV of GIST. What is the basis for that statement?

R277. The concern in the GIST test was that the void distribution at the beginning of the test would be similar to that which would occur if the vessel had blown down from full operating pressure. Equation B.1.4.3 of the SBWR scaling report (NEDC-32288P, Rev 1) can be used to show that the time for the voids to develop will be on the order of

$$t \approx \frac{\rho_{g,r}}{\Gamma_{g,r}}$$

where  $\rho_{g,r}$  is the gas density and  $\Gamma_{g,r}$  is the volumetric net vapor generation rate.  
[[

]]

Q278. The paragraph on the top of page 5-4 says that the initial RPV water level was increased to compensate for GIST’s inability to represent the creation and sustenance of voids in the lower plenum due to stored heat. How does more liquid help represent voids? This paragraph seems to contradict the statement a few lines before about representative thermal-hydraulic conditions in the RPV. Please reconcile these statements reconcile.

R278. The following paragraph from the SBWR scaling report (Page 4-54) provides a better description of what was achieved by increasing the initial water level in the GIST tests,

“The heat release from the RPV metal in SBWR could not be simulated in the GIST tests; the heat stored initially in the RPV wall and its rate of release could not be scaled properly. Thus, voids could not be maintained in the lower plenum and the water level in the core dropped; this was compensated for by increasing the initial RPV water level in the tests. This distortion can be considered in TRACG calculations which can simulate the situation in the tests and in the SBWR”

The additional water was not meant to “help represent void”, but rather to better represent the two phase level which is a combination of liquid and voids. The “earlier statement about representative thermal-hydraulic conditions in the RPV” refers to the time for a void distribution to develop in the RPV at the beginning of the tests as discussed in the response to RAI 277.

- Q279. Page 5-5, second paragraph - Reference is made to section 3.5. This section does not exist in this report.
- R279. This section was deleted from the final version of the report. The reference should be to the ESBWR Design Description, NEDC-33084P, submitted in August 2002. The change will be incorporated into the next revision of the report.
- Q280. There are some discrepancies between the PI groups listed on page 6-2 and those derived in Appendix A of NEDC-32606P, “SBWR Testing Summary Report,” on page A-4. For example, the term  $\square M_{l,r}$  should be  $\square M_{l,o}$ . Please clarify the nomenclature and definitions in order to resolve these discrepancies.
- R280. The equations are consistent but the nomenclature is different for the two reports. Both the way that the PI groups were broken up and the subscript notation were different. In the SBWR, global scaling of the entire system was used and therefore there was a need for local and global reference values. These were indicated by the subscripts “r” and “o”, respectively. Additionally, in the ESBWR scaling report, local reference values were distinguished as those where initial conditions were used and those where they were calculated. These were denoted by the subscripts “o”, and “r”, respectively. This distinction was not made in the older SBWR scaling report. The easiest way to see that the equations are the same is to substitute the reference variables in for the PI groups in both equations and use the subscript “r” in place of “o” in both equations. The resulting equations will be the same. All that is lost in doing this is the distinction of whether a reference variable was an initial condition or not.
- Q281. Equation 6.1-3 is incorrect. The last term on the right hand side is inconsistent with the formulation provided in NEDC-32288P, “SBWR Scaling Report,” page B-12, Equation (B.2-22).
- R281. The “+” sign before the last summation sign on the right hand side of equation 6.1-3 should not be there. The change will be incorporated into the next revision of the report.
- Q282. The elimination of the PCCS pool from the scaling considerations as the ultimate sinks has some significant implications. One clear implication of this approach is the pseudo-resolution of the non-condensable issue. Specifically, consider the statement on page 6-6: “Therefore the change in condensable fraction is set to 5% which will bound the range that would occur after a VB opening moves noncondensibles to the DW and then back to the WW\_”. The

fundamental reason to conduct PANDA testing is indeed to resolve the non-condensable issue after the opening of VBs. The implication of the extent of mixing or segregation bears immediate consequences on the PCCS operation and therefore on the heat removal from the containment. Setting a `_bounding_` value appears quite arbitrary. How is this justified?

- R282. The importance of the PCC pool (and, more generally, PCCS heat removal capacity) from the standpoint of scaling has been addressed in the response to RAI 259, part 1 by evaluation of the terms in the non-dimensional energy equation for the suppression pool. The purpose of the PANDA tests has been addressed in the response to RAI 291, where it was stated the PANDA facility “provided information on noncondensable release over a wide range of timing and rates”. This was done because of the difficulty in predicting the specific noncondensable fraction in the drywell at a given time and covers a range of conditions that will bound those expected in the ESBWR.

The selection of 5% noncondensable fraction is somewhat arbitrary and is used to show how the noncondensable contribution would be scaled for this particular single value. In retrospect, the word “representative” would have been a preferable characterization. It is easy to see that the noncondensable contribution shown in Figure 8-7 (“bubbles” term in the bar chart) would double for twice this fraction and would be ~20% of the value shown if the noncondensable fraction was 1% rather than 5%. The scaling only allows us to show a single value for the noncondensable contribution but there is a range of possible noncondensable fractions depending on the specific case considered. Because of the uncertainty, the tests covered a wide range of noncondensable conditions as discussed above.

- Q283. In the proposed scaling, the condensation phenomena are eliminated by considering a flow of steam and noncondensable gases at the PCCS inlet as if this flow was not determined by the condensation rates within the PCCS. However, the condensation rate is the direct result of the presence of noncondensable gases. The proposed scaling approach does not address this effect, and may result in eliminating important scaling parameters thus misrepresenting the adequacy of the facilities. Explain how the proposed approach addresses this issue. In your explanation, provide a detailed technical justification for this simplification of your scaling approach.

- R283. The condensation rate of the PCC is considered in the bottom-up scaling provided in Sections 3.6 and 4.4.1.3 of the SBWR Scaling Report, NEDC-32288P, Rev 1.

Essentially, the only difference between the ESBWR and earlier pressure suppression systems is the addition of a heat removal device (the PCC heat exchanger) in the flow path between the drywell and the suppression pool. In the earlier designs, all the decay heat energy was deposited in the suppression pool, and rejected from the suppression pool to the ultimate heat sink via the Pool

Cooling Mode of the (active) Residual Heat Removal (RHR) System. In the ESBWR, the flow from the drywell to the suppression pool passes through the PCC heat exchanger, rejecting a large majority of the decay heat to the ultimate heat sink instead of the suppression pool.

It is important to understand that in any pressure suppression containment system, the long-term containment pressure is dominated by the wetwell air space response, not by the drywell<sup>17</sup>. (See the response to RAI 360.) In the latter stages of the LOCA, when the vent flow rate from the drywell to the suppression pool is reduced, the vent flow losses are negligible. During this time the drywell pressure is equal to the wetwell pressure plus the submergence head of the flow path between the drywell and the suppression pool. In the ESBWR there are 2 such flow paths – the main vent, and the PCCS system via the PCC heat exchanger and PCC vent. The PCC vent is at a higher elevation (lower submergence) than the main vent, making this the preferred flow path.

Consider a case where the PCC heat exchanger is replaced with a simple pipe from the drywell to the suppression pool, having the same submergence head. (Although flow losses are small during the PCC heat rejection period, even design this “pipe” such that the overall loss coefficient is the same as the PCC.) In this case the PCC “pipe” flow would be identical to that of the PCC system. The driving pressure difference is the same. The conclusion that is drawn from this analogy is that the PCC inlet flow rate is not a function of the condensation rate within the PCC.

When the PCC heat exchanger – for whatever reason – is incapable of condensing sufficient steam to reject the reactor decay heat, then the pressure at the vent will rise and clear suppression pool water from the vent. The excess energy will be vented to the suppression pool, however the drywell pressure will not exceed the wetwell pressure plus this submergence head. Some of the decay heat energy will be rejected to the environment via the PCC, and the remaining decay heat energy will be deposited in the suppression pool – raising the pool temperature. Thus, it may be seen that the PCC condensation rate is important in limiting the deposition of energy in the suppression pool, the suppression pool temperature, and therefore the wetwell pressure. An additional scaling equation has been added in the response to RAI 259, Part 1 to address this condition.

All of the testing and analysis performed in support of the SBWR and the ESBWR has demonstrated that the PCCS is a self-regulating system. If the condensation capability exceeds the decay heat load, the pressure in the heat exchanger will drop, and the water level in the bottom header and tubes will rise until an equilibrium condition is reached. Note that in this case no flow path

---

17 Earlier BWR pressure suppression containment designs also experienced short-term drywell pressure peaks associated with vent clearing. For BWR/6 plants (Mark III containments) the short-term peak set the drywell design pressure. The long-term response is limiting in the ESBWR

exists from the drywell to the suppression pool and all the decay heat is rejected via the PCCS. If the decay heat load exceeds the condensation capability, then the pressure in the heat exchanger will rise, lowering the water level in the vent until the vent clears and a flow path exists between the drywell and suppression pool. If the cause of the decay heat exceeding the condensation rate was build-up of non-condensable gas within the heat exchanger, then the flow will purge the non-condensables out of the heat exchanger (transferring them to the wetwell air space). The purged heat exchanger will then be capable of rejecting all of the decay heat.

- Q284. Page 6-5 - There is a paragraph titled “RPV Reference Values” which states that the pressure difference between the beginning and end of a phase is the value chosen as reference. Are these pressure values fixed values or do they depend on the transient? How are they fixed if they are fixed? If they are not fixed, what is the rationale to use a variable value as a reference? The same question applies to the statements of the first paragraph on page 6-6.
- R284. The method of determining the reference values is described in Section 7.3. The initial pressure is fixed at the value at the beginning of the test and is not dependent on the transient considered. The test initial pressures for the test covering the late blowdown period are at an intermediate point in the blowdown process. The values were selected based on a trade-off between starting at as high a pressure as possible and the pressure capability of the facilities. The starting pressures are high enough that any disturbances resulting from test initiation would be fully completed before reaching the lower pressures at which GDCS flow initiates. The pressure at the end of the phase is fixed by geometrical considerations which control the time at which the GDCS flow will start as described in Section 7.3.1.
- Q285. The first paragraph of Section 7, page 7-1, discusses about “governing equations summarized in Section 6.” Section 6 has the equations for the control volume introduced in Section 3. Section 7 further states that these equations are “applied to the ESBWR.” Does this mean that it is a working assumption that the control volume equation of Section 3 applies directly to the entire system in every phase of the transient?
- R285. The control volume equation of Section 3 applies to each of the control volumes in the ESBWR (RPV, drywell, wetwell) not the entire integral system. A global momentum method was applied to look at the various volumes and flow paths as an integral system as part of the SBWR scaling report (NEDC-32288P, Rev 1). There was no useful information gained from the exercise. Therefore it has not been repeated as part of this report as described in Section 6.2 of this report. The working assumption is that the control volume equations introduced in Section 3 do apply to each control volume in the system. The specific sources of heat and mass are supplied for each individual control volume as described in Section 7.

- Q286 Provide the derivation of the system equations in Section 7. Specifically, there is a large portion of the transient in which the RPV and the containment interact dynamically. Where are the equations for this system of at least 2-volumes and several connecting paths? How do the PI values compare between equations and between facilities and prototype?
- R286. In the ESBWR there is minimal interaction between the different regions of the ESBWR. We do not believe that a coupled equation with a multiple volume system and flow paths is necessary. The results of test programs and global momentum scaling performed as part of the SBWR program (and documented in the Scaling of the SBWR Related Tests) has supported this conclusion. A brief summary is provided below.

A good indication of possible interactions between system elements is the existence of similar time constants in adjacent system elements. When there is a large difference in time constants for adjacent system regions there is little dynamic interaction between the system elements and resulting in a decoupling of the systems. This concept has been discussed by Zuber in *Hierarchical, Two-Tiered Scaling Analysis, Appendix D to An Integrated Structure and Scaling Methodology for Severe Accident Technical Issue Resolution* where he discusses hierarchical decomposition of systems and the associated differences in time constants.

In the ESBWR there is strong separation in the time constants of adjacent systems. This is typical of pressure suppression systems where the large thermal mass of the suppression pool results in a very long time constant for the wetwell. This minimizes dynamic interactions between the WW and other parts of the system as demonstrated by the stable pressure behavior of the WW in the ESBWR predictions and long-term test results.

There is a short period at the beginning of an accident (when the noncondensable gas is moving from the DW to the WW) when the time constants of the RPV and containment volumes are similar. This is because pressure suppression is not effective at mitigating the effect of noncondensable gas moving to the WW. However, during this time the flow from the RPV is choked decoupling it from the containment, anyhow. This has been discussed in the response to RAI 294.

The PCC has a very short time constant so the PCC pressure rapidly adjusts to the pressure of the DW, which has a much longer time constant, without interactions between their pressures. Similarly the startup times for the connecting pipes in the ESBWR are very short so the pipe flows also reach a quasi steady value based on the pressures in the volumes that they connect.

One possibility for interactions is through the parallel flow paths from the RPV and DW to the WW during the early phases of an accident. This was investigated quantitatively in the SBWR scaling report, *Scaling of the SBWR Related Tests*,

NEDC-32288P. In that report a global momentum method was applied to look at the various volumes and flow paths as an integral system. A set of matrix equations representing the multiple flow paths and volumes was set up and evaluated during different temporal phases. The results of that work are reported in Section 4 of the report. The exercise found that interactions between different flow paths and volumes were negligible.

Supplementary Information for RAIs 259 and 286

The purpose of this response is to address the issue of interactions between the major ESBWR volumes that was raised by the NRC staff and consultants. This is done by supplementing the derivations of the scaling equations in section 6 of the ESBWR Scaling Report. The terminology and nomenclature is the same as in the ESBWR Scaling Report. New terminology is defined in this response.

Interactions between the major ESBWR volumes (RPV, DW, SP and WW) occur as a result of flows between these volumes. The table below shows the important “external” flows that need to be considered during the various phases of the LOCA transient.

[[

]]

In the above table, the flow terms shown in red (bold) represent interaction terms, which are calculated from corresponding pressure differences between the participating

volumes. The other flows are either choked or driven by decay heat or PCC condenser capacity. For the latter, the pressure difference between the volumes becomes the dependent quantity based on the flow rate. In the long term the PCC vent flow consists primarily of noncondensibles that end up in the wetwell gas space. The integrated flow of noncondensibles flowing out of the PCC vent is slightly less than the noncondensibles flowing into the PCCS. This is because the PCCS maintains (on average) a nearly constant noncondensibles inventory such that the condensing capacity matches the decay heat. The temperature of the noncondensibles is close to the PCC secondary temperature of 100 C, so very little sensible energy is added to the suppression pool as the noncondensibles flow through to the wetwell gas space. The terminology NC ~95% implies that 95% of the noncondensibles initially in the drywell are pushed into the wetwell gas space in the early blowdown transient. Most of the remaining 5% will be transported before the GDCS phase. During the GDCS phase vacuum breaker openings occur and some of the noncondensibles are returned to the drywell. These are assumed to be of the order of no more than 5% of the original drywell noncondensibles content, and are re-transported to the wetwell in the long term phase.

The Scaling Report expresses the conservation equations for liquid mass, pressure rate and the energy equation in non-dimensional form to examine the correspondence of the dominant phenomena between the ESBWR and the relevant test facilities. In these equations, interactions between the major volumes (RPV, drywell, SP and wetwell) are represented through the flows between the regions. The flow terms were non-dimensionalized with respect to reference values of the flows. In the following, the flows that are driven by pressure difference are explicitly expressed in terms of these pressure differences, resulting in cross terms involving pressures in connecting volumes. Non-dimensionalized values of the pressure differences are used in the reference terms. The corresponding PI groups indicate the importance of these terms in the scaling of the test facilities.

**Liquid Mass:**

$$\frac{dM_l}{dt} = -\sum_i \frac{\dot{Q}_i}{h_{fg}} + \sum_i W_{l,i} + \sum_i \frac{\Delta h_{sub} W_{l,i}}{h_{fg}} \dots\dots\dots$$

$$-\frac{1}{h_{fg}} \left[ V_{RPV} (1 - \rho_g h'_g) + M_l \left( \frac{\rho_g}{\rho_l} h'_g - h'_f \right) \right] \frac{dP_R}{dt}$$

...(1)

(Equation 3.1-11 of ESBWR Scaling Report)

Some external flows can be related to pressure differences between regions through the momentum equation (except for break and DPV flows that are choked in the blowdown phase, and are not dependent on the receiver pressure and involve no coupling between volumes):

$$\left(\frac{L}{a}\right) \frac{dW_i}{dt} = \Delta P_{ij} - \rho g H_{ij} - \left(\frac{F}{a^2}\right) \frac{W_i^2}{2\rho} \dots\dots\dots(2)$$

(Equation 3.2-3 of ESBWR Scaling Report)

In general, it can be shown that for the ESBWR transients being considered, the inertial terms for the flow paths are negligible in magnitude relative to the other terms. Hence, the momentum equation can be solved for the flow as:

$$W_i = \sqrt{\left(\frac{2\rho a^2}{F}\right) (\Delta P_{ij} - \rho g H_{ij})} \dots\dots\dots(3)$$

Substituting for the flow rates in the liquid mass equation (1):

$$\begin{aligned} \frac{dM_l}{dt} = & -\sum_i \frac{\dot{Q}_i}{h_{fg}} + \sum_i \sqrt{\left(\frac{2\rho a^2}{F}\right) (\Delta P_{ij} - \rho g H_{ij})} + \sum_i \frac{\Delta h_{sub} \sqrt{\left(\frac{2\rho a^2}{F}\right) (\Delta P_{ij} - \rho g H_{ij})}}{h_{fg}} \\ & - \frac{1}{h_{fg}} \left[ V_{RPV} (1 - \rho_g h'_g) + M_l \left( \frac{\rho_g}{\rho_l} h'_g - h'_f \right) \right] \frac{dP_R}{dt} \end{aligned} \dots\dots(4)$$

The nondimensional form of the equation is

$$\begin{aligned} h_{fg}^+ \frac{dM_l^+}{dt^+} = & -\sum_k \Pi_{M,\dot{Q},k} \dot{Q}_k^+ + h_{fg}^+ \sum_i \Pi_{M,W,i} \sqrt{\Delta P_{ij}^+} + \sum_i \Pi_{M,sub,i} h_{sub,i}^+ \sqrt{\Delta P_{ij}^+} \\ & - \left[ \Pi_{M,\dot{P}1} V_{RPV}^+ f_3^+ + \Pi_{M,\dot{P}2} f_4^+ M_l^+ \right] \frac{dP^+}{dt^+} \end{aligned} \dots\dots\dots(5)$$

where

$$f_3 = 1 - \rho_g h'_g; \quad f_4 = \frac{\rho_g}{\rho_l} h'_g - h'_f \quad \text{are thermodynamic properties,}$$

$$\Pi_{M,\dot{Q},k} = \frac{\dot{Q}_{k,o}}{h_{fg,o}} \frac{t_r}{\Delta M_{l,r}}$$

$$\Pi_{M,W,i} = \sqrt{\left(\frac{2\rho a^2}{F}\right) (\Delta P_{ij,o} - \rho g H_{ij,o})} \frac{t_r}{\Delta M_{l,r}}$$

$$\begin{aligned} \Pi_{M,\text{sub},i} &= \frac{\Delta h_{\text{sub},i,o}}{h_{fg,o}} \frac{\sqrt{\left(\frac{2\rho\alpha^2}{F}\right)(\Delta P_{ij,0} - \rho g H_{ij,0})} t_r}{\Delta M_{t,r}} \\ \Pi_{M,\dot{P}1} &= \frac{V_{RPV,o} f_{3,o}}{h_{fg,o}} \frac{\Delta P_r}{\Delta M_{t,r}} \dots\dots\dots(6) \\ \Pi_{M,\dot{P}2} &= \frac{f_{4,o} \Delta P_r}{h_{fg,o}} \frac{M_{t,o}}{\Delta M_{t,r}} \end{aligned}$$

are PI numbers, and

$$\begin{aligned} \Delta M_t^+ &= \frac{M_t - M_{t,o}}{\Delta M_{t,r}}; t^+ = \frac{t}{t_r}; \dot{Q}_k^+ = \frac{\dot{Q}_k}{\dot{Q}_{k,o}}; \Delta P_{ij}^+ = \frac{\Delta P_{ij} - \rho g H_{ij}}{\Delta P_{ij,0} - \rho g H_{ij,0}}; h_{\text{sub},i}^+ = \frac{\Delta h_{\text{sub},i}}{\Delta h_{\text{sub},i,o}}; \\ M_t^+ &= \frac{M_t}{M_{t,o}}; P^+ = \frac{P - P_o}{\Delta P_r}; h_{fg}^+ = \frac{h_{fg}}{h_{fg,o}}; f_3^+ = \frac{f_3}{f_{3,o}}; f_4^+ = \frac{f_4}{f_{4,o}} \end{aligned} \quad (7)$$

are the nondimensional variables. A standard nomenclature for the  $\Pi$  groups is adopted where the first subscript indicates the equation to which the term applies (i.e. mass, pressure), the second one indicates the phenomena represented and the third one indicates the flow path or source. Note that not all flows are replaced by driving head terms (see table on page 1). Some flow based PI groups will remain in the equation as shown in the original equation 6.1-1 of the scaling report. These are not shown here to reduce the complexity of the equation.

[[  $\Delta P_r$

]]

**Temperature (Energy) Equation:**

The temperature of the suppression pool is important to the steam partial pressure in the WW gas space. The temperature change is of course dependent on the energy in the pool. The dimensional form of the full equation is

$$M \frac{de}{dt} = -p \frac{dV}{dt} + \dot{Q} + \sum W_i (h_{o,i} - h_o) + \frac{P}{\rho} \sum W_i \dots\dots\dots(10)$$

(Equation 3.1-6 of the ESBWR Scaling Report)

Substituting for the external flows as before in (10):

$$M \frac{de}{dt} = -p \frac{dV}{dt} + \dot{Q} + \sum \sqrt{\left(\frac{2\rho a^2}{F}\right) (\Delta P_{ij} - \rho g H_{ij})} (h_{o,i} - h_o) \dots\dots\dots (11)$$

$$+ \frac{P}{\rho} \sum \sqrt{\left(\frac{2\rho a^2}{F}\right) (\Delta P_{ij} - \rho g H_{ij})}$$

Non-dimensionalizing:

$$M^+ \frac{de^+}{dt^+} = -\Pi_{e,v} P^+ \frac{dV^+}{dt^+} + \sum_k \Pi_{e,Q,k} \dot{Q}_k^+ + \sum_i \Pi_{e,wh,i} \sqrt{\Delta P_{ij}^+} h_i^+ \dots\dots\dots (12)$$

$$+ \frac{P^+}{\rho^+} \sum_i \Pi_{e,mech,i} \sqrt{\Delta P_{ij}^+}$$

where:

$$\Pi_{e,v} = \frac{P_o \Delta V_r}{M_o \Delta e_r}$$

$$\Pi_{e,Q,k} = \frac{\dot{Q}_{k,o} t_r}{M_o \Delta e_r}$$

$$\Pi_{e,wh,i} = \frac{\sqrt{\left(\frac{2\rho a^2}{F}\right) (\Delta P_{ij,0} - \rho g H_{ij,0}) \Delta h_{i,o} t_r}}{M_o \Delta e_r} \dots\dots\dots(13)$$

$$\Pi_{e, mech, i} = \frac{P_o \sqrt{\left(\frac{2\rho a^2}{F}\right) (\Delta P_{ij,0} - \rho g H_{ij,0}) t_r}}{M_o \Delta e_r \rho_o}$$

and

$$\begin{aligned} e_i^+ &= \frac{e - e_o}{\Delta e_r}; & P^+ &= \frac{P}{P_o}; & dV^+ &= \frac{dV}{\Delta V_r}; & t^+ &= \frac{t - t_o}{t_r}; \\ \dot{Q}_k^+ &= \frac{\dot{Q}_k}{\dot{Q}_{k,o}}; & \Delta P_{ij}^+ &= \frac{\Delta P_{ij} - \rho g H_{ij}}{\Delta P_{ij,0} - \rho g H_{ij,0}}; & h_i^+ &= \frac{h_i - h_o}{\Delta h_{i,o}}; & & \dots\dots\dots(14) \\ \rho^+ &= \frac{\rho}{\rho_o}; & M^+ &= \frac{M}{M_o} \end{aligned}$$

are nondimensional variables.

**Time Rate of Pressure Change**

The dimensional form of the equation is

$$V f_2 \frac{dp}{dt} = \sum_i [W_i (h_{o,i} - h_o)] + \sum_i W_i P^* / \rho + \dot{Q} - P^* \frac{dV}{dt} - V \sum_j \left[ f_{1,j} \frac{dy_j}{dt} \right]$$

.....(15)

(Equation 3.1-7 of the ESBWR Scaling Report)

The right side of the equation contains terms for energy increase due to enthalpy and heat additions, pressurization due to volume changes and fluid addition and changes in constituent fractions.

Substituting for the flow rates in terms of the driving heads in (15):

$$\begin{aligned} V f_2 \frac{dp}{dt} &= \sum_i \left[ \sqrt{\left(\frac{2\rho a^2}{F}\right) (\Delta P_{ij} - \rho g H_{ij})} (h_{o,i} - h_o) \right] \\ &+ \sum_i \frac{P^*}{\rho} \sqrt{\left(\frac{2\rho a^2}{F}\right) (\Delta P_{ij} - \rho g H_{ij})} + \dot{Q} - P^* \frac{dV}{dt} - V \sum_j \left[ f_{1,j} \frac{dy_j}{dt} \right] \end{aligned}$$

.....(16)

Non-dimensionalizing:

$$\begin{aligned} f_2^+ V^+ \frac{dP^+}{dt^+} &= \sum_k \Pi_{P, \dot{Q}, k} Q_k^+ - \Pi_{P, V} P^{*+} \frac{dV^+}{dt^+} + \sum_i \Pi_{P, Wh_i} \sqrt{\Delta P_{ij}^+} h_i^+ \\ &+ \frac{P^{*+}}{\rho^+} \sum_i \Pi_{P, mech, i} \sqrt{\Delta P_{ij}^+} - V^+ \sum_j \Pi_{P, y, j} \left( f_{1,j}^+ \frac{dy_j^+}{dt^+} \right) \end{aligned} \dots\dots\dots(17)$$

where

$$P^* = P + \frac{\partial e}{\partial v} \Big|_{P,y}$$

$$f_{1,j} = \frac{1}{v} \frac{\partial e}{\partial y_j} \Big|_{P,v,y}$$

$$f_2 = \frac{1}{v} \frac{\partial e}{\partial P} \Big|_{v,y}$$

are thermodynamic properties, and

$$\Pi_{P,\dot{Q},k} = \frac{\dot{Q}_{k,o}}{V_o f_{2,o}} \frac{t_r}{\Delta P_r}$$

$$\Pi_{P,V} = \frac{P_o^* \Delta V_r}{\Delta P_r V_o f_{2,o}} \dots\dots\dots (18)$$

$$\Pi_{P,Wh,i} = \frac{\sqrt{\left(\frac{2\rho\alpha^2}{F}\right) (\Delta P_{y,0} - \rho g H_{y,0}) \Delta h_{i,o}}}{V_o f_{2,o}} \frac{t_r}{\Delta P_r}$$

$$\Pi_{P,mech,i} = \frac{\sqrt{\left(\frac{2\rho\alpha^2}{F}\right) (\Delta P_{y,0} - \rho g H_{y,0}) P_o^*}}{V_o f_{2,o} \rho_o} \frac{t_r}{\Delta P_r}$$

$$\Pi_{P,y,j} = \frac{f_{1,j,o} \Delta y_{j,r}}{\Delta P_r f_{2,o}}$$

are PI numbers, and

$$P^+ = \frac{P - P_o}{\Delta P_r}; \quad V^+ = \frac{V}{V_o}; \quad dV^+ = \frac{dV}{\Delta V_r}; \quad t^+ = \frac{t - t_o}{t_r};$$

$$\dot{Q}_k^+ = \frac{\dot{Q}_k}{\dot{Q}_{k,o}}; \quad \Delta P_{y,j}^+ = \frac{\Delta P_{y,j} - \rho g H_{y,j}}{\Delta P_{y,0} - \rho g H_{y,0}}; \quad h_i^+ = \frac{h_i - h_o}{\Delta h_{i,o}}; \quad y_j^+ = \frac{y_j - y_{j,o}}{\Delta y_{i,r}}; \quad \dots\dots\dots(19)$$

$$P^{**} = \frac{P^*}{P_o^*}; \quad \rho^+ = \frac{\rho}{\rho_o}; \quad f_{1,j}^+ = \frac{f_{1,j}}{f_{1,j,o}}; \quad f_2^+ = \frac{f_2}{f_{2,o}}$$

are nondimensional variables. This equation is used for the RPV for the late blowdown and GDCS transition phases and in the containment regions for the long-term phase.

II

II

**[[ Table 286-1 Summary of Driving Head based PI-groups**

NEDO-33083-A

]]

[[Table 286-2 Comparison of Original Scaling Report PI groups and revised Driving Head Based PI groups.

- Q287. The last paragraph on page 7-2 appears to state that each model equation is normalized in each phase with a common reference time, and that this makes distortions resulting from timing differences transparent. It is not clear from the discussion what this means. Are any of the facilities operating at a different time scale than the prototype? What does it mean to use a common reference time? Is it a common definition that may change in numerical value from facility to facility, or is it a rigid choice given by one or more of the facilities? How important (quantitatively and in terms of PIs) are other competing processes during each phase?
- R287. The common reference time is based on a common definition but can have different numerical values from facility to facility due to differences in the reference parameters. The use of common reference times is only relevant when more than one control volume equation is evaluated for the same time period as is the case for the late blowdown and GDCS transition phases in the RPV. During these phases both the pressure rate equation and liquid mass rate equations are evaluated as indicated in Table 7-1. It would be possible to select a blowdown time constant based on the pressure rate equation and a draindown time constant based on the liquid mass equation. Doing so, however, would decouple the scaling of the pressure and mass in the vessel. It is important to maintain the relationship between pressure and mass since the timing of GDCS injection is dependent on the vessel pressure.

Therefore a time constant based on the depressurization rate is used for both the pressure and mass equations, as described at the bottom of page 7-3. Although equation 7.3-3 is used for all of the facilities, the numerical values calculated for the time constants, are different due to differences in the facilities. These time constants are then applied to the mass rate equation also. This cross coupling highlights differences in the depressurization rate and mass loss rate for the different facilities. Also see the response to Question 289.

The relative importance of competing processes can readily be seen in the bar graphs in Figures 7-1 through 7-7. The height of the bar indicates the strength of the process.

- Q288. Immediately after Eq. 7.3-2, the term  $H_{GDCS}$  is introduced. However, this term does not appear in the equation nor in any other portion of the text. Clarify the reference to the “the vertical height of the liquid filled GDCS line”.
- R288. The generic variable  $L_m$  in equation 7.3-2 should be replaced by the variable  $H_{GDCS}$ . The correction will be made in future revisions of the report.
- Q289. In Eq. 7.3-3, the reference time is arbitrarily set although isochronicity was previously established. The right hand side of this equation is of fundamental

relevance to the scaling analysis, describing the energy lost via the ADS is compared with the loss of liquid inventory. This should be the central element of the scaling question in the intermediate portion of the transient. Later, in the scaling results section, it appears that matching the depressurization transient overshadows the key issue: how much water is lost as the pressure drops. Matching the pressure traces is a relatively easy task. It is the inventory relationship to the depressurization that relates directly to the adequacy of a given facility in representing plant behavior. An example of the consequences of this topic will be given in the comments concerning Section 8. Provide a description of the criteria used to evaluate the facilities.

R289. See responses to questions 253 and 287. The relationship between depressurization rate and inventory loss is addressed by using the depressurization time constant for both the pressure rate equation and the liquid mass equation. The time constant for each facility is based on its depressurization rate. Since the duration of the phase is set by these time constants the reference mass loss during the phase represents the mass lost during a similar amount of depressurization and therefore links the depressurization rate and inventory loss rate. If a separate time constant based on the mass equation were used for the mass equation, then it would be possible to show that the pressure rate and inventory loss rate are each well scaled individually, but there would be no indication that the depressurization rates relative to the mass loss rate are similar.

Q 290 The in-vessel, natural-circulation phenomena are not addressed in detail. On page 7-10, flashing is mentioned. This element of the vapor generation formulation is not clearly documented particularly in reference to the overall conditions in the RPV. The novel geometry of the RPV and its effects on the liquid inventory distribution may have a significant impact on these phenomena. How is this effect reflected in the scaling groups?

R290. The thrust of this question appears to be the scaling of the internal flows and flashing in the various regions of the RPV. The pressure differences within the RPV are much smaller than system pressure until the vessel depressurizes close to the containment pressure. Hence, the pressure rate calculated from Equation 6.1-5 is applicable to all regions of the RPV.

[[

]]

[[

]]

[[

]]

[[

]]

[[

]]

[[

]]

[[

]]

[[

]]

[[

]]

**Q291.** In the final paragraph of Section 7.6, “Bottom-up Scaling,” the issue of noncondensable gas mixing and segregation is dismissed. What is the rationale for using the PANDA facility if its data are not used to resolve this issue?

**R291.** The importance of stratification and mixing is in influencing the timing and rate for noncondensables reaching the PCC and the wetwell. As described in the

report *TRACG Application for ESBWR* (NEDC-33083P) a bounding approach is used to address stratification and mixing when applying TRACG to ESBWR analysis. The PANDA tests provided information on noncondensable release over a wide range of timing and rates. This information is useful in ensuring that the most bounding combination of release rate and timing has been applied in the TRACG application. As expected the impact of various release timings and rates on the peak containment pressure is small. The intent of the PANDA tests is not to simulate the stratification and mixing that would be expected in the ESBWR since the relatively simple open geometry cannot possibly simulate the complicated geometry in the drywell of the ESBWR with all of the equipment and relatively confined spaces.

- Q292. The acceptance criterion presented in the report for a well-scaled facility is meaningless unless one can relate the effect of such distortion range on the figure of merit. If the figure of merit is core coolability, it is necessary to show that when a given non-dimensional group is within the acceptability range, its effect on core coolability is within the acceptable range of uncertainties. Describe what figure of merit is used and provide a detailed justification on the acceptance criterion based on the impact that the distortions of important parameters have on the figure of merit.
- R292. The tests are not intended to be prototype tests that will predict actual peak values in the figures of merit (RPV water level and containment pressure). Instead they are used to provide data to qualify the TRACG code so that it can be used to predict the plant response for a wide range of accidents. As such the magnitudes of the processes present in the test should be similar to those expected in the plant so that the TRACG models can be qualified for predicting those processes. This puts a requirement on the magnitude of the processes present in test and plant (we chose 1/3 to 3 criterion) but it does not place any specific requirements on variations in the figure of merit. In addition the dominant processes should be the same in the tests and ESBWR. Clearly certain break points in test and plant behavior, such as core uncover versus no core uncover should be avoided, however.

The 1/3 – 3 criterion was selected to make sure that the phenomena of interest were of the same order of magnitude in the ESBWR and tests. The range 1/3 to 3 results in a total variation of a factor of 9 between the largest and smallest parameter, or approximately 1 order of magnitude. The factor of 3 in either direction also provides separation between the range used to identify phenomena as unimportant. Processes that are a factor of 10 less than the dominant process are considered unimportant.

- Q292 The 1/3 - 3 criterion for acceptance is meaningless unless one can relate the effect of such distortion range on the figure of merit. Presumably the figure of merit is core coolability. Therefore, it is necessary to show that when a given non-dimensional group is within the acceptability range, its effect on core

coolability is within the acceptable range of uncertainties. Provide a detailed justification on the 1/3 – 3 criterion that is based on the impact that the distortions of important parameters have on the figure of merit.

**Supplemental response to RAI 292**

There was a remaining concern that the range of 1/3 to 3 for the ratio of PI groups was not an adequate criteria without further supporting information. This supplemental response addresses that concern.

[[

]]

Following the work of diMarzo [1], a simplified model of the RPV blowdown behavior is used to predict the plant and test performance, including only the key variables needed to predict the behavior with reasonable accuracy. The simplified models were compared against TRACG predictions for the ESBWR, and test data for the test facilities to assure that they are reasonably accurate.

The details of the simplified model approach and implementation are summarized in the paper by diMarzo. The specific application to the ESBWR and test facilities is summarized below. There are several differences and added complications in the ESBWR compared to the situation in diMarzo's paper. For application to the ESBWR and test facilities, a GDCS line break is used since this is the limiting break for RPV liquid inventory. This is also the break considered for the RPV liquid mass in the ESBWR scaling report. For this break, the ESBWR has both steam flow from the vessel due to ADS flow and liquid flow from the broken GDCS line. In addition, the minimum liquid inventory occurs a short time after ECCS injection flow from the GDCS system initiates. The GDCS flow rate is highly dependent on the RPV pressure. Therefore a simple model of the GDCS flow is needed.

The simplified model results in a system of equations for the pressure and inventory in the vessel,

[[

]]

where the following variables are used

$P$  = pressure in vessel

$t$  = time

$I = M_l/M_o$  = liquid inventory in vessel divided by initial inventory

$M_l$  = liquid inventory

$W_{GDCS}$  = GDCS injection flow rate

$Q_{deheat}$  = decay heat

$Q_{stored}$  = stored energy release from vessel wall

In addition the following values are held constant

$M_o$  = Initial inventory in vessel (steam and liquid)

$\rho_l$  = liquid density

$V$  = RPV non solid volume

$F$  = Discharge coefficient for liquid flows out of the vessel

$D$  = Discharge coefficient for vapor flows out of vessel

$R$  = Gas constant

$T$  = temperature in vessel

$h_s$  = GDCS pool subcooling relative to RPV ( $h_{pool} - h_{GDCS}$ )

$h_{fg}$  = enthalpy of vaporization

$a = h_{fg}/RT$

$C_p$  = Specific heat

$A$  = critical flow area

[[

]]

where

$P_{RPV}$  = RPV pressure ( $P$  in the equations above)

$P_{DW}$  = drywell pressure (held constant)  
 $H_{GDCS}$  = hydrostatic head for the GDCS line  
 $H_{mainvent}$  = submergence of the main vent  
 $W_{GDCSrated}$  = rated GDCS flow when the RPV and drywell are at the same pressure  
 $g$  = acceleration due to gravity constant

[[

]]

The last term in equation 292-2, representing the mass stored in the gas space, has been dropped in equation 292-7. This term has a very small impact on the inventory calculation and adds undesirable complexity to the calculation since it contains the pressure derivative.

The non-dimensional variables in equation 292-6 and 292-7 are all in the form,

$$X^+ = \frac{X}{X_0} \quad (292-8)$$

where  $X$  is the variable of interest and  $X_0$  is the reference value for the variable. For all variables except time and areas, the initial values are used as the reference values. For the ADS area, which varies with time, the maximum area is used. The determination of the time reference value is described in a later section.

The PI groups are defined as,

[[

II

[[ Table 292-1 PI group Magnitudes – comparison of scaling report values and simple model values for the ESBWR.

[[

]]

[[ ]]

[[

]]

]]

[[

]]

**References:**

1. di Marzo, Marino, 2001, "A Simplified Model of the BWR Depressurization Transient," Nuclear Engineering Design, **205**, 107-114.

Q293. With reference to the discussion concerning the relationship between pressure and inventory, Figure 8-5 shows excellent agreement in the temporal behavior of the pressure. This result should be directly related to the liquid inventory information depicted in Figure 8-2. Here, during the crucial GDCS phase, the liquid mass results do not appear to be consistent: Giraffe/SIT exhibits three times the magnitude of liquid mass as ESBWR and GIST about one third. Explain why this is an acceptable outcome.

R293. As discussed in the response to RAI 292, the purpose of the tests is to provide data for TRACG qualification so that TRACG can predict the plant response. To satisfy this goal, the test must include the important processes at a similar magnitude to the ESBWR. Since a factor of three difference is the criterion used to satisfy this, it should be expected that the rate of change for a figure of merit could also be different by a factor of three, or so. This should be acceptable also.

Additionally, since the two tests mentioned cover the range of 1/3 to 3, they bound the ESBWR conditions.

In the case of the GDCS flow mentioned above, the fact that the vessels fill faster or slower is of little importance. In fact, when the GDCS flows begin in earnest they dominate all other processes. This becomes a simple filling problem. Since the process is dominated by a single parameter, it would be possible to use an alternate time scaling for this phase (i.e. not 1:1) and end up with the GDCS flow parameters scaled very closely.

Q294. Chapters 6 and 7 discuss the non-dimensionalization of the governing equations and the comparative analysis of the resulting PIs. However, the actual comparisons, in figures 7.1 through 7.7 and 8.1 to 8.7, only have one equation per transient phase. What happened to the other dynamic equations?

R294. A summary of which equations are applied in each region and transient phase is given in Table 7-1 and summarized in Section 7.2 of the report. Section 7.2 of the report has been expanded to provide more detailed discussion of the rationale for application of the scaling equations to different parameters, regions and temporal phases. The revised Section 7.2 is below. This revised version will be incorporated into future revisions of the report. It should be noted that there are multiple evaluations of the equations for some phases. For example Table 7-1 shows two scaling equations being evaluated during the first two transient phases. In the revised version of Table 7-1, below, this has been increased to four equation applications during the late blowdown phase.

Dynamic equations for mass, pressure and energy (or temperature) were developed in Section 6. These equations, in the general form shown there are applicable to all of the volumes in the ESBWR. However, certain parameters are of more interest than others in different volumes and temporal phases. Therefore, the equations are applied only for those parameters, regions and temporal phases that are of interest. The specific applications of the scaling equations to different regions of the ESBWR are summarized in Table 7-1. The motivations for the selected application shown there are summarized below.

The water level in the RPV is of prime interest during the first three temporal phases – late blowdown, GDCS transition, and full GDCS. Therefore, the RPV liquid mass equation is evaluated for these phases. This is indicated by the “M”s in the RPV column of the table. Additionally, the RPV depressurization is important for the first two phases, since it controls the flashing rate and time of GDCS initiation. Thus, the RPV pressure is also considered for the late blowdown and GDCS transition phases. The liquid mass in the RPV during the long-term phase is of minimal interest for scaling since it is a simple case of decay heat boiling off inventory that is replaced by PCC return flow. The dominant parameters influencing the RPV mass are readily identifiable as boiloff

due to decay heat and return flow from the PCC via the return line from the condensate tank. The scaling of the decay heat is demonstrated through the DW pressure scaling (see  $\Pi_{P,mech,ADS}$  and  $\Pi_{P,W,ADS}$  in Figure 7-6) and the PCC scaling is demonstrated through the bottom-up scaling of the PCC given in the response to RAI 259, part 1. The RPV pressure is nearly identical to the drywell pressure during the long-term phase since these volumes are connected by the large DPV pipes. Therefore, the pressure equation for the combined volume is evaluated as indicated by the "P" in the DW column for the long-term phase.

In the long-term phase, the liquid level has recovered in the RPV and the containment pressure is of primary interest. The pressure in the WW sets the containment pressure. The initial increase in containment pressure occurs during the blowdown phase when most of the noncondensibles are moved to the WW. The long-term pressure is controlled by the quantity of noncondensibles in the WW and the energy balance for the WW gas space. Therefore, the pressure equation is evaluated for the WW in the long-term PCCS phase. The DW acts primarily as a conduit for steam to flow to the PCCS and WW during all of the phases considered (this excludes the first few seconds of blowdown which is not considered as part of the ESBWR test program). To assure that this is the case and that none of the sources and sinks of energy in the DW are important, the pressure equation is evaluated for the DW during the long-term phase.

During this long-term phase the change in SP temperature is negligible. The only energy sources for the SP are heat exchange with the gas space above and the very small energy addition associated with occasional bubbling of non-condensable gas through the PCC vent. In addition, the walls provide a small energy sink. Even if all of the energy from the VB leakage flow was directly deposited into the SP region above the PCC vent for 24 hours, with no heat losses from the pool, the temperature increase in this top pool layer would only be on the order of 2 deg C. Therefore the energy equation is not evaluated for the SP during the long-term phase.

During the GDCS and GDCS transition phases, the RPV liquid is subcooled and vapor generation ceases. Without this energy source to the containment, the containment becomes quiescent. Therefore the scaling equations are not applied to the containment during this period. Most of the changes in containment parameters occur during the blowdown period. Additional evaluations of the SP energy and WW pressure have been added as part of these RAI responses (see RAI 259, part 1) to better capture this dynamic period. The updated version of Table 7-1, below, reflects these additions. The drywell pressure is interesting during the very early portion of the blowdown, during vent clearing. However, the response during that period is typical of all pressure suppression containments and has been investigated previously for the operating plants. The tests in the ESBWR program begin at later stages of a LOCA, so no scaling of the initial blowdown period is included in this report.

**Table 7-1 Application of Scaling Equations to ESBWR Phases and Regions**

		<b>Plant Region</b>			
		<b>RPV<sup>5</sup></b>	<b>DW<sup>2</sup></b>	<b>WW gas<sup>3</sup></b>	<b>Suppression Pool</b>
<b>Transient Phase</b>	<b>Late Blowdown (7.5.1)<sup>1,4</sup></b>	M, P	-	P	T
	<b>GDCS Transition (7.5.1)<sup>1,4</sup></b>	M, P	-	-	-
	<b>Full GDCS (7.5.1)<sup>1,4</sup></b>	M	-	-	-
	<b>Long Term PCCS (7.5.2)<sup>1,4</sup></b>	-	P	P	-

1 M = liquid mass equation, P = pressure equation, T = temperature (energy) equation.

2 DW and RPV gas act as one volume during reflood and long-term phases

3 Includes GDCS gas volume

4 Number in parenthesis is section where results are shown

5 The limiting breaks are used for each region: GDCS Line break for the RPV and MSLB for the containment

Q295. Matching the pressure traces in time has some relevance to the overall plant behavior. However, the discrepancies in the RPV liquid inventory recovery are more significant. How can these concluding remarks be tied to the overall discussion on the acceptable range of the distortions outlined in Section 8 of the report?

R295. As stated in RAI responses 292 and 293, the rates of change for figures of merit can be expected to be different by as much as a factor of three, since this is the criterion used for the individual processes. It is not necessary to match the figures of merit any closer than this as discussed in those responses.

### Response to NRC RAI Regarding Scaling Issues – Additional Supplementary Information

(1) Please provide a justification of the distribution of non-condensable gases ([[ ]]) on Page 6 of enclosure 1 to MFN-117 dated October 20, 2003.

Response (1):

[[

]]. Most of the noncondensibles are moved from the drywell to the wetwell during the early part of blowdown, prior to the start of the ESBWR tests. [[

]].

The ESBWR TRACG runs estimate that the noncondensable fraction at the start of the late blowdown period will be in the range of [[ ]]. The test initial conditions reflect this by starting with noncondensable fractions in the drywell in the range of [[

]]. However, it is easy to extrapolate this to other values by looking at the bars in Figure 8-6 and 8-7. For example the approximate impact of the noncondensable movement for PANDA test M7 ([[ ]]) would be approximately [[ ]] that shown in Figure 8-7.

(2) On page 7, same reference, the equations feature the variables  $f_3$  and  $f_4$ . Please provide the units of these properties

Response (2):

The terms  $f_3$  and  $f_4$  are described on page 6-2 of the ESBWR Scaling Report, NEDC-33082P, Rev 0. The definitions and units for these variables are:

$$f_3 = 1 - \rho_g h'_g; \text{ dimensionless}$$

$$f_4 = \frac{\rho_g}{\rho_l} h'_g - h'_f; \text{ units} = \text{m}^3/\text{kg}$$

where,

$h_f$  is the saturated liquid enthalpy,

$h_g$  is the saturated vapor enthalpy,

$\rho_f$  is the saturated liquid density,

$\rho_g$  is the saturated vapor density, and

primes denote derivatives with respect to pressure.

(3) On page 25, same reference, you provided a graph with a comparison of ESBWR and test analytical results. Please update this figure to include the GIST and GIRAFFE test data. You may also consider revising this plot to remove time by plotting delta inventory vs. delta pressure.

Response (3):

The Figure below provides the requested information. The inventory and pressure data have been added for the tests and the data has been replotted as RPV Pressure vs. Inventory. As before the plots show a very similar trend for the ESBWR and tests. Although there are distortions present in the magnitudes as previously identified by the scaling groups, the behavior of inventory relative to pressure is similar for all facilities.

[[

]].

[[

Figure 1. RPV Inventory vs. Pressure Comparison for Simple Model and Test Data for ESBWR and Test Facilities ]]

The following two comments are related to GIRAFFE/SIT test scaling:

(4) The SBWR scaling report [Ref. 7, Table 4.1-20] shows that the GIRAFFE/SIT test is scaled well, [[ ]]. Comparison of the same dimensionless parameter ratio for GIRAFFE/SIT and ESBWR is needed to establish that the test data are applicable for ESBWR.

Reference 7 is NEDC-32288P "Scaling of the SBWR Related Tests". The requested information may be shown graphically in Figure 8-5 of NEDC-33082P. If that is correct then the test data [[

]] for this important parameter. It isn't then clear that interactions XL3 and XL4 are the same for the test and ESBWR. The value of the PI group needs to be provided and the consequences of any differences on these interactions need to be explained.

Response (4):

[[

]]. Values for these parameters are shown graphically in Figure 8-2 and 8-5 of NEDC-33082P, Rev 0, "ESBWR Scaling Report", respectively. Numerical

values are given in Table A-4 and A-10 of the same reference, respectively. The numerical values given in the report are:

[ [

]]

[[

]]. A better measure of the true impact of the differences in the PI groups is given by the supplemental response to RAI 292 given in pages 17 to 25 of enclosure 1 to MFN-117. The graph shown on page 25 of the reference shows that the timing of pressurization rate, GDCS initiation timing, and minimum water level is reasonably well represented in tests. Therefore the distortions present had a minimal impact on the interactions represented by PIRT parameters XL3 and XL4.

(5) The GIRAFFE/SIT data exhibit phenomenon E3 (Cold Water Injection Below >Two-Phase Level) and phenomenon E7 (cold water injection above two-phase level). Please justify your conclusion that these phenomena are not important.

Sections 3.5.3 and 3.5.4 of NEDC-32606P state that based on the results of GIRAFFE/SIT test run GS2: "the issues raised by this phenomenon are not a concern". Test case GS2 exhibited GDCS injection for some periods of time both above and below the two-phase level in the downcomer. The test provides data that may be useful for qualifying the TRACG code to predict these phenomena. However, the conclusion that appears to be reached is that these phenomena are not a concern because the core did not uncover in this run or any other runs. This implies that GE sees no need to have models that accurately predict these phenomena. However, it is not clear why the core not uncovering shows that these phenomena did not play a role in the response. Also, the TRACG code will be used to simulate many events, and it is not apparent from the arguments presented that these phenomena are of no concern. These phenomena were

ranked high and therefore, better justification needs to be provided for not qualifying the code to predict these phenomena.

Response (5):

[[

]].

Moreover, the test findings did not affect the TRACG qualification plan. The effects of these phenomena were present in the test results that were compared against TRACG calculations. The qualification report (NEDE-32725P) shows that the depressurization rate of the RPV, the downcomer level and chimney were all calculated well in the GIRAFFE/SIT tests. [[

]].

## NRC RAIs and Responses

### ESBWR Test and Analysis Program Description (TAPD) NEDC-33079P

Note: RAI responses including data files that cannot be read on a PC are not included.

Q33. Please provide a roadmap for separate effects testing used for TRACG qualification for containment analysis.

R33. **Separate Effects Tests for Containment Applications**

[[

]]

Q177. Comparison of non-dimensional parameters (similar to one presented for SBWR and CRIEPI in Table A.4-1 of NEDC-33079P), or dimension-less groups (PI-Groups) should be derived based on scaling analysis, and their numerical values should be compared for ESBWR with the test facilities in order to provide assurance that the test facility represents the ESBWR design. As indicated in Table 6.1 of NEDC-33079P, GE qualified TRACG code for its application to anticipated transient without scram (ATWS) and Stability events in ESBWR against the following facilities: 1/6 Scale Boron Mixing Test, CRIEPI and Dodewaard. GE, however, did not present comparisons of representative

parameters for ESBWR design and the above facilities in the submittals. The staff, therefore, requests GE to submit scaling analyses for the above mentioned test facilities, and provide comparisons of dimension-less parameters as discussed above, between ESBWR and the test facilities in order for GE to qualify TRACG code for its application to ATWS and stability events in ESBWR against the test facilities.

R177 Comparisons of relevant dimensionless parameters between the 1/6 Scale Boron Mixing Test, CRIEPI and Dodewaard and the ESBWR are provided below.

[[ ]]

[[ ]]

[[

]]

[[ ]]

[[ ]]

[[

]]

[[ ]]

[[ ]]

[[ ]]

[[

]]

[[ ]]

[[

]]

[[

]]

[[

]]

[[

]]

[[

]]

It can be concluded that the 1/6<sup>th</sup> scale mixing tests are reasonable for evaluating the mixing in the ESBWR bypass regions because the density difference between the borated solution and water, the core average void fraction and the leakage loss coefficients are adequately matched. Numerical values for the parameters in the ESBWR and the 1/6<sup>th</sup> Scale Boron Mixing Test are provided in the table below.

**Comparison of Parameters for ESBWR and 1/6<sup>th</sup> Scale Boron Mixing Test**

[[

]]

**CRIEPI Tests**

The CRIEPI tests are natural circulation and stability tests, dominated by flashing instability at low pressure.

The relevant parameters that characterize these phenomena are shown in the table below.

**Comparison of Non-Dimensional Parameters Between ESBWR and CRIEPI**

[[

]]

**Dodewaard Data**

The Dodewaard data have been used to qualify steady state natural circulation performance. The main parameters of interest are the geometrical configuration, flow rate and core and chimney void fractions. [[

]]

**Comparison of Dodewaard and ESBWR Geometry and Steady-State  
Parameters**

[[

]]

Q178. Page xv - For LASL, it is suggested to add a statement in parentheses for clarification. [Los Alamos National Laboratory (LANL) is the current name for LASL].

R178. LASL has been changed to LANL on page xv in Rev.1 of the report.

Q179. Page A-122 - In Table A.5-3, the TRACG analyses for PANDA P-Series tests focus entirely on containment phenomena\*, as confirmed by the information presented in "TRACG Qualification for ESBWR" (NEDC-33080P). We understand that with the exception of P2 test\*, the focus of these PANDA tests is on the long-term cooling containment issues. However, the PANDA P-Series tests are the only ESBWR tests in which the gas space of the gravity driven cooling system (GDCS) pool was connected to the wetwell (WW) gas space. As a result, please revise Table A.5-3 and "TRACG Qualification for ESBWR" to include the vessel parameters such as reactor pressure vessel (RPV) pressure and water level in the data comparison. In addition, other containment parameters such as suppression pool (SP) water level and drywell (DW) water level (from wall condensation) should also be included.

\*One exception is that the reactor pressure vessel (RPV) and GDCS water levels were included in data comparison for the PANDA P2 test, which covered the long-term passive containment cooling system (PCCS) cooling phase and the transition from GDCS injection to the long-term cooling phase.

R179. [[

]]

Q180. Page A-70 - Provide a comparison of the important vessel and containment parameters (such as RPV water level, pressures of RPV and DW and WW, SP level, and GDCS pool level) of the three integral counterpart tests.

R180. Please see the response to question 336.

Q181. Page 1-10 (1st paragraph) - GIST test data have been used in the qualification of TRACG to SBWR and documented in Reference 15 (the GIST report, GEFR-00850, October 1989). As shown in Figs. 4.3-51, 4.3-53, and 4.3-54 of GEFR-00850, the GDCS flow rate predicted by TRACG is good for main steam line break (MSLB - GIST Test B01), acceptable for the GDCS Line Break (GDLB - GIST Test C01A), but poor for the bottom drain line break (BDLB - GIST Test A07 for which the TRACG-calculated total GDCS flow is about half of the data). In comparison, better agreement with GIST data was achieved in the TRACG04A calculations shown in Fig. 5.1-21, Fig. 5.1-23, and Fig. 5.1-12 of "TRACG Qualification for SBWR" (NEDC-32725P, Vol. 2). What are the major

differences (in terms of models, code input, and noding) between TRACG04A and the earlier version of TRACG used for the GIST calculations (GEFR-00850)?

R181. [[

]]

Q182. Page 1-8, Section 1.2.1.3.4 states that "Key model parameters and input variables will be treated conservatively to produce a bounding calculation of the containment parameters of interest (pressure and temperature)." Provide a narrative describing the basis for the decision reached to use conservative as opposed to best-estimate values for key model parameters.

R182. This statement applies to containment analysis. The Qualification Report provides the basis for this approach. TRACG, in conjunction with the coarse noding used for containment analysis, cannot accurately calculate phenomena such as suppression pool stratification and noncondensable mixing and transport in the drywell. Hence, a conservative approach is employed.

Q184 The rationale for selecting the inadvertent ADS actuation event is that it cannot be bracketed by MSLB during the "early" blowdown phase from the initial opening of the safety relief valves (SRVs) to the opening of the depressurization valves (DPVs), because there is no PCCS heat removal until the DPVs are opened. A TRACG calculation for inadvertent ADS actuation is therefore desirable and should last until the transient becomes similar to any LOCAs. Please provide the opening sequence including time delay for the SRVs and DPVs in the inadvertent ADS.

R184. The opening time sequence of the SRV's and DPV's was given in RAI 23. Inadvertent ADS actuation has not been considered as an initiating event for typical accident analysis, but is an event considered in the PRA realm. Inadvertent ADS is beyond the scope of the analysis performed in Chapter 15 and will be covered in Chapter 19 of the Safety Analysis Report.

Q185. In section 2.2.1, the statement is made that "The limiting LOCA ... from the viewpoint of containment pressure, it is likely to be the large steamline break." This statement appears equivocal. Why is the statement not more definitive if the analysis is available?

R185. The steamline break has been shown to be the most limiting break for containment pressure. The statement in the TAPD has been changed to a definitive statement in Revision 1 of the document (Section 2.2.1).

Q186. Page 2-3, Section 2.2.1.1 - The statement is made that, "This setpoint [level 3] is assumed to scram the reactor." Will the level scram setpoint be reached before the drywell pressure scram setpoint?

R186. [[

]]

Q187 Page 2-5, Section 2.2.1.2 - For the last paragraph an elevation diagram would be helpful to the discussion.

R187. Please see Figure 187A and Figure 187B for details.

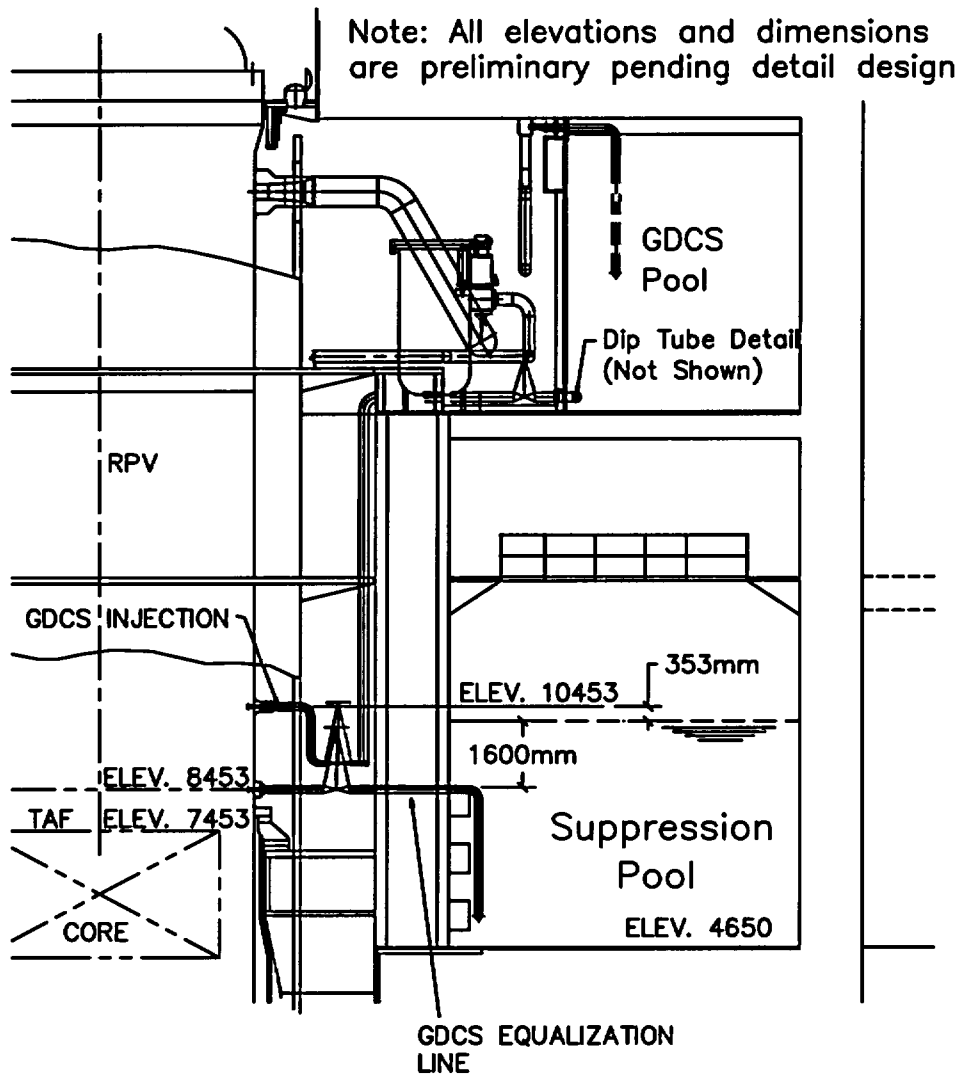
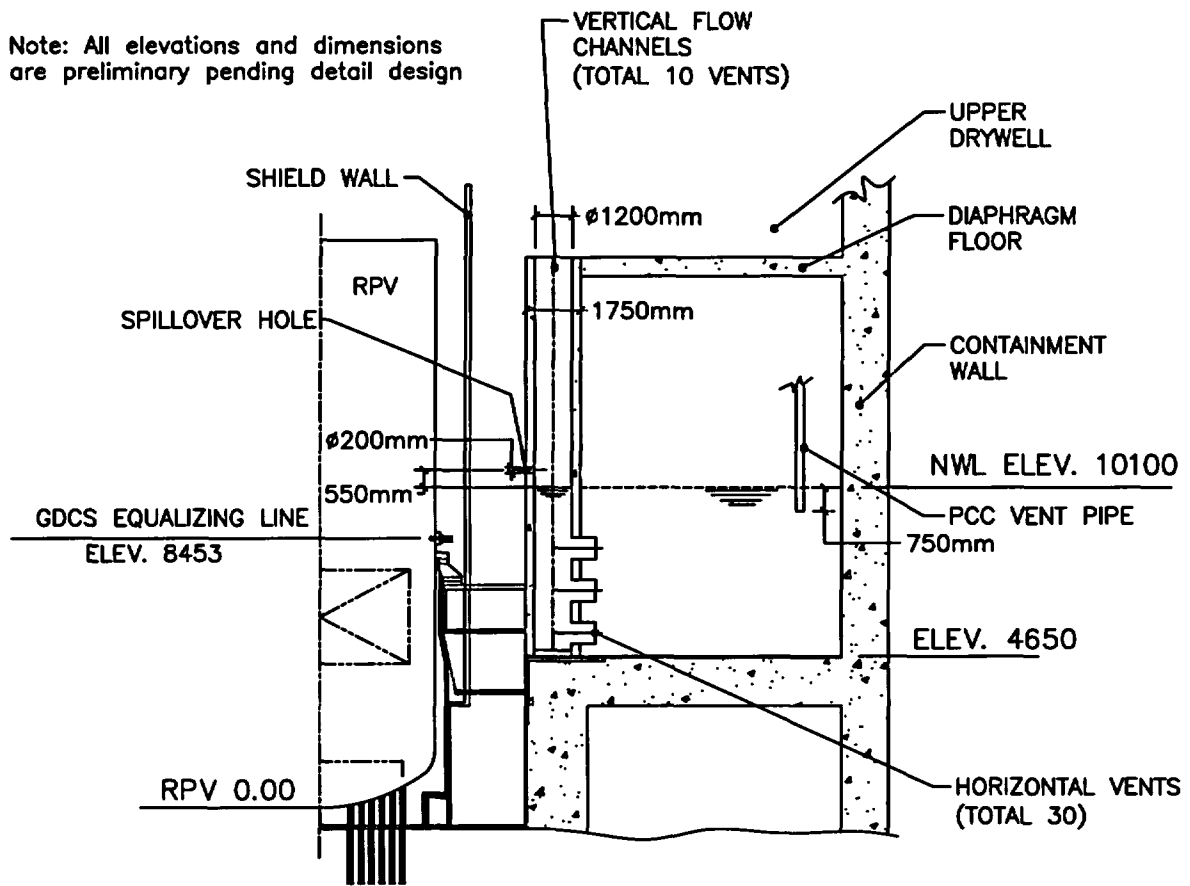


Figure 187A GDCS Equalization Line



**Figure 187B Spillover Hole Configuration**

Q188. In the ESBWR design, how was the relative and absolute submergence of the PCCS vent and the upper most main vent determined?

R188. [[

]]

Q189. Page 2-8, Section 2.2.1.4 - *Long-Term PCCS Period* - The statement is made that, "However, unlike the GDCS line break, the steam generated by the decay heat is condensed and all of it is returned to the vessel via the PCCS Drainage Tank." Why should the two scenarios differ in this regard?

R189. [[

]]

Q190. Page 2-9 (last paragraph) - It is stated that water collected in the drywell can spill into the wetwell through the spillover holes in the pipes connected to the horizontal vents. Please provide a sketch to show the elevation and diameter of the spillover holes and explain why their presence will not adversely affect horizontal vent clearing in a loss of coolant accident (LOCA).

R190. Please see Figure 187B (above) for details of the spillover holes. The holes lead from the annular region of the drywell (region surrounding the RPV) to the vertical vents, which lead to the horizontal vents under the water surface of the suppression pool. The spillover holes are 200 mm in diameter and are located about 550 mm above the normal level of the suppression pool water. One hole leads into each of the ten vertical vent pipes. The spillover holes provide a return path for water, which may accumulate in the lower drywell and the annular region of the drywell during a pipe break accident. The purpose of the spillover holes is to provide a means to limit the draw-down of the suppression pool water and thereby assure the PCCS heat exchanger vent submergence. Since the spillover holes are located above the normal water level in the vertical vents they have no impact upon the vent clearing process. The drywell atmosphere pressurizes the vertical vent water column and forces this level down to the first, second and sometimes even third horizontal vents in order to clear the vents and relieve the pressure differential.

Q191. Page 2-12 (4th paragraph) - Under what conditions will the subcooled water be sprayed into the steam dome of the reactor vessel? Where is the location of the source of the subcooled water?

R191. The subcooled water is sprayed into the steam through the feedwater spargers. The source is from the condensate/feedwater system. The assumption is that the feedwater system (e.g., motor driven pumps) is still available and operating.

Q192. Page 2-13 - Main Steam Isolation Valve (MSIV) Closure Transient - Is this discussion consistent with the scenario in the licensing calculations?

R192. The scenario is based on realistic calculations for the MSIV closure ATWS event. The licensing scenario may incorporate conservatisms to bound uncertainties, but is not expected to be significantly different.

Q193. Page 2-15, Section 2.2.4.4 - While geysering can indeed be "postulated," its actual relevance to the ESBWR is not entirely evident. Is there analysis that would show that it should indeed be considered?

R193. [[

]]

Q194. Page 2-16 - There is a discussion of the conditions for opening the GDCS equalizing lines (between the SP and RPV). (1) Are there any integral test data (e.g., GIRAFFE) that covered PCCS performance after the opening of equalizing lines (to drain SP water into the RPV as expected during GDLB or BDLB)? (2) Is there an analysis or physical evidence to ensure that any manometric oscillation between the connected SP and RPV will not occur or it will not uncover an equalizing line (if the check valve on the equalizing line fails to close when called upon)?

R194. [[

]]

Q195. Page 2-16 - (1) What is the water level in the loop seal (during normal full-power operation) between a passive containment cooling (PCC) unit and its condensate drain tank? (2) Is there any water in the PCC condensate drain tank during normal full-power operation?

R195. (1) The water level is provided as a loop seal, to prevent an open bypass from drywell to wetwell or vice versa. Its height is determined based on maximum long-term pressure differential postulated between the drywell and wetwell. The

normal water level in the loop seal is approximately 2.5 m. To ensure the U-tube water seal on the condensate drain line section is full at all times, level detection instrumentation is provided to signal water level in this U-tube seal and, if a low-level condition is detected, makeup into the U-tube water seal is provided automatically via supply from the Condensate Storage and Transfer System. Level detection instrumentation is also present to detect a condition of water accumulation in the condensate drain tanks. If water level exceeds a pre-determined set-point level, drain valves are opened to drain this water into the drywell equipment drain sump.

(2) The drain tanks should not have any water in them during normal operation (other than minor condensation from moist drywell air). If water level did build up in the tank it would be drained as described in (1) above.

Q196. Page 2-21, Fig. 2-2-5 - The figure shows that the TRACG-calculated PCCS heat removal rate is always lower than the core decay heat power for the MSLB. On page A-8, it is stated that under certain conditions, the PCCS heat removal rate can exceed the core decay power. Are there any TRACG LOCA analyses or integral test data in which the PCCS heat removal rate exceeded decay power for a certain period of time?

R196. The decay heat is higher than the PCC heat removal because of other heat sinks, such as drywell walls. The normal mode of the PCCS is to remove the energy required to balance the net energy input. In scenarios leading to VB openings, heat removal by the PCCS exceeds the net energy input until the drywell pressure drops below the VB setpoint.

Q197. Page 2-22 - Is there a TRACG analysis for an ATWS initiated by inadvertent MSIV closure for the ESBWR (similar to Fig. 2.2-6 obtained for SBWR)?

R197. [[

]]

Q198. Page 2-24 - (1) Provide the reference from which the ESBWR stability map in Fig. 2.2-7 was obtained. (2) Was this figure based on ODYSY computer code calculations? (3) Describe the ESBWR transients represented by the small elliptic area (in the lower left corner of Fig. 2.2-7). (4) If control rods are fully inserted, is there any possibility for the reactor to enter the unstable region shown in this figure?

R198. 1) The stability map shown is a BWR map and is used for assessing margins in operating BWRs [Ref. BWROG Program Option E1A; Also, *ODYSY Application for Stability Licensing Calculations*, NEDC-32992P-A, July 2001]. The design boundary for the ESBWR uses decay ratios that are half of the BWR design limits to provide sufficient margins during normal operation. These values are

consistent with decay ratios in the flow control operating range for jet pump BWRs.

2) [[

]]

3) The elliptic region in the box represents Dodewaard data , and the other ellipse characterizes the estimated range of ESBWR steady state operation. No transient evaluations have been performed as yet for the ESBWR. Two transient scenarios were evaluated for the SBWR and the results shown in the SBWR TAPD (NEDC-32391P, Rev.C). 4) If all rods are fully inserted, the reactor will be at hot shutdown and there is no possibility of entering the unstable region on the map.

Q199. Page 2-25 - Is there a power/flow stability map for ESBWR (similar to Fig. 2.2-8 obtained for SBWR)?

R199. [[

]]

Q200. Page 2-27, Section 2.3 - In many instances, aspects of plant design that may be termed initial and boundary conditions are as important to the analysis as phenomena/processes. While such items are not to be considered part of TRACG qualification, they become part of transient analysis and may be explored in experimental programs. How and at what stage are the relevant aspects of initial and boundary conditions considered vis a vis the phenomena identification and ranking table (PIRT)? Is this aspect considered to be covered by the Bottom-Up process?

R200. [[

]]

Q201. Question was addressed in July 9, 2003, meeting.

R201. No Response Required.

Q202. Page 3-27 (No.2 - B11/4) - It seems that the suction lines of the Reactor Water Cleanup/Shutdown Cooling (SDC) System are connected either to the RPV downcomer annulus or to the RPV bottom head and the injection lines are connected to the RPV via the main feedwater lines. (1) Please provide a sketch to show "inlet and outlet nozzles located diametrically across the downcomer." (2) There is a typographical error in the fourth column, "CFD code calculations show

sort [sic] circuiting will not occur” should be replaced with CFD code calculations show short circuiting will not occur.

R202. Please refer to Figures 202A and 202B for details of the shutdown cooling suction nozzle and the feedwater nozzles.

The typographical error has been corrected in Revision 1 of the report (Page 3-27).

[[

**Figure 202A ESBWR RPV**

]]

**Figure 202B Section View A-A**

Q203. Page 2-49 - It seems that some high-ranked phenomena are missing in Table 2.3-4 (ESBWR PIRT for ATWS), because it does not include any phenomena associated with standby liquid control system (SLCS) which can play an important role in ATWS. For example, the Bottom-Up Process listed in Table

3.2-1 (p. 3-9) has identified two high-ranked SLCS phenomena (Issues C41/1 and C41/2) that are missing in Table 2.3-4. Please explain why Table 2.3-4 does not include these SLCS phenomena.

R203. FMCRD availability is not considered for ATWS events. Availability of the FMCRDs will mitigate the event similar to a normal scram. [[

]]

Q204. Page 2-54, Table 2.3-6 - Should this list include the controllers for feedwater and steam pressure valves?

R204. Control systems are considered in overall plant stability evaluations, but do not influence stability because the time constants are an order of magnitude larger than those for density wave oscillations. Typically, control systems are tuned for optimal performance during plant startup.

Q205 Question was addressed in July 9, 2003, meeting.

R205. No Response Required.

Q206 Page 3-3, Table 3.2-1 - There is a typographical error – “hutdown” should be replaced with “shutdown.”

R206. The typo has been corrected in Revision 1 of the report (Page 3-3).

Q207 Page 3-5 - Please explain why the following phenomena are not ranked high (7 or higher) in the Bottom-Up Process listed in Table 3.2-1 (ESBWR Thermal-Hydraulic Phenomena): (1) Issue No. J/3 - Unique power/flow operating map and natural circulation characteristics, (2) Issue N21/3 - Effect of core inlet subcooling on stability, (3) Issue T10/3 - WW response to long-term heat addition from PCCS vents (Note that a companion issue, Issue T10/5 - Stratification below PCCS vent discharge, is ranked high), (4) Issue T10/9 - Establishes DW to WW pressure drop and PCCS operation, (5) Issue T10/12 - PCCS submergence determines DW to WW, and (6) Issue T15/11 - Replaces drywell GDCS pool. (Note that the explanation for Issue J/3 on p. 3-22 (3.3.6.3 Natural Circulation Characteristics) seems to indicate its importance, because extensive TRACG qualification against test data was conducted on this issue.)

R207. [[

]]

**Q208.** Page 3-5 - There are several questions regarding Table 3.2-1. (1) Please explain the footnote “ESBWR T/H phenomena outlined in gray have not been evaluated. Relative importance was < 5 or phenomena not unique to ESBWR or the system was not safety related.” Note that some of the phenomena outlined in gray are ranked high. (2) Why is Issue B11/11 (carryover/carryunder at lower limit of AS2B test data) an ESBWR-unique phenomenon? What does AS2B stand for? (3) For Issue B11/14 (Bypass leakage), should ATWS be included under “Kind/Phase of Transient”? (4) For Issue B21/3 (break flow of DPV stub tubes), why it is not listed as an ESBWR-unique thermal-hydraulic phenomenon? (5) For Issue C12/2 (Loss of control rod drive system (CRDS) flow), please explain the logic that CRDS pumps trip if GDCS pool level drops by a specified amount. What is C&FWS (not in Abbreviations and Acronyms)? (6) For Issue C41/1, it seems that bulk temperature must be maintained no less than 68 °F (instead of “less than 68 °F”) to prevent precipitation. (7) For Issue E50/3, should “Interaction between DW pressure, RPV pressure” be replaced with “Interaction between WW pressure, RPV pressure” under the “Important T/H Phenomena” column?

**R208.** [[

]]

- Q209. Page 3-18 (last line) - It is stated, "Additional information on ESBWR core stability can be found in Subsection 3.3.7 under Stability and Natural Circulation Characteristics." But Subsection 3.3.7 is for containment phenomena. As a result, should this statement be modified?
- R209. The reference should refer to Section 3.3.6. This has been corrected in Revision 1 of the report (Page 3-18).

Q210. Page 3-19, Section 3.3.1.3 - Since core uncover does not occur, what is the relevance of the section covering flow distribution in the chimney during reflood?

R210. Flow distribution in the chimney during reflood is not important. This issue is rated important for normal operation and stability. The discussion on Page 3-19 has been modified as follows:

[[

]]

This change has been made in Revision 1 of the report.

Q211. Page 3-20, Section 3.3.3.5 - The statement is made that "Analysis clearly demonstrates that it is not possible to produce a sufficient pressure difference between the RPV Isolation Condenser drain line nozzle and the DPV for this to happen." Does the analysis refer to TRACG (page 4-24, 4.4.4) or some other method?

R211. The analysis refers to the TRACG calculations on Page 4-24 and Appendix B. This statement has been added to the text in Revision 1.

Q212. Page 3-22 - The following statement is made: "A related issue is that of "soft" vs. "hard" inlet conditions." Does this refer to the natural circulation flow loop as opposed to one with pumped flow?

R212. Yes, flow configurations with pumped flow are referred to as those with hard inlet conditions.

Q213 Page 3-23, Section 3.3.7.3 - The statement is made that "The vacuum breakers have been redesigned to preclude failure to close." What was the problem with the earlier design? Does this refer to insufficient valve stroke to meet minimum flow requirements (page A-41, A.3.2.4.3)?

R213. Historically, BWRs have used swing check valves to provide wetwell to drywell vacuum breaking. Swing check valves have a pivot pin that rotates with the disk. Gravity acts to close the valve but the closure force is reduced as the valve closes. Despite the proven attributes of swing check valves, the ESBWR design team determined that a specially designed vacuum breaker valve would be desirable to meet the more stringent leak tightness and reliability criteria for passive check valves in the ESBWR.

The vacuum breaker redesign was not prompted by a valve stroke issue; rather, during flow testing of the new valve it was determined that the valve stroke needed to be lengthened to achieve the minimum flow requirements.

Q214 Page 3-23, Section 3.3.7.3 - The statement is made that “A separate isolation valve can be activated in the vacuum breaker.” How will the operator decide to do this? How will the operator know which vacuum breaker is leaking?

R214. Each vacuum breaker is instrumented with four proximity sensors located around the disk periphery. Alarms are provided to the operator for each vacuum breaker which indicate: (1) vacuum breaker leaking (2) vacuum breaker open, or (3) vacuum breaker sensor failure. The operator can then manually initiate isolation valve closure as necessary.

Q215. Page 3-25, Section 3.3.9.2 - It is stated that the capability of the PCCS to vent a large accumulation of the specified noncondensable gas has been demonstrated by analysis. To what analysis does this refer?

R215. The statement referred to a simplified analysis that was performed in the early days of the SBWR program to show that the drywell pressure would rise to clear noncondensibles with conservative assumptions on the mixing and stratification of light noncondensibles. This analysis is no longer relevant with the availability of test data with light noncondensibles in PANTHERS, GIRAFFE/Helium and PANDA. The sentence related to the analysis has been removed from Revision 1 of the report.

Q216. Page 3-25, Section 3.3.9.2 - The following statements were made, “The ... PANDA P-Series tests provide definitive ... data on the issue of whether a light gas degrades the heat transfer of the PCCS more than a heavy gas under natural circulation conditions.” The PANDA results from test P7 indicate (ALPHA-820-0, page 40) that the gas “accumulated in the PCCS and adversely affected PCCS performance ... additional investigations would be necessary to come up with final conclusions.” Please document where the final conclusion has been made.

R216. [[

]]

Q217. Page 3-25, Section 3.3.9.2 - The wording of section 3.3.9.2 is not clear and should be improved.

R217. This section has been rewritten as follows in Revision 1:

[[

]]

- Q218. Page 4-2 - The statement is made that, "...and possible sloshing between the reactor vessel downcomer and the suppression pool through the equalization line..." What could initiate or sustain such sloshing?
- R218. The initial opening of the equalization line valve could result in manometric oscillations between the vessel downcomer and the suppression pool. Any oscillations would be damped out quickly (SBWR Scaling Report, Appendix C) and this scenario will not persist.
- Q219. Page 4-3 (2nd paragraph) - (1) As stated, the passive autocatalytic recombiner (PAR) induced flow velocity in the DW is significantly less than the maximum PCCS inlet flow velocity. How does the PAR-induced flow velocity compare to the average PCCS inlet flow velocity during the long-term PCCS cooling phase (which does not include the GDCS injection phase)? (2) "Primary Containment Cooling System (PCCS)" should be replaced with Passive Containment Cooling System (PCCS).
- R219. (1) This issue is deferred to the certification phase of the ESBWR program as it is outside the current review scope for TRACG application. (2) The typo has been fixed in Revision 1 of the report.
- Q220. Page 4-4, Section 4.1.2 - It is stated that "The high pressure makeup systems consist of the Isolation Condenser, which returns condensed steam to the vessel, and the Control Rod Drive System..." While the Isolation Condenser is a heat removal system, it seems inappropriate to call it a makeup system. Please correct this statement.
- R220. The ICS is an inventory control system rather than a makeup system. It does not add inventory to the vessel from outside the containment but controls the loss of inventory. The sentence has been changed as follows in Revision 1:

Transients end either by reaching a new steady state or by a scram, followed by inventory control using the Isolation Condenser System and the CRD System for high pressure makeup. ~~The high pressure makeup systems consist of the Isolation Condenser, which returns condensed steam to the vessel, and the Control Rod Drive System, which can supply high pressure makeup from the Condensate Storage Tank.~~ System interactions including the effects of these systems have been considered in connection with LOCAs.

Q221. Pages 4-5 to 4-21 - Are there any high-ranked ESBWR phenomena that were not ranked "high" (7 or higher) in the PIRTs for SBWR?

R221. [[

]]

Q222. Page 4-12 - Please explain why Table 4.1-2a (Composite List of Highly Ranked Phenomena for LOCA/Containment) does not list vacuum breaker leakage as a high-ranked phenomenon. Note that based on PIRT parameter definition (p. S-42 of TAPD Supplement 1, "Discussion of PIRT Parameters"), vacuum breaker leakage is not part of "Vacuum breaker mass flow" or "DW/WW boundary leakage." Issue T10/11 (p. 3-14) also shows a high ranking of 9 for VB steam bypass/leakage.

R222. [[

]]

Q223. Page 4-21- Please explain why flashing in the chimney region is not listed as a high-ranked phenomenon in Table 4.1-5a (Composite List of Highly Ranked Phenomena for Stability).

R223. Flashing in the chimney due to static pressure differences is only important at low pressure, for example during startup conditions. Plant startup is covered under operational transients. Stability evaluations in Table 4.1-5a refer to operating pressures where flashing effects in the chimney are insignificant.

Q224. Page 5-2 (3rd paragraph) - There is a typographical error. "Omtario Hydro" should be replaced with "Ontario Hydro."

R224. This has been corrected in Revision 1 of the report (Page 5-2).

Q225. Page 5-13, Section 5.2 - Do the Moss Landing separator tests refer to the design to be used in ESBWR?

R225. [[

]]

Q226. Page 5-13, Section 5.2 - Were any tests performed directed at the question of avoiding backflow leakage in the GDCS drain line from the RPV to the wetwell?

R226. Backflow leakage in the GDCS drain line from the RPV to the wetwell does not have a direct path either during operation or during an accident situation. During operation, the closed squib valve provides the seal between the RPV and either the GDCS pool (via the injection line) or to the wetwell (via the equalizing line). In the event of an inadvertent squib valve actuation, the biased-open check valve will close to prevent backflow.

During an accident scenario when the squib valves have opened, the biased-open check valve prevents any significant backflow leakage from either the RPV to the GDCS pool or from the RPV to the wetwell through the equalizing lines. These check valves are not designed to be totally leak tight therefore some small leakage may result. Please refer to RAI #349 for a discussion of backflow leakage observed during the PANDA tests M9 and P2.

Q227. Page 6-2 - (1) "Table 6.1" should be replaced with "Table 6.1-1" (as shown on the next page and also on the 4th line on Page A-6). (2) On the 4th row (Geysering) and 5th row (Plant startup), "F4" (Geysering during startup) should be replaced with "F5" (see Table 2.3-3 on page 2-47).

R227. The above typos have been corrected in Revision 1 of the report.

Q228. Page A-5 (1st and 5th paragraphs) - Is "the vent tank flow control valve" or "the vent flow control valve" shown in Fig. A.3-2 (Page A-92) as PCV/2?

R228. Yes, the vent tank flow control valve is designated as PCV/2.

Q229. Page A-6, Section A.3.1.1.2, and Page A-16, Section A.3.1.2.2 - What is meant by "Concept Demonstration"? Is this the same as 'proof of principle'?

R229. Yes, the two terminologies are equivalent.

Q230. Page A-30, Section A.3.1.5.4 - It would seem that the key prerequisite to obtaining reasonable agreement between TRACG and GIRAFFE would entail reasonably accurate modeling of facility heat loss. How was this done?

R230. Heat losses in the GIRAFFE/Helium tests were established during facility shakedown tests. During the runs, the facility employed microheaters to balance heat losses to the ambient. Despite the microheaters, heat losses were significant. [[

]]

Q231. Page A-41 (1st paragraph) - Please provide the basis for the hard seat equivalent flow area.

R231. [[

]]

Q232. Page A-42 (3rd paragraph) - Please provide a sketch to show the SLCS injection locations through the core shroud.

R232. The SLCS injects poison directly through the core shroud into the core bypass region. There are four azimuthal locations and four axial locations as shown in Figures 232.1 through 232.4. The dimensions and elevations as shown in the four figures are preliminary and may change during final design.

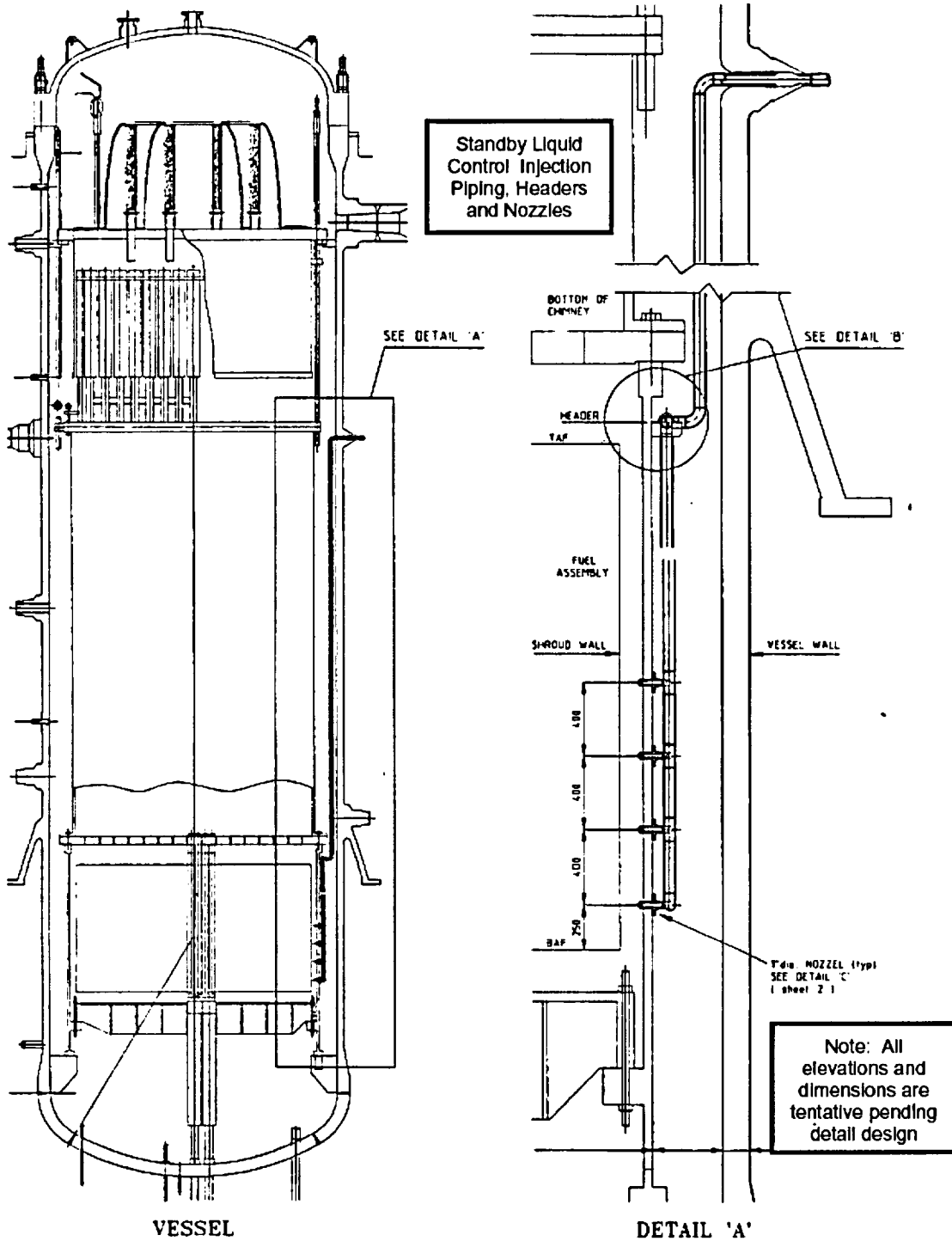
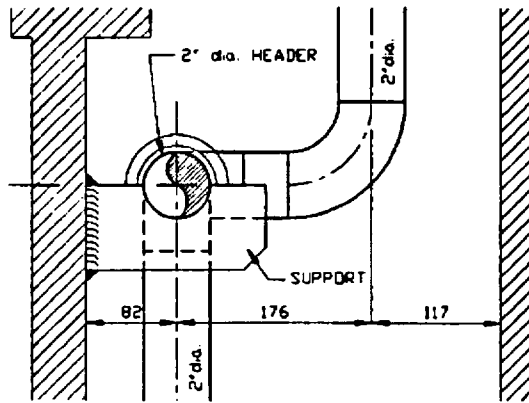


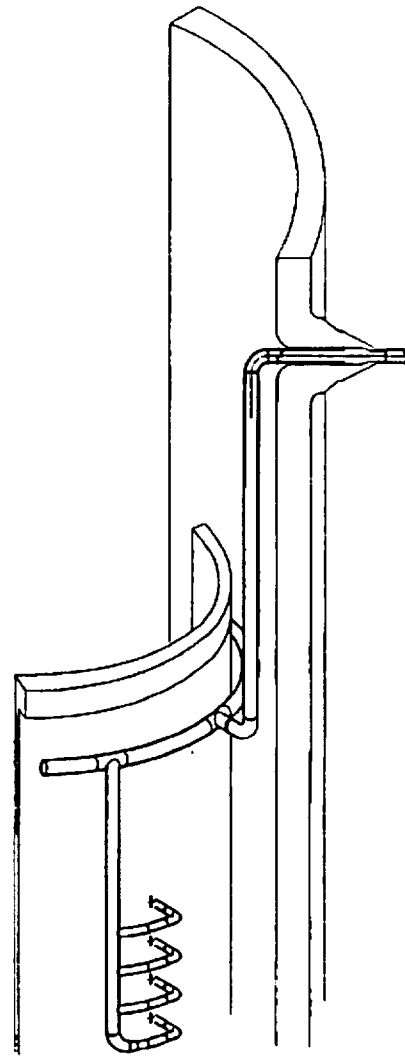
Figure 232 -1



**DETAIL 'B'**  
scale 1:5

Standby Liquid  
Control Injection  
Piping, Headers  
and Nozzles

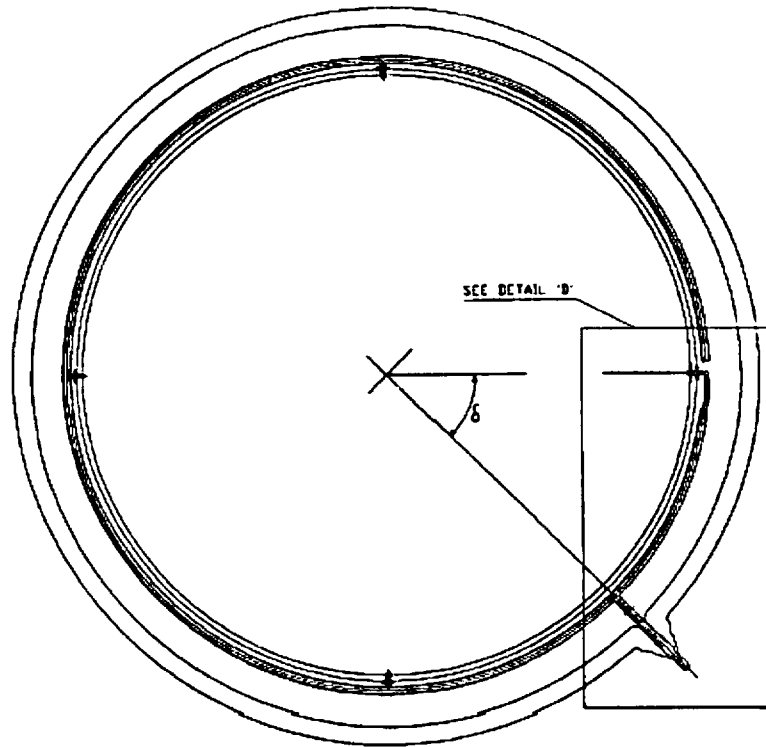
Note: All  
elevations and  
dimensions are  
tentative pending  
detail design



**ISOMETRIC VIEW**  
not to scale

Figure 232-2

Standby Liquid  
Control Injection  
Piping, Headers  
and Nozzles



CROSS SECTIONAL PLAN THRO' VESSEL  
scale 1:50

Note: All  
elevations and  
dimensions are  
tentative pending  
detail design

Figure 232-3

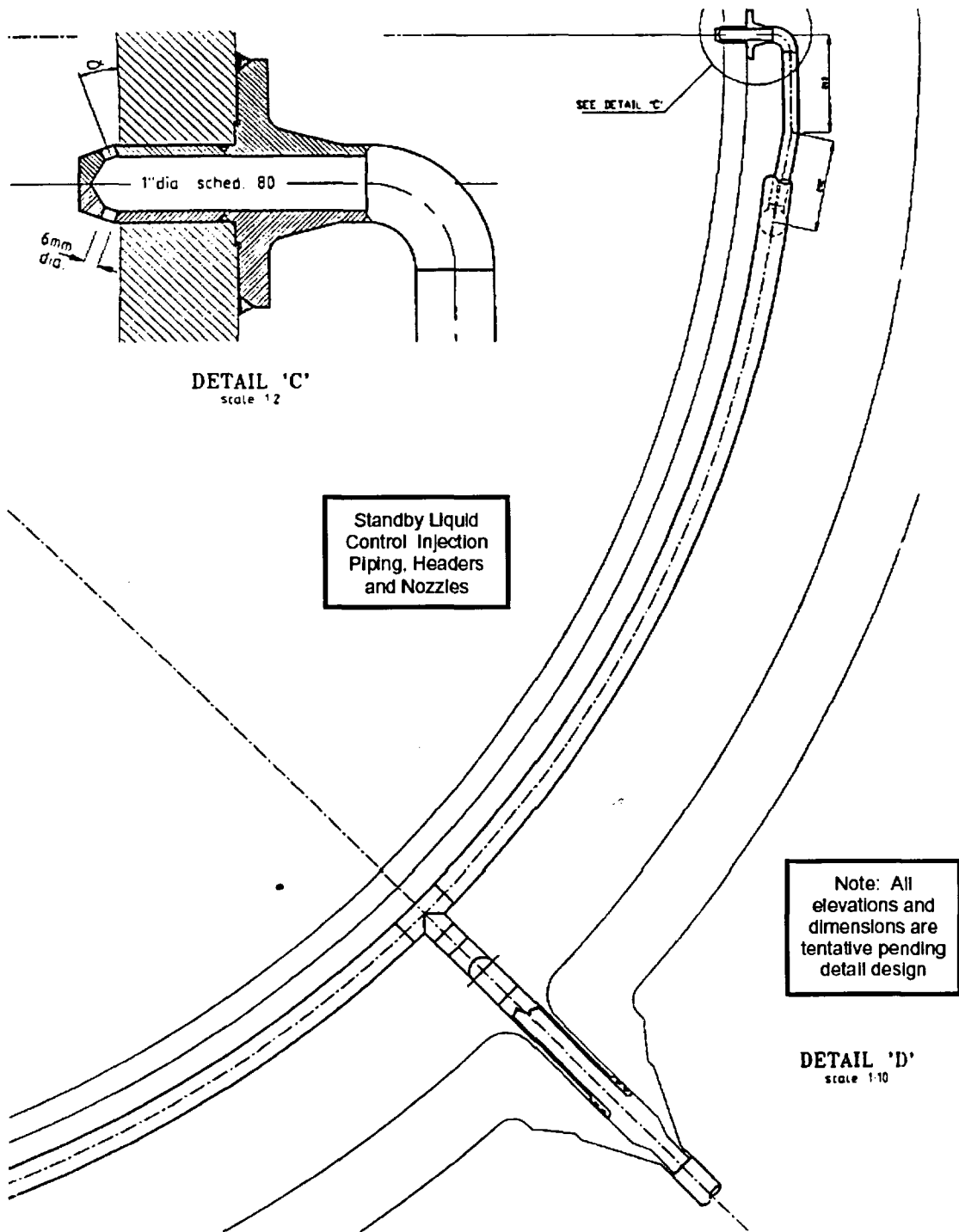


Figure 232-4

- Q233. Page A-42, Section A.4.1 - It is not evident that TRACG is capable of calculating boron mixing. Have the mixing data been shown to be applicable to ESBWR?
- R233. As explained in the report TRACG Qualification for SBWR (NEDC-32725P, Rev. 1) an application procedure has been developed to ensure that TRACG calculates the effects of boron mixing in the bypass conservatively; i.e delays the boron delivery to the core by a reasonable margin. Applicability of the tests was addressed in response to RAI 177 above.
- Q234. Page A-91, Figure A.3-1 - (1) Is the center vertical pipe (supplying steam to condenser tubes) insulated from the PCC pool water in the ESBWR design? Will there be any steam condensation inside the center vertical pipe during PCC operation? (2) Was the center vertical pipe insulated from the PCC pool water in the PANTHERS/PCC tests?
- R234. The center riser pipe is not insulated from the PCC pool water in the ESBWR design and steam condensation is expected in this pipe during PCC operation. The center riser pipe was not insulated from the PCC pool water during the PANTHERS tests.
- Q235. Pages A-94 and A-95 - Are the steam mass flow rates and air mass flow rates shown in Fig. A.3-4 ("Comparison of PANTHERS/PCC Steam-Air Range to SBWR Conditions") and Fig. A.3-5 ("TRACG PANTHERS/PCC Qualification Points") for a single PCC unit in the SBWR?
- R235. Yes, the points refer to a single PCC unit in the SBWR.
- Q236. Page A-96 - Figure A.3-6 shows an IC unit. (1) Is the center vertical pipe (supplying steam to condenser tubes) insulated from the IC pool water in the ESBWR design? Will there be any steam condensation inside the center vertical pipe during IC operation? (2) Was the center vertical pipe insulated from the IC pool water in the PANTHERS/IC tests?
- R236. The center vertical riser pipe of the IC in the ESBWR design is insulated from the IC pool water. Very little steam is expected to condense on the riser pipe during IC operation since the inner pipe wall will be close to actual steam temperature. The PANTHERS/IC test used an IC with a steam riser pipe that was insulated from the IC pool water.
- Q237. Page A-119 - Figure A.4-2 shows four SBWR conditions (at 0.1, 0.2, 0.35, and 0.5 MPa, respectively) in dimensionless subcooling numbers. Is there a similar figure to reflect the corresponding ESBWR conditions?
- R237. The precise startup path for the ESBWR has not yet been fixed. TRACG analysis has been performed to look at possible startup trajectories. [[

]]

Q238. Page B-1 - (1) Please provide the reference for TRACG interaction studies discussed in Appendix B. (2) Please provide a list of all the safety grade systems that are not engineered safety features (e.g., isolation condenser system).

R238. 1) The TRACG interaction studies were reported in the SBWR TAPD, NEDC-32391P, Rev. C.

2) The isolation condenser is the only safety grade inventory control system that is not an engineered safety feature.

Q239. Page B-2, Section B.3 - Why does filling of the isolation condenser (IC) stop at the lower header elevation and not proceed further? Does the elevation of the attachment of the IC drain line to the downcomer uncover, or is it a matter of the gravity head of water that accumulates in the downflow side of the IC system?

R239. The IC condensate drain line nozzle is slightly above the water level when vessel depressurization occurs (ADS). Therefore the nozzle and drain line will be above the annulus water level. The pressure difference between the drain line nozzle and the upstream side of the depressurization valves is not high enough to cause an overall flow reversal in the IC heat exchanger. It is sufficient to reverse the drain flow and support a head of water in the IC up to the lower header.

Q240. Page B-5 - Does the "Min Chimney Level" in Table B.3-1 represent the two-phase mixture level (instead of the collapsed level)?

R240. Yes, Table B3.1 shows the two-phase mixture level.

Q241. Page B-6 - What is the physical reason for large differences in flow rates between the IC drain line and the supply line at  $t < 1.2$  min and at  $t > 5.7$  min during GDLB?

R241. [[

]]

Q242. Page S-3, Section S.1.3.1 - There is considerable discussion of counter-current flow limit (CCFL), however, it is not clear whether CCFL conditions are indeed to be expected or not. If so, where, when, and for how long?

R242. [[

]]

Q243. Page S-3 - It is stated that "Although the core is "covered," the local critical heat flux could be exceeded." Given the conditions of heat flux and void fractions during a LOCA in an ESBWR, how is this possible? In page S-5, it is further stated that, "Film boiling is not expected for the ESBWR LOCA...."

R243. [[

]]

Q244. Page S-8, Section S.1.2.1 - The *Summary* paragraph could perhaps more usefully be placed at the very beginning of Section S.1.3.1 as an introduction. The same is true for subsequent sections.

R244. This has been done in Revision 1 of the document.

Q245. Page S-8, Section S.1.3.2 - It is not evident how TRACG can be expected to represent the flows and locations over time of noncondensable gases. This observation applies to other containment phenomena, such as pool mixing and stratification, spillage of subcooled GDSCS water from the RPV into the drywell, phase separation in the drywell, various plumes, etc. The ability to model non-condensable gases, presumably, is the reason for the statement (page 1-8, 1.2.1.3.4), "Key model parameters and input variables will be treated conservatively to produce a bounding calculation of the containment parameters of interest (pressure and temperature)."

R245. [[

]]

Q246. Page S-10, Section S.1.3.2 - It is stated that "Tests indicate that complete condensation of the steam entering the suppression pool occurs in the pool, even when the gas bubbles contain a significant amount of noncondensable [gases]." On page, S-11 it is, however, stated that "Early in the transient, large bubbles from the horizontal vents lead to level swell in the pool with potential break through the surface..." These two statements are contradictory.

R246. The statement on page S-10 does not apply to the initial air clearing transient. It is intended to apply for the subsequent phase where steam discharges into the suppression pool, accompanied by the remaining noncondensibles.

Q247. Page S-12, Section S.1.3.2 - It is stated that "The pool will be well mixed, and the temperature differences in the pool will not be significant." Why is this to be expected rather than the opposite?

R247. In the early part of the LOCA transient, the PCC pool is subcooled, with a strong natural circulation flow pattern. The heated water near the PCC tubes rises upwards and is replaced by cooler water from the sides of the pool. This stable natural circulation causes the pool to be well-mixed. After a few hours, the pool begins to boil because of the energy deposited in the pool. The vigorous boiling process maintains the pool in a well-mixed mode.

Q248. Page S-12, Section S.1.3.2 - It is also stated that "The region in the center of the tube bundle could trap voids." Explain the mechanism for trapping voids in the center of the tube bundle.

R248. [[

]]

Q249. Page S-13, Section S.1.3.2 - Drywell/Wetwell Boundary. It is stated that "Leakage from the drywell to the wetwell is an important issue for the long term transient." Besides the vacuum breakers, are there any other potential leakage paths that must be considered, such as wall penetrations at the GDCS drain lines, the PCCS and IC vent lines?

R249. [[

]]

Q250. Page S-16, Section S.1.3.3 - It is stated that "For the ESBWR, the flow transient is always gradual during startup and sudden reactivity insertion is not possible." Although the startup is gradual, it would seem that the transition in Richardson Number from stable stratified to mixed could possibly occur over a much shorter time interval.

R250. Thermal stratification in the lower plenum is mitigated by the operation of the Reactor Water Cleanup System. This system removes water from the bottom of the lower plenum and returns it through the cleanup system and heat exchangers to the downcomer. The ESBWR cleanup is unique in that it is combined with the shutdown cooling system. As such the cleanup function subsystem can increase flow during times of potential stratification. In addition, the lower plenum of the RPV has four separate drain lines connected to the two trains of the cleanup system, for greater water removal and mixing.

Q251. Question was addressed in July 9, 2003, meeting.

R251. No Response Required.

Q252. Page S1-iv of Supplement 1 - For LASL, it is suggested to add a statement in parentheses for clarification. [Los Alamos National Laboratory (LANL) is the current name for LASL].

R252. LASL has been changed to LANL in this version of the document (Page S1-iv).

Q360. Page 2-6, 1st paragraph. It is stated that "For design basis accidents, the peak long-term drywell pressure occurs when all the noncondensable gases are present in the wetwell and, consequently, the drywell is nearly pure saturated steam."

Q360.1. Is this statement based on TRACG analysis or test data? Let us compare this statement with the PANDA M3 test data: when the peak DW pressure occurred at around 10,000 seconds (ALPHA-613-0/Page 15), the partial air pressure in the DW was in a range of [[  
]] (ALPHA-613-0/Page 22).

R360.1. Perhaps this statement would better read, "For design basis accidents, the long term drywell pressure is maximized when all the non-condensable gasses are present in the wetwell, and, consequently, the drywell is nearly pure saturated steam." All BWR containment testing and analysis performed over the last 40 years has demonstrated that the drywell pressure may be calculated from the simple relationship:

$$P_{DW} = P_{WW} + P_{SUB} + P_{Vent} \quad (1)$$

Where:

$P_{DW}$  is the drywell pressure  
 $P_{WW}$  is the wetwell air space<sup>1</sup> pressure  
 $P_{SUB}$  is the submergence head of the vent, and  
 $V_{vent}$  is the flow loss through the vent system

In the long term case for the ESBWR the vent system flow losses are negligible, and the submergence head is constant. The wetwell air space pressure is the sum of the partial pressure of the non-condensables and the water vapor pressure associated with the temperature of the suppression pool, i.e.

$$P_{WW} = P_{nc} + P_{vap} \quad (2)$$

and the non-condensable partial pressure may be calculated from the classical equation of state for an ideal gas

$$P_{nc} = \frac{mRT}{V} \quad (3)$$

where:

$p_{nc}$  is the wetwell non-condensable partial pressure  
 $m$  is appropriate gas constant  
 $T$  is the absolute temperature in the wetwell air space, and  
 $V$  is the wetwell air space volume.

Since the wetwell non-condensable partial pressure will be maximized when the wetwell non-condensable mass is maximized, the drywell pressure is maximized when all the non-condensable gasses are present in the wetwell, i.e. purged from the drywell and present in the wetwell. At a given suppression pool temperature, the drywell pressure will be maximized if all the non-condensable mass is in the wetwell.

In practice, the peak drywell pressure occurs at the time of peak suppression pool temperature, while all, or nearly all, the drywell non-condensable inventory has been purged to the wetwell. In the case in point, the drywell pressure would have been a few tenths of a psi higher if complete non-condensable carryover had occurred. In practical application, the peak drywell pressure always occurs when all or nearly all the non-condensable mass is in the wetwell. Note that in the case in question, between 98 and 99% of the non-condensables are in the wetwell.

---

<sup>1</sup> The terminology "wetwell air space" indicates the gas volume above the suppression pool, and does not indicate the presence of "air" – the ESBWR containment is inerted with nitrogen.

Q360.2. Is this range of the noncondensable gas concentration deemed to be negligible (with respect to its adverse impact on the PCC heat removal) so that it would be correct to say that the DW is filled with nearly pure saturated steam?

It should be pointed out that a similar comparison to the GIRAFFE/Helium test data cannot be made for the lack of noncondensable gas concentration data, and an RAI on this issue has been included among those regarding the GIRAFFE tests.

R360.2. No level of non-condensable concentration is “deemed negligible” in the drywell performance analysis. TRACG calculates the non-condensable concentration throughout the drywell, and specifically at the location of the PCCS supply to the heat exchanger, and in the PCC heat exchanger itself. Whatever the non-condensable concentration is, it is accounted for the performance analysis.

It should also be noted that steam condensation within the PCC heat exchanger is not a function of the non-condensable content in the drywell, per-se, but of the non-condensable concentration in the PCC heat exchanger itself. When the non-condensable concentration in the PCC heat exchanger reaches the point where the decay heat can no longer be rejected, the drywell pressure will begin to rise, and this will increase the pressure within the PCC heat exchanger, lead to clearing of the PCC vent, and purge of the non-condensables from the heat exchanger. The presence of this range of non-condensables does not effect the ability of the PCCS to reject heat over a long term, only the time between purges.

There is no question in this RAI, only a statement. However, the response presented to Items (1) and (2) above are not dependant on the gas specie of the non-condensable, and would also apply to GIRAFFE.

Q409. General Electric (GE) topical report, GEFR-00850, is dated October 1989. The TRACG code has undergone changes since that time. Please confirm that the TRACG results presented in this report will be replaced by relevant analyses performed with the code version to be used for ESBWR design analysis.

R409. The GIST vs TRACG comparisons shown in GEFR-00850 have been replaced in Section 5.1 of the report TRACG Qualification for SBWR, NEDC-32725P, Rev.1. The latter calculations were performed with TRACG02. Calculations with TRACG04 are not expected to result in significant differences. This will be confirmed by rerunning sample cases with TRACG04 prior to use of the code for design.

Q410 GE topical report NEDC-33079P, “ESBWR Test and Analysis Program Description (TAPD),” list phenomenon [[

]] – as a medium ranked phenomenon that is covered by the GIST test data for validation of TRACG. The percolation phenomenon that occurred during the main steam line break test [[ ]] was apparently not predicted by the version of TRACG used at that time. Section 4.3.3.1 of the TAPD report offers this as an explanation of the differences in depressurization predictions. While entrainment would not be expected to be as important for the ESBWR design, compared to the GIST facility, due to the presence of steam separators and dryers in the ESBWR, it is nevertheless listed as a medium ranked phenomenon in the phenomenon identification and ranking table (PIRT). As such, one would expect TRACG to be assessed to predict entrainment. Does the version of TRACG to be used for ESBWR design analysis correctly predict the [[

]]? If the GIST data are used to assess TRACG for droplet entrainment, do the important dimensionless groups (e.g. Weber Number, Reynolds Number) cover the range of the ESBWR? If the GIST data are not used, what data are used for TRACG assessment for this medium ranked phenomenon?

- R410. There are several statements made by the reviewer that need to be sorted out. The primary focus of the question appears to be on droplet entrainment. The comment on the percolation phenomenon is irrelevant to the question and has been addressed in another RAI (343). There is no Section 4.3.3.1 in the TAPD. Presumably the reviewer is referring to GEFR-00850.

[[

]]

- Q411 The TAPD report lists a number of phenomena (E8 – break flow, E1 – break uncover, E3 – cold water injection below the 2-phase level, E7 – cold water injection above the 2-phase level) related to the GDCS line break flow where assessment data are provided by the GIST tests. [[

]] Please explain how this limitation of the GIST data is addressed in the TRACG assessment.

R411. [[

]]

Q412 Section A-3.1.4.1 of the TAPD report states that GIST facility is vertically scaled [[ ]]with SBWR, but this appears not to be the case for ESBWR. The electrically heated rods that model the fuel in GIST are [[ ]], whereas the ESBWR fuel rods are [[ ]]. How is this difference in vertical dimension handled in using the GIST data to assess models for ESBWR applications?

R412. [[

]]

Q413 Void distribution in the core region is correctly not included as phenomena that the GIST data cover. The presence of non-prototypical cold surfaces next to every heater rod will tend to increase liquid flow through the rod bundle to the upper plenum. Phenomenon F1, void distribution/2-phase level in the chimney and upper plenum, will be affected by the larger amount of liquid entering this region. How is this addressed when these data are used for TRACG assessment of upper plenum/chimney void distribution?

R413. [[

]]

NEDO-33083-A

## **NRC RAIs and Responses**

**ESBWR Test Report  
NEDC-33081P, Rev 0**

**Note: RAI responses including data files that cannot be read on a PC are not included.**

Q296. Page 2-1, Section 2.2 - In ESBWR Test and Analysis Program Description, (NEDC-33079P) it is stated that the main vents will not open following the blowdown phase. In the PANDA tests, however, the main vents open on a number of occasions. It would be helpful to provide a section that describes the intended typicality and conservatism in each of the tests and the particular aspects that dominate the results in terms of causing the main vents to open when they do.

R296. The main vents open for varying time periods during all of the PANDA tests except Test P6, where the IC was in operation. This behavior is shown by the main vent phase indicators in Figures 19a and b and the thermocouples near the WW end of the main vents (e.g., MTG.MV.1.4) in Figures 20a and b of the test reports. [[

]] The WW pressure increase is mainly the result of transfer of residual DW air with only a small contribution from the increase in WW steam partial pressure. [[

]]

Q297. Page 2-4, Section 2.3.5 - It is stated that "To cover this possibility in Test P6, the IC was valved out of service after seven hours of operation." Why was this time chosen? It would seem that a value closer to one hour would be more appropriate to cover this eventuality.

R297. [[

]] One of the major objectives of the test was to demonstrate the ability of the PCCs to assume the increased heat load after a long period of operation at a reduced load level.

Q334. In the PANDA M-series and P-Series test reports, it is stated that with few exceptions the tests began at about one hour after the reactor scram. For some tests the initial core power was either below (e.g., Test P3) or above (Tests P2 and M7) the equivalent decay power at one hour after the reactor scram as discussed below.

Based on the SBWR decay heat power at one hour after the scram, the equivalent PANDA core power is 1.06 megawatts (MW) (or 1.056 MW as reported on page 22 of ALPHA-606, "PANDA Facility, Test Program and Data Base General Description"). Therefore, the initial core power of a PANDA M-series test should be set at about 1.06 MW if the test is to begin equivalently at one hour after the SBWR scram.

Based on the ESBWR decay heat power at one hour after the scram, the equivalent PANDA core power is 1.07 MW. This is calculated below with a PANDA scaling factor of [[ ]] and a decay heat power at [[ ]] of the full power (based on an ORIGEN calculation for a 10-by-10 boiling water reactor (BWR) fuel bundle at [[ ]]).

[[ ]]= 1.07 MW (or = 1.19 MW if using [[ ]] as the scale for PANDA)

Therefore, the initial core power of a PANDA P-series test for ESBWR should be at 1.07 MW (as a minimum) if the test is to begin equivalently at one hour after the scram. Note that PANDA M-series tests for the SBWR and P-series tests for the ESBWR have practically the same core power (namely, 1.07 MW vs. 1.06 MW), if the scale of PANDA is proved to be [[ ]] of the ESBWR.

Please describe how the core power was calculated and provide a table to list the initial core power and its equivalent time after the reactor scram for all PANDA M-series and P-series tests. If additional power was added to offset heat loss (or some power was subtracted for other reason), a statement should be made to this effect. Please list other initial test conditions in the same table (e.g., similar to the GIRAFFE table on p. 2-106 of NEDC-32606P, "SBWR Testing Summary Report").

R334. The RPV power for the PANDA M-series and P-series tests was calculated from a design specification that is based on the ANSI/ANS-5.1 standard. According to this specification, the shutdown power at one hour from the time of scram is 1.32% of the rated power. The RPV power for the M-series tests was calculated using a rated power of 2000 MW and a [[ ]] This gives an initial (one-hour) power of 1.06 MW. A time-dependent factor was applied to account for the release of stored energy from the RPV structure. This factor [[ ]] and reduced monotonically to 1.0 as the transient proceeded. Thus, the initial RPV heater power for the base-case M-series tests was [[ ]]

The power vs. time for all the M-series tests with the exception of M7 and M9 is given in Table 5.7-8 of Reference 1. The power vs. time for Test M9, which was initiated at an earlier time in the LOCA transient, is given in Table 5.7-9. The initial heater power for Test M9 was set at 1.4 MW, which was the upper limit of the PANDA heater capacity. To compensate for the fact that 1.4 MW is somewhat less than the scaled power at the at the time in the LOCA transient simulated by Test M9, the power was decreased more slowly than the corresponding decay power during the initial portion of the transient. Test M7 was run with a constant power of 1.13 MW. Detailed listings of the thermodynamic initial conditions for the M-series tests are given in Tables 5.7-11 through 5.7-19 of Reference 1.

The P-series tests were originally scaled to a 3600 MW ESBWR with a [[ ]] This gave a one-hour PANDA power of 1.19 MW. With the same [[ ]] applied for RPV structure stored energy, the initial heater power is [[ ]] When the ESBWR power was raised to 4000 MW, the PANDA P-series tests were recharacterized as [[ ]] with the RPV heater power maintained at an initial [[ ]] The variation of heater power with time for each of the P-series tests is shown in the figures labeled Figure Pn-2 (n = test number) in Reference 2. For all tests except P2, the variation of the heater power with time (i.e., ratio of instantaneous power to initial power) was the same for the P-series tests as for the M-series tests. The power vs. time for Test P2 is shown in Table 334.1. Detailed listings of the thermodynamic initial conditions for the P-series tests are given in Tables 2-3 through 2-9 of Reference 2.

Table 334.1  
PANDA Heater Power for Test P2

Time from Scram (s)	Heater Power (MW)
1200 (Test Start)	1.4000
2250	1.4000
2500	1.3549
2940	1.2758
3600	1.2758
3650	1.2646
4000	1.2216
5000	1.1370
6000	1.0604
7000	1.0061
7200	0.9955
8000	0.9627
9000	0.9302
10000	0.9000
12000	0.8717
14400	0.8524

18000	0.8055
20000	0.7837
28800	0.7170

**References**

1. "TRACG Qualification for SBWR", NEDC-32725P, August 2002.
2. "TRACG Qualification for ESBWR, NEDC-33080P, August 2002.
3. "ESBWR Test Report", NEDC-33081P, August 2002.
4. "GIRAFFE SBWR Helium Series Test Report", NEDC-32608P, June 1996.

Q335. It appears that the initial passive containment cooling system (PCCS) vent submergence was set at [[ ]] for PANDA M-series tests, [[ ]] for PANDA P-series tests, and [[ ]] for GIRAFFE/Helium tests and System Interaction tests.

Q335.1. Please explain the basis for selecting this range of PCCS vent submergence [[ ]] in these tests.

R335.1. [[ ]]

]]

In summary, the range of vent submergences in the three test programs had very little effect on the containment pressure and temperature and is judged not to be significant.

Q335.2. Was there any difference in the PCCS vent submergence before and after a test? If so, what was the difference?

R335.2. The increase in PCC vent submergence during the tests was negligible except for PANDA Tests M7 and P3, where it increased by about 0.04 m (Figure 336.2).

Q336.

Q336.1. Please provide a comparison of the important parameters including reactor pressure vessel (RPV), drywell (DW), and wetwell (WW) pressures, suppression pool (SP) level, and PCCS heat removal between PANDA M-series tests and PANDA P-series counterpart tests such as Test M7 vs. Test P3, and Tests M6/8 vs. Test P6.

R336.1. The pressures, suppression pool levels and PCC inlet flow rates for Tests M7 and P3 are compared in Figures 336.1 to 336.3. Similar comparisons for Tests M6/8 and P6 are shown in Figures 336.4 to 336.6.

[[

]]

In summary, the differences between Tests M7 and P3 and between Tests M6/8 and P6 can be explained in terms of differences in the initial and boundary conditions. All four tests show satisfactory PCCS response under a demanding set of conditions.

- Q336.2. Provide a comparison of the important vessel and containment parameters (such as RPV water level, pressures of RPV and DW and WW, SP level, and GDCS pool level) of the three integral counterpart tests (GIRAFFE/Helium H1, PANDA M3, and either PANDA P1 or P4 (for  $t < 4$  hours, without air injection to DW)). This question replaces a previous question (RAI 180). The counterpart tests were not specified in the previous RAI.
- R336.2. Comparisons of RPV heater power, RPV, DW and WW pressures and PCCS flows for PANDA Tests P1 and M3 and GIRAFFE/Helium Test H1 are shown in Figures 336.7 to 336.9. The PCCS flows were judged to be a more useful variable to compare than the water levels because the water levels do not change appreciably during these tests (see, e.g., the plot of WW water levels for Tests M6/8 and P6 in Figure 336.5). Only

in the case of the PANDA early-start tests (M9 and P2) and the tests with the DW initially filled with air (M7 and P3), for which there are no GIRAFFE counterparts, do the pool water levels change significantly.

The first comparison (Figure 336.7) shows the heater powers for the three tests after scaling adjustments. [[

]] Taken together, the comparison of the three tests, encompassing a wide range of scales, shows similar behavior of key response variables. Differences in the details of the responses can be explained. All three tests confirm the satisfactory performance of the PCCS for limiting the long-term containment pressure following a design-basis LOCA.

[[

**Figure 336.1 Pressure Comparison for Tests M7 and P3**

**Figure 336.2 Wetwell Level Comparison for Tests M7 and P3**

**Figure 336.3 PCC Flow Comparison for Tests M7 and P3**

**Figure 336.4 Pressure Comparison for Tests M6/8 and P6**

**Figure 336.5 Wetwell Level Comparison for Tests M6/8 and P6**

**Figure 336.6 PCC and IC Flow Comparison for Tests M6/8 and P6**

**Figure 336.7 RPV Heater Power Comparison for Tests M3, H1 and P1**

**Figure 336.8 Pressure Comparison for Tests M3, H1 and P1**

**Figure 336.9 PCC Flow Comparison for Tests M3, H1 and P1**

]]

**References**

1. "TRACG Qualification for SBWR", NEDC-32725P, August 2002.
2. "TRACG Qualification for ESBWR, NEDC-33080P, August 2002.
3. "ESBWR Test Report", NEDC-33081P, August 2002.
4. "GIRAFFE SBWR Helium Series Test Report", NEDC-32608P, June 1996.

Q337 Data from the passive containment cooling (PCC) vent phase detectors in the PANDA tests do not seem to be fully consistent with the DW and WW pressure data. For example, based on the pressure difference between the DW and WW for PANDA Test M3 shown on ALPHA-613-0/Page15 (M3 Data Transmittal Report), there was continuous PCC venting into WW. In contrast, data from PCC vent phase detectors (on ALPHA-613-0/Page 20) showed continuous PCC venting only at [[ ]] seconds and sporadic PCC venting afterwards. Please provide an explanation.

R337. During the long-term transient in Test M3 and in other similar PANDA tests, there is a pressure difference between the WW and DW, [[  
]] After the start-up of the PCCS and clearing of the initial DW air, there were no vacuum breaker openings in Test M3. The PCCS adjusted its heat removal capacity to meet the changing decay heat simulated in the RPV. After the initial air-clearing transient, flow to the PCCS was nearly all steam so, [[  
]] The pressure difference between the WW and DW was just equal to, or slightly below, the head required to clear the PCC vents so the PCCs [[  
]] as indicated by the vent phase detectors.

Q338 [[

]] Are there any PANDA data regarding the two-phase flow characteristics (e.g., void fraction, pressure drop) in the RPV chimney? Note that this question is in response to the Advisory Committee on Reactor Safeguards (ACRS) interest on the two-phase flow in the ESBWR partitioned chimney, which was reflected in the questions raised in the two recent ACRS meetings.

R338. The reviewer has correctly stated that the hydraulic diameter of the PANDA chimney is similar to that of the SBWR chimney partitions. There were no measurements of chimney pressure drop, so void fraction data are not available. As covered in RAI 179, the RPV in PANDA is primarily a steam generation source. The issue of chimney void fraction distribution is covered elsewhere; e.g. the Ontario Hydro test data (see TAPD Tables 5.1-1a. and 5.3-1a).

Q339. Please provide Paul Sherrer Institute (PSI) document ALPHA-703-0, "PANDA P-Series Test Specification," Dec. 5, 1997. Is there a PSI/TEPSS document comparing pretest predictions with PANDA P-series tests? If so, please provide the document. (Note that on ALPHA-716-0/Page13 for Test P1, it is stated that the global DW/WW pressure response of test data was as expected from pretest calculations.)

R339. Since these tests were used as additional data for TRACG qualification, the key reports were the results, which were provided. The reports readily available to GE on the Panda P series tests have been provided in the ESBWR Test Report NEDC-33081, Rev 0. All the References were not available to GE but attached is the final version of the Test Specification.

The pretest predictions that were done for the program were documented in the attached Reference - "Technology Enhancement for Passive Safety Systems - TEPSS: Final Report", INNO-TEPSS(99)-D20, European Commission, Fourth Framework Programme on Nuclear Fission Safety, Contract FI4I-CT95-0008. Since these tests were used as additional data for the qualification of TRACG after the tests were run, the pre-test predictions were of limited interest.

Q340. [[

]]

R340. [[

]]

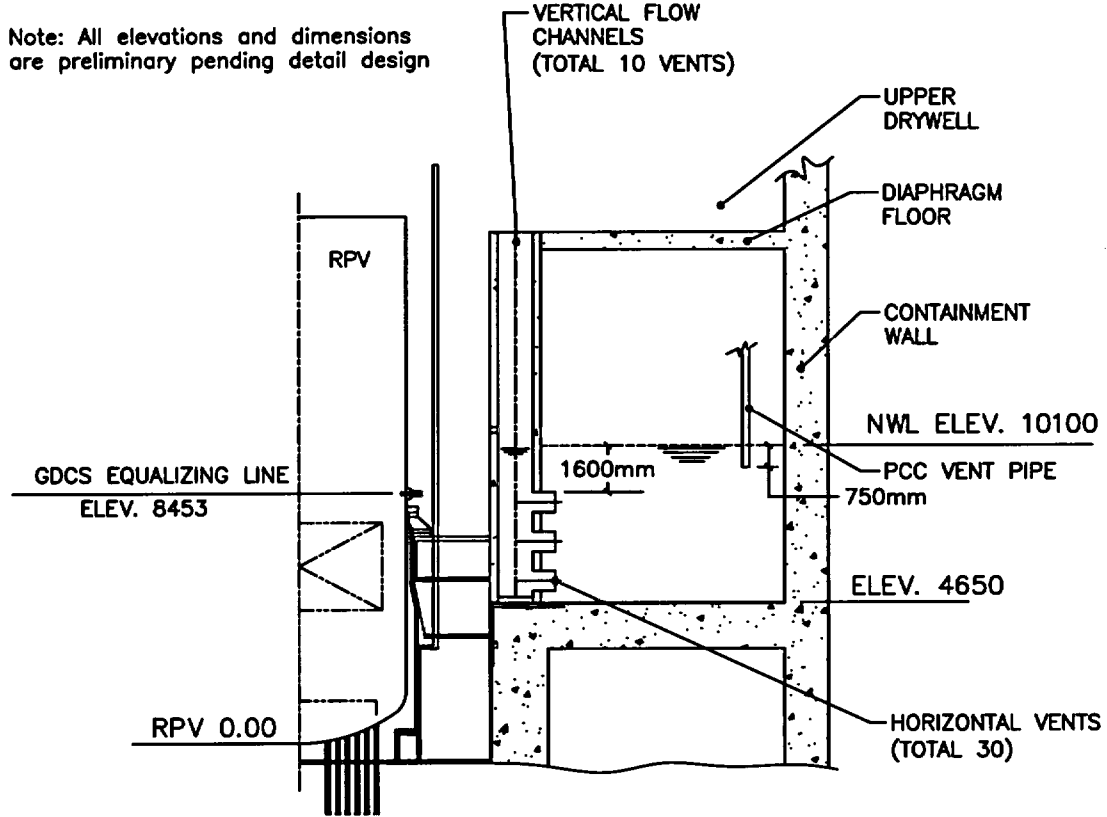


Figure 340.1 PCC Vent Submergence

Q341. What is the technical basis for setting the vacuum breaker (VB) opening pressure at 0.5 psi (i.e., the valve opens when the WW pressure exceeds the DW pressure by this amount)? We understand that the DW and WW can stand a maximum pressure differential of 3 psid. Has GE performed any TRACG sensitivity calculations or integral systems tests to determine the sensitivity of the peak containment pressure in a loss of coolant accident (LOCA) with respect to the VB opening pressure?

R341. [[

]]

Q342. [[ ]] Has GE performed any TRACG analysis to determine how much safety margin that the PCCS has? In other words, what is the minimum PCCS heat removal capacity required to prevent the peak containment pressure from exceeding its design value for the main steam line break (MSLB)?

R342. No TRACG analysis has been performed to determine the minimum PCCS heat transfer capacity to prevent the containment from exceeding the design pressure. We currently show more than adequate margin below the containment design pressure with the current PCCS design.

Q343. [[

]]

R343. [[

]]

Q344. [[

]]

R344. [[

]]

Q345. The DW water levels were measured in the PANDA tests but were not reported. Please provide this data?

R345. In both the PANDA M-series and P-series tests, DW levels were measured. These measurements were identified as instrument channels ML\_D1 and ML\_D2. Plots of these measurements for the M-series P-series tests are shown below as Figures 345.1 to 345.16. The water accumulation in the DW, even in the longest PANDA tests, [[

[[

]]

**Figure 345.1. Test P1/8 Drywell Levels**

**Figure 345.2. Test P2 Drywell Levels**

**Figure 345.3. Test P3 Drywell Levels**

**Figure 345.4. Test P4 Drywell Levels**

**Figure 345.5. Test P5 Drywell Levels**

**Figure 345.6. Test P6 Drywell Levels**

**Figure 345.7. Test P7 Drywell Levels**

**Figure 345.8 Test M2 Drywell Levels**

**Figure 345.9. Test M3 Drywell Levels**

**Figure 345.10. Test M3A Drywell Levels**

**Figure 345.11. Test M3B Drywell Levels**

**Figure 345.12. Test M6/8 Drywell Levels**

**Figure 345.13. Test M7 Drywell Levels**

**Figure 345.14. Test M9 Drywell Levels**

**Figure 345.15. Test M10A Drywell Levels**

**Figure 345.16. Test M10B Drywell Levels**

]]

Q346. Page 2-3, 3rd paragraph.

R346. This RAI is perceptive, in that the question of non-condensable content in the drywell is probably one of the largest uncertainties in overall BWR pressure suppression system performance, and has been so since the earliest test and analysis.

Prior to providing specific response to the 3 specific questions in this RAI, it will be helpful to state some general observations on BWR pressure suppression performance.

The initial response to a primary system break within the containment – independent of break size – is the same for the ESBWR design and earlier BWR designs, including the Mark I, II, III and ABWR configurations. The only significant difference between the ESBWR containment and its predecessors is the method of decay heat removal through the passive PCCS system instead of active pool cooling modes of the Residual Heat Removal systems of current plants. No EBWR-specific testing was necessary during the early blowdown period for the ESBWR, precisely for this reason.

Prior to the ESBWR, GE calculated containment performance using the NRC approved M3CPT model described in NEDO-20533 and NEDO-20533 Supplement 1. [[

]] For main steam line and recirculation line breaks, this methodology typically calculates near-complete purge of non-condensables into the wetwell in less than 10 seconds (for example Figure 3B-10 of GESSAR II – 22A7007).

The TRACG containment model used for the ESBWR is more complex than the previous M3CPT model. [[

]] For break locations in the upper drywell, non-condensables are purged in a few tens of seconds. However, in this situation, the non-condensables in the lower drywell are first compressed, and then bleed out slowly beginning in the GDCS period.

Also, from a PCCS performance standpoint, the extent of non-condensable transport during the blowdown period is largely irrelevant, since quenching of the drywell steam contents with GDCS overflow water will open the drywell to wetwell vacuum breakers, and reintroduce non-condensables previously purged to the wetwell into the drywell.

Q346.1. It seems incorrect to say that the ESBWR LOCA analysis shows that essentially all of the initial inventory of the DW inerting gas is forced into the WW “within a matter of seconds,” because the time required depends on the break size and location. Even for the MSLB, it will take more than a matter of seconds to move nitrogen gas to the WW. Please revise this statement.

R346.1. The wording will be changed to read, “during a period of time much shorter than the reactor blowdown period.”

Q346.2. Please provide the TRACG-calculated time (in seconds) to move a major portion (e.g., 90% or higher) of the nitrogen gas from DW to the WW for the MSLB, GDLB, and BDLB (base cases only, no parametric studies).

R346.2. As noted earlier in the response, TRACG calculates the inventory in each drywell node, it is difficult to provide a direct answer to this question. For example, in the MSLB case, the top upper drywell calculation provided 90% transport times of 1.0, 12.0, and 13.5 seconds for the top 3 levels. Since in the MSLB there is no flow through the lower drywell, the 90% transport time for this volume is much longer on the order of 50 hours.

In the BDLB case, the bottom 4 levels are essentially cleared of nitrogen in less than 2 seconds, while 90% transport times are on the order of 100 seconds for the top 2 levels. Since there is flow through the lower

drywell with a BDLB, a mechanism exists to purge the non-condensables, and this volume has a 90% transport time of about 2 hours.

GDLB information is not available at this time.

Q346.3. Please modify the following statement: "Thus, when the ESBWR PCCS is called upon to assume the decay heat load, it is expected that it will face a minimal challenge from residual noncondensable gas in the inlet mixture," to reflect the issue discussed in question 346.1 above.

R346.3. The wording is correct as written. The model does show that the vast majority of the non-condensable drywell inventory has been purged to the wetwell air space during the blowdown period. Note that this wording is in the description of the PANDA P3 test. The purpose of this test was to demonstrate that the PCC will function adequately, even if the expected conditions are not experienced in the plant.

Q347. Page 2-3, 4th paragraph. [[

]] Please provide the basis for the decay heat load estimate at one hour after the scram.

R347. The RPV power for Test P3 was [[ ]] To force the system into an asymmetric mode, all of the RPV steam flow to DW1 was valved off and the PCC1 unit on DW1 was valved out. This was in contrast to the similar test (M7) in the M-series, which had all three PCC units in service. To compensate for the one PCC unit out of service, the P3 RPV power level was reduced to approximately two-thirds of the scaled one-hour decay power.

Q348. Page 2-4, last paragraph.

Q348.1. What is the technical basis to selecting a leakage path between the DW and WW of  $1 \text{ cm}^2 (A/\sqrt{K})$  (where A is defined as the leakage area and K is defined as the loss coefficient) of  $1 \text{ cm}^2$  for design basis accident evaluations.

R348.1. [[

]]

Q348.2. Since this leakage path is set at 1 cm<sup>2</sup> in the TRACG LOCA analyses, does it imply that K = 1?

R348.2. [[

]]

Q349. Pages 3-1 (last paragraph) and 3-3 (Fig. 3-1). It is stated that [[

]]

Q349.1. [[

]]

R349.1. [[

]]

Q349.2. [[

]]

R349.2. [[



[[

**Figure 349.1. RPV and GDCS Levels for PANDA Tests M9 and P2**

]]

Q349.3. How many VB openings occurred in Test P2?

R349.3. There were two VB openings in Test P2. One occurred very close to the start of the test and a second occurred at about 7000s. The times of the VB openings are shown in Figure 21a of the P2 test report that was included in the Reference 3 submittal.

Q349.4. [[

]]

R349.4. [[

]]

Q349.5. Why was the peak DW pressure in Test P2 about 0.1 bar lower than in Tests P4 and P1/8?

R349.5. The lower DW pressure is associated with the lower WW pressure that results from the increase in the effective WW gas space as the GDCS pool drains to the RPV.

Q349.6. Why did the DW pressure decrease much faster at around 8000 seconds in Test P2 than in Tests P4 and P1/8?

R349.6 The flow of subcooled GDCS water to the RPV contributed to the DW pressure decrease in Test P2.

**References**

1. "TRACG Qualification for SBWR", NEDC-32725P, August 2002.
2. "TRACG Qualification for ESBWR, NEDC-33080P, August 2002.
3. "ESBWR Test Report", NEDC-33081P, August 2002.
4. "GIRAFFE SBWR Helium Series Test Report", NEDC-32608P, June 1996.

Q350. Page 3-4, Fig. 3-2.

Q350.1. Does each data point shown in Fig. 3-2 represent the WW pressure increase between the end of the test and the beginning of the test? In other words,  $\Delta P_{nc}$  (of x-axis) =  $P_{nc}$  (at the end of the test in the WW) –  $P_{nc}$  (at  $t = 0$  in the WW), and  $\Delta P$  (of y-axis) = WW pressure (at the end of the test) – WW pressure (at  $t = 0$ ).

R350.1. Yes, that is what is plotted.

Q350.2. Why did H1 and M3 fall below the 45-degree line? What is the physical implication?

R350.2. The results for Tests M3 and H1 show that the WW pressure increase was essentially equal to the increase in the noncondensable pressure.  
[[

]]

Q350.3. An improvement could be made to Fig. 3-2 by making the y-axis at the same length as the x-axis so that the 45-degree line would be truly the 45-degree line.

R350.3. The reviewer's suggestion has been incorporated in the replot of Figure 3-2, shown below as Figure 350.1.

[[

**Figure 350.1 WW Pressure Increase vs. Increase in Noncondensable Partial Pressure**

]]

Q351. ALPHA-716-0/Page 18 (Fig. 3 for Test P1/8).

Q351.1. Explain why the main steam line flow rate rose continuously between 0 and 900 seconds, as shown in Fig. 3. In other words, why didn't the peak flow rate occur at  $t = 0$  seconds?

R351.1. The increase in steam flow rate during the first few minutes of Test P1/8 is the result of the heater bringing the RPV liquid to boil-off conditions. This also includes pressurization of the DW and start-up of the PCCS. This flow increase is part of the start-up transient for the test. Similar behavior can be observed in the other PANDA tests.

Q351.2. [[

]]

R351.2. [[

]]

Q352. ALPHA-716-0/Page 19 (Fig. 4). What was the reason for a drastic drop in the PCC1 feed flow rate at around 12,600 seconds (immediately after VB opening) as shown in Fig. 4?

R352. The drop in PCC flow is the result of the PCCS ingesting air following the vacuum breaker opening. As discussed in earlier responses, the flow to the PCC is driven by the pressure difference between the DW and the PCCS. When air enters the PCC, the pressure in the PCC increases because of the degradation of the condensation heat transfer. In response, the DW pressure increases and opens the PCC vents.

Q353. ALPHA-716-0/Page 20 (Fig. 5). [[

]]

R353. [[

]]

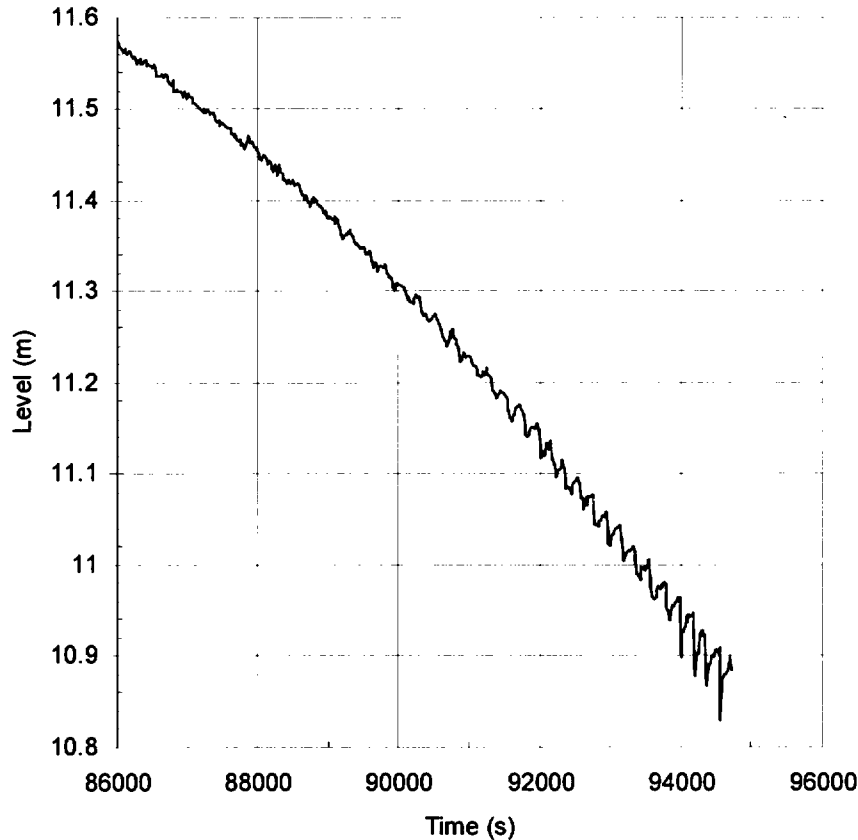


**Figure 353.1. RPV Collapsed Level in Test P1/8**

Q354. ALPHA-716-0/Page 24 (Fig. 9). As shown in Fig. 9 and stated on ALPHA-716-0/Page 14 (1st paragraph), the continuous temperature rise in the WW1 gas temperatures (MTG.S1.1 and MTG.S1.3) was due to DW steam condensation inside the main vent pipes (located inside the WW gas space) during the first 11 hours (39,600 seconds).

Q354.1. In contrast, what caused the gas temperature of MTG.S1.6 to decrease between 21,000 and 40,000 seconds?

R354.1. The measurement referred to in this question (MSTG.S1.6) was near the top of WW 1 and slightly removed from the location where the main vent entered the WW gas space. We have concluded that this instrument was outside the zone of influence of the main vent. After initial heat-up from pressurization and venting during the first 1000 seconds, the temperature in this region may have actually cooled slightly due to system heat losses. The decrease referred to in the question is much less than one degree so the effect is small.

Q354.2. What was the reason for the suppression pool surface temperature (MTS.S1.1) exceeding the gas temperatures (MTG.S1.6 and MTG.S1.3) for a large portion of the test duration?

R354.2. We believe the temperature differences referenced here were due to spatial temperature variations in the WW. The pool surface was hotter than the air space because [[

]]

The pool surface temperature was also measured by a floating probe that measured three temperatures: one about 1 cm. below the surface; one at the surface; and a third about 1 cm. above the surface. The temperature reported was the surface temperature but, with few exceptions, these three temperatures were within a degree of each other. The air space temperatures higher up and away from the surface [[

]]

Q354.3. Explain why the VB opening at around 3.5 hours (12,600 seconds) was not reflected in the WW gas temperatures.

R354.3. When the vacuum breaker opened at 3.5 hours, air flowed out of the WW. If there were any response, it would have been a slight local cooling of the gas space. With some effort, one might attribute the very slight decrease in the temperature recorded by MTG.S1.6 at the time of vacuum breaker opening to this outflow. Any effect on the bulk temperature in the large WW airspace above the pool would be small.

Q355. ALPHA-716-0/Pages 26, 28, and 30. Comparing the PCC upper tube temperatures in PCC1 (Figs. 11a), PCC2 (Fig. 12a), and PCC3 (Fig. 13a), only the PCC1 tube gas temperature experienced a large decrease immediately after VB opening (at around 3.5 hours or 12,600 seconds). Does this decrease imply that at around 3.5 hours, the opening of VB1 occurred before the opening of VB2 so that DW1 received a larger portion of the noncondensable gas vented from the WW?

R355. This is a reasonable conclusion by the reviewer although it cannot be supported by direct experimental evidence. It is likely that the amount of air entering DW1 was similar to that entering DW2 but, with only one PCC on DW1, the effect on the PCC1 temperatures was greater than for the two PCC units connected to DW2.

Q356. ALPHA-716-0/Page 32. Why was the air partial pressure at mid-height of DW2 (MPG.D2.2) greater than that near the DW2 bottom (MPG.D2.3) as shown in Fig. 14?

R356. [[

]]

Q357. ALPHA-716-0/Page 33.

Q357.1. Why there was more air in WW2 (MPG.S2) than in WW1 (MPG.S1) by about 0.08 bar (1 psi)? Was this caused by the venting of two PCC units to WW2 (vs. the venting of only one PCC unit to WW1)?

R357.1. The greater air partial pressure in WW2 throughout the test was due to the test initial conditions (Table 6.1 of the test report). The initial difference persisted throughout the test but did not have a detrimental effect on the test results or on the accomplishment of the test objectives.

Q357.2. Why was the VB opening at around 3.5 hours (12,600 seconds) not reflected in the air partial pressure in the WW?

R357.2. Since the vacuum breaker flow was out of the WW airspace, there was no change in the ratio between the air and steam partial pressures. Any change would have to be due to a global air space pressure change resulting from the vacuum breaker opening. As can be seen from the plot of Figure 1 of the test report, the WW and DW pressures, the WW airspace is so large, that the vacuum breaker opening had a negligible effect on the WW pressure and therefore we would expect no change in the WW air partial pressure.

Q358. ALPHA-716-0/Pages 36 to 38. As shown in Fig. 18, all three PCC vent lines were not cleared between 20,000 and 40,000 seconds, while Fig. 5 (ALPHA-716-0/Page 20) shows continuous steam condensation in the PCC units. Does this imply that the PCC units are capable of condensing steam even when their vent lines are not cleared and are blocked with water?

R358. Yes, the PCCS is able to operate without venting. It is only necessary that the system maintain a sufficient length of condensing surface in the tubes to match the RPV heat load. The period cited was after the vacuum breaker opening when the DW had been cleared of air and the flow to the PCCs was nearly pure steam. There was a gradual buildup of noncondensable which led to vent clearing at about 50,000 seconds.

Q359. ALPHA-716-0/Pages 41 to 42.

Q359.1. Please provide an instrumentation diagram to show where these main vent thermocouples were located.

R359.1. The main vent instrument locations are shown in Figures 359.1 and 359.2. The thermocouples used to measure gas temperatures are

identified as MTG.MV1.1 - 4 and MTG.MV2.1 - 4. Dimensions are in millimeters.

**Main Vent 1 Line**

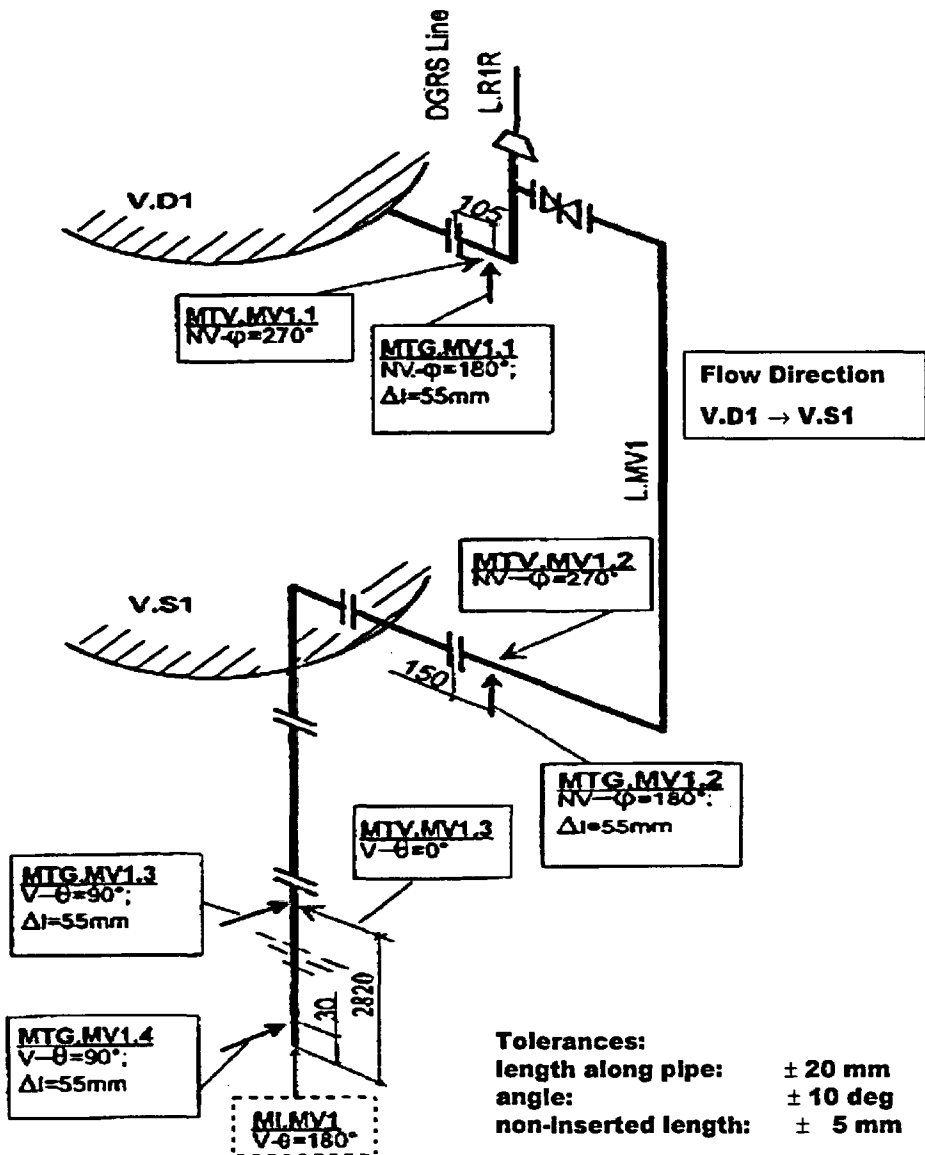


Figure 359.1. Main Vent 1 Instrument Locations

### Main Vent 2 Line

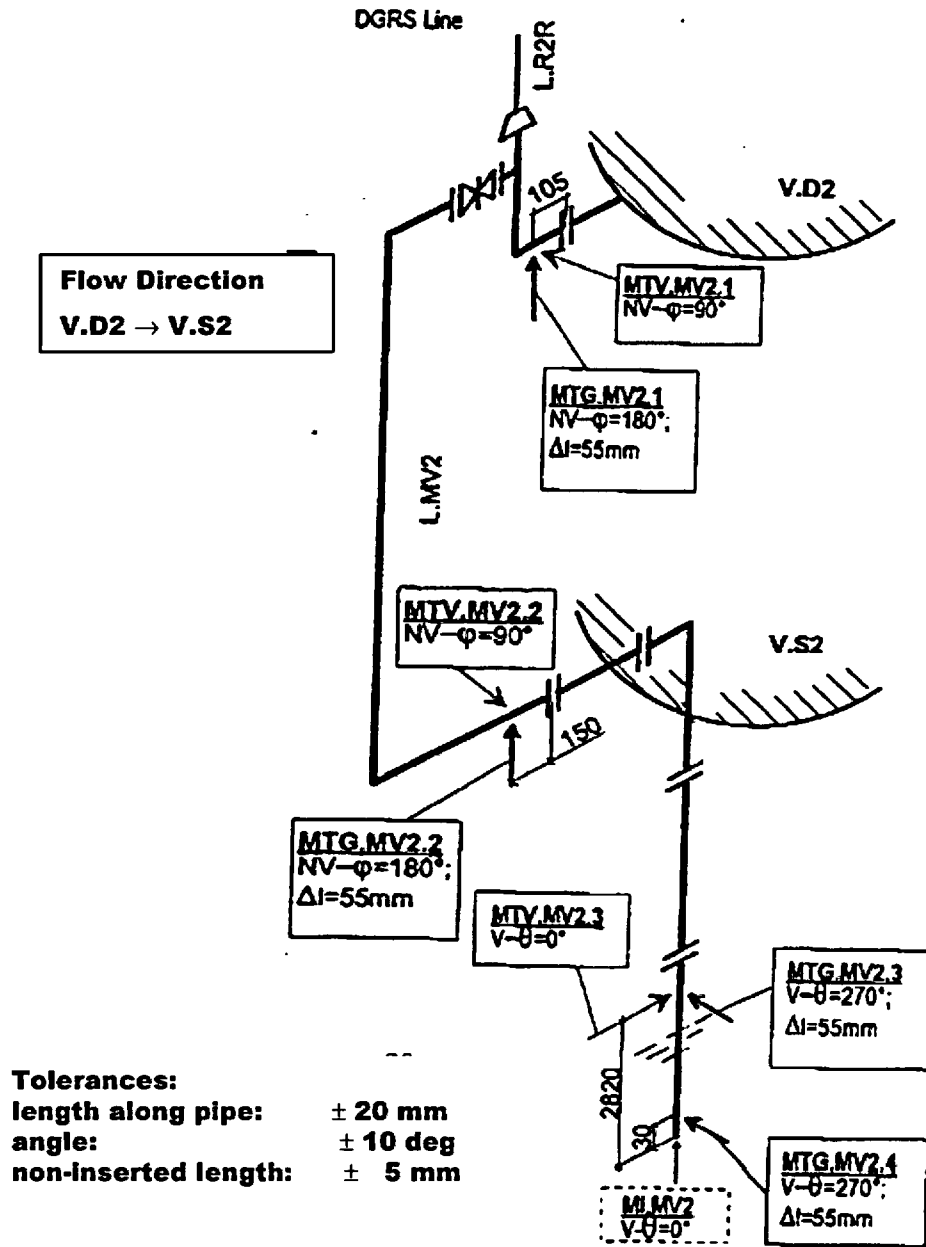


Figure 359.2. Main Vent 2 Instrument Locations

Q359.2. Explain why there was a rapid decrease in the temperatures of MTG.MV1.2 and MTG.MV1.3 at around 40,000 seconds.

R359.2. [[

]]

Q359.3. Explain why there was a temperature drop and recovery of MTG.MV1.3 at around 10,000 seconds.

R359.3. The temperature drop and recovery at 10,000 seconds is nearly coincident with the vacuum breaker opening. The main vent temperatures are responding to the DW pressure decrease prior to vacuum breaker opening and the subsequent pressure increase as flow to the PCCS decreases.

NEDO-33083-A

## NRC RAIs and Responses

### SBWR Testing Summary Report NEDC-32606P

Note: RAI responses including data files that cannot be read on a PC are not included.

Q334. In the PANDA M-series and P-Series test reports, it is stated that with few exceptions the tests began at about one hour after the reactor scram. For some tests the initial core power was either below (e.g., Test P3) or above (Tests P2 and M7) the equivalent decay power at one hour after the reactor scram as discussed below.

Based on the SBWR decay heat power at one hour after the scram, the equivalent PANDA core power is 1.06 megawatts (MW) (or 1.056 MW as reported on page 22 of ALPHA-606, "PANDA Facility, Test Program and Data Base General Description"). Therefore, the initial core power of a PANDA M-series test should be set at about 1.06 MW if the test is to begin equivalently at one hour after the SBWR scram.

Based on the ESBWR decay heat power at one hour after the scram, the equivalent PANDA core power is 1.07 MW. This is calculated below with a PANDA scaling factor of [[ ]] and a decay heat power at [[ ]] of the full power (based on an ORIGEN calculation for a 10-by-10 boiling water reactor (BWR) fuel bundle at [[ ]]).

[[ ]]= 1.07 MW (or = 1.19 MW if using [[ ]] as the scale for PANDA)

Therefore, the initial core power of a PANDA P-series test for ESBWR should be at 1.07 MW (as a minimum) if the test is to begin equivalently at one hour after the scram. Note that PANDA M-series tests for the SBWR and P-series tests for the ESBWR have practically the same core power (namely, 1.07 MW vs. 1.06 MW), if the scale of PANDA is proved to be [[ ]] of the ESBWR.

Please describe how the core power was calculated and provide a table to list the initial core power and its equivalent time after the reactor scram for all PANDA M-series and P-series tests. If additional power was added to offset heat loss (or some power was subtracted for other reason), a statement should be made to this effect. Please list other initial test conditions in the same table (e.g., similar to the GIRAFFE table on p. 2-106 of NEDC-32606P, "SBWR Testing Summary Report").

R334. The RPV power for the PANDA M-series and P-series tests was calculated from a design specification that is based on the ANSI/ANS-5.1 standard. According to this specification, the shutdown power at one hour from the time of scram is 1.32% of the rated power. The RPV power for the M-series tests was calculated using a rated power of 2000 MW and a [[ ]]. This gives an initial (one-hour) power of 1.06 MW. A time-dependent factor was applied to account for the release of stored energy from the RPV structure. This factor [[ ]] and reduced monotonically to 1.0 as the transient proceeded. Thus, the initial RPV heater power for the base-case M-series tests was [[ ]].

The power vs. time for all the M-series tests with the exception of M7 and M9 is given in Table 5.7-8 of Reference 1. The power vs. time for Test M9, which was initiated at an earlier time in the LOCA transient, is given in Table 5.7-9. The initial heater power for Test M9 was set at 1.4 MW, which was the upper limit of the PANDA heater capacity. To compensate for the fact that 1.4 MW is somewhat less than the scaled power at the at the time in the LOCA transient simulated by Test M9, the power was decreased more slowly than the corresponding decay power during the initial portion of the transient. Test M7 was run with a constant power of 1.13 MW. Detailed listings of the thermodynamic initial conditions for the M-series tests are given in Tables 5.7-11 through 5.7-19 of Reference 1.

The P-series tests were originally scaled to a 3600 MW ESBWR with a [[ ]]. This gave a one-hour PANDA power of 1.19 MW. With the same [[ ]] applied for RPV structure stored energy, the initial heater power is [[ ]]. When the ESBWR power was raised to 4000 MW, the PANDA P-series tests were recharacterized as [[ ]] with the RPV heater power maintained at an initial [[ ]]. The variation of heater power with time for each of the P-series tests is shown in the figures labeled Figure Pn-2 (n = test number) in Reference 2. For all tests except P2, the variation of the heater power with time (i.e., ratio of instantaneous power to initial power) was the same for the P-series tests as for the M-series tests. The power vs. time for Test P2 is shown in Table 334.1. Detailed listings of the thermodynamic initial conditions for the P-series tests are given in Tables 2-3 through 2-9 of Reference 2.

Table 334.1  
PANDA Heater Power for Test P2

<b>Time from Scram (s)</b>	<b>Heater Power (MW)</b>
1200 (Test Start)	1.4000
2250	1.4000
2500	1.3549
2940	1.2758
3600	1.2758
3650	1.2646
4000	1.2216
5000	1.1370
6000	1.0604
7000	1.0061
7200	0.9955
8000	0.9627
9000	0.9302
10000	0.9000
12000	0.8717
14400	0.8524

18000	0.8055
20000	0.7837
28800	0.7170

**References**

1. "TRACG Qualification for SBWR", NEDC-32725P, August 2002.
2. "TRACG Qualification for ESBWR, NEDC-33080P, August 2002.
3. "ESBWR Test Report", NEDC-33081P, August 2002.
4. "GIRAFFE SBWR Helium Series Test Report", NEDC-32608P, June 1996.

Q335. It appears that the initial passive containment cooling system (PCCS) vent submergence was set at [[ ]] for PANDA M-series tests, [[ ]] for PANDA P-series tests, and [[ ]] for GIRAFFE/Helium tests and System Interaction tests.

Q335.1. Please explain the basis for selecting this range of PCCS vent submergence [[ ]] in these tests.

R335.1. [[ ]]

]]

In summary, the range of vent submergences in the three test programs had very little effect on the containment pressure and temperature and is judged not to be significant.

Q335.2. Was there any difference in the PCCS vent submergence before and after a test? If so, what was the difference?

R335.2. The increase in PCC vent submergence during the tests was negligible except for PANDA Tests M7 and P3, where it increased by about 0.04 m (Figure 336.2).

Q337. Data from the passive containment cooling (PCC) vent phase detectors in the PANDA tests do not seem to be fully consistent with the DW and WW pressure data. For example, based on the pressure difference between the DW and WW for PANDA Test M3 shown on ALPHA-613-0/Page15 (M3 Data Transmittal Report), there was continuous PCC venting into WW. In contrast, data from PCC vent phase detectors (on ALPHA-613-0/Page 20) showed continuous PCC venting only at  $[t < \sim 8500\{3\}]$  seconds and sporadic PCC venting afterwards. Please provide an explanation.

R337. During the long-term transient in Test M3 and in other similar PANDA tests, there is a pressure difference between the WW and DW,  $[[ \quad ]]$  After the start-up of the PCCS and clearing of the initial DW air, there were no vacuum breaker openings in Test M3. The PCCS adjusted its heat removal capacity to meet the changing decay heat simulated in the RPV. After the initial air-clearing transient, flow to the PCCS was nearly all steam so,  $[[ \quad ]]$  The pressure difference between the WW and DW was just equal to, or slightly below, the head required to clear the PCC vents so the PCCs  $[[ \quad ]]$  as indicated by the vent phase detectors.

Q336.  $[[ \quad ]]$

$[[ \quad ]]$  Are there any PANDA data regarding the two-phase flow characteristics (e.g., void fraction, pressure drop) in the RPV chimney? Note that this question is in response to the Advisory Committee on Reactor Safeguards (ACRS) interest on the two-phase flow in the ESBWR partitioned chimney, which was reflected in the questions raised in the two recent ACRS meetings.

R338. The reviewer has correctly stated that the hydraulic diameter of the PANDA chimney is similar to that of the SBWR chimney partitions. There were no measurements of chimney pressure drop, so void fraction data are not available. As covered in RAI 179, the RPV in PANDA is primarily a steam generation source. The issue of chimney void fraction distribution is covered elsewhere; e.g. the Ontario Hydro test data (see TAPD Tables 5.1-1a. and 5.3-1a)

Q339. Please provide Paul Sherrer Institute (PSI) document ALPHA-703-0, "PANDA P-Series Test Specification," Dec. 5, 1997. Is there a PSI/TEPSS document comparing pretest predictions with PANDA P-series tests? If so, please provide the document. (Note that on ALPHA-716-0/Page13 for Test P1, it is stated that the global DW/WW pressure response of test data was as expected from pretest calculations.)

R339. Since these tests were used as additional data for TRACG qualification, the key reports were the results, which were provided. The reports readily available to GE on the Panda P series tests have been provided in the ESBWR Test Report NEDC-33081, Rev 0. All the References were not available to GE but attached is the final version of the Test Specification.

The pretest predictions that were done for the program were documented in the attached Reference - "Technology Enhancement for Passive Safety Systems - TEPSS: Final Report", INNO-TEPSS(99)-D20, European Commission, Fourth Framework Programme on Nuclear Fission Safety, Contract FI4I-CT95-0008. Since these tests were used as additional data for the qualification of TRACG after the tests were run, the pre-test predictions were of limited interest.

Q340. [[

]]

R340. [[

]]

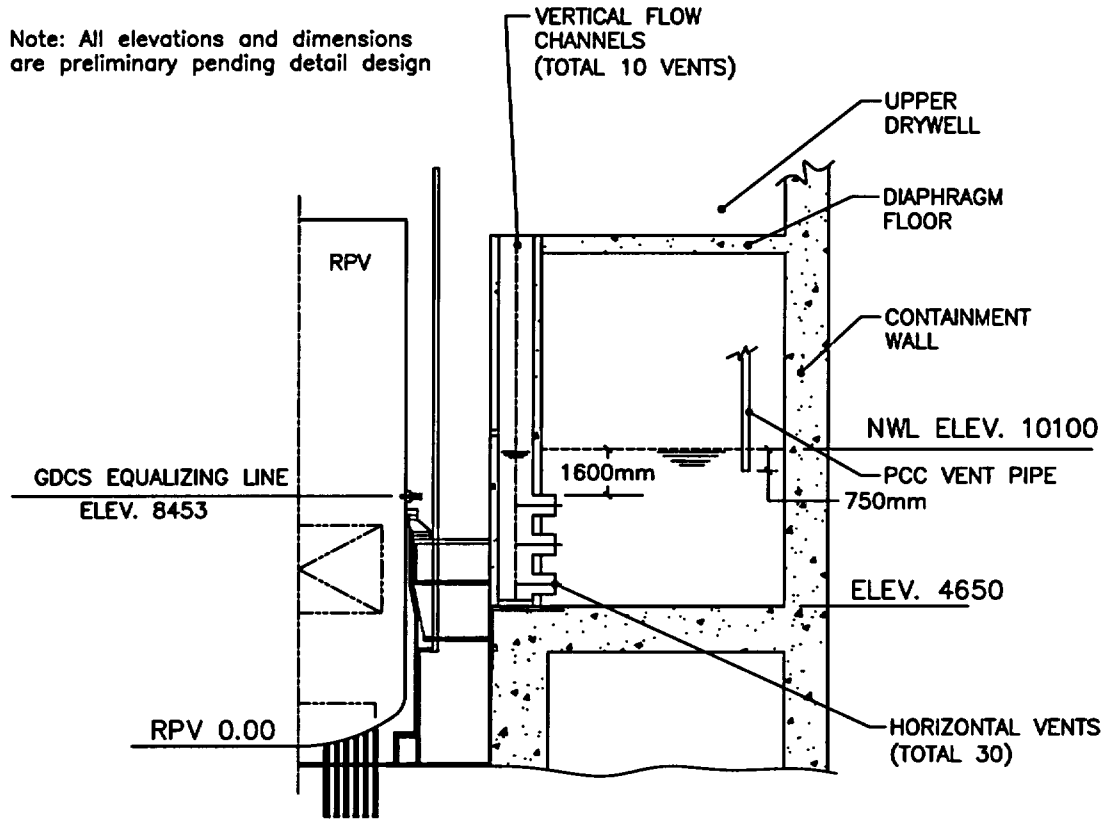


Figure 340.1 PCC Vent Submergence

Q341. What is the technical basis for setting the vacuum breaker (VB) opening pressure at 0.5 psi (i.e., the valve opens when the WW pressure exceeds the DW pressure by this amount)? We understand that the DW and WW can stand a maximum pressure differential of 3 psid. Has GE performed any TRACG sensitivity calculations or integral systems tests to determine the sensitivity of the peak containment pressure in a loss of coolant accident (LOCA) with respect to the VB opening pressure?

R341. [[

]]

Q342. [[ ]] Has GE performed any TRACG analysis to determine how much safety margin that the PCCS has? In other words, what is the minimum PCCS heat removal capacity required to prevent the peak containment pressure from exceeding its design value for the main steam line break (MSLB)?

R342. No TRACG analysis has been performed to determine the minimum PCCS heat transfer capacity to prevent the containment from exceeding the design pressure. We currently show more than adequate margin below the containment design pressure with the current PCCS design.

Q343. [[

]]

R343. [[

]]

Q344. [[

]]

R344. [[

]]

Q345. The DW water levels were measured in the PANDA tests but were not reported. Please provide this data?

R345. In both the PANDA M-series and P-series tests, DW levels were measured. These measurements were identified as instrument channels ML\_D1 and ML\_D2. Plots of these measurements for the M-series P-series tests are shown below as Figures 345.1 to 345.16. The water accumulation in the DW, even in the longest PANDA tests, [[ ]]

[[

**Figure 345.1. Test P1/8 Drywell Levels**

**Figure 345.2. Test P2 Drywell Levels**

**Figure 345.3. Test P3 Drywell Levels**

**Figure 345.4. Test P4 Drywell Levels**

**Figure 345.5. Test P5 Drywell Levels**

**Figure 345.6. Test P6 Drywell Levels**

**Figure 345.7. Test P7 Drywell Levels**

**Figure 345.8 Test M2 Drywell Levels**

**Figure 345.9. Test M3 Drywell Levels**

**Figure 345.10. Test M3A Drywell Levels**

**Figure 345.11. Test M3B Drywell Levels**

**Figure 345.12. Test M6/8 Drywell Levels**

**Figure 345.13. Test M7 Drywell Levels**

**Figure 345.14. Test M9 Drywell Levels**

**Figure 345.15. Test M10A Drywell Levels**

**Figure 345.16. Test M10B Drywell Levels**

]]

Q348. Page 2-4, last paragraph.

Q348.1. What is the technical basis to selecting a leakage path between the DW and WW of  $1 \text{ cm}^2 (A/\sqrt{K})$  (where A is defined as the leakage area and K is defined as the loss coefficient) of  $1 \text{ cm}^2$  for design basis accident evaluations.

R348.1. [[

]]

Q348.2. Since this leakage path is set at  $1 \text{ cm}^2$  in the TRACG LOCA analyses, does it imply that  $K = 1$ ?

R348.2. [[

]]

Q360. Page 2-6, 1st paragraph. It is stated that “For design basis accidents, the peak long-term drywell pressure occurs when all the noncondensable gases are present in the wetwell and, consequently, the drywell is nearly pure saturated steam.”

Q360.1. Is this statement based on TRACG analysis or test data? Let us compare this statement with the PANDA M3 test data: when the peak DW pressure occurred at around 10,000 seconds (ALPHA-613-0/Page 15), the partial air pressure in the DW was in a range of [[  
]] (ALPHA-613-0/Page 22).

R360.1. Perhaps this statement would better read, “For design basis accidents, the long term drywell pressure is maximized when all the non-condensable gasses are present in the wetwell, and, consequently, the drywell is nearly pure saturated steam.” All BWR containment testing and analysis performed over the last 40 years has demonstrated that the drywell pressure may be calculated from the simple relationship:

$$P_{DW} = P_{WW} + P_{SUB} + P_{Vent} \quad (1)$$

Where:

$P_{DW}$  is the drywell pressure  
 $P_{WW}$  is the wetwell air space<sup>1</sup> pressure  
 $P_{SUB}$  is the submergence head of the vent, and  
 $V_{vent}$  is the flow loss through the vent system

In the long term case for the ESBWR the vent system flow losses are negligible, and the submergence head is constant. The wetwell air space pressure is the sum of the partial pressure of the non-condensables and the water vapor pressure associated with the temperature of the suppression pool, i.e.

$$P_{WW} = p_{nc} + p_{vap} \quad (2)$$

and the non-condensable partial pressure may be calculated from the classical equation of state for an ideal gas

$$p_{nc} = \frac{mRT}{V} \quad (3)$$

where:

$p_{nc}$  is the wetwell non-condensable partial pressure

---

<sup>1</sup> The terminology “wetwell air space” indicates the gas volume above the suppression pool, and does not indicate the presence of “air” – the ESBWR containment is inerted with nitrogen.

$m$  is appropriate gas constant  
 $T$  is the absolute temperature in the wetwell air space, and  
 $V$  is the wetwell air space volume.

Since the wetwell non-condensable partial pressure will be maximized when the wetwell non-condensable mass is maximized, the drywell pressure is maximized when all the non-condensable gasses are present in the wetwell, i.e. purged from the drywell and present in the wetwell. At a given suppression pool temperature, the drywell pressure will be maximized if all the non-condensable mass is in the wetwell.

In practice, the peak drywell pressure occurs at the time of peak suppression pool temperature, while all, or nearly all, the drywell non-condensable inventory has been purged to the wetwell. In the case in point, the drywell pressure would have been a few tenths of a psi higher if complete non-condensable carryover had occurred. In practical application, the peak drywell pressure always occurs when all or nearly all the non-condensable mass is in the wetwell. Note that in the case in question, between 98 and 99% of the non-condensables are in the wetwell.

- Q360.2. Is this range of the noncondensable gas concentration deemed to be negligible (with respect to its adverse impact on the PCC heat removal) so that it would be correct to say that the DW is filled with nearly pure saturated steam?

It should be pointed out that a similar comparison to the GIRAFFE/Helium test data cannot be made for the lack of noncondensable gas concentration data, and an RAI on this issue has been included among those regarding the GIRAFFE tests.

- R360.2. No level of non-condensable concentration is “deemed negligible” in the drywell performance analysis. TRACG calculates the non-condensable concentration throughout the drywell, and specifically at the location of the PCCS supply to the heat exchanger, and in the PCC heat exchanger itself. Whatever the non-condensable concentration is, it is accounted for the performance analysis.

It should also be noted that steam condensation within the PCC heat exchanger is not a function of the non-condensable content in the drywell, per-se, but of the non-condensable concentration in the PCC heat exchanger itself. When the non-condensable concentration in the PCC heat exchanger reaches the point where the decay heat can no longer be rejected, the drywell pressure will begin to rise, and this will increase the pressure within the PCC heat exchanger, lead to clearing of the PCC vent, and purge of the non-condensables from the heat

exchanger. The presence of this range of non-condensables does not effect the ability of the PCCS to reject heat over a long term, only the time between purges.

There is no question in this RAI, only a statement. However, the response presented to Items (1) and (2) above are not dependant on the gas specie of the non-condensable, and would also apply to GIRAFFE.

Q361. Pages 2-9 (last paragraph) and 2-25 (Fig. 2.1-2).

Q361.1. When the PCC vent tank was closed, was the vent valve shown in Fig. 2.1-2 (on top of the vent tank on the right-hand-side) shut off? If so, the pressure in the vent tank would rise if the pure steam flow into the PCC was not completely condensed.

R361.1. For the pure steam test, the vent tank vent valve was closed. The pressure in the PCC corresponded to that required for complete condensation. Tests were conducted by establishing the initial flow conditions. Incomplete condensation would cause the system pressure to rise until complete condensation occurred. The inlet pressure was allowed to stabilize while maintaining full condensation. After 10 minutes of steady performance (no change in inlet pressure), the data were taken. [[

]]

Q361.2. For the PANTHERS/PCC steady-state pure steam tests, did the vent tank pressure ever rise?

R361.2. During the steady-state pure steam tests after the test conditions were established (see response to (1) above), the vent tank pressure did not rise.

Q361.3. What action was taken if the vent tank pressure began to rise? (There seem to be two options: either reducing the pure steam flow rate to the PCC until the vent tank pressure stops rising and eventually reaches an equilibrium pressure, or maintaining the pure steam flow rate to the PCC until the vent tank pressure rises to a higher equilibrium pressure.)

R361.3. During each of the steady-state pure steam tests, the flow rate to the test apparatus was held constant and the vent tank pressure did not change. While setting up each test, the steam flow rate was first established and then the pressure in the system was allowed to change to that required to have complete condensation.

Q362. Page 2-10, 1st paragraph. Explain how the vent tank pressure was controlled in the steam-air steady-state tests.

R362. For the air-steam mixture tests, both the vent and drain lines were open. The vent tank flow control valve controlled the vent tank pressure. However, the test condition was specified by the inlet pressure. The downstream vent tank pressure along with the condenser performance controlled the inlet pressure. After setting up the test and 10 minutes of steady-state operation (constant inlet pressure), the data were taken. There was no adjustment of the vent tank flow control valve during data collection. [[

]]

Q363. Page 2-10, 3rd paragraph.

Q363.1. Please provide a basis for the statement that main vent clearing occurs within a few seconds of the LOCA (e.g., BDLB or GDLB).

R363.1. As was discussed in the response to RAI 346, the initial response to a primary system break within the containment – independent of break size – is the same for the ESBWR design and earlier BWR designs, including the Mark I, II, III and ABWR configurations. The only significant difference between the ESBWR containment and its predecessors is the method of decay heat removal through the passive PCCS system instead of active pool cooling modes of the Residual Heat Removal systems of current plants. No EBWR-specific testing was necessary during the early blowdown period for the ESBWR, precisely for this reason.

Main vent clearing is dominated by the inertia of the water in the vent system and the pressurization rate in the drywell following a primary system breach, which is dependant on drywell volume and break size. BWR/2 through BWR/6 containments have Design Basis Accident (i.e. MSLB or recirculation line break) drywell pressurization rates on the order of 20 psi/sec, and main vent clearing times between about 0.5 and 1.0 sec. These designs also demonstrate a short-term drywell pressure peak associated with the vent clearing process that is near the long-term peak value for BWR/2 through BWR/5. The short-term drywell peak pressure is the maximum for BWR/6 plants.

The ABWR and ESBWR designs have break areas to drywell volume ratios some what less than these earlier designs. Hence, the drywell pressurization rate is lower, but the vent system inertia is also less due to the shortened horizontal vent in these designs. The ABWR SAR does not report vent clearing times, due to the dominance of the long term pressure response in that design.

The ESBWR containment performance is also dominated by the long-term response. There is a short-term drywell pressure peak, but it is much less than the long term pressure. The MSLB vent clearing times calculated for the ESBWR are 0.7, 1.0, and 1.4 seconds for the three levels of vents, respectively.

Q363.2. What is the duration of main vent clearing for the MSLB?

R363.2. The top main vents will remain "open" throughout the reactor blowdown and GDCS transition period, although the phenomenon main vent chugging will occur, resulting in an intermittent opening during the latter stages. The TRACG calculated duration of main vent flow is about 600seconds.

Q364. Page 2-13, 2nd paragraph. Please provide a drawing of a spectacle flange.

R364. A spectacle flange, sometimes called a spectacle blind or figure 8 flange, is used in piping systems to allow normal flow in one configuration and to blank off or stop flow or pressure when the spectacle (blank) is reversed. A spectacle could be used where a local leak rate test is required and a component must be isolated in order to leak test. Please see the following figures representing the spectacle or blind piece and the flange unit.



**FIGURE 364.1 SPECTACLE OR BLIND OR FIGURE 8**

The following sketch will also represent the flange plus blind configuration.

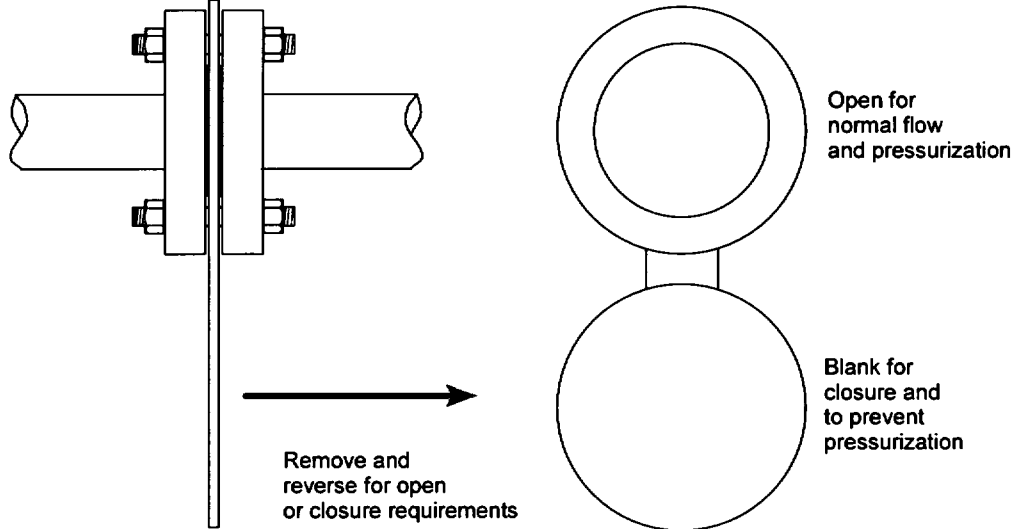


**FIGURE 364.2 SIMPLIFIED SKETCH OF SPECTACLE FLANGE**

- Q365. Page 2-14, last paragraph. Please explain the statement that “the pressure corresponds to that required to condense all of the given steam at zero air fraction.”
- R365. The pure-steam PCC tests determined the required pressure to result in complete condensation for different steam flow rates. Tests were setup by establishing the initial flow conditions and then allowing the pressure to fluctuate until a steady value was reached.

[[

]]

- Q366. Page 2-24, Fig. 2.1-1.

Q366.1. What is the large vertical pipe connected to the lower header of the PANTHERS PCC shown in the left hand sketch of Fig. 2.1-1?

R366.1. The large vertical pipe is somewhat out of proportion for this sketch. This is the guard pipe that surrounds the condensate return and vent line,

which are exiting the bottom horizontal header of the PCC heat exchanger. The guard pipe penetrates the concrete top slab of the containment and protects both the concrete and the pipes. This sketch is somewhat misleading and a better representation can be found in Figure 3.2 of "Thermal-Hydraulic Data Report of Panthers-PCC Tests, S. Botti, R. Silverii (SIET 00393RP95).

Q366.2. Why is this pipe not shown on the right hand sketch of Fig. 2.1-1?

R366.2. The guard pipe was left out in the right hand sketch. Again please refer to Figure 3.2 of "Thermal-Hydraulic Data Report of Panthers-PCC Tests, S. Botti, R. Silverii (SIET 00393RP95).

Q367. Page 2-27, Fig. 2.1-4.

Q367.1. As shown in Fig. 2.1-4, the pressure drop between the PCC top header and the bottom header is negligible. Are there any data to support this statement? Is this statement inapplicable to the steady-state and transient PANTHERS/PCC tests?

R367.1. Yes, we have data from the PANTHERS/PCC prototype heat exchanger test that supports the very low pressure drop. Delta pressure gauges DPT016 and DPT026, measured the pressure differential between the steam header and the condensate header for both heat exchanger shells.

The statement is applicable to the steady-state and transient PANTHERS/PCC tests.

Q367.2. [[

]]

R367.2. The vent line from the PCC heat exchanger was not submerged for the PANTHERS/PCC test. Also the top vent submergence is not applicable for the PANTHERS/PCC test since this is a component test only and not an integral systems test such as PANDA.

The Figure 2.1-4 referenced in the question is an expansion of Figure 2.1-3, which shows the PCC operating modes and ranges. Figure 2.1-4 shows how the PANTHERS/PCC tests covered the ranges and modes of the PCC operation. On Figure 2.1-4, vent, submergence, top vent submergence and vacuum breaker setpoint values are representative values and aren't applicable to the PANTHERS/PCC tests.

Please refer to RAI Number 335 response for discussion of vent submergence and its impact upon the containment pressure and

temperature for the integrated tests. In summary, the range of vent submergences in the three integrated test programs had very little effect on the containment pressure and temperature and is judged not to be significant.

Q367.3. The VB setpoint of 2.1 kPa (0.30 psi) seems to be too low. Should the ESBWR/SBWR VB setpoint equal 3.45 kPa (0.50 psi)?

R367.3. [[

]]

Q368. Page 2-30, Fig. 2.1-7. What is the PANTHERS/PCC heat rejection rate with inlet steam flow at 5 kg/s and zero air mass fraction?

R368. [[

]]

Q369. Page 2-46, Fig. 2.2-1. The left hand sketch of Fig. 2.2-1 shows a large vertical pipe which is bigger in diameter than the vertical pipe housing of the isolation condenser (IC) vertical inlet line as shown in the middle sketch. Please explain this discrepancy.

R369. The large vertical pipe shown in the left hand sketch is a bit out of proportion. It is in fact the vertical steam supply line and its surrounding guard pipe. The steam supply pipe branches into two horizontal supply lines at the top of the pool. The vertical steam supply line is located inside of the larger guard pipe. A better representation can be found in Figure 3.2 of "Panthers-IC Test Report, R. Silverii (SIET 00458RP95).

Q370. Page 2-54, 1st paragraph. To avoid confusion, it seems appropriate to replace the statement, "The PCC/IC pools were isolated for this and all subsequent tests, " with the following statement: "The PCC/ICs pools were not interconnected for this and all subsequent tests."

R370. The statement will be changed to read, "The PCC/ICs pools were not interconnected for this and all subsequent tests."

Q371. Page 2-54, 2nd paragraph. It appears incorrect to say that Test M2 is a repeat of Test M3, because all the break flow was directed into DW2 in Test M2.

R371. The reviewer's comment is accepted. The meaning of "repeat" in this context was that the initial conditions and RPV heater power vs. time were the same.

Q372. Page 2-54, last paragraph. Please quantify the bypass area that is ten times the scaled SBWR design value (in cm<sup>2</sup>).

R372. Test M6/8 was conducted with a [[  
]] The corresponding PANDA  $A/\sqrt{K} = 0.4 \text{ cm}^2$ .

Q373. Page 2-61, last paragraph. Please explain the statement: "A design limitation of the test facility which does not permit two-phase flow from the RPV to the DW through the steam lines." Is this a concern to PANDA tests?

R373. Not permitting two-phase or liquid flow through the steam lines is not a concern for the PANDA tests. Only steam due to decay heat boil-off leaves the RPV during the long-term cooling phase of the ESBWR LOCA. As a practical matter, this requirement was placed on the PANDA facility to avoid damaging the low-flow measurement instrumentation in the steam line.

Q374. Page 2-67, 4th paragraph. Please add a figure to show the RPV, DW, and WW pressures and the PCC inlet mass flow rates (or add two separate figures if it is preferred). [[

]]

R374. [[

]] Figures 336.1 and 336.2 (RAI336) show the RPV, DW and WW pressures and the PCC inlet flow rates for Test M7.

Q375. Page 2-68, 2nd paragraph. Please provide a comparison of air concentration (or partial air pressure) in the DW between Tests M3 and M9 to support the statement that more air remained in the DW in Test M9 than in Test M3.

R375. The reason for the pressure difference between Tests M3 and M9 is a slightly lower noncondensable inventory in Test M9. This was primarily associated with

the fact that in Test M9 the initial GDCS pool level is about 3.3 m above the GDCS level in Test M3.

Q376. Page 2-75, Fig. 2.3-5.

Q376.1. In Fig. 2.3-5, how many times did VB open in PANDA Test M3A? It appears that there were only three VB openings based on the DW pressure drops shown in Fig. 2.3-5 (excluding the small pressure drop at 13,000 seconds), but the figure legend stated four VB openings in Test M3A.

R376.1. In Test M3A there were two periods where there were one or more vacuum breaker openings. These periods followed the last two of the four PCC pool refillings. The Figure 2.3-5 legend indicates the number of actual vacuum breaker openings that occurred in each of these periods. For Test M3A, there were four openings following the third refilling and one following the last refilling. Similarly, in Test M3B there were two openings following the last refilling. The multiple openings in each period were in quick succession and confined to the brief interval in which the DW pressure was depressed.

Q376.2. As stated on p. 2-63 (2nd paragraph), M3B showed decreases in the DW pressure when the PCC pools were refilled (Fig. 2.3-8). This statement appears to be true with one exception; Fig. 2.3-5 shows no DW pressure decrease for M3B at around 11,000 seconds when the PCC pools were refilled. What is the rationale for this exception?

R376.2. All of the DW pressure decreases in Figure 2.3-5 were the result of PCC pool refilling. Water was added to the PCC pool four times in Test M3B: at around 12,000s, 27,000s, 44,000s and 62,000s. Times are approximate because each pool refilling took place over a short time period. In the DW pressure plot (Figure 2.3-5), there are three distinct pressure decreases as the result of pool water additions and the corresponding enhancement of PCCS heat removal. The magnitude of the pressure decreases becomes larger with time as the PCC heat load decreases and a smaller fraction of the condenser tube length is required to condense the steam. This is evidenced by the fact that the first refilling did not produce a noticeable drop in the DW pressure and the last refilling was followed by a DW pressure decrease that resulted in two vacuum breaker openings.

Q377. Page 2-77, Fig. 2.3-7. Was the tube wall temperature shown in Fig. 2.3-7 measured at the inside surface of the condenser tube?

R377. No, the tube wall temperature shown in Figure 2.3-7 was derived from a thermocouple, soldered at the bottom of a groove that is about in the middle of the tube wall thickness.

Q378. Page 2-79, Fig. 2.3-9. Why was the DW pressure of Test M2 (asymmetric steam flow to the DW) lower than that of Test M3 in Fig. 2.3-9?

R378. In Test M2, all the steam flow was to DW2 and steam could only enter DW1 through the DW crossover pipe. Air in the DW1 region below the crossover pipe did not mix effectively with the incoming steam and remained stratified. This resulted in less air being transferred to the WW and, consequently, slightly lower WW and DW pressures in Test M2.

Q379. Page 2-80, Fig. 2.3-10. Since the DW pressure of Test 10A (2 PCC units) was either lower or the same as that of Test M3 (3 PCC units) as shown in Fig. 2.3-10, does this imply that 2 PCC units were sufficient to remove the decay heat for these PANDA tests?

R379. The fact that the DW pressures levels out at just [[ ]] for both Tests M3 and M10A does show that two PCC units are sufficient to remove the decay heat. The fact that the long-term pressures for the two tests are essentially the same is the result of two compensating effects. As stated in the response to RAI378, the asymmetric steam flow to DW2 allows stratification of noncondensable in DW1 and thereby lowers the pressure. The valving out of PCC1 for Test M10A [[

]] an amount that approximately balanced the effect of less noncondensable transfer so that the long-term pressures from the two tests were about the same.

Q380. Page 2-101, next to the last paragraph. It is stated that “The core heater in the facility simulated the decay heat following a scram with 1:400 scale adjusted for stored energy effects.”

Q380.1. Please explain how the GIRAFFE core power was adjusted for the stored energy effects.

R380.1. The term, “adjusted for stored energy effects” is a misnomer. Additional RPV bundle power was supplied in GIRAFFE not for stored energy per se, but to partially account for heat transfer from the GIRAFFE vessels to the environment.

GIRAFFE was an outdoor facility, and it was determined early in the program that additional energy would need to be added to the facility to account for heat losses from the various facility pressure vessels to the ambient.

The GIRAFFE SBWR Helium Series Test Report, NEDC-32608P, (previously provided to the USNRC via MFN-091-96 dated June 24, 1996) describes the processes used to ameliorate these effects. Section 3.7 of that report describes the facility characterization tests that were performed. Facility heat losses were compensated for by insulation, microheater power (trace heating elements located inside the vessel insulation), and additional RPV bundle heater power.

Q380.2. Quantify this core power adjustment in a table by dividing the initial core power in the GIRAFFE tests (listed in Table 2.5-2 on p. 2-105, Table 2.5-3 on p. 2-106, and Table 2.6-2 on p.2-119) into two parts – the equivalent decay heat power for GIRAFFE (scaled from the SBWR after the scram) and the adjustment to the core power (in kW).

R380.2. Appendix B of NEDC-32608P provides the results of the facility characterization tests. The core power was increased by a constant 27kW to account for the heat losses. Table 2.2 of NEDC-32608P states that the initial heater power was 93 kW. Table B-1 of the same report describes that 27 kW of this was added for heat loss compensation. The difference is 66 kW which is the exact results of the 2000 MW rated (SBWR), divided by a scale factor of 400, and multiplied by the one-hour shutdown power fraction of 0.0132.

Q381. Pages 2-103 (1st paragraph) and 2-111 (Fig. 2.5-5). [[

]]

R381. Test H2 was run with essentially no nitrogen in the D/W<sup>1</sup> – only helium and had no VB openings. [[

]]

<sup>1</sup>There was a very small amount (0.1%) of nitrogen measured in the D/W, due to the residual nitrogen from the previous test.

Q382. Pages 2-103 (3rd paragraph) and 2-109 (Fig. 2.5-3). [[

]]

Q382.1. Does GE agree or disagree with this comment? Give us a reason for disagreement.

R382.1. GE does disagree with the comment.

[[

---

<sup>2</sup> The ESBWR design pressure is 60 psia. GE recognizes that inconsistencies exist in the ESBWR Design Description Report, NEDC-33084P, and this will be rectified in the next revision of that report

]]

Q382.2. [[

]]

R382.2. The direct gas sampling results from the GIRAFFE/He tests were successful, and reported in NEDC-32608P, "GIRAFFE SBWR Helium Series Test Report", Tables 6.1 through 6.6. This document was provided to the NRC via MFN-091-96 dated June 24, 1996. The data is again provided below for reference.

[[

**Table 6.1. Direct Gas Sampling Results for Test H1**

**Table 6.2. Direct Gas Sampling Results for Test H2**

**Table 6.3. Direct Gas Sampling Results for Test H3**

**Table 6.4. Direct Gas Sampling Results for Test H4**

**Table 6.5. Direct Gas Sampling Results for Test T1**

**Table 6.6. Direct Gas Sampling Results for Test T2**

]]

- Q383. Page 2-103 (last paragraph). There are no figures in this report to compare the important parameters of the two GIRAFFE tie-back tests (T1 and T2) and the previous GIRAFFE test for which Test T1 was a tie-back test. Please provide figures to compare the important parameters (e.g., DW/WW/RPV pressures, PCC condensate flow rate, etc.)
- R383. GIRAFFE testing was performed by Toshiba Corporation, a GE technical associate in Japan. The GIRAFFE/He and GIRAFFE/SIT programs were run in accordance with JEAG-4101 quality assurance guidelines. JEAG-4101 is the Japanese equivalent of ASME NQA-1 in the United States. Early GIRAFFE testing in support of the SBWR concept was not performed in full compliance with JEAG-4101.

GIRAFFE/He “tie-back” tests T1 and T2 were performed with a dual purpose. First, these tests form an integral part of the comprehensive data base for evaluation of the effects of lighter than steam non-condensables, but it was also hoped that by performing these two tests as repeats of tests not having met full quality assurance requirements, that the size of the acceptable GIRAFFE data base could be expanded. Unfortunately, this proved not to be possible. While key parameters were compared, and it was concluded that the tie-back tests provided repeatable results to the earlier tests, there was sufficient doubt caused by the quality assurance situation that the earlier GIRAFFE tests were not used in support of the SBWR.

None of the earlier GIRAFFE test data is cited in the TRACG qualification information for either the SBWR or the ESBWR.

### **R383. SUPPLEMENTARY INFORMATION FOR RAI383**

A figure comparing the DW and WW pressures from GIRAFFE Test T1 and the earlier GIRAFFE test that T1 “tied back” to is attached below. The earlier test, performed in 1992, was designated “Phase 2 MSLB”. The initial conditions for these two tests were nominally identical. The two sets of pressures are in good overall agreement. [[

Comparison of DW and WW Pressures from GIRAFFE Tests: Phase 2 MSLB and T1

]]

Q384. Page 2-105, last line. Was the GDCS injection completed before the test initiation for all the GIRAFFE/Helium tests?

R384. Yes. These tests were initiated at the one-hour point in the LOCA when the GDCS tank has completely drained. The statement in the report that, "The GDCS pool level should be positioned in hydrostatic equilibrium with the RPV level..." makes this clear.

Q385. Pages 2-112 (4th and 5th paragraphs) and 2-114 (3rd paragraph).

Q385.1. Is a GIRAFFE 3-tube IC unit with two tubes plugged and only one tube operational equivalent to one IC condenser in the SBWR (which has three IC condensers)?

R385.1. No. The GIRAFFE 3-tube IC condenser with two tubes plugged is equivalent to two SBWR IC condensers.

Q385.2. [[

]]

R385.2. The statement in the 5<sup>th</sup> paragraph is correct.

Q386. Pages 2-112 (last paragraph) and 2-118 (Table 2.6-1). As stated, a single GDCS pool in GIRAFFE is equivalent to all three GDCS pools in the SBWR, and only one of the three GDCS pool would have pool-to-RPV flow under a GDLB with a single failure of a GDCS injection valve (Table 2.6-1) connected to one of the two remaining intact pools. We have two questions regarding this statement.

Q386.1. Is it correct to say that for a GDLB in the SBWR concurrent with an injection line valve failure on another GDCS pool, two out of the three GDCS pools can still provide water injection to the RPV? Each of the three GDCS pools in the SBWR has two injection lines connected to the RPV; if an injection line fails to open because of a valve failure, the other line can still provide water from this pool to the RPV.

R386.1. Your statement is correct for the SBWR configuration. Two out of three pools will drain to the vessel, with the draining of one of the pools being somewhat slower due to the failed injection valve on that pool. Also to be perfectly accurate, if one GDCS line breaks on pool A (for example), and one (out-of-two) injection valves fail on pool B, some of the water from pool A will still drain to the vessel, while the majority of water from pool A will drain to the lower drywell.

Q386.2. Similarly for a GDLB in the ESBWR with an injection line valve failure, how many GDCS pools (a total of four in the ESBWR) are available to provide water injection to the RPV?

R386.2. For the ESBWR design, one division of GDCS was added so that there are now four divisions. There are still only three water pools. Two divisions share one pool. With a GDCS line break the majority of one pool will drain to the lower drywell

Q389. Page 2-129, Fig. 2.6-9.

Q389.1. What was the IC condensate flow rate for Test GS2 in comparison to the PCCS condensate flow rate shown in Fig. 2.6-9?

R389.1. The IC condensate flow rate was not measured in the GIRAFFE/SIT tests. The condensate return line in the GIRAFFE Test Facility was not instrumented to measure flow rate.

Q389.2. There is a typographical error in Fig. 2.6-9 for which the unit of pressure should be in "MPa" instead of "kPa."

R389.2. GE agrees. The change will be incorporated into the next revision of the report.

Q390. Page 10, Section 2.2, item (c): What constitutes a "large fluctuation" of tube-side heat transfer and flow rates?

R390. This particular objective was more for qualitative than quantitative judgment. It was recognized early in the test program that during startup and shutdown of the IC heat exchanger, transient conditions would be experienced, especially steam and condensate flows. This objective was geared more towards the steady state conditions to confirm steady, consistent (and predictable) operation of the unit. The test personnel were looking for any excessive variations in the indications for heat transfer and the various flow parameters.

Q391. On page 11, item (h): An elbow flow meter is mentioned on this page. Also, on page 17 the "elbow flow meter" is mentioned twice, indicating that there are two of these devices. Why are the instruments not mentioned in the instrumentation description or data reduction? What happened to this data?

R391. The elbow flow meters were installed in the steam supply and condensate return lines in order to see what dP transients were experienced during startup of the IC condenser. They were not intended to be used for actual flow measurement devices for the prototype test series. The actual SBWR/ESBWR system design uses such elbow flow meters to measure gross, excess flow should either line break during standby or operation. The elbow-tap flow meters measure the dP at the 90° elbow and will send a signal to the Leak Detection system in order to isolate the system in the event of a major pipe break. Startup transients are critical for this mode of leak detection since the transient could provide a spurious trip and isolation of the system.

The table of instrumentation shows the two elbow-tap dP transmitters as follows:

- steam = DP EFM1, instrument TMD 155
- condensate = DP EFM2, instrument TMD-160

Refer to Appendix A, "Instrument List", Table A.1.

Both were recorded and exist on the data tapes. For an example of the data, refer to Section 8.2.3, Page 43 and Figure 8.33.

Q392. Page 11, item (k): The vibrations measured in this test are representative of one half of the actual structure and function of the IC. How are the measured vibrations scaled to take this into account?

R392. The acceleration measurements were made primarily for the purpose of evaluating vibration characteristics and detection of possible condensation water hammer loads. The vibration measurements were not intended to be scaled and represent

the movement and vibration of one heat exchanger. The vibration instrumentation was used to monitor for gross or serious problems during the startup, operation or shutdown of the heat exchanger operation.

The first ESBWR reactor and plant will be tested per Regulatory Guide 1.68, "Preoperational and Initial Startup Test Programs for Water cooled Power Reactors". Just like any first of a kind reactor it will be instrumented and tested for various effects such as pipe expansions or contractions and unusual or unexpected vibrations. The tests during the initial startup phase will include thoroughly testing the overall isolation condenser system, during its startup, operation and shutdown. The final heat exchanger design, as installed in the ESBWR reactor will be treated as a part of this test program. The entire system will be fully tested and accepted as part of a strenuous pre-operational and startup test program.

Q393. Page 12, Section 3.1, item (e): It is noted that there are several departures from prototypical dimensions of the main steam supply line. Please, explain the nature, extent and impact of these non-typical dimensions.

R393. Item (e) of Section 3.1, is referring to the steam supply line and the point at which the steam exits the test facility pressure vessel. For the test the steam was extracted at the top of the steam vessel. The SBWR/ESBWR steam line for the IC's exit the side of the top section of the pressure vessel.

For the test the steam was supplied to the IC heat exchanger through a 10" Schedule 80 pipe up to the steam supply line for the IC itself. The 10" pipe then expands into a 12" Schedule 80 pipe which is the same size as the ICS design for SBWR/ESBWR. Both the test specimen and the actual IC design use a 12" Schedule 80 steam supply line feeding four individual steam lines to the top headers. The steam inlet to the IC component test specimen is the same as the actual design. The 10" line from the vessel allows a better velocity representation in order to measure the steam flow. The steam flow in the 12" inlet line for the test exchanger was ~50% of the actual steam flow in the final dual exchanger design.

Q394. Page 12, item (g): What is meant by the phrase "prototypical as is practical □" What is the condensate drain line prototypical of? Since the IC in the test a half-unit full-scale IC, is the area of the drain line one-half of the area of the actual drain line? The schematics suggest that the full IC will have a single drain line. The underlying assumption is that doubling the size of the tested IC would double the drain line flow. Please provide the basis for this assumption. In addition, the dynamic response of a half drain line, or even a full drain line with half-unit IC would be different from the prototype. How are these differences accounted for in the test and the analysis?

R394. "Prototypical as is practical" means that within reason, good engineering judgment and economics, an effort was made to simulate the actual heat exchanger design.

The drain line is prototypical of the actual heat exchangers drain line and was tested with exactly the same size piping as the double heat exchanger design. The drain lines from two heat exchangers join and are routed back to the ESBWR reactor pressure vessel. The drain line flow for the test was about 50% of the flow to be experienced in the actual design since only one module or heat exchanger unit was tested. Total drain line flow is just a matter of basic design, considering the maximum velocity and therefore pressure drop of the drain line as part of the whole IC system. Again, there was no attempt to simulate a prototypical IC system only test the heat exchanger component.

Q395 Page 13, Section 3.2: It is stated that since the facility includes a half-unit full-scale IC, scaling analysis is not necessary. Please explain how the dynamic response of the flow and the system vibration aspects were accounted for in the scaling analysis.

R395. Please refer to RAI 392 through 394 above and the general response above.

Q396 Page 16, Section 3.5.1: The last paragraph in this sections suggests that there may be a steam flow into the system that is not being measured. Is this statement correct? Please provide additional details regarding this steam flow and any impact it may have on the test results.

R396. Steam flow to the test specimen (heat exchanger) is measured. The superheated steam is supplied through two lines to the test (pressure vessel), one a 5" line and one a 3" line. Both lines of superheated steam are reduced in pressure through pressure control valves and desuperheated with water sprays. The total steam is mixed at a mixing tee and then passes to the vessel. The saturated steam leaves the vessel after first passing through a separator unit and dryer unit. The total steam flow to the IC heat exchanger is measured for test purposes at the exit of the vessel. The 3" superheated steam flow into the mixing tee is not measured but is desuperheated and mixed. The total steam flow is measured once it leaves the pressure vessel. The detailed P&ID of the test facility shows this arrangement.

Q397 Bottom of page 16: There is a typographical error, it should read "steam" instead of "staam."

R397. The word "steam" is misspelled as "staam".

Q398 On page 17, Section 3.6: It is stated that the IC returns to the vessel [[ ]] below the water level. Is this the collapsed water level or the two-phase water level? If it is the two-phase water level, how is this level detected or measured?

R398. Please refer to the description of the reactor pressure vessel in Section 3.5.2 of the report and Figure 1.2. The test vessel is designed to simulate the presence of the RPV. The ICS is designed strictly as a natural circulation driven steam condenser, relying upon the difference in densities between the steam leg versus the cooler condensate leg. The pressure vessel acts as a return vessel for the condensate and input source for the steam similar to a BWR. There is a level of saturated water that sits in the lower part of the vessel with steam being first desuperheated and then injected into the vessel and to the steam space above the normal water level. The normal water level is fixed at about 7 meters from the vessel bottom. The condensate is allowed to return to the vessel at about 4.12 meter below the normal water level (~2.88 m above bottom). Section 6.3 describes how the vessel water level is measured.

Q399 Section 3.6, bottom of page 17: [[  
 ]]

R399. The actual design of the ICS for the SBWR and ESBWR has a requirement for minimum slope of the drain line at 1/25 or 4%. Therefore the test facility requirement meets the design requirement.

Q400 The top paragraph of page 18 discusses the characteristic time of valves, specifically to simulate the prototypic valve opening of the IC return. It is not clear in this report or in the NEDC-33082P, "ESBWR Scaling Report," how the characteristic time of the IC system compares to the other dynamic (and simultaneous) aspects of the system response. It is also not clear whether the dynamic response characteristic of the IC return line was considered in the design of the test or in the analysis of the data. Please explain if and how these dynamic features of the test were analyzed in the context of scaling and data sufficiency.

R400. Again, this was not an attempt to prototypically test an IC system only the heat exchanger component. The test condensate return valves were used to simulate the opening of the actual design condensate valve. The two test valves were actually a 4" ball valve and a 2" valve in parallel. The small valve was opened first followed by the quick opening of the 4" valve. The initial time for opening the 4" valve was selected at two seconds. During the shakedown testing, two seconds was found to be too rapid, causing some water hammer in the test loop. After some shakedown testing it was discovered that by opening the 2" for about 25 seconds followed by opening the 4" valve, the water level drop in the heat exchanger could be better controlled and no water hammer was experienced. The actual opening time of the current design is about 30 seconds.

Q401 Section 3.7 on page 18: The vent lines are described in detail. Are the vent lines prototypical?

R401. The vent lines in the actual design are at the same locations as the single unit used for testing. The ESBWR design has both a top header vent and a lower header vent. In the design the vent lines are ¾" Schedule 80 pipe, the same size as those in the tested vent lines.

Q402 Section 4.9 on page 23: The scribe marks used to measure permanent strains are described. It is stated in the report that the results are not yet available. Are these results now available? Were there any permanent deformations of the system? Please provide the detailed results from the measurement of the scribe marks.

R402. These scribe marks were not measured at the conclusion of the test program. There was no known permanent deformations of the heat exchanger.

Q403 Were the data acquisition systems discussed on page 24 synchronized?

R403. Yes, the data acquisition systems were monitored and synchronized by the common supervisory computer per the detailed procedures of the test facility (SIET).

Q404 Page 35, Section 7.1: It is suggested that tests to examine the effect of inlet pressure could be conducted consecutively. If a test has already been performed, the water in the IC return line would be warmer than it was during the initial test, thus varying the head available in the IC line. How was this effect addressed in the experiments?

R404. The procedure for this test sequence required the heat exchanger pool be brought to saturation temperature (~100°C) before collecting the steady state data. This provided somewhat of a fixed pool temperature for the condensate as it exited the pool. In addition the procedure called for holding at the new inlet pressure to stabilize for at least 10 minutes and to verify steady-state conditions per their test procedure. Once steady-state was confirmed the data was recorded for 30 minutes. Primarily there is stabilization of conditions between tests.

Q405 The test matrix for the startup demonstration of the IC consisted of a single test. How is it demonstrated that this test encompasses the expected phenomena, given that the IC return line is not entirely prototypical, even assuming that the half-unit IC and the return pipe behave in a prototypical fashion? What basis, analytical or experimental, supports the sufficiency if the test data for this component? According to the conclusions in Section 9, this test was not conducted. Was the test conducted after the test report was written?

R405. [[

]]

During the initial startup test program for the ESBWR (refer to RAI 392) the startup of the IC system will be demonstrated during a full closure of the main steam isolation valves (i.e., transient conditions).

## NRC RAIs and Responses

TRACG Qualification for SBWR  
NEDC-32725P, Rev. 1

**Note: RAI responses including data files that cannot be read on a PC are not included.**

Please provide the following TRACG input decks:

**Q330.3 Ontario Hydro Void Fraction Tests TRACG deck**

Please provide both the pre-test and post-test calculation input decks for Tests 15\_1 and 23\_4.  
( Page 4.1-1 of TRACG SBWR qualification for SBWR.)  
Need 1-Tube model and eight tube models.  
Test T12, T13, T11 and T02 input decks.

R330.3 The requested input decks were provided to the NRC separately.

**Q330.5 PANTHER PCC TRACG qualification input decks**

Please provide both the pre-test and post-test calculation input decks for Tests 15\_1 and 23\_4.  
( Page 4.1-1 of TRACG SBWR qualification for SBWR.)  
Need 1-Tube model and eight tube models.  
Test T12, T13, T11 and T02 input decks

R330.5 The requested input decks were provided to the NRC separately.

**Update of ESBWR TRACG Qualification for NEDC-32725P  
Using the 9-Apr-2004 Program Library Version of  
TRACG04**

**Table of Contents**

1.0	INTRODUCTION .....	4
2.0	SEPARATE EFFECTS TESTS .....	5
2.1	Toshiba Low Pressure Void Fraction Tests .....	5
2.2	Ontario Hydro Void Fraction Tests .....	9
3.0	COMPONENT PERFORMANCE TESTS .....	13
3.1	PANTHERS PCC Performance .....	13
3.2	PANTHERS IC Performance .....	20
3.3	PANDA PCC Performance.....	24
3.4	Suppression Pool Stratification Tests .....	26
4.0	INTEGRAL SYSTEMS TESTS.....	33
4.1	GIST.....	33
4.2	GIRAFFE Helium Tests .....	38
4.3	GIRAFFE Systems Interactions Tests .....	43
4.4	One-Sixth Scale Boron Mixing Tests .....	53
4.5	PSTF Mark III Containment Response.....	62
4.6	4T/Mark II Containment Response.....	64
4.7	PANDA Transient Tests (M-Series).....	68
5.0	NATURAL CIRCULATION AND FLOW OSCILLATION TESTS .....	73
5.1	Analysis of February 1992 Startup of Dodewaard Natural Circulation BWR .	73
5.2	CRIEPI Low Pressure Oscillation Tests.....	85
5.3	PANDA Exploratory Tests .....	87
6.0	REFERENCES .....	89

## **1.0 INTRODUCTION**

The purpose of this supplement is to present an updated subset of the qualification studies presented in NEDC-32725P, "TRACG Qualification for SBWR", Rev. 1, August 2002 using the 9-April-2004 GENE Program Library version of TRACG04. This update provides assurance that the conclusions drawn from the qualification studies performed with earlier versions of TRACG remain valid. The 9-April-2004 version of TRACG is the version used to calculate the results presented in the ESBWR Application Report and, as such, the updated qualification studies are consistent with the results presented in the Application Report.

The presentations in this supplement are arranged in the same sequence as in NEDC-32725P, i.e., separate effects tests, component performance tests, integral systems tests and natural circulation and flow oscillation tests. Each of the qualification studies in NEDC-32725P is represented by an updated calculation for at least one of the tests included in the original study. To make this supplement reasonably self-contained, each section includes a brief description of the test facility and test matrix and the TRACG model of the facility. The test(s) selected for the update are identified and results are presented in the form of compound figures that show both the original and updated comparisons between the TRACG calculations and the test results. To facilitate reference to the more detailed descriptions in NEDC-32725P, the figure numbers used for the original TRACG vs. data comparisons in that report have been retained.

## 2.0 SEPARATE EFFECTS TESTS

### 2.1 Toshiba Low Pressure Void Fraction Tests

The Toshiba low-pressure void fraction tests were conducted in a 16-rod bundle at pressures of 0.50 and 1.00 MPa. An X-ray CT scanner was used to measure the void fraction at an elevation of 45 mm above the top of the heated length. Data were obtained at the two pressures for equilibrium qualities at the end of the heated section in the range of 0 to 12%. The test series analyzed for the original TRACG qualification [6-1, Section 3.1] consisted of: (1) Test Series 300 at a pressure of 1.00 MPa and a mass flux of 1390 kg/m<sup>2</sup>-s; (2) Test Series 400 at a pressure of 1.00 MPa and a mass flux of 833 kg/m<sup>2</sup>-s; and (3) Test Series 110 at a pressure of 0.50 MPa and a mass flux of 1390 kg/m<sup>2</sup>-s. Each test series consisted of five tests covering a range of bundle powers and corresponding exit qualities.

All 15 of the original comparisons between TRACG calculations and the test data were repeated with the 9-Apr-2004 version of TRACG04. The TRACG model simulates the test section with a CHAN component consisting of an unheated bottom cell, 24 equal-length cells covering the heated length and an unheated top cell. The updated comparisons between the TRACG calculations and the measured void fractions are shown together with the original comparisons in Figures 3.1-5 through 3.1-7. The figures show the calculated and measured void fractions plotted vs. the equilibrium exit quality.

[[

]]

[[

**Figure 3.1-5. TRACG Calculations of Toshiba CT Void Data  
(1.00 MPa and 1390 kg/m<sup>2</sup>-s)  
Upper – Original [6-1] Lower – TRACG04 (9-Apr-2004) ]]**

[[

**Figure 3.1-6. TRACG Calculations of Toshiba CT Void Data  
(1.00 MPa and 833 kg/m<sup>2</sup>-s)  
Upper – Original [6-1] Lower – TRACG04 (9-Apr-2004) ]]**

[[

**Figure 3.1-7. TRACG Calculations of Toshiba CT Void Data  
(0.50 MPa and 1390 kg/m<sup>2</sup>-s)  
Upper – Original [6-1] Lower – TRACG04 (9-Apr-2004) ]]**

## 2.2 Ontario Hydro Void Fraction Tests

Void data at high pressure and high temperature were obtained in a 12.4-m long, 52-cm I.D. vertical pipe using the pump test facility of Ontario Hydro Technologies (OHT) in Canada. The temperature and flow through the test section were controlled. Two-phase flow was created by draining water from the test loop into a storage tank. The two-phase mass flux in the test section was varied from 600 to 2200 kg/m<sup>2</sup>-s during the tests. A multi-detector gamma densitometer was used to measure local void fraction. The cross-sectional average of the void fraction measurements was used for comparison with the TRACG calculations.

For both the original [6-1, Section 3.2] and updated void fraction comparisons, a test at a nominal temperature of 280° C (6.4 MPa) was analyzed with TRACG. The major feature of the TRACG model is a 13-cell TEE component with Cells 4 through 13 representing the vertical test section. Cell 9 corresponds to the location where the void fraction was measured. Figures 3.2-6 through 3.2-8 show the updated and original comparisons between the TRACG calculation and the void measurements. Figures 3.2-6 and 3.2-7 show comparisons between the calculated void fraction and three of the void fraction measurements over 20-s time periods with average void fractions of approximately 0.5 and 0.75, respectively. [[

]] Figure 3.2-8 shows the original and updated TRACG vs. data comparisons over the duration of the test. In this figure, the void data were averaged over successive 36-second segments. [[

]]

[[

**Figure 3.2-6. Local Void Fluctuations (near 2000s) at Nominal Temperature of 280°  
C  
Upper – Original [6-1] Lower – TRACG04 (9-Apr-2004) ]]**

[[

**Figure 3.2-7. Local Void Fluctuations (near 2500s) at Nominal Temperature of 280°  
C  
Upper – Original [6-1] Lower – TRACG04 (9-Apr-2004) ]]**

[[

**Figure 3.2-8. Comparison of TRACG and Time-Averaged Data – Average  
Void Fraction at Nominal Temperature of 280° C  
Upper – Original [6-1] Lower – TRACG04 (9-Apr-2004) ]]**

### 3.0 COMPONENT PERFORMANCE TESTS

#### 3.1 PANTHERS PCC Performance

The PANTHERS PCC (Passive Containment Condenser) test facility consisted of a prototype PCC unit, secondary-side pool, steam supply, air supply and vent and condensate tanks. Steady-state performance testing was conducted by supplying a specified steam/air mixture to the PCC with the secondary-side pool saturated at atmospheric conditions. The measurements included PCC inlet and outlet (vent and drain) flows and the pressures in the vent and condensate tanks. (The pressure in the condensate tank was maintained in equilibrium with the condenser inlet line.) For air/steam tests, the inlet pressure was controlled and the measured vent flow was used to determine the condensation efficiency of the unit. For pure-steam tests, the inlet pressure was allowed to stabilize at whatever level was required to achieve complete condensation. Transient noncondensable accumulation tests were performed by closing the vent and allowing the noncondensable gas (air or helium) to accumulate within the PCC. Transient pure-steam tests were performed by varying the secondary-side pool water level. For both types of transient tests, the inlet pressure was the primary response variable of the system.

The original set of comparisons between PANTHERS PCC test measurements and corresponding TRACG calculations [6-1, Section 4.1] consisted of three steady-state pure-steam tests, nine steady-state steam/air tests and four transient tests. The present update repeats the TRACG calculations for all three steady-state pure-steam tests (T41\_1, T43\_2 and T49\_1), two steady-state steam/air tests (T15 and T23) and one transient test (T54 – variable pool water level). The main feature of the TRACG model is a single PIPE component with eight cells representing the 496 condenser tubes in the PANTHERS PCC unit. Additional components represent the inlet and outlet headers, the inlet, drain and vent piping and the secondary-side pool.

Figure 4.1-14 shows the original and updated comparisons between the measured and calculated inlet pressures for the three steady-state pure-steam tests. Figures 4.1-16a and b and 4.1-18a and b show the original and updated comparisons between the measured and calculated condenser efficiency (inlet flow minus vent flow divided by inlet steam flow) and pressure drop (condensate tank to vent tank) for Tests T15 and T23. The efficiency and pressure drop are plotted vs. the condenser inlet pressure. Finally, Figure 4.1-28 shows the original and updated comparisons between the measured and calculated inlet pressure plotted vs. the secondary-side pool collapsed level for Test T54. [[

]]

[[

**Figure 4.1-14. Comparison of TRACG and PANTHERS Inlet Pressure for Pure  
Steam Tests  
Upper – Original [6-1] Lower – TRACG04 (9-Apr-2004) ]]**

[[

**Figure 4.1-16a. Comparison of TRACG and PANTHERS Efficiency for Test 15  
Upper – Original [6-1] Lower – TRACG04 (9-Apr-2004) ]]**

[[

**Figure 4.1-16b. Comparison of TRACG and PANTHERS Pressure Drop for Test 15**  
**Upper – Original [6-1] Lower – TRACG04 (9-Apr-2004) ]]**

[[

**Figure 4.1-18a. Comparison of TRACG and PANTHERS Efficiency for Test 23  
Upper – Original [6-1] Lower – TRACG04 (9-Apr-2004) ]]**

[[

**Figure 4.1-18b. Comparison of TRACG and PANTHERS Pressure Drop for Test 23  
Upper – Original [6-1] Lower – TRACG04 (9-Apr-2004) ]]**

[[

**Figure 4.1-28. Comparison of TRACG and PANTHERS Inlet Pressure for Test 54  
Upper – Original [6-1] Lower – TRACG04 (9-Apr-2004) ]]**

### 3.2 PANTHERS IC Performance

The PANTHERS IC (Isolation Condenser) test facility consisted of a prototype IC module, a steam supply vessel, a vent tank and associated piping. The IC unit represented one module of the two-module prototype heat exchanger. The IC module was installed in a secondary-side water pool under atmospheric conditions. Steady-state and transient tests were performed. For the steady-state tests, the inlet steam flow was specified and the condenser pressure was allowed to stabilize at the level required to achieve complete condensation. Transient tests included noncondensable buildup and variable secondary-side pool water level with the condenser inlet pressure as the primary response variable. For the noncondensable buildup tests, the condenser pressure was allowed to stabilize at the specified inlet steam flow before noncondensable injection was initiated.

The original set of comparisons between PANTHERS IC test measurements and corresponding TRACG calculations [6-1, Section 4.2] consisted of three steady-state tests and three transient tests. The main feature of the TRACG model is a single PIPE component with eight cells representing the 120 condenser tubes in the one-module PANTHERS IC unit. Additional components represent the inlet and outlet headers, inlet, drain and vent piping, the steam supply vessel and the secondary-side pool. The present update repeats the TRACG calculations for the three steady-state tests (T02, T06 and T11) and the initial steady states that preceded the two noncondensable buildup tests (T12 and T13). The full transient simulation of Test T12 (noncondensable buildup) was also repeated.

Figure 4.2-4 shows the original and updated comparison between the measured and calculated steady-state inlet pressures for Tests T02, T06, T11, T12 and T13. Figures 4.2-7 and 4.2-8 show the original and updated comparisons between the measured and calculated inlet pressure and IC heat removal vs. time for the transient noncondensable buildup test T12. [[

]]

[[

**Figure 4.2-4. Comparison of TRACG and PANTHERS for Steady-State Tests  
Upper – Original [6-1] Lower – TRACG04 (9-Apr-2004) ]]**

[[

**Figure 4.2-6. Comparison of TRACG and PANTHERS Inlet Pressure Transient for  
Test 12  
Upper – Original [6-1] Lower – TRACG04 (9-Apr-2004) ]]**

[[

**Figure 4.2-7. Comparison of TRACG and PANTHERS Heat Transfer for Test 12**  
**Upper – Original [6-1] Lower – TRACG04 (9-Apr-2004) ]]**

### 3.3 PANDA PCC Performance

The original TRACG qualification for the SBWR included steady-state PCC performance tests conducted at the PANDA test facility in Switzerland. The PANDA test facility represents all of the features necessary for an integrated system simulation of the long-term post-LOCA transient including a detailed representation of the Passive Containment Cooling System (PCCS). Each of the three PCC units in the PANDA facility has twenty full-scale condenser tubes and an isolatable secondary-side water pool. The unit designated as PCC3 was used for the steady-state performance tests. The drywell vessels were isolated and a pipe was installed to deliver steam directly from the simulated reactor pressure vessel to the inlet of PCC3. For steam/air tests, air was injected into the inlet line at a point downstream of the steam measurement location and the pressure was controlled by adjusting the venting rate to the outside environment from the wetwell airspace at the discharge end of the PCC3 vent. For pure-steam tests, the vent line to the wetwell was closed and the pressure self-adjusted to the level required for complete condensation. The test matrix consisted of four pure-steam tests and six steam/air tests.

For the original qualification, TRACG calculations were made for all ten tests [6-1, Section 4.3]. The main feature of the TRACG model is a PIPE component representing the 20 condenser tubes. Additional components represent the upper and lower headers and the inlet, drain and vent piping. The present update repeats the TRACG calculations for all ten tests. Figure 4.3-4 shows the updated and original comparisons between the measured and calculated condenser efficiency (fraction of inlet steam flow condensed) for the six steam/air tests. Figure 4.3-5 shows the updated and original comparisons between the measured and calculated condenser pressure for the four pure-steam tests. [[

]]

[[

**Figure 4.3-5. Comparison of TRACG Calculations of Condenser Inlet Pressure with PANDA Measurements (Pure-Steam Tests) ]]**

### 3.4 Suppression Pool Stratification Tests

Two series of blowdown tests to investigate suppression pool stratification were conducted in the Mark III Pressure Suppression Test Facility (PSTF). One series was performed with full-scale vents (the 5707 series) and a second series was performed with one-third area scaled vents (the 5807 series). The test facility included a pressure vessel with electric heaters to simulate the reactor pressure vessel (RPV), a drywell (DW) vessel, an RPV-to-DW blowdown line, a wetwell (WW) vessel and the DW-to-WW vents. Test parameters included the break size and the initial WW pool temperature. Tests were conducted by pressurizing the RPV, opening the blowdown line and recording the DW and WW pressure and temperature response. The test instrumentation included a radial/axial array of thermocouples in the WW pool that provide data for assessing pool stratification.

The original TRACG qualification [6-1, Section 4.4] was performed for one test from the full-scale vent series (5707-01) and one test from the one-third area scaled vent series (5807-29). The principal elements of the TRACG model are a VSSL component that includes representations of the DW and WW volumes and a set of three TEE components to model the vent system. A FILL component is used to supply the measured break flow to the DW. An additional feature of the model is the use of the TRACG control system to regulate mixing within the WW pool on the basis of the vapor flows through the top, middle and bottom horizontal vents. A similar procedure is used in the TRACG model of the ESBWR plant to ensure that suppression pool stratification effects are bounded.

For the qualification update, the calculation was repeated for Test 5807-29. Updated comparisons between calculated and measured WW pool temperatures are shown along with the original comparisons in Figures 4.4-8 through 4.4-13. The initial WW pool temperature was 24° C. Temperature vs. time comparisons are made for six regions (volumes) in the WW pool as defined in the following table:

Volume	Radial Position	Axial Span (m)
1/2	Inner/Outer	0.00 – 0.10
3/4	Inner/Outer	0.10 – 0.74
5/6	Inner/Outer	0.74 – 2.94

The pool is divided at mid-radius to form the inner and outer volumes. The axial positions of the volume boundaries are relative to the position of the free surface. For reference, the axial positions of the three horizontal vent centerlines are 2.2m, 3.6m and 5m. Thus, Volumes 1 through 4 are above the top vent while Volumes 5 and 6 subtend the level of the top vent. [[

]]

[[

**Figure 4.4-8. Temperature Profile of Volume 1 – Test 5807-29  
Upper – Original [6-1] Lower – TRACG04 (9-Apr-2004) ]]**

[[

**Figure 4.4-9. Temperature Profile of Volume 2 – Test 5807-29  
Upper – Original [6-1] Lower – TRACG04 (9-Apr-2004) ]]**

[[

**Figure 4.4-10. Temperature Profile of Volume 3 – Test 5807-29  
Upper – Original [6-1] Lower – TRACG04 (9-Apr-2004) ]]**

[[

**Figure 4.4-11. Temperature Profile of Volume 4 – Test 5807-29  
Upper – Original [6-1] Lower – TRACG04 (9-Apr-2004) ]]**

[[

**Figure 4.4-12. Temperature Profile of Volume 5 – Test 5807-29  
Upper – Original [6-1] Lower – TRACG04 (9-Apr-2004) ]]**

[[

**Figure 4.4-13. Temperature Profile of Volume 6 – Test 5807-29  
Upper – Original [6-1] Lower – TRACG04 (9-Apr-2004) ]]**

## 4.0 INTEGRAL SYSTEMS TESTS

### 4.1 GIST

The GDCS Integrated Systems Test (GIST) facility simulated the ESBWR plant components and features that could affect the performance of the Gravity Drain Coolant System. These include the reactor pressure vessel (RPV), upper and lower drywell (UDW and LDW) and the wetwell (WW). The GIST RPV included a lower plenum, guide tube, heated channel, bypass, upper plenum, standpipe (chimney), downcomer and steam dome. The RPV was equipped with an Automatic Depressurization System (ADS) and the facility was capable of simulating a main steamline break (MSLB), a GDCS line break (GDLB) and a bottom drain line break (BDLB). Principal measurements included RPV dome pressure, GDCS flow rate and pressure taps that could be used to infer liquid inventories in the heated channel, bypass and downcomer. [[

]]

Five GIST tests representing different breaks were included in the original TRACG qualification study [6-1, Section 5.1]. The TRACG model represents the GIST RPV with a VSSL component and the tall cylindrical DW and WW tanks with PIPE components. The VSSL component includes all of the GIST RPV features described above. A CHAN component is used for the heated channel. A pair of PIPE components connecting the downcomer with the lower plenum represents the annulus region.

The GDCS line break (Test C01A) was selected for the present update. Updated comparisons of the TRACG04 calculations with the measurements for Test C01A are shown along with the original comparisons in Figures 5.1-19, 5.1-23, 5.1-27 and 5.1-31. Figure 5.1-19 compares the measured and calculated RPV steam dome pressures. [[

]]

[[

**Figure 5.1-19. Comparison of RPV Pressure (Test C01A)  
Upper – Original [6-1] Lower – TRACG04 (9-Apr-2004) ]]**

[[

**Figure 5.1-23. Comparison of GDCS Flow (Test C01A)**  
**Upper – Original [6-1] Lower – TRACG04 (9-Apr-2004) ]]**

[[

**Figure 5.1-27. Comparison of Annulus Pressure Drop  
Upper – Original [6-1] Lower – TRACG04 (9-Apr-2004) ]]**

[[

**Figure 5.1-31. Comparison of Core Pressure Drop (Test C01A)  
Upper – Original [6-1] Lower – TRACG04 (9-Apr-2004) ]]**

## 4.2 GIRAFFE Helium Tests

The GIRAFFE helium test series provides a qualification basis for the startup and operation of the ESBWR passive containment cooling system (PCCS) in the presence of noncondensibles that are both heavier (nitrogen) and lighter (helium) than steam. In addition to the PCCS, the GIRAFFE facility included representations of the reactor pressure vessel (RPV), drywell (DW), wetwell (WW), gravity drain cooling system (GDSC) and isolation condenser system (ICS). The GIRAFFE PCCS consisted of a heat exchanger, upper steam box, lower water box and three connecting heat exchanger tubes. A steam supply line from the DW to the steam box, a drain line from the water box to the GDSC pool, a vent line from the water box to the WW pool and a secondary-side pool with a steam vent to the atmosphere completed the system. Test measurements included PCCS temperatures and flows, and pressures, temperatures and gas samples in the upper and lower DW and the WW. The test series simulated the PCCS startup phase, beginning at one hour from the initiation of the LOCA, of a main steamline break with the noncondensable gas environment as the principal test parameter. The ICS was not in service for these tests.

The tests included in the original TRACG qualification [6-1, Section 5.2] study were: H1 (the “base case”) with a prototypical mixture of steam and nitrogen in the DW at test start; H2 with helium instead of nitrogen in the DW at test start; H3 with a mixture of steam, nitrogen and helium in the DW at test start; H4 with nitrogen only in the DW at test start but with helium slowly bled in over time; and T2 with an initial DW nitrogen concentration three times greater than H1 and no helium. The TRACG model uses a VSSL component to model the RPV, upper DW, WW and PCCS secondary-side pool. Three individual PIPE components are used to represent the three PCCS condenser tubes. Test H1 was selected for the current qualification update.

Updated comparisons between the TRACG calculations and the GIRAFFE measurements are shown together with the original comparisons in Figures 5.2-9 (DW and WW pressures), 5.2-12 (nitrogen partial pressure in the upper and lower portions of the condenser tubes), 5.2-13 (nitrogen partial pressure in the upper and lower DW) and 5.2-14 (nitrogen partial pressure in the WW). The “measured” PCC nitrogen partial pressures are inferred from total pressure and temperature measurements by assuming saturated steam conditions. The nitrogen partial pressures in the DW and WW are obtained from the gas sampling measurements.

[[

]]

[[

**Figure 5.2-9. H1: Drywell and Wetwell Pressure**  
**Upper – Original [6-1] Lower – TRACG04 (9-Apr-2004) ]]**

[[

**Figure 5.2-12. H1: PCC Nitrogen Partial Pressure**  
**Upper – Original [6-1] Lower – TRACG04 (9-Apr-2004) ]]**

[[

**Figure 5.2-13. H1: Drywell Nitrogen Partial Pressure**  
**Upper – Original [6-1] Lower – TRACG04 (9-Apr-2004) ]]**

[[

**Figure 5.2-14. H1: Wetwell Nitrogen Partial Pressure**  
Upper – Original [6-1] Lower – TRACG04 (9-Apr-2004) ]]

### 4.3 GIRAFFE Systems Interactions Tests

The GIRAFFE systems interaction test series provides a qualification basis for the performance of the ESBWR emergency core cooling system (ECCS) during the transition from the late blowdown phase of a LOCA to the startup of the gravity drain cooling system (GDCS) and the subsequent reflood of the reactor vessel. The major features of the GIRAFFE test facility were described in Section 4.2. The principal differences in the facility as configured for the systems interaction tests were the inclusion of the isolation condenser system (ICS) and the initiation of the tests from a reactor pressure of 1.03 MPa. The GIRAFFE ICS was similar to the PCCS but for these tests flow was only permitted through one of the three ICS tubes. Key measurements included RPV, DW and WW pressures, break and GDCS flows, and chimney, bypass and downcomer water levels.

The systems interaction test series included: Test GS1 (the base case) simulating a GDCS line break with a single DPV failure and no PCCS or ICS operation; Test GS2 simulating a GDCS line break with a single DPV failure and parallel PCCS and ICS operation; Test GS3 simulating a bottom drain line break with a single DPV failure and PCCS and ICS operation; and Test GS4 simulating a GDCS line break with a GDCS valve failure in one of the remaining GDCS lines and PCCS and ICS operation. All four of the systems interaction tests were included in the original TRACG qualification study [6-1, Section

5.3]. The principal feature of the TRACG model is a VSSL component with various regions of the r-z geometry representing the test facility components that simulated the reactor pressure vessel (RPV), upper drywell (UDW), wetwell (WW), the GDCS pool and the PCC and IC secondary-side pools. One-dimensional components are used to model the GDCS lines, the middle and lower drywells and the PCC and IC primary systems. Test GS1 was selected for the present update of the TRACG qualification.

Updated comparisons of the TRACG04 calculations with the measurements for Test GS1 are shown along with the original comparisons in Figures 5.3-12 (RPV dome pressure), 5.3-13 (DW pressure), 5.3-14 (WW pressure), 5.3-19 (chimney collapsed level), 5.3-20 (channel delta-P), 5.3-21 (bypass collapsed level), 5.3-22 (downcomer collapsed level) and 5.3-23 (GDCS flow). [[

]]

[[

**Figure 5.3-12. GS1 – RPV Dome Pressure**  
**Upper – Original [6-1] Lower – TRACG04 (9-Apr-2004) ]]**

[[

**Figure 5.3-13. GS1 – DW Pressure**  
**Upper – Original [6-1] Lower – TRACG04 (9-Apr-2004) ]]**

[[

**Figure 5.3-14. GS1 – Wetwell Pressure**  
**Upper – Original [6-1] Lower – TRACG04 (9-Apr-2004) ]]**

[[

**Figure 5.3-19. GS1 – Chimney Collapsed Level**  
**Upper – Original [6-1] Lower – TRACG04 (9-Apr-2004) ]]**

[[

**Figure 5.3-20. GS1 – Channel Delta-P**  
**Upper – Original [6-1] Lower – TRACG04 (9-Apr-2004) ]]**

[[

**Figure 5.3-21. GS1 – Bypass Collapsed Level**  
**Upper – Original [6-1] Lower – TRACG04 (9-Apr-2004) ]]**

[[

**Figure 5.3-22. GS1 – Downcomer Collapsed Level**  
**Upper – Original [6-1] Lower – TRACG04 (9-Apr-2004) ]]**

[[

**Figure 5.3-23. GS1 – GDCS Flow**  
**Upper – Original [6-1] Lower – TRACG04 (9-Apr-2004) ]]**

#### 4.4 One-Sixth Scale Boron Mixing Tests

A series of tests was conducted in a 1/6-scale mockup of a BWR/5 to examine the mixing behavior of a boron solution injected into the reactor coolant via the Standby Liquid Control System (SLCS). The test facility simulated the flow resistances of the core and bypass regions and could be run under either forced or natural circulation. The tests were conducted at atmospheric pressure and air was injected into the channels to simulate steam voids. Sodium thiosulfate was used to simulate the sodium pentaborate used in BWRs. The concentration of the sodium thiosulfate was adjusted to simulate the prototypical density difference between the much hotter reactor coolant and the injected salt solution in a BWR. In the test, the injected solution was actually 54K hotter than the simulated circulating coolant so that temperature measurements could be used to supplement direct specific gravity measurements as a means of determining the local concentration of the salt solution. Test 342 in the test series, which was performed under natural circulation with the salt solution injected in the upper plenum, was chosen for the original qualification study [6-1, Section 5.4] and is most representative of the conditions in an ESBWR

The objective of the qualification study was to show that TRACG could be used to model the transport of the boron solution through the bypass, core and lower plenum regions. The principal element of the TRACG model is a VSSL component with ten axial levels and four radial rings representing the facility reactor pressure vessel (RPV). From bottom-to-top, the level structure in the VSSL component models the lower plenum, core and bypass, upper plenum and steam dome. The three inner rings represent the region inside the shroud and the outer ring the downcomer. The core model represents 560 channels, apportioned within the three inner rings. The channels and other RPV components (e.g., control rod guide tubes) are modeled with PIPE and TEE components. Two TRACG models were used in the original qualification study. [[

The TRACG models were run at prototypical reactor conditions (7.24 MPa and 561 K) to simulate the density difference that was artificially introduced in the test by adjusting the concentration of the salt in the injected solution. ]]

Updated comparisons between the Model 1 TRACG calculations and the test results are shown along with the original comparisons in Figures 5.4-3 through 5.4-10. The comparisons are in terms of mixing coefficients at various locations in the regions representing the flow channels, bypass and plenums. The mixing coefficient is defined as the local concentration of the sodium thiosulfate divided by the global average concentration. [[

]]

[[

**Figure 5.4-3. Channel at 41-in. Center: Well-Mixed Model  
Upper – Original [6-1] Lower – TRACG04 (9-Apr-2004) ]]**

[[

**Figure 5.4-4. Channel at 55-in. Middle: Well-Mixed Model  
Upper – Original [6-1] Lower – TRACG04 (9-Apr-2004) ]]**

[[

**Figure 5.4-5. Channel at 41-in. Periphery: Well-Mixed Model  
Upper – Original [6-1] Lower – TRACG04 (9-Apr-2004) ]]**

[[

**Figure 5.4-6. Bypass at 41-in. Center: Well-Mixed Model**  
**Upper – Original [6-1] Lower – TRACG04 (9-Apr-2004) ]]**

[[

**Figure 5.4-7. Bypass at 55-in. Middle: Well-Mixed Model  
Upper – Original [6-1] Lower – TRACG04 (9-Apr-2004) ]]**

[[

**Figure 5.4-8. Bypass at 41-in. Periphery: Well-Mixed Model  
Upper – Original [6-1] Lower – TRACG04 (9-Apr-2004) ]]**

[[

**Figure 5.4-9. Lower Plenum at 14-in. Middle: Well-Mixed Model  
Upper – Original [6-1] Lower – TRACG04 (9-Apr-2004) ]]**

[[

**Figure 5.4-10. Upper Plenum Center: Well-Mixed Model  
Upper – Original [6-1] Lower – TRACG04 (9-Apr-2004) ]]**

#### 4.5 PSTF Mark III Containment Response

Tests were conducted in the General Electric Pressure Suppression Test Facility (PSTF) in support of the original Mark III pressure suppression containment design, which uses a horizontal vent system similar to that employed in the ESBWR. Emphasis in the tests was placed on vent clearing phenomena that influence the magnitude of the short-term peak in the drywell (DW) pressure following a large-break LOCA. The test facility included an electrically heated pressure vessel (RPV) connected to a DW via a blowdown line. The blowdown line had a rupture disk to simulate the rupture of a main steam line and a critical flow venturi to set the break size. The DW vessel was connected via a discharge duct to a set of horizontal vents that discharged to a wetwell (WW) vessel that was open to the atmosphere. The key test measurement is the DW pressure. The complete test matrix included tests with one, two and three horizontal vents.

Test Series 5703, which was run with three horizontal vents and, accordingly, is most representative of the ESBWR design was selected for the original TRACG qualification [6-1, Section 5.5]. Test Series 5703 included three tests with two different break sizes and differing top vent submergences. The TRACG model uses a VSSL component to represent the PSTF DW and WW and a TEE component to represent the RPV. The horizontal vent system is modeled by a set of three interconnected TEE components. Test 5703-01, which had a break size of 63.5 mm (venturi diameter) and a top vent submergence of 2.06m, was selected for the updated qualification.

Updated and original comparisons of the calculated and measured DW pressure for Test 5703-01 are shown in Figure 5.5-5. [[

]]

[[

**Figure 5.5-5. Drywell Pressure Response – TRACG vs. Measured Data, Test 5703-01**  
**Upper – Original [6-1] Lower – TRACG04 (9-Apr-2004) ]]**

## 4.6 4T/Mark II Containment Response

A series of blowdown tests, designated Test Series 5101, was conducted in the Pressure Suppression Test Facility (PSTF) to provide supporting data for the Mark II vertical-vent containment design. Test Series 5101 used the same steam generator and drywell vessels as the PSTF Mark III tests described in Section 4.5. The major difference in the test facility as configured for the Mark II tests was the use of a vessel designated as the Temporary Tall Test Tank (4T) to simulate the Mark II wetwell and vertical vent system. The 5101 test series included seven tests representing two break sizes, three vent submergences and a range of initial WW pool temperatures. Tests were conducted with both closed and open wetwells. The key measurements are the DW and WW pressures.

The original TRACG qualification study [6-1, Section 5.6] included all seven tests performed with a closed WW. The principal element of the TRACG model is a VSSL component that includes both the DW and WW of the test facility. One-dimensional components are used to model the steam generator, blowdown line and DW-to-WW vent line. Test 5101-34, which had a break size (venturi diameter) of 76.2 mm, vent submergence of 4.112 m and initial WW pool temperature of 20.6° C was selected for the updated calculation.

Updated comparisons of the measured and calculated DW pressure, WW pressure and DW-to-WW pressure difference as functions of time are shown together with the original comparisons in Figures 5.6-5 through 5.6-7. [[

]]

[[

**Figure 5.6-5. Drywell Pressure Response for Test 5101-34 - TRACG vs. Measured Data  
Upper – Original [6-1] Lower – TRACG04 (9-Apr-2004) ]]**

[[

**Figure 5.6-6. Wetwell Airspace Pressure for Test 5101-34 – TRACG vs. Measured Data  
Upper – Original [6-1] Lower – TRACG04 (9-Apr-2004) ]]**

[[

**Figure 5.6-7. Drywell-to-Wetwell Pressure Differential for Test 5101-34 – TRACG vs.  
Measured Data  
Upper – Original [6-1] Lower – TRACG04 (9-Apr-2004) ]]**

#### 4.7 PANDA Transient Tests (M-Series)

The original TRACG qualification for the SBWR included nine transient tests (the M-series) performed at the PANDA test facility in Switzerland. The PANDA facility has all of the features necessary for an integrated system simulation of the ESBWR long-term post-LOCA transient, including a detailed representation of the Passive Containment Cooling System (PCCS). Additional PANDA components represent the reactor pressure vessel (RPV), drywell (DW), wetwell (WW), Isolation Condenser System (ICS) and Gravity-Driven Cooling System (GDCS). The M-series test matrix consisted of Tests M3, M3A, M3B, M2, M10A, M10B, M6/8, M7 and M9. Test M3 (the “base case”) was a simulation of the long-term cooling phase following a LOCA caused by a guillotine rupture of one of the main steam lines. Tests M3A and M3B repeated the Test M3 transient scenario while examining possible alternatives for configuring and refilling the PCC and IC secondary-side pools. Tests M2, M10A and M10B examined the influence of asymmetric distributions of the DW steam-air mixture on the startup and long-term performance of the PCCS. Test M6/8 considered system interaction effects associated with parallel operation of the ICS and the PCCS and the effect of a direct bypass of steam from the DW to the WW gas space. Test M7 addressed the issue of PCCS startup from a condition representing the upper limit of initial DW noncondensable inventory. Test M9 examined PCCS performance during the transition from the GDCS-injection phase to the long-term cooling phase of the post-LOCA transient. Measurements included pressures, temperatures, flows and noncondensable gas (air) concentrations.

For the original qualification study [6-1, Section 5.7], TRACG calculations were performed for all nine of the M-series tests. The M-series PANDA TRACG input model represents the DW, WW and GDCS vessels within a VSSL component. The RPV, PCCS, ICS and the piping that interconnects the PANDA vessels are represented by one-dimensional PIPE, TEE, VLVE, CHAN, BREK and FILL components. The procedures used to initiate and control the tests in the PANDA facility were directly simulated in the TRACG model. Tests M3 (the base case) and M10B (all steam directed to DW1 and PCC1 out of service) were selected for the current update.

Updated comparisons between TRACG calculations and PANDA M-series measurements for Tests M3 and M10B are shown in Figures M3-1 and M10B-1 (DW and WW pressures) and M3-2 and M10B-2 (PCC inlet flows). (In the updated comparisons, the test measurements have been decimated 10:1 to facilitate plotting with EXCEL.) [[

]]

[[

**Figure M3-1. Drywell and Wetwell Pressures for Test M3  
Upper – Original [6-1] Lower – TRACG04 (9-Apr-2004) ]]**

[[

**Figure M3-2. PCC Inlet Flows for Test M3**  
**Upper – Original [6-1] Lower – TRACG04 (9-Apr-2004) ]]**

[[

**Figure M10B-1. Drywell and Wetwell Pressures for Test M10B**  
**Upper – Original [6-1] Lower – TRACG04 (9-Apr-2004) ]]**

[[

**Figure M10B-2. PCC Inlet Flows for Test M10B**  
**Upper – Original [6-1] Lower – TRACG04 (9-Apr-2004) ]]**

## **5.0 NATURAL CIRCULATION AND FLOW OSCILLATION TESTS**

### **5.1 Analysis of February 1992 Startup of Dodewaard Natural Circulation BWR**

The original TRACG SBWR qualification study included a simulation of the 1992 startup of the Dodewaard natural circulation reactor in the Netherlands following a refueling outage [6-1, Section 6.2]. The startup measurements showed early establishment of circulation flow and no evidence of reactor instability. The Dodewaard reactor (subsequently shut down permanently) was a natural circulation BWR with internal free surface steam separation and a maximum thermal power output of 183 MWt. In January 1992, the reactor was shut down for annual maintenance and refueling. On February 15 and 16, 1992 the reactor startup was performed in accordance with the normal startup procedure. Measurements included: thermal power; pressure; main steamline flow; collapsed water level; downcomer subcooling, pressure difference and velocity; and bypass temperature and velocity.

The TRACG simulation of the Dodewaard startup was repeated using the 9-Apr-2004 version of TRACG04. The TRACG input model uses a VSSL component to model the Dodewaard reactor vessel. The VSSL cells are arranged in 16 axial levels and four radial rings. The three inner rings contain the core and the chimney and the outer ring contains the downcomer. Four CHAN components are used to represent the fuel. One-dimensional PIPE components are used to model the control rod guide tubes.

Updated comparisons between TRACG calculations and the Dodewaard startup measurements are shown along with the original comparisons in Figures 6.2-4 through 6.2-14. In Figure 6.2-4, the TRACG thermal power, derived from the measured neutron flux power by averaging, is compared with the thermal power calculated from a heat balance using the Dodewaard measurements. The TRACG thermal power is an input to the startup calculation. Figures 6.2-5 and 6.2-6 compare the TRACG and Dodewaard pressure and steam flow. In the first phase of the simulation (0-25,000s) the steam flow is prescribed (via a FILL component) and the pressure is calculated. In the second phase of the transient (25,000 to 70,000s), the pressure is prescribed (via a BREK component) and the steam flow is calculated. Figure 6.2-7 compares TRACG and measured water level; Figures 6.2-8 and 6.2-9 compare TRACG and measured downcomer subcooling and velocity; Figures 6.2-10 and 6.2-11 compare TRACG and measured differential pressures in the downcomer; Figures 6.2-12 and 6.2-13 compare TRACG and measured bypass temperature and velocity; and Figure 6.2-14 compares TRACG and measured feedwater sparger flow. [[

]]

[[

**Figure 6.2-4. Comparison of Measured and Calculated Thermal Power  
Upper – Original [6-1] Lower – TRACG04 (9-Apr-2004) ]]**

[[

**Figure 6.2-5. Comparison of Measured and Calculated Pressure  
Upper – Original [6-1] Lower – TRACG04 (9-Apr-2004) ]]**

[[

**Figure 6.2-6. Comparison of Measured and Calculated Steam Flow**  
**Upper – Original [6-1] Lower – TRACG04 (9-Apr-2004) ]]**

[[

**Figure 6.2-7. Comparison of Measured and Calculated Water Level  
Upper – Original [6-1] Lower – TRACG04 (9-Apr-2004) ]]**

[[

**Figure 6.2-8. Comparison of Measured and Calculated Downcomer Local  
Subcooling  
Upper – Original [6-1] Lower – TRACG04 (9-Apr-2004) ]]**

[[

**Figure 6.2-9. Comparison of Measured and Calculated Downcomer Velocity  
Upper – Original [6-1] Lower – TRACG04 (9-Apr-2004) ]]**

[[

**Figure 6.2-10. Comparison of Measured and Calculated Short Range Downcomer  
Pressure Differences DP1 and DP2  
Upper – Original [6-1] Lower – TRACG04 (9-Apr-2004) ]]**

[[

**Figure 6.2-11. Comparison of Measured and Calculated Short Range Downcomer  
Pressure Difference DP3  
Upper – Original [6-1] Lower – TRACG04 (9-Apr-2004) ]]**

[[

**Figure 6.2-12. Comparison of Measured and Calculated Bypass Temperatures  
Upper – Original [6-1] Lower – TRACG04 (9-Apr-2004) ]]**

[[

**Figure 6.2-13. Comparison of Measured and Calculated Bypass Velocity**  
**Upper – Original [6-1] Lower – TRACG04 (9-Apr-2004) ]]**

[[

**Figure 6.2-14. Comparison of Measured and Calculated Sparger Flow  
Upper – Original [6-1] Lower – TRACG04 (9-Apr-2004) ]]**

## 5.2 CRIEPI Low Pressure Oscillation Tests

The original TRACG qualification included comparisons between TRACG calculations and data from low-pressure thermal-hydraulic oscillation tests performed in the CRIEPI test facility in Japan [6-1, Section 6.3]. The CRIEPI test loop consisted of two electrically heated channels, a chimney, a separator/upper plenum, downcomer, preheater and subcooler. Tests were conducted at pressures of 0.2, 0.35 and 0.5 MPa. Principal measurements included the inlet temperature and the flow rate.

The original TRACG qualification study included comparisons of calculated and measured downcomer inlet velocities as functions of inlet subcooling at pressures of 0.2 and 0.5 MPa with a power of 2.5 kW per channel. The TRACG model uses CHAN components to model each of the heated channels and a VSSL component for the upper plenum/separator tank. A BREK component connected to the VSSL is used to impose the pressure boundary condition and PIPE components are used for the chimney and downcomer. For the current update, the 0.5 MPa results were recalculated. Figure 6.3-10 shows the updated and original comparisons of downcomer inlet velocity vs. inlet subcooling. [[

]]

[[

**Figure 6.3-10. Steady-State Flow Comparison (P = 0.5 MPa)**  
**Upper – Original [6-1] Lower – TRACG04 (9-Apr-2004) ]]**

### 5.3 PANDA Exploratory Tests

The PANDA test facility was used to conduct a series of exploratory tests (designated the E-Series) to investigate and clarify the nature of pressure and steam flow oscillations that were observed during some of the facility shakedown tests. The configuration of the PANDA facility for the E-Series was essentially the same as for the steady state S-series tests described in Section 3.3. In this configuration, the RPV steam flow is directed to passive containment condenser unit PCC3 and condensate is returned to the RPV via the GDCS line. The sensitivity of the steam flow oscillations to RPV power, RPV water level and air fraction in the PCCS inlet flow was investigated. The full test matrix consisted of Tests E1A and E1B with the initial RPV water level below the top of the chimney and Tests E1C, E2 and E3 with the initial RPV water level above the top of the chimney.

The original qualification study [6-1, Section 6.4] consisted of TRACG simulations of Tests E1C and E2. These two tests were similar except that in Test E2 the power level was decreased by 50% during the test. Both of these tests were characterized by well-defined oscillations. In Test E2, the oscillations stopped after the power was reduced. The TRACG model for the PANDA E-Series tests models the RPV with a CHAN component for the electrically heated rod bundle, PIPE and TEE components, respectively, for the chimney and downcomer and a VSSL component for the upper plenum. Additional PIPE components represent the steam line from the RPV to PCC3 and the GDCS return line. BREK and FILL components, respectively, are used to specify the steam line pressure and the PCC3 condensate return via the GDCS line. The basis for this simplification was the conclusion that the PCC3 unit was not a causative factor for the steam flow oscillations. The Test E2 simulation was selected for the current update.

Figure 6.4-18 shows the updated and original comparisons between the calculated and measured RPV steam flow for Test E2. [[

]]

[[

**Figure 6.4-18. Steam Flow to PCC3 for Test E2**  
**Upper – Original [6-1] Lower – TRACG04 (9-Apr-2004) ]]**

## **6.0 REFERENCES**

- 6-1. NEDC-32725P, "TRACG Qualification for SBWR", Rev. 1, August 2002

**NRC RAIs and Responses**

**TRACG Model Description  
NEDE-32176P, Rev. 2**

**Note: RAI responses including data files that cannot be read on a PC are not included.**

Q32. Comparison of the TRACG Model Description report, NEDE-32176P, Revision 2, with Revision 1 indicates that significant material essential to the ESBWR review has been expunged without indication in the text. For example, Table 6.0-1 has had significant containment items removed and yet the table is not indicated as modified from Rev. 1. Section 7.11, Containment Components, has been removed in its entirety. There are also numerous missing sections related to "Wall Friction and Form Losses" which address containment modeling. Please provide appropriate revisions to the text to incorporate all material pertaining to the containment modeling that has been expunged in going from Revision 1 to Revision 2 of NEDE-32176P.

R32. Revision 2 of the TRACG Model Description report, NEDE-32176P removed discussion of the containment-related topics to simplify NRC review of the document for AOOs. The ESBWR reports reference both Revision 1 and Revision 2 of the Model Description document to provide the needed information for the containment application. The next revision of the Model Description report will integrate the removed sections with Revision 2.

Q34 What are "k" and "B" in Eq. 3.2-8 and how are they specified?

R34. k [[  
defined in the nomenclature in Section 3.1.1 and Section 6.1.7.3. B<sub>s</sub> is defined in the nomenclature in Section 3.1.1. [[

]]

Q35 Section 3.3 - When values of solution from the balance equations are restricted by critical flow or counter current flow limit (CCFL), is the time step repeated with smaller time, or are flows adjusted and calculation proceeds?

R35. The velocity is set to the [[  
]] The critical flow model is described in Section 6.3 and the CCFL is described in Section 6.1.7.2. [[

]]

Q36 Equation 4.1-5 - The heat transfer coefficients for different phases are multiplied by the same surface area. During the boiling regime, the surface will either have

liquid or vapor in contact but not both. Please explain why this has been done or correct the equations. Same question for Eq. 4.2-1.

R36. The flow regime map is described in Section 5. and the wall heat transfer is described in Section 6.6. If liquid is in contact with the wall as in single phase liquid convection or nucleate boiling, [[ ]] If vapor is in contact with the wall as in single phase vapor convection or film boiling, [[ ]] as described in Section 6.6.8. Also see the response for Q58.

Q37 Is there guidance on when to use the implicit or explicit option for conduction calculation?

R37. [[ ]] calculations. See page 21 of the TRACG02A User's Manual (NEDC-32956P).

Q38. Equation 5.1-4 is used for developing criterion for transition from bubbly to annular flows. The equation implies that volume flux is much larger than 1 m/s. What happens during low flow conditions?

R38. The assumption is made (TRACG02) that [[ ]] This is true for most practical BWR applications. For example in a BWR fuel bundle the volumetric flux for rated conditions range from [[ ]] m/sec., while the drift flux velocity range from [[ ]] m/sec. For low flow such as natural circulation the volumetric flux range from [[ ]] However, the excellent comparison to void fraction data shown in NEDE-32177P demonstrates the applicability of the model. For TRACG04 the assumption that the drift velocity can be neglected is not made. This modification will be documented in Revision 3 of the TRACG Model LTR.

Q39. Equation 5.1-20 - How is  $E_1$  defined?

R39. As it is stated in the line just below: "where [[ ]] given by Equation 5.1-17..." The nomenclature is confusing. [[ ]]

[[ ]]  
The confusing nomenclature will be clarified in Revision 3 of the TRACG Model LTR.

Q40. Based on Fig 5.1-3, Ishii's original model is as good as the modified one. Why is there a need to modify it?

R40. The reason is given in the first paragraph of Section 5.1.2.2 just before Equation 5.1-17: [["

]]

Q41. Table 6.0-1 addresses the question of applicability of TRACG for a vessel. However, TRACG is also used for containment modeling. Is there a similar table for containment?

R41. Yes, containment components are included in Table 6.0-1 in NEDE-32176, Revision 1. These are not documented in Rev. 2 since the NRC was not asked to review the containment model for the AOO applications. The documentation for the containment components will be included in Revision 3 of the TRACG Model LTR.

Q42. Why doesn't Table 6.0-1 include a steam separator?

R42. The separator models and the range of assessment are described in Section 7.7. Note in particular Figures 7.7-3 to 7.7-7. The omission of the separator from Table 6.0-1 will be corrected in Revision 3 of the TRACG Model LTR.

Q43. Interpretation of terms for Eq. 6.1-5, provides a definition for  $\alpha$ . The same symbol is used for more than one purpose. What is the basis that these symbols are identical?

R43. [[

]] The assumption however was adopted for all flow regimes for consistency. The excellent comparison to void fraction data shown in NEDE-32177P (Section 3.1) demonstrates the applicability of the model.

Q44 Please provide a comparison between Eq. 3.1-30 and 6.1-2. Why do the gravity terms have different signs?

R44. Different sign conventions were used in the two sections. In Section 3, the acceleration of gravity is  $-9.81\text{m/sec}^2$  for vertical up-flow. Section 6.1, which was extracted from Reference 6.1-2 uses the opposite sign convention where the acceleration of gravity is  $9.81\text{m/sec}^2$  for vertical up-flow. This discrepancy will be corrected in the next revision of the report.

- Q45. Equations 6.1-6 and 6.1-7 - Why are steady inertia terms neglected?
- R45. The interfacial shear model is based on the two assumptions stated in Section 6.1.1 in the TRACG Model Description:
- For adiabatic and steady-state conditions, the two-fluid model and the drift flux model are equivalent, and drift flux parameters can be used to characterize the relative velocity, and the phase and flow distributions.
  - The correlations for the interfacial shear and drag, as well as wall friction, as derived from adiabatic steady-state conditions, are applicable for transient conditions.
- For adiabatic and steady state conditions in a straight fluid channel without any area changes there is no acceleration of the fluid and the  $\frac{\partial}{\partial t}$  as well as the  $\frac{\partial}{\partial x}$  terms are zero.
- Q46. Equation 6.1-10 - The 'g' term (gravity) is missing.
- R46. This is a typographical error, 'g' is missing in the last term of Equation 6.1-10. Down-stream applications of the equation correctly include the 'g' term. This will be corrected in the next revision of the report.
- Q47. Equation 6.1-21- What type of averaging is implied on both sides of the equation?
- R47.  $\langle \rho \rangle$  is defined by  $\langle \rho \rangle = \frac{1}{A} \int \rho dA$ , where the average indicated by  $\langle \rangle$  is the cross-sectional average.
- Q48. Critical Weber number is for the upper limit on the droplet size distribution. Is the GE recommended value conservative for LOCA application?
- R48. The critical Weber number defines the maximum stable droplet size,  $We_{crit}$  was chosen as a representative size for the average droplet size. The excellent comparison to void fraction data shown in NEDE-32177P demonstrates the applicability of the model. Comparisons to integral effects LOCA tests such as TLTA and FIST as shown in NEDE-32177P also demonstrates the adequacy of the model. It should furthermore be kept in mind, that TRACG is not intended to be conservative but best estimate. Conservative estimates for the critical safety parameters are obtained as described in the application methodology LTR.
- Q49. Below Eq. 6.1-63, there is reference to Eq. 5.1-25. Where is this equation?
- R49. This reference should be to Equation 5.1-23. This will be corrected in the next revision of the report.



to the fact that the spacers will break up the bubbles in a fuel channel an upper limit of half the hydraulic diameter was chosen. For a fuel channel, which has the smallest hydraulic diameter of the BWR components, this would lead to an upper limit of [ ]. The lower limit of 0.0005 m was chosen to prevent the interfacial heat transfer from becoming too large, which can lead to numerical difficulties. For very large interfacial heat transfer rate, the phases will be in thermal equilibrium and the results are not very sensitive to the exact value of the interfacial heat transfer. For typical operating conditions, the bubble sizes will be in the range of [ ], and the number density will be in the range of [ ], and are therefore not affected by the limits. Similar arguments are applied for droplet flow, in order to keep the interfacial heat transfer within reasonable bounds. The good comparison to the void fraction and heat transfer data shows that these limits do not adversely affect the results.

- Q55. Section 6.5.4.1 (annular flow regime) - How is the noncondensable gas concentration estimated at the interface? The saturation temperature will depend on this concentration.
- R55. The [ ] is used, however, for condensation a degradation of the condensation due to the local accumulation of noncondensable gas at the interface is correlated in the factor  $C_{ncg}$  as described at the end of Section 6.5.4.1..
- Q56. Section 6.5.4.1 (annular flow regime) - Why is the heat transfer coefficient modified on the liquid side?
- R56. The heat transfer on the liquid side is not modified; it is calculated from the conduction across a thin liquid film and is given by Equation 6.5-18 in NEDE-32176P. The heat transfer on the vapor side is based on a modification to the model developed by Theofanous. The original model as developed by Theofanous is given by:

$$St = 0.02 \sqrt{\frac{L}{D}}$$

In TRAC-PF1/MOD1 the model was modified by removing the shape factor term:

$$St = 0.02 = \frac{h}{\rho C_p v}$$

The justification is given in Section 4.1.1 of NUREG/CR-5069. The justification considers that a constant Stanton number falls within the range of the available data. This model was carried over to other TRAC versions including TRACG. The final justification for the use of this model is based on the qualification in

NEDE-32177P. The vapor side heat transfer coefficient for annular flow is only significant for conditions where significant vapor super heat is present. Qualifications against test data for such conditions are contained in Sections 3.2, 5.1 and 5.2 of NEDE-32177P.

Q57. Please check Eq. 6.5-29. When pipe is half full and  $\alpha=0.5$ , does this expression reduce to the correct limit?

R57. Equation 6.5-29 is based on the following assumptions. [[

]] Figure 57-1 shows the void fraction, the surface area per unit volume assuming a smooth surface, the surface area per unit volume assuming a wavy surface and Equation 6.5-29 as function of the liquid height.

[[

Figure 57-1 Surface Area for Stratified Flow ]]

[[

]]

Q58. Section 6.6 describes the heat transfer coefficient at the wall. In section 3.1, Eqs. 3.1-19 and 3.1-20 indicate that the heat transfer coefficient accounts for the

fraction of the wall in contact with one or the other phase. However, heat transfer coefficients in Section 6.6 do not indicate this. Please explain.

- R58. The logic for the selection of the heat transfer coefficients is given Section 6.6.2 and shown in Table 6.6.1. This Table is repeated here for convenience.

Table 6.6.1 Selection Logic for Wall Heat Transfer

[[

]]

[[

]]

[[  $\dots$  ]] (6.6-37)

where

[[  $\dots$  ]] (6.6-38)

and:

$h_{NB}(T_{CHF})$  = Nucleate boiling heat transfer coefficient evaluated at  $T_{CHF}$   
 $h_{FB}(T_{min})$  = Film boiling heat transfer coefficient evaluated at  $T_{min}$ .

In Equation 6.6-37, the first term is heat transfer to the liquid and the second term is heat transfer to the vapor. This equation could therefore be expressed as:

[[ ]] (6.6-37a)

and

[[ ]] (6.6-37b)

Q59. Section 6.6.10.3 - The applicability of the Tien-Gonzalez correlation was based on CORECOOL code. Was there any assessment done with TRACG?

R59. Functional testing was done for correct implementation. Qualification was not done for the TRACG AOO submittal as [[  
 ]] Qualification has been performed  
 and will be included for the TRACG LOCA submittal.

Q60. Section 6.6.6 - Four critical heat flux criteria are described. What options are used and where in ESBWR? What correlation is used for flow reversal or very low flows in the channel (Modified Zuber is excluded from the channel components)?

R60. [[

]]

Q61. Equation 6.6-64 - What is “Rem” and where is it defined?

R61. The definition for  $Re_m$  was inadvertently missed. [[

[[ ]]

]]

Q62. Equation 6.6-65 - How is “ $\rho_m$ ” defined?

R62. The density of the gas mixture ( $\rho_m$ ) is the [[  
]]

Q63. Equation 6.6-68 - What effect does “ $f_{l,other}$ ” cover ?

R63. According to Section 3.6 of [[

]]

Q64. Section 6.6.11 - Lighter than steam (helium) or heavier than steam (air) have different flow near the interface and may affect the film thickness differently. Where is this effect considered?

R64. The factor [[

]]Other mechanisms  
not explicitly considered will be reflected in the degradation factors [[

]]

Q65 Section 6.6.11 - What condensation model is used in containment? How much is the uncertainty in the correlation? How does condensation affect the early pressure peak during steam line break LOCA?

R65. For condensation in the containment, the option that is selected uses the minimum condensation heat transfer coefficient from the Uchida correlation and the Kuhn-Schrock Peterson (K-S-P) correlation with the shear enhancement factor ( $f_{1shear}$ ) set to 1. The applicability to containment is discussed near the end of Section 6.6.11.1. For condensation in tubes, the K-S-P has a standard deviation of 7.4% compared to pure steam data and a standard deviation of 17.6% when compared to Kuhn's 70 steam-air tests as indicated in the first part of Section 6.6.11.3. The application for steam condensation in the containment is discussed later in Section 6.6.11.3. The various correlations are compared with each other in Figure 6.6-15 and they are compared to the data from Dehbi in Figure 6.6-16. For containment applications, *TRACG Application for ESBWR, NEDC-33083P* suggests using [[

]]

In general, the long-term heat transfer is dominated by conduction through the wall. As a result, any error in the condensation rate that in turn affects the heat transfer coefficient has essentially no impact on the total amount of condensed steam and the long-term containment response. The question rightly implies a concern with the short-term pressure response where the condensation rate could have some impact on the peak pressure. To address this concern, sensitivity studies have been performed to assess how potential variations in steam condensation in the containment impact the calculated peak containment pressure for a simulated steam line break LOCA. The sensitivity results are summarized in Table 65-1. The results for cases 1, 2 and 3 are not distinguishable within the numerical noise. This indicates two things: (1) The K-S-P correlation with  $f_{1shear}=1$  is providing a lower condensation rate than the Uchida correlation and (2) the calculated value for  $f_{1shear}\approx 1$ . Case 4 shows that the impact of the condensation rate on the peak pressure must be relatively small because even a 25% increase in the heat transfer area for the drywell walls only causes a slight decrease in the peak pressure.

Table 65-1 Drywell Peak Pressure Sensitivity for Steam Line Break LOCA

Case #	Description	Peak Pressure (psia)
1	Reference (recommended for containment): Minimum of K-S-P with $f_{1shear}=1$ and Uchida	39.717
2	K-S-P with $f_{1shear}=1$	39.727
3	K-S-P with calculated $f_{1shear}$	39.727
4	Reference with 25% increase in heat transfer	39.419

	area	
--	------	--

Q66. Section 7.7 - The high void core region in the steam separator is assumed to have solid body rotation and the liquid film will also have swirl with tangential velocity decreasing towards the wall (no slip). Please explain the basis of liquid film tangential velocity described in Eq. 7.7-2.

R66. [[

]]

Q67. Figures 7.7-6 and 7.7-7 show upper and lower bands for carry under. There are expressions for upper limit for carryunder. Are there similar expressions for lower limit?

R67. The upper and lower bands shown in Figures 7.7-6 and 7.7-7 are the upper and lower boundaries for the experimentally observed carry under.

Q68. Section 7.5.2 (p. 7.5-10 to 7.5-18) - Are there specific references for the development of the various correlations and the associated parameters, such as Eqs. 7.5-9, 7.5-13, 7.5-15, 7.5-16?

R68. There are many questions on the dynamic gap model. This model has been extensively reviewed previously and is already approved by the NRC. The fuel gap conductance models in Sections 7.5.2 and 7.5.3 are identical to the SAFER/GESTR models approved by the NRC, and also reviewed in the TRACG application for AOOs (Ref. NEDE-23785-PA, Vol. 1 and 2). The reference number is [7.5-4].

Q69. Section 7.5.2.2 (p. 7.5-12) - What is the physical significance of the effective hot radial thermal gap  $R_{eff}$ ?

R69. See Eqs. (7.5-21) and (7.5-22). [[

]]

The fuel gap conductance models in Sections 7.5.2 and 7.5.3 are identical to the SAFER/GESTR models approved by the NRC, and also reviewed in the TRACG application for AOOs.

Q70. Section 7.5.2.2 (p. 7.5-13) - What criteria are used to determine the gases to be considered in the calculation of the gas conductivity?

R70. The gases that are considered are those that are prevalent in the gap. Helium is obviously important because of the initial backfilling of helium. [[

]] The fission gas production of some isotopes of xenon (Xe) and krypton (Kr) are also important because their fission yield rates compared to the decay times are large enough that these gases exist in sufficient amounts and for long enough times that they can be released from the UO<sub>2</sub> pellet into the gap.

The fission yields and the half-lives are not the only consideration. For example, cesium is produced in large amounts but is not present as a gas in the gap in any appreciable amounts because it readily reacts chemically and is effectively removed as a gas by a number of processes. Olander discusses these processes in Chapter 12 of his book<sup>[70-1]</sup>. Chapter 13 of Olander's book discusses fission gas production in the fuel pellet and the release mechanisms are discussed in Chapter 15. Ultimately, the only fission gases that accumulate in the gap in any appreciable amounts are the stable (or longer half-life) isotopes of Xe and Kr as stated in Section 15.3.6. [[

]]

The fuel gap conductance models in Sections 7.5.2 and 7.5.3 are identical to the SAFER/GESTR models approved by the NRC, and also reviewed in the TRACG application for AOOs.

References for R70

[70-1] Olander, Donald R.; Fundamental Aspects of Nuclear Reactor Fuel Elements, TID-26711-P1, U.S. Dept. of Energy Office of Scientific and Technical Information, 1976.

Q71 Section 7.5.2.2 (p. 7.5-13) - What is the basis for the gases assumed in the gap of a perforated clad?

R71. The response to Q70 provides the basis for modeling the gases in the gap prior to clad perforation. [[

]]

The fuel gap conductance models in Sections 7.5.2 and 7.5.3 are identical to the SAFER/GESTR models approved by the NRC, and also reviewed in the TRACG application for AOOs. The model for composition of the gases in the gap after perforation was also approved by the NRC in 1981<sup>[71-4]</sup>.

References for R71

- [71-1] *The GESTR-LOCA and SAFER Models for the Evaluation of the Loss-of-Coolant Accident, Volume II*, NEDE-23785-1-PA, Revision 1, October 1984, page 4-31.
- [71-2] *General Electric Company Analytical Model for Loss-of-Coolant Analysis in Accordance with 10CFR50 Appendix K – Volume 1*, NEDE-20566-P-A, Class III, September 1986, page I-108,109.
- [71-3] *CHAST05 Core Heatup Analysis Model Technical Description*, NEDO-21426, November 1977, pages 4-4,5.
- [71-4] Letter, R. L. Tedesco (NRC) to G. G. Sherwood (GE) dated February 4, 1981, “Acceptance for Referencing of Topical Report NEDE-20566P, NEDO-20566-1 Revision 1 and NEDE-20566-4 Revision 4”.

Q72. Section 7.5.2.2 (p. 7.5-13) - Do the constants in Eq. 7.5-14 depend on the relative mix of steam and hydrogen?

R72. [[

]]

The fuel gap conductance models in Sections 7.5.2 and 7.5.3 are identical to the SAFER/GESTR models approved by the NRC, and also reviewed in the TRACG application for AOOs.

Q73. Section 7.5.2.3 (p. 7.5-15) - The section on fuel pellet gap conductance has defined several “gaps.” Which ‘hot gap size’ does the model refer to in relation to the calculation of the contact pressure  $P_c$ ?

R73. [[

]]

The fuel gap conductance models in Sections 7.5.2 and 7.5.3 are identical to the SAFER/GESTR models approved by the NRC, and also reviewed in the TRACG application for AOOs.

Q74. Section 7.5.2.4 (p. 7.5-16) - What is the basis for the constant in Eq. 7.5-24?

R74. [[

]]

The fuel gap conductance models in Sections 7.5.2 and 7.5.3 are identical to the SAFER/GESTR models approved by the NRC, and also reviewed in the TRACG application for AOOs.

Q75. Section 7.5.2.5 (p. 7.5-16) - Does  $R_{ref}$  vary with time and how?

R75. [[

]]

The fuel gap conductance models in Sections 7.5.2 and 7.5.3 are identical to the SAFER/GESTR models approved by the NRC, and also reviewed in the TRACG application for AOOs.

Q76. Section 7.5.2.5 (p. 7.5-16) - How does the thermal expansion coefficient of the fuel take into consideration the effects of burnup, such as densification and relocation?

R76. The effects of burnup [[ ]] See the response for Q75.

Q77. Section 7.5.2.6.1 (p. 7.5-17) - How are the inputs  $F_r$  and  $F_{kx}$  determined?

R77. [[

]]

The fuel gap conductance models in Sections 7.5.2 and 7.5.3 are identical to the SAFER/GESTR models approved by the NRC, and also reviewed in the TRACG application for AOOs.

Q78. Section 7.5.2.6.2 (p. 7.5-18) - Does Eq. 7.5-30 still apply if  $P_{ci}$  is less than zero?

R78. [[

]]

The fuel gap conductance models in Sections 7.5.2 and 7.5.3 are identical to the SAFER/GESTR models approved by the NRC, and also reviewed in the TRACG application for AOs.

- Q79. Section 7.5.2.7 (p. 7.5-18) - Is there any documented comparison between the gap conductance calculated by TRACG and other referenced GE models and codes?
- R79. The fuel gap conductance models in Sections 7.5.2 and 7.5.3 are identical to the SAFER/GESTR models approved by the NRC, and also reviewed in the TRACG application for AOs.

The TRACG implementation was verified against SAFER as part of the TRACG testing. An example of this testing is shown in Figure 79-1. The comparison was done for a small break LOCA case. The initial values agreed perfectly and small differences developed during the transient due to differences in the hydraulic model.

[[

Figure 79-1 TRACG to SAFER Gap Conductance Comparison.

]]

Q80. Section 7.5.3.2 (p. 7.5-19) - Does the cladding perforation model apply only to the core location of maximum linear heat generation rate (LHGR)?

R80. The perforation model applies to any point along the fuel rod. Normally perforation would be expected to occur at the point of peak LHGR, but perforation could occur for an LHGR less than the PLHGR, if the temperature is higher at that location.

Q81. Section 7.5.3.1 (p. 7.5-19) - Why does subscript 'f' refers to two different variables in Eqs. 7.5-33 and 7.5-34?

R81. [[  
]]

The fuel gap conductance models in Sections 7.5.2 and 7.5.3 are identical to the SAFER/GESTR models approved by the NRC, and also reviewed in the TRACG application for AOOs.

Q82. Section 7.5.3.1 (p. 7.5-20) - How is Eq. 7.5-35 developed?

R82. [[  
  
  
  
  
  
  
  
  
  
]]

The fuel gap conductance models in Sections 7.5.2 and 7.5.3 are identical to the SAFER/GESTR models approved by the NRC, and also reviewed in the TRACG application for AOOs.

Q83. Section 7.5.3.1 (p. 7.5-20) - How is the factor determined for Eq. 7.5-36?

R83. [[  
  
  
  
]]

The fuel gap conductance models in Sections 7.5.2 and 7.5.3 are identical to the SAFER/GESTR models approved by the NRC, and also reviewed in the TRACG application for AOOs.

Q84. Section 7.5.3.2 (p. 7.5-20) - What are the subscripts 'g', 'l' and 'v', 'w', and 'pl' in Eqs. 7.5-37 to 7.5-39?

R84. The subscripts in question are defined as follows:

- "g" and "v" - vapor outside of clad,
- "l" - liquid outside of clad,
- "w" - unheated cladding,
- "pl" - plenum.

The fuel gap conductance models in Sections 7.5.2 and 7.5.3 are identical to the SAFER/GESTR models approved by the NRC, and also reviewed in the TRACG application for AOs.

Q85. Section 7.5.3.2 (p. 7.5-20) - Is the gas temperature in the fuel the same as the plenum gas temperature?

R85. No, the volume to temperature ratio in the fuel column is determined using Eq. (7.5-35).

The fuel gap conductance models in Sections 7.5.2 and 7.5.3 are identical to the SAFER/GESTR models approved by the NRC, and also reviewed in the TRACG application for AOs.

Q86. Section 7.5.3.3 (p. 7.5-21) - Besides the gas conductivity, does the state of a perforated clad affect the gap conductance in other ways?

R86. [[

]]

The fuel gap conductance models in Sections 7.5.2 and 7.5.3 are identical to the SAFER/GESTR models approved by the NRC, and also reviewed in the TRACG application for AOs.

Q87. Sections 7.5.2 and 7.5.3 - Is it possible to summarize parameters that are axially dependent and those that are not?

R87. The fuel gap conductance models in Sections 7.5.2 and 7.5.3 are identical to the SAFER/GESTR models approved by the NRC, and also reviewed in the TRACG application for AOs. The axial resolution in the modeling has not been changed.

[[

]]

- Q88. Section 7.9 - Is a heat exchanger component used for ICS and PCCS modeling?
- R88. The ICS and PCCS heat exchangers are modeled using the standard PIPE and TEE components coupled with the component to component heat transfer models. Condensation heat transfer is given by the models described in Section 6.6.11.
- Q305. Figure 6.6-16 in the TRACG Model Description reports uses the units "WALLS/m<sup>2</sup>K" for the average heat transfer coefficient. Should these units be "watts/m<sup>2</sup>-K?"
- R305. Yes, the units should be watts/m<sup>2</sup>-K. The typographical error will be corrected in the next revision of the Model Description report.

Q306. Equation 6.5-28 in NEDE-32176P is used for mass and heat exchange at a free surface, and is reported to be taken from "Heat Transfer," Third Edition, J.P. Holman.

Q306.1. Provide the specific text (page) in Holman from which the equation is taken, or provide its derivation. Discuss the units as this form does not appear to be consistent with standard formulations.

R306.1. The correlation for the free natural convection in air above a horizontal surface comes from J. P. Holman, Heat Transfer, 3<sup>rd</sup> Edition, New York: McGraw-Hill, Inc. 1972, Table 7-2, and is in British units given by:

$$h = 0.22(\Delta T)^{1/3}$$

Converting this expression to SI units gives:

$$h = 5.6783 * 0.22(1.8 * \Delta T)^{1/3} = 1.52(\Delta T)^{1/3}$$

In 4<sup>th</sup> Edition of Holman, Table 7-2 the coefficient has been reduced slightly and gives the same equation in SI units as:

$$h = 1.43(\Delta T)^{1/3}$$

This correlation was modified to simulate natural free convection in a medium other than air by multiplying by the ratio of the conductivities:

$$h = 1.43 \frac{k_v}{k_{air}} (\Delta T)^{1/3}$$

Using a value of 0.03171 for the conductivity of air at 373K, the above expression becomes:

$$h = 1.43 \frac{k_v}{0.0317} (\Delta T)^{1/3} = 45.11k_v (\Delta T)^{1/3}$$

This above coefficient matches Equation 6.5-28 in NEDE-32176P (45.04) to within 0.2%.

The original model as implemented into TRAC, contained a unit conversion error and also used an unrealistic low value for the

---

<sup>1</sup> This conductivity is consistent with the expression in TRACM (NUREG/CR-6724), where the conductivity of air is given by  $k_v = 2.091E - 4 * T_v^{0.846}$ . A value of 0.0313 is obtained at a temperature of 373K.

conductivity of air. The original expression from 3<sup>rd</sup> Edition of Holman was converted incorrectly to metric units as:

$$h = 5.6783 * 0.22(\Delta T / 1.8)^{1/3} = 1.027(\Delta T)^{1/3}$$

It also used an unrealistic low value of the 0.0228 for the conductivity of air that originated from TRAC-PF1/MOD1 (NUREG/CR-5069). Using this value with the above equation gives:

$$h = 1.027 \frac{k_v}{0.0228} (\Delta T)^{1/3} = 45.04k_v (\Delta T)^{1/3}$$

Q306.2. How was the Sparrow-Uchida degradation factor obtained? Does the correction factor include any bias based on the Sparrow or Uchida data? Is it a “best-estimate” correction? What is the uncertainty in this correction factor and is it considered in the calculations?

R306.2. The precise origin of the tabulated values that are referred to as the Sparrow-Uchida degradation factors is not known. There is reason to believe (as will be demonstrated) that these values were obtained by merging the separate results from Sparrow and Uchida. The tabulated values in the code are used to degrade the condensation heat transfer at the free surface between the mixture and vapor regions when a water level is predicted. The values are tabulated in the code as the ratio of air-to-steam density and are presented graphically in Figure 6.5-1 of NEDE-32176P, Rev. 2. That figure has been reproduced here as Figure 306-1 and additional curves have been added to allow the Sparrow-Uchida degradation curve to be compared with the curves attributed individually to Uchida and Sparrow.

The curve marked “Sparrow 100” in Figure 306-1 is obtained from Figure 10.4 from Collier’s book. Collier’s book is cited in NEDE-32176P, Rev. 2 as Reference [6.5-11]. Collier attributes this and 3 other curves shown in his Figure 10.4 to Minkowycz and Sparrow. The “Sparrow 100” curve that is shown here is the forced convection curve corresponding to a bulk mixture temperature of 100 C. It is clear that all four of the “Sparrow” curves are for relatively low mass fractions for air in steam over the range from 0.0 to 0.1. Here in Figure 306-1, the lowest point in the Sparrow curve has been extrapolated assuming the same slope as suggested by the previous two points.

The so-called Uchida correlation as presented in Eq. 6.6-81 of NEDE-32176P, Rev. 2 cannot apply for relatively low mass fractions because it obviously predicts the wrong trend as the mass of air approaches zero and in fact is undefined in the limit of zero air mass. For Uchida, the functional form of the degradation factor is obvious but the composite

heat transfer coefficient (HTC) must be divided by the undegraded heat transfer coefficient (HTCo) to obtain the degradation function. Appropriate values for HTCo are in the range from around 40 to 70 ( $W/m^2/K$ ). The plots presented here uses  $HTCo = 64.19$  to convert the Uchida heat transfer coefficient expression into the degradation function.

Notice from Figure 306-1 that a transition from the Uchida to the Sparrow degradation functions is needed because the degradation factor due to Uchida alone increases unrealistically for the smaller air mass fractions. The suggested Uchida-Sparrow form does not have this undesirable behavior.

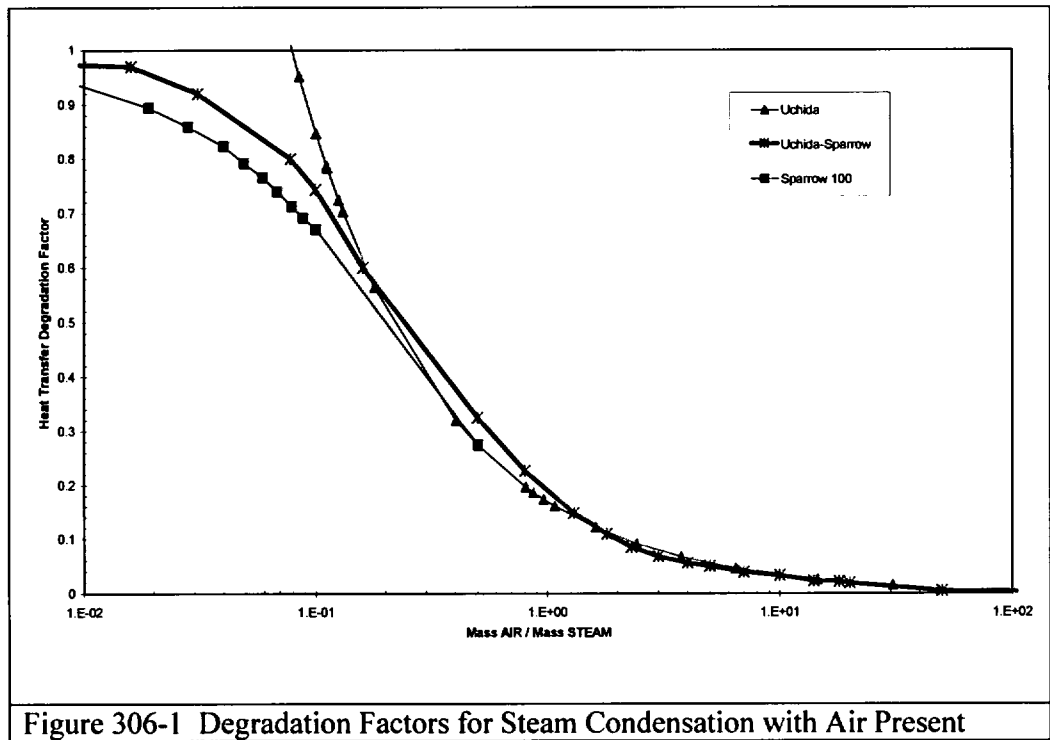
The three curves from Figure 306-1 are replotted in Figure 306-2 using a different abscissa. The abscissa and the V-S and KSP curves in Figure 306-2 are the same as those from Figure 6.6-14 of NEDE-32176P, Rev. 2 except the scale has been expanded to illustrate the similarity between the correlations for very low air mass fractions. As seen in Figure 306-2, the Uchida-Sparrow form predicts the same trend as the Vierow-Schrock (V-S) and Kuhn-Schrock-Peterson (KSP) forms as the air mass fraction becomes smaller except that Uchida-Sparrow gives less degradation than V-S and KSP. Some difference is expected since Uchida-Sparrow is based on a flat surface where V-S and KSP are based on flow inside tubes.

The additional "Sparrow 25" curve in Figure 306-2 corresponds to the curve from Figure 10.4 of Collier's book that represents forced convection at a bulk mixture temperature of 25 C. Notice the similarities between the "Sparrow 25" and KSP curves. The difference between "Sparrow 25" and "Sparrow 100" suggests that the degradation of heat transfer at the mixture-vapor surface due to the presence of air becomes less important as the bulk temperature increases. Similarly, the degradation becomes less important as the pressure is increased. For general TRACG applications, the higher Sparrow-Uchida curve corresponding to higher pressures and temperatures is expected to be more appropriate.

The Uchida-Sparrow degradation factor is intended for use as a best-estimate (unbiased) correlation for stratified mixture-vapor surfaces corresponding to a water level. The uncertainty for Uchida-Sparrow is estimated to be roughly the same as the uncertainty for KSP. Since KSP has an overall uncertainty of 17.6% for steam-air tests but only 7.4% for pure steam tests, the RMS difference attributed to the degradation factor is estimated to be 16%. (A 20% value is suggested as an appropriate uncertainty for KSP on page 6.6-44 of NEDE-32176P, Rev. 2.)

[[

]]



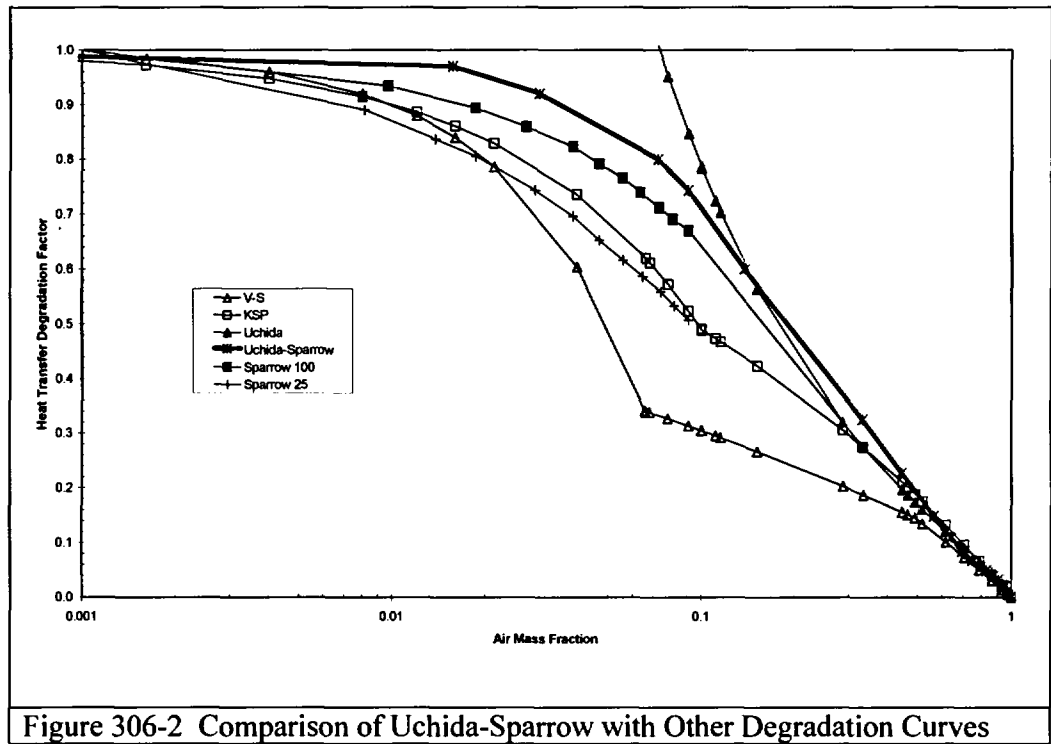


Figure 306-2 Comparison of Uchida-Sparrow with Other Degradation Curves

NEDE-32178P Rev. 1  
GE PROPRIETARY INFORMATION

**Figure 4.2-14 Effect of the Variation of Interfacial Heat Transfer (PIRT 96) on Steam  
Condensation and Wetwell Pressure for SBWR**

Additional information to R306. [[

]]

**WW5: Heat Sources/Sinks**

This PIRT phenomenon is controlled by condensation and wall/structure heat transfer. The uncertainties are the same as the values established for DW2.

**WW6: 3-D Effects in Suppression Pool**

The basic phenomenon associated with this PIRT is the stratification in the suppression pool. Temperature stratification in the pool is important, since it will affect the heat transfer to and from the airspace, which will affect the containment temperature and pressure. Pool stratification data from large-scale tests have shown that the condensed steam from the main vent discharge heats the portion of the pool above the vent. The TRACG model predicts complete mixing of steam discharged from the main vent, SRV, and PCC, with little or no stratification. Based on TRACG sensitivity studies (discussed in Section 4.1.3), a bounding model was developed which forces stratification in the pool by setting the cell face areas of the adjacent cells at levels below the entry point of steam to zero. This prevents mixing between the cells on that level and the energy flow is mixed only with cells at and above entry level.

{

}

**Figure 4.2-14 Effect of the Variation of Interfacial Heat Transfer (PIRT 96) on Steam  
Condensation and Wetwell Pressure for SBWR**

{

}

**Figure 4.2-15 Comparison of PANDA Test M3 Wetwell Airspace Temperature with  
TRACG Predictions for WW1 Pressure.**

**Supplementary Information in Response to RAI 306**

The correlation used for interfacial heat transfer at a horizontal 'level' (e.g. surface of the suppression pool) in TRACG is attributed to Holman. This correlation is given in metric units as

$$h = 1.43 (\Delta T)^{1/3} \quad (1)$$

It was generalized in TRACG by explicitly accounting for the conductivity of the fluid, as:

$$h = 45.04 k(\Delta T)^{1/3} \quad (2)$$

This correlation is strictly applicable only to the case of turbulent flow over a solid horizontal plate with the hot side facing up.

In TRACG, this equation is applied to both sides of the interface (liquid to interface and vapor to interface). So the temperature condition of a hot horizontal plate facing up (or cold plate facing down) will not be met for both sides. For the situation of turbulent flow over a hot horizontal plate facing down, an alternate correlation is available as:

$$h = 0.12 (\Delta T/L)^{1/4} \text{ (British units)} \quad (3)$$

$$h = 0.59 (\Delta T/L)^{1/4} \text{ (Metric units)} \quad (4)$$

For  $L = 2 \text{ m}$  and  $\Delta T = 100\text{K}$ , Equation 1 gives a heat transfer coefficient of  $6.6 \text{ W}/(\text{m}^2\text{K})$ ; Equation 4 gives a value of  $1.57 \text{ W}/(\text{m}^2\text{K})$ .

[[

]]

Reference:

[306-1]W. H. McAdams, Heat Transmission, Third Edition, McGraw-Hill, New York, 1954, pages 172 and 180.

Q307. In NEDE-32176P, Rev 1, it is stated that “If the containment contains significant amounts of horizontal surface area, care should be taken to model this area with a non-horizontal equivalent area since no condensation heat transfer will be predicted using  $g \cdot \cos(0^\circ) = 0.0$ .”

Q307.1. For the ESBWR, is this a concern? If so, how are horizontal surfaces treated in the calculations? Provide a description of the heat structures (wall, piping, etc.) considered in the calculations in the drywell, the suppression pool and the wetwell and the mass and heat transfer correlations being used for condensation, convection and, if appropriate, radiation (based on the expected flow regime - laminar or turbulent, and orientation - vertical or horizontal). Identify the horizontal surfaces that are being treated as non-horizontal.

R307.1. See the response to RAI298 for the discussion of ESBWR containment heat structures and the representation of non-vertical heat slabs in the containment portion of the TRACG model, which has only vertical heat slabs. It should be mentioned that most containment internal heat structures other than a few vertical wall heat slabs in the ESBWR design were conservatively ignored. The heat transfer correlations used for containment modeling are discussed in the response to RAI65.

Q307.2. In Section 7.11, it is stated that the Uchida correlation is available as an option for a lower bound for condensation, which would be consistent with guidance provided in Standard Review Plan. Is this option used in the calculations?

R307.2. Yes, the Uchida correlation is available as an option for a lower bound for condensation. However, this option is not used in the base case calculation. Results of sensitivity study show that the impact of using this option on the long-term DW pressure is small, about +0.2 psi.

In general, the vertical heat slabs have a very small impact on both the short-term and long-term DW pressure. Sensitivity studies were performed by changing the surface areas of the vertical heat slabs in the DW/WW wall and the WW outer wall. [[

]] In summary, the impact of condensation modeling on peak DW pressure is small, especially in comparison to the margin to the design pressure [[ ]]

Q308. In NEDE-32176P, Rev. 1, it is stated that wall friction correlations are used in the same way as in other codes, like GOTHIC “which are specifically meant for containment analysis, and have been expensively qualified for these applications.” Provide a reference to the qualification of the TRACG 3-D treatment of wall friction for containment calculations.

In addition, it appears that the modeling in TRACG is based on a presumed flow pattern (ref. Fig. 6.2-1), which is reflected in the nodalization. It is also stated that when large 3-D cells are used, the error could be larger when using the fully developed flow correlations. Only one comparison is made for two cells of approximately equal size based on an assessment of the Reynolds number. The basic data used to develop the models is based on flow in pipes with diameters in the range of a few to several millimeters, or flow in rod bundles. Based on these observations is the treatment of wall friction on containment surfaces modeled in a conservative manner? Provide a justification for applying the models to these surfaces. How does the error in the wall friction influence the integrated system response, keeping in mind that there are several models used for containment, which have errors, or uncertainties identified with them?

R308. [[

]]

It should be noted that wall friction in large open volumes is not a significant factor in the pressure distribution within the containment. The dominant pressure differences are between different regions of the containment. These pressure

drops are through restrictions such as horizontal vents and the PCCS, which are typically pipes and readily amenable to the calculation of pressure drop.

Most containment codes (e.g. CONTAIN [Code Manual for CONTAIN 2.0: A Computer Code for Nuclear Reactor Containment Analysis, NUREG/CR-6533, December 1997]) treat the whole drywell as one cell, and wall friction and pressure gradients within this large cell are not even considered. This again points out the lack of importance of the wall friction correlations used in TRACG for the calculation of the overall containment pressure and temperature response.

(It should be noted that small pipes in BWRs have diameters of several centimeters rather than millimeters as stated in the question.)

### Q312. Flow Regime Maps

The flow regime maps provide the critical information about the interfacial area density and the shape for the two-fluid formulation.

The ESBWR containment consists of many regions where two-phase flow conditions exist. These regions vary in size and orientation. The drywell and suppression chamber (wetwell) consists of large volumes, which may have a condensate film on the walls and droplets in the gas phase. The suppression pool receives an inflow from a jet mixture of noncondensable gas and steam which will break-up in bubbles. There are also other liquid pools with free surfaces. The horizontal vents undergo vent clearing and two-phase flow during early blowdown. The heat exchangers of the PCCS have small diameter tubes with downward film flow on the wall.

The transition between annular flow and dispersed flow regimes is defined by entrainment inception. However, no information about entrainment inception is provided in NEDE-32176P. The entrainment rate correlation described in the report, is based on pipe data with diameters less than 0.032 meters and, therefore, the entrainment correlation does not appear to apply to any part of the containment except the PCCS tubes.

A liquid film is expected on the heat structures and liquid droplets in the drywell atmosphere. However, the droplet field can not be predicted by the entrainment criteria in the code as the mechanism is fogging and not shear at the interface. Therefore, the flow regime map does not appear to apply to the drywell and suppression chamber.

Q312.1. Justify the use of the flow regime map for calculating flows (velocities) near containment surfaces and for intercell flow between the large, 3-D cells used to model the containment volumes. It appears that the nodalization drives the determination of flow regimes and that there could be an inconsistency description of the flow regime (and cell fluid

properties) at a 3-D cell boundary, which does not represent a physical structure.

- R312.1. TRACG uses a relatively simple flow regime map as shown in Figure 5.1-1 of NEDE-32176P, which consists basically of two distinct patterns: (a) liquid-continuous at low void fractions, and (b) vapor-continuous at high void fractions. A transition zone separates the two primary regimes. The liquid-continuous regime applies to the single-phase liquid flow and bubbly/churn flow regimes. The vapor-continuous regime applies to the annular, dispersed droplet and vapor flow regimes. The transition regime involves churn to annular and churn to droplet regimes depending on the void fraction, flow rate and other variables.

The same flow regime map is used for vertical and horizontal flows. For horizontal flow at low velocities, a transition to stratified flow is calculated based on a critical Froude number.

These flow regimes were primarily intended for pipe geometries, but have also been successfully applied to large three-dimensional cells, e.g. in the lower plenum of the reactor vessel. The key output from the flow regime map is the choice of the interfacial shear model that determines the void fraction in these cells. Void fractions calculated in large plena of reactor vessels are reasonable and agree with data obtained from tests facilities such as PSTF and EBWR [NEDE-32177P].

[[

}}

In summary, the TRACG flow regimes, while simple, should be adequate for containment calculations. This is substantiated by comparisons of TRACG calculations with Mark II and Mark III simulations in the PSTF for the short term blowdown (TRACG Qualification for SBWR, NEDC-32725P, Rev.1, Sections 5.5 and 5.6) and the PANDA test facility for the long term response (Section 5.7).

- Q312.2. Describe the model for entrainment inception from films on the containment walls.
- R312.2. The entrainment correlation used in TRACG is described in Section 5.1.2 of NEDE-32176P. When a cold surface with a temperature less than the saturation temperature is present in a vapor occupied cell, condensation will be initiated with a film forming on the wall. TRACG calculates the fraction entrained as droplets based on the correlation for the entrained fraction, which is a function of the vapor velocity and the liquid Reynolds number. The remaining liquid is available to form a film on the wall. The liquid film flow rate is checked against the minimum required to form a stable film over the surface. Smaller amounts of liquid will only cover the surface partially. As the liquid flow rate increases, a part of the film will be entrained as droplets, depending on the vapor velocity.

Q312.3. There is also a question about the applicability of the pipe flow regime map to the drywell, the suppression chamber (wetwell), the suppression pool and to the downward flow in the PCCS tubes and return lines and the vertical sections of the horizontal vents. The Tables 6.1-1 and 6.2-1 (NEDE-32176P, Rev 1) summarize GE's assessment of flow regime maps for different containment regions. The indirect assessment through interfacial shear and mass transfer data base covers the pressure, void fraction and mass flux range, but the diameter range is not covered for the drywell and suppression chamber and there is a large ("by about 15%") uncertainty in applying the correlations to these volumes.

How is this uncertainty treated in the calculations? How was the uncertainty value obtained and could it be larger? How does the uncertainty in the interfacial shear and mass transfer influence the integrated system response, keeping in mind that there are several models used for containment which have errors or uncertainties identified with them?

R312.3. The applicability of the flow regime map to the large drywell, wetwell and suppression pool regions was addressed in response to (312.1) above. [[

]]

Q313. Wall Friction

Wall friction and momentum transfer is important in the PCCS tubes and the horizontal vents. The friction on the containment walls is also computed in the code. The single phase friction factors are calculated from the curve fit to Moody's diagram, which is valid for pipe flows. The data base covers a very large Reynolds number range. However, the applicability to the drywell geometry and large diameter channels is questionable. This model was assessed with the data base limited to small diameters, which covers the PCCS tubes, but is too small for horizontal vent. Furthermore, the two-phase multipliers were based on the data with lower steam qualities while in the drywell and in the horizontal vents, the quality could be close to 100%. Furthermore, it is not clear if the two-phase multiplier is valid for down flow as expected in the PCCS tubes and in the horizontal vents.

Q313.1. Provide justification for using this model for the PCCS tubes, the horizontal vents and the containment wall structures.

R313.1. Wall friction is not an important phenomenon in the large containment volumes. Please see the response to RAI 308 for a more detailed discussion.

[[

]]

Q313.2. There is another uncertainty in the implementation of the friction factors in the 3-D component used for containment. It is not clear how the friction factor in the transverse direction are estimated from the Moody's curve, which was developed from vertical tube flows.

How is the traverse friction factor obtained for use in the large 3-D cells? How is friction handled on horizontal surfaces, for example the drywell floor or the diaphragm floor?

R313.2. Transverse friction factors are only calculated for cells that have frictional resistance in the transverse direction. An example is the flow through control rod guide tubes in the lower plenum of the reactor vessel. The loss coefficient due to contraction and expansion through the rows of guide tubes leads to a transverse friction coefficient. These are typically form losses and not Moody friction factors. In the open drywell volume there are no transverse resistances to flow. The wall friction is calculated from cell center to cell center, based on the velocity, which is calculated at the cell interface. Thus, the component of the cell velocity parallel to the wall is used in the calculation of the wall shear. Friction at a horizontal surface (such as the floor) will be calculated using the horizontal component of the velocity in the cell next to the floor. The standard wall friction correlations will be employed in this calculation based on the Reynolds number that uses the scalar value of the velocity vector. The magnitude of the velocity is very close to the component of the velocity parallel to the wall.

Q313.3. An additional uncertainty is in the partitioning of the wall friction contribution between two phases. The correlations for single phase flow along with two-phase multiplier are for mixture models and are being used for two-fluid formulations. The report does not indicate the method used to dividing wall friction between the two phases.

Describe the method (model) for dividing the wall friction between the two phases.

R313.3. [[

]]

Q314. Wall Heat Transfer

Wall heat transfer occurs in every component in the containment. The important areas are heat transfer to vertical and horizontal structures and inside and outside of the PCCS tubes.

The single phase heat transfer is based on Dittus-Boelter for forced flow and McAdams correlation for free convection on vertical walls. However, applicability of these correlations for large open spaces has not been shown.

The Dittus-Boelter correlation was developed from pipe data and requires the hydraulic diameter for the Reynolds (Re) number calculation. Similarly, the McAdam's correlation also requires the hydraulic diameter for computing the Grashof (Gr) number. These correlations have been implemented with hydraulic diameter based on cell size. If the cell hydraulic diameter is computed with only the wetted perimeter, the hydraulic diameter may be correct.

Q314.1. Provide a justification for using these correlations for the containment surfaces. It would be more appropriate to use correlations for flat plates, which are based on wall length. Can it be shown that the use of an appropriately calculated hydraulic diameter to represent the structure characteristic length will result in a conservative heat transfer calculation? Will laminar conditions exist in the containment (for example based on Gr number) for which additional correlations would be needed? In this case, or if a correlation for a flat plate were to be used to better represent the structure, the hydraulic diameter (characteristic length) would not necessarily cancel out based on a  $Gr^{1/3}$  correlation.

R314.1. [[

]]

Q314.2. The correlations used to model heat transfer require an estimate of the Reynolds number, but it is not shown how it is estimated. For the 3-D formulation, there are three components of velocity and the code document does not indicate which component of the velocity is used to estimate the Reynolds number. The other uncertainty is in the use of the cell edge velocity. As the cells are large, the velocity is averaged over a large area and the effect of a no slip condition at the wall is negligible. The correlations were developed from pipe flow data where the average velocity is affected much more by the no slip condition at the wall. Furthermore, the wall heat transfer is partitioned between two phases but it is not explained how this partitioning is performed.

How is the Reynolds number obtained for use in these correlations?  
How does the uncertainty in obtaining the Reynolds number influence the integrated system response, keeping in mind that there are several models used for containment, which have errors, or uncertainties identified with them?

R314.2. [[

]]

Q314.3. Describe the method (model) for dividing the heat transfer between the two phases.

R314.3. [[

]]

Q314.4. For horizontal surfaces, TRACG uses the same heat transfer correlation as for vertical walls. The assessment provided indicates that for large  $Gr \times Pr$ , the heat transfer coefficient is significantly over predicted.

Provide an assessment of the effect of this discrepancy on the long term pressure calculation. How does the uncertainty in obtaining the heat transfer from horizontal surfaces influence the integrated system response, keeping in mind that there are several models used for containment which have errors or uncertainties identified with them?

R314.4. [[

]]

Q314.5. The heat transfer from a floor will be different than from a ceiling. This is not distinguished in the code. How is this difference treated in the calculations?

R314.5. TRACG uses the same heat transfer correlation for free convection from hot surfaces facing up or down. As stated in response to the previous parts of this RAI, the correlation is in good agreement with data for the former situation but overestimates the heat transfer for the latter case. See response above for further discussion of the impact of the assumption.

Q314.6. The other area of importance is heat transfer due to condensation on cold surfaces. With the accumulation of noncondensable gases, the condensation rate will degrade. TRACG models this heat transfer with the Nusselt's correlation for condensation and degradation due to noncondensable gas through use of the minimum value from the Kuhn-Schrock-Peterson (K-S-P) correlation, which was derived from vertical pipe data, and the Uchida correlation. The data base for these correlations covers pressure up to 4.5 bars which is appropriate for containment application.

In principle, the staff accepts such an approach. However, the applicability of this model to the containment analysis needs to be discussed in more detail given the fact that the nodalization may affect the noncondensable gas concentration near the interface and therefore, the heat transfer degradation.

R314.6. [[

]]

Q314.7. How was the degradation factor obtained? Does the correction factor include any bias based on the data used to develop the degradation factor? Is it a “best-estimate” correction? What is the uncertainty in this correction factor and is it considered in the calculations?

R314.7. In the K-S-P correlation, the factor  $f_2$  accounts for the degradation due to noncondensibles. It is obtained by correlating the ratio of the condensation heat transfer coefficient with noncondensibles to the heat transfer coefficient without noncondensibles. The form of the correlation is given in Section 6.6 of the TRACG Model Description [NEDE-32176P]. It is intended to be a best fit to the data. The uncertainty in the K-S-P correlation was addressed in the TRACG Application Report [NEDC-33083P] and is excerpted below.

[[

]]

Q314.8. The two-phase flow in the PCCS tubes is modeled with the conventional approach for a film flow regime. The critical aspect of this component is the heat transfer inside the tubes. The correlation used by TRACG for single phase flow and condensation heat transfer is appropriate as it was developed from tube data of the same diameter as the PCCS tube, and for pressures up to 5 bars.

However, implementation as described in Section 6.6.11.1 has an apparent error in Eq 6.6-60. The average heat transfer coefficient is a function of the length over which averaging was done and a derivative with respect to [z] should account for this dependency. This model should be revisited and if simplifying assumptions are being made, describe the derivation of the equation as presented.

R314.8. Equation 6.6-60 is correct. This can be readily verified by recognizing that

$$\bar{h}(z) = \frac{1}{z} \int_0^z h(x) dx$$

Combining with Equation 6.6-59 and Equation 6.6-56,

$$Re_l = \frac{4}{\mu_l h_{fg}} (T_s - T_w) \int_0^z h(x) dx$$

Differentiating with respect to z,

$$\frac{d(Re_l)}{dz} = \frac{4h}{\mu_l h_{fg}} (T_s - T_w)$$

### **Supplemental Information for RAI 314.1**

Question:

PCCS Performance During Blowdown

In response to RAI 314.1, it was stated that the PCCS removes about 15% of the blowdown energy. In response to RAIs 335 and 340, it was stated that the PCCS vent submergence is deep enough to avoid stratification but not so deep that it stops the vent function.

1. Provide a road map locating the source of data that demonstrates the PCCS performance (to condensing steam) during the blowdown portion of the event. Under these conditions (flow rates, steam and noncondensable fractions) will the PCCS condense 100% of the steam?
2. If the PCCS cannot condense 100% of the steam, provide a road map locating the source of the data that demonstrates that the PCCS vent submergence is low enough to condense the steam in the suppression pool, such that only noncondensable gases enter the wetwell.

Response:

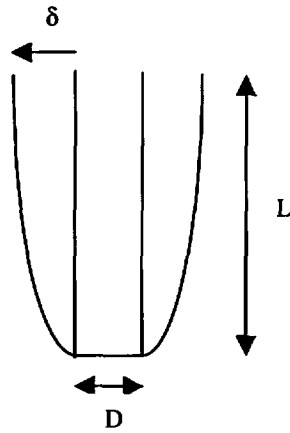
1. The attached Figure 1 shows the flow rates through the PCCS calculated by TRACG for the first 2000 seconds of the transient. The flow is for 3 PCC units lumped into one in the TRACG model. Hence the flow per PCC is the flow shown in the figure divided by 3. Most of the flow in this phase flows through the main vents. The PCC flow varies from approximately [ ]. Figure 2 shows the noncondensable partial pressure at the PCC inlet during the same time period. After clearing out the noncondensibles above the steam line break location in the first couple of seconds, the flow is essentially all steam until 10 minutes into the transient.

The flow rate of [ ] is within the test database of the PANTHERS tests. At PANTHERS, a full SBWR-scale PCC unit was tested over a steam flow range between [ ]. Steam-air tests were also conducted over the same steam flow range combined with an air flow range of [ ] (Table A.3-2 of ESBWR TAPD, NEDC-33079P). The ESBWR PCC has similar dimensions but has [ ] tubes.

The steam only tests were conducted allowing the PCC pressure to adjust such that all the incoming steam was condensed. Figure 4.1-14 in NEDC-32725P, TRACG Qualification for SBWR, Vol. 1, shows that TRACG calculated the required pressure to condense the steam flow conservatively. (The data point on the right side of the figure corresponds to a steam flow rate of [ ]). Figure 1 also shows that a part of the steam flowing through the PCCs is not condensed. The uncondensed steam flow drops from [ ] to a small value at 300s. Beyond this time, a combination of increase in PCC pressure and reducing steam flow through the PCCs allows the PCC condensing capacity to catch up with steam flow.

2. The most relevant data for condensation efficiency of steam discharged through the PCC vent can be found in Reference 1. In the LINX test facility, tests were performed with a vent pipe with an I.D. of 40 mm and submergences ranging from 37.5 to 75 cm. Steam flow rates ranged up to 50 g/s. This mass flux corresponds to a flow rate of [ ] in an ESBWR-size vent of [ ]. The test data showed that the steam was fully condensed in all the tests, with even low submergences until the pool temperature got to a few degrees below saturation. At typical subcoolings, the steam was condensed at a distance of 10 to 15 cm ( $L/D = 3$  to 4) above the vent discharge. A simple argument can be made that condensation will be complete for a pipe of a different size at the same  $L/D$  or less when the mass flux is the same. Assuming equal  $L/D$ , the required submergence is of the order of [ ].

[Justification: For a discharge steam flow rate  $W$ , assume an interfacial area  $A_i$  is needed for complete condensation. The steam flows upward a distance  $L$  as a growing thermal plume around the vent pipe of diameter  $D$  until it is condensed. The required interfacial area is proportional to the plume volume.



For a given subcooling,

$$W = k_1 A_i = k\pi D\delta L$$

$$W/\pi D^2 = k\delta L/D$$

$\delta$  varies as  $L^{1/2}$  to  $L$

Thus,

$$W/\pi D^2 = KL^{1.5 \text{ to } 2}/D$$

For the same mass flux, the condensation length  $L$  will vary as the diameter to the  $1/2$  to  $2/3$  power.]

In the time frame of interest, the main vents are also open. The mixing in the suppression pool will be far greater than that for a PCC vent discharging into a quiescent pool. This will help condensation of the steam even more efficiently.

Reference 1: C. De Walsche, F. de Cachard, "Experimental Investigation of Condensation and Mixing during Venting of Steam/Non-Condensable Gas Mixture into a Pressure Suppression Pool", ICONE-8565, Proceedings of ICONE 8, 8<sup>th</sup> International Conference on Nuclear Engineering, April 2-6, 2000, Baltimore, MD, USA

[[

**Figure 1: TRACG plot: 3 PCC inlet and vent flow for 2000 sec**

]]

Figure 2: TRACG plot: 3 PCC inlet total and air partial pressure for 2000 sec

**Q315. Interfacial Momentum Transfer**

Interfacial momentum transfer occurs at interfaces and affects the distribution of the liquid and vapor phases and therefore the void fraction. It is important to predict the void fraction accurately as it has an effect on heat transfer and the two-phase multipliers for wall friction and local pressure loss coefficients. The containment has many regions where interfacial momentum transfer needs to be modeled, such as the film on the wall (or the spillover from the vessel in the drywell), the droplet phase, the PCCS tube film flow, the flow in the horizontal vents and the flows over liquid surfaces in the GDCS tank, the suppression pool and the condensate pools that might be created in the drywell or other regions.

The general approach in TRACG is to use mixture information or a drift flux correlation and to partition it into interfacial shear for different regimes. The description lacks an assessment of the applicability of this approach to model the containment. The areas where the models may not be applicable include the drywell, the horizontal vents and the suppression pool. In the drywell area, the liquid will be in the form of films on structures and fog in the atmosphere. The flow regime maps will not predict a film flow and therefore, the code may select, for example, a dispersed flow regime. Furthermore, the fogging in the bulk due to the cooling of the steam will likely lead to a droplet flow regime. However, the size of the drops should not be determined from a Weber number equal to 12 as this critical Weber number represents the largest drop size, while a fog will consist of much smaller drops. The fogging phenomenon will produce a spectrum of drop sizes which cannot be represented by a drop size calculated from the critical Weber number, and thus resulting in a different behavior of the droplets.

Q315.1. Provide a discussion of the applicability of the TRACG models to address these issues for interfacial momentum transfer- void fraction, two phase multipliers for wall friction, drop formation and the treatment of drops, and interfacial momentum - as they relate to the evaluation of containment performance.

R315.1. [[

]]

Q315.2. The other area where the applicability of TRACG is not certain is in the horizontal vents as the interfacial shear was derived from vertical flow data and it may not apply to horizontal vents. No assessment has been presented for its application to the horizontal vent flows.

Provide a discussion of the applicability of the interfacial shear model in TRACG for the horizontal vents.

R315.2. [[

]]

Q315.3. The suppression pool receives a mixture of steam and noncondensable gases from different sources (horizontal vents, safety relief valves and PCCS). The steam condensation will depend upon the residence time of the bubble and the interfacial area. The report does recognize the difficulty of modeling the pools (see the text below Eq. 6.1-33, NEDE-32716P).

If the void fraction is over-predicted, then the interfacial shear is under predicted and bubbles will have larger residence time and larger interfacial area leading to more condensation. It is recognized that the design philosophy for the vents to the suppression pool is such that 100% of the steam is condensed in the pool (no steam escapes the pool surface into the wetwell gas space).

TRACG handles the condensation of the steam in the suppression pool based on the Bubbly/Churn flow model described in Section 6.1.3 of NEDE-32716P, but does not account for degradation due to the presence of noncondensable gases. Are the expected conditions (pressure, hydraulic diameter and mass flow rate) within the range for which the model is applicable? Is it conservative to neglect the degradation from the presence of noncondensable gases? How is the over-prediction of the void fraction addressed in the calculations?

R315.3. The reviewer apparently misunderstood the text below equation 6.1-33. The data for low vapor flow rates in a pool were used to develop a correlation for the drift velocity under these conditions. This correlation is given in Equations 6.1-34 and 6.1-35. For large hydraulic diameters and low volumetric fluxes, TRACG modifies the coefficient in the drift

velocity (Equation 6.1-30) according to Equation 6.1-34. TRACG calculations are compared with the data of Wilson and Bartolomei in the report TRACG Qualification NEDE-32177P, Rev.2, Section 3.1.3. The agreement between the measured and predicted void fractions is excellent. The range of deviations is between  $\pm 2\%$ .

[[

]]

Q315.4. Are there any data and are there any TRACG comparisons to that data where the vent submergence was not low enough to prevent steam from escaping the pool?

R315.4. There are no data where a significant amount of uncondensed steam escaped from the pool surface. The vent submergences are designed to prevent this occurrence.

#### Q316. Interfacial Heat and Mass Transfer

The heat and mass transfer at the interface are related and predictions of one will provide an estimate of the other. The model consists of predicting the flow regime, interfacial area density and heat transfer coefficients at the interface.

Q316.1. It is our understanding that the liquid side interfacial heat transfer coefficient is obtained from a correlation developed for heat transfer over evaporating drops. Provide a description of the physical process being modeled and justify its use for this situation.

R316.1. TRACG uses the Lee-Ryley correlation for the vapor side interfacial heat transfer for droplet flow.

$$\text{Nu}_d = 2 + 0.74\sqrt{\text{Re}_d} \text{Pr}_v^{0.33}, \quad \text{Re}_d = \frac{\rho_v v_{rd} d_d}{\mu_v}$$

This correlation was developed from data for evaporating droplets. Since the flow around a droplet is very similar to the flow around a vapor bubble for bubbly flow, it is assumed that the same correlation is applicable to the liquid side interfacial heat transfer for bubbly flow. For liquid, the Prandlt number dependence was dropped, since  $\text{Pr} \approx 1$  for water.

$$Nu_b = 2 + 0.74\sqrt{Re_b}$$

$$Re_b = \frac{\rho_l v_{rb} d_b}{\mu_l}$$

TRAC-M (NUREG/CR-6724) uses a combination of the Whittaker correlation for low Reynolds numbers and the Chen & Mayinger correlation for high Reynolds numbers to calculate the liquid side interfacial heat transfer for bubbly flow:

$$Nu_b = 2 + (0.4\sqrt{Re_b} + 0.06 Re_b^{2/3}) Pr_l^{0.4} \quad \text{Low Re (Whittaker)}$$

$$Nu_b = 0.185 Re_b^{0.7} \sqrt{Pr_l} \quad Re < 10^4 \text{ (Chen \& Mayinger)}$$

$$Nu_b = 116.7 \sqrt{Pr_l} \quad Re > 10^4 \text{ (Chen \& Mayinger)}$$

These correlation are compared in Figure 316-1 for Pr = 1.0.

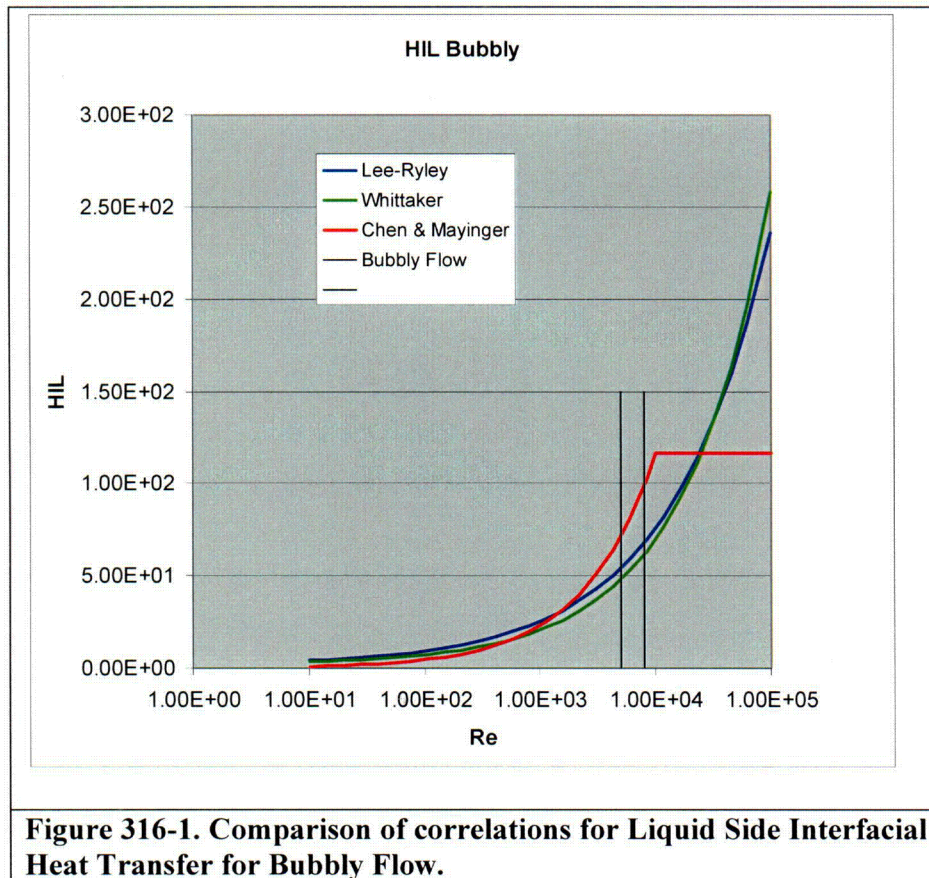


**Figure 316-1. Comparison of correlations for Liquid Side Interfacial Heat Transfer for Bubbly Flow.**

For bubbly flow the Reynolds number for the bubbles are typically in the range of 5000 to 8000. For this range the Whittaker correlation is 10% lower than the Lee-Ryley correlation, and the Chen & Mayinger correlation is approximately 40% higher than the Lee-Ryley correlation. These differences are compatible with the uncertainty range for the correlations.

The good comparison to void fraction data and plant transient data as demonstrated in the TRACG Qualification (NEDE-32177P) justifies the application of the Lee-Ryley for the interfacial heat transfer. In the TRACG application (NEDE-32178P) a factor of 2 (-50%, +100%) uncertainty is assumed for liquid side interfacial heat transfer. This uncertainty more than covers the difference between the above correlations.

Q316.2. It is our understanding that the vapor side interfacial heat transfer coefficient is obtained from the conduction heat transfer solution for a solid sphere with a correction for internal convection and the degradation due to noncondensable gases is accounted with the a degradation factor. If this is correct, provide a description of the physical process being modeled and justify its use for this situation.

R316.2. Assuming no flow inside a vapor bubble, the heat transfer between the vapor in the bubble and the interface, is given by thermal conduction. For a spherical particle with an equilibrium temperature profile, the heat transfer due to thermal conduction is equivalent to a heat transfer coefficient given by:

$$h_{iv,b} = \frac{2}{3} \pi^2 \frac{k_v}{d_b}$$

Due to the movement of the bubble relative to the liquid, there will be natural circulation inside the bubble. An empirical factor  $2.7(\mu_l/\mu_v)$  is applied as an enhancement to the pure conduction heat transfer to give Equation 6.5-9 in the TRACG Model Description (NEDE-32176P):

$$h_{iv,b} = \frac{2}{3} \pi^2 \frac{k_v}{d_b} [2.7 \frac{\mu_l}{\mu_v}]$$

For typical bubbly flow, this correlation gives a heat transfer coefficient in the range of 2000-8000. TRAC-M, for comparison, uses a constant value of 1000 without any justification.

It is assumed that steam and air are mixed perfectly inside a bubble, and no degradation is applied for condensation heat transfer. This is a

reasonable assumption given the internal circulation and the small size of the bubbles.

For bubbly flow, the interfacial heat transfer is the dominant heat transfer to the vapor, and with the assumption that the interface is at the saturation temperature, the vapor temperature will follow the saturation temperature. The thermal time constant for the bubbles with the heat transfer coefficient given by the above expression or the value from TRAC-M will typically range from 75 msec. to less than 1 msec.

With the only significant heat transfer to bubbles coming from the interface, which is at the saturation temperature, and the low thermal heat capacity of the bubbles, the results are insensitive to the exact value of the vapor side interfacial heat transfer.

**List of Changes in TRACG04 between the ESBWR Version Provided to the NRC  
and 9-Apr-2004 Program Library Version**

Changes that might affect ESBWR results slightly

[[

]]

Changes that apply to operating BWR LOCA/AOO calculations

[[

]]

Output capabilities added

[[

]]

Corrections/changes to avoid abortions and improve reliability

[[

]]

Response to NRC Question on Model LTR NEDE-32176 (Rev 1 and 2)  
Equation 6.6-61

Question:

On page 6.6-38 for NEDE-32176P, rev 1, third equation, it appears that there is an extra term that should not have been included in the equation. This is the hfg term. Please take a look at this equation, and let us know whether the equation is correct.

Response:

There are typographical errors in Equations 6.6-61 (indicated above) and in Equation 6.6-62. These are corrected in the attached corrected Page 6.6-38 for NEDE-32176 Rev. 1.

These equations are intermediate steps in the derivation of Equation 6.6-67 for the Nusselt condensation heat transfer coefficient. Equation 6.6-67 is correct in the report. The implementation of the equation for the condensation heat transfer coefficient in TRACG has been checked and is also correct.

A simple energy balance yields:

$$\Gamma(z) = \frac{\bar{h}(z)}{h_{fg}} (T_s - T_w) z \quad (6.6-59)$$

where  $\bar{h}(z)$  is the average value of the film heat transfer coefficient  $h_{ref}$  from the start of condensation to  $z$ .

Combining Equations 6.6-56 and 6.6-59 and differentiating

$$d(Re_\ell) = \frac{4h_{ref}}{\mu_\ell h_{fg}} (T_s - T_w) dz \quad (6.6-60)$$

Now, combining Equations 6.6-58 and 6.6-60

$$\frac{2}{3} Re_\ell^{-1/3} = 0.052 \frac{g^{1/3} \rho_\ell^{2/3} k_\ell}{\mu_\ell^{2/3}} \cdot \frac{1}{4h_{ref}} \quad (6.6-61)$$

Using Equations 6.6-54 and 6.6-61 and solving for  $\delta$  gives the turbulent film thickness

$$\delta = 51.3 \left( \frac{\mu_\ell^2}{\rho_\ell^2 g Re_\ell} \right)^{1/3} \quad \text{or} \quad \delta = 32.3 \left( \frac{\mu_\ell^3}{\rho_\ell^2 g \Gamma} \right)^{1/3} \quad (6.6-62)$$

for  $Re_\ell > 2000$ .

As stated above, the two-part correction takes the form:

$$h_{\text{condensation}} = f_1 f_2 h_{ref} \quad (6.6-63)$$

where  $f_1$  is a factor greater than unity, which accounts for increased heat transfer due to shearing (thinning) of the condensate film layer. The factor,  $f_2$ , is less than unity and accounts for the decrease in heat transfer resulting from the presence of noncondensibles.

The factor  $f_1$  is given by:

$$f_1 = 1 + 2.88 \times 10^{-5} Re_m^{1.18} \quad \text{for } Re_\ell \leq 1000 \quad (6.6-64)$$

with the limit of  $f_1 \leq 3$  and

$$f_1 = 1 \quad \text{for } Re_\ell > 2000$$

## **NRC RAIs and Responses**

**TRACG Qualification  
NEDE-32177P, Rev. 2**

**Note: RAI responses including data files that cannot be read on a PC are not included.**

- Q89. Section 3.1.1.1 (p. 3-4) - The 8x8 rod bundle simulated a top-peaked power distribution. Was the power to the rods uniform? Are the heat fluxes noted in Table 3.1-2 axially averaged values for all 64 rods?
- R89. The axial power distribution was top peaked. The radial rod to rod power distribution was [[  
]] The axial peaking was approximately 1.55 and the local rod to rod peaking was [[  
]] The heat flux in Table 3.1-2 is the [[  
]] for all the rods.
- Q90. Section 3.1.1.2 (p. 3-6) - What is the uncertainty in using a single channel TRACG model to simulate a rod bundle test? Was the sub-channel effect negligible in the FRIGG test?
- R90. TRACG uses a one-dimensional model for the fuel channel and calculates channel average properties. The void fraction measurement from the FRIGG utilized eight individual X-ray beams and produced the average void fraction for the channel. [[

]]

- Q91. Section 3.1.1.5 (p. 3-10) - The sensitivity study investigated the effect of axial nodalization. How are sub-channel effects and the sensitivity to multiple parallel channels addressed?
- R91. TRACG utilizes a one-dimensional model for the fuel channel. [[  
]], see Section 6.1 in NEDE-32176P. The GEXL correlation for critical power empirically [[  
]] See also the response to Question 90.

Qualification for parallel channels has been addressed in the SSTF qualification in the TRACG Qualification LTR (NEDE-32177P) Sections 4.3 and 5.3, and has also been addressed in the nodalization studies on channel grouping in the TRACG Qualification LTR (NEDE-32177P) Section 6.9.

- Q92. Section 3.1.3 (p. 3-14 to 3-17) - In the Bartolomei tests void fraction was measured at different elevations. How is the void fraction shown in Figure 3.1-13 derived from the test data? A hot water coil provided heating to the test section and there should be an axial variation in the vapor volumetric flux in the heated

section. Are the void fraction data shown in Figure 3.1-13 taken in the unheated section above the hot water coil?

- R92. The void fraction measurements in the Bartolomei test were obtained from gamma ray attenuation data obtained in the adiabatic region above the heater coils. The test facility and the data are described in: G. G. Bartolomei, V. A. Suvorov and S. A. Tevlin, "Hydrodynamics of Steam Generation a Two-Circuit Nuclear Power Plant," Teploenergetika 10(1), p 52-57, 1963.
- Q93. Section 3.1.4 (p. 3-18) - The inlet quality for the chimney section was determined by mass and energy balance. Did the energy balance take into consideration that a fraction of the fission energy was not deposited in the core?
- R93. In a typical BWR approximately [[ ]] of the energy is deposited in the fuel rods. The remaining energy is deposited directly in the water in the fuel channel and in the bypass between the fuel channels. Since the flow in the chimney is the sum of the in channel and bypass flow, it does not matter where the energy is deposited.
- Q94. Section 3.1.5.3 (p. 3-26) - In Figure 3.1-22, the maximum level deviation is not within the measurement uncertainty as the report stated. Please explain.
- R94. The report states that the level is within the measurement uncertainty over most of the test, but that the deviation increases to [[ ]] at the end of the test. This statement is for test 5803-01, where the level comparison is shown in Figure 3.1-24. For this test the measurement uncertainty is [[ ]]. Figure 3.1-22 is test 5801-15, and for this test it is stated at the top of page 3-26 that the maximum deviation is [[ ]]. For this test the measurement uncertainty is [[ ]].  
The 5803 test series are liquid blow down tests. In these tests there is very little flashing before the uncover of the break location. Therefore the water level is very well defined and the measurement accuracy is given by the accuracy of the pressure drop measurement. The 5801 test series are steam blow down tests. In these tests, the pressure decreases rapidly immediately after the break and there is a large amount of flashing below the level. Therefore the uncertainty in determining the two-phase level is significantly larger.
- Q95. Section 3.1.5.3 (p. 3-27) - In Figure 3.1-23, would the use of measured break flow (Fig. 3.4-12) as a boundary condition result in better agreement with pressure data?
- R95. The simulations were made to test both the critical flow and the void fraction models together. No attempt was made to use the measured break flow.
- Q96. Section 3.2.1 (p.3-36) - Is there any reason the negative temperature deviation is so much higher in Figure 3.2-3 than the other 3 comparisons?

- R96. In test 3.06.6B the peak temperature was approximately [[ ]] higher at the 3.6m elevation than at the 2.4m elevation. TRACG predicted this trend for both tests. However in test 3.08.6C the test showed a peak temperature that was approximately [[ ]] less at the 3.6m elevation than at the 2.4m elevation. There is no apparent reason for this difference in the observed trend.
- Q97. Section 3.2.2.4 (p. 3-40) - In Figure 3.2-9, how does the rod number correspond to the position of the rods in the 8x8 bundle?
- R97. The rod numbers from 1 to 64 for the 8X8 bundle are shown in Figure 97-1. Rod number [[ ]] In Figure 3.2-9, the numbers [[ ]] There is an error in Figure 3.2-9. The legends between data and TRACG have been reversed and thus TRACG underpredicts the peak temperature by [[ ]] rather than overpredicting the temperature by [[ ]]. In either case, [[ ]] is a very small error on a peak cladding temperature of approximately [[ ]] The rod temperature is conservatively overpredicted for the peripheral rods (1 and 64) because the local vapor temperature in the vicinity of the cold channel box is less than the bulk vapor temperature. In Figure 3.2-7, the rod group for rod 28 in Figure 97-1 should have been rod group 10. These typographical errors will be corrected in the next revision of the report.

1	2	3	4	5	6	7	8
9	10	11	12	13	14	15	16
17	18	19	20	21	22	23	24
25	26	27	28	29	30	31	32
33	34	35	36	37	38	39	40
41	42	43	44	45	46	47	48
49	50	51	52	53	54	55	56
57	58	59	60	61	62	63	64

Figure 97-1. Rod Numbers for the CSHT Test Facility

- Q98. Section 3.3.2 (p. 3-43) - In Figure 3.3-2, the legends for the data points are missing.

R98. The legends for the data points are shown in the attached Figure 3.10-1.  
[[

Figure 3.10-1. CSHT Facility CCFL Test Data

]]

Q99. Section 3.4.1.2 (p. 3-48) - The axial temperature profiles are shown in Figure 3.4-5 and not in Section 3.4-5.

R99. This will be corrected in the next revision.

Q100. Section 3.4.1.2 (p. 3-48) - What was the uncertainty of the pressure measurement?

R100. The uncertainty in the pressure measurement for the Marviken critical flow tests is 90 kPa [Reference 100.1].

Reference 100.1: TRACC-M/F77, Version 5.5 Developmental Assessment Manual, NUREG/CR-6730, Vol.1, page 4.3-2, July 2001.

Q101. Section 3.4.1.5 (p. 3-48) - Why did TRACG predict much higher break flow rate than the data for the initial 5 seconds for both Tests 15 and 24?

R101. Due to the high sonic velocity in subcooled liquid the break flow is expected to increase to its maximum value almost instantaneously. The transit time for a sonic wave in the subcooled liquid in the nozzle and discharge pipe is approximately 5 msec. This behavior is calculated by TRACG. The delay in the measured break

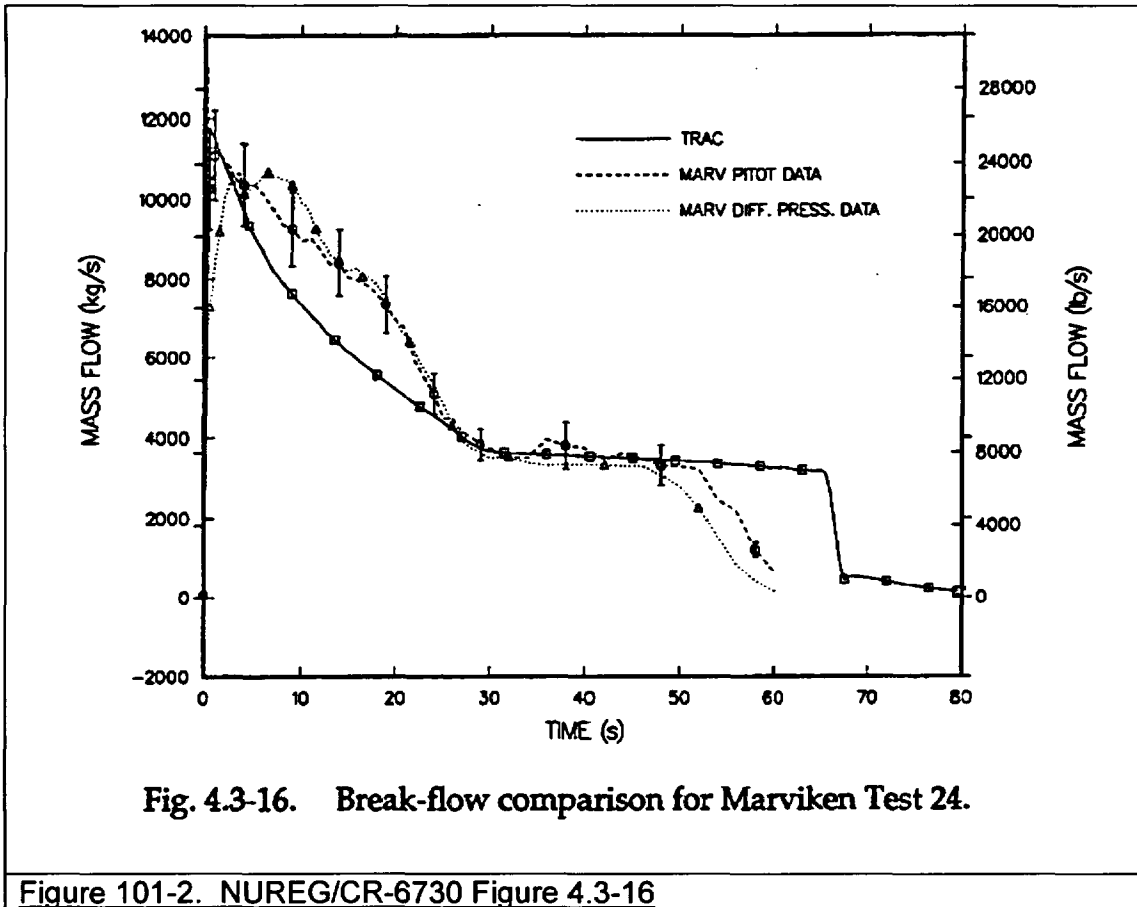
flow as seen most clearly in test 24 is most likely due to lag in the instrumentation.

The TRACG comparison to the measured break flow for Marviken test 24 is shown in Figure 101-1. The measured break flow is based on a measurement of the liquid inventory in the vessel. The measurement uncertainty for this measurement is 15-20% (TRAC-M Development Assessment Manual, NUREG/CR-6730). There was also a Pitot tube measurement of the flow. This measurement is most reliable for single-phase conditions. Both measurements are shown in Figure 4.3-16 from NUREG/CR-6730. This Figure is shown below in Figure 101-2. It is seen that the flow measurement from the Pitot tube is in very close agreement with the calculated flow in the initial 5 seconds of the test.

[[

]]

**Figure 101-1. NEDE-32177P Figure 3.4-8 Comparison of Break Flow for Marviken Test 24**



Q102. Section 3.4.1.5 (p. 3-56) - In Figure 3.4-8, what is the cause of the 20 second delay in the TRACG prediction of the transition to pure steam flow?

R102. For test 24 the measured break flow is [[  
]] for the liquid blow down phase and [[  
]] for the two-phase  
blow down phase. This is shown in Table 3.4-2. As a result of this difference the  
two-phase level drops down to the break location earlier in the test than in the  
calculation.

Q103. Section 3.4.2 (p. 3-59) - What is the cause of the flow spikes predicted by  
TRACG in Figures 3.4-11 through 3.4-13?

R103. In PSTF test 5801-15 the two-phase level [[  
]] This is evident from a comparison of  
Figures 3.1-17 and 3.1-22. [[  
]] seen in  
Figure 3.4-11. The initial spike in the break flow seen in Figures 3.4-12 and 3.4-  
13 is the [[  
]] This period correspond to the initial fast depressurization seen in  
Figures 3.1-23 and 3.1-25. The [[  
]]

Q104. Section 3.5 (p. 3-64) - Where is the documentation for the TRACG qualification  
of the pressure drop for the core bypass flow paths?

R104. TRACG uses loss coefficients for the leakage paths based on experimental data.  
These data were obtained for operating BWRs, but the dominant leakage paths  
should be similar for the ESBWR. The models for the leakage and bypass flow  
paths are described in NEDE-32785-1-PA. Also, see Section 7.5.1 of NEDE-  
32176P, Rev. 2 and Reference 7.5-1 that it cites.

Q105. Section 3.5.1 (p. 3-65) - How do the thermal-hydraulic characteristics of the  
ATLAS test bundle simulating GE9 fuel compare with the ESBWR fuel  
assembly?

R105. The fuel bundles used for the demonstration analysis in the ESBWR application  
methodology are of the GE12 design. The actual fuel design to be loaded into the  
ESBWR will likely be different based on the timing, but will use the latest  
licensed GNF fuel.

The GE12 design utilizes a 10 x 10 fuel rod array, which includes 78 full-length  
fuel rods, 14 part length fuel rods and 2 large central water rods. The active fuel  
length is approximately 3.05 m (10 ft) compared to the active fuel length of  
approximately 3.66 m (12 ft) for operating BWRs. A comparison of the principal  
dimensions between GE9 and the ESBWR GE12 bundle are shown in the table  
below.

[[

While the data for the two lattices are compared as requested, it is important to mention that GE/GNF perform full scale tests of all fuel designs prior to use. Thus, a more relevant comparison would be between full-length and shorter GE12 designs for which all parameters are matched except for active fuel length. Pressure drop data and GEXL correlation coefficients are available for full-length GE12 designs. Transient tests have also been performed to validate the application of the GEXL correlation for GE12 fuel. ]]

The pressure drop correlations (friction, spacers, tieplates, etc) are applicable to the shorter length fuel. [[

]]

Q106 Section 3.6.1.2 (p. 3-70) - For the TRACG qualification calculations, the first rod in the ATLAS test bundle to undergo burnout was known a priori from the test result. For the LOCA analysis of an ESBWR how will the first rod to burnout be identified? How is the flow distribution to the 'hot rod' channel and the other lumped channels determined?

R106. The rod with the [[ ]] is the first rod to enter boiling transition, because that is how the [[ ]] for the rods in the bundle is calculated. [[

]] Subchannel effects are not considered in the TRACG analysis – an assumption that has been validated over many years of experience. TRACG represents the core with a combination of individual high power fuel channels and groups of fuel channels lumped together with averaged characteristics. The flow distributions to these channels are solved for with the constraint of a common pressure drop from the lower to upper plenum.

- Q107. Section 3.6.3 (p.3-72) - Are there any TRACG qualifications for burnout prediction under low pressure, low flow, and near saturation conditions that are expected in a LOCA for the ESBWR?
- R107. For the FIST small break LOCA test, the dryout occurs for low flow and low pressure conditions. See Section 5.2.3. For the TLTA boil off test, the dryout occurs for low flow and low pressure. See Section 5.1.1.
- Q108. Section 5.1.1 (p. 5-1) - The boiloff test was conducted at a pressure of 2.76 MPa. Has there been assessment of low pressure boiloff that would be more representative of ESBWR post-LOCA conditions?
- R108. Integral tests such as GIST and GIRAFFE/SIT show no boiling transition at low pressures. The Zuber correlation used under these conditions has a wide pressure data base.

Q109. Section 5.1.1.3 (p. 5-4) - How is the uncertainty in the measured nodal void fraction related to the smoothing of the data?

R109. The measured pressure drop showed fluctuations which were removed in the smoothed data. The smoothed data were then converted to a void fraction assuming that the measured pressure drop is entirely due to the static head. The magnitude of the fluctuations in the pressure drop plus the uncertainty in the pressure drop measurement when converted to an equivalent static head corresponds to a 5% uncertainty in average void fraction between the pressure tap locations.

Q110. Section 5.1.1.3 (p. 5-4) - Figures 5.1-3 to 5.1-6 showed the comparison between measured and calculated void fraction. How are the weighted average void fractions derived from the calculated nodal void fractions?

R110. The weighted average void fraction is the sum of the node length multiplied with the void fraction over the distance between the measurement locations divided by the sum of the node lengths. Thus the weighted average void fraction represents the average void fraction between the measurement locations.

Q111. Section 5.1.1.4 (p. 5-4) - What is the sensitivity of the calculated results to TRACG nodalization?

R111. No nodalization studies were done for this test. The nodalization strategy is derived from sensitivity studies on separate effects tests.

Q112. Section 5.1.3.3 (p. 5-37) - Was TRACG able to calculate the lower plenum bulk flashing at about 16 sec. after the uncover of the recirculation line suction inlet?

R112. Yes, this is clearly seen in Figure 5.1-36

Q330 Please provide the following TRACG input decks:

Q330.4 PSTF level swell test TRACG input decks

Please provide both the pre-test and post-test calculation input decks for Tests 15\_1 and 23\_4. ( Page 4.1-1 of TRACG SBWR qualification for SBWR.)  
Need 1-Tube model and eight tube models.  
Test T12, T13, T11 and T02 input decks

R330.4 PSTF level swell test TRACG input decks provided separately on CD.

Supplemental Information for RAI 330.4

The experimental data for the PSTF 5803\_1 and 5803\_2 tests are summarized in the following tables. These tables present Level (“\_L”), Pressure (“\_P”), and Break flow (“\_W”) versus time. For 5803\_1 test, SI units (second, m, MPa, kg/s) are used. For 5803\_2 test, British units (second, ft, psia, lb/s) are used.

[[

---

[[ ]]

---

]]

[[

]]

[[

[[

]]

]]

\

[[\_\_\_\_\_

]]

## **NRC RAIs and Responses**

**TRACG Qualification for ESBWR  
NEDC-33080P, Rev. 0**

**Note: RAI responses including data files that cannot be read on a PC are not included.**

Q25 General Electric (GE) topical report NEDC-33080P, "TRACG Qualification for ESBWR," dated August, 2002, describes qualification studies of the TRACG computer code performed for ESBWR. This report documents two additional validation studies performed specifically in support of ESBWR. The test data used for these studies are from the P-Series containment tests performed at the PSI PANDA test facility in Switzerland and from the elevated-pressure hydrodynamic instability tests performed at the CRIEPI/SIRIUS test facility in Japan.

Title 10 of the *Code of Federal Regulations* (10 CFR) Part 52.47(b)(2) states that certification of a standard design which differs significantly from light water reactor designs or utilizes simplified, inherent, passive or other innovative means to accomplish its safety functions will be granted only if each safety feature of the design has been demonstrated either through analysis, appropriate test programs, experience, or a combination.

Part 52.48 describes that applications filed under this subpart will be reviewed for compliance with 10 CFR Part 20, Part 50 and its appendices, ... and as those standards are technically relevant to the design proposed for the facility. Part 52.48 thus invokes appropriate aspects of Part 50, including Appendix B quality assurance (QA) requirements.

For SBWR design certification qualification test program activities GE met Part 50, Appendix B by implementing their latest NRC approved "Nuclear Energy Business Operations Quality Assurance Program Description" (topical report), NEDO-11209-04A, Revision 8. Additionally, NEDG-31831, "SBWR Design and Certification Program Quality Assurance Plan," was developed by GE to fulfill the QA requirements of the SBWR reactor design and certification program. NEDG-31831 meets the requirements of ANSI/ASME NQA-1-1983 and its NQA-1a-1983 addenda, which includes specific requirements related to "Qualification Tests." NEDG-31831 provides that design and testing work performed by international technical associates will be performed to their internal QA programs acceptable to the regulatory authorities of their respective countries as evaluated by GE for compliance with the provisions of ANSI/ASME NQA-1-1983.

The staff is not clear as to what GE considers tests being "*confirmatory in nature.*" Please describe what "*confirmatory in nature*" encompasses and how GE plans to use the data from the PANDA-P series tests conducted at PSI in Switzerland and the SIRIUS two-phase flow instability tests conducted in CRIEPI, Japan. It is our understanding that data from these tests is going to be used to support the ESBWR design and be part of the ESBWR design certification application. If this is the case, please describe how these tests and test data meet the GE topical report and NQA-1 quality requirements for testing related activities.

R25. Rev 1.

[[

]]

The following corrections will be made to NEDC-33080P, "TRACG Qualification for ESBWR" to clarify the GE position.

<b>Errata for NEDC-33080P</b>			
<b>No.</b>	<b>Location</b>	<b>Original</b>	<b>Revised</b>
1	Section 1, p. 1-1, 1 <sup>st</sup> paragraph, 1 <sup>st</sup> sentence	This report describes qualification studies of the TRACG computer code performed for the European Simplified Boiling Water Reactor (ESBWR).	This report describes confirmatory qualification studies of the TRACG computer code performed for the ESBWR.
2	Section 1, p. 1-1, 3 <sup>rd</sup> paragraph, 1 <sup>st</sup> sentence	The present report documents two additional validation studies performed specifically in support of the ESBWR.	The present report documents two confirmatory validation studies performed for the ESBWR.
3	Section 1, p. 1-1, 3 <sup>rd</sup> paragraph, last sentence	The CRIEPI/SIRIUS tests extended the previous CRIEPI investigation of hydrodynamic instability at low pressure to cover the pressure range from ESBWR startup to full-power operation.	The CRIEPI/SIRIUS tests augmented the previous CRIEPI investigation of hydrodynamic instability at low pressure to confirm the application of TRACG over the pressure range from ESBWR startup to full-power operation.
4	Section 1, p. 1-1, 4 <sup>th</sup> paragraph	(Add sentence to end of paragraph.)	The thermal-hydraulic phenomena of importance to the performance of the ESBWR were identified in the PIRT Tables provided in the ESBWR TAPD [1-3]. No additional phenomena of importance were identified for the ESBWR relative to the earlier SBWR study. Thus the existing data base that was available for the SBWR program is sufficient for the validation of TRACG for the ESBWR as well.

<b>Errata for NEDC-33080P</b>			
5	Section 2.1, p. 2-1, 2 <sup>nd</sup> paragraph, 1 <sup>st</sup> sentence	To support the extension of the TRACG qualification activity to the ESBWR, an ESBWR-specific PANDA test program was performed.	To confirm the application of the TRACG SBWR qualification activity to the ESBWR, an ESBWR-specific PANDA test program was performed.
6	Section 2.2, p. 2-3, 3 <sup>rd</sup> paragraph, 3 <sup>rd</sup> sentence	Subsequent tests incorporated variations of key parameters and addressed specific thermal-hydraulic phenomena which are considered to be of potential importance for calculation of long-term post-LOCA behavior in the ESBWR.	Subsequent tests incorporated variations of key parameters and addressed specific thermal-hydraulic phenomena that are relevant to the confirmation of TRACG qualification for the calculation of long-term post-LOCA behavior in the ESBWR.
7	Section 2.3.3, p. 2-11, 1 <sup>st</sup> paragraph, 1 <sup>st</sup> sentence		
8	Section 2.6.1, p. 2-30, 3 <sup>rd</sup> paragraph, 1 <sup>st</sup> sentence		
9.	Section 2.6.2, p.2-31, 1 <sup>st</sup> paragraph, 4 <sup>th</sup> and 5 <sup>th</sup> sentences		

<b>Errata for NEDC-33080P</b>			
10	Section 3.1, p. 3-1, 1 <sup>st</sup> paragraph, last sentence	The study described here was undertaken to provide a qualification basis for the use of TRACG to predict two-phase flow instability at higher pressures.	The study described here was undertaken to provide a confirmatory qualification basis for the use of TRACG to predict two-phase flow instability over the ESBWR pressure range.
11	Section 3.1, p. 3-1, 2 <sup>nd</sup> paragraph, 6 <sup>th</sup> sentence	The objective was to extend the TRACG qualification base for prediction of thermal-hydraulic oscillatory conditions in a natural circulation reactor from startup to normal operation.	The objective was to confirm the application of TRACG for prediction of thermal-hydraulic oscillatory conditions in a natural circulation reactor from startup to normal operation.
12	Section 3.7, p. 3-6, 2 <sup>nd</sup> paragraph, last sentence	The results of these comparisons show that TRACG is capable of predicting the dependence of the oscillation characteristics (amplitude and period) on the relevant system parameters.	The results of these comparisons confirm that TRACG is capable of predicting the dependence of the oscillation characteristics (amplitude and period) on the relevant system parameters.
13	Section 3.7, p. 3-6, 4th paragraph, 1 <sup>st</sup> sentence	The results of these simulations, together with those presented in References 3-8 and 3-9, show that TRACG is capable of predicting thermal-hydraulic instabilities, including geysering, flashing-induced instability at low system pressure and density wave oscillation at relative high system pressure.	The results of these simulations, together with those presented in References 3-8 and 3-9, confirm that TRACG is capable of predicting thermal-hydraulic instabilities, including geysering, flashing-induced instability at low system pressure and density wave oscillation at relatively high system pressure.

## 1. INTRODUCTION

This report describes confirmatory qualification studies of the TRACG computer code performed for the ESBWR. ~~This report describes qualification studies of the TRACG computer code performed for the European Simplified Boiling Water Reactor (ESBWR).~~ It supplements the material in the generic TRACG qualification report [1-1] and the TRACG qualification report for the SBWR [1-2]. Computer code qualification, as defined at GE Nuclear Energy, incorporates the process of validation of the code against data or alternate engineering calculations. Validation is part of the process of “qualifying” the computer code for design application.

The generic TRACG qualification report [1-1] includes a comprehensive collection of TRACG qualification studies applicable to BWR-related separate effects, component, integral system and reactor tests. These tests cover a wide range of phenomena and configurations representative of BWR conditions for loss-of-coolant accidents (LOCAs), operational transients and density wave oscillation. Most of these test data are also applicable to the ESBWR, as discussed in the ESBWR Test and Analysis Program Description (TAPD) [1-3]. Reference 1-2 supplemented the TRACG generic qualification by documenting an extensive set of validation studies performed as part of the earlier SBWR program. All of the Reference 1-2 studies are considered to be directly applicable to the ESBWR [1-3].

The present report documents two confirmatory validation studies performed for the ESBWR. ~~The present report documents two additional validation studies performed specifically in support of the ESBWR.~~ The test data used for these studies are from the P-series containment tests performed at the PANDA test facility in Switzerland and from the elevated-pressure hydrodynamic instability tests performed at the CRIEPI/SIRIUS test facility in Japan. The PANDA P-series tests extended the previous PANDA investigation of SBWR post-LOCA long-term containment cooling to confirm the post-LOCA performance of the higher-power ESBWR with its modified containment configuration. The CRIEPI/SIRIUS tests augmented the previous CRIEPI investigation of hydrodynamic instability at low pressure to confirm the application of TRACG over the pressure range from ESBWR startup to full-power operation. ~~The CRIEPI/SIRIUS tests extended the previous CRIEPI investigation of hydrodynamic instability at low pressure to cover the pressure range from ESBWR startup to full-power operation.~~

This report is one of several documents that provide the information necessary for the validation of the TRACG computer code and its application for ESBWR design analysis. The relationship of this report to the generic TRACG qualification report [1-1] and the SBWR qualification report [1-2] was addressed above. The other relevant reports are the ESBWR Test and Analysis Program Description [1-3], the ESBWR Test Report [1-4], the ESBWR Scaling Report [1-5], the TRACG Model Description [1-6], and the TRACG Application for ESBWR [1-7]. A unifying element of the ESBWR documentation is reference to a set of “PIRT” phenomena that have been judged to be of significance for the calculation of ESBWR safety parameters. The PIRT acronym derives from the Phenomena Identification and Ranking Tables that are used to identify and prioritize the phenomena in relation to the safety parameters. The thermal-hydraulic phenomena of importance to the performance of the ESBWR were identified in the PIRT Tables provided in the ESBWR TAPD [1-3]. No additional phenomena of importance were identified for the

ESBWR relative to the earlier SBWR study. Thus the existing data base that was available for the SBWR program is sufficient for the validation of TRACG for the ESBWR as well.

TRACG is being qualified for ESBWR licensing analyses of operational transients, LOCA-ECCS and LOCA-containment. A detailed description of the application methodology is provided in Reference 1-7. There are differences in the application approach for the three types of events. Operational transients are being addressed within the framework of the Code Scaling, Applicability and Uncertainty (CSAU) methodology [1-8]. For LOCA-ECCS, the CSAU process will be followed to identify the uncertainties in the TRACG models, correlations and parameters

## 2. PANDA TRANSIENT TESTS P1-P8

### 2.1 Introduction

Reference 2-1 describes a comprehensive qualification of the TRACG computer code [2-2 and 2-3] for analysis of the SBWR. A major element of the TRACG SBWR qualification program was a series of integral systems tests performed in the PANDA test facility at the Paul Scherrer Institute (PSI) in Switzerland. The PANDA facility was designed to model the long-term cooling phase of the SBWR LOCA. It includes the Passive Containment Cooling System (PCCS), the Isolation Condenser System (ICS) and the Gravity Drain Cooling System (GDCCS). The SBWR test matrix (known as the M-series) included, in addition to a design-basis LOCA simulation, a series of tests designed to challenge both the performance of the passive safety systems and the ability of TRACG to predict that performance. The most significant conclusion from the SBWR PANDA qualification activity [2-1] was that TRACG accurately calculates post-LOCA containment pressurization and is well-suited to the calculation of post-LOCA containment transients involving interactions between the passive safety systems.

To confirm the application of the TRACG SBWR qualification activity to the ESBWR, an ESBWR-specific PANDA test program was performed. ~~To support the extension of the TRACG qualification activity to the ESBWR, an ESBWR-specific PANDA test program was performed.~~ The PANDA facility was modified to represent the ESBWR and a test matrix, designated as the "P-series", was defined. The P-series consisted of eight transient tests representing design-basis and beyond design-basis post-LOCA conditions [2-4]. The purpose of this section is to present the results of TRACG post-test calculations for the P-series tests as an extension to the qualification reported in Reference 2-1. The post-test analyses of the transient tests were performed by an ESBWR PANDA analysis team, with participation from PSI in Switzerland, where the tests were conducted, and the General Electric Company (GE) in the United States. The calculations were performed with the TRACG04 version of the code.

The remainder of this section is organized as follows. Section 2.2 presents a brief description of the PANDA test facility and the P-series test matrix. Section 2.3 discusses the applicability of the PANDA transient data to the ESBWR and includes a rationale for each of the P-series tests. Section 2.4 provides a description of the PANDA TRACG input model used for the post-test analyses. For each test, there is a summary table of the measured thermodynamic conditions at the start of the test which were used for the initialization of the various components in the TRACG model. Section 2.5 presents the results of the post-test calculations on a test-by-test basis and includes a quantitative evaluation of the accuracy of the TRACG predictions. Section 2.6 discusses the results of the study with reference to key ESBWR phenomena and presents a final set of conclusions.

### 2.2 Test Facility and Test Matrix

The PANDA test facility was originally designed to model the long-term cooling phase of the loss-of-coolant accident (LOCA) for the SBWR. In its original configuration, it was a 1/25 volume-scaled, full-height simulation of the SBWR primary system and containment and

MFN 03-142  
Enclosure 2

included the major components necessary to simulate the SBWR system response during the long-term phase of the LOCA. These components include the containment drywell (DW), the

cooling phase and represents the starting point for most of the PANDA simulations of ESBWR post-LOCA behavior.

The long-term cooling phase of the LOCA is defined as starting at one hour from the occurrence of the break. Conditions at this time in the LOCA transient were derived from ESBWR TRACG calculations. The calculations show that the one-hour thermodynamic conditions throughout the system are relatively stable. The effect of subcooling of RPV water by GDCS injection is just on the verge of being overcome by the decay power. The pressure difference between the RPV and DW is just sufficient to maintain flow of the boiloff steam through the break and the open depressurization valves. To remove the energy added to the DW, the PCCS must first purge residual noncondensable gases from the DW to the WW and, accordingly, the pressure difference between the DW and WW is just sufficient to clear the PCC vents.

One of the compromises made in the original design of the PANDA test facility was to not scale the volume of water available to replace boiloff in the SBWR and, by extension, the ESBWR PCCS. In the ESBWR, this volume, which extends outside the individual PCC pools, is sufficient to maintain coverage of no less than 50% of the condenser tube length for 72 hours. In PANDA, only the water in the four individual pools (three PCC pools and one IC pool) is available to replace boiloff. Capability was originally provided to either interconnect or isolate the individual pools and to provide replacement water through fittings in the pool bottoms. It was subsequently decided that the ability to directly assess individual PCC and IC heat transfer through the boildown of the individual pools outweighed the advantage of allowing refill from the pools for condenser units (typically, the IC) that were not in service for a given test. With the exception of Test P1/8, the duration of the P-series tests was short enough to preclude uncovering of the condenser tubes by pool boildown.

The P-series test matrix is described in detail in Reference 2-4. Test P1 was a base-case simulation of the ESBWR LOCA long-term cooling phase following a MSLB. Subsequent tests incorporated variations of key parameters and addressed specific thermal-hydraulic phenomena that are relevant to the confirmation of TRACG qualification for the calculation of long-term post-LOCA behavior in the ESBWR. ~~Subsequent tests incorporated variations of key parameters and addressed specific thermal-hydraulic phenomena which are considered to be of potential importance for calculation of long-term post-LOCA behavior in the ESBWR.~~ Test P2 was configured to start at an earlier time in the transient and provided data during the transition from the GDCS injection phase to the long-term cooling phase. Test P3 demonstrated PCCS start-up capability with initially non-condensable-filled DW vessels and PCC units, representing the upper limit of initial DW noncondensable inventory. In addition, Test P3 examined the influence of asymmetric distributions of steam and air in the DW on the startup and long-term performance of the PCCS by releasing all of the RPV steam to DW2. To further challenge the system, the PCC unit on DW1 was valved out of service. Test P4 included the delayed release of non-condensable gas into the DW to simulate the effect of noncondensable hideout in regions of the ESBWR DW that are not directly exposed to mixing by the steam jets emanating from the RPV. Test P5 was similar to Test P4 but further challenged the system by valving one of the PCC units out of service. Test P6 considered system interaction effects associated with parallel operation of the PCCS and ICS and the effect of a postulated direct bypass of steam from the

MFN 03-142  
Enclosure 2

DW to the WW air space. Test P6 was started with the Isolation Condenser (IC) in operation in parallel with the PCCs. Later in the test, a DW-to-WW leakage path was opened to simulate a possible steam bypass. At a still later time, the IC was valved out,

MFN 03-142  
Enclosure 2

MFN 03-142  
Enclosure 2

|

MFN 03-142  
Enclosure 2

MFN 03-142  
Enclosure 2

|

MFN 03-142  
Enclosure 2

MFN 03-142  
Enclosure 2

|

### 3. SIRIUS TWO-PHASE FLOW INSTABILITY TESTS

#### 3.1 Introduction

A potential concern during the design of the ESBWR [3-1, 3-2] was the startup process. The design uses a chimney installed on the top of the core to enhance the natural circulation core flow. Experiments have shown that hydraulic oscillations can occur under low pressure and low power conditions during the startup process of a natural-circulation reactor. These hydraulic oscillations include geysering [3-3], flashing-induced instability at low system pressure (0.1 – 0.5 MPa) [3-4], and density wave oscillation at relatively high system pressure (1.0 – 7.2 MPa) [3-5]. In previous studies, TRACG has been successfully qualified against test facility and plant stability data [3-6 and 3-7]. TRACG has also been qualified against geysering data and flashing induced instability data at low system pressure [3-8, 3-9, 3-10]. The study described here was undertaken to provide a confirmatory qualification basis for the use of TRACG to predict two-phase flow instability over the ESBWR pressure range. ~~The study described here was undertaken to provide a qualification basis for the use of TRACG to predict two phase flow instability at higher pressures.~~

10

TRACG analyses were performed to simulate the two-phase flow instability data at relatively high pressure from the SIRIUS loop at the Central Research Institute of the Electric Power Industry (CRIEPI) in Japan. The SIRIUS loop was designed to investigate thermal-hydraulic instabilities in natural-circulation BWRs. In previous qualification studies, TRACG has been qualified against stability data from operating plants and test facilities, including flashing-induced instability data at low pressure from the SIRIUS test facility [3-10]. The TRACG comparisons described here include the dependence of the amplitude and period of the oscillations on heat flux, inlet subcooling and system pressure. Comparisons are also made in terms of stability maps in the plane of inlet subcooling versus heat flux. The objective was to confirm the application of TRACG for prediction of thermal-hydraulic oscillatory conditions in a natural circulation reactor from startup to normal operation. ~~The objective was to extend the TRACG qualification base for prediction of thermal hydraulic oscillatory conditions in a natural circulation reactor from startup to normal operation.~~ The evaluation includes a comparison between the nominal operating condition of the ESBWR and the measured stability map at a system pressure of 7.2 MPa to demonstrate the margin to instability in terms of inlet subcooling.

11

#### 3.2 Test Facility and Test Matrix

The SIRIUS test facility was constructed at CRIEPI in Japan to investigate thermal-hydraulic instabilities in BWRs. The test facility was based on non-dimensional scaling of the original SBWR design [3-1] with 70% of the chimney height of the prototype. A schematic of the SIRIUS test facility is shown in Figure 3-1. The test loop consists of two electrically heated channels (1.7-m high), chimney (5.4-m high), separator (upper plenum), downcomer, preheater and subcooler. The total length of the downcomer section is about 30 m. Water temperature at the channel inlet was measured by thermocouples and the flow rate was measured by an orifice flow meter [3-4].

MFN 03-142  
Enclosure 2

Detailed measurements of the pressure drop across different sections of the test loop under forced liquid flow conditions were previously performed at the SIRIUS test facility in order to obtain local loss coefficients. The test facility is divided into eight regions (see Figure 3-1) and

agreement between the TRACG results and the data. The key results and conclusion from these comparisons are summarized below.

For cases with sinusoidal oscillations, the shape and amplitude of the oscillations in inlet velocity and void fraction depend on inlet subcooling, heat flux and system pressure. Detailed comparisons between test observations and TRACG calculations were made for cases covering a wide range of inlet subcoolings at low, medium and high heat fluxes and medium and high pressures. The results of these comparisons confirm that TRACG is capable of predicting the dependence of the oscillation characteristics (amplitude and period) on the relevant system parameters. ~~The results of these comparisons show that TRACG is capable of predicting the dependence of the oscillation characteristics (amplitude and period) on the relevant system parameters.~~

12

The results of these simulations, together with those presented in References 3-8 and 3-9, confirm that TRACG is capable of predicting thermal-hydraulic instabilities, including geysering, flashing-induced instability at low system pressure and density wave oscillation at relatively high system pressure. ~~The results of these simulations, together with those presented in References 3-8 and 3-9, show that TRACG is capable of predicting thermal hydraulic instabilities, including geysering, flashing induced instability at low system pressure and density wave oscillation at relative high system pressure.~~ These qualification studies demonstrate that TRACG can be used to analyze the thermal-hydraulic oscillatory conditions in a natural circulation reactor from start-up to normal operation. Based on comparison of the measured stability map to the ESBWR startup trajectory [3-15] and nominal operating condition (Figure 3-15), the SIRIUS test results support the conclusion that the ESBWR design has significant core inlet subcooling margin to the hydraulic instability region.

13

- Q113. The document reviewed does not include the information regarding the physical dimensions of the PANDA test facility. Please provide a reference that contains the relevant dimensions of the various components (vessels, tanks, heat exchangers, pressure differential to open vacuum breaker, etc.) of the facility. Please also provide the scaling ratios (vs. ESBWR) of the individual components (or any deviations from 1/45 ratio).
- R113. The PANDA test facility dimensions are given in Reference 1, which was transmitted to the NRC via a letter to Joseph Sebrosky, dated August 16, 2002. The basic dimensions of the facility have not changed since that document was issued, although the vessel connections were modified to reflect the ESBWR configuration as described in References 2 and 3. For scaling comparisons, it is the parameter groups identified as "PI-groups" in the scaling report that are important rather than individual parameters. The PI-groups for ESBWR and PANDA are compared in Reference 4. The numerical values required to calculate ESBWR-to-PANDA ratios of individual parameters are given in Reference 5 but the ratios are not listed since they are not as relevant to the scaling comparison as the PI-groups.

**References**

1. *PANDA Facility, Test Program and Data Base General Description (DTR Umbrella Report)*, Alpha-606-0, PSI, May 1996 (Non-Proprietary).
  2. *ESBWR Test Report*, NEDC-33081P, August 2002 (Section 2.2).
  3. *ESBWR Scaling Report*, NEDC-33082P, Rev 0, December 2002 (Section 5.5).
  4. *Ibid.* (Section 8).
  5. *Ibid.* (Appendix A).
  6. *TRACG Qualification for SBWR*, NEDC-32725P, V. 1, Rev. 1, August 2002 (Section 4.1).
  7. *Ibid.* (Section 4.3)
  8. *TRACG Qualification for ESBWR*, NEDC-33080P, August 2002.
  9. *TRACG Application for ESBWR*, NEDC-33083P, September, 2002 (Section 3.3.1.1.3).
  10. *Ibid.* (Section 3.3.1.1.1).
  11. *Ibid.* (Section 3.3.1.1.2).
  12. *TRACG Qualification for SBWR*, NEDC-32725P, V. 1, Rev. 1, August 2002 (Appendix B).
  13. *TRACG Application for ESBWR*, NEDC-33083P, September, 2002 (Figure 3.7-2).
- Q114. One of the main purposes of the PANDA tests was to support the use of TRACG to model the post-LOCA behavior of ESBWR containment. However, the

nodalization of the PANDA test facility (Figure 2-3 of NEDC-33080P) is substantially different from that of ESBWR (presented in Figure 2-2 of NEDC-33080P and Figure 2.7-1 of NEDC-33083P, TRACG Application for ESBWR). For example, azimuthal nodalization of the VESSEL component was utilized to represent various components in PANDA, while radial nodalization was utilized to model them in ESBWR.

R114. The nodalizations used for PANDA and for the ESBWR are not substantially different. They appear different because the PANDA nodalization models the different pressure vessels as two-ring sectors while the ESBWR model uses two complete rings to model the corresponding regions. Both of these nodalizations preserve rotational symmetry so there is no difference between using a sector or a complete ring. The PANDA facility, with its paired DW and WW vessels, was specifically designed to investigate the effects of asymmetry on the operation of the passive safety systems and, while PANDA is a scaled version of the ESBWR in terms of volumes and elevations, there are some nodalization differences that result from inherent geometric differences. However, the nodalizations of both PANDA and the ESBWR use a similar level structure and the numbers of cells used to represent corresponding region volumes are similar. There are differences in the level structure where boundaries are modeled, but the overall nodalization approach between the two is similar. The use of two rings of the TRACG VSSL component for the modeling of the RPV, DW, WW, GDCS pool and PCCS pools in both PANDA and the ESBWR is a key similarity. Two rings is the minimum required to represent an upflow/downflow circulation pattern within the vessels.

Q114.1. Was there any attempt to use similar nodalizations between the ESBWR and PANDA simulations? If not, please explain why these differences should not be an issue in using the PANDA analytical results to validate the TRAC simulation of the ESBWR analysis, considering that nodalization is an important element of the validation.

R114.1. The nodalization used for PANDA does attempt to follow the important characteristics of the nodalization used for the ESBWR. As noted above, there are many similarities between PANDA and the ESBWR models, particularly with respect to the radial and axial nodalizations of the PANDA vessels representing the ESBWR RPV, DW, WW, GDCS and PCCS pools. The ESBWR represents the WW with a single azimuthal sector and two rings while the two PANDA WW vessels are each represented by a single sector and two rings. (An objective of the PANDA test program was to demonstrate the adequacy of the axisymmetric modeling of the DW and WW in the ESBWR.) The same numbers of cells and levels are used for the liquid and vapor regions in each of the PANDA WW vessels as are used to model the wetwell pool and air-space in the ESBWR. A similar strategy is used to model the DW, although the ESBWR DW runs the full length of the model and, consequently, has more levels than the PANDA DW. Again, two rings

and a single sector are used for the ESBWR DW and for each of the PANDA DW vessels. The level and cell arrangement in the PCC pools and the nodalization of the condensers themselves are the same in both the ESBWR and PANDA TRACG models. The RPV nodalization in both the ESBWR and PANDA models has two rings and a similar number of levels. For both nodalizations, the cells which represent the various volumes in the model are arranged in several levels with two rings and, as there are no lateral or azimuthally connected cells, the same form of the governing equations is used to calculate flow between cells. The nodalization differences between the two models are believed to be superficial and substantially outweighed by the similarities.

Q114.2. In view of the importance of the noncondensable gas distribution in DW and its potential impact on the PCCS performance, the nodalization of the DW is of considerable interest. Both in PANDA and ESBWR, the DW is modeled with four axial nodes. However, the DW in PANDA is represented by two radial rings and also includes two small axial nodes (to represent the connecting pipes) in the middle, while the DW in ESBWR is represented by four radial rings with relatively evenly distributed four axial nodes. It seems that these are quite dissimilar nodalizations. Please discuss the possible impact of this nodalization difference in using the PANDA analyses for the validation of TRACG code. Does this imply that the DW nodalization would not be a significant factor?

R114.2. The responses presented earlier in this section have pointed out that both the PANDA and ESBWR nodalizations employ two rings (not four) to model all major regions in the containment. The two relatively short axial cells in the PANDA DW model are specifically related to the DW connecting pipe. This is a PANDA-unique feature that facilitated the simulation of asymmetric effects and their potential impact on the performance of the PCCS. There would be no technical basis for replicating this aspect of the nodalization in the ESBWR model. [[

]] The objective of the PANDA TRACG qualification was to confirm the adequacy of the code in a realistic application framework. Accordingly, the DW nodalization

was chosen to be representative of the region of the ESBWR DW represented in PANDA with no special component to ensure noncondensable holdup. Delayed release of noncondensable in PANDA was addressed by Tests P4 and P5.

Q114.3. The heat transfer in the poolside film may be a significant factor to determine the PCCS capability to remove heat. Please discuss the nodalization of the PCCS pool (it is not clear from the document) and its impact on the heat transfer in the outside surface of the PCCS pipes. The discussion should include the number of radial cells used and the effect of nodalization on the internal natural circulation and heat transfer in the pool (vs. using one cell radially). Were there any measurements which will help to determine the pool side heat transfer coefficients? List any tests or studies to validate this model/nodalization. Were there any sensitivity calculations regarding the pool side nodalization? Was the variation between parallel tubes accounted for? Was the changing level elevation accounted for in calculating the heat transfer coefficients (or effective heat transfer area)? Is the same nodalization used for ESBWR?

R114.3. The PCC pool and condenser modeling used for both PANDA and the ESBWR were verified against extensive component test data, including [[

]] In these tests, the pool-side and gas-side heat transfer modeling as well as the pool, condenser tube and header nodalizations were verified by comparisons to data over a range of conditions simulating those expected in the post-LOCA transient. The PANTHERS comparisons included a [[

]] Both the PANDA and ESBWR TRACG simulations account for the pool level decrease associated with boiloff and its effect on the poolside heat transfer coefficient and the effective condenser heat transfer area.

#### References

1. *PANDA Facility, Test Program and Data Base General Description (DTR Umbrella Report)*, Alpha-606-0, PSI, May 1996 (Non-Proprietary).
2. *ESBWR Test Report*, NEDC-33081P, August 2002 (Section 2.2).
3. *ESBWR Scaling Report*, NEDC-33082P, Rev 0, December 2002 (Section 5.5).
4. *Ibid.* (Section 8).
5. *Ibid.* (Appendix A).

6. *TRACG Qualification for SBWR*, NEDC-32725P, V. 1, Rev. 1, August 2002 (Section 4.1).
7. *Ibid.* (Section 4.3)
8. *TRACG Qualification for ESBWR*, NEDC-33080P, August 2002.
9. *TRACG Application for ESBWR*, NEDC-33083P, September, 2002 (Section 3.3.1.1.3).
10. *Ibid.* (Section 3.3.1.1.1).
11. *Ibid.* (Section 3.3.1.1.2).
12. *TRACG Qualification for SBWR*, NEDC-32725P, V. 1, Rev. 1, August 2002 (Appendix B).
13. *TRACG Application for ESBWR*, NEDC-33083P, September, 2002 (Figure 3.7-2).

Q115. The post-test results are presented in Section 2.5. Were there any attempts to do the pre-test or blind calculations? If not, why not? If there were, were any significant differences between the pre- and post-test results observed? Were any parameters adjusted during the post-test analyses? If yes, what were they? Were the same adjustment made to the ESBWR analyses?

R115. Blind pretest calculations were not done for the P-series tests described in Reference 8. Double-blind pretest calculations were done for three of the earlier M-series tests and the steady-state PANDA PCC tests documented in Revision 1 of NEDC-32725P. The M-series pretest calculations predicted the peak DW pressure within [[ ]]. The pretest calculations indicated that the prediction of WW temperature could be improved by reducing the vapor space nodalization from [[ ]]

]] This change was incorporated for the M-series post-test calculations and was also implemented in the E/SBWR containment model. At the close of the M-series post-test calculations, it was concluded that certain procedures should be implemented in the application methodology for E/SBWR containment calculations to ensure adequate consideration of the potential implications of mixing and stratification in large containment volumes. These procedures [[ ]]

]] The M-series post-test calculations also indicated that the TRACG PANDA model could be improved by representing the large DW crossover pipe by two TRACG PIPE components that would permit the simulation of back and forth circulation through the connecting pipe. This change, which was unique to the PANDA facility and had no counterpart for the ESBWR model, was incorporated in the TRACG model for the post-test calculation of the P-series tests. The other major change in the TRACG model from the M-series to the P-series was to make the RPV and the PCCS pools part of the TRACG VSSL component. The major reason for this change was to bring the PANDA model

into correspondence with the representation of these regions in the ESBWR model. The only change made in the model in the course of the P-series post-test calculations was to raise the inlet to the IC steam line to prevent liquid from entering the line. This change had no implication for the ESBWR model.

## References

1. *PANDA Facility, Test Program and Data Base General Description (DTR Umbrella Report)*, Alpha-606-0, PSI, May 1996 (Non-Proprietary).
2. *ESBWR Test Report*, NEDC-33081P, August 2002 (Section 2.2).
3. *ESBWR Scaling Report*, NEDC-33082P, Rev 0, December 2002 (Section 5.5).
4. *Ibid.* (Section 8).
5. *Ibid.* (Appendix A).
6. *TRACG Qualification for SBWR*, NEDC-32725P, V. 1, Rev. 1, August 2002 (Section 4.1).
7. *Ibid.* (Section 4.3)
8. *TRACG Qualification for ESBWR*, NEDC-33080P, August 2002.
9. *TRACG Application for ESBWR*, NEDC-33083P, September, 2002 (Section 3.3.1.1.3).
10. *Ibid.* (Section 3.3.1.1.1).
11. *Ibid.* (Section 3.3.1.1.2).
12. *TRACG Qualification for SBWR*, NEDC-32725P, V. 1, Rev. 1, August 2002 (Appendix B).
13. *TRACG Application for ESBWR*, NEDC-33083P, September, 2002 (Figure 3.7-2).

Q116. The time step sizes sometimes influence the results of the calculations. Are the time step sizes of the PANDA analysis similar to those of ESBWR analysis (maximum as well as average)? What was the basis of the time step selections?

R116. TRACG chooses its timestep in accordance with an internal logic that continuously optimizes the accuracy and efficiency of the calculation. The only control imposed by the user is to supply a maximum and minimum timestep. TRACG will not use a timestep larger than the specified maximum and it will stop if its built-in accuracy criteria require it to use a timestep smaller than the specified minimum. In addition, the user may divide the duration of the calculation into segments and vary the specified maximum and minimum timesteps from segment to segment. The ESBWR containment calculation uses a maximum timestep of [[            ]] for the first hour of the simulation and [[            ]] thereafter. The minimum timestep is [[            ]] for the first hour and [[            ]] thereafter. For the PANDA runs, which involved deliberately imposed and relatively abrupt transient changes, the maximum timestep ranged from 0.02 to 0.2 s and the minimum timestep was [[            ]] except for a short



Q117.1. Should this phenomenon repeat periodically, since the excess heat removal capability still exists?

R117.1. An important operating characteristic of the PCCS is [[

]] If the heat removal capacity of the system falls below the DW heat load, [[

]]

Q117.2. If the high heat removal capacity reduces the  $\Delta p$ , shouldn't the PCCS heat removal and  $\Delta p$  balance eventually at some equilibrium? (It should be noted that the PCCS inlet flow rates in Figure P1/8-3 and the PCCS heat removal in Figure P1/8-2 did not decrease markedly during this period when the  $\Delta p$  decreases.)

R117.2. The flow to the condenser units is [[

II

Figure 117.2.1. TRACG Pressure Differences for PANDA Test P4

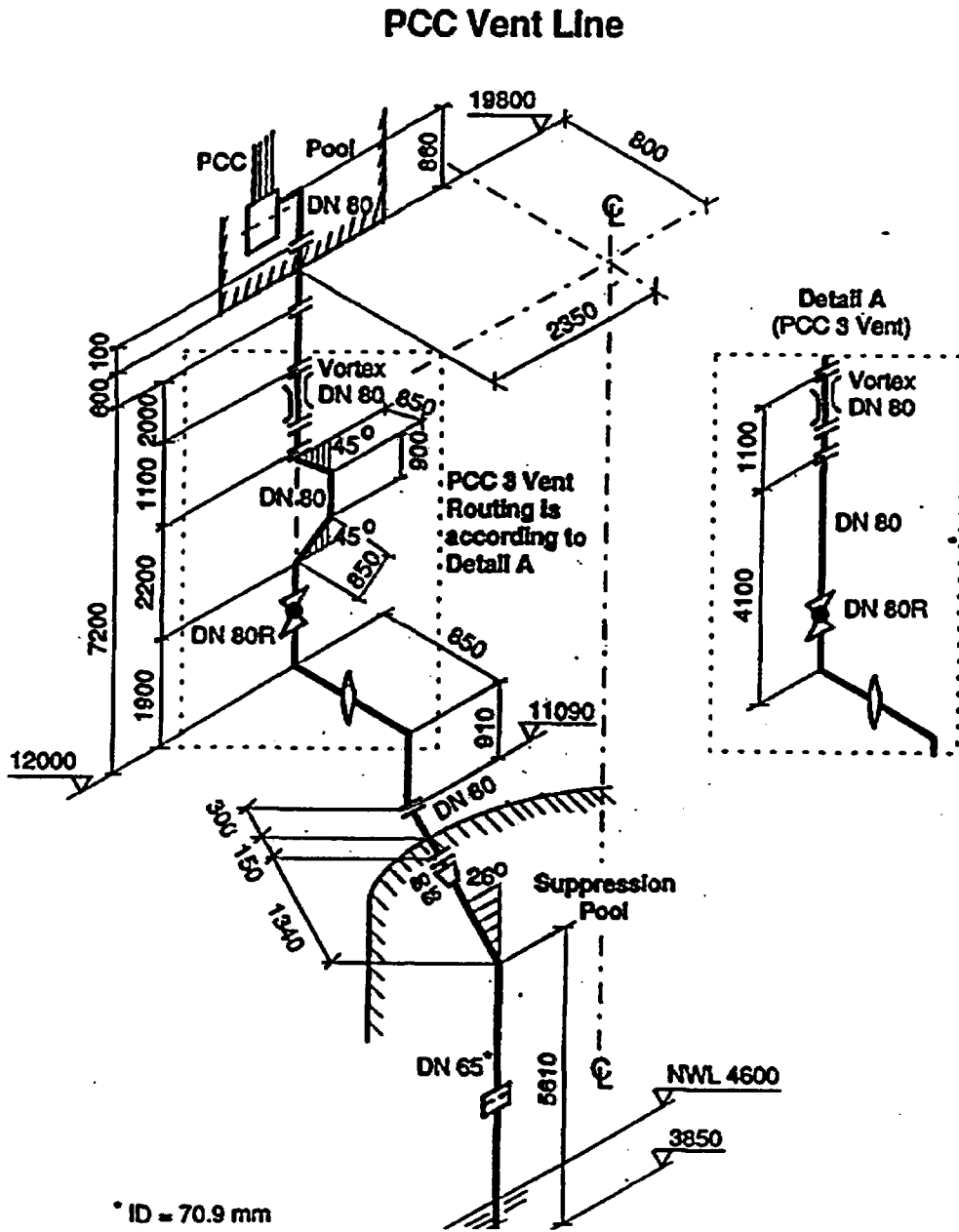
[[Supplementary Information for RAI 117.2

**PCC to WW Pressure Difference vs Vent Phase Indication**

]]

Supplementary Information for RAI 117.2

PCC Vent Pressure Tap – Located on downstream side of vortex flow meter



- Q117.3. The DW pressure drops happened at considerably different times for the test and the analysis for some tests, (about 12000 and 8000 sec for P1, 7000 and 13000 seconds for P2, 22000 and 12000 sec for P6). It happens earlier for test than analysis for some tests, and later for some other tests. Please discuss how this discrepancy and inconsistency will affect the ESBWR DW calculation.
- R117.3. TRACG had a varying degree of success in predicting the timing of the first VB opening. The results ranged from [[

]] The integrated energy removal by the PCCS will match the decay heat input over the long term even though there are intermediate periods where the heat removal exceeds or lags behind the decay heat.

Q117.4. Were similar drops in the DW pressure and  $\Delta p$  also observed in this period in the ESBWR analysis?

R117.4. Yes. The ESBWR post-LOCA containment pressure response shows similar drops in the DW pressure. Typically, about [[  
]] are observed in the course of a  
72-hour ESBWR analysis [13].

#### References

1. *PANDA Facility, Test Program and Data Base General Description (DTR Umbrella Report)*, Alpha-606-0, PSI, May 1996 (Non-Proprietary).
2. *ESBWR Test Report*, NEDC-33081P, August 2002 (Section 2.2).

3. *ESBWR Scaling Report*, NEDC-33082P, Rev 0, December 2002 (Section 5.5).
4. *Ibid.* (Section 8).
5. *Ibid.* (Appendix A).
6. *TRACG Qualification for SBWR*, NEDC-32725P, V. 1, Rev. 1, August 2002 (Section 4.1).
7. *Ibid.* (Section 4.3)
8. *TRACG Qualification for ESBWR*, NEDC-33080P, August 2002.
9. *TRACG Application for ESBWR*, NEDC-33083P, September, 2002 (Section 3.3.1.1.3).
10. *Ibid.* (Section 3.3.1.1.1).
11. *Ibid.* (Section 3.3.1.1.2).
12. *TRACG Qualification for SBWR*, NEDC-32725P, V. 1, Rev. 1, August 2002 (Appendix B).
13. *TRACG Application for ESBWR*, NEDC-33083P, September, 2002 (Figure 3.7-2).

Q118. For tests P1 and P2, substantial  $\Delta p$  between the DW and WW (P1-1a and P2-1a) and flow to PCCS (P1-3 and P2-3) are maintained throughout the tests. This should imply either noncondensable gases or steam is flowing to WW and, therefore, the WW pressure should increase. However, the WW pressure remains constant (P2-1) or declines (P1-1). Please discuss if this observation is correct, and, if correct, please explain why. (Does this mean that there is no  $\Delta p$  between the PCCS and WW, and thus no flow?)

R118. The characteristic state of the PCCS condenser units is [[

]] The flow into the  
condenser is [[

]] Over large time periods of the post-LOCA transient, [[

]] Over the  
long term, however, the amount of noncondensable purged to the WW is [[

]]

Q119. In general, the code does not seem to predict  $\Delta p$  (between DW and WW) very well for the PANDA tests, although it shows good matches for the magnitudes of the pressure and overall heat removal. In view that the  $\Delta p$  is the important variable in determining the performance of PCCS, please discuss how the PANDA results can be used for the validation of TRACG.

R119. Following the initial blowdown and PCCS startup, the PCCS operates [[

that TRACG correctly simulates [[ ]] The PANDA tests confirmed ]]

Q120. Editorial comments:

Q120.1. Definitions of the TRACG variables in the figures are not provided. While some of variables are obvious, some are difficult to figure out. Some examples are D1L12C1-TR in Figure P1/8-15, or D2L12C2-TR in Figure P1/8-16, etc.

R120.1. The following table describes the notation used for the TRACG variables in all of the comparison plots:

Figure	Notation	Quantity	Location
1	DW1	Pressure (bar)	DW1
1	WW1	Pressure (bar)	WW1
1a	DW-WW	Pressure Difference (bar)	DW1-WW1
2	IC	Power (kW)	IC
2	PCC1	Power (kW)	PCC1
2	PCC23	Power (kW)	PCC23
2	TOT PCC/IC	Power (kW)	Total Condenser Power
3	PCC1	Inlet Flow (g/s)	To PCC1
3	PCC23	Inlet Flow (g/s)	To PCC23
3	IC	Inlet Flow (g/s)	To IC
4	RPV lev	Collapsed Level (m)	RPV
4	GDCS lev	Collapsed Level (m)	GDCS Pool
5	PCC1	Collapsed Level (m)	PCC1 Pool
5	PCC23	Collapsed Level (m)	PCC23 Pool
5	IC	Collapsed Level (m)	IC Pool
6	N/A		
7	IC/UH	Temperature (C)	IC Upper Header
7	IC/C1	Temperature (C)	IC Cell 1
7	IC/C3	Temperature (C)	IC Cell 3
8	IC/C4	Temperature (C)	IC Cell 4
8	IC/C6	Temperature (C)	IC Cell 6
8	IC/C8	Temperature (C)	IC Cell 8

Figure	Notation	Quantity	Location
8	IC/LH	Temperature (C)	IC Lower Header
9	P1/UH	Temperature (C)	PCC1 Upper Header
9	P1/C1	Temperature (C)	PCC1 Cell 1
9	P1/C3	Temperature (C)	PCC1 Cell 3
10	P1/C4	Temperature (C)	PCC1 Cell 4
10	P1/C6	Temperature (C)	PCC1 Cell 6
10	P1/C8	Temperature (C)	PCC1 Cell 8
10	P1/LH	Temperature (C)	PCC1 Lower Header
11	P23/UH	Temperature (C)	PCC23 Upper Header
11	P23/C1	Temperature (C)	PCC23 Cell 1
11	P23/C3	Temperature (C)	PCC23 Cell 3
12	P23/C4	Temperature (C)	PCC23 Cell 4
12	P23/C6	Temperature (C)	PCC23 Cell 6
12	P23/C8	Temperature (C)	PCC23 Cell 8
12	P23/LH	Temperature (C)	PCC23 Lower Header
13	Same as Fig. 11		
14	Same as Fig. 12		
15	D1L9C1	Temperature (C)	DW1; Level 9; Inner Ring
15	D1L9C5	Temperature (C)	DW1; Level 9; Outer Ring
15	D1L12C1	Temperature (C)	DW1; Level 12; Inner Ring
15	D1L12C5	Temperature (C)	DW1; Level 12; Outer Ring
16	D2L9C2	Temperature (C)	DW2; Level 9; Inner Ring
16	D2L9C6	Temperature (C)	DW2; Level 9; Outer Ring
16	D2L12C2	Temperature (C)	DW2; Level 12; Inner Ring
16	D2L12C6	Temperature (C)	DW2; Level 12; Outer Ring
17	W1L6C1	Temperature (C)	WW1; Level 6; Inner Ring
17	W1L6C5	Temperature (C)	WW1; Level 6; Outer Ring
17	W1L7C1	Temperature (C)	WW1; Level 7; Inner Ring
17	W1L7C5	Temperature (C)	WW1; Level 7; Outer Ring
18	W1L3C1	Temperature (C)	WW1; Level 3; Inner Ring
18	W1L3C5	Temperature (C)	WW1; Level 3; Outer Ring
18	W1L4C1	Temperature (C)	WW1; Level 4; Inner Ring
18	W1L4C5	Temperature (C)	WW1; Level 4; Outer Ring
18	W1L5C1	Temperature (C)	WW1; Level 5; Inner Ring
18	W1L5C5	Temperature (C)	WW1; Level 5; Outer Ring
19	W2L6C1	Temperature (C)	WW2; Level 6; Inner Ring
19	W2L6C5	Temperature (C)	WW2; Level 6; Outer Ring
19	W2L7C1	Temperature (C)	WW2; Level 7; Inner Ring
19	W2L7C5	Temperature (C)	WW2; Level 7; Outer Ring
20	W2L3C1	Temperature (C)	WW2; Level 3; Inner Ring
20	W2L3C5	Temperature (C)	WW2; Level 3; Outer Ring
20	W2L4C1	Temperature (C)	WW2; Level 4; Inner Ring
20	W2L4C5	Temperature (C)	WW2; Level 4; Outer Ring

Figure	Notation	Quantity	Location
20	W2L5C1	Temperature (C)	WW2; Level 5; Inner Ring
20	W2L5C5	Temperature (C)	WW2; Level 5; Outer Ring
21	D1L9C1	Air Partial Pressure (bar)	DW1; Level 9; Inner Ring
21	D1L9C5	Air Partial Pressure (bar)	DW1; Level 9; Outer Ring
21	D1L12C1	Air Partial Pressure (bar)	DW1; Level 12; Inner Ring
21	D1L12C5	Air Partial Pressure (bar)	DW1; Level 12; Outer Ring
22	D2L9C2	Air Partial Pressure (bar)	DW2; Level 9; Inner Ring
22	D2L9C6	Air Partial Pressure (bar)	DW2; Level 9; Outer Ring
22	D2L12C2	Air Partial Pressure (bar)	DW2; Level 12; Inner Ring
22	D2L12C6	Air Partial Pressure (bar)	DW2; Level 12; Outer Ring
23	VB1-LEAK	VB1 Leakage Flow (g/s)	DW1 to WW1 via VB1

Q120.2. It appears there is an error in Table 2-11 (Page 2-43). The elevation of instrument MTG.D1.2 is denoted as 38 m from tank bottom.

R120.2. The entries for MTG.D1.2 and MTG.D2.2 should be “5.78m from tank bottom”.

Q121. In Figure P1/8-1a, when the VB opens, the  $\Delta p$  quickly increased (restored) to the level before the VB opening.

R121. This behavior is typical of the PCCS performance. [[

]]

Q121.1. Please explain why the DW pressure increases above the WW pressure. Is this due to a temporary decrease in the PCCS heat removal capability caused by the noncondensable gases in the DW?

R121.1. Yes. The PCCS heat removal capability is temporarily degraded by the ingestion of noncondensable. The increased pressure allows the condenser units to [[  
]]

Q121.2. Why does the PCCS performance deteriorate so much when the noncondensable gas concentration increases very little (Figure P1/8-21 shows the concentration in DW is less than 0.3%, i.e., noncondensable gas partial pressure of 0.005 bar) after the VB opening. Is this an indication of impact of a very small amount of noncondensable gases on the PCCS performance?

R121.2. There are [[

]]

Q121.3. When the vacuum breaker (VB) opened at 12,000 seconds in P1, the noncondensable gas concentration in DW increased slightly (to 0.005 bar) (Figure P1/8-21). However, when the VB opened in P2 (Figures P2-21 and -22), it increased to 0.3 bar. Please explain why the DW noncondensable gas concentration increases are so different between these two tests.

R121.3. The transients leading to the VB openings in Tests P1 and P2 are [[

]]

Q122. Figure P1/8-2 shows a sustained deficit of the heat removal by the PCCS. Yet, the DW/WW pressures essentially remain constant during the whole test. Please explain why the cumulative effect of this heat removal deficit is not exhibited in the pressure? Wouldn't this eventually be an issue when it continues for 72 hours (259,200 seconds)?

R122. The results shown in Figure P1/8-2 [[

]]

#### References

1. *PANDA Facility, Test Program and Data Base General Description (DTR Umbrella Report)*, Alpha-606-0, PSI, May 1996 (Non-Proprietary).
2. *ESBWR Test Report*, NEDC-33081P, August 2002 (Section 2.2).
3. *ESBWR Scaling Report*, NEDC-33082P, Rev 0, December 2002 (Section 5.5).
4. *Ibid.* (Section 8).
5. *Ibid.* (Appendix A).
6. *TRACG Qualification for SBWR*, NEDC-32725P, V. 1, Rev. 1, August 2002 (Section 4.1).
7. *Ibid.* (Section 4.3)

8. *TRACG Qualification for ESBWR*, NEDC-33080P, August 2002.
9. *TRACG Application for ESBWR*, NEDC-33083P, September, 2002 (Section 3.3.1.1.3).
10. Ibid. (Section 3.3.1.1.1).
11. Ibid. (Section 3.3.1.1.2).
12. *TRACG Qualification for SBWR*, NEDC-32725P, V. 1, Rev. 1, August 2002 (Appendix B).
13. *TRACG Application for ESBWR*, NEDC-33083P, September, 2002 (Figure 3.7-2).

Q123. Figure P1/8-1a shows  $\Delta p$  is zero around 35,000 sec for the analysis, but Figure P1/8-3 shows a sustained PCCS inlet flow. Please explain what is the driving force for this flow at this time. If this is condensation driven, is this an indication that PCCS does not need  $\Delta p$  (DW-WW) to operate, at least when the noncondensable gas concentration is low?

R123. Yes, the PCCS inlet flow [[

]]

Q124. For Test P1/8, it appears that the code does not predict the  $\Delta p$  very well in the period of 0-50,000 seconds (the  $\Delta p$  decreased to zero periodically for the analysis, while a sustained  $\Delta p$  was observed in the test after initial dip). In view that the  $\Delta p$  is the driving force of the PCCS (it also impacts on the VB opening, which influence the noncondensable gas concentration in the DW), please discuss how the results of simulation of this test can be used to validate the code.

R124. As stated in the response to RAI 123, [[

]] The PANDA tests (M-series and P-series) demonstrated the validity of this assertion by subjecting the system to a wide range of challenges and showing that the important features of the response (the range of drywell and wetwell pressures and integrated energy removal) could be adequately predicted by TRACG.

Q125. Figure P1/8-5 shows that the PCCS pool level decreases to the lower header upper edge in 100,000 seconds. Is this representative of the ESBWR PCCS pool level in this time period? In view that the ESBWR containment cooling is expected to last 72 hours (259,200 seconds), please discuss why this depletion of pool water is acceptable.

R125. One of the compromises made in the design of the PANDA test facility was to not scale the volume of water available to replace boiloff in the ESBWR PCCS. [[

]] This is more than sufficient to remove the decay heat load.

Q126. The test and calculated gas and liquid temperatures in the WW are substantially different (Figures P1/8-17 through P1/8-20). While the calculated temperatures are constant, the test temperatures are shown to initially increase and then decrease (at around 20,000 seconds for liquid and around 40,000 seconds for the gas).

R126. Please see the responses to the individual questions below.

Q126.1. Please explain this difference between the tests and analyses, discussing why this test can be used for the TRACG validation for ESBWR in spite of this difference.

R126.1. A characteristic of the TRACG simulation of PANDA is to [[

]]

Q126.2. Please explain why the test WW liquid and gas temperatures start decreasing at about 25,000 seconds and 40,000 seconds, respectively, in the test when seemingly nothing else happens.

R126.2. The rise in the WW gas temperature stops at approximately [[

]] The PANDA main vents correctly simulate the ESBWR during the time that there is flow through them from the DW to the suppression pool. [[

]]

Q126.3. Please also explain why the WW gas temperature continues to increase between 20,000-40,000 seconds, while the pool surface temperature starts to decrease at about 25,000 seconds.

R126.3. As described above, the increase in the WW gas temperature was [[

]]

Q126.4. Beyond 40,000 seconds, both the WW gas and liquid temperatures continue to decrease in the test. Where does the energy go during this period (i.e., what cools the WW gas and liquid)?

R126.4. The WW gas is primarily [[

]]

Q127. The purpose of this test is “to examine PCCS behavior and system interactions during the transitional period from the end of blowdown to the initiation of long-term cooling” (Section 2.3.1). However, “the comparison was adversely affected by the leaky check valve,” (Section 2.5.2.1) and consequently it appears difficult to derive any conclusions for the period when it was intended to be studied. Please explain why this test is still relevant.

R127. The objective of Test P2 was to demonstrate the PCCS response early in the post-LOCA transient, [[

]]

Q128. In Section 2.5.2.1, measured and calculated DW and WW pressures and the DW-to-WW pressure difference for test P2 are compared in Figures P2-1 and 1a. It is explained that the cause for discrepancies was due to equipment malfunction and that it was not important as calculated pressures were in line with the measurement. However, Figure P2-1a clearly shows a substantially different trend.

R128. While there are differences in the [[  
overall pressure responses are similar. The major difference is [[ ]]

]] The  
predicted and observed phenomena are similar but the [[  
]]

Q128.1. Please explain this discrepancy between the test and analysis and justify why TRACG is applicable to ESBWR LOCA calculation despite this discrepancy, in view that the  $\Delta p$  is the driving force of the PCCS and also affects the GDCS flow rate.

R128.1. As described in prior responses, [[  
]] The driving force for flow to the PCCS from the DW in this  
period [[

]] Both the test and the TRACG simulation are  
valid demonstrations of the behavior of the ESBWR during and following the late  
stage of GDCS injection.

Q128.2. Why does the test  $\Delta p$  rise initially in the test? Since there is no steam generation during this period, it seems the  $\Delta p$  should be near zero.

R128.2. As seen in Figure P2-2, RPV heater power [[  
]] It is  
believed that the brief initial RPV (and DW) pressure rise in the test was [[  
]] In this test, the initial RPV conditions [[

]]

Q129. Figure P2-1 shows a pressure difference between the DW pressures of the test and calculation in the initial phase (GDCS injection phase), which is substantial at this phase. Therefore, it seems that the code does not simulate this phase very well. Please explain the cause of this difference and discuss the significance of this difference in the TRACG validation.

R129. It is believed that the [[

]] The measurements indicate that [[

]]

Q130. Figure P2-3 shows the PCCS inlet flow and  $\Delta p$  between DW and WW (figure P2-1a) for the calculation. Please explain what is the driving force of this PCCS flow during the period from 5,000 to 13,000 seconds and from 15,000 to 20,000 seconds. Figure P2-3 also shows that the PCCS heat removal rates are similar for the test and calculation, while the  $\Delta p$ 's are substantially different between the test and calculation (for example, during 15,000-20,000 seconds). Please explain why the PCCS performance is not affected by the  $\Delta p$ .

R130. The flow to the PCCS in this period is [[  
]] As shown in the figure accompanying the response to RAI 117.2,  
the [[

]]

Q131. Figure P2-4 shows the calculated level difference between RPV and GDCS at a specified WW-DW pressure difference (Figure P2-1a) and corresponding water level. Since the WW pressure is lower than DW, shouldn't the GDCS tank level be higher than the RPV by at least the same amount? Please explain.

R131. The GDCS tank level is not related to the RPV level by [[

]]

Q132. Figures P2-18 and p2-20 show the WW water surface temperature peaked at about 7,000 seconds and then decreased. Please explain what mechanism contributed to this cooling. On the other hand, the same figures show that the calculated liquid temperature increases steadily. Please discuss what impact this discrepancy would have in using the TRACG for ESBWR analyses.

R132. The rise in the measured WW surface temperature (floating temperature probe) was [[

]]

Q133. Figures P2-21 and P2-22 show steady increases of the noncondensable gas in the DW for the calculation while the noncondensable gas concentration rises quickly and remains at that level for the test. Since the period in which the VB is open is much shorter for the test, it appears that the noncondensable gas flow rate is much higher during the short period when the VB was open for the test. Please compare the noncondensable gas flow rates when the VB are open for the test and calculation and explain the disparity of the flow rates, so the staff can assess how well the TRACG simulates the VB flow rates.

R133. Figures P2-21 and P2-22 compare the air partial pressure from [[

]]

Q134. It is stated in Section 2.5.3.1 that “TRACG’s calculation of the air purging rate from DW2 and portions of DW1 above the connecting pipe are in good agreement with the measurements (Figures P3-21 and 22).”

R134. Please see the responses to the individual questions below.

Q134.1. However, Figure P3-22 shows very high degree of stratification of air partial pressure in DW2 for the calculation, while relatively uniform distribution for the test during the initial 10,000 seconds (the period when it matters most in terms of the noncondensable gases). Please discuss how GE drew the conclusion of “good agreement” from this figure.

R134.1. Figure P3-22 shows air partial pressure measurements near the top (MPG\_D2\_1), in the middle (MPG\_D2\_2) and at the bottom (MPG\_D2\_3) of DW2. The measurement locations are close to the vessel centerline. [[

]]

Q134.2. Figure P3-21 and Figure P3-15 show TRACG was unable to simulate the trapped noncondensable gas in DW2. Please explain how this TRACG shortcoming is handled in ESBWR analyses.

R134.2. Figure P3-21 shows comparisons of measured and calculated air partial pressures in DW1, which was isolated in this test. [[

]]

Q135. These tests are intended to investigate the effect on PCCS performance of the delayed release of noncondensable gas from a region of the DW not directly accessible to RPV steam flow. However, the results (test as well as analysis) show that the noncondensable gases are quickly swept to the WW once the injection stops similar to what happens earlier. Then the system repeats similar behavior observed at the beginning of the tests, at slightly higher pressure. In other words, these tests don't seem to provide any more information than obtained in P1. To address the impact of slow seepage (bleeding) of a small amount of noncondensable gases through the PCCS and possible degradation of PCCS capability to remove heat in the presence of these gases, could a small amount of noncondensable gas (in the order of 1% or less) be continuously injected to the DW during the test? Are there any such test data available?

R135. Tests P4 and P5 adequately demonstrate the manner in which the PCCS would respond to the ingestion of a slug of noncondensable at any time during the long-term post-LOCA transient. [[

]]

Q136. Test P6 was performed to “consider system interaction effects associated with parallel operation of the ICS and PCCS and the effect of a direct bypass of steam from the DW to the WW air space.” Why are these effects combined in one test? Is the bypass of steam more important when the ICS and PCCS operate together? It seems these two unrelated effects make it harder to understand the results.

R136. Test P6 was composed of a [[

]] In addition to information on single and multiple system interactions, it is believed that Test P6 provided a more meaningful challenge for TRACG than would a series of tests involving only single interactions.

Q137. Why does the  $\Delta p$  decrease slower for P6 (Figure P6-1a) compared to P1 (Figure P1/8-1a), when less steam is sent to the DW in P6?

R137. The rate of decrease of the DW pressure is primarily determined [[

]]

Q138. It appears that the  $\Delta p$  decreases to zero at about 20,000 seconds and again at about 40,000 sec (Figure P6-1a) for the test, because of the VB leakage bypassing steam from the DW to the WW. However, Figure P6-2 shows that the PCCS still removes most of the heat at these time periods. What is the driving force of the PCCS flow and why does the PCCS still work when  $DP=0$ ?

R138. As discussed in the responses to prior questions, the [[

]]

Q139. What was the cause of the sudden blip of  $\Delta p$  for the calculation at about 42,000 seconds, when seemingly nothing else happens? The concern is whether this kind of anomaly may show up somewhere else in the TRACG calculations of ESBWR.

R139. The “blip” in the TRACG DW pressure at about 42,000 s is [[

]]

Q140. Figure P6-23 shows that TRACG substantially over-predicted the VB leakage flow rate during 15,000-25,000 seconds (the period when IC operation and VB opening overlapped), while it gave a good match after 25,000 seconds. Please discuss this inconsistency and its implication in TRACG application to ESBWR. The concern is when to trust the TRACG calculation of the VB leakage rate and when not to.

R140. The VB leakage is [[

]]

Q141. In Section 2.6.2.2, it is stated that "PCC tube gas temperature comparisons indicate that, for given inlet conditions, TRACG requires a somewhat greater length of the condenser tubes to achieve complete condensation." However, this point was not discussed in any individual test. Please explain how this conclusion is derived from the tests.

R141. This conclusion is reached by comparing the calculated and measured positions [[

]] The more important point is that both the test and the calculation show that the PCCS has significant margin relative to the long-term decay heat load.

#### References

1. *PANDA Facility, Test Program and Data Base General Description (DTR Umbrella Report)*, Alpha-606-0, PSI, May 1996 (Non-Proprietary).
2. *ESBWR Test Report*, NEDC-33081P, August 2002 (Section 2.2).
3. *ESBWR Scaling Report*, NEDC-33082P, Rev 0, December 2002 (Section 5.5).
4. *Ibid.* (Section 8).
5. *Ibid.* (Appendix A).

6. *TRACG Qualification for SBWR*, NEDC-32725P, V. 1, Rev. 1, August 2002 (Section 4.1).
  7. Ibid. (Section 4.3)
  8. *TRACG Qualification for ESBWR*, NEDC-33080P, August 2002.
  9. *TRACG Application for ESBWR*, NEDC-33083P, September, 2002 (Section 3.3.1.1.3).
  10. Ibid. (Section 3.3.1.1.1).
  11. Ibid. (Section 3.3.1.1.2).
  12. *TRACG Qualification for SBWR*, NEDC-32725P, V. 1, Rev. 1, August 2002 (Appendix B).
  13. *TRACG Application for ESBWR*, NEDC-33083P, September, 2002 (Figure 3.7-2).
- Q142. In Section 2.6.2.3, it is stated that “a relatively large uncertainty in poolside heat transfer could be tolerated without adversely affecting the ability of TRACG to calculate the behavior of the PCCS in context of an overall systems model of the containment.” Please discuss how this conclusion was determined, and provide specific data, if any, to support this conclusion.
- R142. The basis for this statement is that the poolside thermal resistance represents [[
- ]]
- Q143. In Section 2.6.2.8, it is stated that, “The modeling features described above have minimal impact on the calculation of system pressure and lead to a conservative prediction of WW gas temperature. The WW pressure is primarily set by the inventory of noncondensable gas with a minor contribution from the partial pressure of the steam in the gas space. The steam partial pressure is, in turn, set by the temperature at the surface of the SP [suppression pool].”
- R143. Please see the responses to the individual questions below.
- Q143.1. Please explain why the modeling leads to a conservative prediction of WW gas temperature.
- R143.1. The modeling features cited [[
- ]]
- Q143.2. In the long term, the containment pressure is determined by the partial pressure of the steam in the gas space in addition to the non-condensable gas mass in the WW gas space, which is determined by the liquid surface temperature, which is determined by how much of the uncondensed steam in the PCCS is deposited in the WW water. How well the PCCS performs eventually affects the WW liquid temperature and WW pressure. Please discuss why the partial pressure of the steam in the gas space is a minor contributor to the WW pressure. Please note that WW4 is ranked as high in the phenomena identification and ranking table (PIRT) for ESBWR Containment/LOCA.

R143.2. The word "minor" was in reference to the relative contributions of the noncondensable and the steam. [[

]]

**Update of ESBWR TRACG Qualification for NEDC-33080P Using the 9-  
Apr-2004 Program Library Version of TRACG04**

**Table of Contents**

1.0	INTRODUCTION .....	34
2.0	INTEGRAL SYSTEMS TESTS .....	35
2.1	PANDA Transient Tests (P-Series) .....	35
3.0	NATURAL CIRCULATION AND FLOW OSCILLATION TESTS .....	40
3.1	SIRIUS Two-Phase Flow Instability Tests .....	40
4.0	REFERENCES .....	42

## 1.0 INTRODUCTION

The purpose of this supplement is to present an updated subset of the qualification studies presented in NEDC-33080P, "TRACG Qualification for ESBWR", Rev. 0, August 2002 using the 9-April-2004 GENE Program Library version of TRACG04. This update provides assurance that the conclusions drawn from the qualification studies performed with earlier versions of TRACG remain valid. The 9-April-2004 version of TRACG is the version used to calculate the results presented in the ESBWR Application Report and, as such, the updated qualification studies are consistent with the results presented in the Application Report.

The presentations in this supplement are arranged in the same sequence as in NEDC-33080P, i.e., the PANDA P-Series integral systems tests followed by the SIRIUS two-phase flow instability tests. Each of these qualification studies is represented by an updated calculation for at least one of the tests included in the original study. To make this supplement reasonably self-contained, each section includes a brief description of the test facility and test matrix and the TRACG model of the facility. The test(s) selected for the update are identified and results are presented in the form of compound figures that show both the original and updated comparisons between the TRACG calculations and the test results. To facilitate reference to the more detailed descriptions in NEDC-33080P, the figure numbers used for the original TRACG vs. data comparisons in that report have been retained.

## 2.0 INTEGRAL SYSTEMS TESTS

### 2.1 PANDA Transient Tests (P-Series)

A confirmatory PANDA test program designated as the P-series was performed after the facility was modified to incorporate specific features of the ESBWR design. As in the case of the prior M-series tests, the emphasis was on the long-term cooling phase of a LOCA caused by a main steamline break (MSLB). To more closely represent the ESBWR containment configuration, the PANDA facility was modified to connect the GDCS gas space to the WW gas space instead of to the DW as for the M-series. The P-series test matrix consisted of Tests P1, P2, P3, P4, P5, P6, P7 and P8. Test P1 was a base-case simulation of the long-term cooling phase following a MSLB LOCA. Test P2 was configured to cover the transition from the GDCS injection phase to the long-term cooling phase. Test P3 demonstrated PCCS startup from a condition representing the maximum initial inventory of noncondensable gas in the DW. Tests P4 and P5 addressed long-term cooling performance with the delayed release of noncondensable gas in the DW. Test P6 addressed parallel operation of the ICS and PCCS and the direct bypass of DW steam to the WW gas space. Test P7 addressed PCCS performance in the presence of a noncondensable gas (helium) that is lighter than steam. Test P8, performed as an extension of Test P1, addressed PCCS behavior with the secondary-side pool water level below the bottom of the condenser upper headers.

For the August 2002 ESBWR qualification study [4-1, Section 2], TRACG calculations were performed for all of the P-series tests. The TRACG input model for the P-series tests differed from that used for the M-series primarily by the inclusion of the RPV and the PCC and IC secondary-side pools in the VSSL component along with the DW, WW and GDCS pool. The model was, of course, modified to represent the connection of the GDCS gas space to the WW gas space. As for the M-series, the method used to initiate and control the TRACG transient simulations closely followed the procedure used in the PANDA facility. Test P4 (delayed injection of DW noncondensable) and P6 (parallel operation of the ICS and PCCS and DW-to-WW steam bypass) were selected for the current qualification update.

Updated comparisons between TRACG calculations and PANDA P-series measurements for Tests P4 and P6 are shown in Figures P4-1 and P6-1 (DW and WW pressures) and P4-3 (PCC inlet flows) and P6-3 (IC and PCC inlet flows). [[

]]

[[

**Figure P4-1. Drywell and Wetwell Pressures for Test P4**  
**Upper – Original [4-1] Lower – TRACG04 (9-Apr-2004) ]]**

[[

**Figure P4-3. PCC Inlet Flows for Test P4**  
**Upper – Original [4-1] Lower – TRACG04 (9-Apr-2004) ]]**

[[

**Figure P6-1. Drywell and Wetwell Pressures for Test P6  
Upper – Original [4-1] Lower – TRACG04 (9-Apr-2004) ]]**

[[

**Figure P6-3. IC and PCC Inlet Flows for Test P6**  
**Upper – Original [4-1] Lower – TRACG04 (9-Apr-2004) ]]**

### 3.0 NATURAL CIRCULATION AND FLOW OSCILLATION TESTS

#### 3.1 SIRIUS Two-Phase Flow Instability Tests

The ESBWR TRACG qualification included simulation of two-phase flow instability tests performed in the SIRIUS loop of the CRIEPI test facility in Japan. The SIRIUS loop was designed to investigate thermal-hydraulic instabilities in natural-circulation BWRs. The test loop consisted of two electrically heated channels, a chimney, upper plenum/separator, downcomer, preheater and subcooler. Test measurements included the channel inlet flow and temperature. Data were collected at a fixed system pressure by maintaining constant channel power while using the preheater to vary the channel inlet subcooling. (The recorded inlet subcooling values were based on the upper plenum pressure.) Pressure drop, flow and temperature data were recorded at each subcooling. With these data, it was possible to estimate the subcooling that marked the transition from stable to oscillatory flow at each power level.

The original qualification study [4-1, Section 3] included TRACG simulation of testing sequences performed at system pressures of 2.0 and 7.2 MPa. For the current update, the TRACG04 simulation of the 2.0 MPa test sequence at a power corresponding to a channel heat flux of  $190 \text{ kW/m}^2$  was repeated. Figure 3-3 shows the updated and original comparisons between calculated and measured stable inlet velocities as functions of inlet subcooling. [[

]]

[[

]]

[[

**Figure 3-3. Comparison of Measured and Calculated Steady-State Inlet Velocities as a Function of Inlet Subcooling at 2.0 MPa and 190 kW/m<sup>2</sup>**  
Upper – Original [4-1] Lower – TRACG04 (9-Apr-2004) ]]

#### **4.0 REFERENCES**

- 4-1. NEDC-33080P, "TRACG Qualification for ESBWR", Rev. 0, August 2002.